

# **OptiSystem**

## Tutorials - Volume 2

Optical Communication System Design Software

---

Version 7.0  
for Windows® XP/Vista





---

# OptiSystem

## Tutorials - Volume 2

Optical Communication System Design Software

---

### **Copyright © 2008 Optiwave**

All rights reserved.

All OptiSystem documents, including this one, and the information contained therein, is copyright material.

No part of this document may be reproduced, stored in a retrieval system, or transmitted in any form or by any means whatsoever, including recording, photocopying, or faxing, without prior written approval of Optiwave.

### **Disclaimer**

Optiwave makes no representation or warranty with respect to the adequacy of this documentation or the programs which it describes for any particular purpose or with respect to its adequacy to produce any particular result. In no event shall Optiwave, its employees, its contractors or the authors of this documentation, be liable for special, direct, indirect, or consequential damages, losses, costs, charges, claims, demands, or claim for lost profits, fees, or expenses of any nature or kind.

## **Technical support**

If you purchased Optiwave software from a distributor that is not listed here, please send technical questions to your distributor.

### **Optiwave**

**Tel** (613) 224-4700

**Fax** (613) 224-4706

**E-mail** [support@optiwave.com](mailto:support@optiwave.com)

**URL** [www.optiwave.com](http://www.optiwave.com)

### **Canada/US**

### **Cybernet Systems Co., Ltd.**

**Tel** +81 (03) 5978-5414

**Fax** +81 (03) 5978-6082

**E-mail** [owtech@cybernet.co.jp](mailto:owtech@cybernet.co.jp)

**URL** [www.cybernet.co.jp](http://www.cybernet.co.jp)

### **Japan**

### **Optiwave Europe**

**Tel** +33 (0) 494 08 27 97

**Fax** +33 (0) 494 33 65 76

**E-mail** [support@optiwave.com](mailto:support@optiwave.com)

**URL** [www.optiwave.eu](http://www.optiwave.eu)

### **Europe**

---

# Table of contents

---

<b>Introduction .....</b>	<b>1</b>
<b>Raman amplifiers .....</b>	<b>3</b>
<b>100 nm bandwidth flat-gain Raman amplifier—Average power model.....</b>	<b>5</b>
<b>Flattening the gain of broadband Raman amplifier with</b>	
<b>multipump configuration.....</b>	<b>13</b>
<b>Optimizing the pump power and frequencies of</b>	
<b>Raman amplifiers for gain flatness .....</b>	<b>19</b>
<b>Raman Amplifier - Dynamic Model.....</b>	<b>25</b>
<b>SOA amplifiers.....</b>	<b>31</b>
<b>SOA gain saturation—Gaussian pulses .....</b>	<b>33</b>
<b>SOA gain saturation—Comparison with experimental results.....</b>	<b>43</b>
<b>SOA gain saturation—Chirped and super Gaussian pulses.....</b>	<b>47</b>
<b>SOA Gaussian pulse—Gain recovery .....</b>	<b>55</b>
<b>SOA pulse compression.....</b>	<b>65</b>
<b>SOA as a wavelength converter (FWM) .....</b>	<b>73</b>

SOA as a wavelength converter (XGM).....	79
SOA In-line amplifier.....	85
Wideband SOA characterization.....	93
Wavelength conversion in a wideband SOA .....	97
<b>Waveguide amplifiers .....</b>	<b>99</b>
Improved gain characteristics in high-concentration	
Er <sub>3</sub> +/Yb <sub>3</sub> + codoped glass waveguide amplifiers .....	101
<b>Dispersion management.....</b>	<b>107</b>
Dispersion compensation schemes—a system perspective.....	109
Compensation of dispersion with Ideal dispersion component.....	117
Compensation of dispersion with Fiber Bragg Grating component .....	121
Uniform Fiber Bragg Grating as a filter.....	127
Compensation of dispersion with OptiGrating .....	139
Dispersion compensation using subsystems .....	147
Maximum-likelihood sequence estimation (MLSE) equalizer .....	153
DFE - Decision-Feedback Equalizer .....	157
Dispersion compensation using electronic equalization.....	161
<b>Lightwave systems .....</b>	<b>163</b>
Optimizing the power and dispersion compensation for	
nonlinear RZ transmission.....	175
10 Gb/s single channel transmission in standard mode fibers (SMF) .....	179

<b>40 Gb/s single channel transmission in standard mode fibers (SMF) .....</b>	<b>185</b>
Engineering the fiber nonlinearities and dispersion .....	193
System design — Power budget .....	197
Time Division Multiplexing (TDM).....	199
Optical Time Domain Multiplexing (OTDM) Design .....	193
Broadband optical system based on a Passive Optical Network (BPON).....	203
Optical code-division multiple-access system (OCDMA) .....	205
Free Space Optics (FSO).....	207
Coherent Optical Transmission.....	209
System Performance Analysis Using Script Automation .....	219
<b>WDM systems .....</b>	<b>225</b>
Comparison of RZ and NRZ modulation formats for 40 Gb/s systems .....	227
16 channel WDM system design.....	243
WDM Components—Tunable filters .....	269
WDM components—AWG demultiplexer .....	249
Broadcast star coupler .....	273
Optical cross-connects .....	275
Configurable optical add-drop multiplexer.....	277
Advanced modulation formats .....	279
Conventional duobinary transmitter .....	293
Modified duobinary transmitter .....	295
Interferometer characterization .....	297

<b>Solitons and soliton systems.....</b>	<b>303</b>
Fundamental and higher order solitons .....	305
Interactions of optical solitons .....	311
Decay of higher order solitons in the presence of third-order dispersion .....	317
Decay of higher order solitons in the presence of intrapulse Raman scattering	323
Decay of higher order solitons in the presence of self-steepening .....	331
Stability of solitons in birefringent optical fibers .....	337
Orthogonal Raman gain .....	345
Average soliton regime .....	351
SOA as in-line amplifier in soliton communication systems.....	359
<b>Metro systems .....</b>	<b>367</b>
Power level management in optical Metro networks.....	369
Migrating to 10Gbps in Metro networks.....	389
Negative dispersion fiber for Metro networks .....	395
Interchannel crosstalk in Metro networks .....	403
WDM Ring—Wavelength independent subscriber equipment .....	407
<b>Digital modulation .....</b>	<b>411</b>
Digital modulation—DPSK .....	413
Digital modulation—OQPSK .....	431
Digital modulation—QAM .....	433
Manchester and PAM Coding/Decoding .....	435

<b>CATV .....</b>	<b>437</b>
Using OptiSystem to analyze CATV systems.....	439
<b>Multimode .....</b>	<b>451</b>
Differential Mode Delay and Modal Bandwidth .....	453
Encircled Flux.....	461



---

## Introduction

---

The most effective way for you to become familiar with OptiSystem is to complete the tutorials and read the advanced simulation projects in this document. You will learn how to use the software by solving problems.

### Advanced simulation project sections

- [Raman amplifiers](#)
- [SOA amplifiers](#)
- [Waveguide amplifiers](#)
- [Dispersion management](#)
- [Lightwave systems](#)
- [WDM systems](#)
- [Solitons and soliton systems](#)
- [Metro systems](#)
- [Digital modulation](#)
- [CATV](#)
- [Multimode](#)

**Notes:**

---

## Raman amplifiers

---

This section contains the following advanced and illustrative simulation projects.

- 100 nm bandwidth flat-gain Raman amplifier—Average power model
- Flattening the gain of broadband Raman amplifier with multipump configuration
- Optimizing the pump power and frequencies of Raman amplifiers for gain flatness
- Raman Amplifier - Dynamic Model

**Notes:**

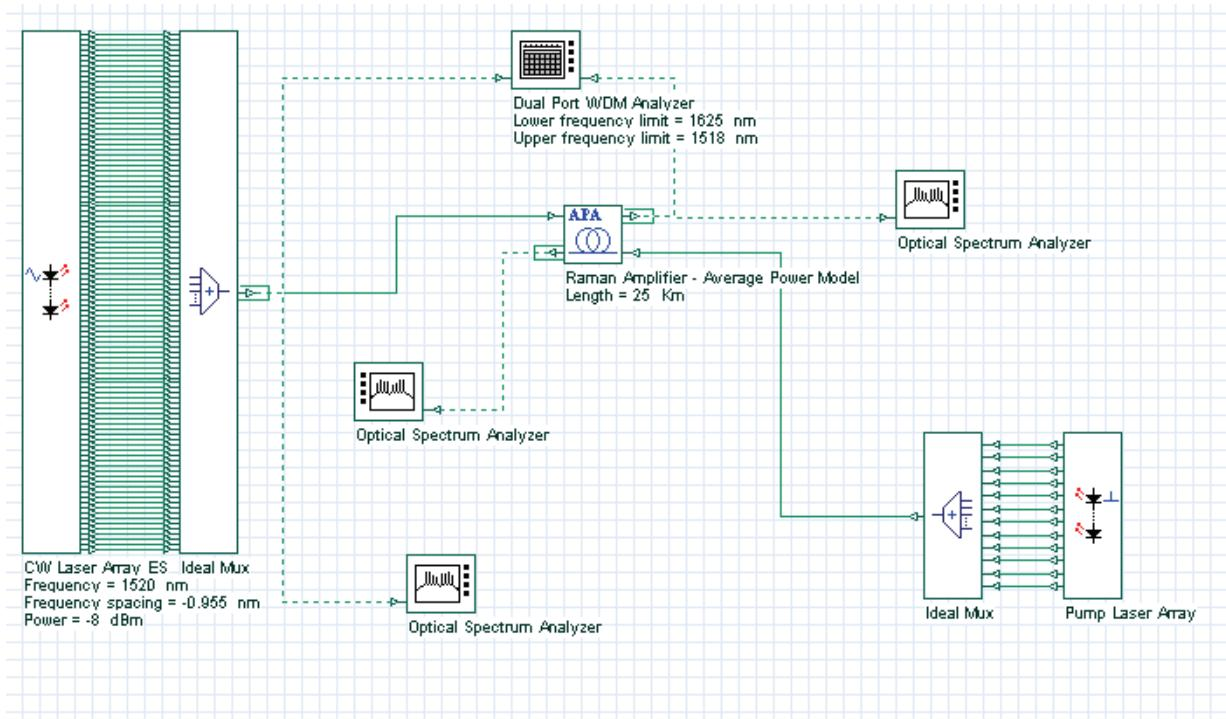
# 100 nm bandwidth flat-gain Raman amplifier—Average power model

This lesson shows the performance of the Average power model in analysis of the 100 nm bandwidth Raman amplifier with multiwavelength backward pump. The parameters considered are close to those used in the experiment of [1]. The same experimental situation has been modeled by means of Average power model in [2].

As is well known one of the largest challenges for the Raman amplifiers is to overcome the bandwidth limitations of EDFA. The above referenced experimental paper shows the possibility to perform gain-equalized Raman gain over 100 nm using a proper asymmetric channel allocations and powers of the pumps.

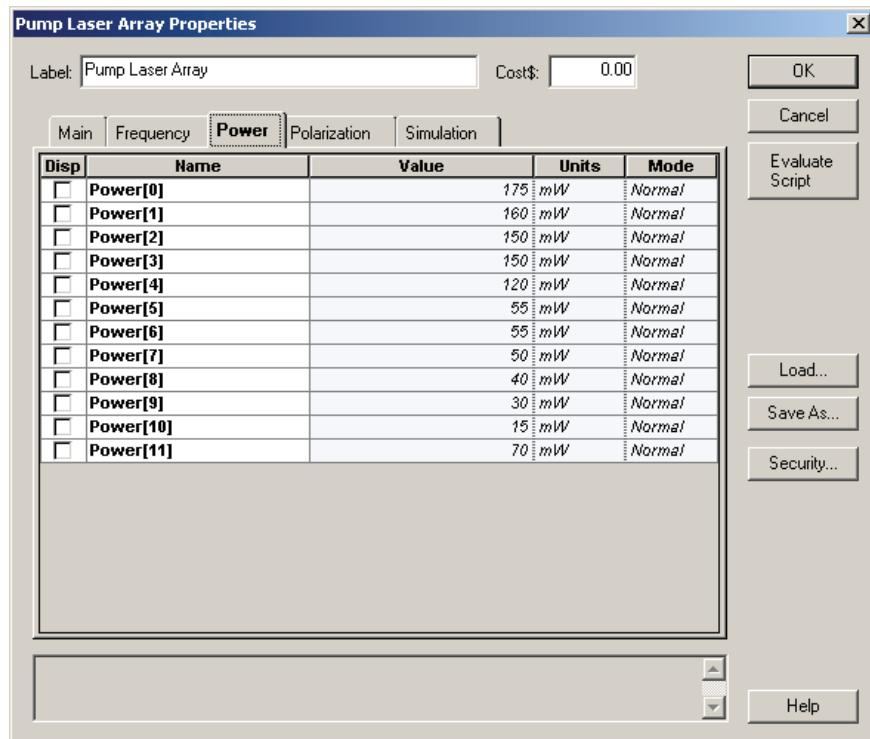
Our project is shown in [Figure 1](#).

**Figure 1 Project Layout for analysis of the Raman gain**



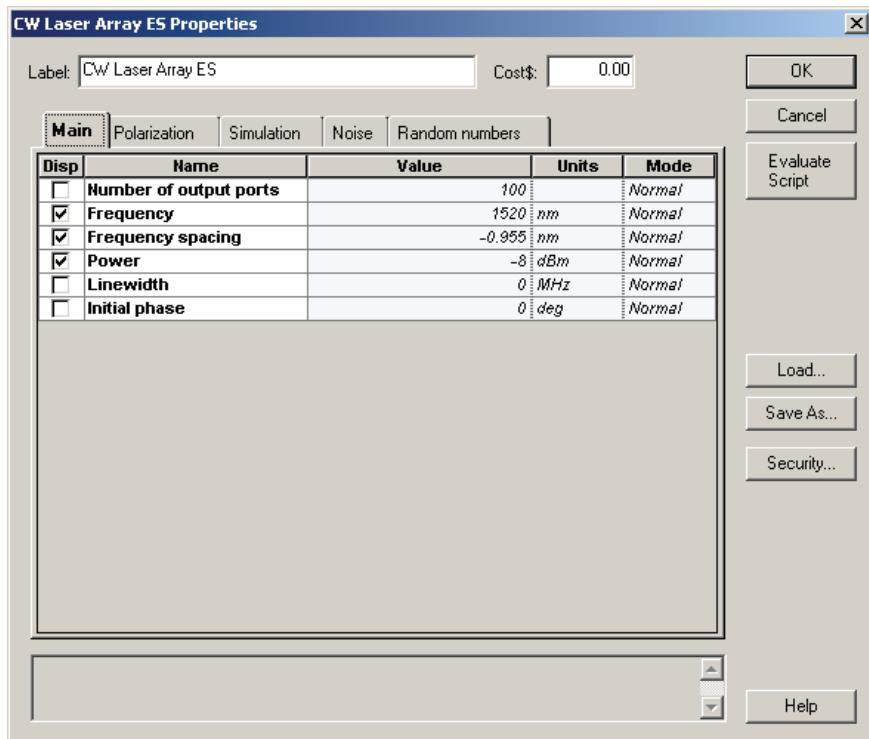
Following the data of [1], the spectral location and the magnitudes of the twelve backward pumps are arranged between 1405 and 1510 nm. The exact values for the locations and power of the pumps are shown in [Figure 2](#). The pump powers are different than those presented in [1].

Figure 2 Backward pumps locations and powers



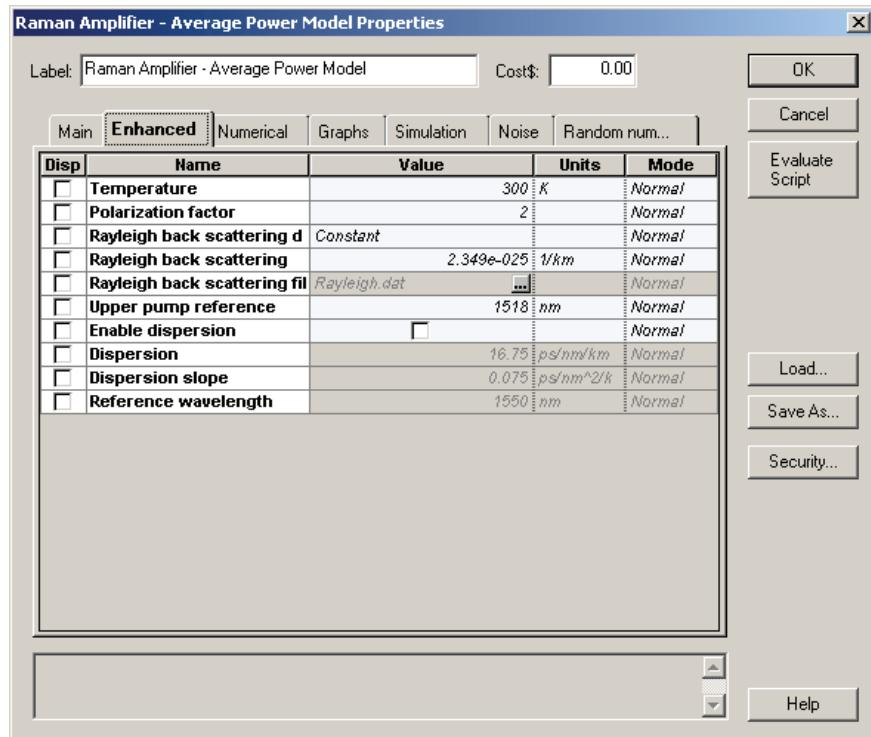
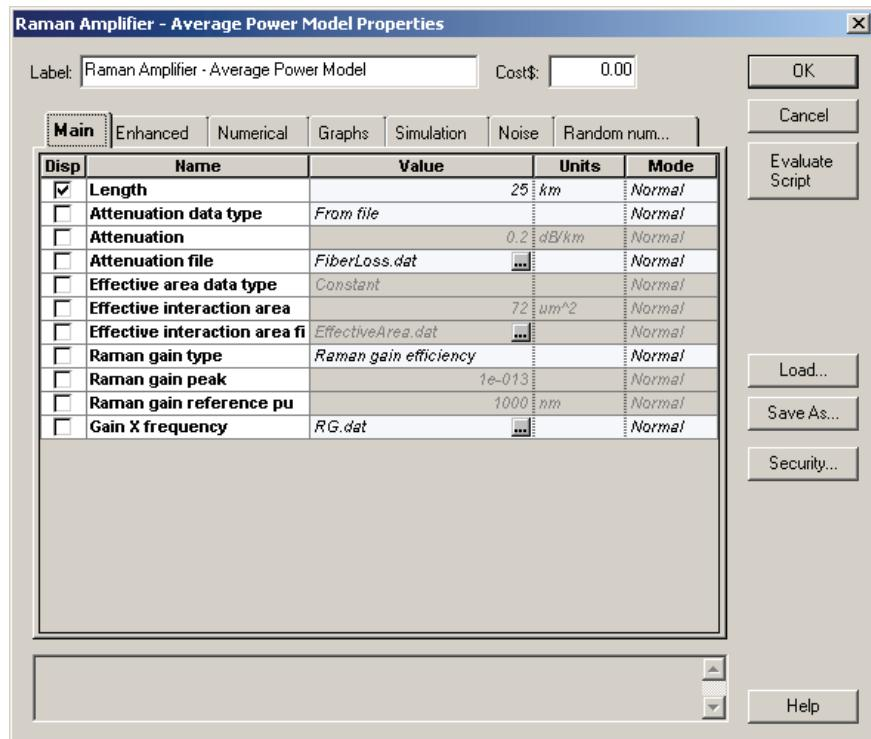
Signals in 100 channels are from 1520 to approximately 1620 nm with spacing equal to 0.955 nm. The power is set to -8 dBm power. For generation of these signals we use a laser array with the above parameters.

Figure 3 100 nm bandwidth signals



The amplifier has following parameters: length  $L = 25$  km, amplifier absolute temperature = 300 K, polarization factor = 2. The background loss and the Raman gain efficiency are defined through files. These parameters are introduced in the tabs of the Raman component:

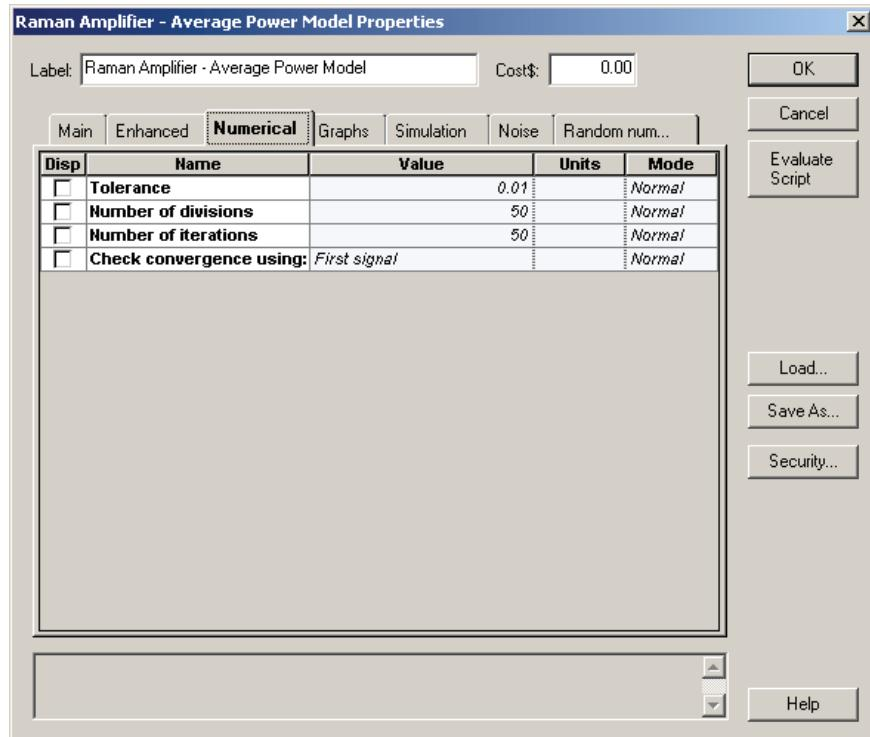
Figure 4 Amplifier parameters



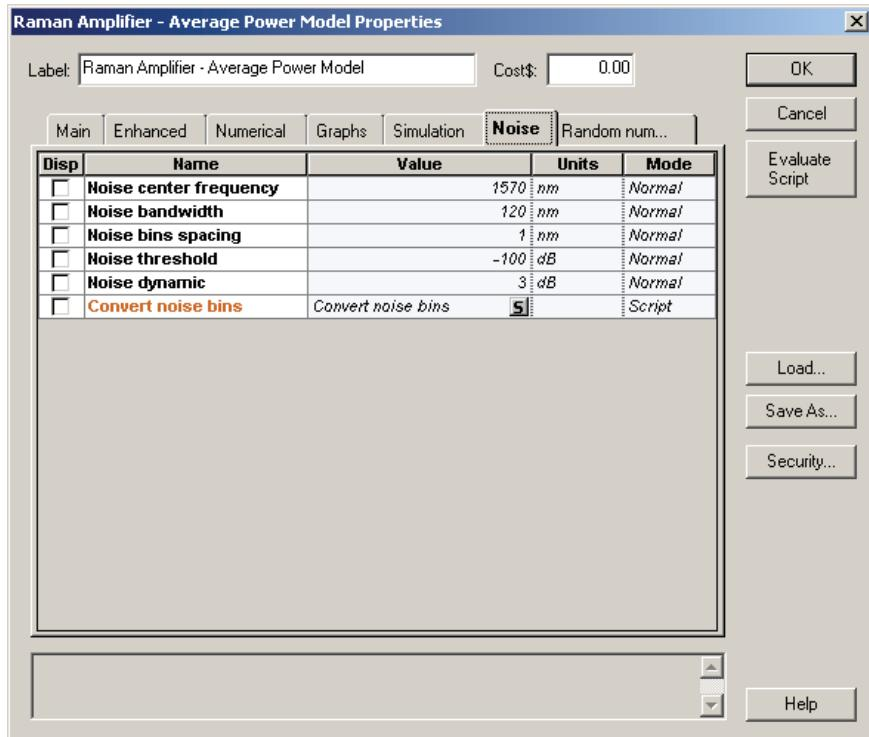
As we can see, when the gain type is set to "Raman gain efficiency", the effective area and Raman peak are disabled. The upper pump reference is set to 1518 nm, after the amplifier is pumped up to 1510 nm and the signals start from 1520 nm.

The tab "Numerical" is used to set the numerical parameters for the calculation. The number of amplifier sections is set to 50 and convergence will be checked using all the signals.

**Figure 5 Numerical settings**

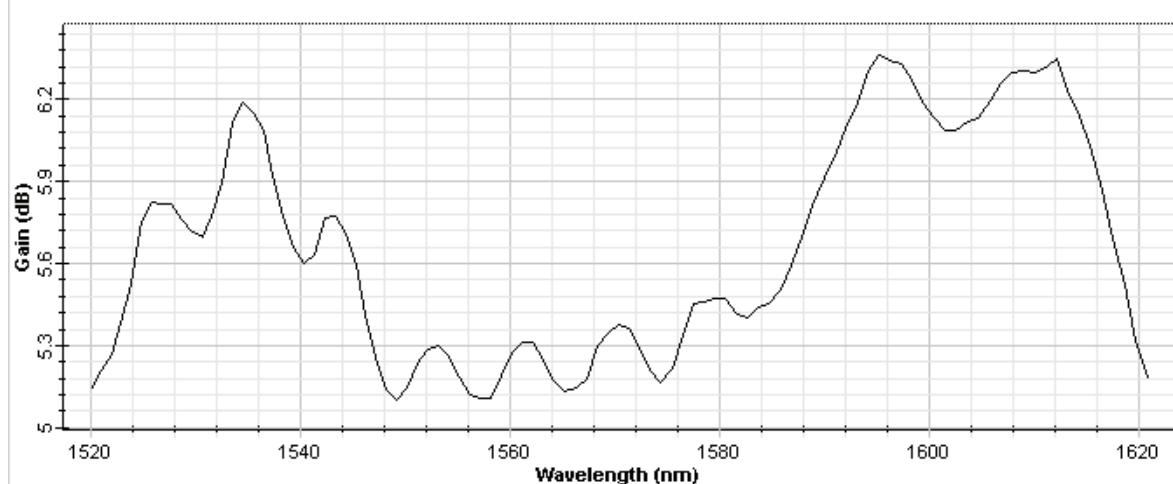


The description of ASE is given in [Figure 6](#).

**Figure 6 Description of ASE**

Note that the noise bins cover all the signal area and that the spacing between them is the same of the channels being transmitted that are illustrated on the next figure.

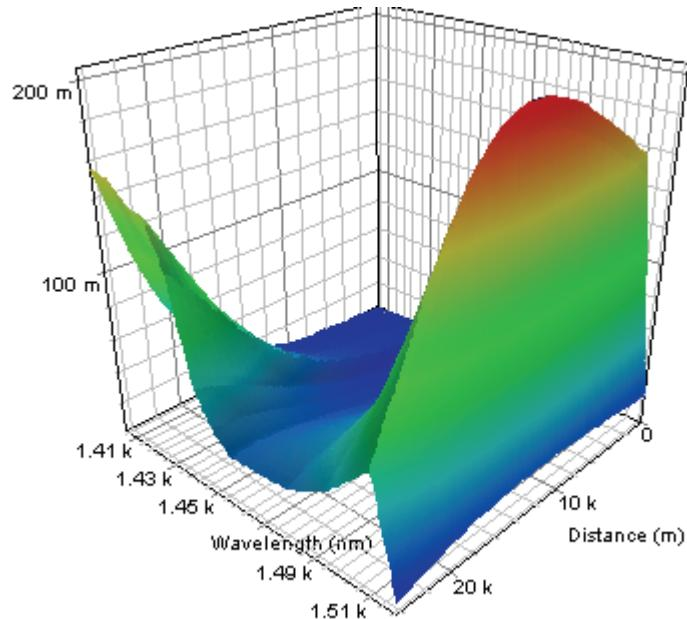
For such parameters the obtained gain for all the channels is shown in [Figure 7](#).

**Figure 7 Gain for the layout described above**

This figure has to be compared with Figure 2 of [2].

The next phenomenon analyzed, is pump depletions due to Raman energy transfer that can be seen on the next figure. The qualitative picture of the energy transfers between the lower wavelengths to the higher ones is very well demonstrated in [Figure 8](#).

**Figure 8 Counter-propagating pump**



In this lesson we have shown the performance of the Average power model for description of the 100 nm bandwidth flat-gain Raman amplifiers.

## References:

- [1] Y. Emori, K. Tanaka, and S. Namiki, "100 nm bandwidth flat-gain Raman amplifiers pumped and gain -equalised by 12-wavelength-channel WDM laser diode unit", Electronics Letters, Vol. 35, No. 16, pp. 1355-1356, 1999.
- [2] B. Min, W. J. Lee, N. Park, "Efficient Formulation of Raman Amplifier Propagation Equations with Average Power Analysis", IEEE Photonics Technology Letters, Vol. 12, No. 11, November 2000.



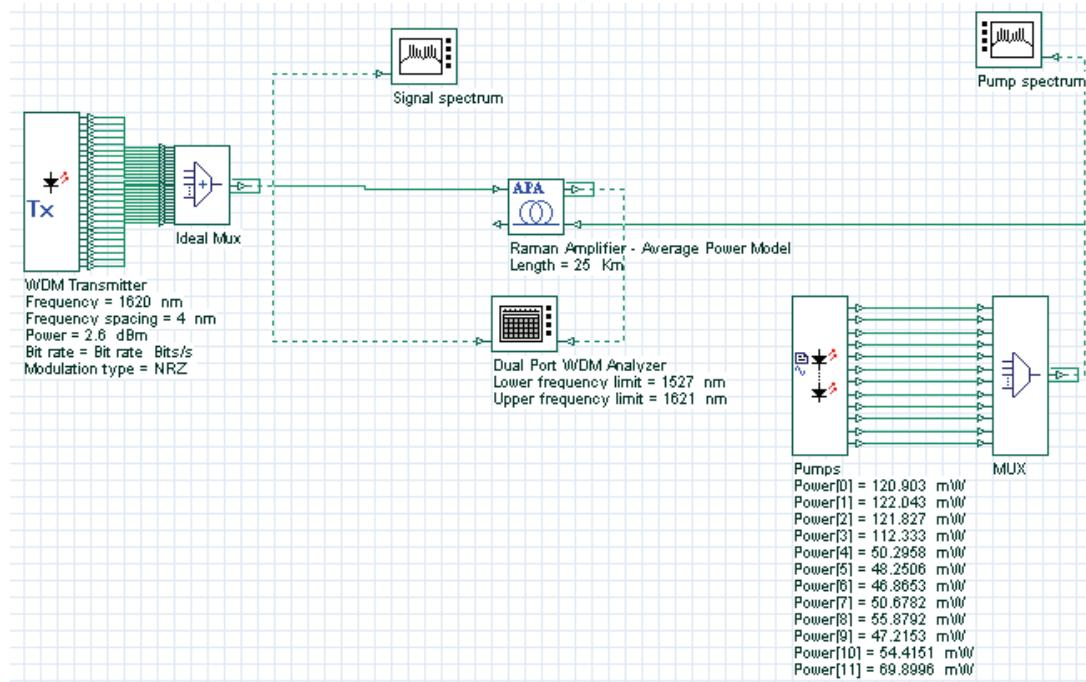
# Flattening the gain of broadband Raman amplifier with multipump configuration

In this lesson, we will use the gain flattening type of optimization to optimize the pump powers for flattening the gain of a Raman amplifier.

Fiber Raman amplifiers are recently getting much more attention in WDM systems due to their greatly extended bandwidth and distributed amplification with the installed fiber as gain medium [1]. It has been shown that the bandwidth of the amplifier can be further increased and a better gain flatness can be obtained by using more than one pump at different wavelengths [1]-[9]. In this example, we use optimization of pump powers to design a gain-flattened Raman amplifier by using 12-wavelength-channel WDM LD unit. We also compare the simulation results with the experimental findings of [9].

The project is **BroadBand Flat Gain Raman Amplifier Average Model.osd**. The project layout is as shown in [Figure 1](#). Channels are between 1528 and 1620 nm with 4 nm separation, and average power of each channel is 0 dBm. The fiber used as gain medium is a 25 km SMF fiber with 9.9e-014 m/W peak Raman gain coefficient. A 12 wavelength-channel WDM high power pump LD unit is used for pumping. The spacing in the short wavelength section (Pump I) (1405-1457.5 nm) is 7.5 nm (~1 THz). The spacing in the long wavelength section (Pump II) (1465-1510 nm) is 15 nm (~2 Thz).

**Figure 1 Raman amplifier with multipump configuration**

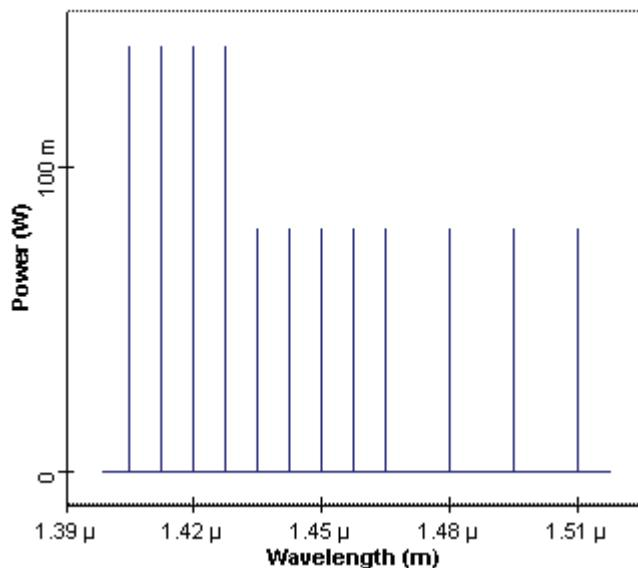


To set up the optimization, you need to insert a new **MPO Optimization** into the project. Then you need to select the Gain Flattening type of optimization in the **Main** tab. Finally you need to add the pump powers in the **Parameters** tab and Gains in the **Results** tab.

In this example, we will show how much flatness you can get before optimization and after optimization. In the **Parameters** tab, after adding pump powers to the selected list, starting pump powers are selected to be 140 mW for the first 4 pumps, and 80 mW for the remaining. Minimum and maximum pump powers are selected to be 20 mW and 160 mW, respectively.

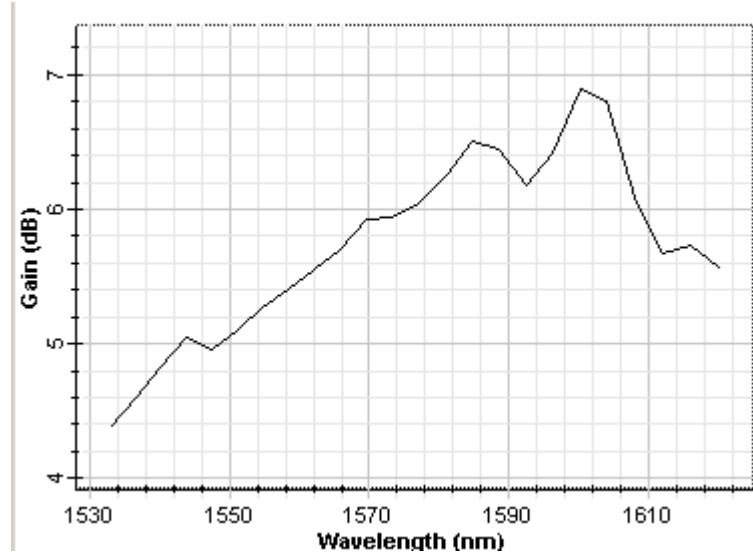
[Figure 2](#) shows the initial pump power spectrum.

**Figure 2 Initial pump power spectrum**



With this pump configuration we observed the gain shown in [Figure 3](#).

The obtained gain flatness was 2.5 dB, maximum gain was 6.9 dB.

**Figure 3 Gain and noise figure spectrums before the optimization is applied**

We selected the Gains for all channels from **Dual Port WDM Analyzer** in the **Results** tab of the optimization tool. You can easily do this by selecting multiple results from the results browser and adding them to the selected list.

Target gain is 3.0 dB as inserted in Target Value of this tab. Number of Goals to Achieve Exactly is same as the number of channels. This is automatically done when you add each result to the selected list and you can not change this value for Gain Flattening type of optimization.

In the **Constraints** tab, Ratio Max/Min Gain (dB) from the **Dual Port WDM Analyzer** is selected and added to the Constraint list. To do so, go to the **Constraint** tab and click **Add**, and in the **New Constraint** window, select **Bind Result** type and click **OK**.

In the **Select Results** window, add Ratio Max/Min Gain (dB) from **Dual Port WDM Analyzer**. As a constraint, gain flatness < 1.5 dB is required. Enter this on the **Constraint** tab by selecting Less than option.

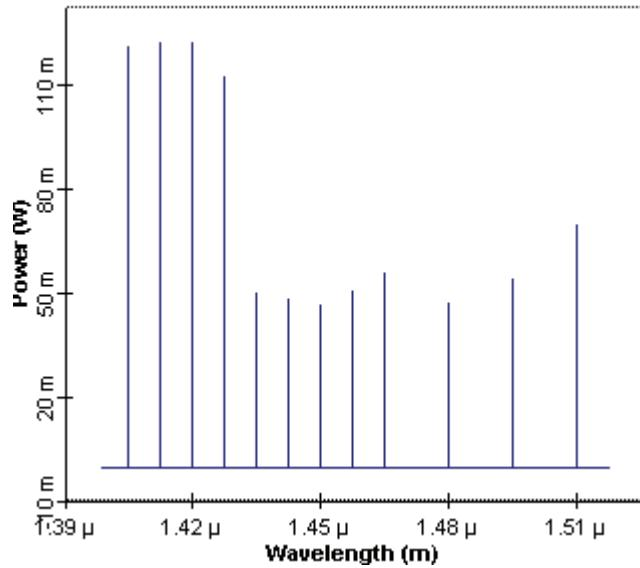
Note that no unit for parameters and results is indicated in the optimization tool. The units of parameters and results in the optimization tool are taken to be same as the ones that are given in the project layout for the corresponding parameter or result.

The optimization parameters in **Advanced** tab are as follows:  
Result Termination Tolerance is 0.1, Constraint Termination Tolerance is 0.1, and Parameter Termination Tolerance is 0.05.

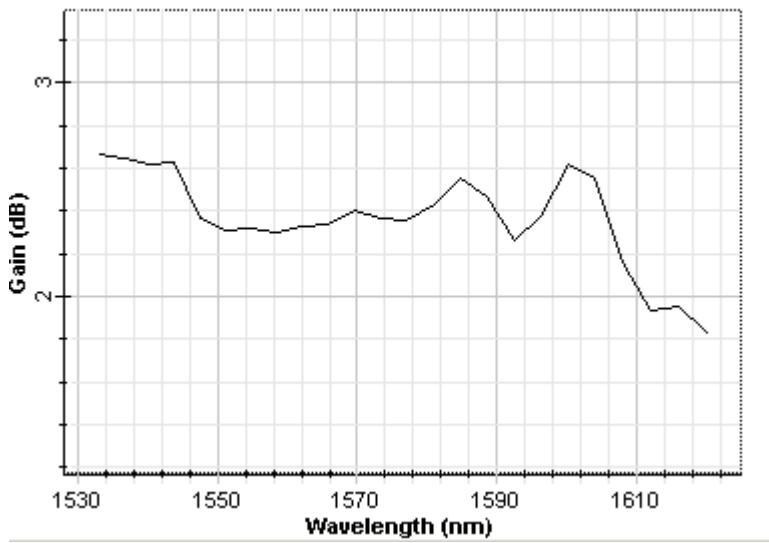
After setting up the optimization, run the optimization.

**Note:** It may take up to 20 minutes to get the results.

Optimum pump powers are obtained after 44 passes. The pump power spectrum after the optimization is shown in [Figure 4](#). Note the agreement of pump power allocation with the experimental findings of [9].

**Figure 4 Optimized pump power spectrum**

Gain spectrum, in this case, is shown in [Figure 5](#). Gain flatness achieved in [9] was  $\sim 1$  dB (\*\* 0.5 dB). We have observed somewhat better gain flatness, compared to this value. After the optimization, achieved forward gain flatness is 0.8 dB and maximum gain is 2.8 dB.

**Figure 5 Gain as measured by Dual Port WDM Analyzer, after the optimization is applied**

## References

- [1] Mohammed N. Islam, "Raman amplifiers for telecommunications", IEEE J. Select. Top. Quan. Elect. 8, 548 (2002).
- [2] Y. Emori, et al., "Broadband flat-gain and low-noise Raman amplifiers pumped by wavelength-multiplexed high power laser diodes", Opt. Fib. Tech. 8, 107 (2002).
- [3] V. E. Perlin and H. G. Winful, "On distributed Raman amplification for ultrabroad-band long-haul WDM systems", J. Lightwave Tech. 20, 409 (2002).
- [4] V. E. Perlin and H. G. Winful, "Optimal design of flat gain wide band fiber Raman amplifiers", J. Lightwave Tech. 20, 250 (2002).
- [5] M. Yan, et al., "Automatic design scheme for optical fiber Raman amplifiers backward pumped with multiple laser diode pumps", IEEE Photon. Tech. Lett. 13, 948 (2001).
- [6] S. Namiki and Y. Emori, "Ultrabroad-band Raman amplifiers pumped and gain-equalized by wavelength division multiplexed high power laser diodes", IEEE J. Select. Top. Quan. Elect. 7, 3 (2001).
- [7] P.C. Reeves-Hall, et al., "Dual wavelength pumped L- and U-band Raman amplifier", Elect. Lett. 37, 883 (2001).
- [8] Xiang Zhou, et al., "A simplified model and optimal design of a multi-wavelength backward pumped fiber Raman amplifier", IEEE Photon. Tech. Lett. 13, 945 (2001).
- [9] Y. Emori, et al., "100 nm bandwidth flat-gain Raman amplifiers pumped and gain equalized by 12-wavelength channel WDM laser diode unit", Elect. Lett. 35, 1355 (1999).

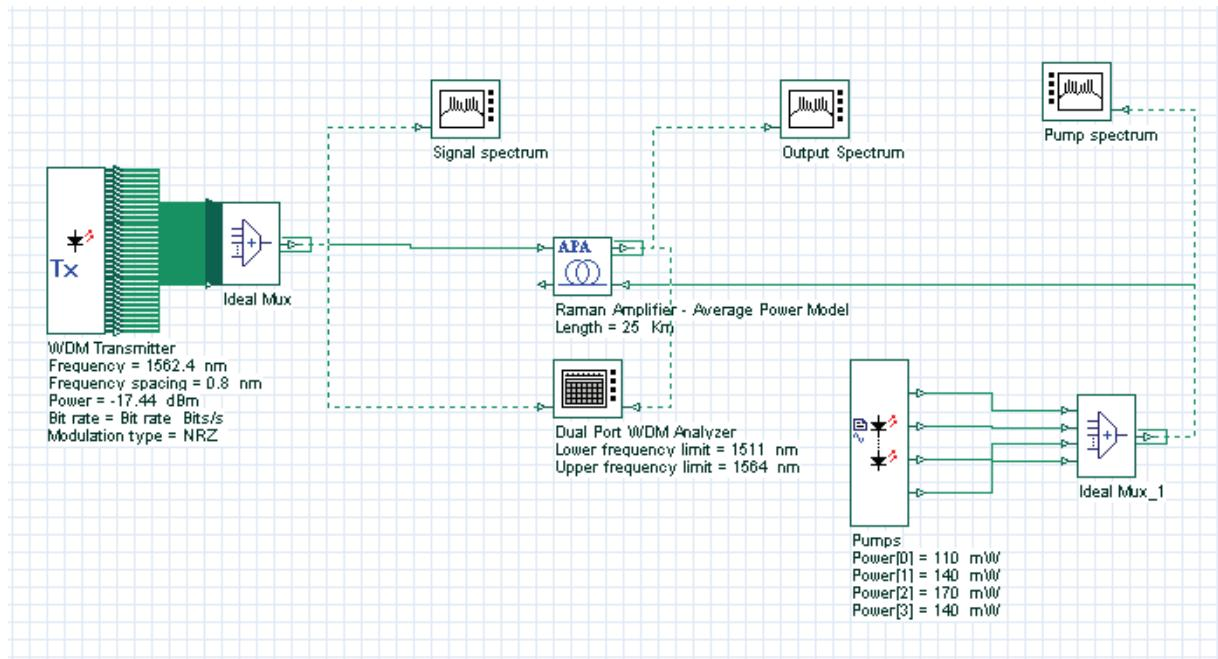
**Notes:**

# Optimizing the pump power and frequencies of Raman amplifiers for gain flatness

In this example, we show that the **Gain Flattening** type of optimization can be used to design multi-wavelength pumped Raman amplifiers with a flattened gain. Given amplifier specifications such as signal level, required gain profile, and number of allowed pump channels, the optimization procedure can generate a combination of pump wavelengths and input powers that would result in the gain profile approximating the specified one as close as possible.

Note that this optimization may require a huge number of iteration since interaction between channels and pumps are very complicated. Therefore it is very important to give good estimated initial values, especially for pump wavelengths, to the optimizer to lower the required number of iterations. For example, a general guideline to estimate the pump channel locations is given in [1].

**Figure 1 Multi-pump configuration project layout**



The project is **Optimizing the pump power and frequencies Average Model.osd**. It contains two versions of the same project, named **Initial** with the initial pump configuration and **Optimized** with the optimized pump configuration and a MPO setup.

The project layout is as shown in [Figure 1](#). 64 channels between 1512 and 1562.4 nm with 0.8 nm separations are multiplexed. The average power of each channel is -20 dBm. We have used our **Average Power Raman amplifier** model to simulate the amplifier. This model allows a fast and accurate estimation of the amplifier gain. For

more information on this model please refer to component description. The fiber used as gain medium is a 25 km fiber with 9.5e-014 m/W peak Raman gain coefficient. The effective area of the fiber is 55 micron square. The loss of the fiber is 0.2 dB/km. We are only interested in the frequency domain response of the amplifier. Therefore, we have done the simulation with **Parameterized** signals. To do so, we have selected **Parameterized** option from **Signals** tab of the **Initial Parameters** window. To set the upper pump frequency, go to **Enhanced** tab of the **Raman Amplifier** component and set **Upper pump reference** parameter to 1510 nm. In this example, a **Dual Port WDM Analyzer** measures amplifier gain and gain flatness. To limit the measurement window within signal spectrum, we set lower and upper frequency limits from the **Main** tab of **Dual Port WDM Analyzer** properties dialog box. These values are 1511 nm and 1564 nm, respectively.

Four CW pump signals with initial powers shown in [Figure 2](#) are used for backward pumping. Initial wavelengths and powers of these pumps are also given in [Table 1](#). These parameters are chosen as in [2] for comparison. Initial configuration is shown in the Layout named "Initial".

**Figure 2** Initial pump power allocation

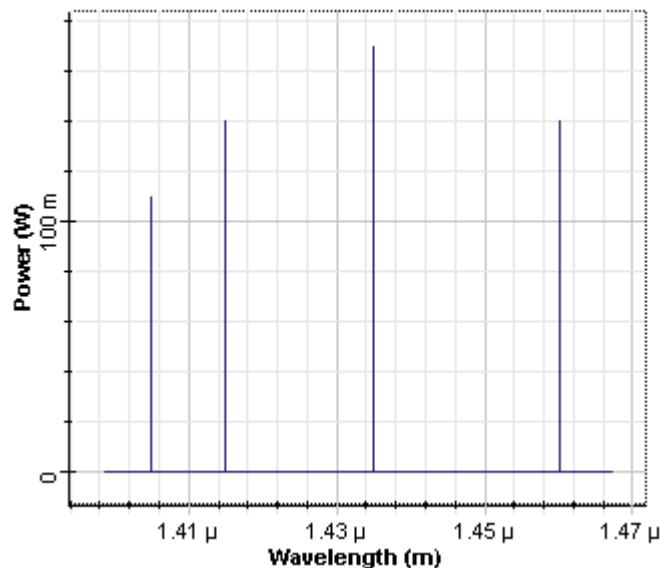
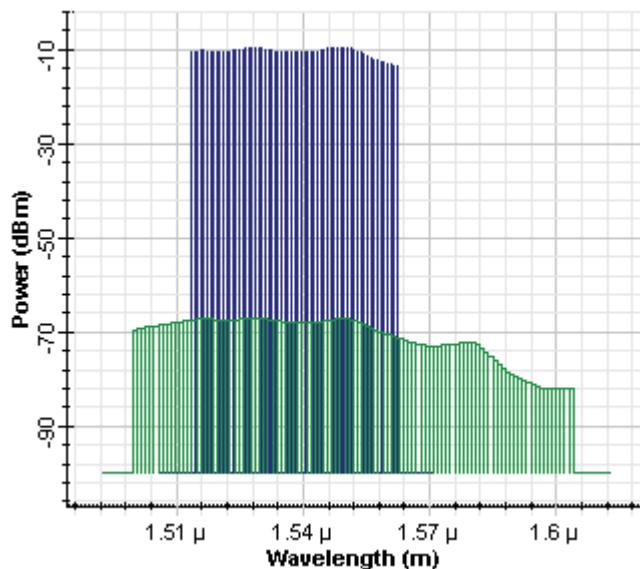


**Table 1** Initial pump parameters

Wavelength (nm)	(10)Power (mW)
1405.0	110.0
1415.0	140.0
1435.0	170.0
1460.0	140.0

With this initial pump configuration, we observed the output power spectrum as shown in [Figure 3](#). The obtained gain flatness was 4 dB, maximum forward gain was 10.5 dB. These values can be seen by double clicking on **Dual Port WDM Analyzer**. To see the gain flatness (Ratio max/min Gain in dB) and maximum forward gain (Max Value Gain in dB), go to **Details** tab of this component.

**Figure 3 Output power spectrum before the optimization**



The optimized configuration is shown in the Layout named "Optimized". In the optimization setup. We have selected the **Gain Flattening** type of optimization in the **Main** tab. In the **Parameters** tab, pump powers and frequencies are added to the table. Minimum and maximum pump powers are selected to be 0 and 300 mW, respectively. Minimum and maximum pump wavelengths are selected to be 1400 nm and 1500 nm, respectively. In the **Results** tab, we selected the Gains for all channels from dual port WDM analyzer to add the table. Target gain is 10.0 dB as inserted in Target Value of this tab. Number of Goals to Achieve Exactly is same as the number of channels and automatically set.

In the **Constraints** tab, we have added Gain Flatness (Ratio Max/Min Gain) as a constraint. Gain flatness is measured by the **Dual Port WDM Analyzer**. As a constraint, gain flatness less than 1.5 dB is required. As an extra constraint, we limit the total pump power to between 500 mW and 1000 mW. This is required to make sure that we can get a gain as high as required. Without forcing this constraint, we have seen that amplifier can be optimized with good gain flatness, but with a gain of about 4 dB. Note also that no unit for parameters and results is indicated in the optimization tool. The units of parameters and results in optimization tool are taken to be same as the ones that are given in project layout for the corresponding parameter or result.

In the **Advanced** tab, Result Termination Tolerance is 0.1, Constraint Termination Tolerance is 0.1, and Parameter Termination Tolerance is 0.1.

Optimum pump powers and wavelengths are obtained after 32 calculations. Pump power spectrum after the optimization is shown in Fig. 4. Optimum pump parameters are also shown in Table 2. Also note that, there is not a unique set of optimum parameters. Therefore, optimization procedure can obtain different set of parameters depending on the starting parameter values.

**Figure 4 Pump power spectrum**

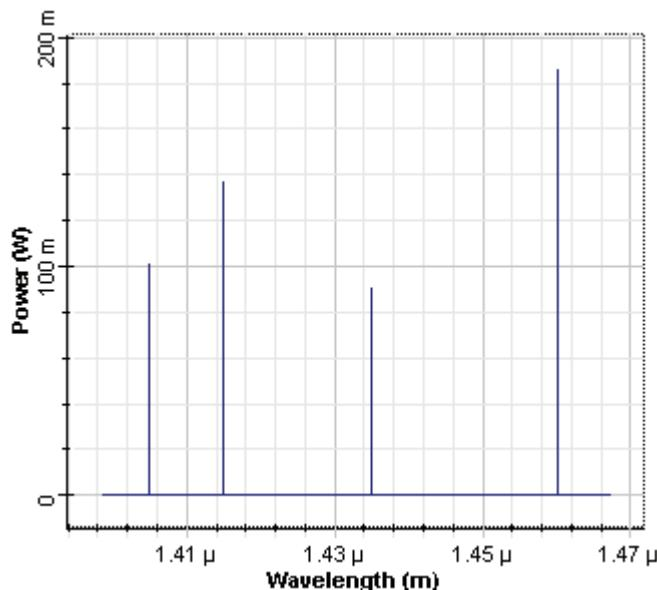


**Table 2 Optimum pump parameters**

Frequency (nm) Power (mW)

Frequency (nm)	(11)Power (mW)
1405.0	101.2
1415.0	136.4
1435.0	90.0
1460.0	186.08

For this specific example, we have found that for the given set of requirements, optimization procedure only needs to adjust the pump powers. As can be seen from Table 2, pump frequencies are kept at the original values. As stated before, there is not a unique set of optimum parameters.

Output power spectrum after the optimization is shown in Figure 5. Gain flatness achieved in [2] was ~2.6 dB. We have observed a better gain flatness, comparing to this value. After the optimization, achieved forward gain flatness is 1.5 dB, maximum forward gain is ~9 dB. Initial and optimized gain spectrums are shown in Figure 6 for comparison.

Figure 5 Output power spectrum after the optimization

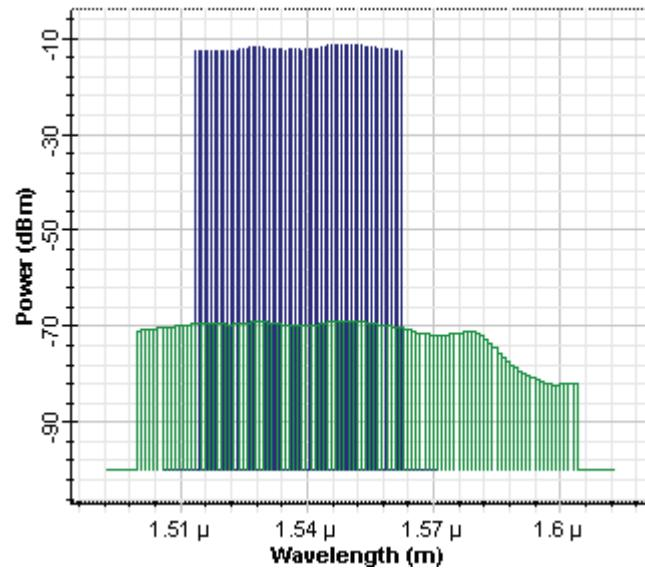
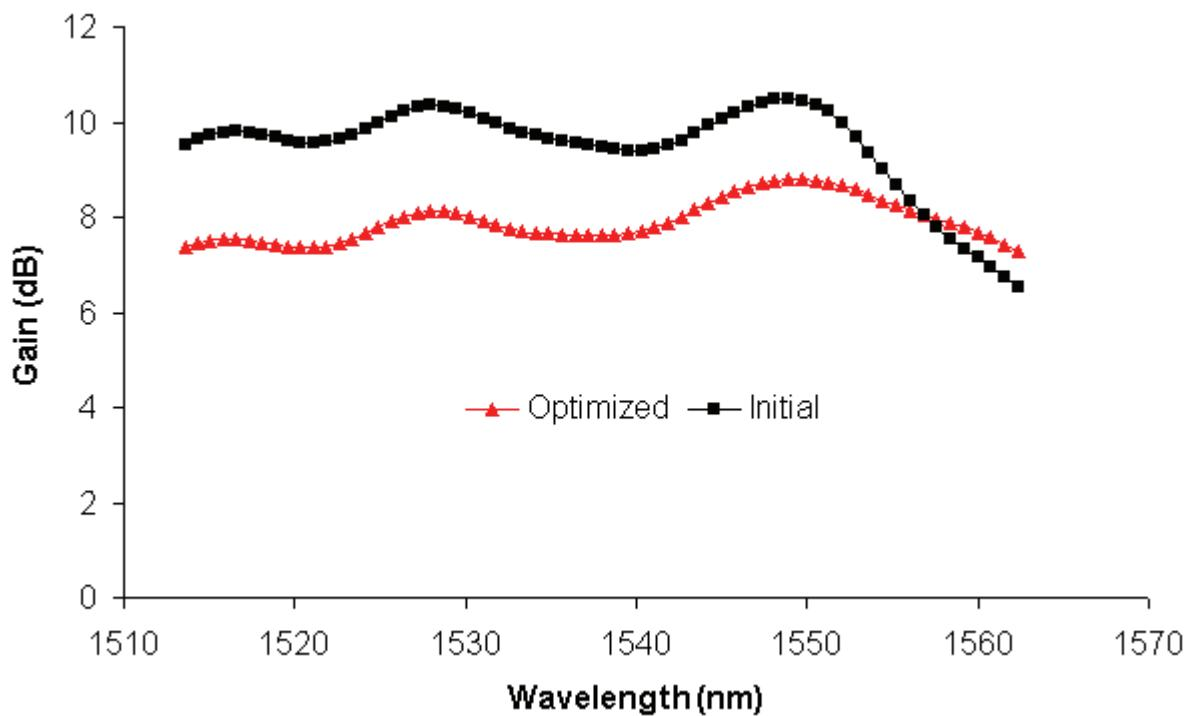


Figure 6 Gain spectrums, before and after optimization is applied



## References:

- [1] Y. Emori, et al., "Broadband flat-gain and low-noise Raman amplifiers pumped by wavelength-multiplexed high power laser diodes", Opt. Fib. Tech. 8, 107 (2002).
- [2] M. Yan, et al., "Automatic design scheme for optical fiber Raman amplifiers backward pumped with multiple laser diode pumps", IEEE Photon. Tech. Lett. 13, 948 (2001).



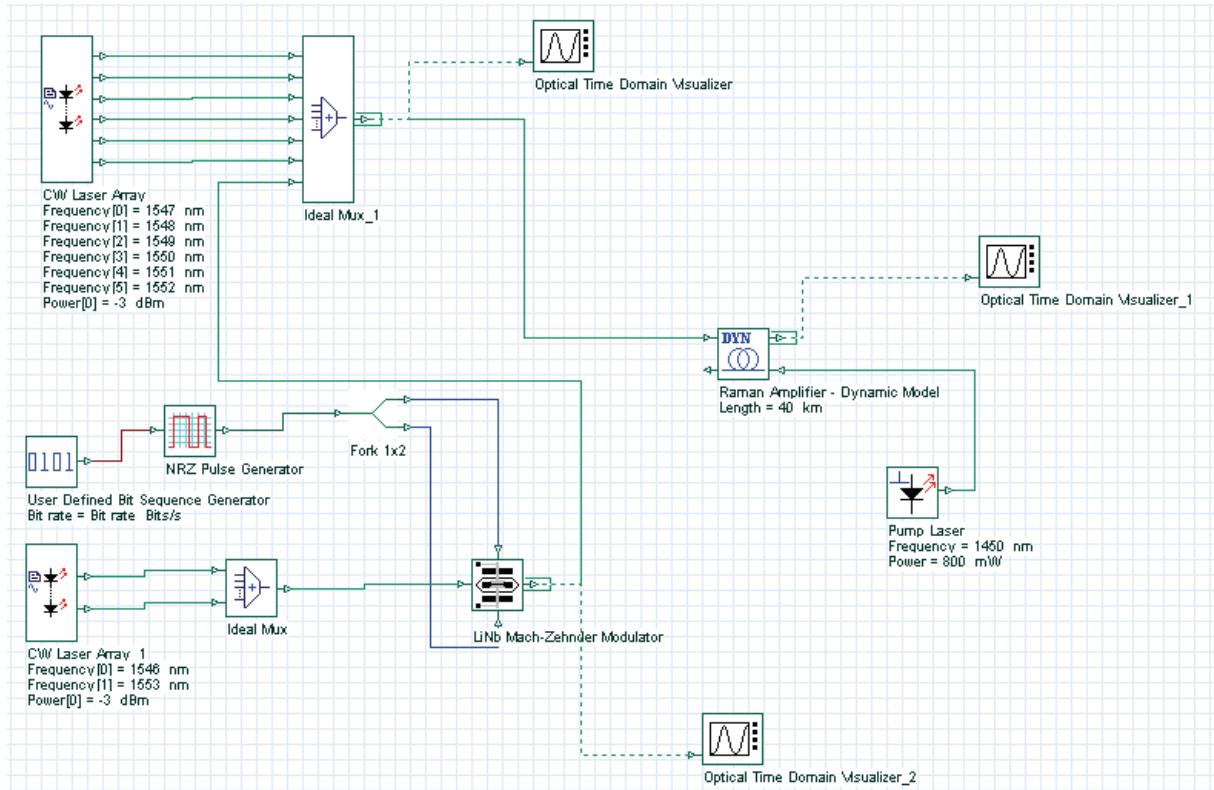
# Raman Amplifier - Dynamic Model

This lesson demonstrates generating the transients based on add-drops in signals in a Raman amplifier.

In this example, we simulate a counter-pumped Raman amplifier for a small number of signals. Then the results are compared with the ones found in the literature.

The project consists of a simple model as shown in [Figure 1](#).

**Figure 1 Project Layout for analysis of the Raman gain**



The amplifier has following parameters: length  $L = 40$  km, amplifier absolute temperature = 300 K, polarization factor = 2. The background loss and the Raman gain efficiency are defined through files. These parameters are introduced in the tabs of the Raman component:

Figure 2 Amplifier parameters

Raman Amplifier - Dynamic Model Properties																																																																	
Label: Raman Amplifier - Dynamic Model			Cost\$: 0.00	<input type="button" value="OK"/> <input type="button" value="Cancel"/> <input type="button" value="Evaluate Script"/> <input type="button" value="Load..."/> <input type="button" value="Save As..."/> <input type="button" value="Security..."/> <input type="button" value="Help"/>																																																													
Main	Enhanced	Numerical	Graphs	Simulation	Noise																																																												
<table border="1"> <thead> <tr> <th>Disp</th> <th>Name</th> <th>Value</th> <th>Units</th> <th>Mode</th> </tr> </thead> <tbody> <tr><td><input checked="" type="checkbox"/></td><td>Length</td><td>40</td><td>km</td><td>Normal</td></tr> <tr><td><input type="checkbox"/></td><td>Attenuation data type</td><td>From file</td><td></td><td>Normal</td></tr> <tr><td><input type="checkbox"/></td><td>Attenuation</td><td>0.2</td><td>dB/km</td><td>Normal</td></tr> <tr><td><input type="checkbox"/></td><td>Attenuation file</td><td>C:\Raman\DSF_Attenuation</td><td>[...]</td><td>Normal</td></tr> <tr><td><input type="checkbox"/></td><td>Effective area data type</td><td>Constant</td><td></td><td>Normal</td></tr> <tr><td><input type="checkbox"/></td><td>Effective interaction area</td><td>72</td><td>μm<sup>2</sup></td><td>Normal</td></tr> <tr><td><input type="checkbox"/></td><td>Effective interaction area fi</td><td>EffectiveArea.dat</td><td>[...]</td><td>Normal</td></tr> <tr><td><input type="checkbox"/></td><td>Raman gain type</td><td>Raman gain efficiency</td><td></td><td>Normal</td></tr> <tr><td><input type="checkbox"/></td><td>Raman gain peak</td><td>1e-013</td><td></td><td>Normal</td></tr> <tr><td><input type="checkbox"/></td><td>Raman gain reference pu</td><td>1000</td><td>nm</td><td>Normal</td></tr> <tr><td><input type="checkbox"/></td><td>Gain X frequency</td><td>D:\Raman\RG.in</td><td>[...]</td><td>Normal</td></tr> </tbody> </table>						Disp	Name	Value	Units	Mode	<input checked="" type="checkbox"/>	Length	40	km	Normal	<input type="checkbox"/>	Attenuation data type	From file		Normal	<input type="checkbox"/>	Attenuation	0.2	dB/km	Normal	<input type="checkbox"/>	Attenuation file	C:\Raman\DSF_Attenuation	[...]	Normal	<input type="checkbox"/>	Effective area data type	Constant		Normal	<input type="checkbox"/>	Effective interaction area	72	μm <sup>2</sup>	Normal	<input type="checkbox"/>	Effective interaction area fi	EffectiveArea.dat	[...]	Normal	<input type="checkbox"/>	Raman gain type	Raman gain efficiency		Normal	<input type="checkbox"/>	Raman gain peak	1e-013		Normal	<input type="checkbox"/>	Raman gain reference pu	1000	nm	Normal	<input type="checkbox"/>	Gain X frequency	D:\Raman\RG.in	[...]	Normal
Disp	Name	Value	Units	Mode																																																													
<input checked="" type="checkbox"/>	Length	40	km	Normal																																																													
<input type="checkbox"/>	Attenuation data type	From file		Normal																																																													
<input type="checkbox"/>	Attenuation	0.2	dB/km	Normal																																																													
<input type="checkbox"/>	Attenuation file	C:\Raman\DSF_Attenuation	[...]	Normal																																																													
<input type="checkbox"/>	Effective area data type	Constant		Normal																																																													
<input type="checkbox"/>	Effective interaction area	72	μm <sup>2</sup>	Normal																																																													
<input type="checkbox"/>	Effective interaction area fi	EffectiveArea.dat	[...]	Normal																																																													
<input type="checkbox"/>	Raman gain type	Raman gain efficiency		Normal																																																													
<input type="checkbox"/>	Raman gain peak	1e-013		Normal																																																													
<input type="checkbox"/>	Raman gain reference pu	1000	nm	Normal																																																													
<input type="checkbox"/>	Gain X frequency	D:\Raman\RG.in	[...]	Normal																																																													

Raman Amplifier - Dynamic Model Properties																																																																											
Label: Raman Amplifier - Dynamic Model			Cost\$: 0.00	<input type="button" value="OK"/> <input type="button" value="Cancel"/> <input type="button" value="Evaluate Script"/> <input type="button" value="Load..."/> <input type="button" value="Save As..."/> <input type="button" value="Security..."/> <input type="button" value="Help"/>																																																																							
Main	Enhanced	Numerical	Graphs	Simulation	Noise																																																																						
<table border="1"> <thead> <tr> <th>Disp</th> <th>Name</th> <th>Value</th> <th>Units</th> <th>Mode</th> </tr> </thead> <tbody> <tr><td><input type="checkbox"/></td><td>Temperature</td><td>300</td><td>K</td><td>Normal</td></tr> <tr><td><input type="checkbox"/></td><td>Polarization factor</td><td>2</td><td></td><td>Normal</td></tr> <tr><td><input type="checkbox"/></td><td>Rayleigh back scattering d</td><td>From file</td><td></td><td>Normal</td></tr> <tr><td><input type="checkbox"/></td><td>Rayleigh back scattering</td><td>5e-005</td><td>1/km</td><td>Normal</td></tr> <tr><td><input type="checkbox"/></td><td>Rayleigh back scattering fil</td><td>C:\mfreitas\Research\Rayl</td><td>[...]</td><td>Normal</td></tr> <tr><td><input type="checkbox"/></td><td>Upper pump reference</td><td>1500</td><td>nm</td><td>Normal</td></tr> <tr><td><input type="checkbox"/></td><td>Enable dispersion</td><td><input type="checkbox"/></td><td></td><td>Normal</td></tr> <tr><td><input type="checkbox"/></td><td>Dispersion</td><td>16.75</td><td>ps/nm/km</td><td>Normal</td></tr> <tr><td><input type="checkbox"/></td><td>Dispersion slope</td><td>0.075</td><td>ps/nm<sup>2</sup>/k</td><td>Normal</td></tr> <tr><td><input type="checkbox"/></td><td>Reference wavelength</td><td>1550</td><td>nm</td><td>Normal</td></tr> <tr><td><input type="checkbox"/></td><td>Group delay data type</td><td>From file</td><td></td><td>Normal</td></tr> <tr><td><input type="checkbox"/></td><td>Group delay</td><td>4900000</td><td>ps/km</td><td>Normal</td></tr> <tr><td><input type="checkbox"/></td><td>Group delay file</td><td>P:\Marcio\Samples\Dynamic</td><td>[...]</td><td>Normal</td></tr> </tbody> </table>						Disp	Name	Value	Units	Mode	<input type="checkbox"/>	Temperature	300	K	Normal	<input type="checkbox"/>	Polarization factor	2		Normal	<input type="checkbox"/>	Rayleigh back scattering d	From file		Normal	<input type="checkbox"/>	Rayleigh back scattering	5e-005	1/km	Normal	<input type="checkbox"/>	Rayleigh back scattering fil	C:\mfreitas\Research\Rayl	[...]	Normal	<input type="checkbox"/>	Upper pump reference	1500	nm	Normal	<input type="checkbox"/>	Enable dispersion	<input type="checkbox"/>		Normal	<input type="checkbox"/>	Dispersion	16.75	ps/nm/km	Normal	<input type="checkbox"/>	Dispersion slope	0.075	ps/nm <sup>2</sup> /k	Normal	<input type="checkbox"/>	Reference wavelength	1550	nm	Normal	<input type="checkbox"/>	Group delay data type	From file		Normal	<input type="checkbox"/>	Group delay	4900000	ps/km	Normal	<input type="checkbox"/>	Group delay file	P:\Marcio\Samples\Dynamic	[...]	Normal
Disp	Name	Value	Units	Mode																																																																							
<input type="checkbox"/>	Temperature	300	K	Normal																																																																							
<input type="checkbox"/>	Polarization factor	2		Normal																																																																							
<input type="checkbox"/>	Rayleigh back scattering d	From file		Normal																																																																							
<input type="checkbox"/>	Rayleigh back scattering	5e-005	1/km	Normal																																																																							
<input type="checkbox"/>	Rayleigh back scattering fil	C:\mfreitas\Research\Rayl	[...]	Normal																																																																							
<input type="checkbox"/>	Upper pump reference	1500	nm	Normal																																																																							
<input type="checkbox"/>	Enable dispersion	<input type="checkbox"/>		Normal																																																																							
<input type="checkbox"/>	Dispersion	16.75	ps/nm/km	Normal																																																																							
<input type="checkbox"/>	Dispersion slope	0.075	ps/nm <sup>2</sup> /k	Normal																																																																							
<input type="checkbox"/>	Reference wavelength	1550	nm	Normal																																																																							
<input type="checkbox"/>	Group delay data type	From file		Normal																																																																							
<input type="checkbox"/>	Group delay	4900000	ps/km	Normal																																																																							
<input type="checkbox"/>	Group delay file	P:\Marcio\Samples\Dynamic	[...]	Normal																																																																							

As we can see, when the gain type is set to "Raman gain efficiency", the effective area and Raman peak are not chosen. The upper pump reference is set to 1500nm, after



the amplifier is pumped at 1450 nm and the signals start from 1546 nm.

The tab "Numerical" is used to set the numerical parameters for the calculation. As we do not need a very accurate gain calculation in order to observe the transients, we set the number of divisions to 50 and the tolerance to just 0.01. It will make the execution much shorter. The convergence will be checked using all the signals.

**Figure 3 Numerical settings**

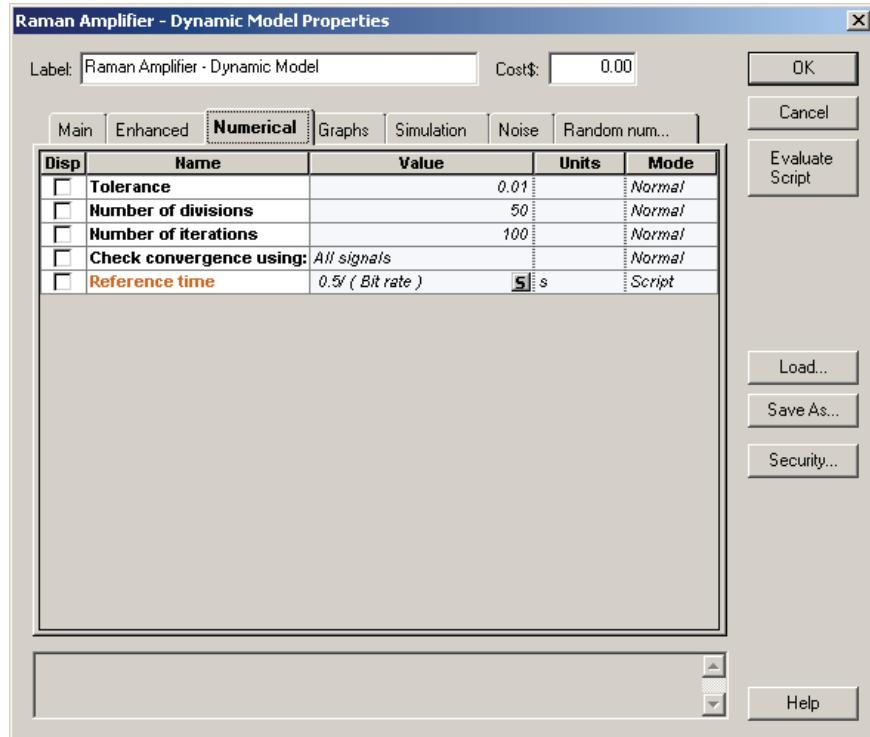
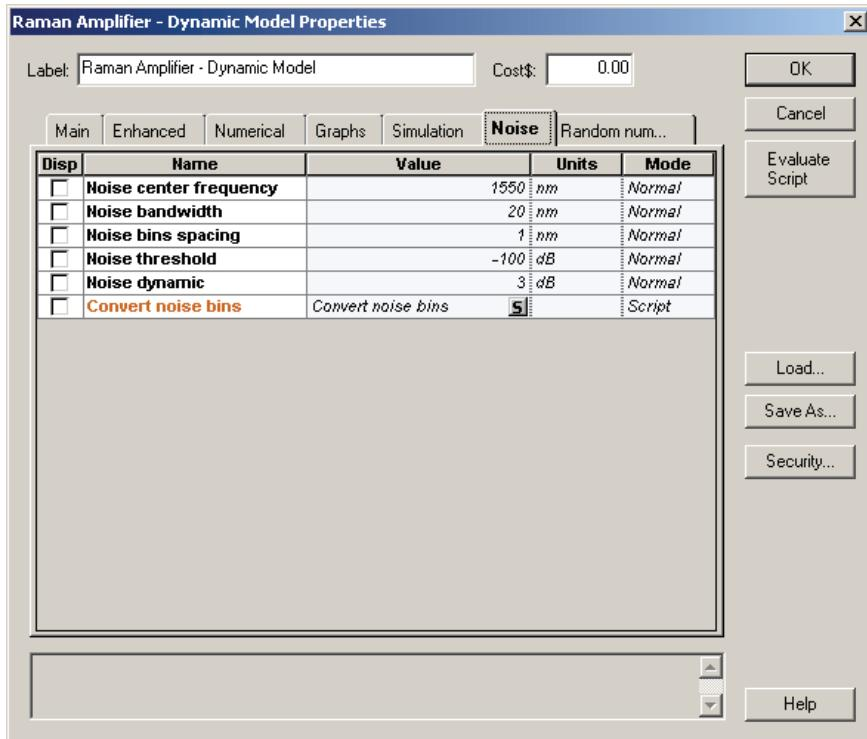


Figure 4 Description of ASE



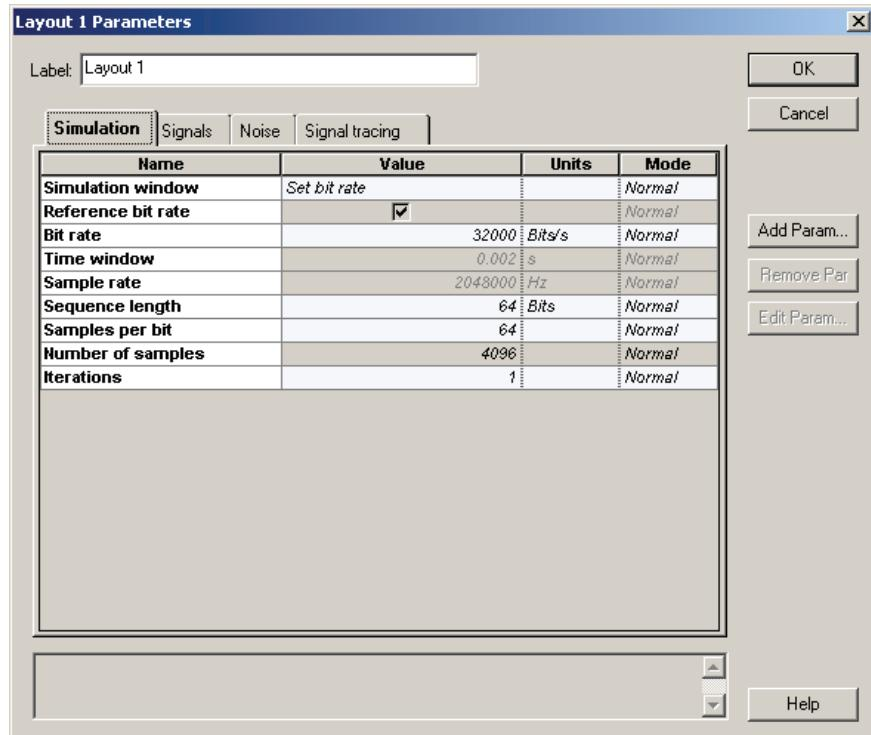
We transmit 8 channels located between 1546 and 1553 nm and -3 dBm power per channel. We have defined three iterations where we drop/add 2, 4 or 6 channels out of the 8 transmitted. After this is done, we compare the surviving-channel-power fluctuation as a function of time. We chose the signal with wavelength equal to 1546, as the surviving one that we will monitor.

A very important setting is the sample rate that will define the size of the time step  $\Delta t$ .

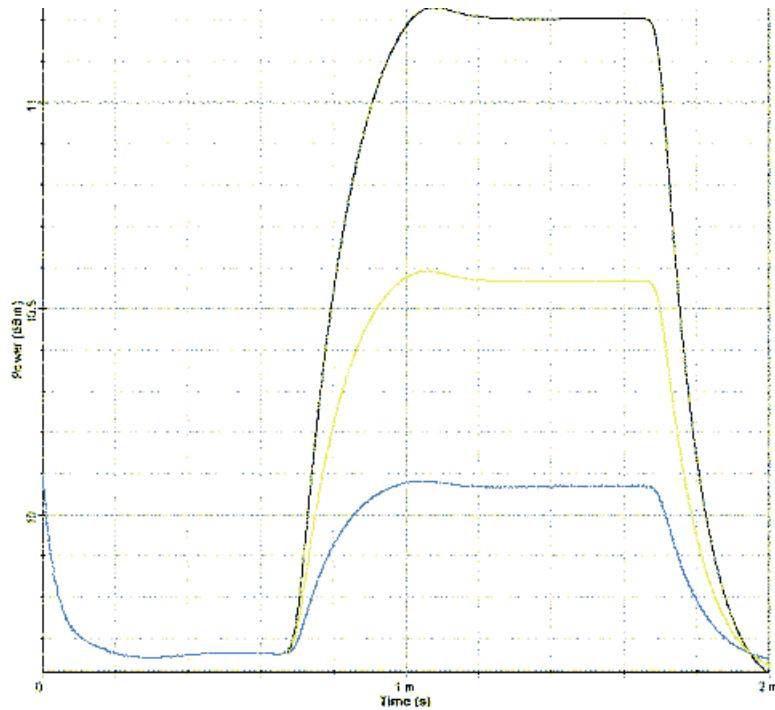
According to [1], the ratio of time and space bins must be

$$\Delta t / \Delta z \leq 4 \times 10^{-9} [\text{s/m}] \quad \text{independently of the Raman fiber length.}$$

In the present case, the space bin is set equal to 800m, so the time bin must be at least  $3.2 \times 10^{-6}$ . Therefore, the number of samples must be at least  $1.25 \times 10^3$ , and we set it to 4096, which is supposed to be more than necessary for the current problem.

**Figure 5 Layout parameters**

The surviving channel power fluctuation is displayed [Figure 6](#).

**Figure 6 Surviving-channel-power fluctuation as a function of time when 2, 4 or 6 out of 8 channels are dropped/added**

## Reference:

- [1] M. Karasek, M. Menif, "Protection of surviving channels in pump-controlled gain-locked Raman fibre amplifier", Optics Communications 210 (2002) 57-65.



---

## SOA amplifiers

---

This section contains the following advanced simulation projects.

- SOA gain saturation—Gaussian pulses
- SOA gain saturation—Comparison with experimental results
- SOA gain saturation—Chirped and super Gaussian pulses
- SOA Gaussian pulse—Gain recovery
- SOA pulse compression
- SOA as a wavelength converter (FWM)
- SOA as a wavelength converter (XGM)
- SOA In-line amplifier
- Wideband SOA characterization
- Wavelength conversion in a wideband SOA

**Notes:**

# SOA gain saturation—Gaussian pulses

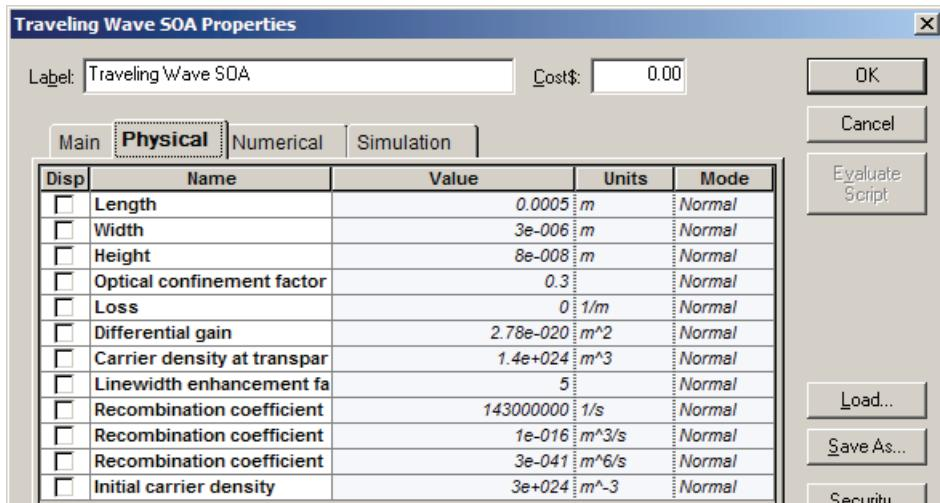
---

Amplification of ultra-short optical pulses in SOA produces considerable spectral broadening and distortion due to the non-linear phenomenon of self-phase modulation. The physical mechanism behind SPM is gain saturation, which leads to intensity-dependent changes of refractive index in response to variations in carrier density. Signal-gain saturation in SOA is caused by a reduction of the population inversion in the active layer due to an increase in stimulated emission. Gain saturation characteristics are especially important in optical repeaters and multi-channel amplifiers which require high-power operation.

This lesson discusses the effect of gain saturation induced self-phase modulation on the amplification of Gaussian pulse. We will consider the pulses with pulse width much shorter than the carrier lifetime. The carrier wavelength of the Gaussian pulse is 1.55 mm.

See [Figure 1](#) for the SOA parameters.

**Figure 1 SOA parameters**



For these SOA physical parameter default values, the following parameter values are obtained:

- Carrier lifetime  $t_C \sim 1.4$  ns
- Saturation energy  $E_{sat} \sim 3.7$  pJ
- Amplification factor  $G_0 = 29$  dB

As a typical value of the line width, the enhancement factor  $\alpha = 5$  is used. Note that for now, the internal losses are zero. This enables a comparison with existing analytical solutions (see the reference at the end of the lesson). The results of this

comparison are similar to the results from the SOA component. Later in this lesson, the influence of the internal losses will be analyzed.

Gaussian pulse with the following parameters was considered

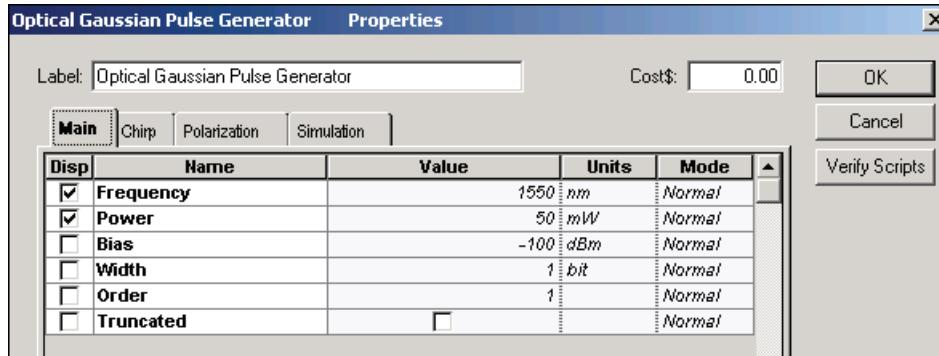
Energy  $E_0 \sim 0.73 \text{ pJ}$

$T_{\text{FWHM}} = 14 \text{ ps} \rightarrow P \sim 50 \text{ mW}$

Note the high value of the initial pulse power. It is the best way to demonstrate the basic qualitative features of gain-saturation induced properties of the pulse amplification. The influence of the value of the initial pulse power will be discussed later in this lesson.

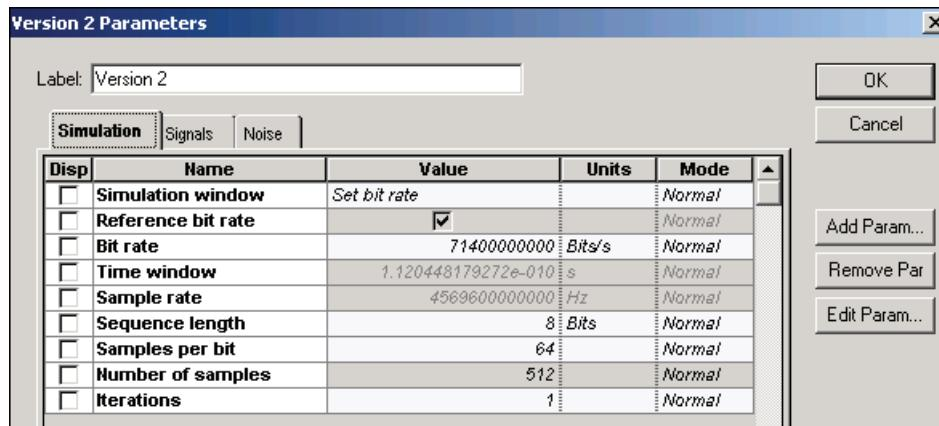
To obtain the required carrier wavelength and power, the following Optical Gaussian Pulse Generator parameters are set (see Figure 2).

**Figure 2 Optical Gaussian Pulse Generator Main parameters**



To obtain the Gaussian pulse with the desired  $T_{\text{FWHM}} = 14 \text{ ps}$ , the following global parameters have been set (see Figure 3).

**Figure 3 Global parameters**

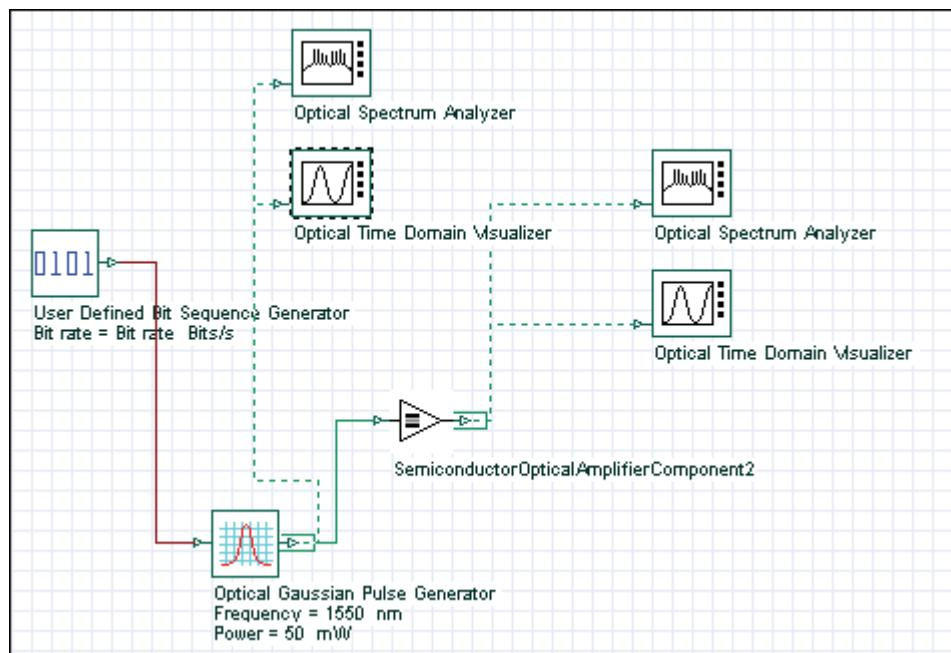


As a result of the set parameters  $\rightarrow T_0/t_C \sim 0.006$  and  $E_0/E_{\text{sat}} \sim 0.2$

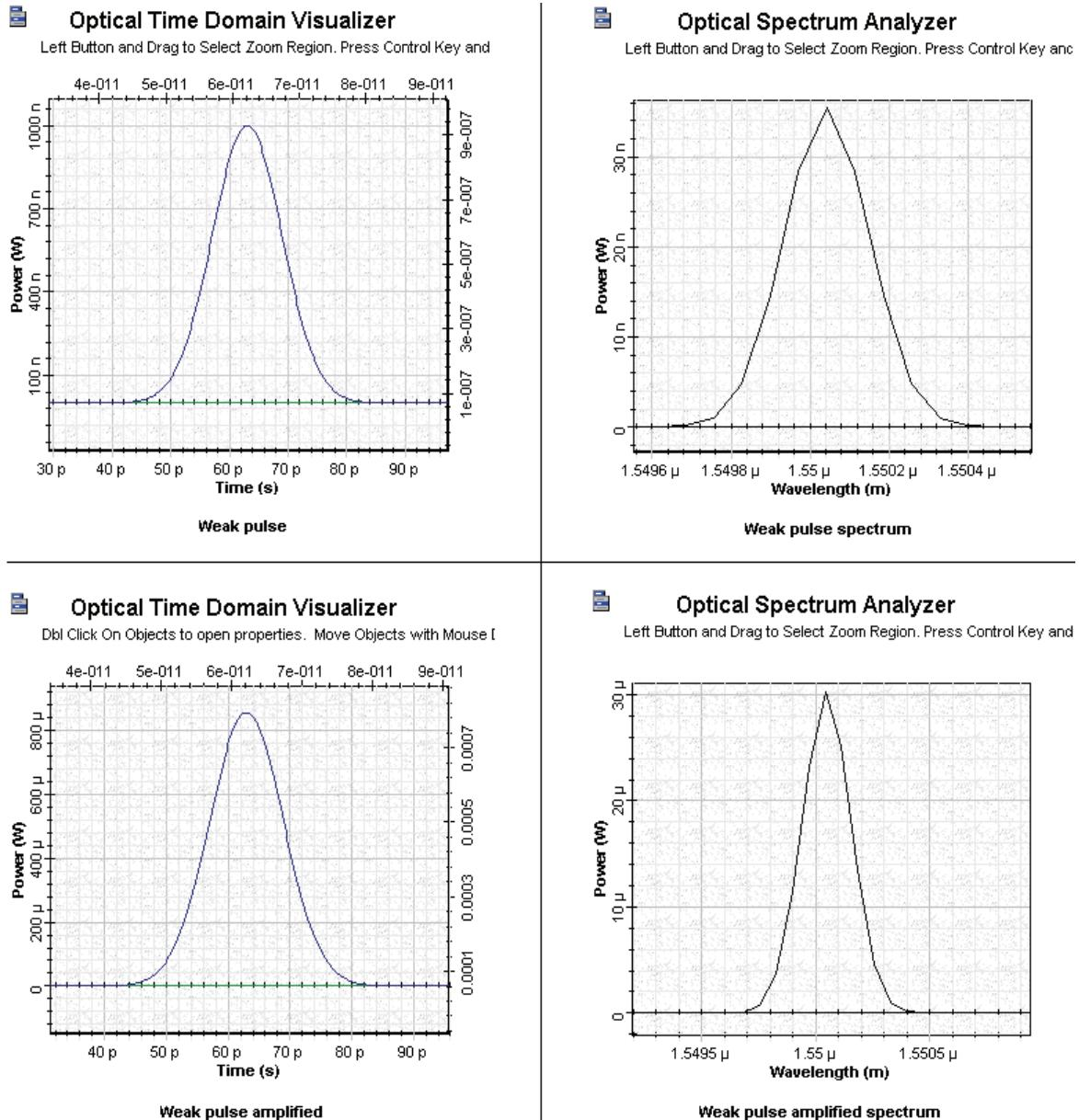
According to the first ratio, the input pulse width is much smaller than the carrier lifetime. The second ratio shows that the pulse energy is comparable with the SOA saturation energy.

See [Figure 4](#) to view the project in which the amplification of the Gaussian pulse with SOA will be analyzed.

**Figure 4 SOA Gain Saturation project layout**



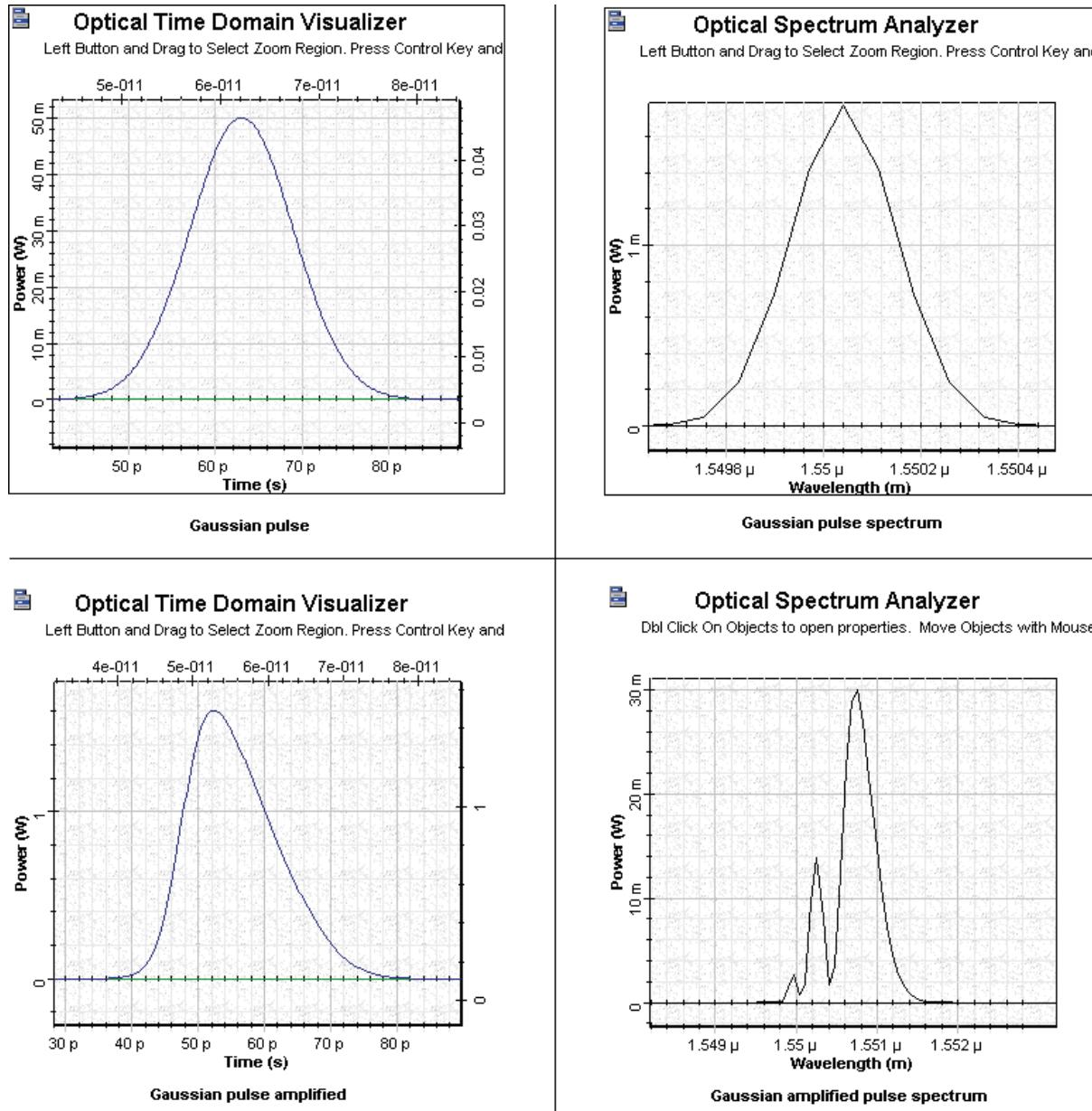
To illustrate the appearance of the gain saturation induced effects, [Figure 5](#) shows the shape and the spectra of the weak and amplified Gaussian pulse at  $P_{in}$  0.001 mW.

**Figure 5 SOA weak and amplified pulse**

Comparison of the two time figures shows that the pulse is amplified in the unsaturated region. No qualitative changes in the spectra of the amplified pulse are evident.

Figure 6 shows the shape and spectra of the initial Gaussian pulse which will be amplified in the saturation region.



**Figure 6 SOA Gaussian pulse and amplified Gaussian pulse in saturation region**

**Figure 6** reveals that the amplified pulse becomes asymmetric — the leading edge is sharper than the trailing edge.

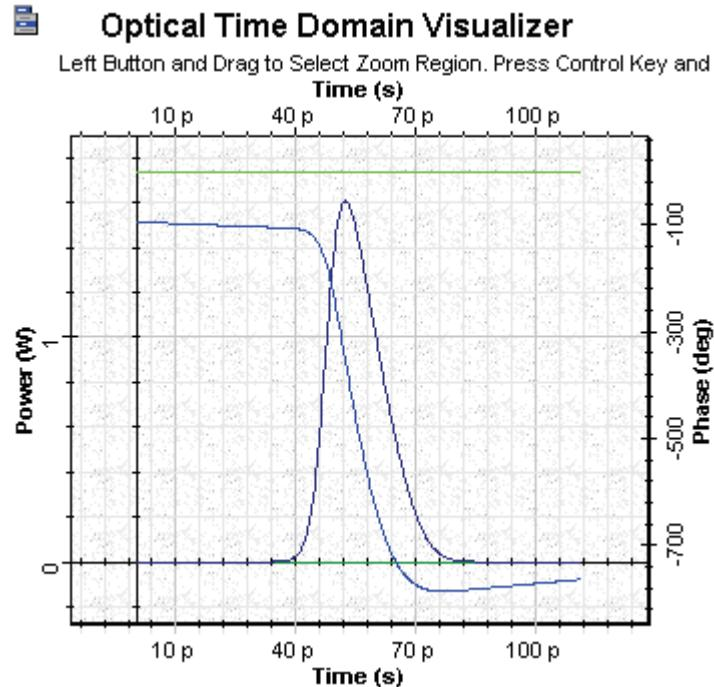
**Note:** The sharpening of the leading edge is a common feature of all amplifiers.

The pulse spectrum of the amplified pulse reveals features that are specific to the SOA.

The spectrum develops a multi-peak structure. The dominant peaks shift toward longer (red) wavelengths. This red shift increases with the increased amplification factor. The red shift observed in this figure is  $\sim 0.001$  mm  $\sim 120$  GHz.

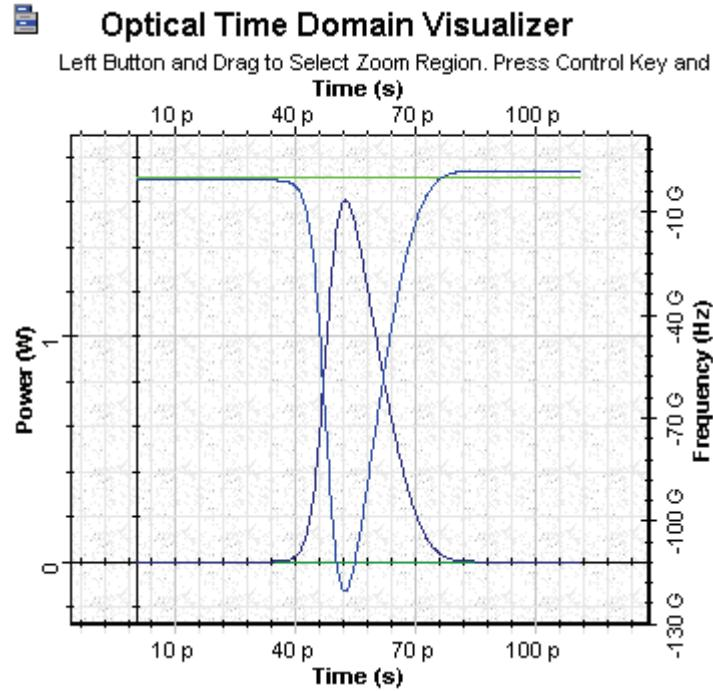
[Figure 7](#) shows a phase of the pulse together with its shape. It is important to note that the phase follows the time evolution of the gain. For such a short pulse, the gain has no time to recover ( $T_0/t_C \sim 0.006$ ).

**Figure 7 SOA Gaussian pulse with saturation 50 mW final time phase**



[Figure 8](#) shows the gain saturation-induced chirp across the pulse together with its shape. Note that the initial Gaussian pulse is unchirped.



**Figure 8** SOA Gaussian pulse with saturation 50 mW final time chirp

The gain saturation induced chirp is negative across the entire pulse. Therefore, the instantaneous frequency is downshifted (the red shift) from the incident frequency. Because the induced chirp increases towards the trailing part of the pulse, the chirp is positive. From the theory of propagation of phase modulated pulses in the medium with group velocity dispersion [3], it follows that the appearance of a positive chirp can be used for pulse compression in the medium with anomalous group velocity dispersion. This application of the gain saturation induced chirp will be considered in SOA gain saturation—Chirped and super Gaussian pulses.

The influence of the initial power, optical confinement factor, and inner losses on the observed properties will now be analyzed. Note that in the model used in [1] and [2], the inner losses have been neglected.

First we will see how the shape and spectrum of the amplified Gaussian pulse (for the same pulse and SOA parameters as above) change as a function from the initial pulse power. The values of the initial power considered were  $P = 5, 10, 20, 30$ , and  $50$  mW. In the first case,  $E_0/E_{\text{sat}} \sim 0.02$ .

To obtain these results, use the sweep mode (see Figure 9).

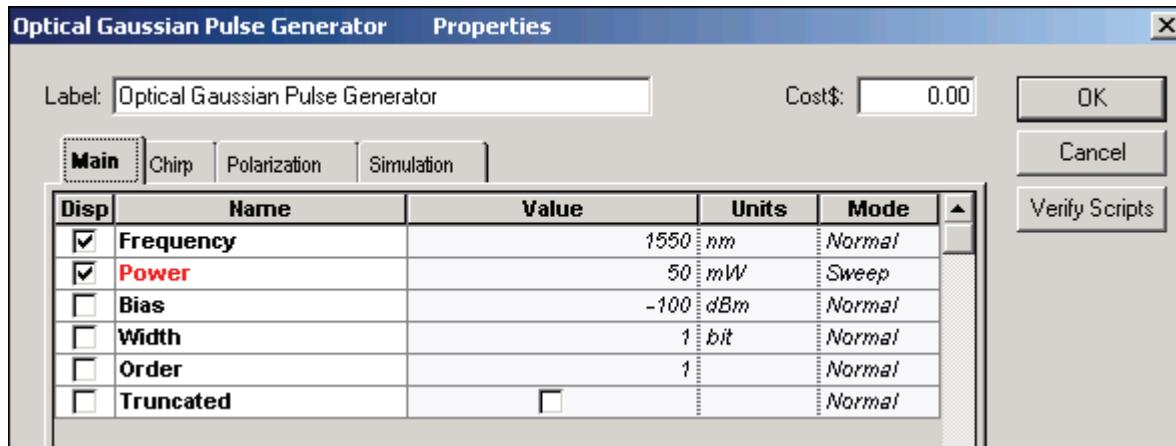
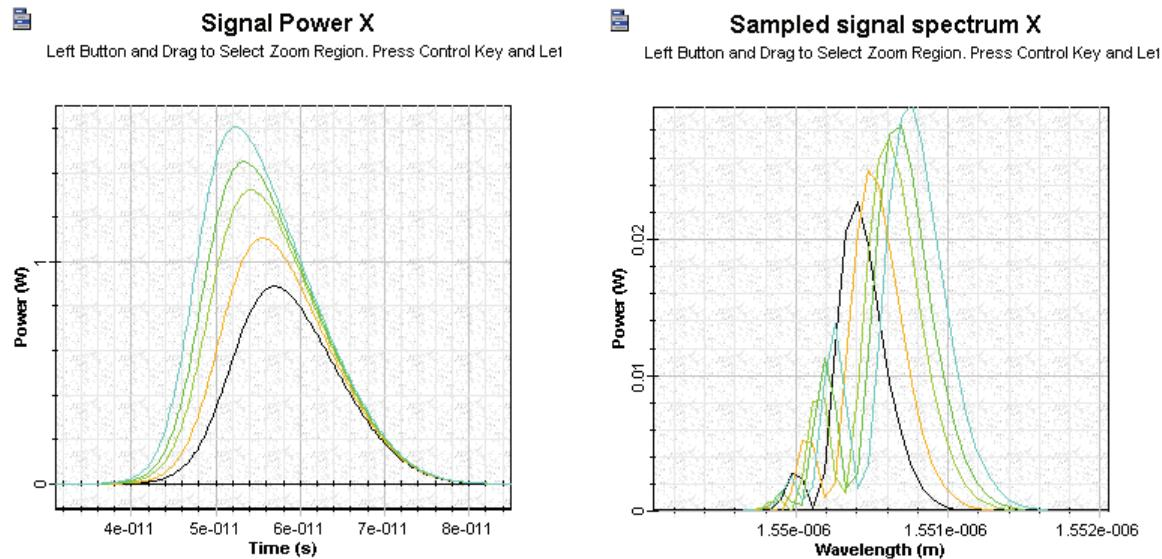
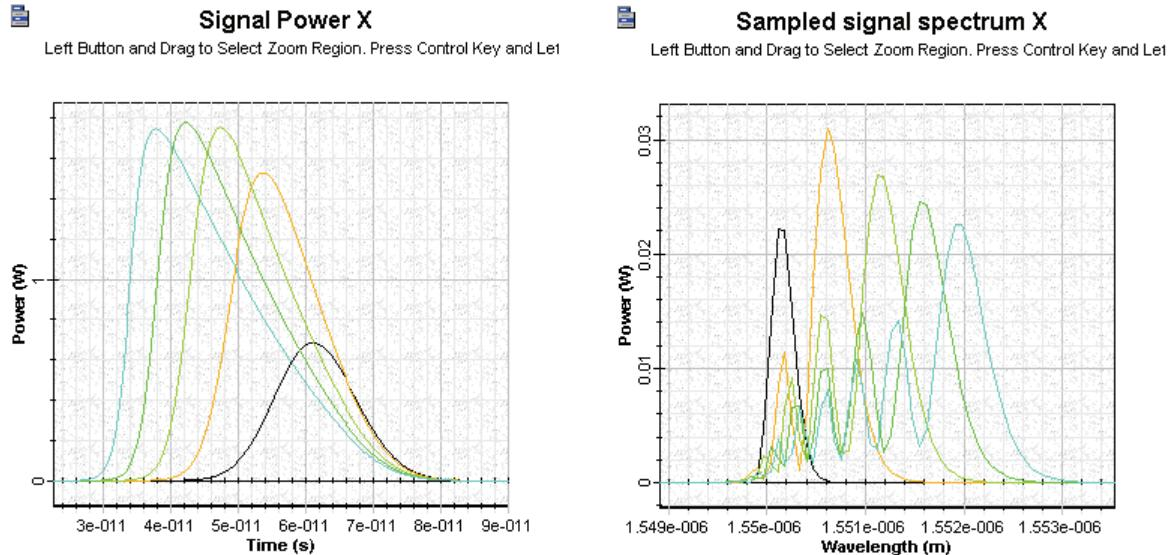
**Figure 9 SOA Gaussian Pulse Generator parameters**

Figure 10 shows the shape and spectrum of the amplified Gaussian pulse as a function from the initial power.

**Figure 10 SOA Gaussian pulse signal**

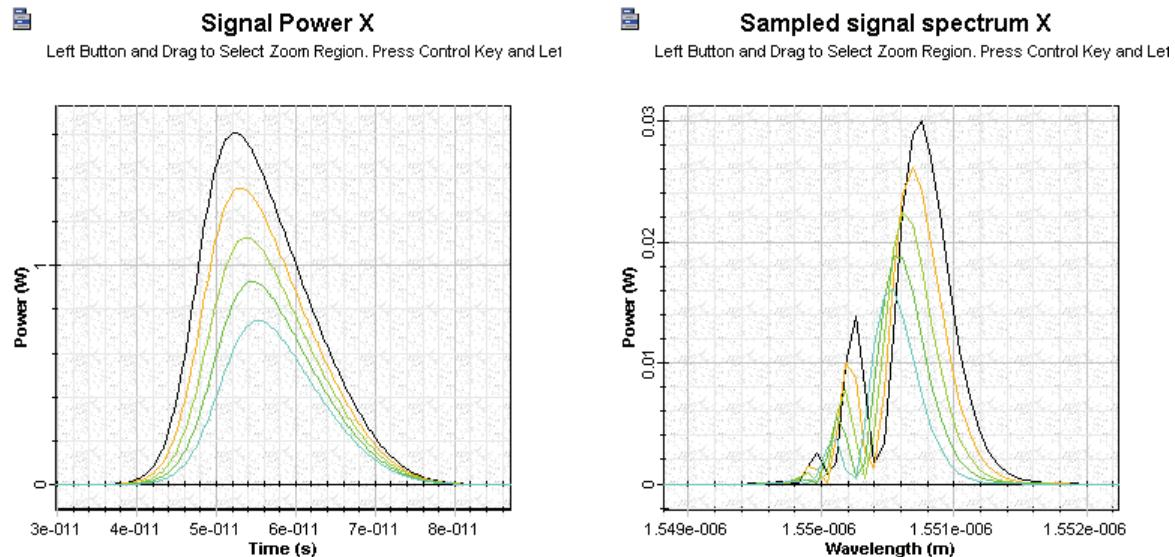
As expected, an increase in the ratio  $E_0/E_{\text{sat}}$  (for fixed pulse width) leads to an increase in the number of peaks in the spectrum and an increase of the red shift.

Figure 11 shows the shape and spectrum of the amplified Gaussian pulse (for the same pulse and SOA parameters as above) as a function from the optical confinement factor. The value of the optical confinement factor considered are  $\Gamma = 0.1, 0.2, 0.3, 0.4, 0.5$

**Figure 11 SOA amplified Gaussian pulse signal**

The optical confinement factor influences the pulse shape and spectrum.

[Figure 12](#) shows the shape and spectrum of the amplified Gaussian pulse (for the same pulse and SOA parameters as above) as a function from the internal losses. The value of internal losses considered are: 0, 1000, 2000, 3000, and 4000 (1/m).

**Figure 12 SOA amplified internal loss Gaussian pulse signal**

In contrast to the optical confinement factor, the internal losses do not influence the pulse shape and spectrum.



In this lesson, we have observed the basic properties of the isolated Gaussian pulse amplification with SOA component of OptiSystem software for gain saturation.

- Both the shape and the spectrum of the amplified pulses are asymmetric
- The spectrum develops multi-peak structure with well-expressed red shift

The obtained results are in complete agreement with previously published results [1] and [2].

## References

- [1] G.P. Agrawal and N.A. Olsson, "Self-phase modulation and spectral broadening of optical pulses in semiconductor laser amplifiers", IEEE Journal of Quantum Electronics, Vol. 25, pp. 2297-2306, 1989.
- [2] G.P. Agrawal, "Fiber-Optic Communication Systems", 2nd Edition, John Wiley & Sons Inc., 1997.
- [3] G.P. Agrawal, "Nonlinear Fiber Optics," 3rd Edition, Academic Press, 2001.



# SOA gain saturation—Comparison with experimental results

---

This lesson applies the results from [SOA gain saturation—Gaussian pulses](#) for interpretation of the experimental results on the amplification of Gaussian pulse with SOA obtained in [1]. The aim of [1] was to report the first investigation of the spectral characteristics of pulse amplification in SOA.

Parameters of SOA given in the paper are:

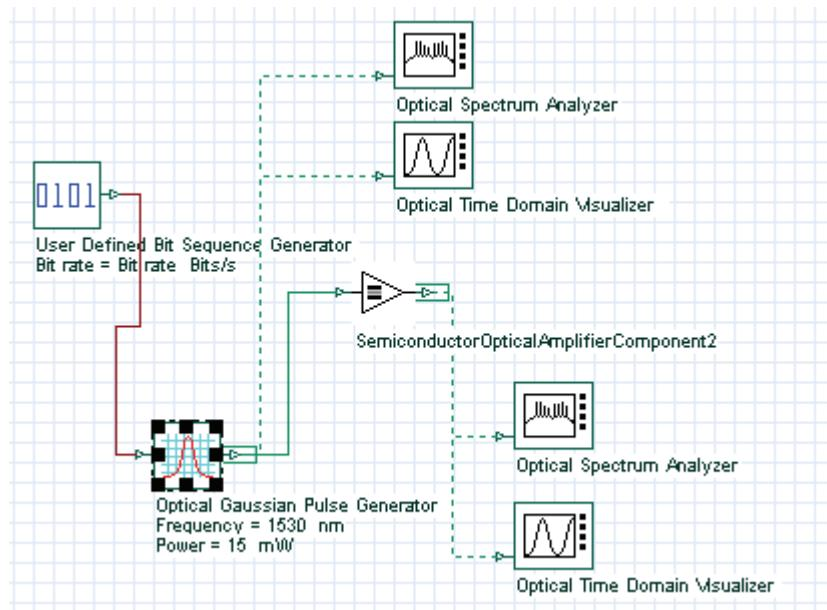
Saturation energy  $E_{\text{sat}} \sim 6 \text{ pJ}$ , and the values of the amplification factor: For a drive current of 30 mA  $\rightarrow G_0 \sim 11 \text{ dB}$  and for a drive current of 130 mA  $\rightarrow G_0 \sim 30 \text{ dB}$ .

There is no information about the carrier lifetime, which makes it impossible to determine the exact value of the ratio  $T_0/t_C$ . There is also no information about the inner losses of the amplifier. Note that model used in [1] does not take into account the inner losses of the amplifier.

The input Gaussian pulse parameters in the experiment are:  $T_{\text{FWHM}} = 15.6 \text{ ps}$ , and input pulse energy  $E_0 \sim 0.18 \text{ pJ} \rightarrow E_0 / E_{\text{sat}} \sim 0.03$ , where the pulse width is much shorter than the carrier lifetime.

The experiment has been analyzed in the framework of the layout in [Figure 2](#).

**Figure 1 SOA Gain Saturation comparison project layout**



The following global parameters and **Optical Gaussian Pulse Generator** parameters have been used (see [Figure 2](#) and [Figure 3](#)).

**Figure 2 Global parameters**

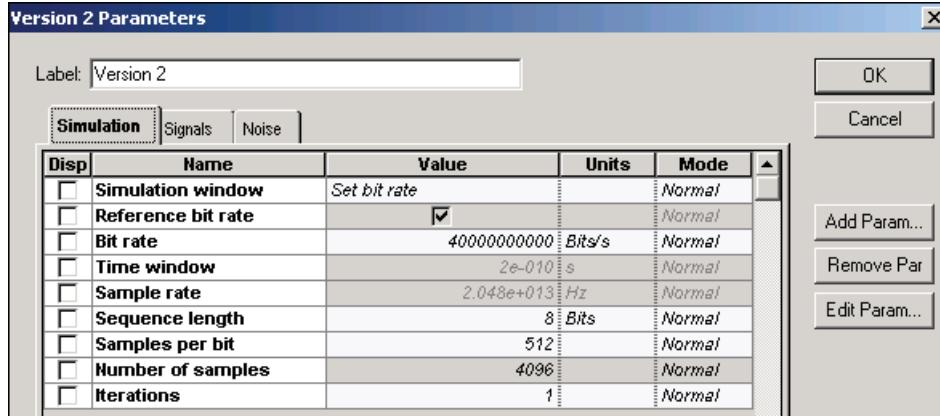
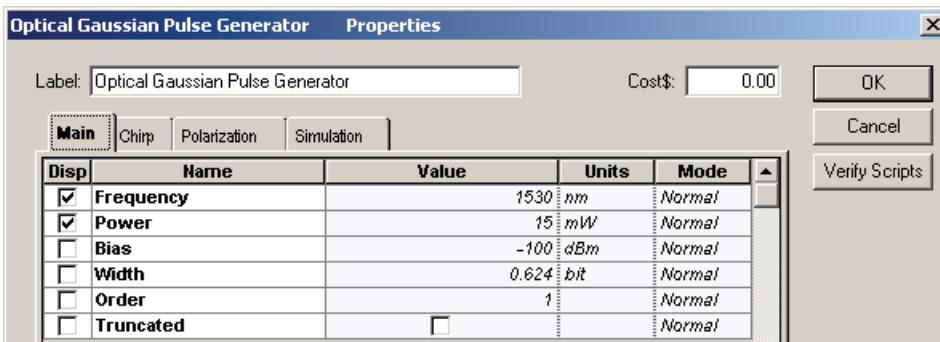
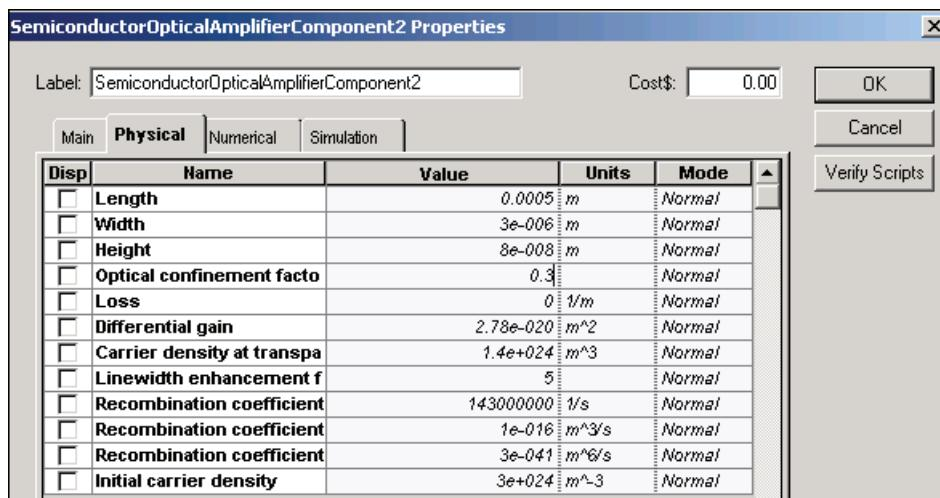


**Figure 3 Optical Gaussian Pulse Generator Main parameters**



We will use the Bit Rate  $B = 40$  Gb/s. Therefore,  $T_B = 25$  ps. To obtain  $T_{FWHM} = 15.6$  ps, a duty cycle of 0.624 was used. To obtain a single pass gain of  $\sim 30$  dB in the experiment, we used the following SOA parameters (see [Figure 4](#)).

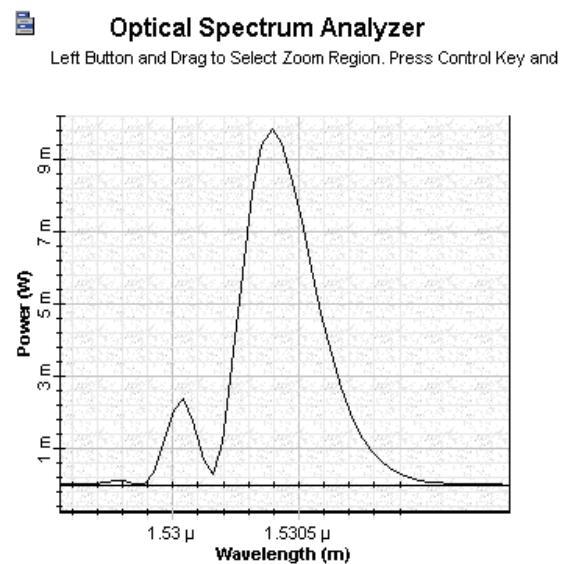
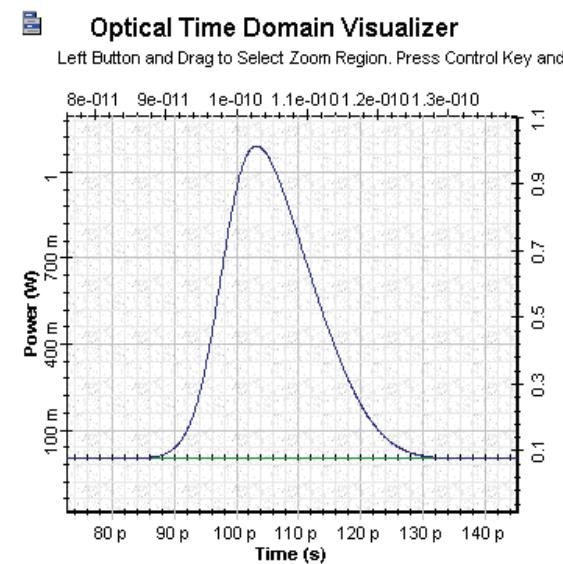
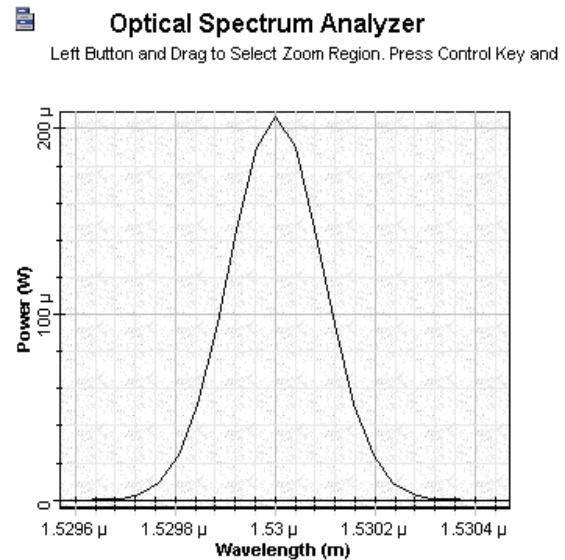
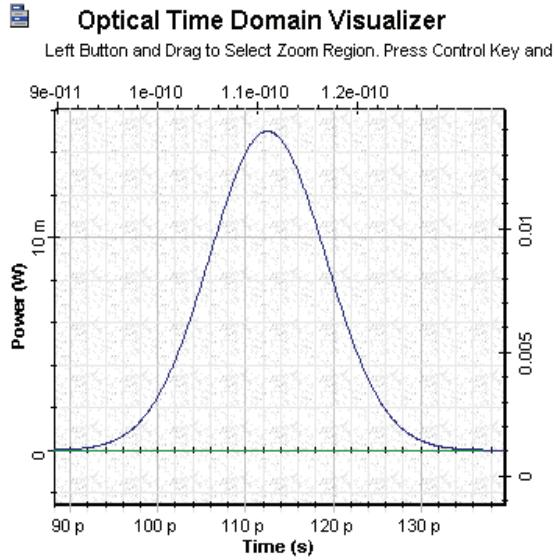
**Figure 4 SOA parameters**



Note that for these estimations, the influence of the inner losses is neglected. The corresponding saturation energy  $E_{\text{sat}}$  is approximately 5 pJ. To satisfy the experimental condition  $E_{\text{in}}/E_{\text{sat}} \sim 0.003$ , the pulse peak power 15 mW is used.

Figure 5 shows the shape in time and in frequency domain of the initial and amplified pulses.

**Figure 5 Time and frequency domain of initial and amplified pulses**



The spectrum of the amplified pulse clearly shows the following properties:

- peak output wavelength is red shifted with  $\sim 0.3$  nm
- secondary peak appears approximately 0.4 nm below the main peak
- main peak is broadened considerably
- experimentally observed value for the red shift of the peak wavelength is 0.31 nm and the measured peak separation is 0.4 nm

As we can see, our numerical observations are in very good agreement with the experimental and model results of [1].

In this lesson, the experimental results of [1] were compared to the results of our SOA model. A good qualitative and quantitative agreement has been established.

## References

- [1] N.A. Olsson and G.P. Agrawal, "Spectral shift and distortion due to self-phase modulation of picosecond pulses in 1.5 mm amplifiers", Appl. Phys. Lett, Vol. 55, pp. 13-15, 1989.
- [2] G.P. Agrawal and N.A. Olsson, "Self-phase modulation and spectral broadening of optical pulses in semiconductor laser amplifiers", IEEE Journal of Quantum Electronics, Vol. 25, pp. 2297-2306, 1989.



# SOA gain saturation—Chirped and super Gaussian pulses

---

This lesson continues to study the effect of gain saturation induced self-phase modulation on the amplification of optical pulses. We will concentrate on the pulses with different shape and initial frequency shift. The chirped Gaussian input pulses are the pulses which are usually produced from directly modulated semiconductor lasers.

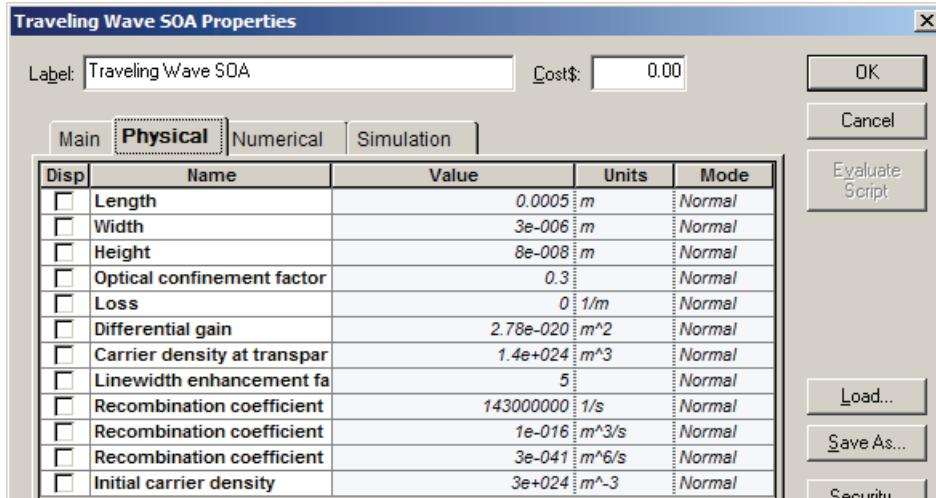
As in [SOA gain saturation—Gaussian pulses](#), we will consider the pulses with a pulse width much shorter than the carrier lifetime. The carrier wavelength of the Gaussian pulse is 1.55 mm.

In first part of this lesson, we will look at chirped Gaussian pulses. In the second part of this lesson, we will look at super Gaussian pulses.

## Saturation of amplification of chirped Gaussian pulse

See [Figure 1](#) for the SOA parameters.

**Figure 1** SOA parameters



For these SOA physical parameter default values, the following parameter values are obtained:

- Carrier lifetime  $t_C \sim 1.4$  ns
- Saturation energy  $E_{sat} \sim 3.7$  pJ
- Amplification factor  $G_0 = 29$  dB

As a typical value of the line width, the enhancement factor  $\alpha = 5$  is used.

Gaussian pulse with the following parameters was considered:

- Energy  $E_0 \sim 0.73 \text{ pJ}$
- $T_{\text{FWHM}} = 14 \text{ ps} \rightarrow P \sim 50 \text{ mW}$

Chirp line width enhancement factor = 5

To obtain the required carrier wavelength and power, the following chirped and super **Optical Gaussian Pulse Generator** parameters are selected (see [Figure 2](#) and [Figure 3](#)).

**Figure 2 Chirped Gaussian Pulse Generator parameters**

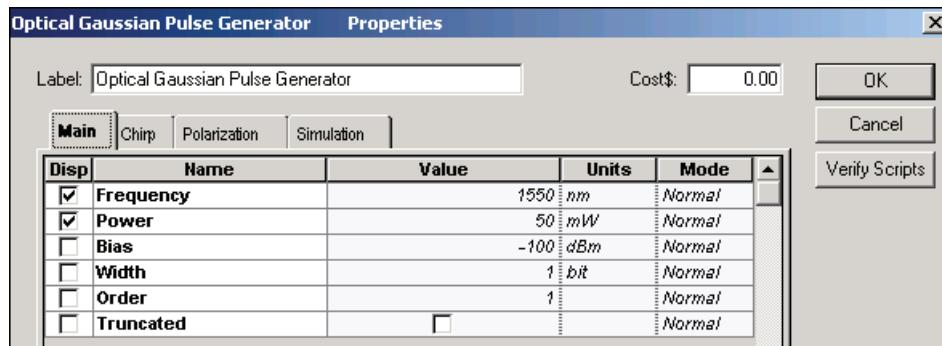
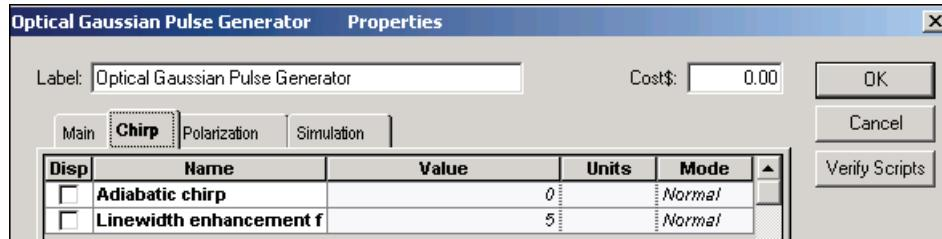
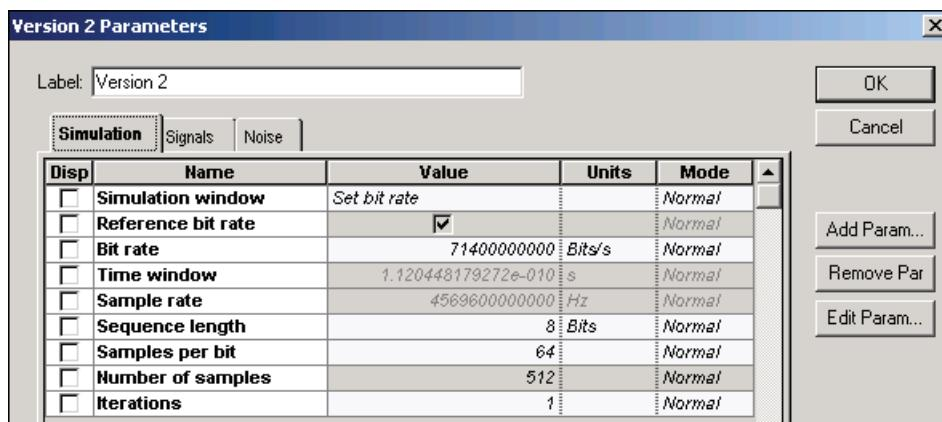


**Figure 3 Super Gaussian Pulse Generator parameters**



To obtain the chirped and super Gaussian pulse with desired  $T_{\text{FWHM}} = 14 \text{ ps}$ , the following global parameters are selected (see [Figure 4](#)).

**Figure 4 Gaussian pulse global parameters**



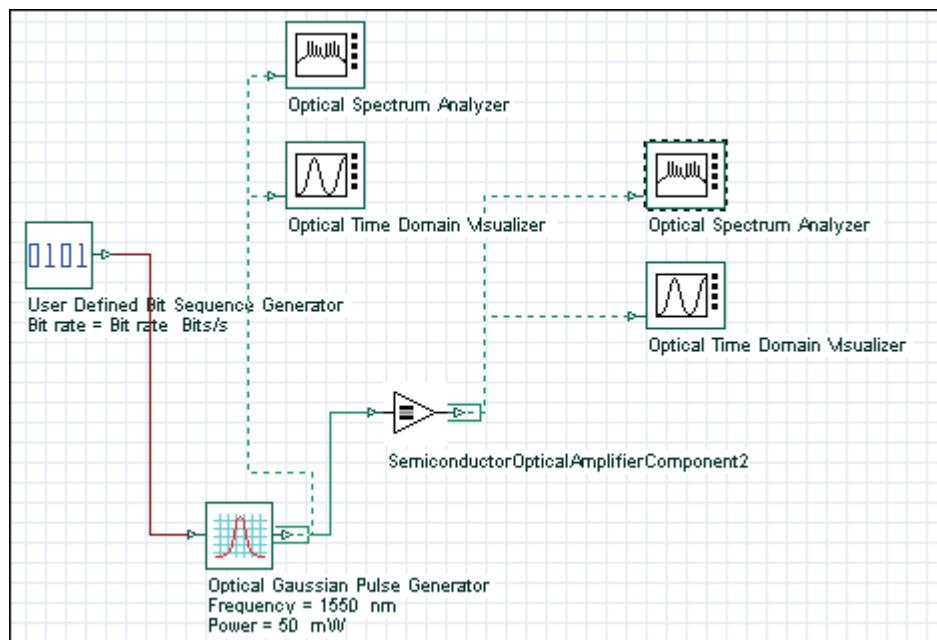
As a result of selecting these parameters:

$$T_0 / t_C \sim 0.006 \text{ and } E_0 / E_{\text{sat}} \sim 0.2$$

According to the first ratio, the input pulse width is much smaller than the carrier lifetime. The second ratio shows that the pulse energy is comparable with the SOA saturation energy.

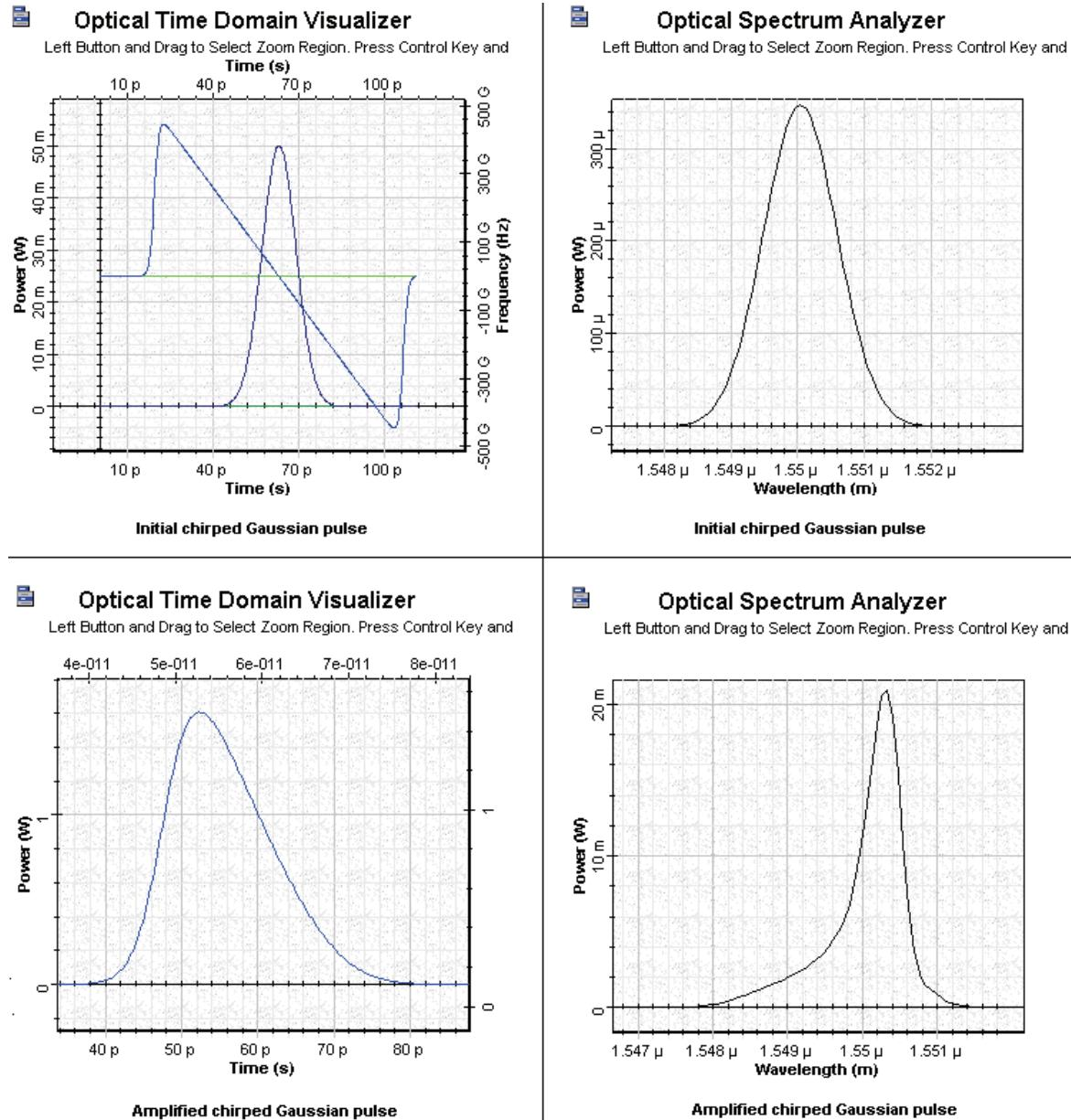
[Figure 5](#) shows the project framework in which the amplification of the Gaussian pulse with SOA will be analyzed.

**Figure 5 SOA Gaussian pulse project layout**



[Figure 6](#) shows the shape and spectrum of the initial and amplified chirped Gaussian pulses.

**Note:** The frequency in the first graph decreases with time across the pulse, which is usually referred to as negative chirp.

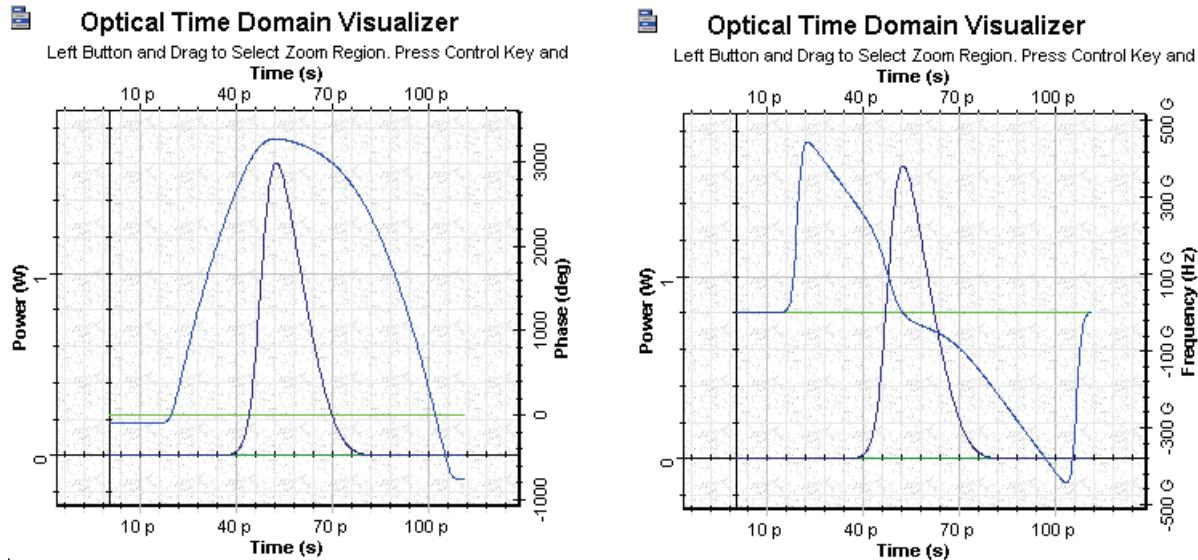
**Figure 6 Initial and amplified chirped Gaussian pulses**

The first graph shows the expected sharpening of the leading edge. Note the different form of the output pulse spectrum and the reduced red shift in comparison with the amplified Gaussian pulse.

[Figure 7](#) shows the gain saturation-induced chirp across the pulse and the deformation of the initial negative chirp after amplification.



**Figure 7 Gain saturation-induced chirp across the pulse and deformation of the initial negative chirp after amplification**



For negative initial chirp the gain saturation induced red shift decreases. (Compare the red shift from the figure with pulse spectrum with this of the amplified Gaussian pulse from [SOA gain saturation—Gaussian pulses](#).) For the opposite sign of initial chirp, the spectrum shifts even more to the red side than in the case of zero initial chirp.

## Saturation of amplification of super Gaussian pulse

The additional pulse parameter considered for the super Gaussian pulse is  $m = 3$ .

**Note:** The pulse is now without initial chirp.

To obtain the additional order parameter, the following **Optical Gaussian Pulse Generator** parameters are selected (see [Figure 8](#)).

**Figure 8 Super Gaussian Parameters**

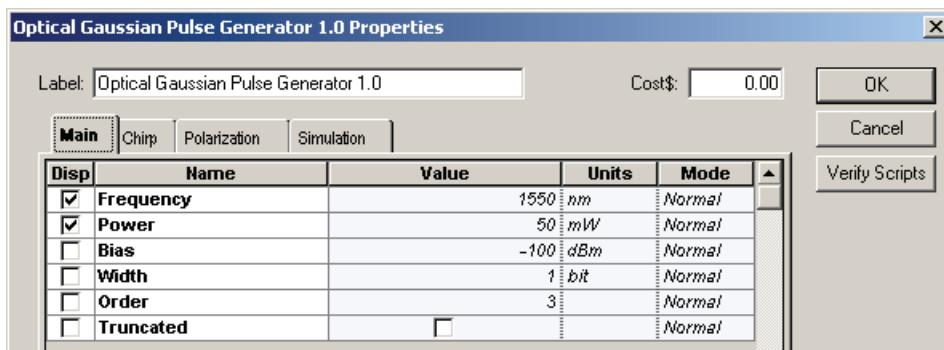
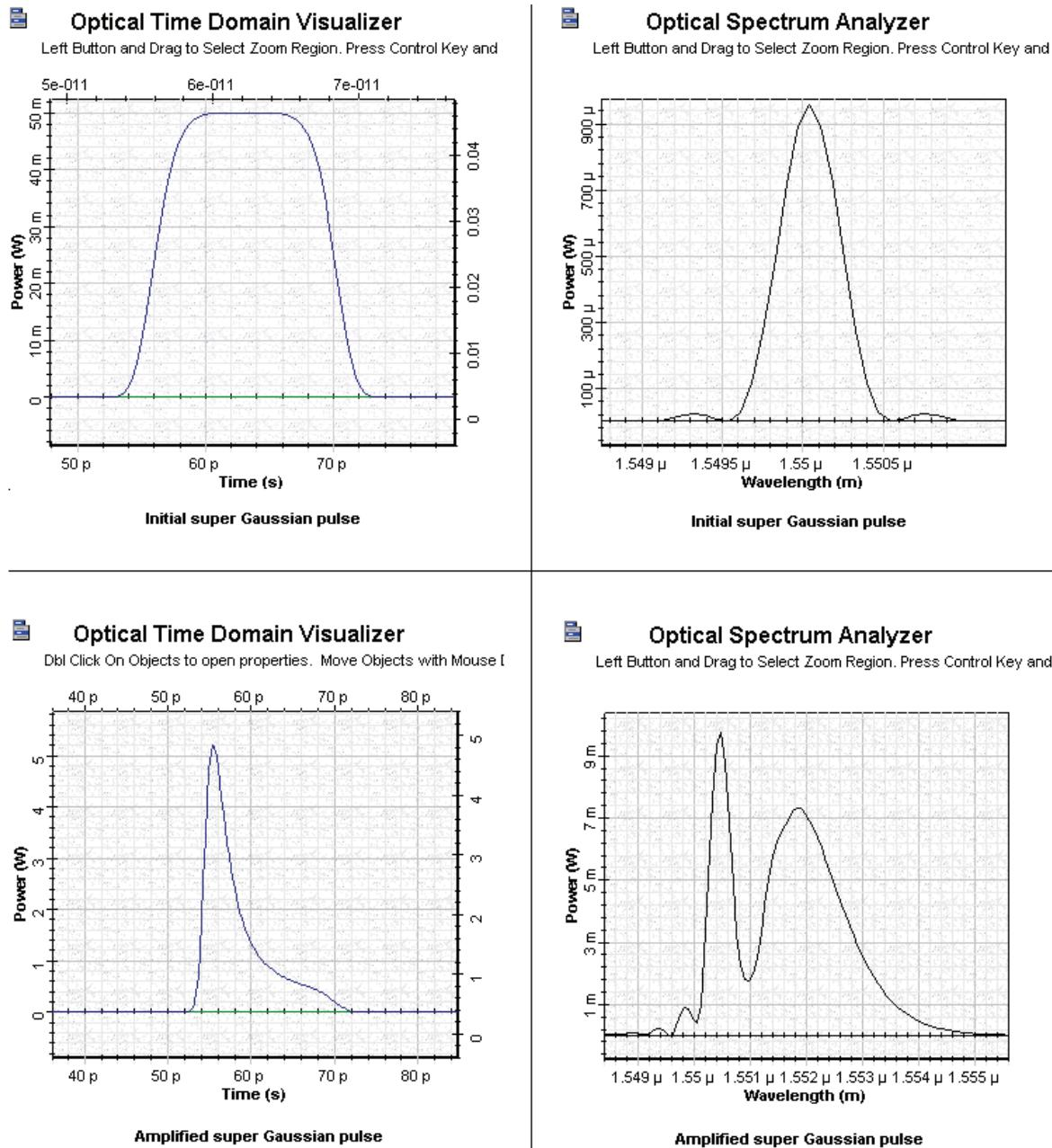


Figure 9 shows the shape and spectra of the initial and amplified super Gaussian pulse.

**Figure 9 Initial and amplified super Gaussian pulse**



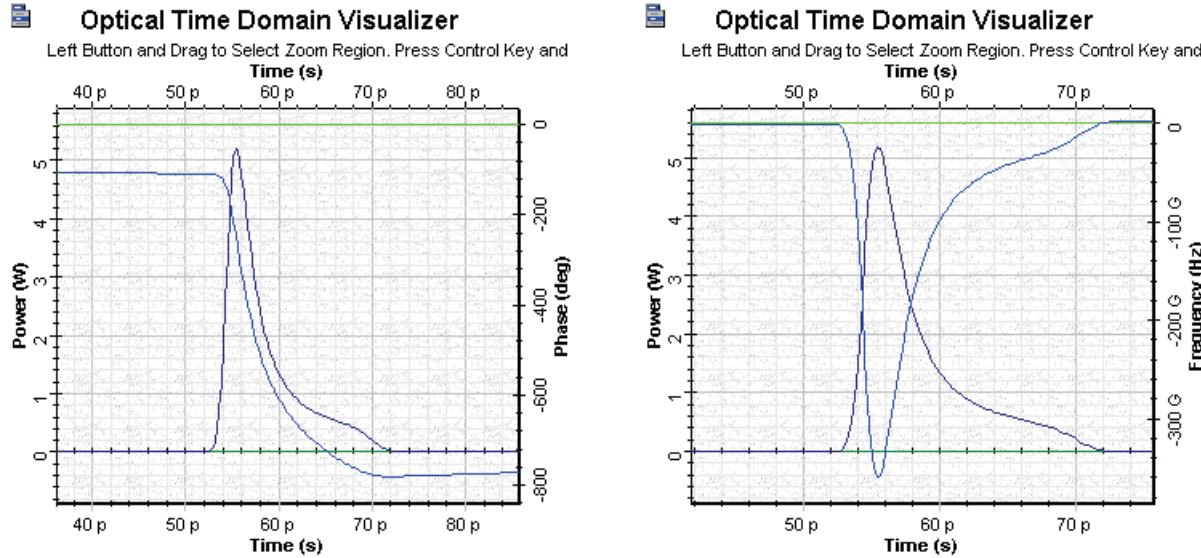
The output pulse has a long tail on the trailing edge and appears to be narrower than the input pulse. This situation is very different from the case of the amplification of the Gaussian pulse where the  $T_{FWHM}$  of the output pulse was larger than the  $T_{FWHM}$  of the input pulse.



The spectrum of the output spectrum has a multi-peak structure and a very well-expressed red shift. Comparing this spectrum with the spectrum of the amplified Gaussian pulse, we can see that it is different. Therefore, the form of the spectrum and the amount of the red shift strongly depends on the initial pulse shape.

[Figure 10](#) shows the shape and spectrum phase of the gain saturation-induced chirp across the pulse.

**Figure 10 Amplified super Gaussian pulse phase and pulse frequency**



This lesson described the basic properties of the chirped and super Gaussian pulse amplification with SOA component of OptiSystem software. We have shown that the shape and spectrum pulse distortions with an amplification of SOA strongly depends on the shape and initial frequency modulation of the pulse. These properties can be very important when pulses produced by directly modulated semiconductor lasers are amplified.

The obtained results are in complete agreement with the results published in [1] and [2].

## References

- [1] G.P. Agrawal and N.A. Olsson, "Self-phase modulation and spectral broadening of optical pulses in semiconductor laser amplifiers", IEEE Journal of Quantum Electronics, Vol. 25, pp. 2297-2306, 1989.
- [2] G.P. Agrawal, "Fiber-Optic Communication Systems", 2nd Edition, John Wiley & Sons Inc., 1997.



# SOA Gaussian pulse—Gain recovery

---

In the previous three lessons, we assumed that the input pulse was much shorter than the carrier lifetime. When the pulse width becomes comparable to the carrier lifetime, the saturated gain has time to recover during the pulse. The recovery effect influences the shape and spectrum of the amplified pulse.

This lesson studies this influence. Three subtopics will be discussed:

- Partial gain recovery
- Complete gain recovery
- Appearance of gain-saturation induced self-phase modulation

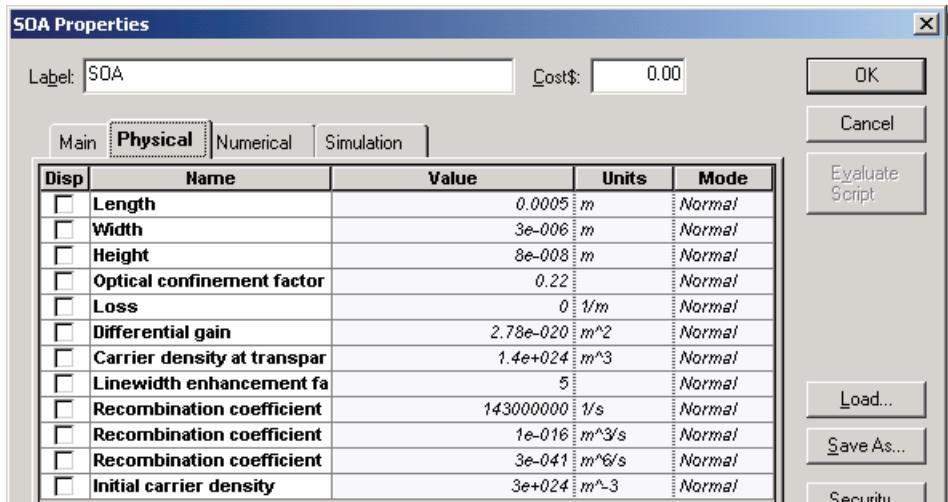
## SOA parameters

The carrier lifetime  $t_C \sim 1.4$  ns,  $\Gamma = 0.22$ ,  $E_{sat} = 5$  pJ.

The unsaturated single pass amplifier gain  $\sim 30$  dB. Inner loss = 0 makes the comparison with [1] possible.

See [Figure 1](#) for SOA Physical parameters.

**Figure 1 SOA parameters**



## Partial gain recovery

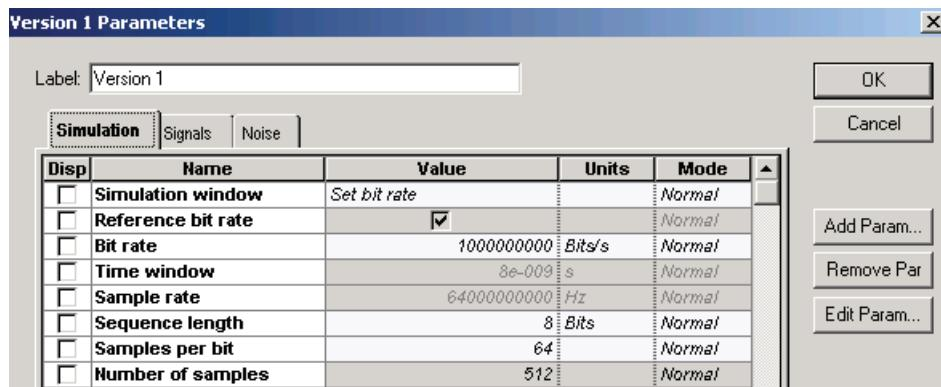
Because the carrier lifetime of our SOA is  $t_C \sim 1.4$  ns, pulse widths have to be smaller than 1.4 ns in order to be able to see the partial gain recovery. Keeping the ratio  $E_{in}/E_{sat}$ , we will consider the influence of increasing the pulse duration, which will approach but remain smaller than the carrier lifetime.

Calculation parameters:

- Bit rate at  $B = 1$  GHz, consequently  $T_B = 1$  ns.

See [Figure 2](#) for the global parameters.

**Figure 2 Global parameters**



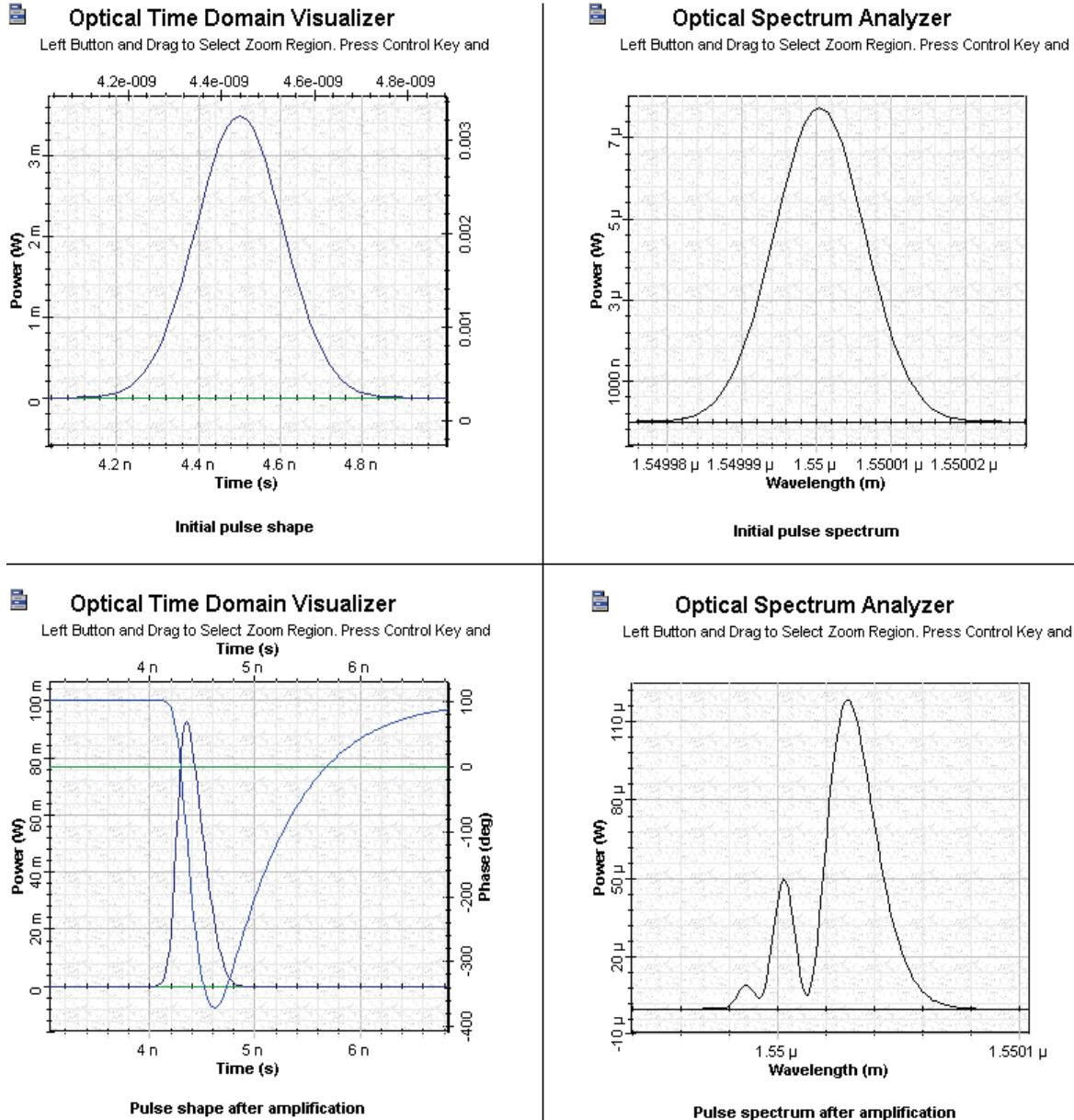
We will consider three pulse widths — 0.25ns, 0.5 ns, and 1 ns. In all three cases, the ratio  $E_{in}/E_{sat} = 0.1$  will remain constant.

## Pulse 1 parameters

- Duty cycle 0.25,  $T_{FWHM} \sim 0.25$  ns  $\rightarrow T_0 \sim 0.14$  ns,  $P_{in} = 3.5$  mW
- Therefore:  $T_0/t_C \sim 0.1$  and  $E_{in}/E_{sat} \sim 0.1$

Figure 3 shows the shape and spectra of the initial and amplified pulses for Pulse 1.

**Figure 3 SOA Gaussian Pulse 1 initial and amplified pulses**

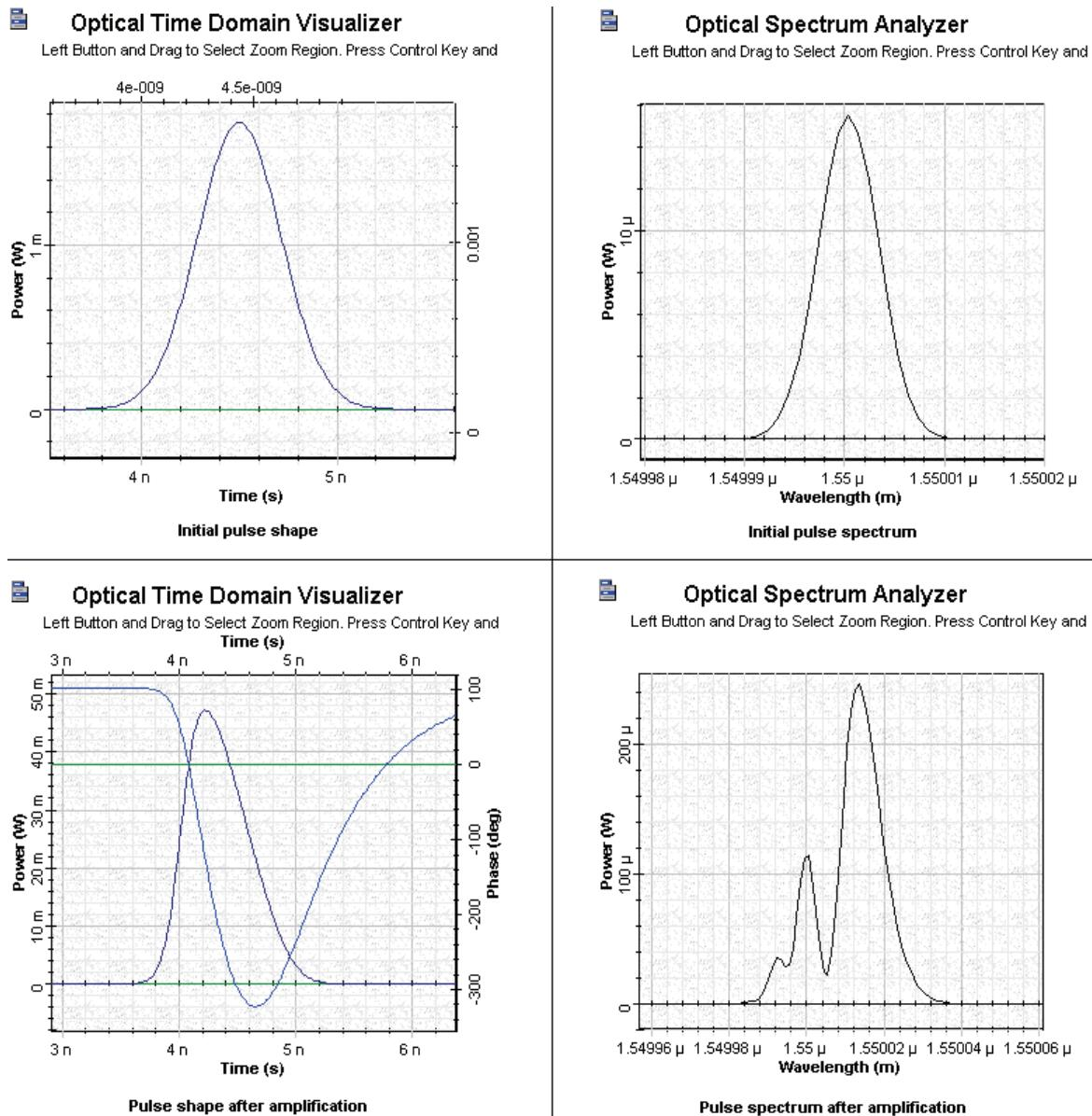


## Pulse 2 parameters

- Duty cycle 0.5,  $T_{FWHM} \sim 0.5$  ns  $\rightarrow T_0 \sim 0.28$  ns,  $P_{in} = 1.75$  mW
- Therefore:  $T_0 / t_C \sim 0.2 \rightarrow E_{in} / E_{sat} = 0.1$

Figure 4 shows the shape and spectra of the initial and amplified pulses for Pulse 2.

**Figure 4 SOA Gaussian Pulse 2 initial and amplified pulses**

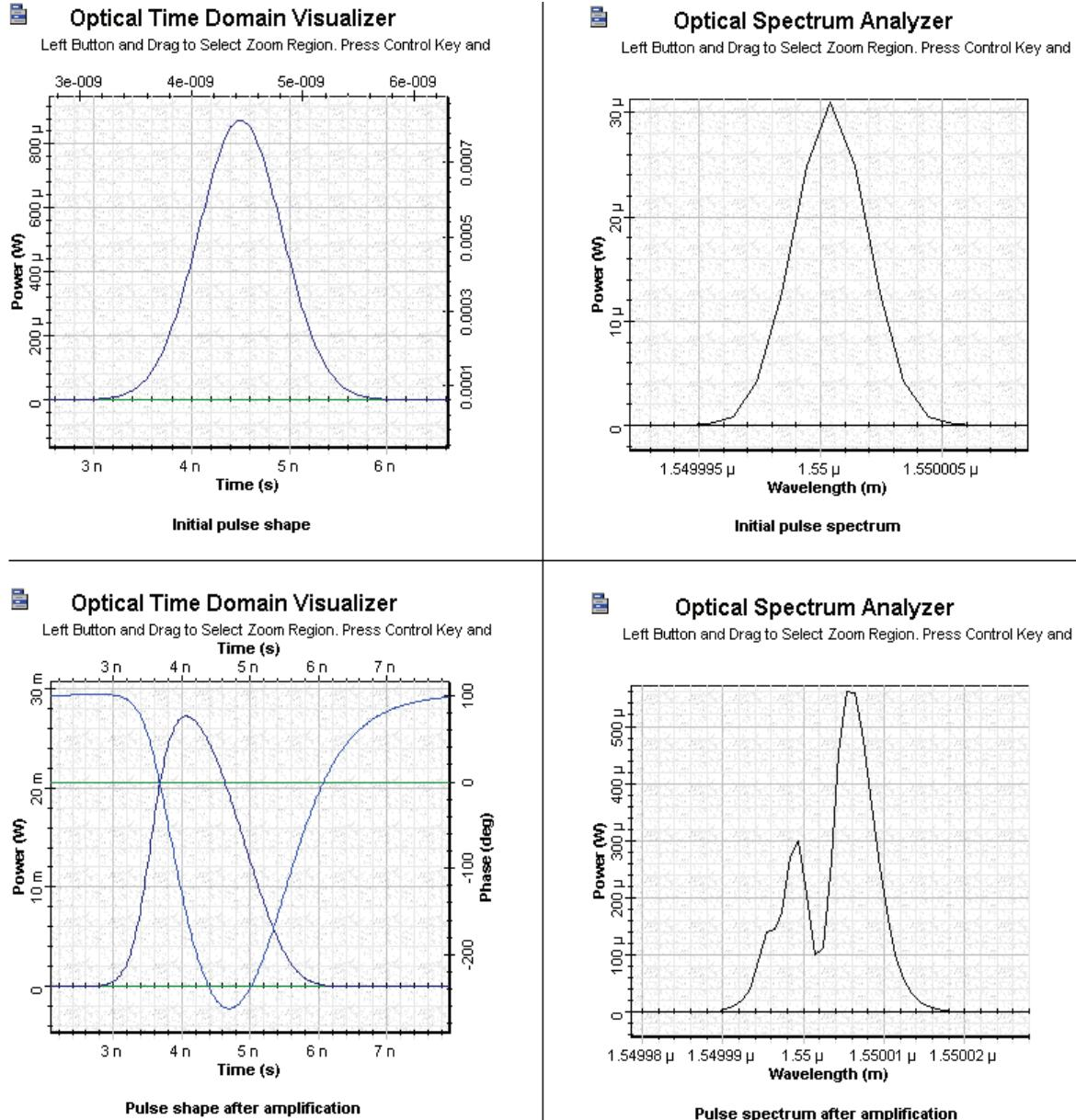


### Pulse 3 parameters

- Duty cycle 1,  $T_{FWHM} \sim 1 \text{ ns} \rightarrow T_0 \sim 0.567 \text{ ns}$ ,  $P_{in} = 0.875 \text{ mW}$
- Therefore:  $T_0 / t_C \sim 0.4$  and  $E_{in}/E_{sat} = 0.1$

Figure 5 shows the shape and spectra of the initial and amplified pulses for Pulse 3.

**Figure 5 SOA Gaussian Pulse 3 initial and amplified pulses**



The following properties for these three amplified pulses can be distinguished.

- By increasing the pulse width and keeping the ratio  $E_{in}/E_{sat} = 0.1$ , the pulse shape becomes less asymmetrical and broader than the input pulse.
- By increasing the pulse width, the spectrum becomes less asymmetrical and the spectral shift decreases. Note the behavior of the phase shown in the shapes of amplified pulses.

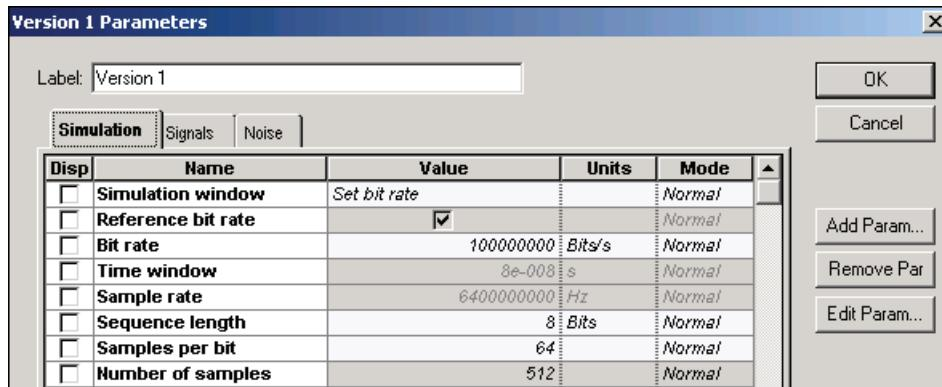
As the phase of the amplified pulse brings information for the gain, the gain does not have enough time to recover completely. (Compare the gain evolution in these three examples with the results of [SOA gain saturation—Gaussian pulses](#).)

### Complete gain recovery (quasi-CW operation)

With the carrier lifetime of our SOA at  $t_C \sim 1.4$  ns, we will consider pulses with widths larger than 1.4 ns.

Bit rate  $B = 100$  MHz, consequently  $T_B = 10$  ns.

**Figure 6 SOA Gaussian Pulse Simulation parameters**



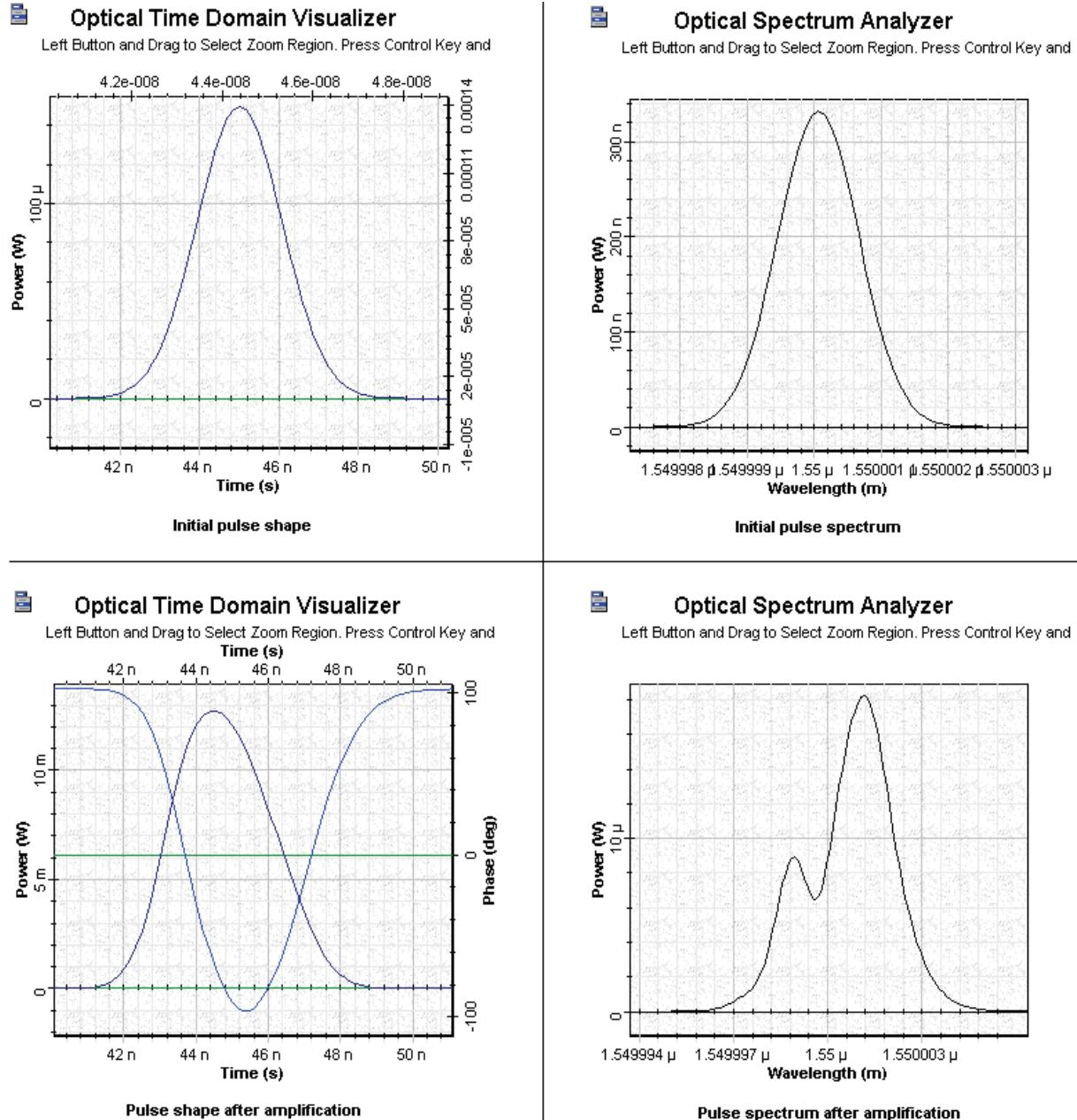
We will consider three pulse widths — 2.5ns, 5 ns, and 10 ns. In all three cases, the ratio  $E_{in}/E_{sat} = 0.1$  will remain constant.

## Pulse 4 parameters

- Duty cycle 0.25,  $T_{FWHM} \sim 2.5 \text{ ns} \rightarrow T_0 \sim 1.4 \text{ ns}$ ,  $P_{in} = 0.15 \text{ mW}$
- Therefore:  $T_0/t_C \sim 1.8$  and  $P_{in}/P_{sat} = 0.04$

Figure 7 shows the shape and spectra of the initial and amplified pulses for Pulse 4.

**Figure 7 SOA Gaussian Pulse 4 initial and amplified pulses**

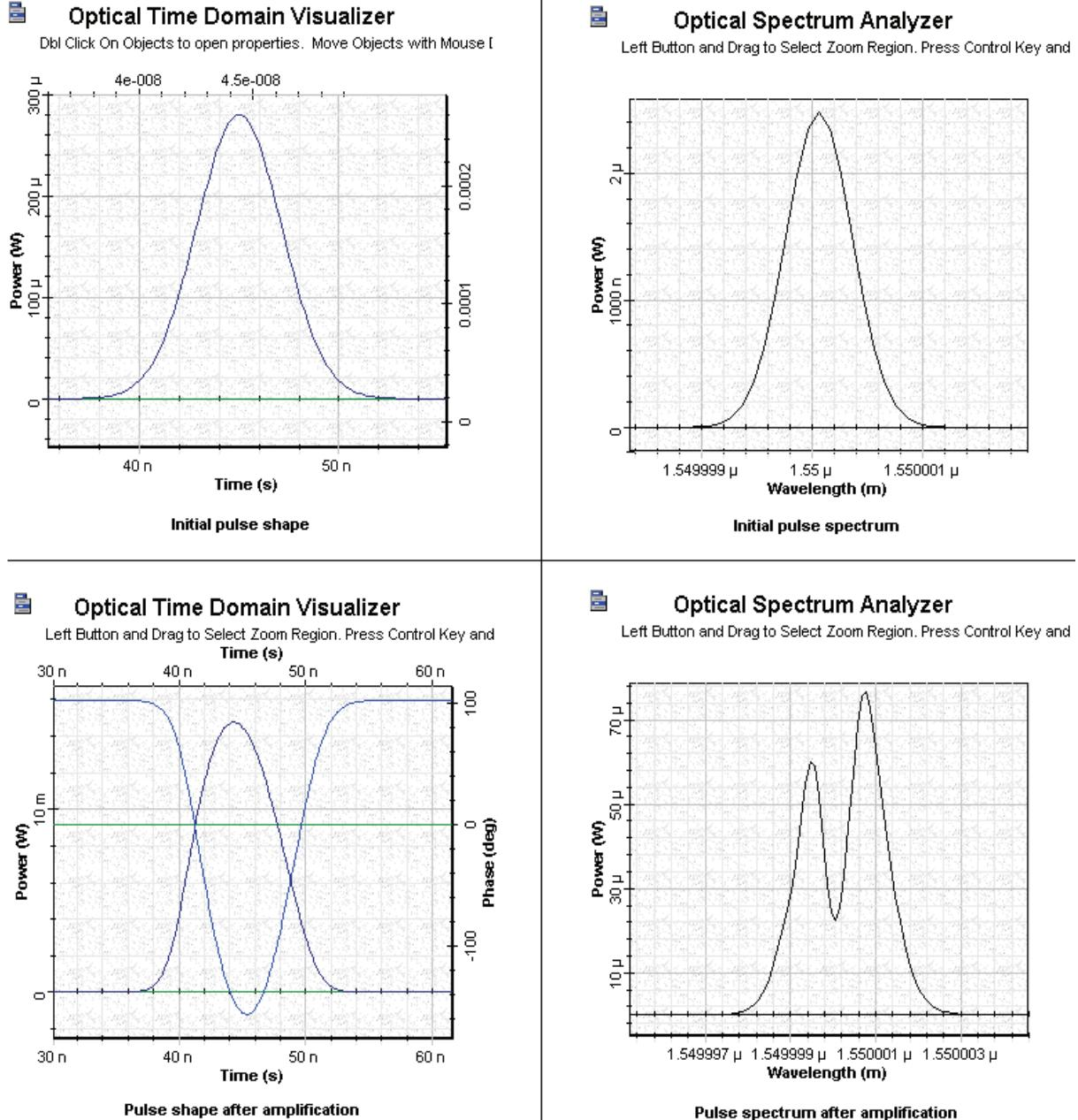


## Pulse 5 parameters

- Duty cycle 0.5,  $T_{FWHM} \sim 5 \text{ ns} \rightarrow T_0 \sim 2.83 \text{ ns}$ ,  $P_{in} = 0.28 \text{ mW}$
- Therefore:  $T_0/t_C \sim 3.6$  and  $P_{in}/P_{sat} = 0.08$

Figure 8 shows the shape and spectra of the initial and amplified pulses for Pulse 5.

**Figure 8 SOA Gaussian Pulse 5 initial and amplified pulses**

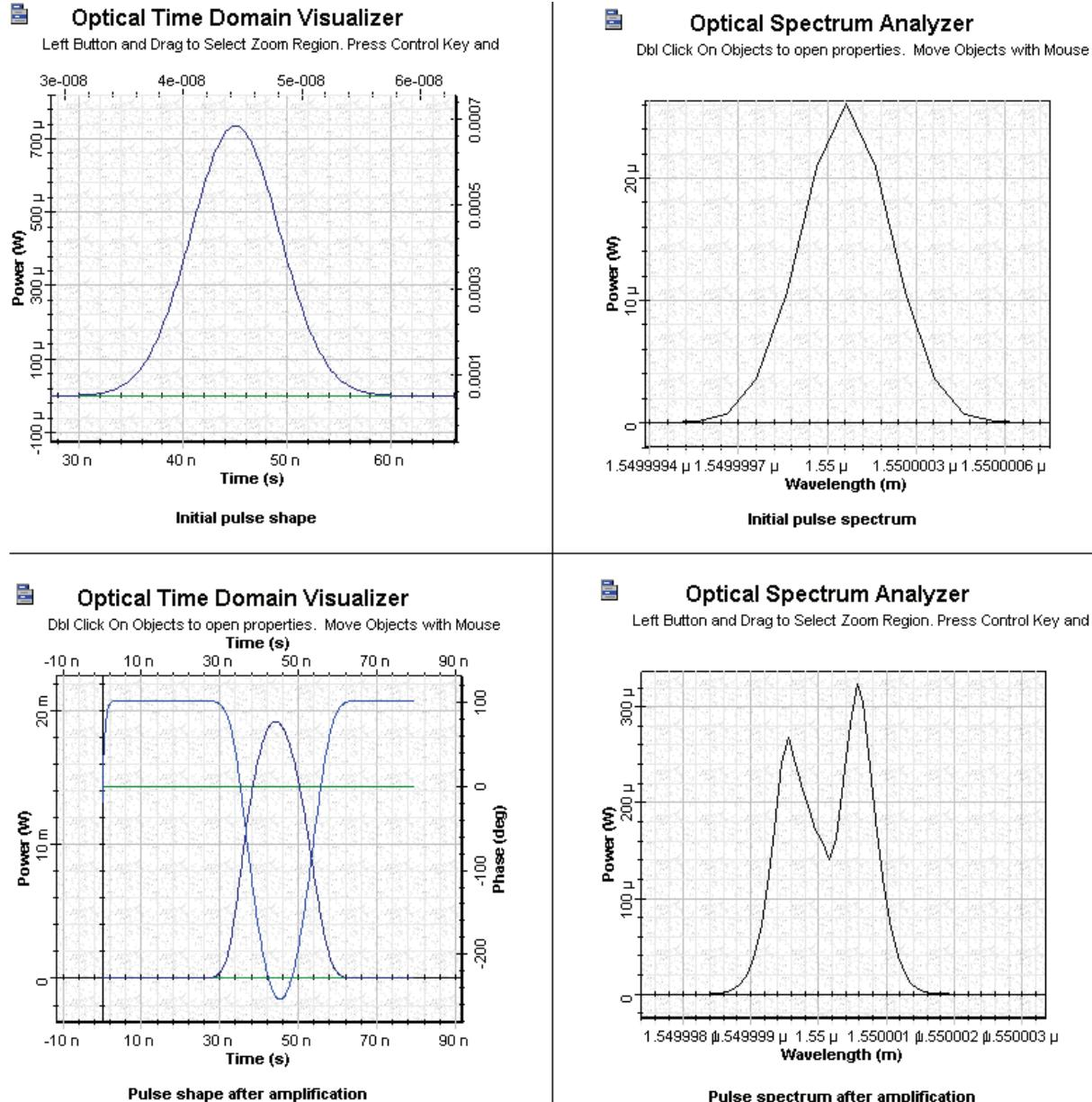


## Pulse 6 parameters

- Duty cycle 1,  $T_{FWHM} \sim 10 \text{ ns} \rightarrow T_0 \sim 5.67 \text{ ns}$ ,  $P_{in} = 0.736 \text{ mW}$
- Therefore:  $T_0/t_C \sim 7.1$  and  $P_{in}/P_{sat} = 0.2$

Figure 9 shows the shape and spectra of the initial and amplified pulses for Pulse 6.

**Figure 9 SOA Gaussian Pulse 6 initial and amplified pulses**



The following properties for these three amplified pulses can be distinguished.

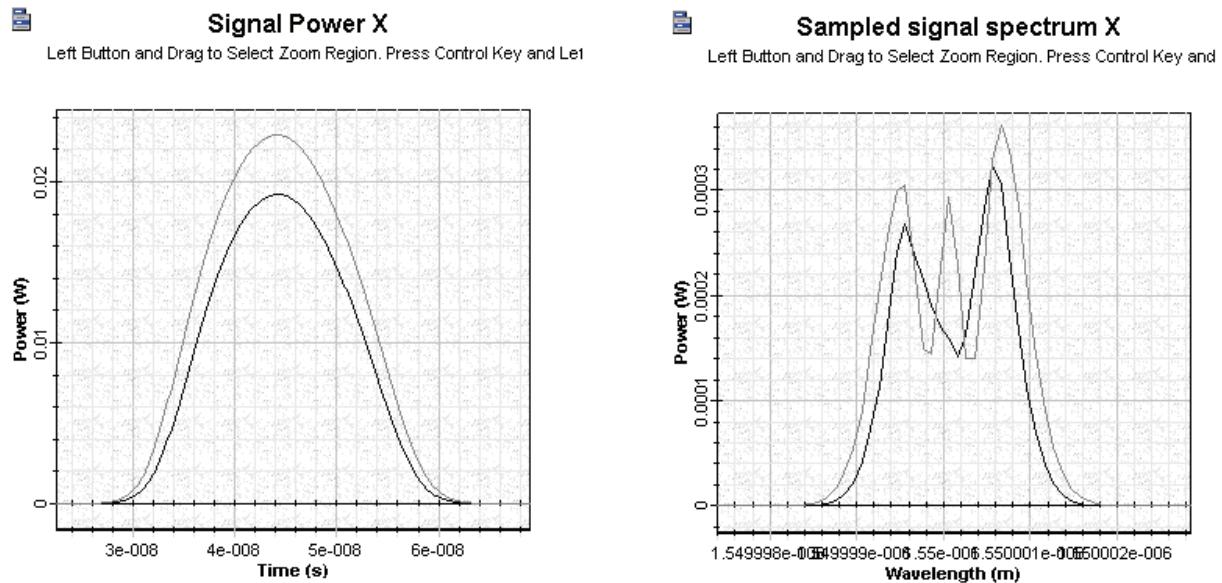
- By increasing the pulse width well above the carrier lifetime, the shapes of the amplified pulses are much more symmetrical. The shapes also become much broader than the shapes of the corresponding initial pulses.
- By increasing the pulse width, the spectrum of the amplified pulses becomes less asymmetrical and the red shift continuously decreases.

The phase is shown in the figures of the shapes of amplified pulses. We see that for these pulses, the gain has time to recover completely.

### Appearance of gain-saturation induced self-phase modulation

Now we will compare the results of Pulse 6 ( $P_{in}/P_{sat} = 0.2$ ) with the results for  $P_{in}/P_{sat} = 0.4$ . We will make this comparison by increasing the initial power 10 times. [Figure 10](#) shows the results of this comparison for the shapes and spectra of the amplified pulses.

**Figure 10 Comparison of results for  $P_{in}/P_{sat} = 0.2$  with  $P_{in}/P_{sat} = 0.4$**



The spectra obtained in the complete gain recovery examples (especially in the last example) exhibit a structure similar to that of the pulse obtained in the propagation in medium with Kerr nonlinearity [2]. This spectra allows the introduction of the concept of gain saturation-induced self-phase modulation [1]. These kinds of spectra are only possible when the pulses are longer than the carrier lifetime.

## References:

- [1] G.P. Agrawal and N.A. Olsson, "Self-phase modulation and spectral broadening of optical pulses in semiconductor laser amplifiers", IEEE Journal of Quantum Electronics, Vol. 25, pp. 2297-2306, 1989.
- [2] G.P. Agrawal, "Nonlinear Fiber Optics," 3rd Edition, Academic Press, 2001.



# SOA pulse compression

---

This lesson applies the results from [SOA gain saturation—Gaussian pulses](#) to analyze the possibility for compression of weak picosecond pulses. As mentioned in [SOA gain saturation—Gaussian pulses](#), one of the main results of the gain saturation induced self-phase modulation in SOA is the formation of positive chirp of the pulse in the process of amplification. Using the theory of propagation of phase modulated optical signals in dispersive medium [1], we know that, depending on the signs of the chirps of signal and the chirp of the dispersive medium, different scenarios are possible.

For equal signs of chirps, the dispersion effect is amplified. In the case of different signs of the chirps, the effect of pulse dispersion can be reduced, effectively leading to pulse compression. To use the positive chirp created in the process of pulse amplification in SOA for compression, we have to propagate the pulse with the dispersive media that creates negative chirp. The media can be standard mode optical fiber used for wavelengths larger than the zero dispersion wavelength — in other words, in the region of anomalous group velocity dispersion. This idea has been proposed and realized in [2]. In this lesson, we will use our SOA component to try to interpret the results obtained in [2].

The following SOA parameters are used in [2]:

Unsaturated single pass gain	$G_0 \sim 30$ dB
Line width enhancement factor	$\alpha = 5$
Saturation energy	$E_{\text{sat}} \sim 6$ pJ
Ratio $E_{\text{in}} / E_{\text{sat}}$	varied over the range 0.01 to 0.2

A typical value for the carrier lifetime is 200 – 300 ps. We consider pulses with the condition  $T_0/T_{\text{sat}} \ll 1$  to be valid. We expect the appearance of effects connected to the gain saturation-induced self-phase modulation using these general conditions.

To analyze this situation, we use following global parameters:

- Bit rate  $B = 40$  Gb/s  $\rightarrow T_B = 25$  ps.

We consider pulses with  $T_{\text{FWHM}} = 25$  ps  $\rightarrow T_0 \sim 15$  ps. [Figure 1](#) shows the global parameters.

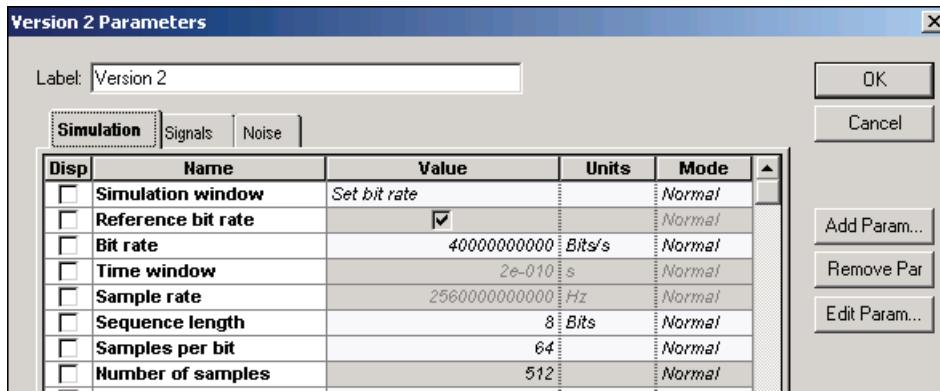
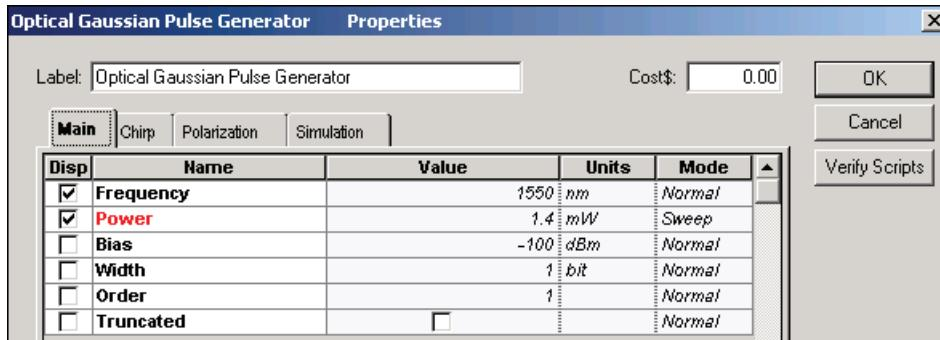
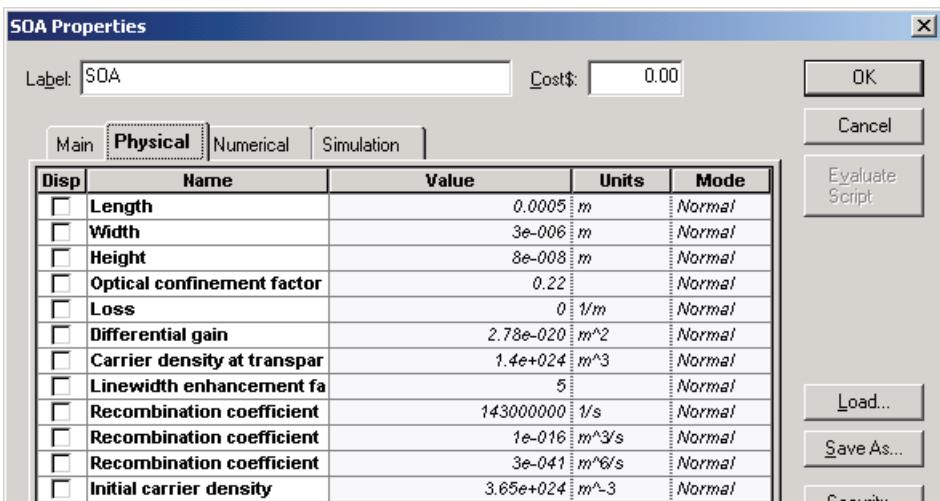
**Figure 1 Global parameters**

Figure 2 shows the **Optical Gaussian Pulse Generator Main** parameters.

**Figure 2 Optical Gaussian Pulse Generator Main parameters**

According to the default values of the SOA component, the carrier lifetime is  $t_C \sim 1.4$  ns and the saturation energy is  $E_{sat} \sim 5$  pJ. Figure 3 shows the SOA **Physical** parameters.

**Figure 3 SOA Pulse Compression Physical parameters**

To satisfy the conditions  $T_0 / T_{sat} \ll 1$  and  $E_{in} / E_{sat} \sim 0.01$  to  $0.2$ , we can use the Gaussian pulse with  $T_0 \sim 15$  ps with  $T_0 / T_{sat} \sim 0.011$  and initial peak pulse powers are 3 mW, 30 mW, and 60 mW (which correspond to  $E_{in} / E_{sat} = 0.01, 0.1,$  and  $0.2$  respectively).

Dispersion length  $L_D$  in standard mode fiber ( $D \sim 16$  ps /nm.km) for pulse with  $T_0 \sim 15$  ps will be  $L_D \sim 11$  km.

Figure 4 shows the **Optical Fiber** main parameters.

**Figure 4 Fiber Main parameters**

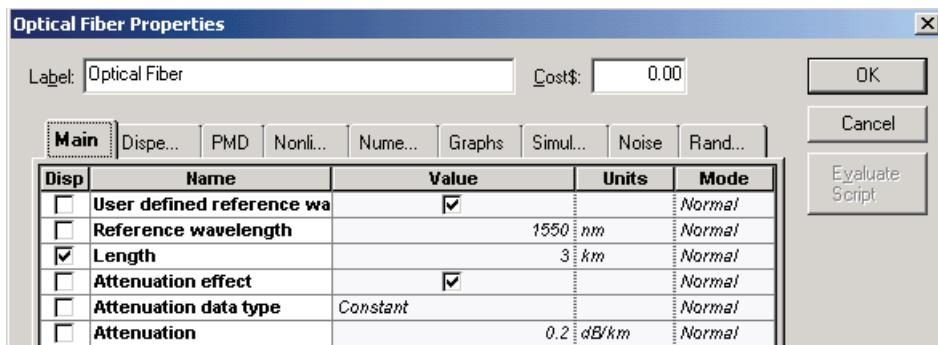
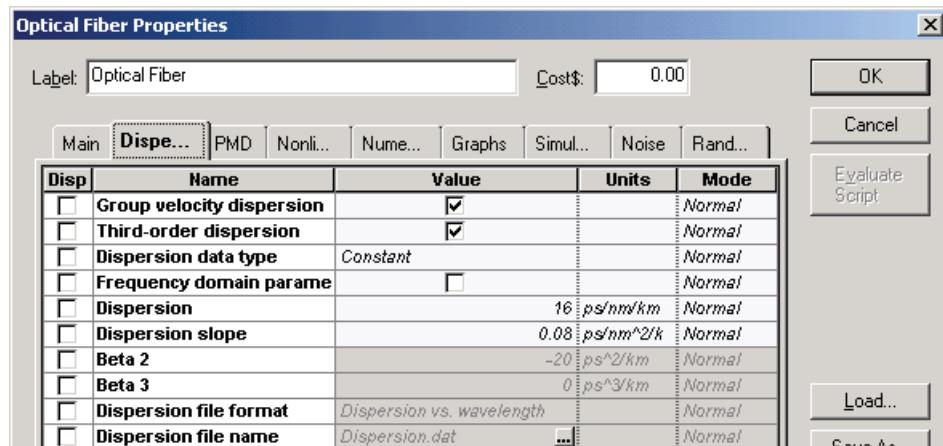


Figure 5 shows the **Optical Fiber** dispersions parameters.

**Figure 5 Fiber Dispersions parameters**



To satisfy the condition  $L_C / L_D \sim 0.3$  given in [1], where  $L_C$  is the length of the fiber used for compression the  $L_C \sim 3.3$  km has been used.

Figure 6 shows the **SOA Pulse Compression** project layout.

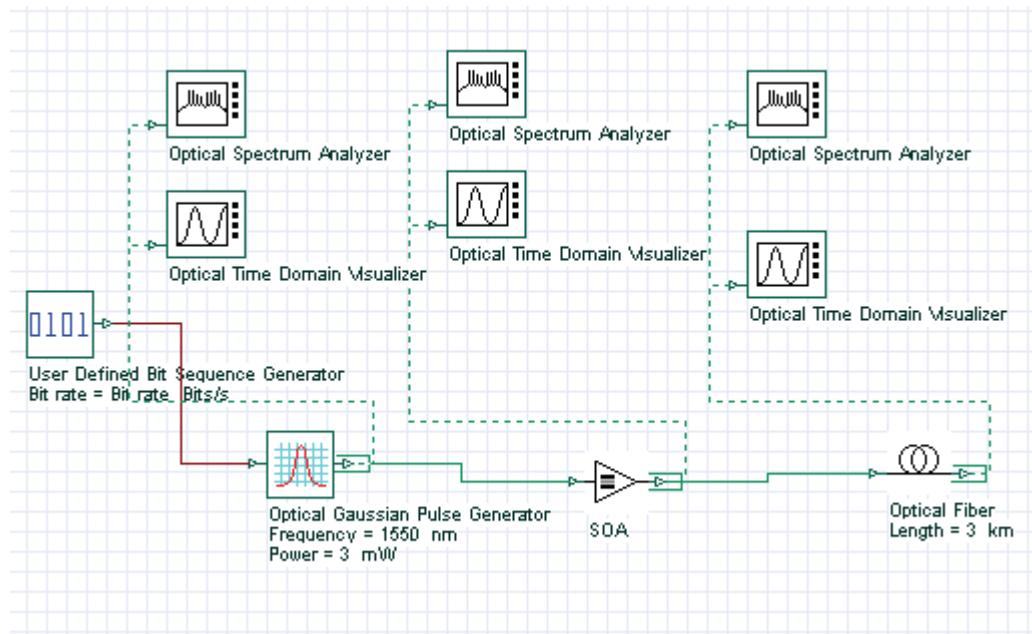
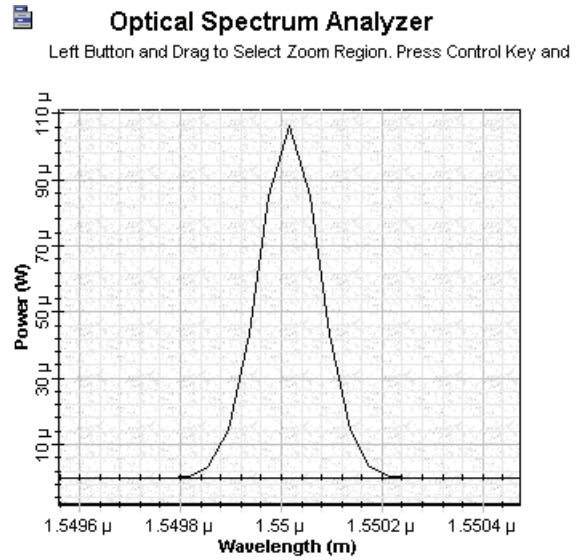
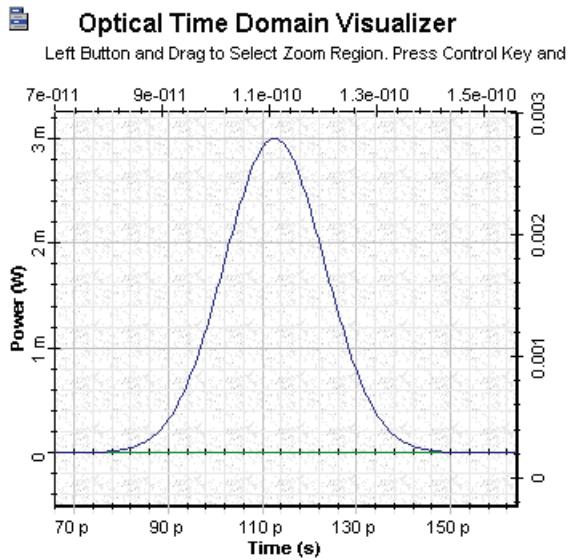
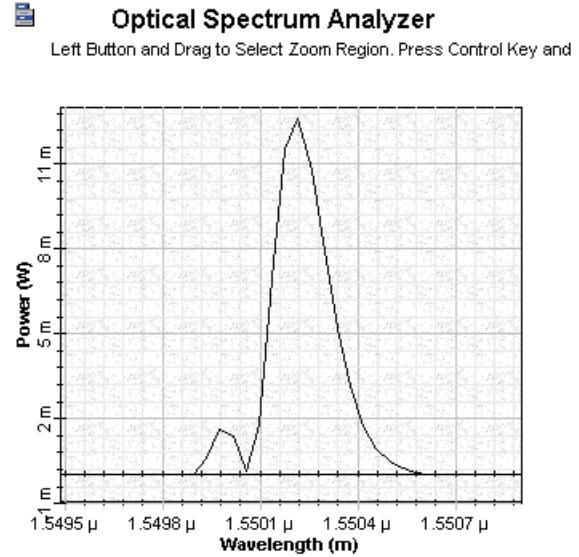
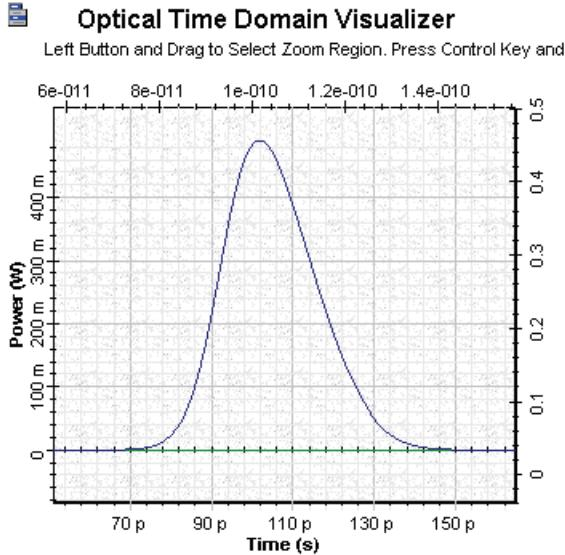
**Figure 6 SOA Pulse Compression project layout**

Figure 7 shows the initial pulse shape and spectrum with  $T_{FWHM} = 25$  ps and with the initial peak pulse power of 3 mW.

**Figure 7 Initial pulse**

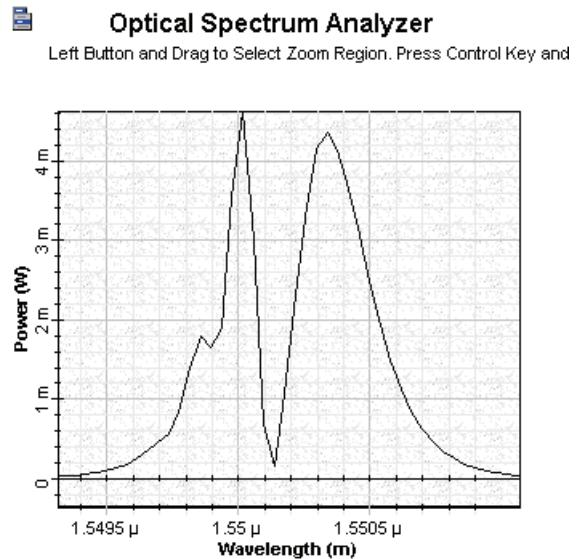
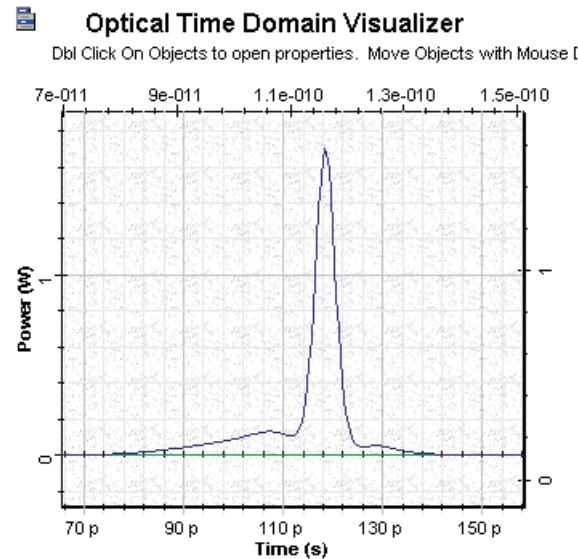
**Figure 8** shows the shape (with corresponding positive induced chirp) and spectrum of the amplified pulse with SOA where  $G_0 = 30$  dB and the line width enhancement factor is  $\alpha = 5$ .

**Figure 8 Amplified pulse**



**Figure 9** shows the shape and spectrum of the amplified pulse passed through a 3 km standard mode fiber.

**Figure 9 OTDV and OSA amplified pulse passed through 3 km standard mode fiber**



The comparison of the width of the pulse after the fiber shows a compression factor of about 7 times with the peak power enhanced by a factor of several hundreds. There are two important physical facts regarding the last shape figure.

- There is a broad pedestal on the leading side of the pulse, which can be explained by the negative chirp in the leading part of the pulse. This leads to increased dispersion of this part of the pulse.
- Regarding the shift of the pulse towards later times — sequence from the red shift of central frequency of the amplified pulse in anomalous group velocity dispersion leads to time delay of the pulse.

As mentioned in [2], the compression factor depends on several input parameters, such as the pulse energy, pulse width, amplifier gain, and compressor length. For non-optimal parameters, another type of phenomenon may occur (for example, pulse breaking).

[Figure 10](#) shows the pulse shapes and spectra with the initial peak powers of 3 mW, 30 mW, and 60 mW.

**Figure 10 Shape and spectra of pulses with 3, 30, and 60 mW peak power**

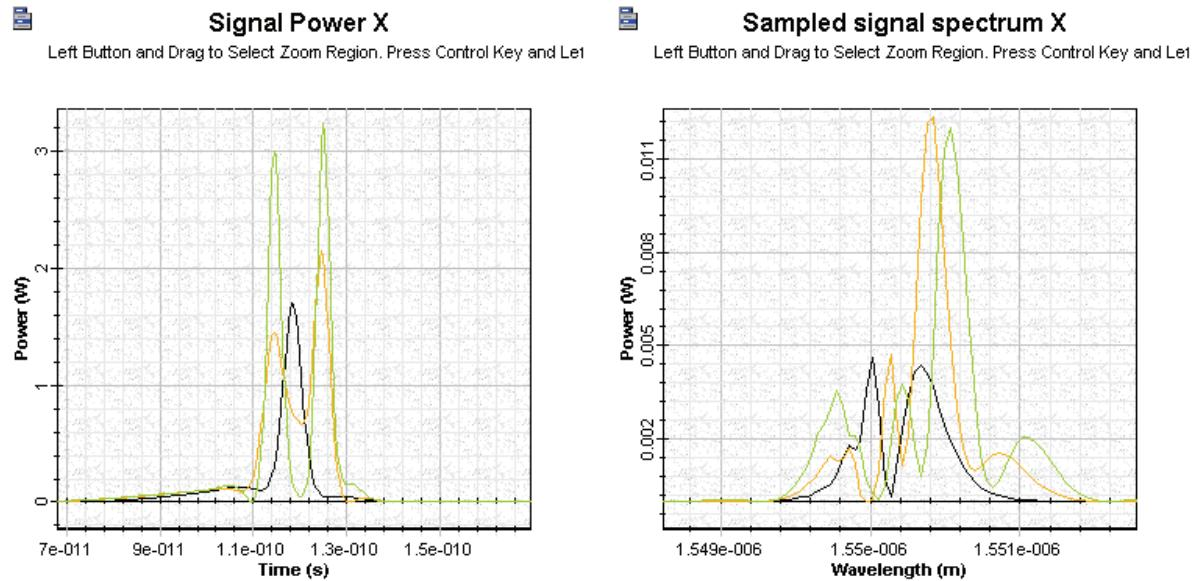


Figure 10 shows that a larger input peak power can lead to pulse breaking phenomenon with connected complicated spectra structure.

This lesson demonstrated the pulse compression of weak pulses (peak energy smaller than pJ) based on the use of the gain saturation-induced self-phase modulation effect in SOA.

## References

- [1] G.P. Agrawal, "Nonlinear Fiber Optics," 3rd Edition, Academic press, 2001.
- [2] G.P. Agrawal and N.A. Olsson, "Amplification and compression of weak picosecond optical pulses by using semiconductor laser amplifier", Optics Letters, Vol. 14, pp. 500-502, 1989.

**Notes:**

## SOA as a wavelength converter (FWM)

---

This lesson demonstrates the application of traveling wave SOA as a wavelength converter using the four-wave mixing effect.

Four-wave mixing (FWM) is a nonlinear effect that takes place when two waves (signal and pump) at different wavelengths are injected into an SOA. A third optical field is generated at the device output, with frequency  $W_c = 2W_p - W_s = W_p - \Omega$ , where  $W_p$  and  $W_s$  are the frequencies of the pump and signal field respectively, and  $\Omega = W_s - W_p$  is detuning between signal and pump.

Several physical phenomena can generate FWM in SOA. When detuning at the order of several GHz, the main mechanism is the carrier density pulsation induced by the signal-pump beating. The carrier density pulsation appears because of the stimulated emission. Our SOA component can handle generation mechanism of FWM. For higher values of detuning, carrier pulsation is no longer effective, and FWM is created from two fast intraband relaxation processes:

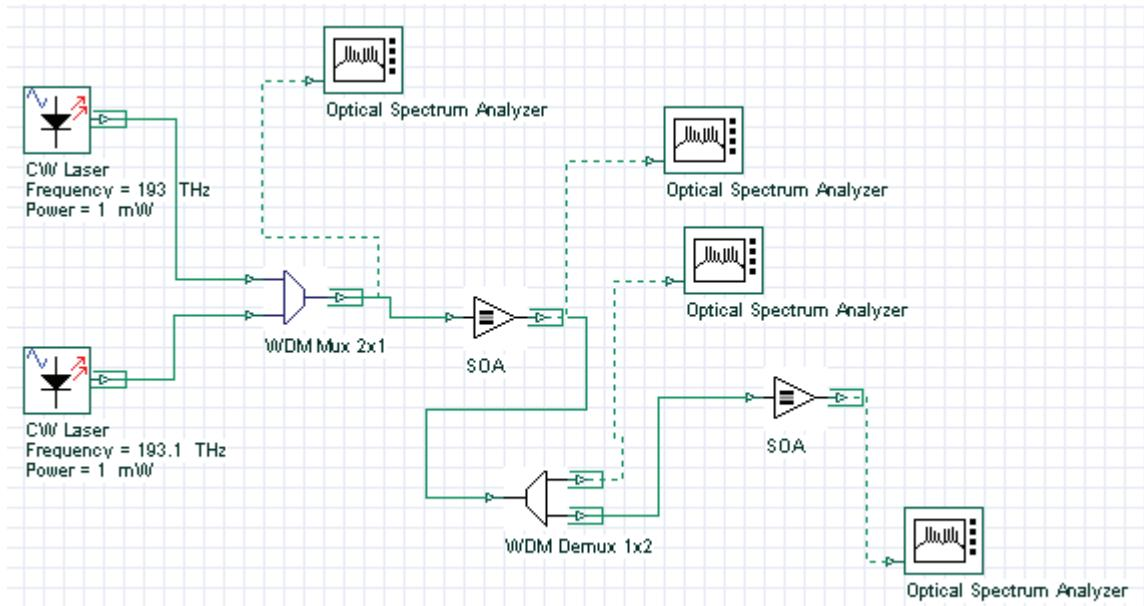
- spectral hole burning
- carrier heating

As their characteristic times are of the order of hundreds of femtoseconds, they become important for values of detuning greater than 1THz [2] and [3].

The main advantage of frequency conversion based on FWM is independence of the modulation format and the bit rate. An additional advantage of this technique is the inversion of the signal spectrum and the resulting reversal of the frequency chirp. This property can be used to achieve dispersion compensation. The main disadvantage of the FWM converter is its low conversion efficiency [2] and [3].

To realize this idea, two CW signals are multiplexed and then launched into SOA, as shown in [Figure 1](#).

Figure 1 Two multiplexed CW signals



Using this project, we will demonstrate the principle of carrier density pulsation induced FWM in SOA. To demonstrate this, two CW signals with carrier frequencies 193 and 193.1 THz and the power of 1 mW (without line widths, initial phases, and polarizations) are multiplexed with the help of WDM Mux 2x1 and launched in SOA. Figure 2, Figure 3, and Figure 4 show the WDM and SOA parameters.

Figure 2 WDM Mux 2x1 Main parameters

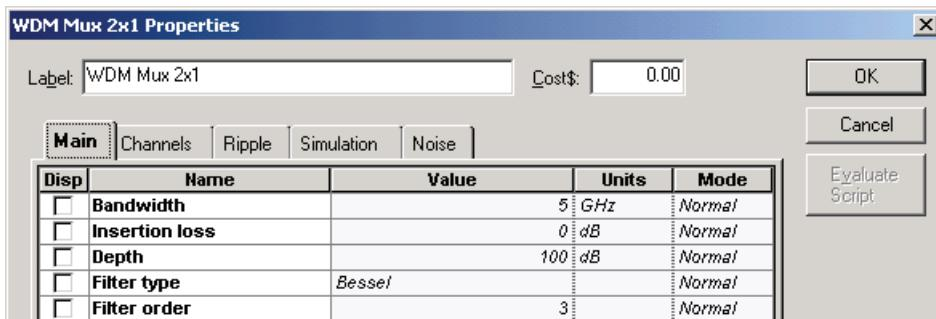
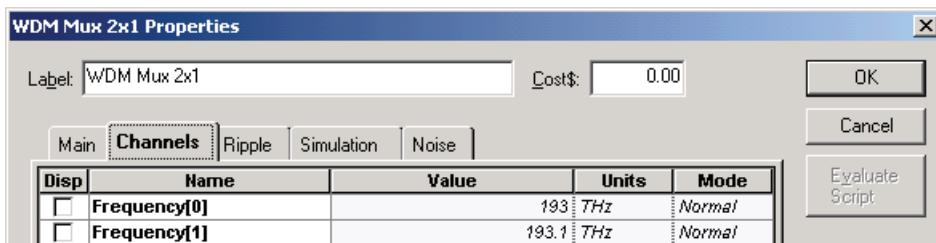


Figure 3 WDM Mux 2x1 channels



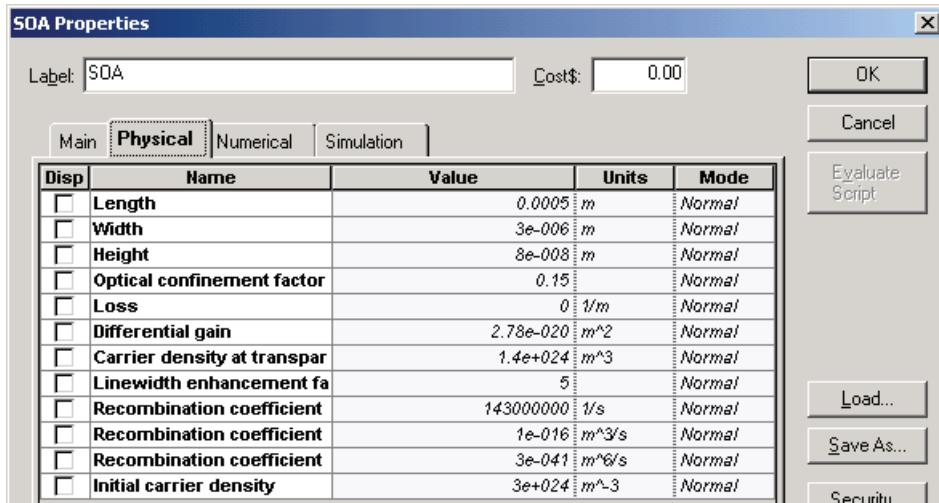
**Figure 4 SOA Physical parameters**

Figure 5 shows signal power after the WDM Mux 2x1.

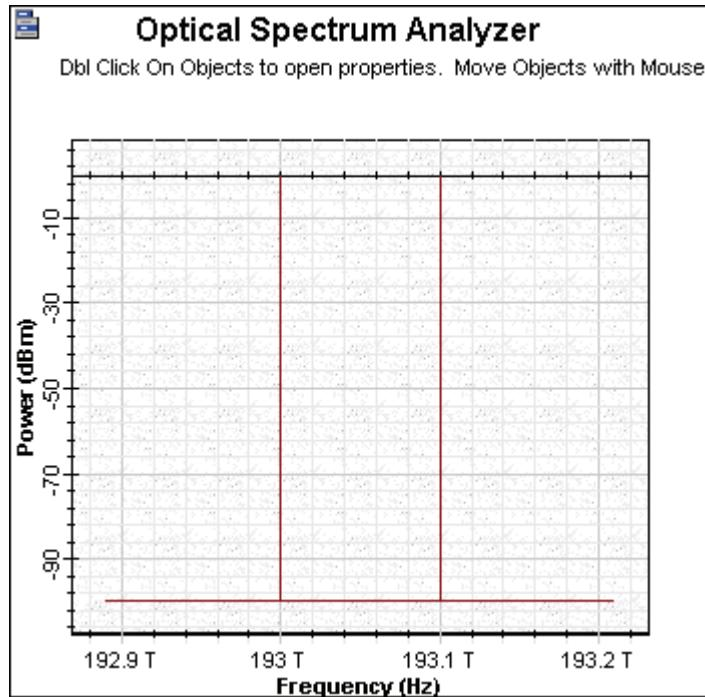
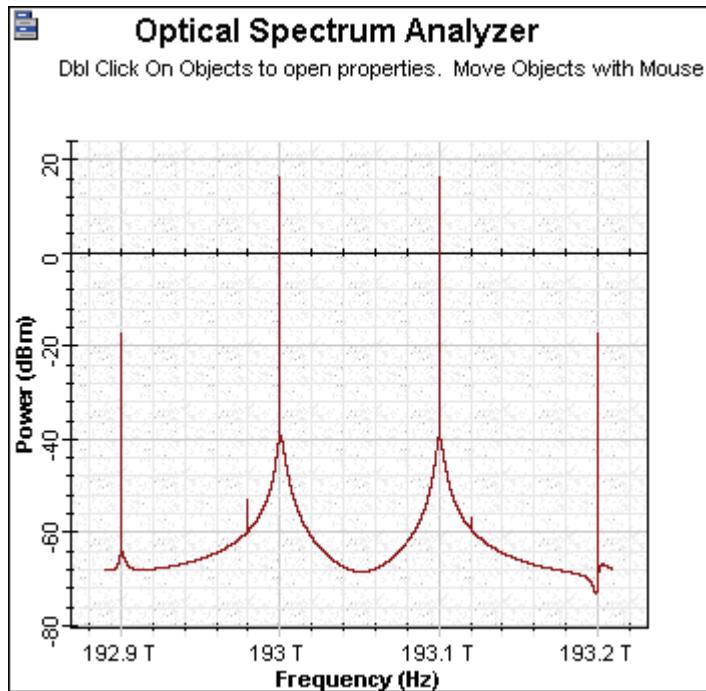
**Figure 5 Signal power after the WDM Mux 2x1**

Figure 6 shows the signal power after the first SOA.

Figure 6 Signal power after the first SOA



In Figure 6, we can see the power generated from the new FWM frequencies at 192.9 THz and 193.2 THz respectively. With the following demultiplexer, we separate the frequencies into 193.1 THz and 193.2 THz. The demultiplexer **Channels** parameters have been changed (see Figure 7).

Figure 7 WDM Demux 1x2 channels

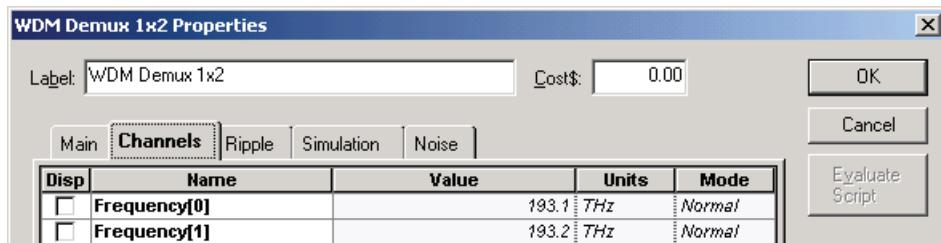
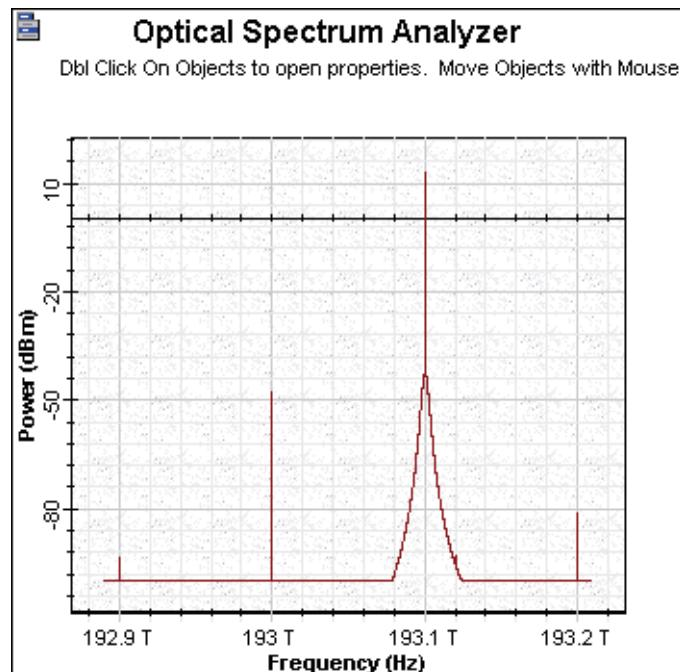
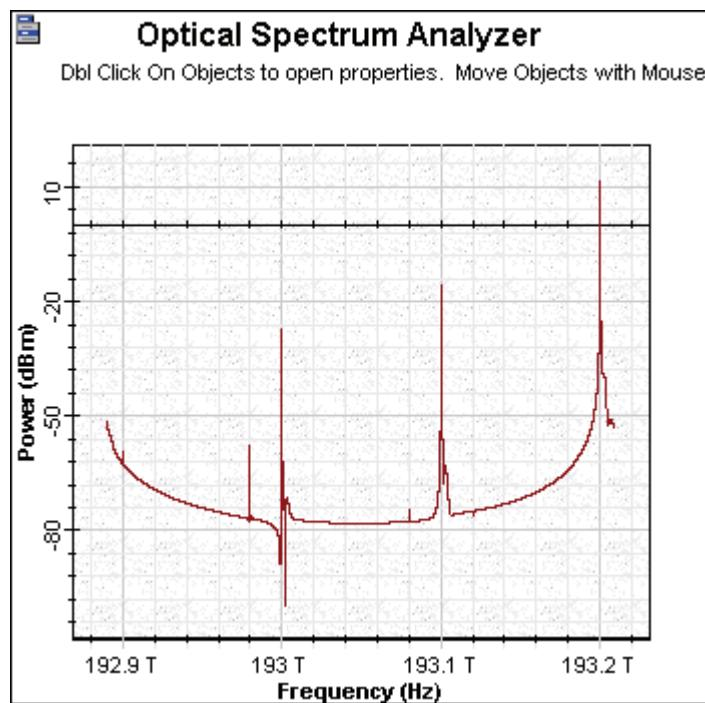


Figure 8 shows the spectrum in the channel at 193.1 THz after demultiplexing.

**Figure 8** Channel spectra at 193.1 THz after demultiplexing

To obtain a better signal from the FWM at 193.2 THz after demultiplexing, we amplify the signal with the second SOA with the same properties as the first one. [Figure 9](#) shows the resulting spectrum.

**Figure 9** Improved signal from the FWM at 193.2 THz after demultiplexing

The result of the second amplification FWM generated signal at 193.2 THz with power comparable with the result of the initial CW signal at 193.1 THz is obtained.

This lesson demonstrated the principal possibility of application of traveling wave SOA as a wavelength converter using four-wave mixing.

## References:

- [1] Terji Durhuus, Benny Mikkelsen, Carsten Joergensen, Soergen Danielsen, and Kristian Stunkjaer, "All-optical wavelength conversion by semiconductor optical amplifier", Journal of Lightwave Technology, Vol. 14, pp. 942-954, 1996.
- [2] G.P. Agrawal, "Fiber Optic Communication Systems", 2nd Edition, John Wiley & Sons Inc., 1997.
- [3] R.Sabella and P.Ludgi, "High speed optical communications", Kluwer Academic Publishers, 1999.



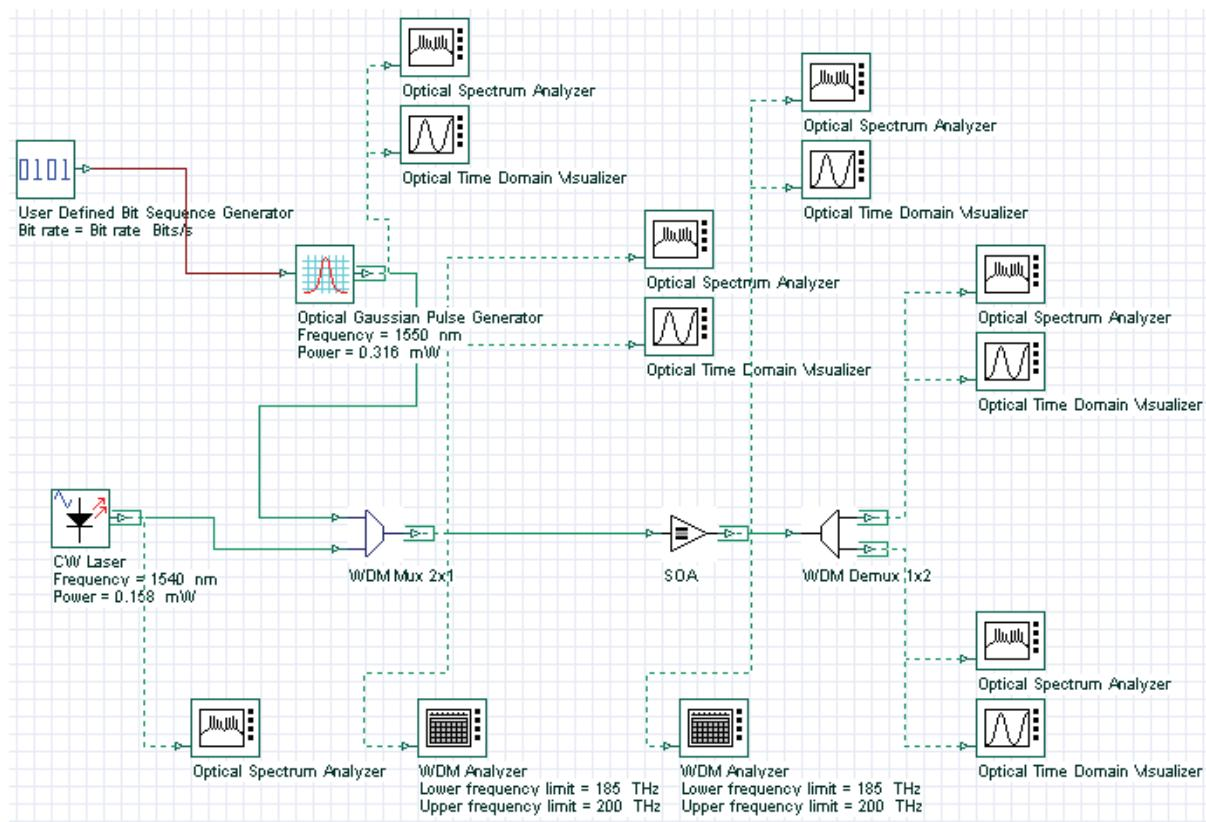
# SOA as a wavelength converter (XGM)

This lesson demonstrates the application of traveling wave SOA as a wavelength converter using cross-gain saturation effect.

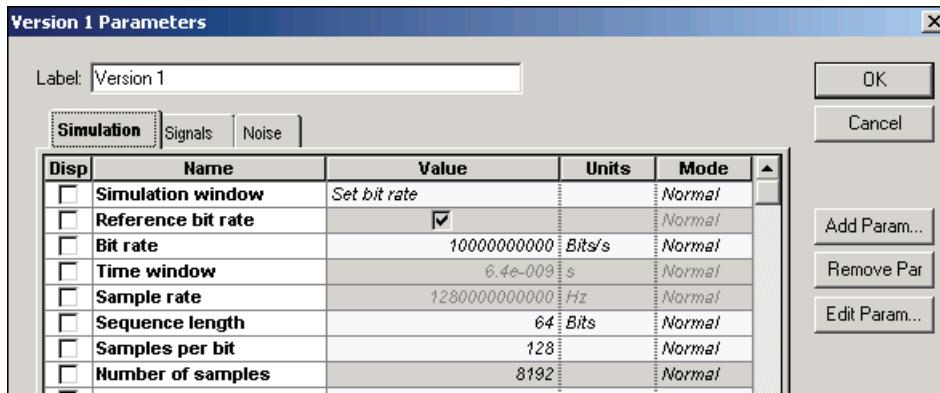
The principle use of the cross-gain modulation in SOA is as an intensity-modulated input signal that modulates the gain in the SOA via gain saturation effect. A continuous wave signal at the selected output wavelength is modulated by the gain variation. After the SOA, the continuous wave signal carries the same information as the intensity modulated signal. The input signal and the CW signal can be launched either co-directionally or counter-directionally into the SOA. A co-propagation scheme is considered here.

To realize this idea, the intensity-modulated input signal and a CW signal are multiplexed and then launched into SOA, as shown in [Figure 1](#).

**Figure 1** Multiplexed intensity-modulated input signal and CW signal



To demonstrate conversion at 10 Gb/s requires following global parameters (see [Figure 2](#)).

**Figure 2 Simulation parameters**

The intensity-modulated input signal and a CW signal have carrier wavelengths of 1550 and 1540 nm (or frequency separation from 1.25 GHz) and powers of 0.316 mW and 0.158 mW (without line widths, initial phases, and polarizations). The signals are multiplexed with the help of WDM Mux 2x1 and launched in SOA.

Figure 3 shows the **Optical Gaussian Pulse Generator** parameters.

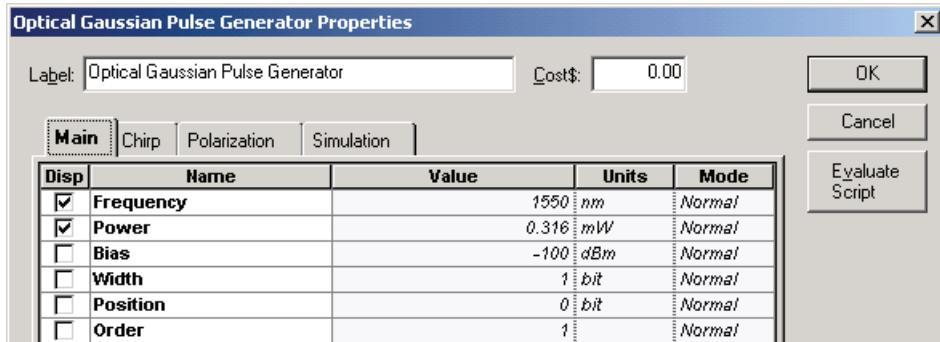
**Figure 3 Optical Gaussian Pulse Generator Main parameters**

Figure 4 shows the shape and spectrum of the intensity modulated signal.

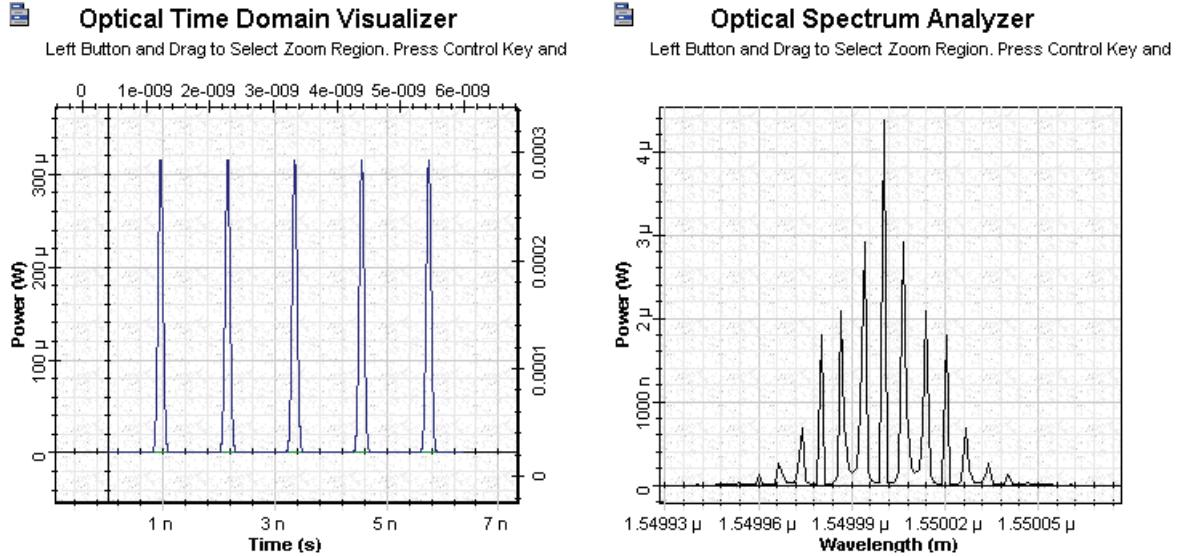
**Figure 4 Shape and spectrum of the intensity modulated signal**

Figure 5 shows the multiplexer parameters and channels.

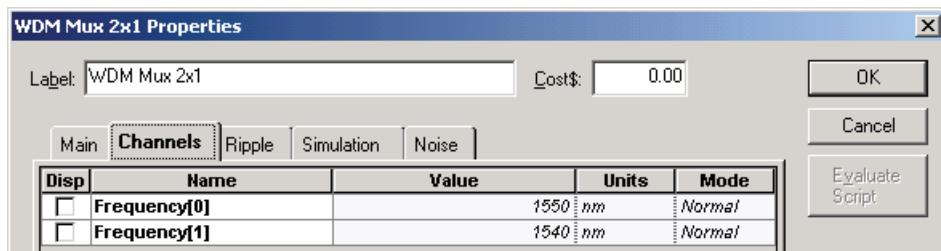
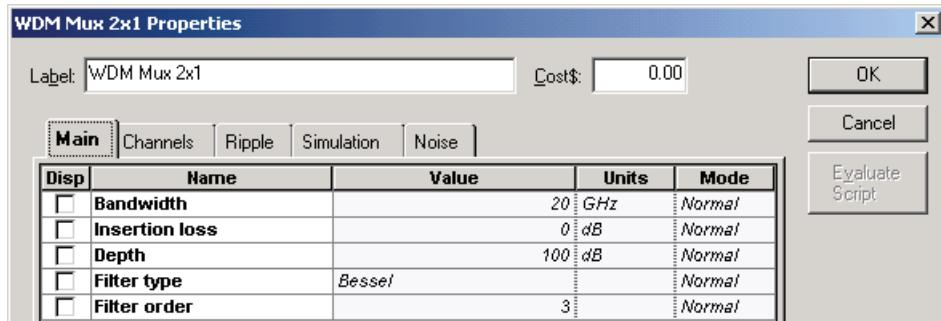
**Figure 5 WDM Mux 2x1 Main parameters and channels**

Figure 6 shows the shape of the WDM Mux 2x1 signal after multiplexing.

**Figure 6 Shape of WDM Mux signal**

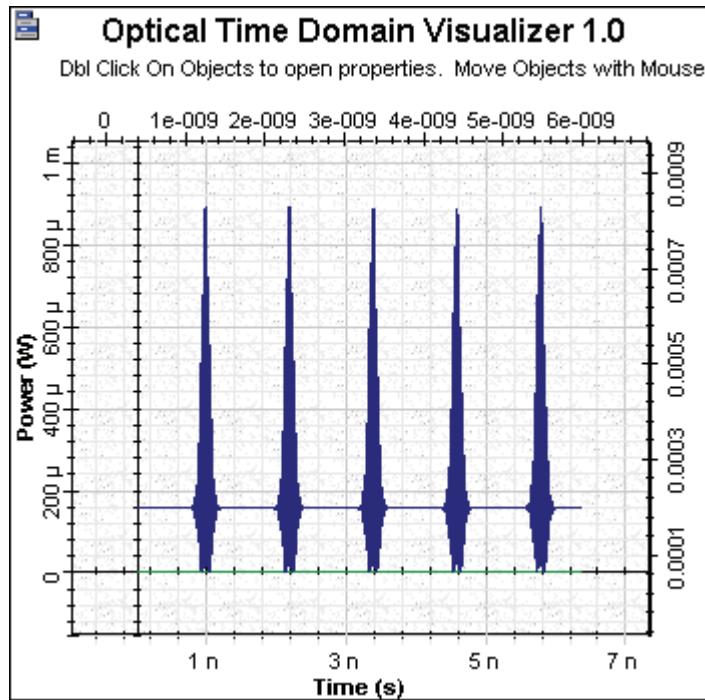
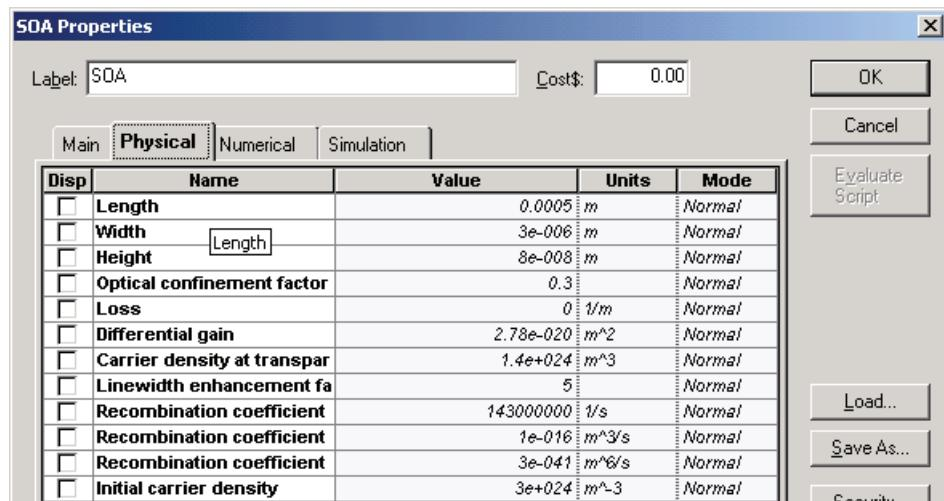


Figure 7 shows the SOA Physical parameters.

**Figure 7 SOA Physical parameters**

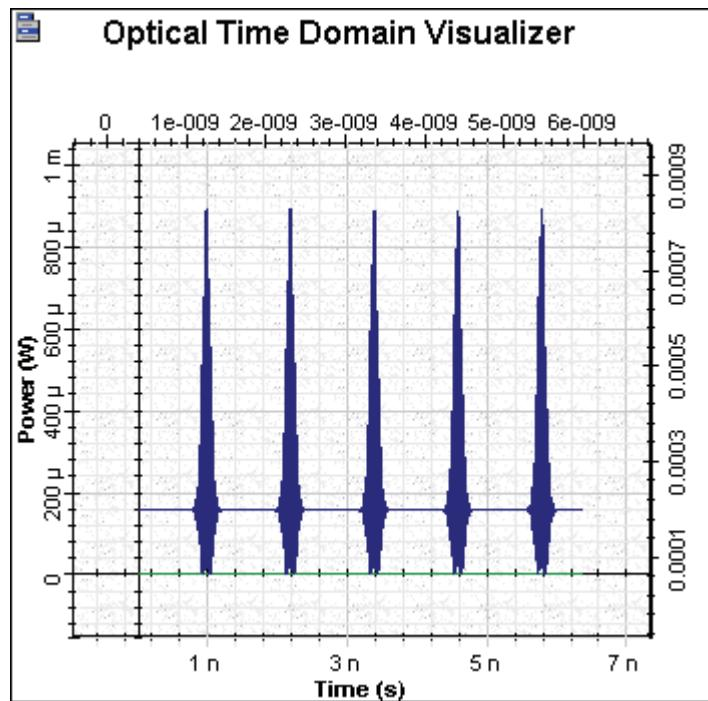


These amplifier parameters give the unsaturated single pass gain  $G_0 \sim 30$  dB.

Figure 8 shows the form of the amplified signal.



Figure 8 Amplified signal



The amplified signal passed through the demultiplexer, which has properties similar to the multiplexer. Figure 9 shows the signal shape and spectrum at  $\lambda = 1550$  nm after the demultiplexer.

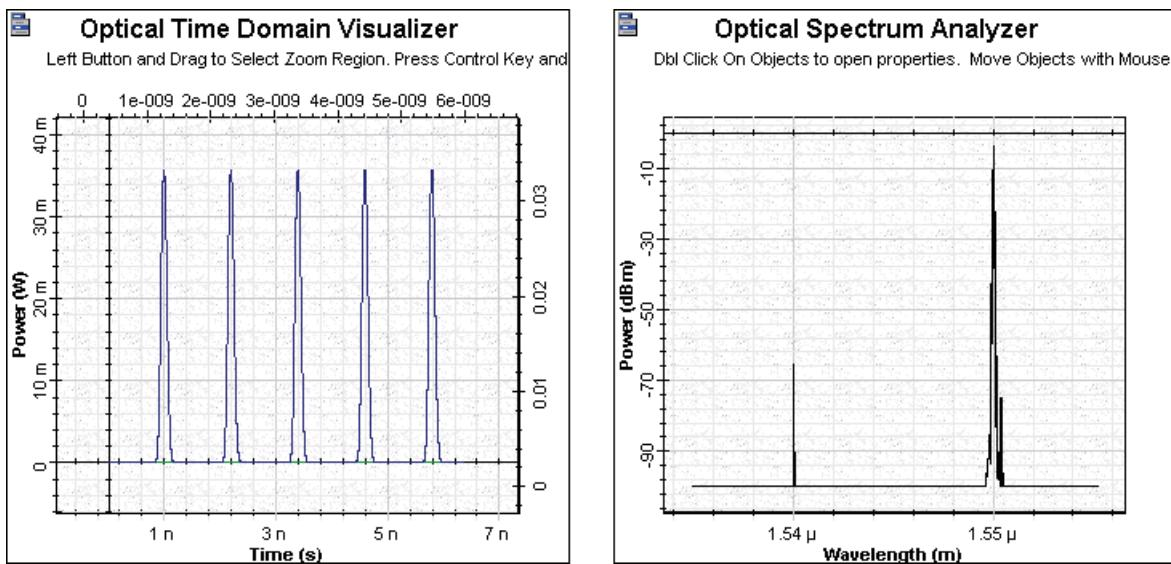
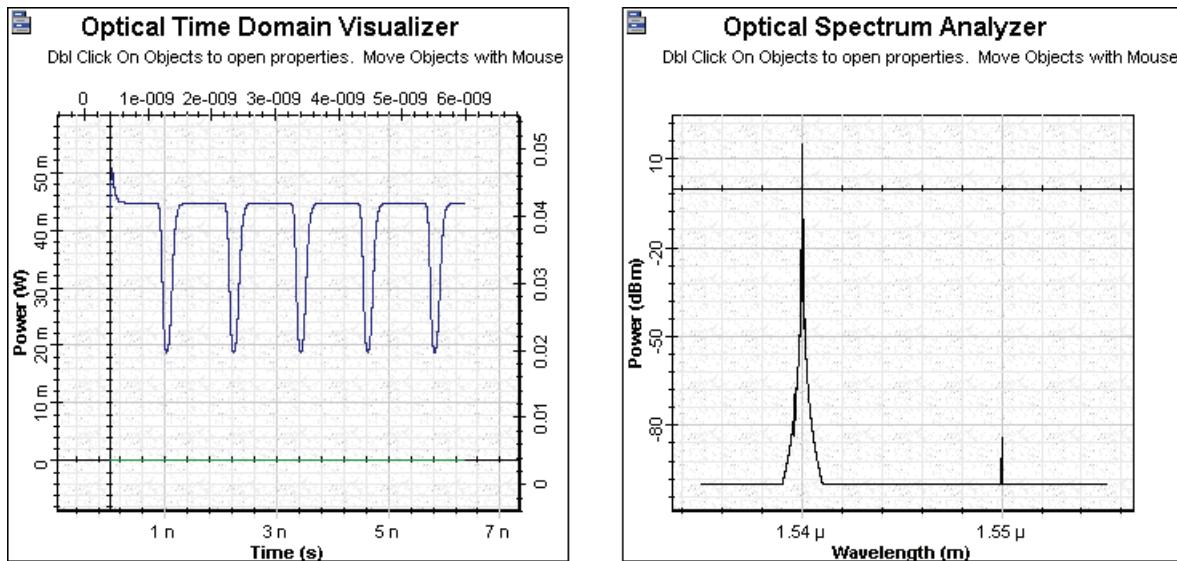
Figure 9 Shape and spectrum of the signal at  $\lambda = 1550$  nm

Figure 10 shows the signal shape and spectrum at  $\lambda = 1540$  nm after the demultiplexer.

**Figure 10 Shape and spectrum of the signal at  $\lambda = 1540$  nm**



The inversion of the signal can be clearly seen.

This lesson demonstrated the application of traveling wave SOA as a wavelength converter using cross-gain saturation effect.

## References

- [1] Terji Durhuus, Benny Mikkelsen, Carsten Joergensen, Soergen Danielsen, and Kristian Stunkjaer, "All-optical wavelength conversion by semiconductor optical amplifier", Journal of Lightwave Technology, Vol. 14, pp. 942-954, 1996.
- [2] G.P. Agrawal, "Fiber Optic Communication Systems", 2nd Edition, John Wiley & Sons Inc., 1997.
- [3] R. Sabella and P. Ludgi, "High speed optical communications", Kluwer Academic Publishers, 1999.



# SOA In-line amplifier

One possible way to upgrade an existing network from previously installed standard optical fibers is to exploit the 1.3 mm optical window, where the step index fibers have a zero-dispersion wavelength using SOA.

The advantages of using SOA as in-line single-channel optical amplifiers are:

- low dispersion of the SMF at this carrier wavelength
- attractive features of semiconductor optical amplifiers

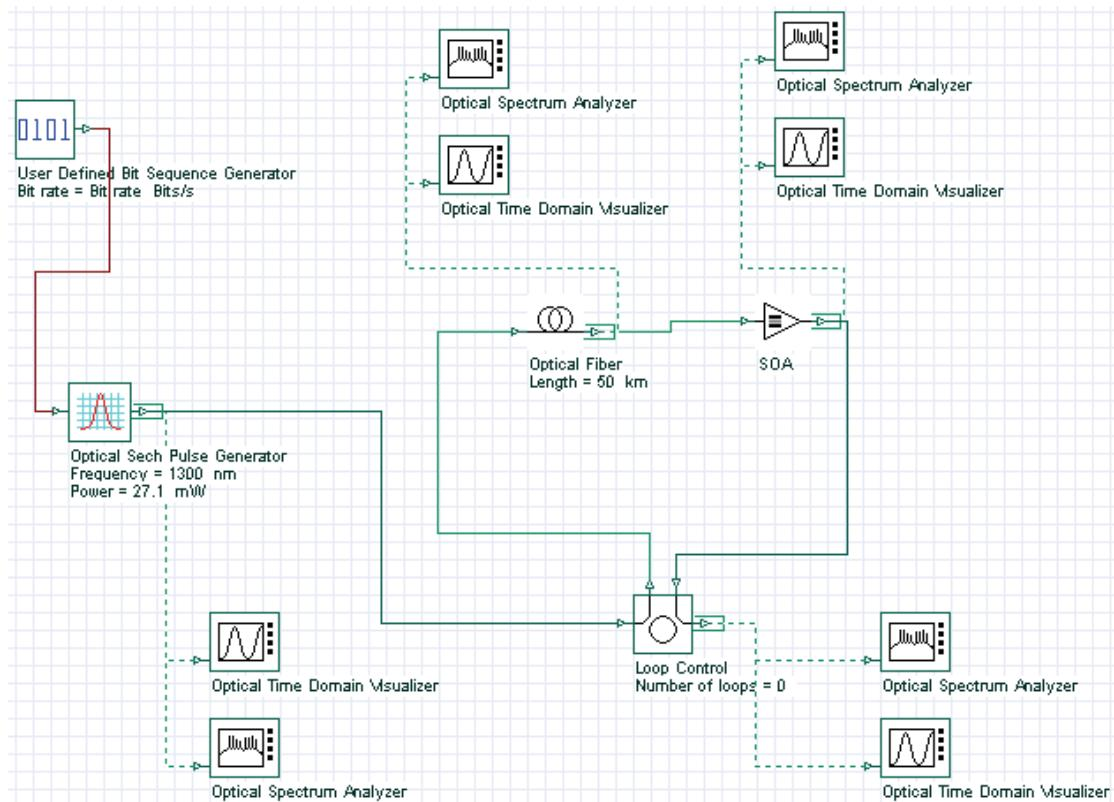
Two disadvantages of using SOA as in-line single-channel optical amplifiers are:

- gain-saturation effects, which lead to non-equal amplification of pulses in the pattern (so called pattern effect)
- chirp that the pulse acquires after amplification

This lesson demonstrates the pattern effect at 10 Gb/s transmission over a 500 km optical link consisting of SMF and in-line SOA's [1]. We will try to use parameters similar to the parameters in [1].

[Figure 1](#) shows the project layout.

**Figure 1 Layout of pattern effect at 10 Gb/s transmission over 500 km optical link**



The following global and pulse parameters are used to achieve transmission at 10 Gb/s (see [Figure 2](#) and [Figure 3](#)).

**Figure 2 Simulation parameters for transmission at 10 Gb/s**

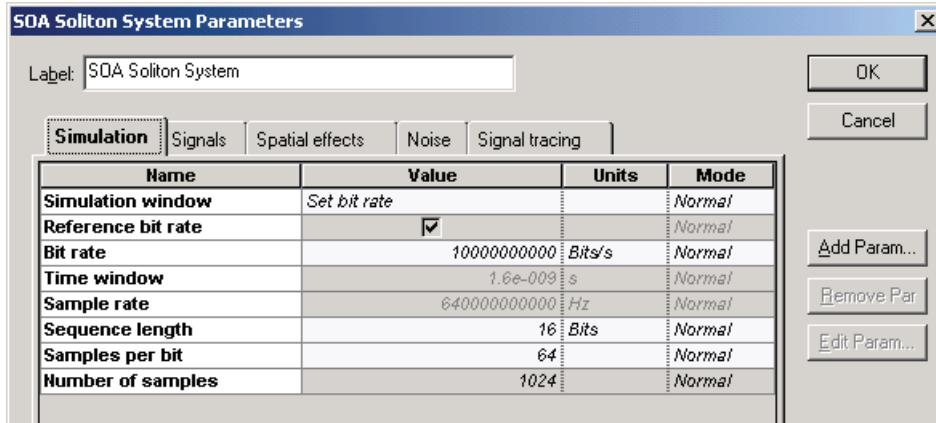
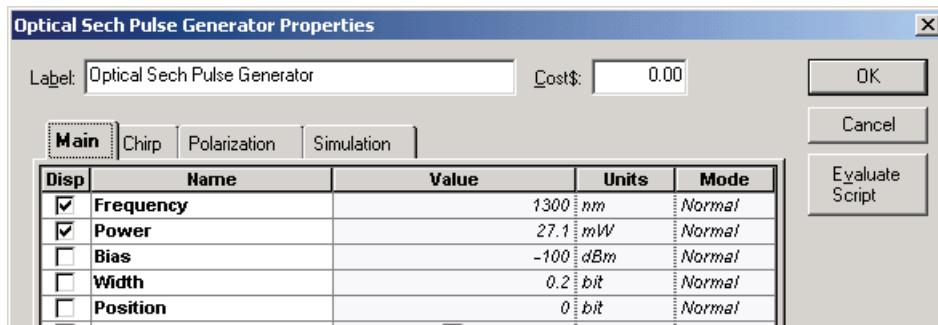


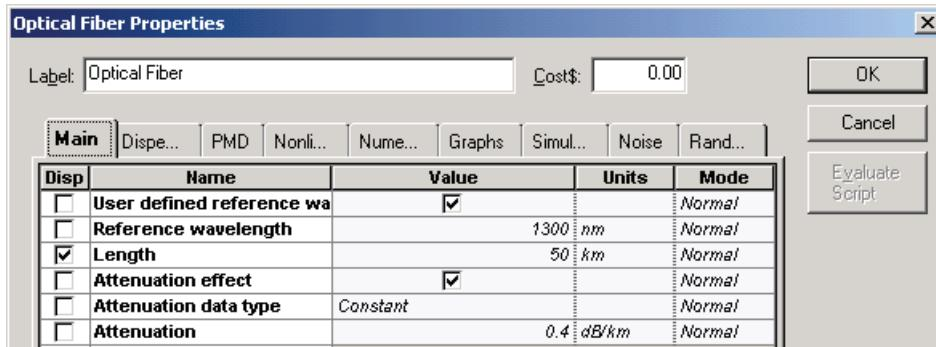
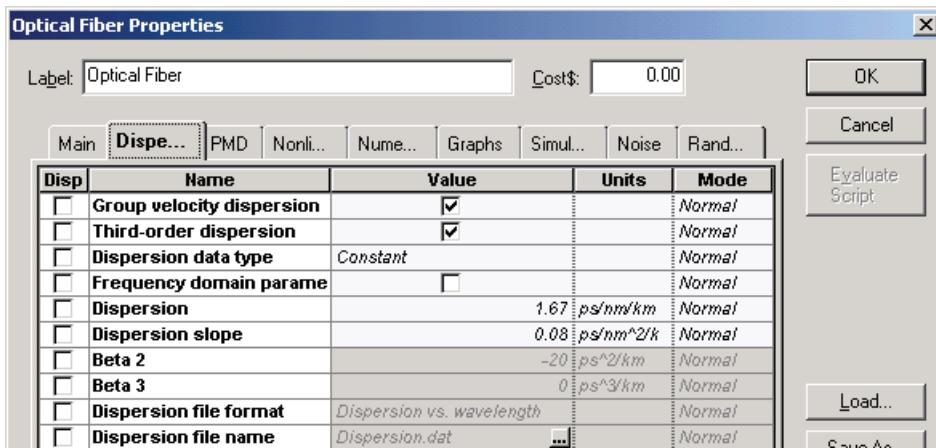
**Figure 3 Optical Sech Pulse Generator Main parameters for transmission at 10 Gb/s**



We fixed  $B = 10 \text{ Gb/s} \rightarrow T_B = 100 \text{ ps}$ .

Sequence length	16 bits
Carrier wavelength of the pulse	$\lambda \sim 1300 \text{ nm}$
$T_{\text{FWHM}} = 20 \text{ ps}$	$\rightarrow T_0 = 0.567 T_{\text{FWHM}} \sim 11.34 \text{ ps}$
Input peak power	21.7 mW

[Figure 4](#) and [Figure 5](#) show the selected fiber parameters.

**Figure 4 Nonlinear Dispersive Fiber Main parameters****Figure 5 Nonlinear Dispersive Fiber Dispersions parameters**

We will consider SMF with a length of 50 km and losses of 0.4 dB/km.

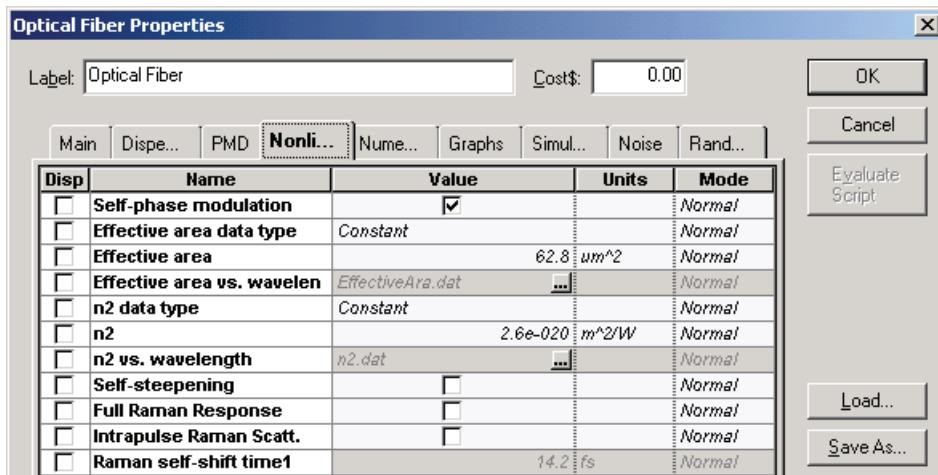
$$K_2 = \frac{(-\lambda^2 D)}{(2\pi c)} \sim -1.5(\text{ps}^2/\text{km}) \rightarrow D = 1.67(\text{ps}/\text{nm.km}) \rightarrow L_D = T_0^2 / |K_2| \sim 85\text{km}$$

**Note:** The effects of group delay and third order of dispersion are not taken into account.

After each fiber, the signal is amplified with SOA. Therefore,  $L_A \sim 50$  km. The condition  $L_A < L_D$  is satisfied.

Figure 6 shows the nonlinear parameters.

Figure 6 Nonlinear Dispersive Fiber NonLinear parameters



The Kerr nonlinearity coefficient

$$\gamma = \frac{n_2 w_0}{c A_{\text{eff}}}$$

for the fixed values of nonlinear refractive index

$$n_2 = 2.6 \cdot 10^{-20} [\text{m}^2/\text{W}], w_0/c = 2\pi/\lambda = 2\pi/1.3 \cdot 10^{-6} [\text{m}^{-1}], (A_{\text{eff}} = 62.8 [\mu\text{m}^2])$$

will be:

$$\gamma = 2 \left[ \frac{1}{\text{km} \cdot \text{W}} \right]$$

The linear losses for 50 km SMF are 20 dB. This is unsaturated single pass gain required from SOA. To obtain this gain, the following parameters have been used (see Figure 7 and Figure 8).

Figure 7 SOA Main parameters

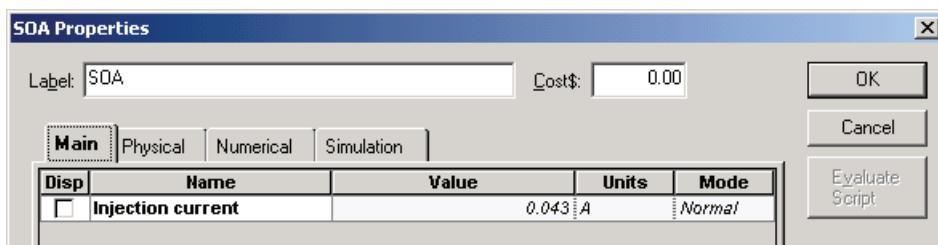
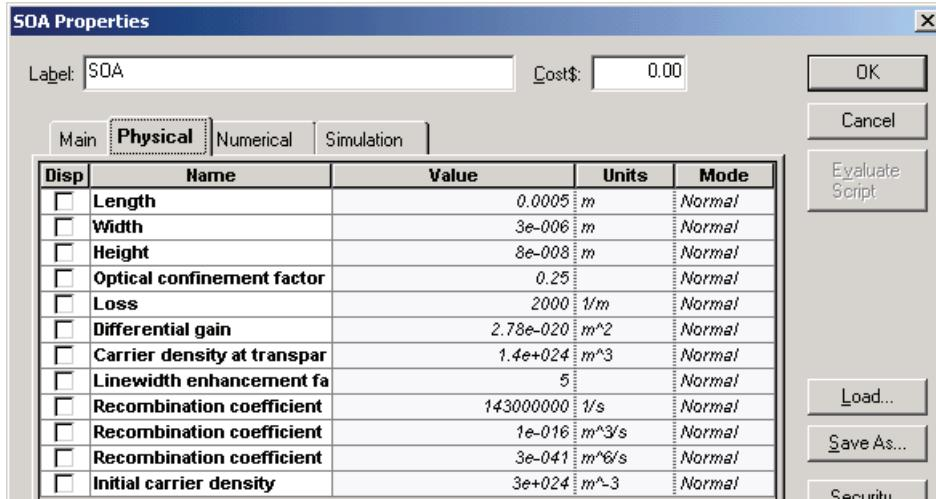


Figure 8 SOA Physical parameters

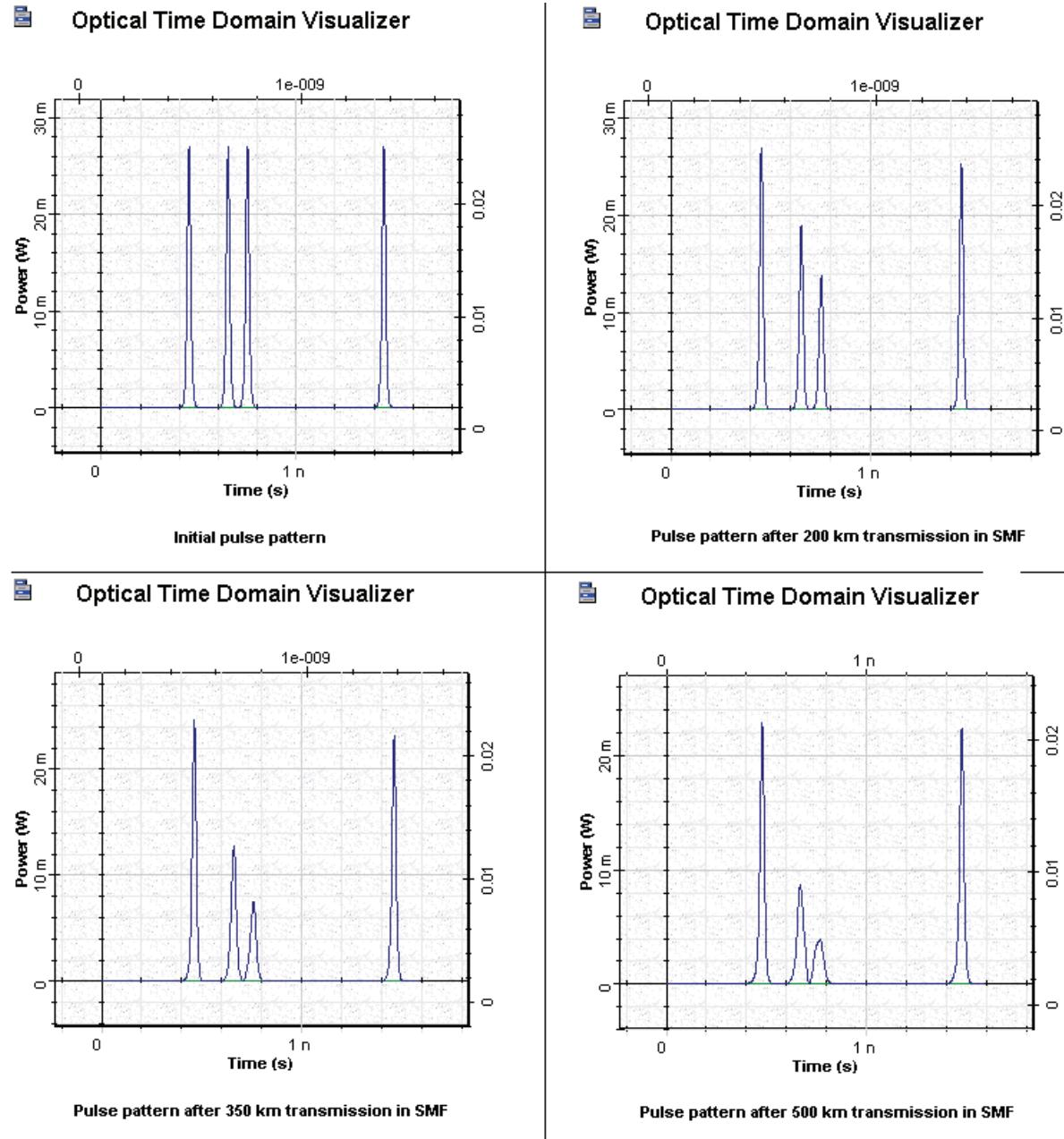


The inner losses are  $2000[m^{-1}]$  and the line width enhancement factor = 5.

$P_{sat} \sim 30$  mW and carrier lifetime  $t_C = 200$  ps in [1]. Therefore,  $E_{sat} \sim 6$  pJ. Our default values of the SOA component are  $\Gamma = 0.25 \rightarrow E_{sat} \sim 5.2$  pJ.

Figure 9 shows the initial pattern of pulses, and the same pattern of pulses after 200, 350, and 500 km transmission in SMF and periodic amplification with SOA at every 50 km.

Figure 9 SOA pulse patterns



In this figure, we can see the pattern effect that leads to a reduction in the gain of the pulses after the first one in the first group. Regarding our default parameters, the carrier lifetime is approximately 1.4 ns even for the last pulse, which is at a distance of approximately 1 nm from the first one. There is not enough time for the gain to recover completely.

This lesson demonstrated two basic problems associated with using the SOA as an in-line amplifier:

- pattern effect, which is a consequence of the gain saturation properties of the SOA
- nonlinear crosstalk [3]

## References:

- [1] M. Settembre, F. Matera, V. Hagele, I. Gabitov, A. W. Mattheus, and S. Turitsyn, "Cascaded optical communication systems with in-line semiconductor optical amplifiers", Journal of Lightwave Technology, Vol. 15, pp. 962-967, 1997.
- [2] F. Matera and M. Settembre, "Study of 1.3 mm transmission systems on standard step-index fibers with semiconductor optical amplifiers", Optics Communications, Vol. 133, pp.463-470, 1997.
- [3] G.P. Agrawal, "Fiber Optic Communication Systems", 2nd Edition, John Wiley & Sons Inc., 1997.

**Notes:**

# Wideband SOA characterization

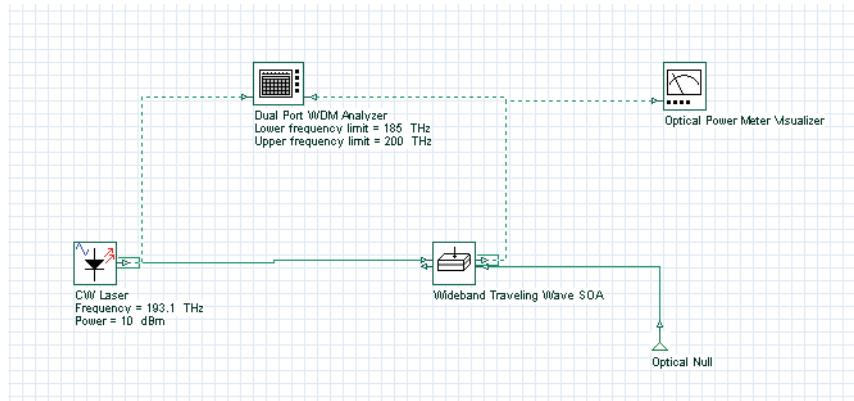
---

The objective of this lesson is to characterize a semiconductor optical amplifier (SOA) through simulations.

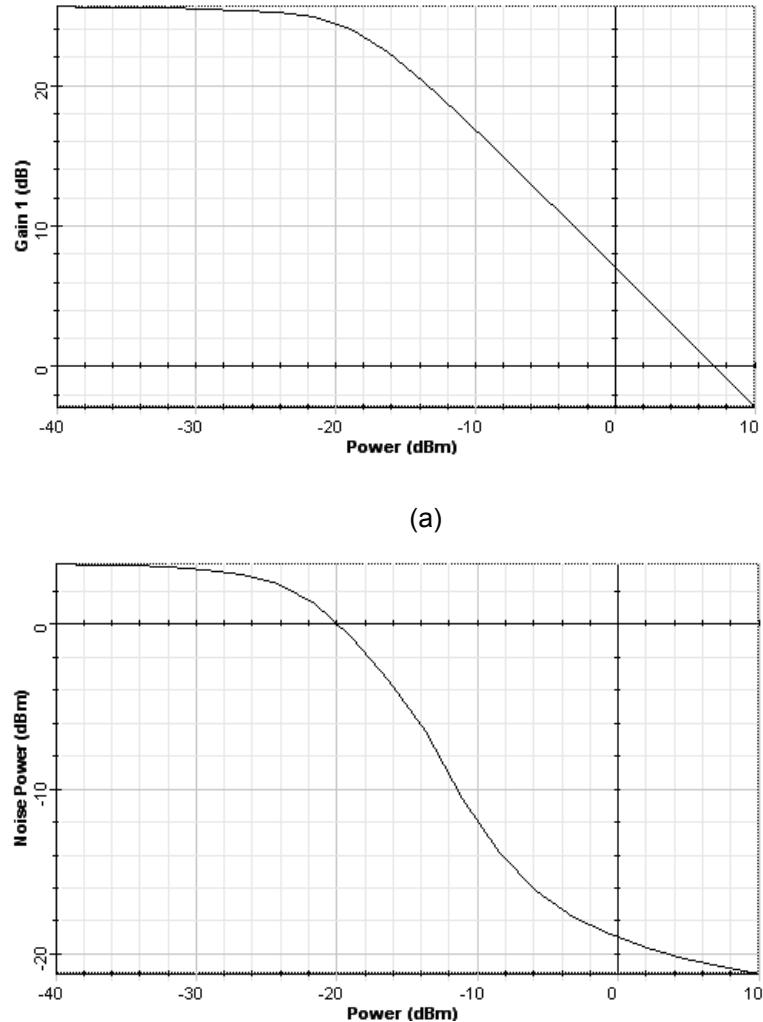
Initially, we are going to characterize the SOA response to the variation in the input signal power.

Figure 1 shows the system layout used in the simulation. We put the power parameter in the CW laser in sweep mode and it was varied from -40 dBm to 10 dBm.

**Figure 1 Gain and ASE power system layout**

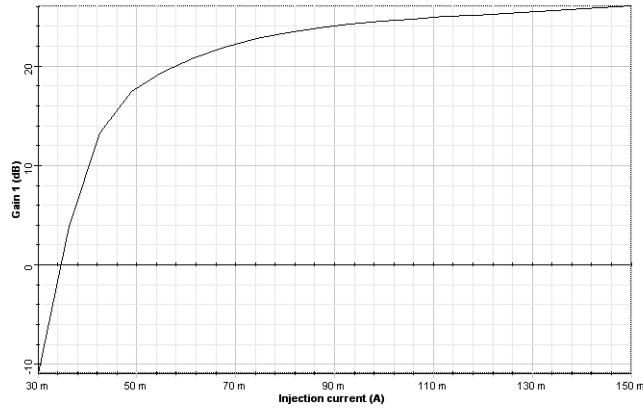


The signal gain and total forward ASE power is shown in Figure 2.

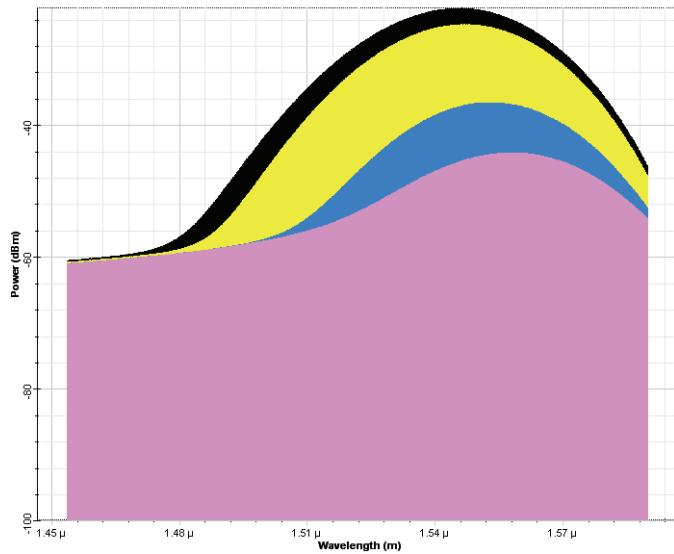
**Figure 2 (a) Signal gain and (b) total ASE power at the SOA output**

In the second part, the injection current parameter is varied from 30 mA to 150 mA. The Input signal power was kept at -30 dBm.

Figure 3 shows the signal gain results obtained in the simulation.

**Figure 3 Signal gain x injection current**

Finally, we analyze the variation the noise spectrum when the input signal power changes. In this case, the forward noise was analyzed. Figure 4 shows the spectra for 4 different input powers: -30 dBm, -20 dBm, -10 dBm and 0 dBm. We can see the increase in the noise peak power with the decrease in the input signal power.

**Figure 4 Noise spectra for different input signal powers**

**Notes:**

# Wavelength conversion in a wideband SOA

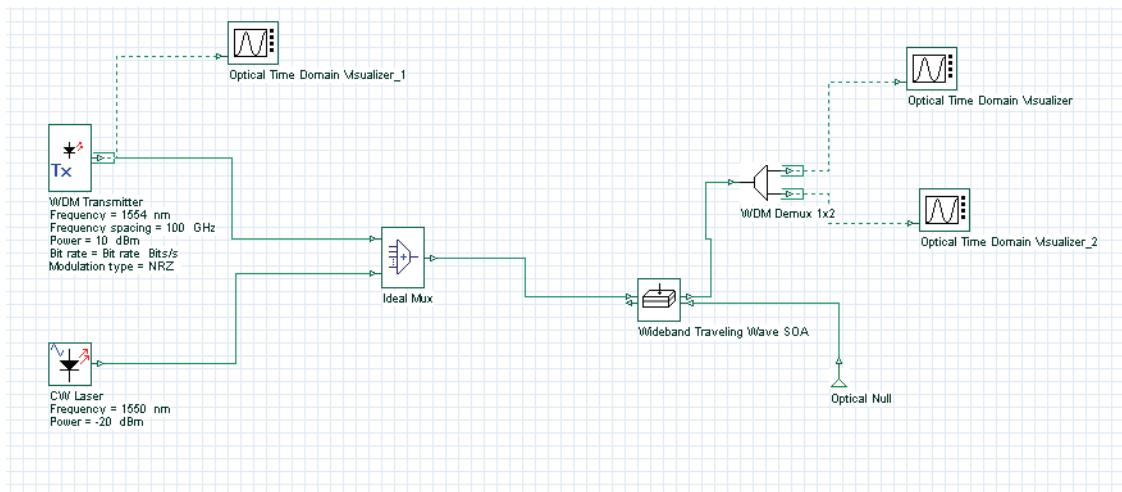
---

The objective of this lesson is to demonstrate the wavelength conversion using the wideband SOA component.

Based on the results from the lesson "Wideband SOA Characterization", we have designed a wavelength converter using the cross-gain modulation method.

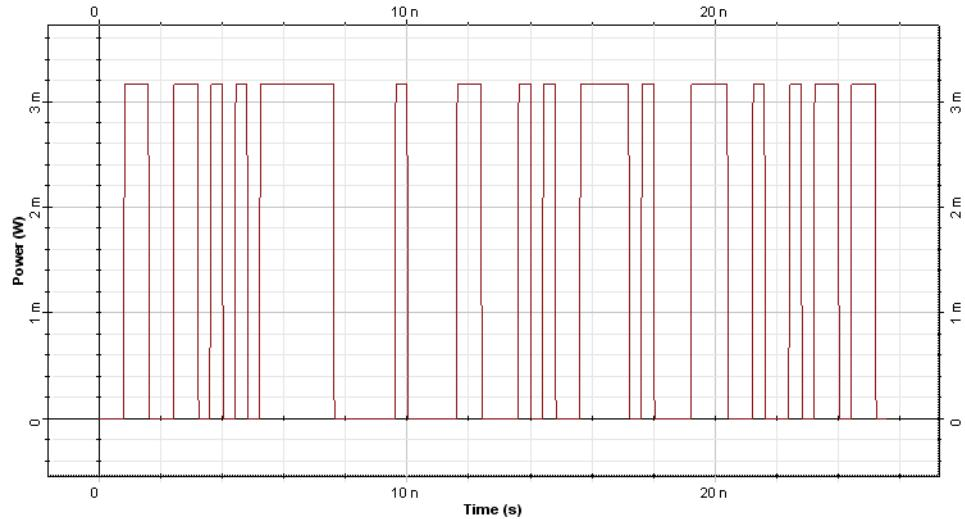
The system designed is shown in Figure 1.

**Figure 1** Wavelength converter system layout



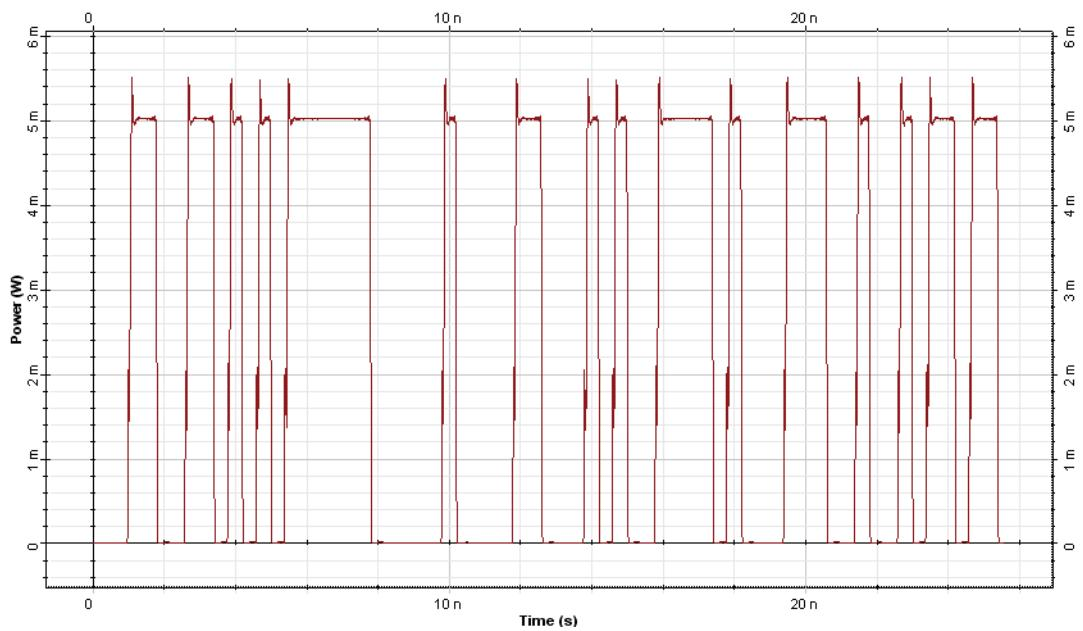
In the simulation, the original information modulated at the signal at 1554 nm will be converted to the wavelength at 1550 nm. See Figure 2.

**Figure 2 Original modulated signal at 1554 nm**



Based on the cross gain modulation, the initial CW signal at 1550 nm is modulated at the SOA and the output signal at 1550 becomes the signal shown in Figure 3.

**Figure 3 Wavelength converted signal at 1550 nm**



---

## Waveguide amplifiers

---

This section contains the following advanced simulation project.

- Improved gain characteristics in high-concentration Er<sup>3+</sup>/Yb<sup>3+</sup> codoped glass waveguide amplifiers

**Notes:**

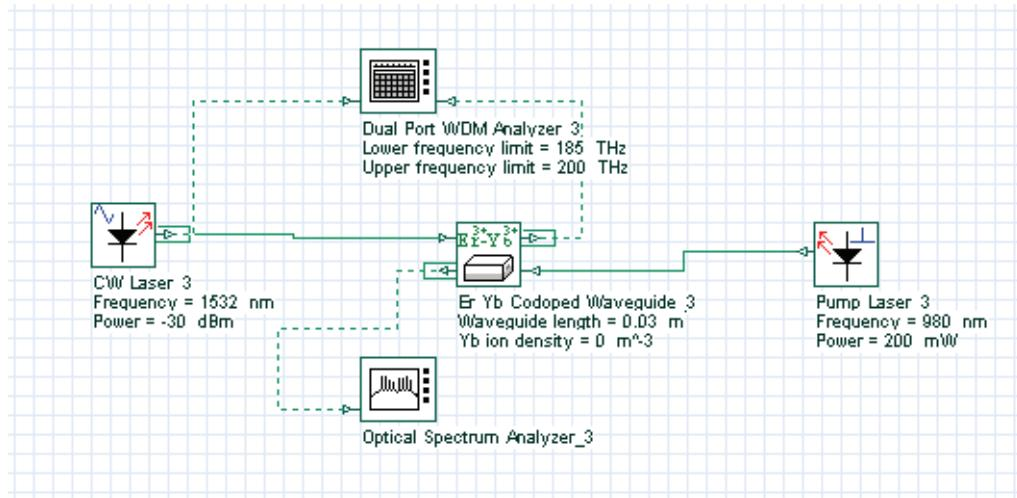
# Improved gain characteristics in high-concentration Er<sup>3+</sup>/Yb<sup>3+</sup> codoped glass waveguide amplifiers

This lesson will prove that we can achieve high gain with a short device length if we use a high-concentration Er<sup>3+</sup>/Yb<sup>3+</sup> codoped glass waveguide amplifier.

In this example, we simulate a codoped waveguide amplifier and show that the efficient Yb<sup>3+</sup> to Er<sup>3+</sup> energy transfer is a useful mechanism to reduce performance degradation due to Er<sup>3+</sup> ion-ion interactions [1].

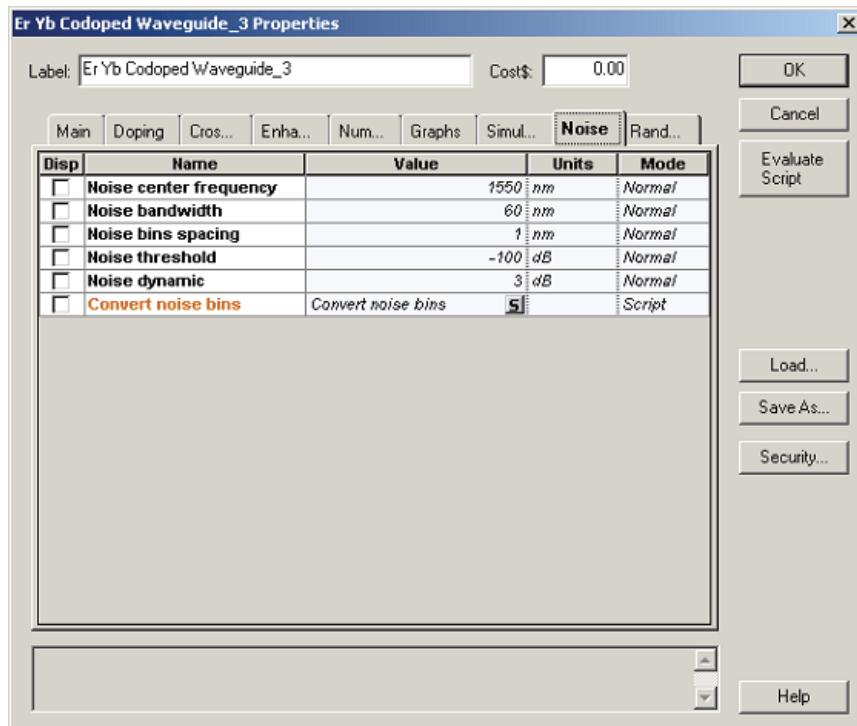
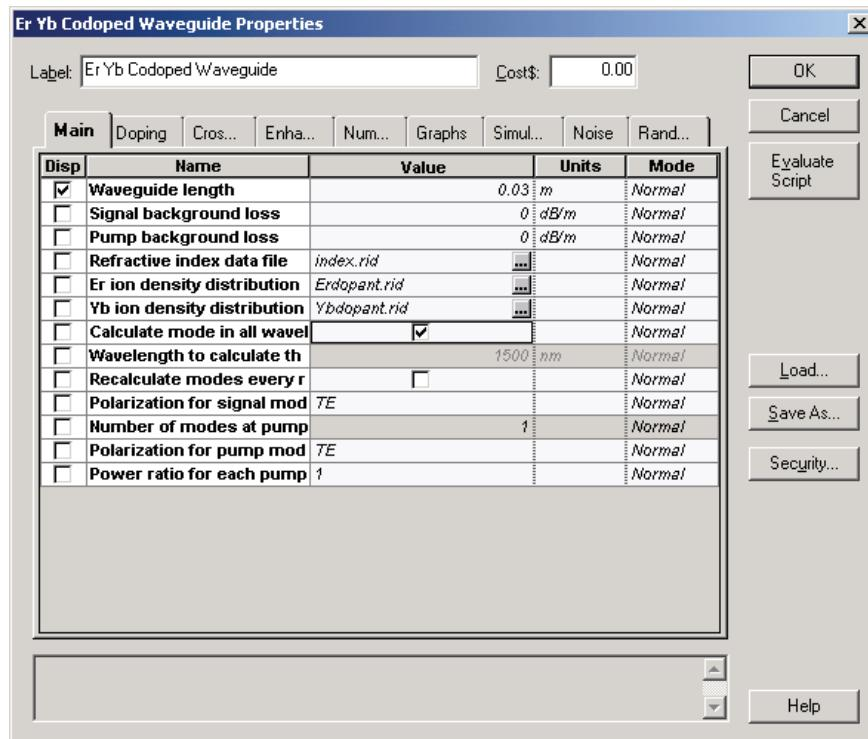
The project consists of different layouts that work together in order to generate the different graphs that we need. All these layouts have the form shown in [Figure 1](#).

**Figure 1** Project Layout for analysis of the Waveguide Amplifier component



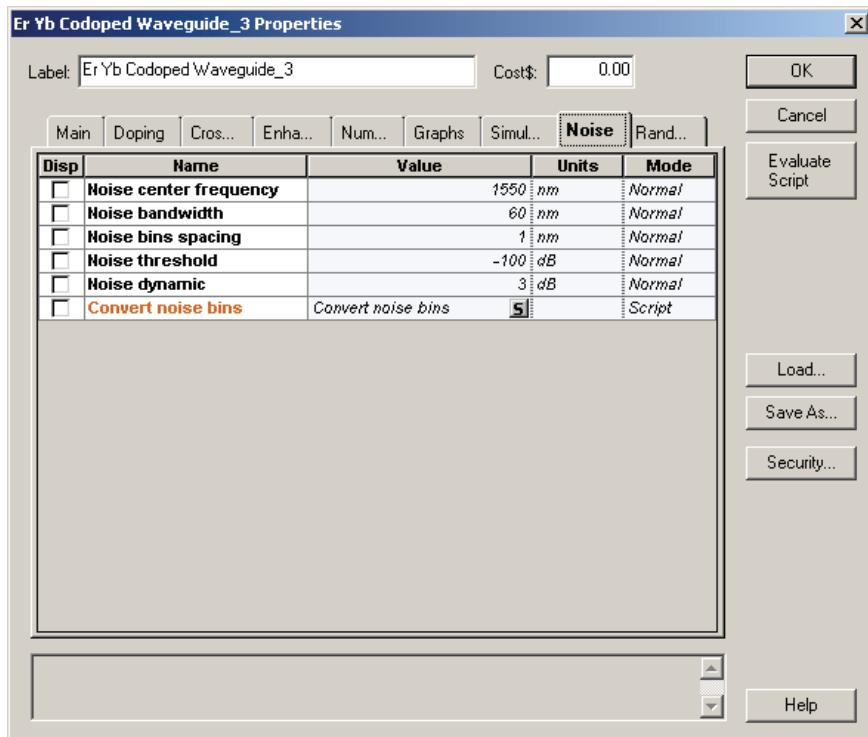
The basic parameters for the waveguide amplifier component, extracted from [1], do not change, so for all layouts we will have the following common parameters (as displayed in [Figure 2](#)), not including the waveguide length.

Figure 2 Waveguide amplifier parameters



The refractive index file was defined using OptiBPM 6.0, and defines a channel that has a narrow square core  $2 \times 2 \mu\text{m}^2$ , and a refractive-index difference of 0.04 ( $n_{co} = 1.55$ ,  $n_{cl} = 1.51$ ). These parameters have been chosen in order to ensure single-mode operation at pump and signal wavelengths (980 and 1532 nm, respectively), polarization independent signal gain, and at the same time, to have a good field confinement on the active region [1]. ASE definition, as described in Figure 3, is kept the same through all the different layouts.

**Figure 3 Description of ASE**



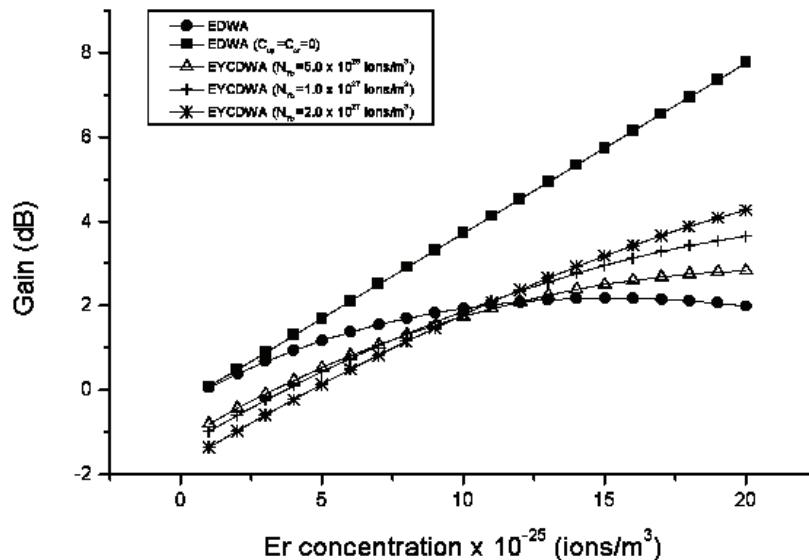
The layouts "EDWA x Er concentration", "EDWA ( $C_{up} = C_{cr} = 0$ ) x Er concentration", "EYCDWA x Er concentration (Yb concentration =  $1.0 \times 10^{27}$ )", "EYCDWA x Er concentration (Yb concentration =  $2.0 \times 10^{27}$ )" and "EYCDWA x Er concentration (Yb concentration =  $5.0 \times 10^{26}$ )" are intended to produce a valuable comparison among these different amplifiers. The values used in the Doping tab are displayed in Figure 4.

Figure 4 Erbium data

Sweeps	Er Yb Codoped Wave	Er pump excess loss	Er signal excess loss
	Er ion density [m^-3]		
1	1e+025	15	11.8
2	2e+025	16.17368421053	12.72105263158
3	3e+025	17.34736842105	13.64210526316
4	4e+025	18.52105263158	14.56315789474
5	5e+025	19.69473684211	15.48421052632
6	6e+025	20.86842105263	16.40526315789
7	7e+025	22.04210526316	17.32631578947
8	8e+025	23.21578947368	18.24736842105
9	9e+025	24.38947368421	19.16842105263
10	1e+026	25.56315789474	20.08947368421
11	1.1e+026	26.73684210526	21.01052631579
12	1.2e+026	27.91052631579	21.93157894737
13	1.3e+026	29.08421052632	22.85263157895
14	1.4e+026	30.25789473684	23.77368421053
15	1.5e+026	31.43157894737	24.69473684211
16	1.6e+026	32.60526315789	25.61578947368
17	1.7e+026	33.77894736842	26.53684210526
18	1.8e+026	34.95263157895	27.45789473684
19	1.9e+026	36.12631578947	28.37894736842
20	2e+026	37.3	29.3

Using the erbium ion density, erbium signal loss, and erbium pump loss as shown above; we perform simulations for an amplifier of 3 cm pumped at 980 nm and different ytterbium concentrations in the case of EYCDWA (Figure 5). By these simulations, it is clear that increasing the Ytterbium concentration, Yb<sup>3+</sup> to Er<sup>3+</sup> energy transfer progressively reduces the negative effect due to Er<sup>3+</sup> ion-ion interactions only at high-erbium concentrations.

Figure 5 Signal gain versus erbium concentration ( $P_p=200\text{mW}$ ,  $P_s=1\mu\text{W}$ ,  $L=3\text{cm}$ )



For the layouts "Yb concentration (3 cm)", "Yb concentration (4 cm)" and "Yb concentration (5 cm)", the doping values change (see [Figure 6](#)).

**Figure 6 Ytterbium data**

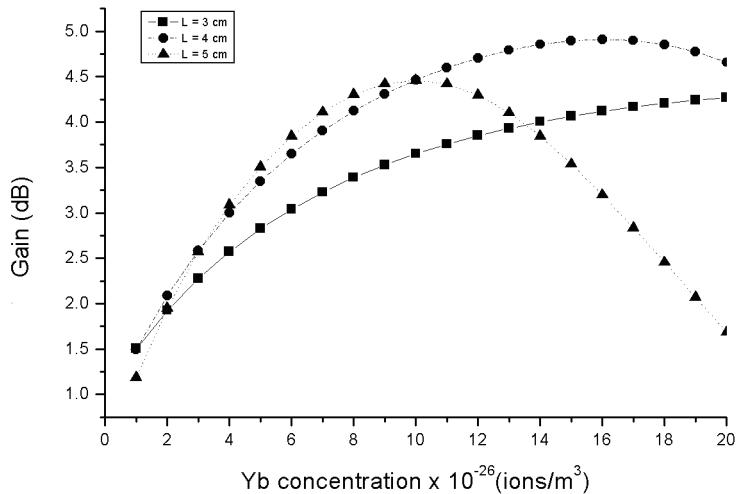
The screenshot shows a software interface titled "Parameter Sweeps". On the right side, there are buttons for "OK", "Cancel", "Help", and "Assign Values...". Below these are several "Spread Tools" buttons: "Linear...", "Exp...", "Log...", "Formula...", "Gaussian...", "LogNormal...", "Uniform...", and "Discrete...". The main area contains a table with the following data:

Sweeps	Er Yb Codoped Wave	Yb pump excess los	Yb signal excess los	Yb ion density [ $m^{-3}$ ]
1	30.5	24	1e+026	
2	32.10526315789	25.26315789474	2e+026	
3	33.71052631579	26.52631578947	3e+026	
4	35.31578947368	27.78947368421	4e+026	
5	36.92105263158	29.05263157895	5e+026	
6	38.52631578947	30.31578947368	6e+026	
7	40.13157894737	31.57894736842	7e+026	
8	41.73684210526	32.84210526316	8e+026	
9	43.34210526316	34.10526315789	9e+026	
10	44.94736842105	35.36842105263	1e+027	
11	46.55263157895	36.63157894737	1.1e+027	
12	48.15789473684	37.89473684211	1.2e+027	
13	49.76315789474	39.15789473684	1.3e+027	
14	51.36842105263	40.42105263158	1.4e+027	
15	52.97368421053	41.68421052632	1.5e+027	
16	54.57894736842	42.94736842105	1.6e+027	
17	56.18421052632	44.21052631579	1.7e+027	
18	57.78947368421	45.47368421053	1.8e+027	
19	59.39473684211	46.73684210526	1.9e+027	
20	61	48	2e+027	

For the Ytterbium concentration defined above, an EYCDWA pumped at 980 nm, with a fixed-erbium doping level, has the profile defined in [Figure 7](#). This graph shows that higher gain can be reached by increasing the Ytterbium concentration. Nevertheless, by increasing the waveguide length, there is an optimum Ytterbium concentration above which the gain is reduced.



Figure 7 Signal gain versus Ytterbium concentration ( $P_p=200\text{mW}$ ,  $P_s=1\mu\text{W}$ ,  $L=3\text{cm}$ ,  $N_{Er}=2.0 \cdot 10^{26} \text{ ions/m}^3$ )



As we see a quantitatively good agreement with the paper considered is observed. Furthermore, we showed that OptiSystem is suitable to support the development of EYCDWA, a very promising area for optical signal processing techniques.

## References

- [1] F. Di Pasquale and M. Federighi, "Improved Gain Characteristics in High-Concentration Er3+/Yb3+ Codoped Glass Waveguide Amplifiers", IEEE Journal of Quantum Electronics, vol. 30, no. 9, September 1994, 2127-2131.

---

## Dispersion management

---

This section contains the following advanced and illustrative simulation projects.

- Dispersion compensation schemes—a system perspective
- Compensation of dispersion with Ideal dispersion component
- Compensation of dispersion with Fiber Bragg Grating component
- Uniform Fiber Bragg Grating as a filter
- Compensation of dispersion with OptiGrating
- Dispersion compensation using subsystems
- Maximum-likelihood sequence estimation (MLSE) equalizer
- DFE - Decision-Feedback Equalizer
- Dispersion compensation using electronic equalization

**Notes:**



# Dispersion compensation schemes—a system perspective

---

In this section, we will show how dispersion compensation schemes affect the system performance. The pulse broadening effect of chromatic dispersion causes the signals in the adjacent bit periods to overlap. This is called intersymbol interference (ISI). Broadening is a function of distance as well as dispersion parameter D. The dispersion parameter is given in ps/nm/km and changes from fiber to fiber. It is also a function of wavelength. D is usually about 17 ps/nm/km in the 1.55 μm wavelength range for a standard single mode fiber (SMF). It is at a maximum of 3.3 ps/nm/km in the same window for a dispersion-shifted fiber (DSF). Nonzero dispersion fiber (NDF) has a chromatic dispersion between 1 and 6 ps/nm/km or -1 and -6 ps/nm/km.

For externally modulated sources, transmission distance limited by chromatic dispersion is [1]

$$L < \frac{2\pi c}{16|D|\lambda^2 B^2}$$

When  $D=16 \text{ ps}/(\text{km-nm})$  and at  $2.5 \text{ Gbps}$ ,  $L \approx 500 \text{ km}$ , whereas it drops to  $30 \text{ km}$  at  $10 \text{ Gbps}$  bit rate.

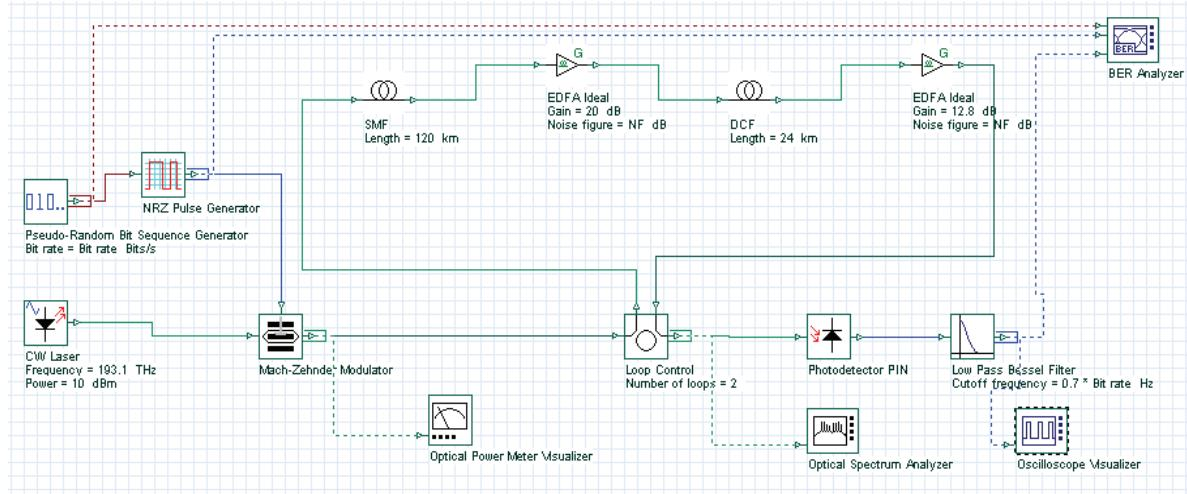
Several techniques, including Dispersion Compensating Fiber or Fiber Bragg Grating, can be used to compensate the accumulated dispersion in the fiber. In the following example we will show three different schemes, pre-, post-, and symmetrical compensation, to compensate the fiber dispersion. First we will use dispersion compensating fibers (DCFs). We will then show how the amount of accumulated dispersion from the dispersion compensator affects the performance. In this case, we will use an ideal dispersion compensating module (DCM) as the dispersion compensator to show the idea.

## Pre-, post-, and symmetrical-compensation by using DCF

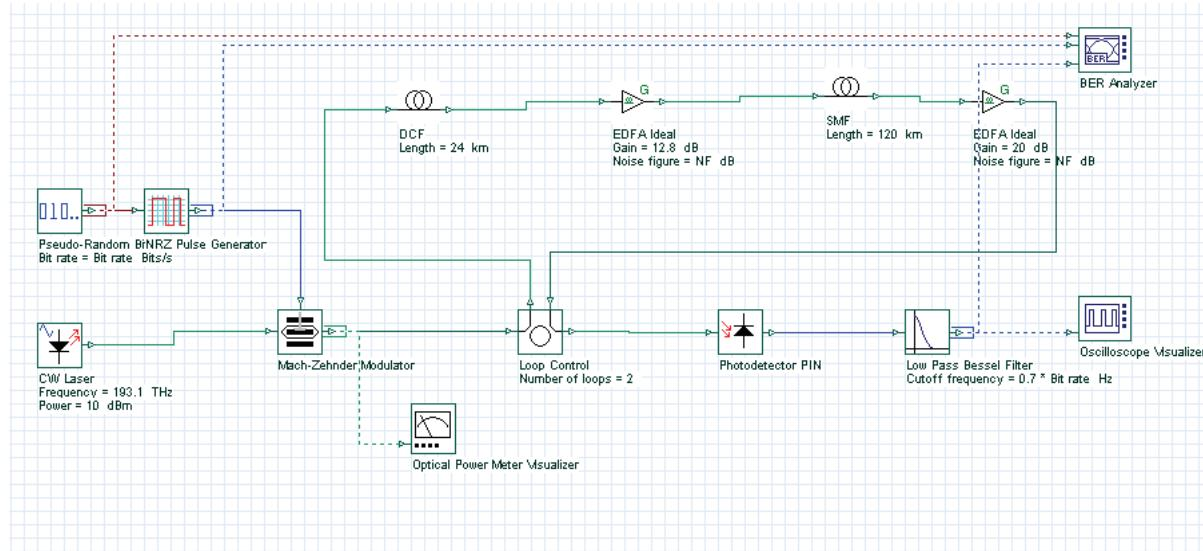
Pre-, post-, and symmetrical compensation configurations are shown in [Figure 1](#), [Figure 2](#), and [Figure 3](#). In our simulations, we have used optical amplifiers after each fiber to compensate for the span loss. The dispersion parameter of SMF is 120 km long and 16 ps/nm-km. Therefore, total accumulated dispersion is  $16 \times 120 = 1920 \text{ ps/nm}$ . This much dispersion can be compensated by using a 24 km long DCF with -80 ps/km-nm dispersion. Total transmission distance is  $120 \times 2 = 240 \text{ km}$  for each cases. In the post-compensation case, DCF is placed after SMF. In the symmetrical compensation case, fiber placement follows the sequence of SMF, DCF, DCF, SMF.

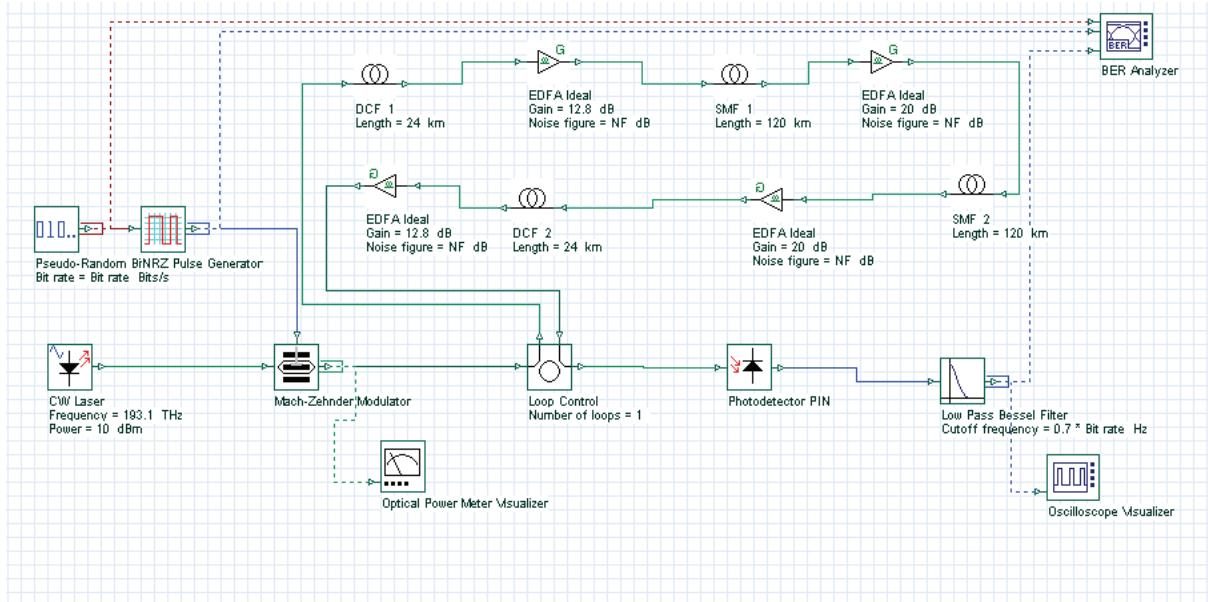


**Figure 1 Dispersion post-compensation**



**Figure 2 Dispersion pre-compensation**



**Figure 3 Dispersion symmetrical-compensation**

For these three cases, the project is found in the following file: **Dispersion compensation pre post symmetrical.osd**. In these simulations, we have used NRZ modulation formats. Receiver sensitivity is -28 dBm for 2.5 Gbps and -25 dBm for 10 Gbps. (Thermal noise of the PIN is  $2.048e^{-23W/Hz}$ .) Simulation results are shown in [Figure 4](#) and [Figure 5](#). [Figure 4](#) shows Q factor of received signal versus transmitted signal power for these three schemes at 2.5 Gbps bit rate. [Figure 5](#) shows the same graph for the 10 Gbps bit rate. To simulate the designs in 10 Gbps, you need to set the global parameter bit rate to 10 Gbps. From these figures, we can conclude that the best performance is obtained by using symmetrical dispersion compensation. The worst case is dispersion pre-compensation. This can also be seen from the eye diagrams given in [Figure 5](#). These results are in complete agreement with the results found in the literature [2] [3].

Figure 4 Q factor verses signal power at 2.5 and 10 Gbps bit rates for pre-, post-, and symmetrical dispersion compensations

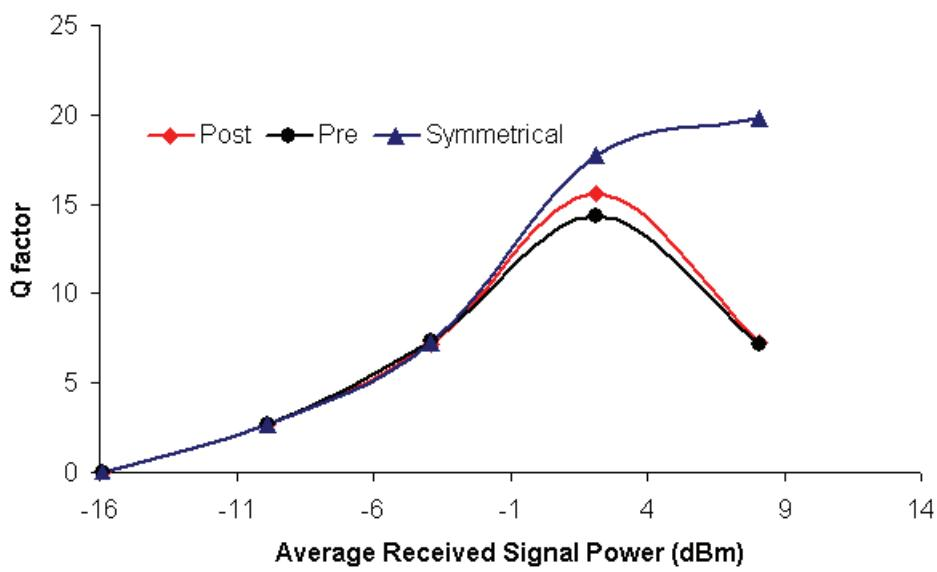
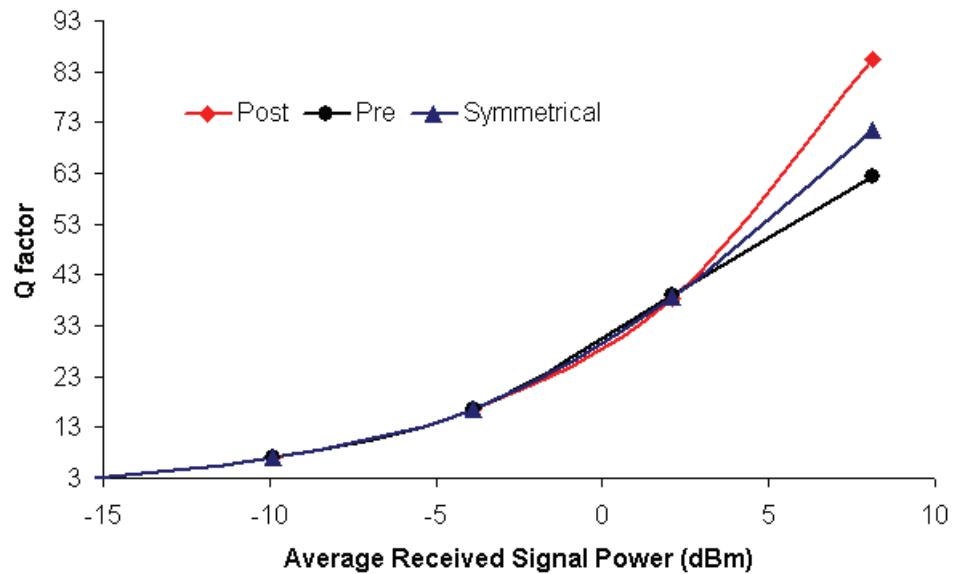
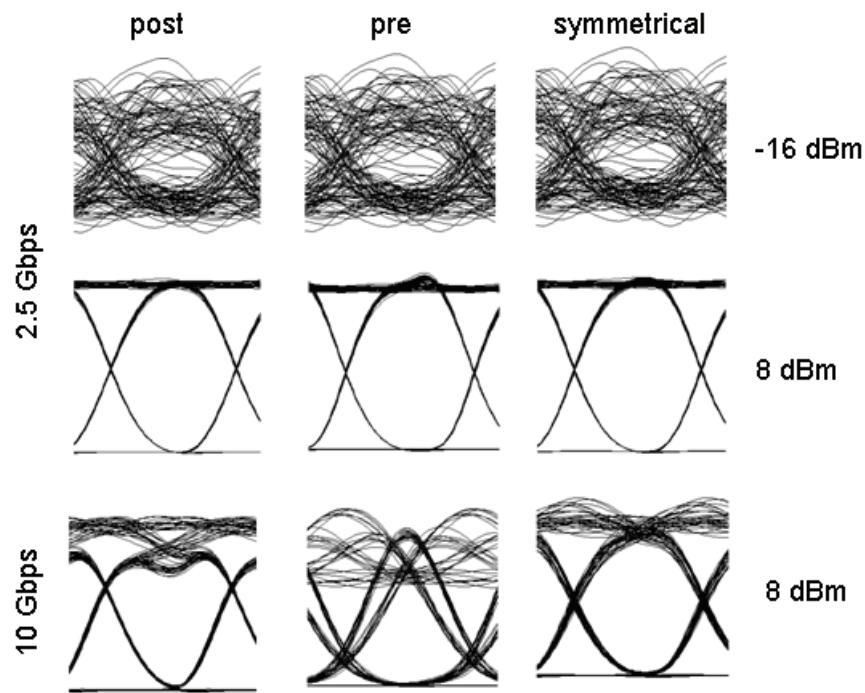


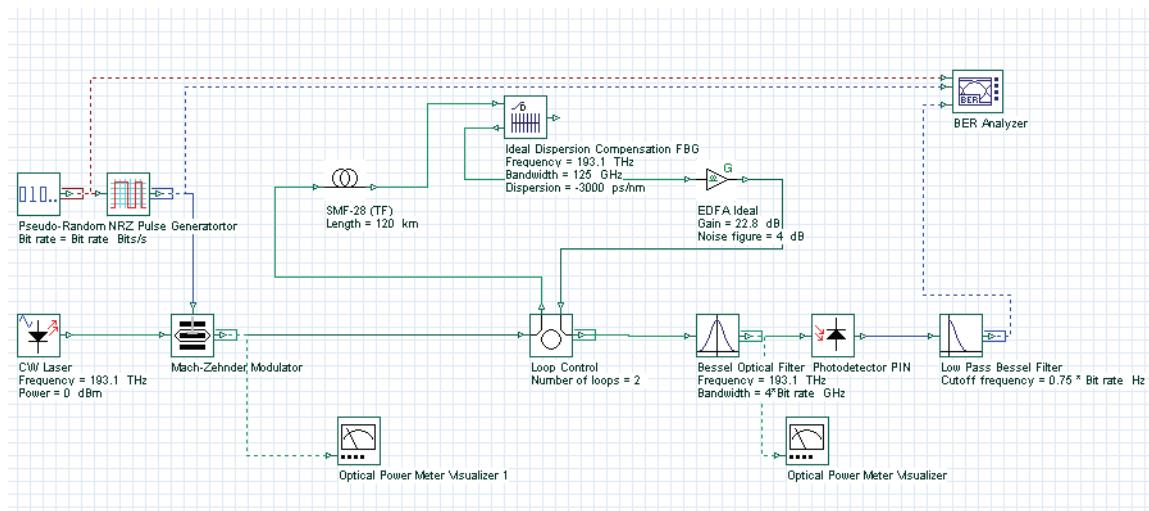
Figure 5 System performance at 2.5 and 10 Gbps bit rates for pre-, post-, and symmetrical dispersion compensations. The eye diagrams are shown for -12 and 10 dBm signal powers.



## Dispersion compensation by using DCM

We will now show how the amount of compensating dispersion affects system performance. We will use an Ideal Dispersion Compensation FBG as the dispersion compensation module (see [Figure 6](#)). In this case, we selected a post-compensation scheme because it is simple compared to the symmetrical compensation scheme. All schemes perform similar in low power regions. Project is given in [Dispersion compensation post with FBG.osd](#).

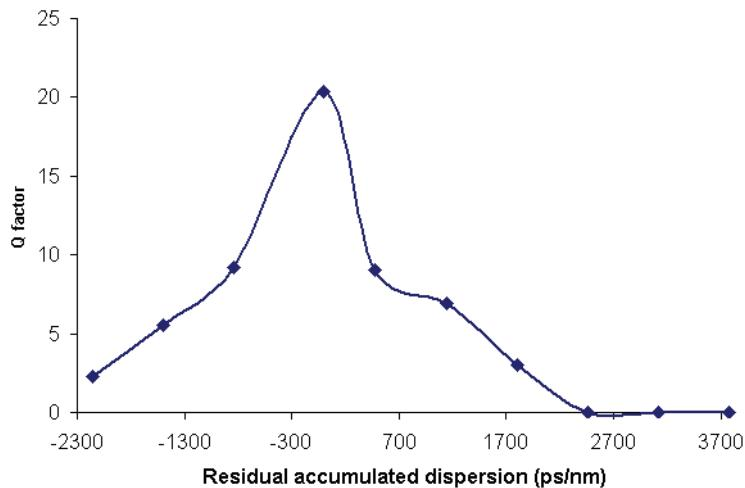
**Figure 6** Dispersion compensation by using DCM



The total accumulated dispersion of the SMF is  $16 \times 120 = 1920 \text{ ps/nm}$ . We swept the total dispersion of FBG from -30 to -3000 ps/nm. The bit rate is set to 10 Gbps. In this simulation, we want to investigate the dispersion-limited performance of the system. To avoid triggering fiber nonlinearity, we keep the received power at -3 dBm. Effects of residual dispersion to nonlinear effects will be considered in other examples.

[Figure 7](#) shows Q factor versus residual dispersion. This simulation shows that in the linear regime (low power), completely compensating fiber dispersion gives the best result. Over-compensating degrades the system performance.



**Figure 7 Q-factor versus residual dispersion**

## References:

- [1] G. P. Agrawal, Fiber Optic Communication Systems, Wiley-Interscience, 1997.
- [2] R. Ramaswami and K. N. Sivarajan, Optical Networks: A practical Perspective, Morgan Kaufmann, 1998.
- [3] M. I. Hayee and A. E. Willner, "Pre- and post-compensation of dispersion and nonlinearities in 10-Gb/s WDM systems", IEEE Photon. Tech. Lett. 9, pp. 1271, 1997.

**Notes:**

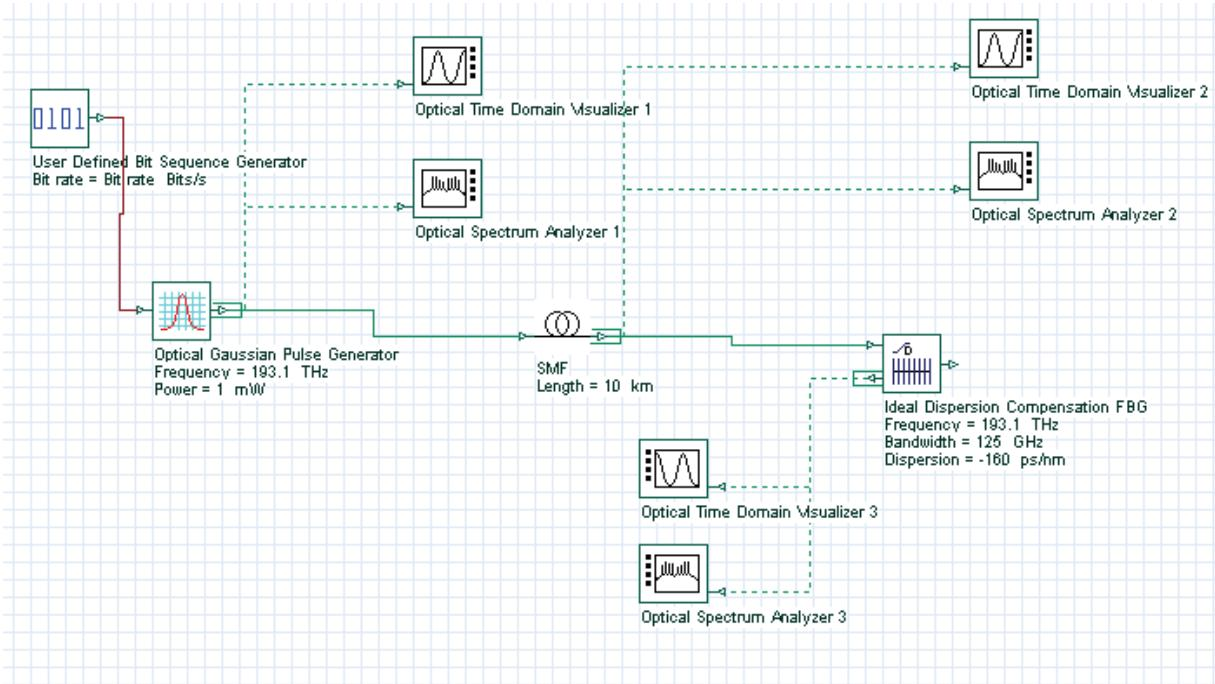


# Compensation of dispersion with Ideal dispersion component

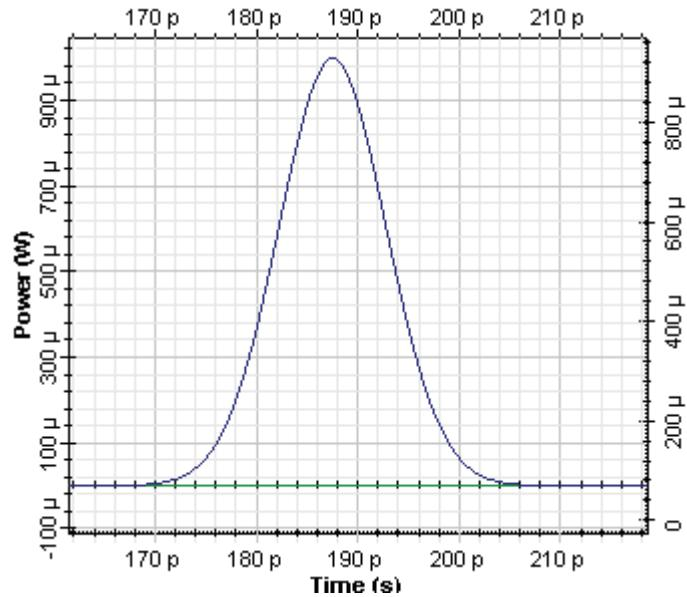
This lesson demonstrates the possibility for dispersion compensation with the help of ideal dispersion component in OptiSystem.

The project layout is shown in [Figure 1](#).

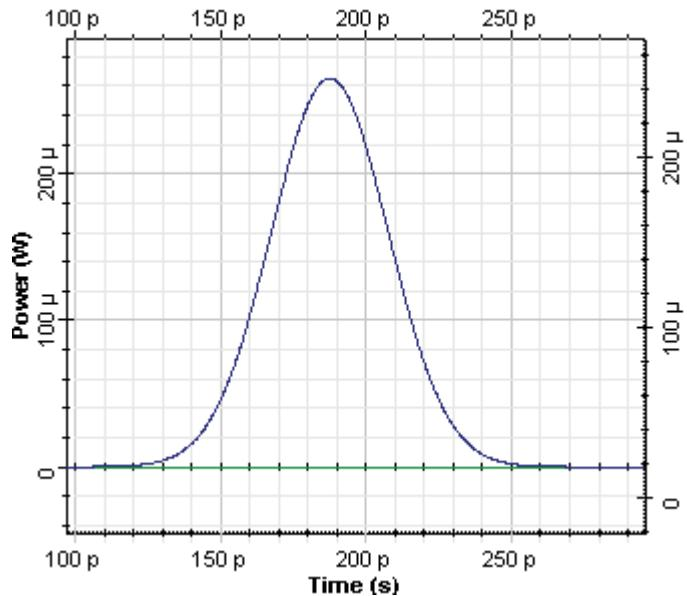
**Figure 1 Project Layout for dispersion compensation with ideal dispersion component in OptiSystem**



The following shape was generated in the Optical Gaussian pulse generator with an initial 12.5 ps pulse and global parameters of a 40 Gb/s bit rate and a 0.5 times bit slot.

**Figure 2 Initial gaussian pulse**

The pulse was launched in 10 km SMF. As a result of this propagation, the width of the pulse increases approximately four times.

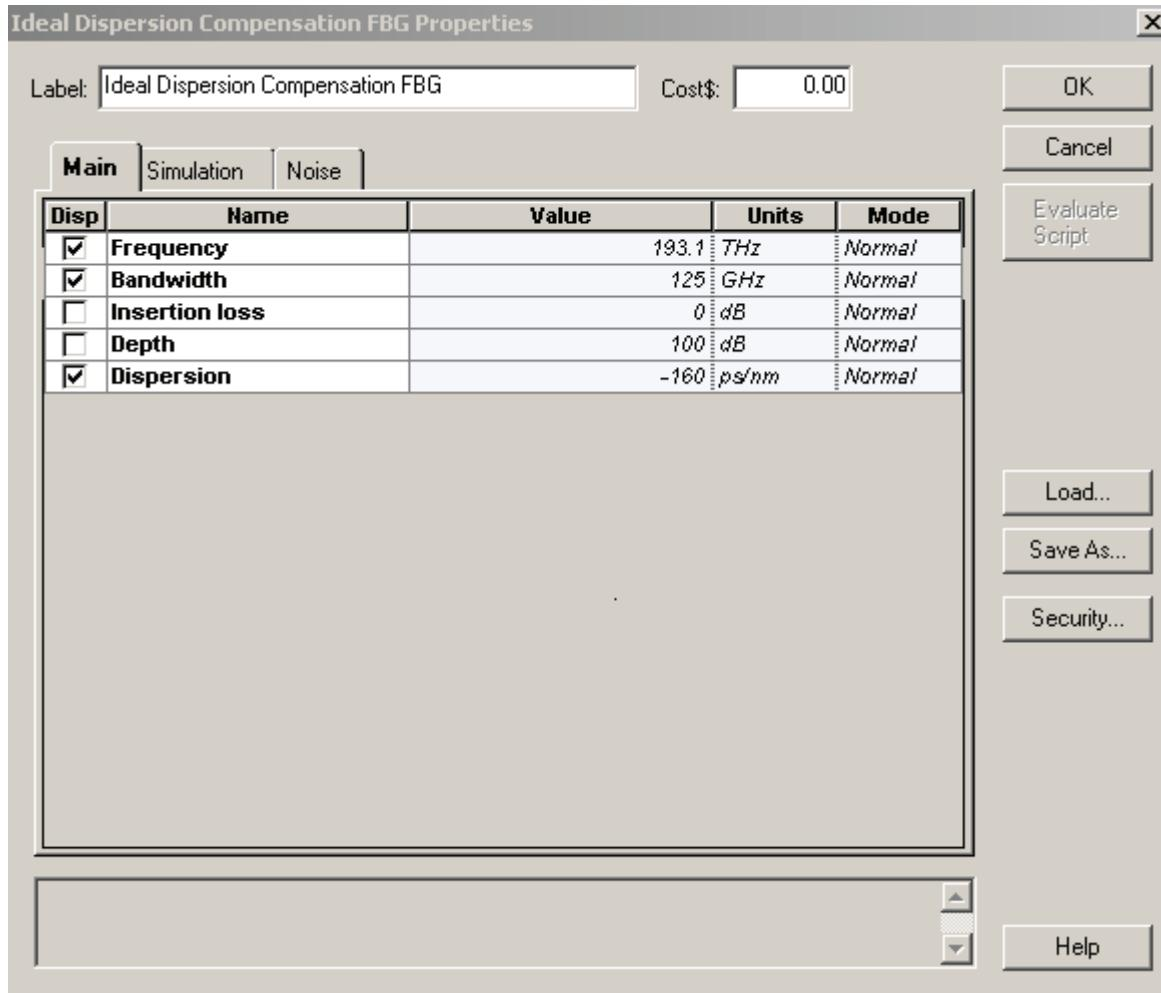
**Figure 3 Gaussian pulse after 10 km propagation in SMF**

After 10 km propagation in SMF, the accumulated dispersion is 160 ps/nm. In order to compensate for this accumulated dispersion, the corresponding option Dispersion in



the Main tab of the Ideal Dispersion Compensation component is fixed as - 160 ps/nm. The central frequency and corresponding bandwidth (in this case ~ 3 times the bit rate) has to be properly chosen. The corresponding tab with these parameters for this component is shown in [Figure 4](#).

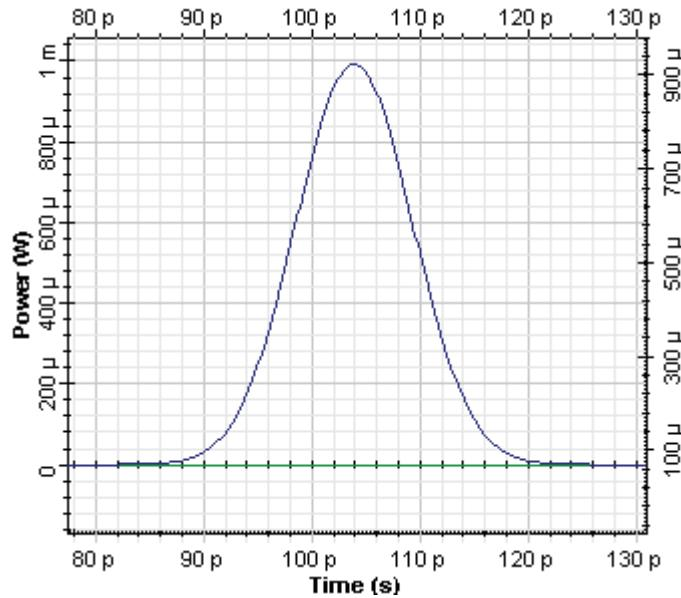
**Figure 4 Parameters of Ideal Dispersion Compensation component**



The result of dispersion compensation performed with the Ideal Dispersion Compensation component is shown in [Figure 5](#).

## COMPENSATION OF DISPERSION WITH IDEAL DISPERSION COMPONENT

**Figure 5 Pulse after dispersion compensation with Ideal Dispersion Compensation component**



As we could expect, an exact compensation of accumulated dispersion was achieved.

In conclusion, we have shown in this session how to use an Ideal Dispersion Compensation component in OptiSystem for dispersion compensation.



# Compensation of dispersion with Fiber Bragg Grating component

This lesson demonstrates the possibility for dispersion compensation with the help of fiber Bragg Grating created with the Fiber Grating component. This component allows design of apodized and chirped fiber gratings that are able to provide dispersion compensation in optical system.

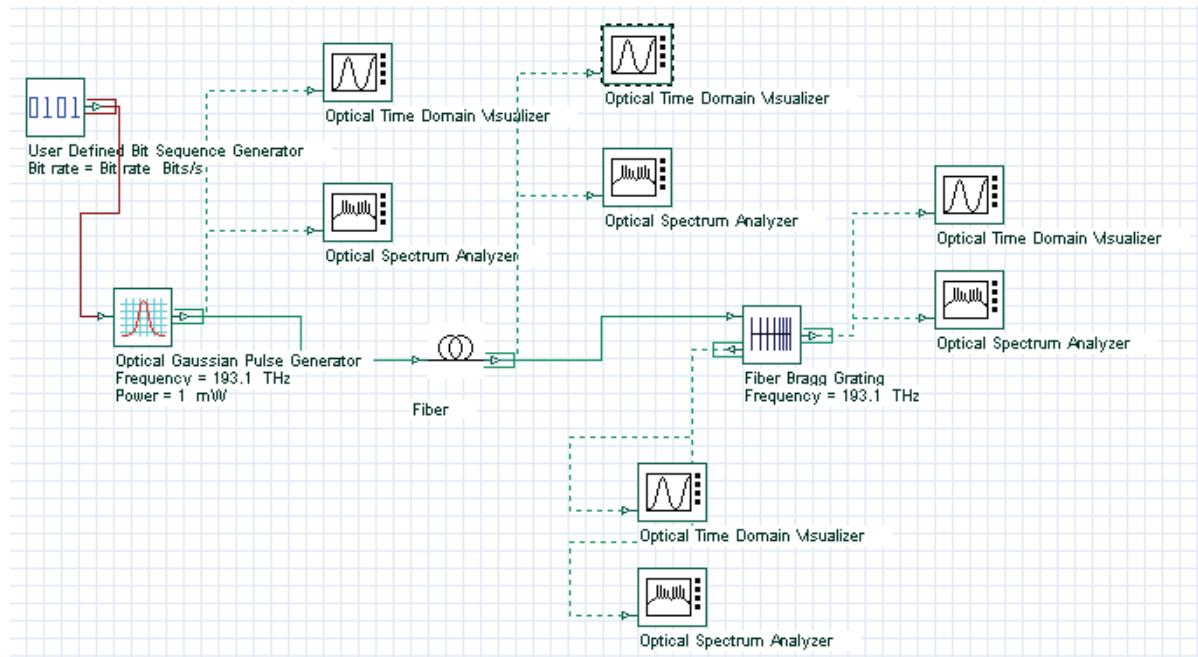
The physical idea behind this compensation is following: creating of an apodised linear chirped grating allows us to create a \*\* time delay between different spectral components of the signal.

For example, in SMF at  $1.55\mu\text{m}$ , group velocity dispersion creates a negative chirp of the pulses, which means that the higher frequencies (which propagate faster) are in the leading part of the pulse and the lower (propagating slower) in the trailing one.

Because of this different velocity of propagation of different spectral components, the pulse spreads. If we create fiber grating with period linearly reducing along the grating, because the higher frequencies will reflect after longer propagation in the grating a time delay between lower and higher frequency components will appear which is just opposite to this created in the SMF. Therefore propagating and reflecting our pulse in this device will allow to compensate the dispersion broadening of our pulse.

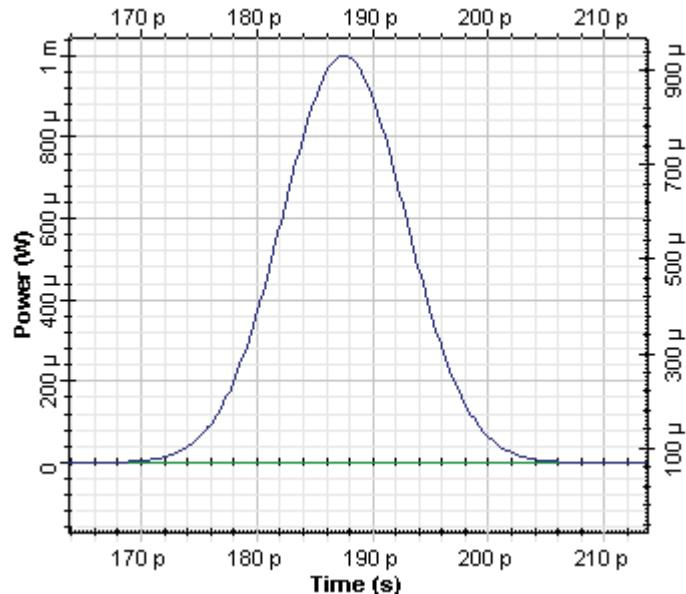
[Figure 1](#) shows the project layout.

**Figure 1 Project Layout for dispersion compensation with Fiber Bragg grating component in OptiSystem**



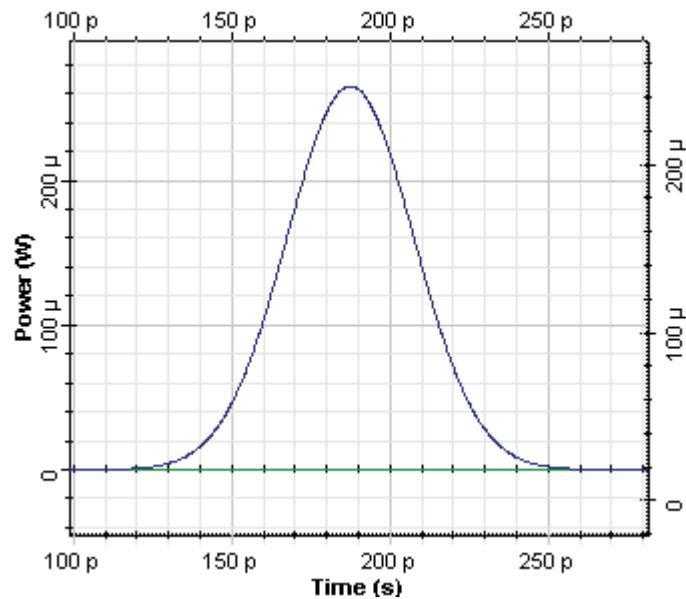
The following shape was generated in the Optical Gaussian pulse generator with an initial 12.5 ps pulse and global parameters of a 40 Gb/s bit rate and a 0.5 times bit slot.

**Figure 2 Initial Gaussian pulse**



The pulse was launched in 10 km SMF. As a result of this propagation, the width of the pulse increases approximately four times.

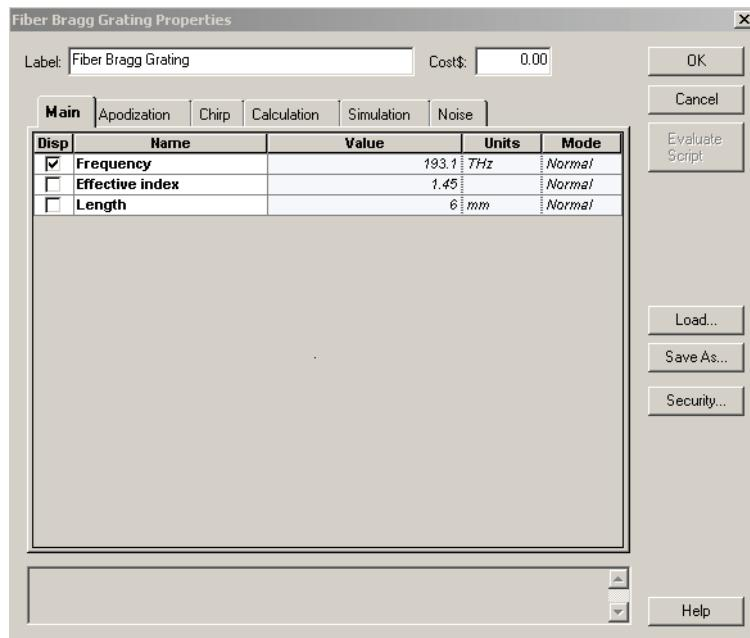
**Figure 3 Gaussian pulse after 10 km propagation in SMF**



Fiber Bragg Grating with following properties has been used: frequency 193.1 THz, effective index =1.45, length = 6 mm, apodization uniform, index of modulation 0.0001, linear chirp with a linear parameter 0.0001, number of segments 101 and maximum number of spectral points 1000.

Note that this linear chirping reduces the period of grating during the propagation of the pulse in the grating. Therefore the higher frequencies will travel more in the grating before being reflected than the lower one. The corresponding tabs with these parameters of fiber grating are shown below.

**Figure 4 Parameters of uniform, apodized, linear chirped Fiber Bragg Grating**



## COMPENSATION OF DISPERSION WITH FIBER BRAGG GRATING COMPONENT

**Fiber Bragg Grating Properties**

Label:	<input type="text" value="Fiber Bragg Grating"/>	Cost\$:	<input type="text" value="0.00"/>	
<input type="button" value="Main"/> <input type="button" value="Apodization"/> <input type="button" value="Chirp"/> <input type="button" value="Calculation"/> <input type="button" value="Simulation"/> <input type="button" value="Noise"/>				
<b>Disp</b>	<b>Name</b>	<b>Value</b>	<b>Units</b>	<b>Mode</b>
<input type="checkbox"/>	Chirp function	Linear		Normal
<input type="checkbox"/>	Linear parameter	0.0001	um	Normal
<input type="checkbox"/>	Quadratic parameter	0.0001	um	Normal
<input type="checkbox"/>	Square root parameter	0.0001	um	Normal
<input type="checkbox"/>	Cubic root parameter	0.0001	um	Normal
<input type="checkbox"/>	Chirp filename	ChirpPeriod.dat	<input type="button" value="..."/>	Normal

OK

Cancel

Evaluate Script

Load...

Save As...

Security...

Help

**Fiber Bragg Grating Properties**

Label:	<input type="text" value="Fiber Bragg Grating"/>	Cost\$:	<input type="text" value="0.00"/>	
<input type="button" value="Main"/> <input type="button" value="Apodization"/> <input type="button" value="Chirp"/> <input type="button" value="Calculation"/> <input type="button" value="Simulation"/> <input type="button" value="Noise"/>				
<b>Disp</b>	<b>Name</b>	<b>Value</b>	<b>Units</b>	<b>Mode</b>
<input type="checkbox"/>	Number of segments	101		Normal
<input type="checkbox"/>	Max. number of spectral p	1000		Normal

OK

Cancel

Evaluate Script

Load...

Save As...

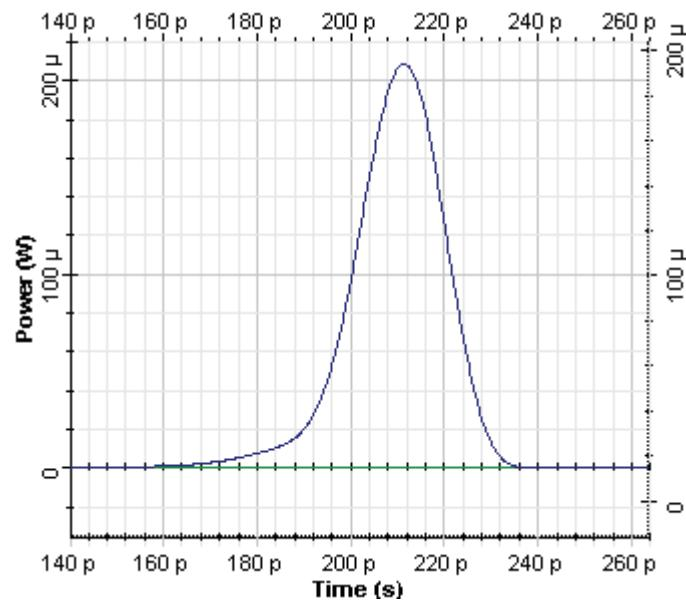
Security...

Help

The result of dispersion compensation performed from this fiber grating component is obtaining of a pulse with approximately 20 ps width.



Figure 5 Pulse after dispersion compensation with fiber grating with uniform apodization and linear chirp



**Notes:**

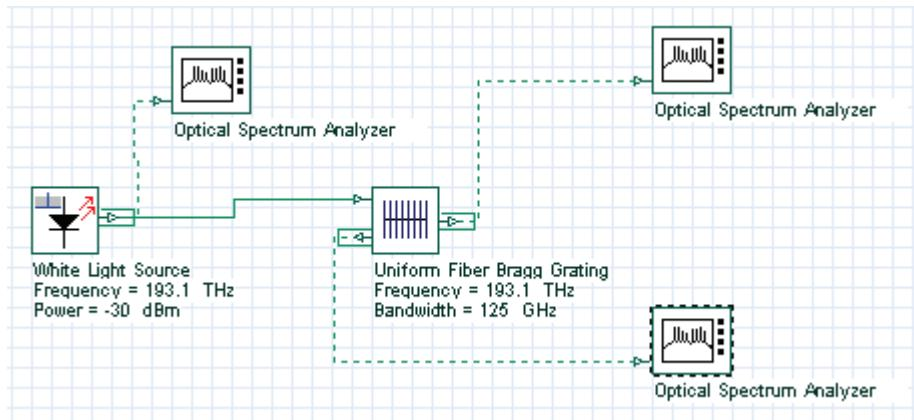


# Uniform Fiber Bragg Grating as a filter

This lesson demonstrates the application of the uniform fiber Bragg grating component in OptiSystem as a filter.

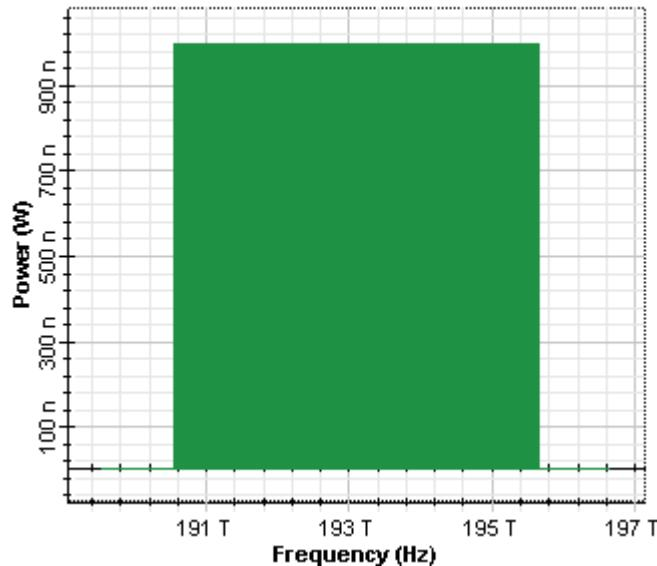
This lesson has two project layouts. In the first one, a white light source is used. In the second one, a Gaussian pulse is used. The first project layout is shown in [Figure 1](#)

**Figure 1** Project Layout for filter with uniform fiber Bragg grating component in OptiSystem



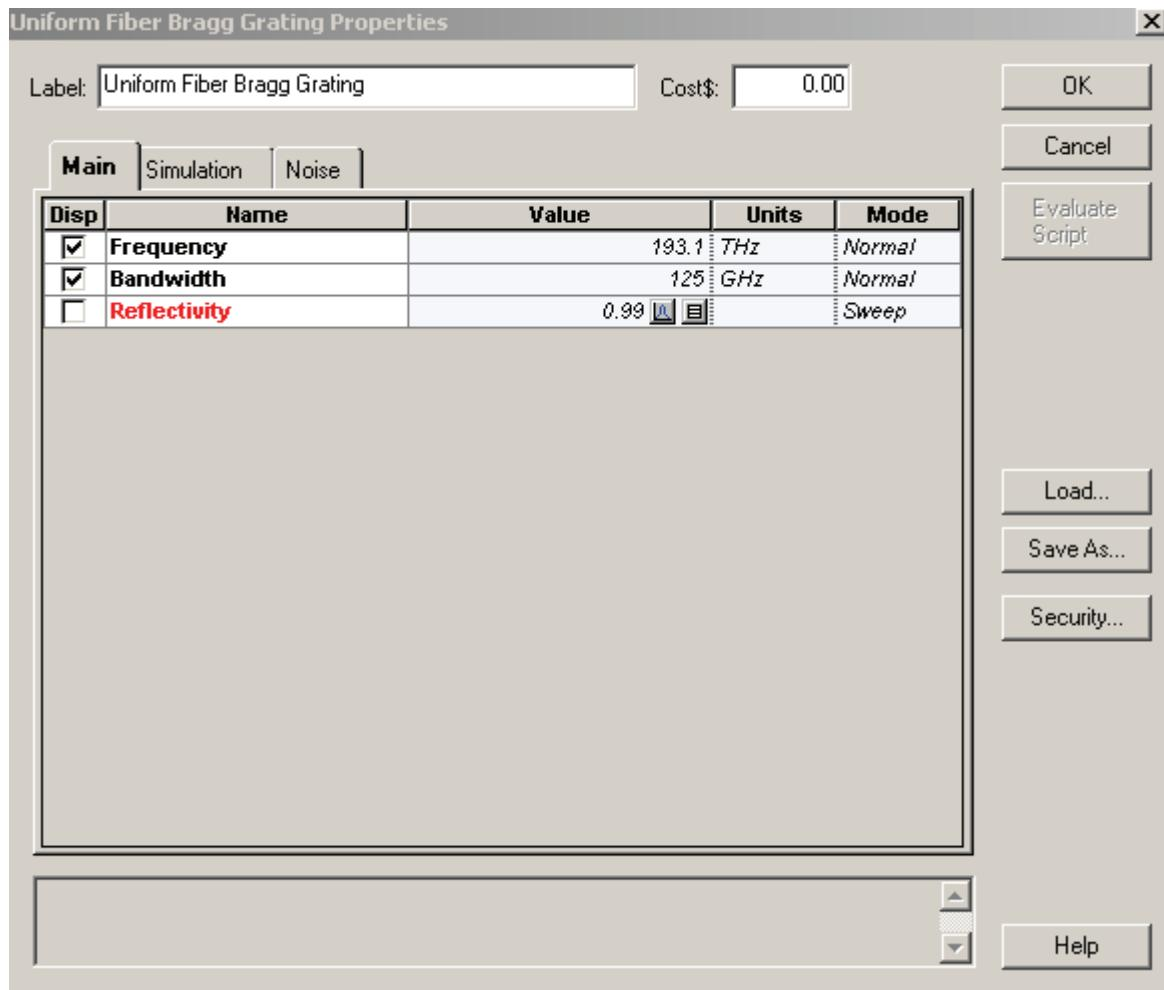
The initial spectrum has the form shown in [Figure 2](#).

**Figure 2** Initial spectrum of white light source

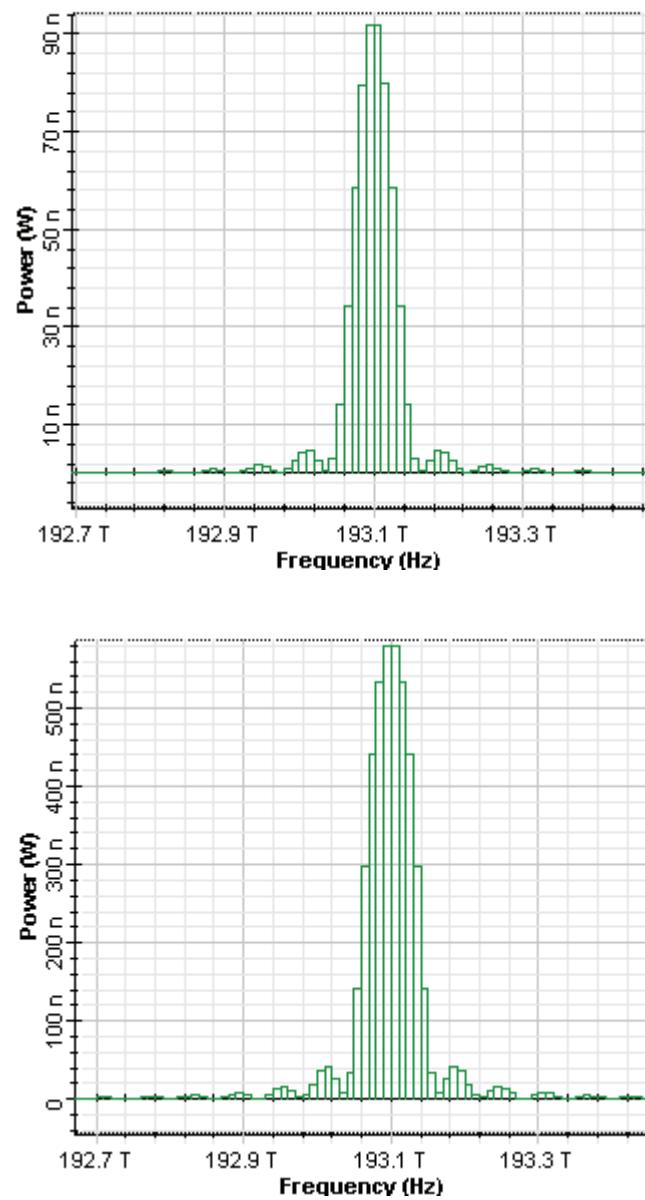


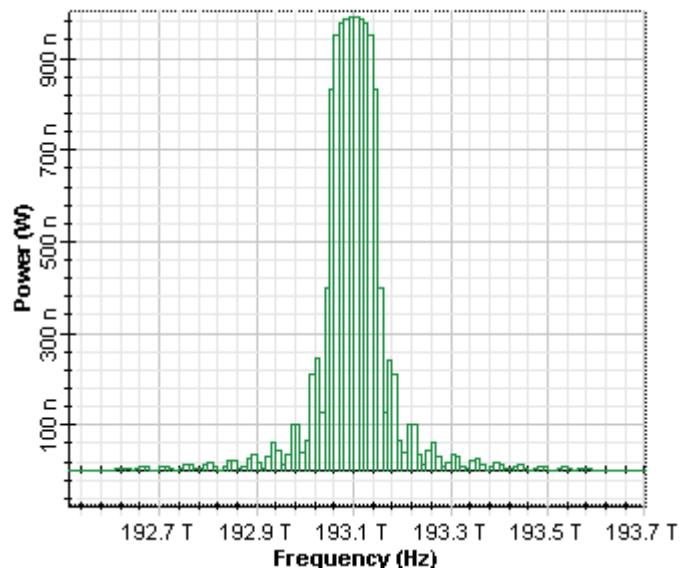
This layout include sweeps on the Reflectivity in the Main tab of the fiber Bragg grating component.

Figure 3 Main tab of the uniform fiber Bragg grating



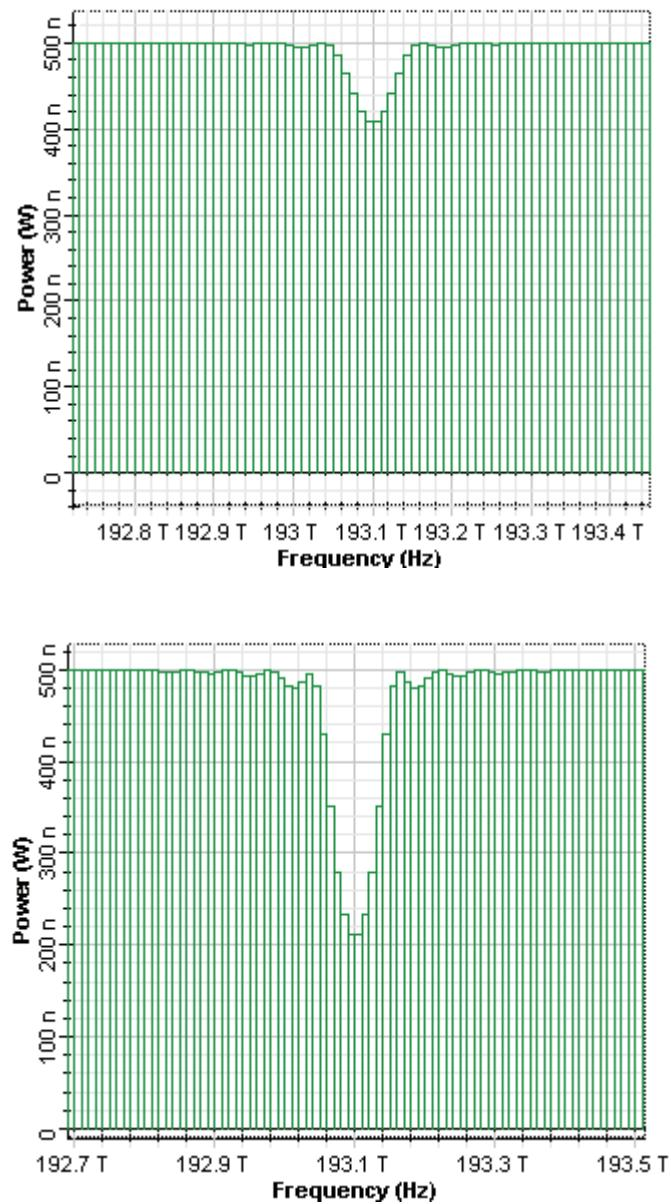
Because the reflectivity is connected with the product of coupling length and the length of the gratings (according to the existing exact solution [1]), this sweep corresponds to the change in the coupling length and/or the length of the grating. The comparison of the corresponding reflection spectrum is shown in Figure 4.

**Figure 4** Reflected spectrums from uniform Bragg grating for 0.19, 0.59 and 0.99 reflectivity

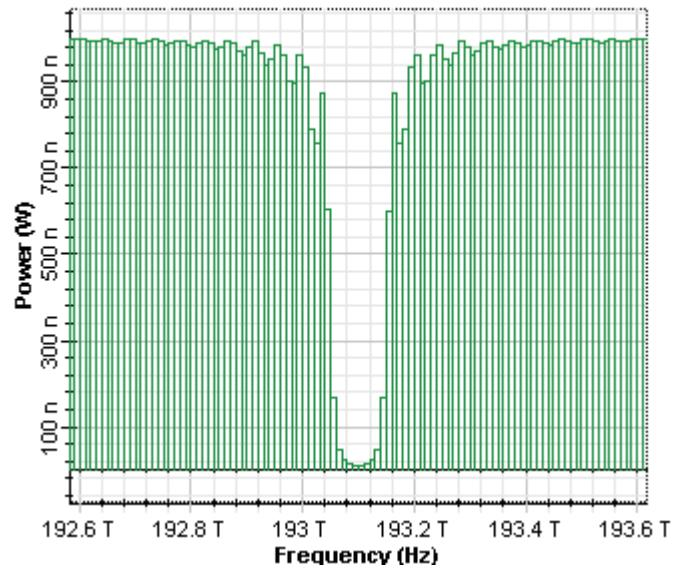


Obtained results are in a good agreement with what could be inferred from the exact solution for the amplitude reflection coefficient of uniform grating [1]. The corresponding transmission spectrums are shown in [Figure 5](#).



**Figure 5** Transmitted spectrums from uniform Bragg grating for 0.19, 0.59 and 0.99 reflectivity

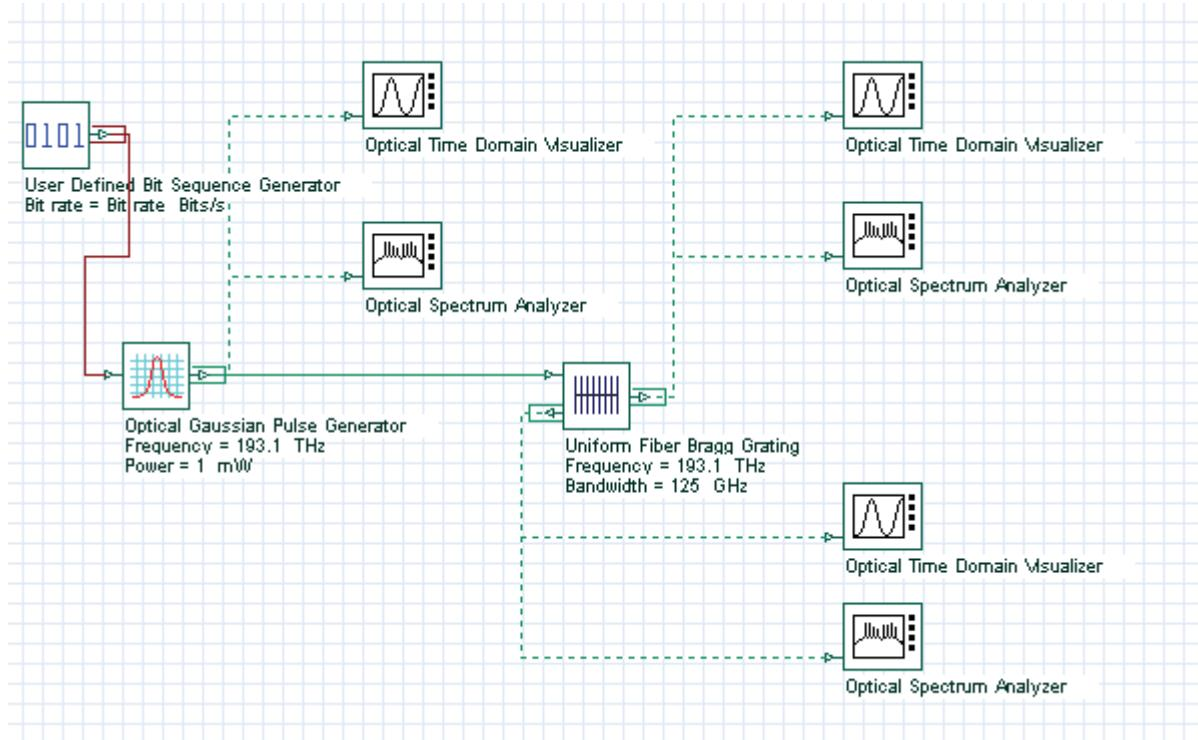
## UNIFORM FIBER BRAGG GRATING AS A FILTER



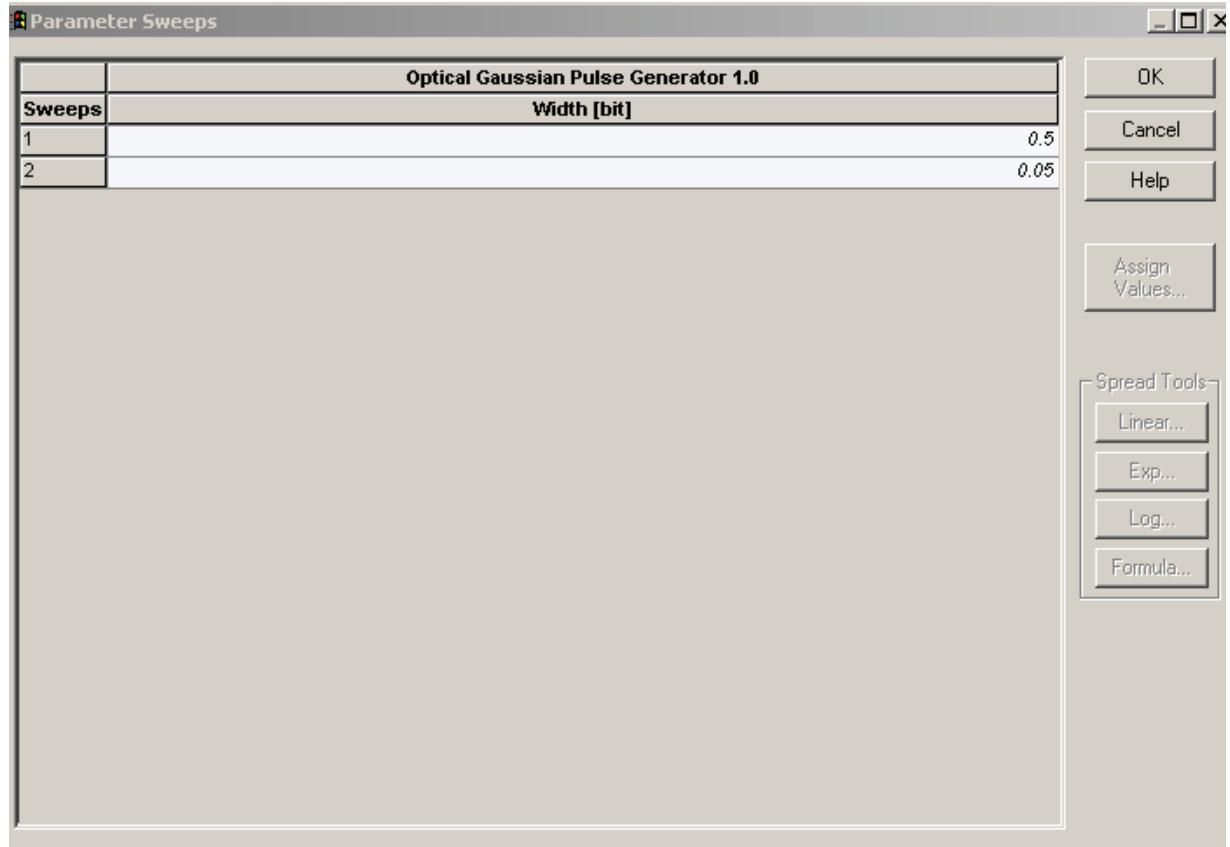
In the second layout, a filter action is demonstrated on the spectrum of Gaussian pulse.



**Figure 6 Project Layout for filter with uniform fiber Bragg grating component in OptiSystem using the Gaussian pulse**



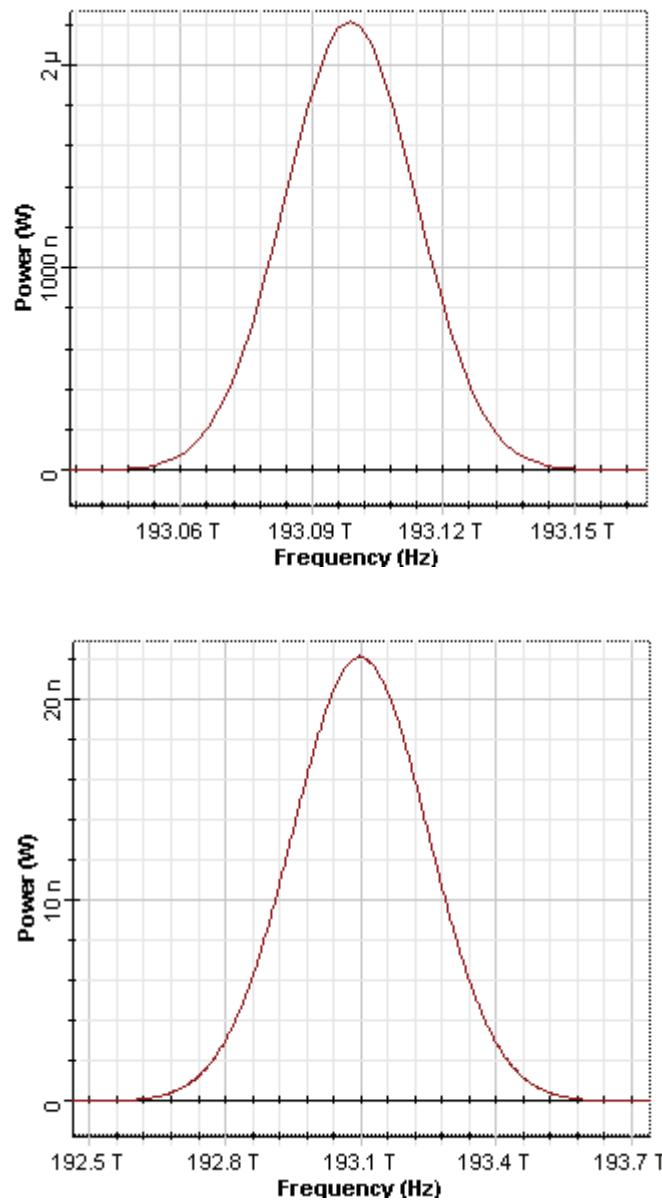
A sweep with the pulse width (0.5 and 0.05 duty cycle in the main tab of Gaussian generator) and respectively with the spectrum of the Gaussian pulses is performed.

**Figure 7 Sweep of the duty cycle**

The spectrum of initial Gaussian pulses are presented in [Figure 8](#)

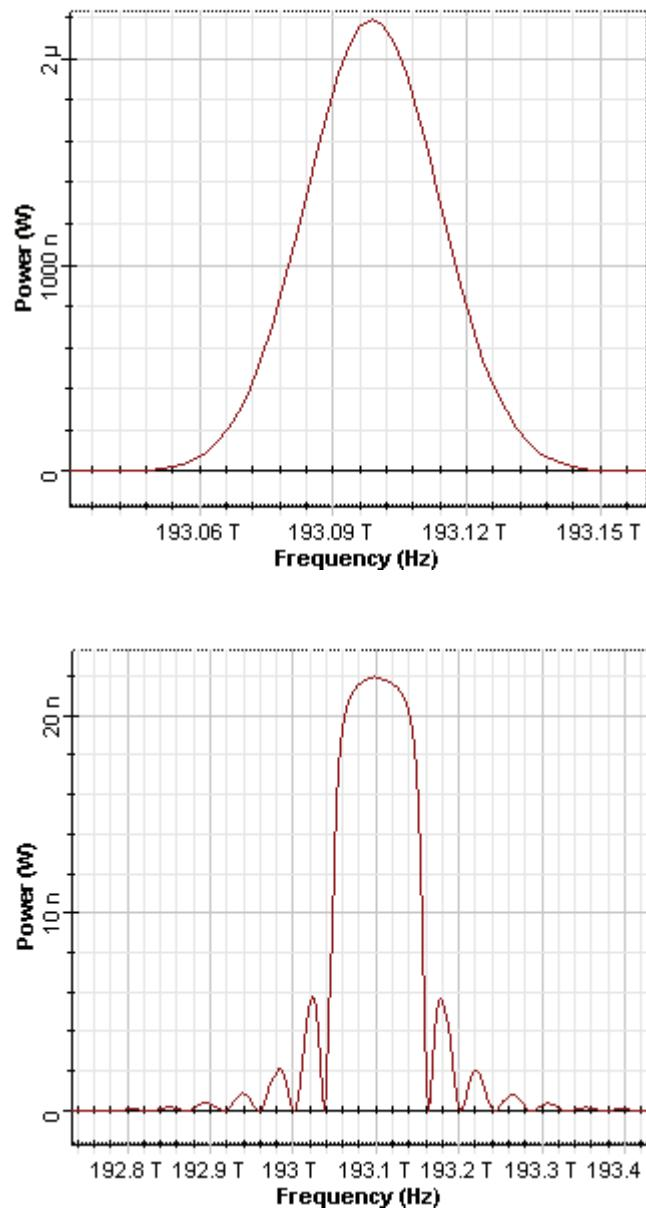


Figure 8 Initial spectrums of the Gaussian pulses, duty ratio 0.5 and 0.05 (12.5 ps and 1.25 ps, respectively)



The obtained reflection spectrums are presented in Figure 9.

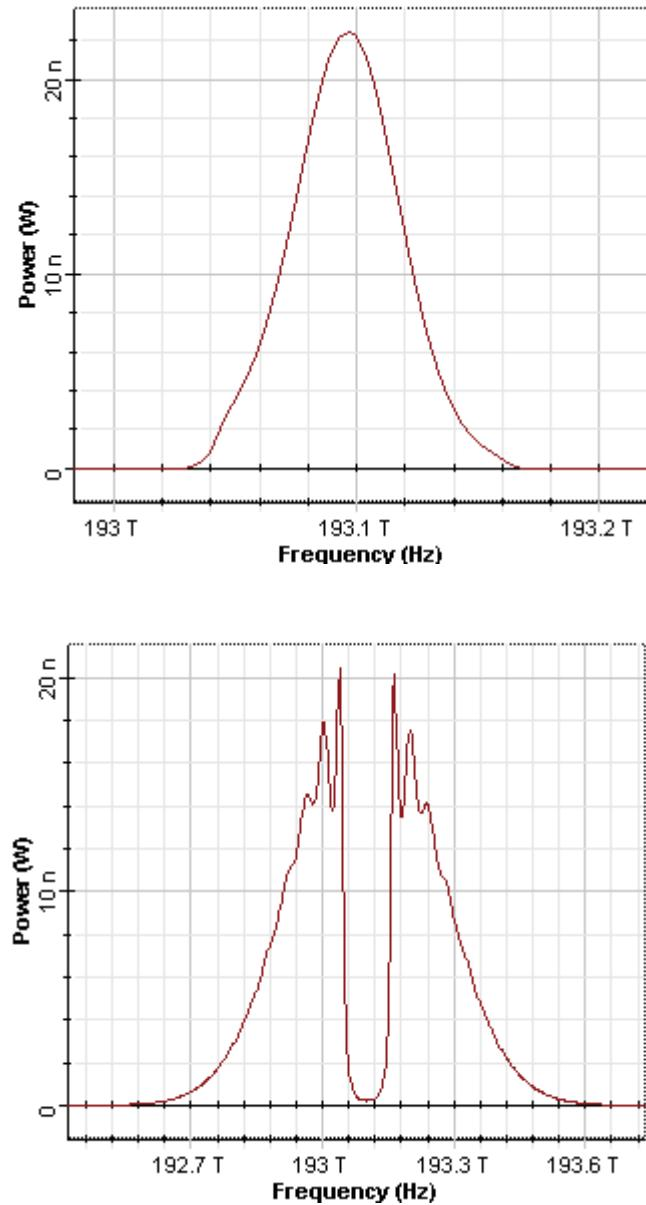
Figure 9 Reflected spectrums of the Gaussian pulses, duty ratio 0.5 and 0.05, respectively



The corresponding transmission spectrums are shown in [Figure 10](#).



**Figure 10 Transmitted spectrums of the Gaussian pulses, duty ratio 0.5 and 0.05, respectively**



As we can see, because in the second case the bandwidth of the grating (125 GHz) is much smaller than the pulse spectrum, a part of the spectrum of the pulse is reflected.

In conclusion, we have demonstrated the uniform fiber Bragg grating component in OptiSystem as a filter.

## References

- [1] S.Chang, Physics of Optoelectronics Devices, Wiley Series in Pure and Applied Optics, 1995.



# Compensation of dispersion with OptiGrating

---

This lesson demonstrates how OptiSystem can work with OptiGrating to design a proper dispersion compensation element in optical systems. The idea behind it is to use the additional possibilities provided by OptiGrating for design of fiber gratings.

The physical idea behind this compensation is following: creating of a linear chirped grating allows us to create a time delay between different spectral components of the signal.

For example, in SMF at 1.55 μm group velocity dispersion creates a negative chirp of the pulses, which means that the higher frequencies (which propagate faster) are in the leading part of the pulse and the lower (propagating slower) in the trailing one.

Because of this different velocity of propagation of different spectral components, the pulse spreads. If we create fiber grating with period linearly reducing along the grating, because of the fact that the higher frequencies will reflect after longer propagation in the grating, a time delay between lower and higher frequency components will appear which is just opposite to this created in the SMF.

Therefore propagating and reflecting our pulse in this device will allow to compensate the dispersion broadening of our pulse.

The dispersion coefficient  $D_g$  [ps/nm.km] for the linearly chirped fiber Bragg grating is given by the following simple expression [1]:

$$D_g = \frac{2n}{c\Delta\lambda_{chirp}}$$

where  $n$  is the average mode index,  $c$  is light velocity,  $\Delta\lambda_{chirp}$  is the difference in the Bragg wavelengths at the two ends of the grating (note that this quantity is given by the total chirp parameter in the grating definition tab in the Grating Manager of OptiGrating).

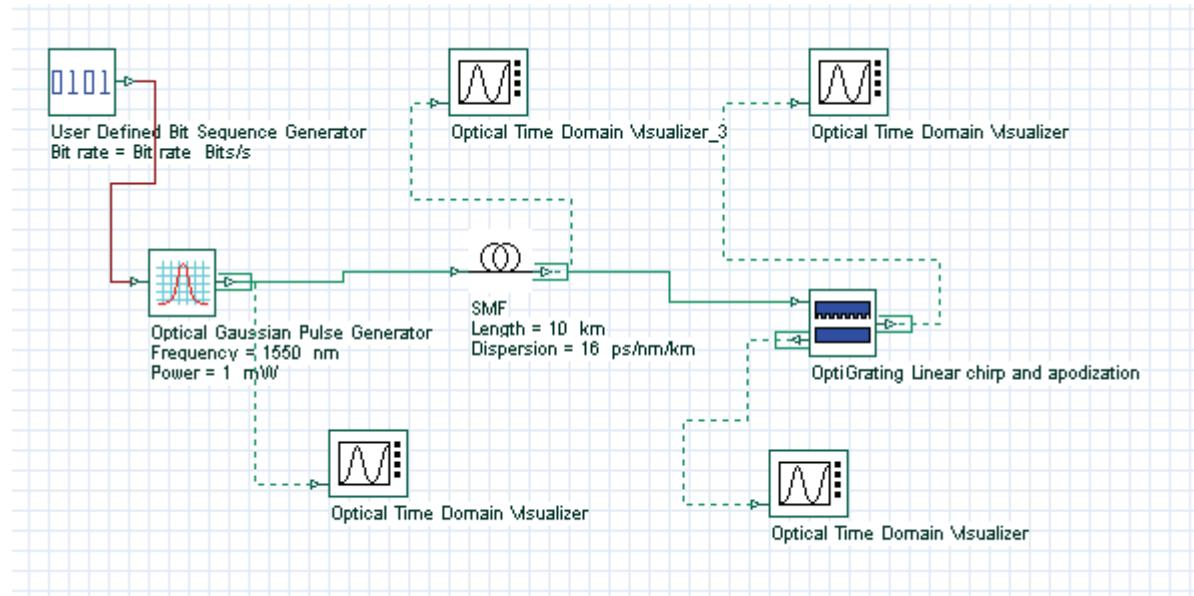
In the first layout:

- a. Linear chirped fiber Bragg grating. Linear chirped FBG.txt

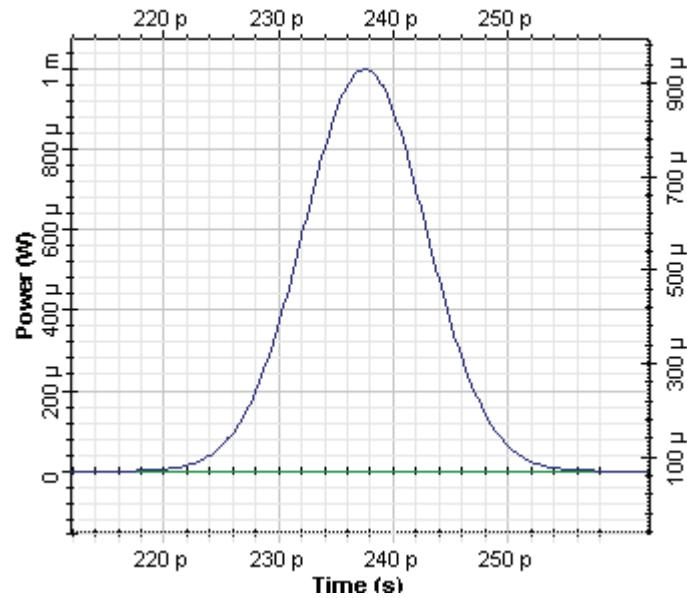
The aim of the first layout is to accomplish dispersion compensation in OptiSystem with the help of a fiber grating with linear chirp generated in accordance with the above formula.

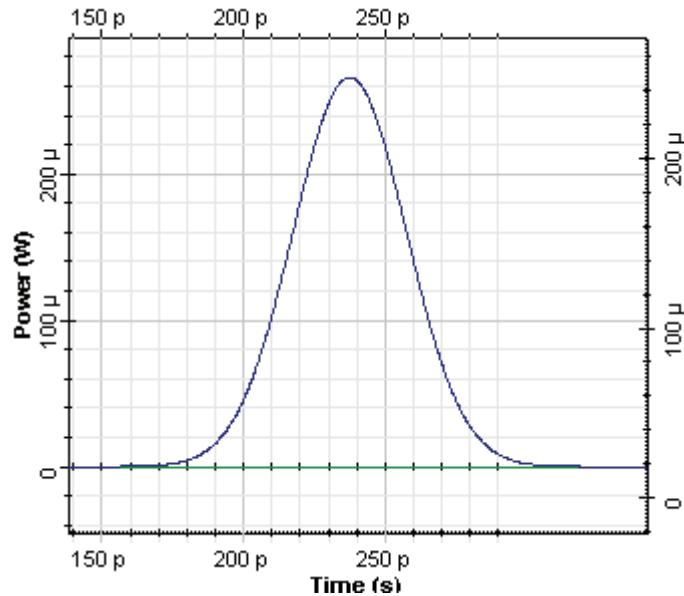
The project under consideration is in [Figure 1](#).



**Figure 1 Project Layout for dispersion compensation with fiber grating with linear chirp**

For bit rate 40 Gb/s and with 0.5 times bit slot, in the Optical Gaussian pulse generator, an initial 12.5 ps pulse was generated and propagated in 10 km SMF. Initial pulse and output from the SMF pulses are shown in [Figure 2](#) and [Figure 3](#).

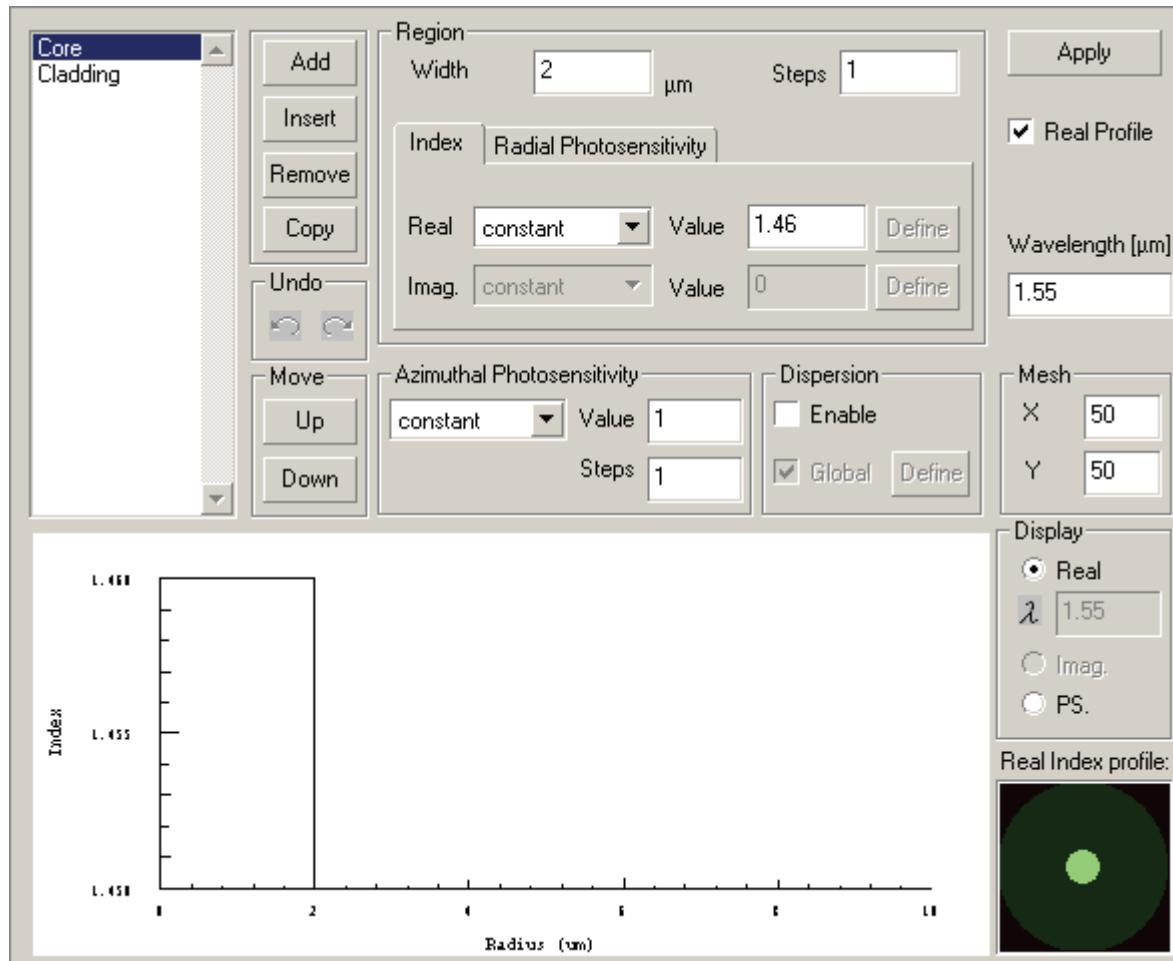
**Figure 2 Initial pulse**

**Figure 3** Pulse after 10 km propagation in SMF

As a result of dispersion, the pulse width increases to approximately 50 ps. The accumulated dispersion after 10 km propagation in SMF is of 160 ps/nm.

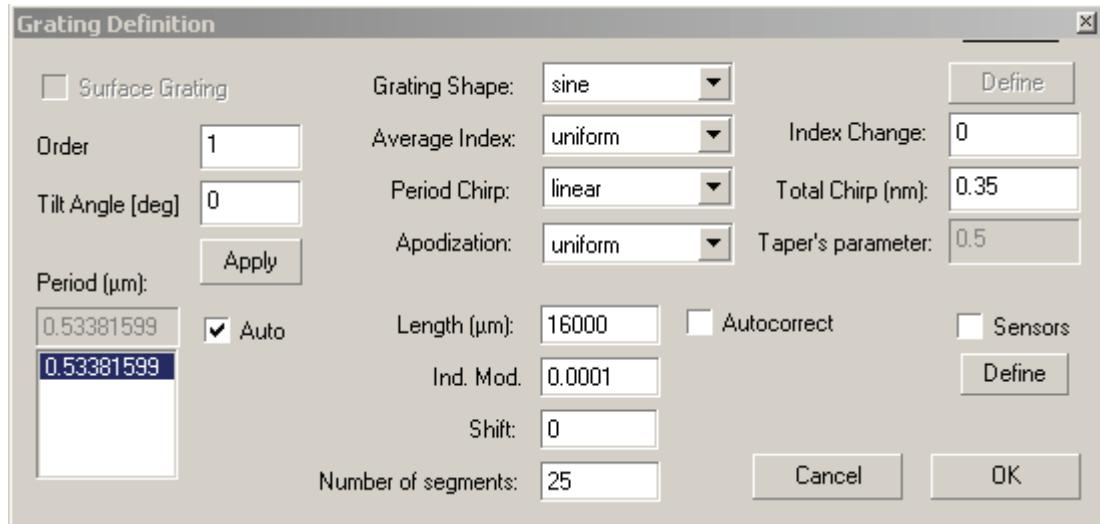
In order to compensate for the accumulated dispersion, we will use FBG designed by means of the file **Linear chirped FBG.ifo** in OptiGrating. The corresponding data for the fiber and the grating is shown in [Figure 4](#) and [Figure 5](#).

Figure 4 Core data



Step-index fiber with the widths of the core (refractive index 1.46) and the cladding (refractive index 1.45) 2 $\mu\text{m}$  and 8 $\mu\text{m}$ , respectively.

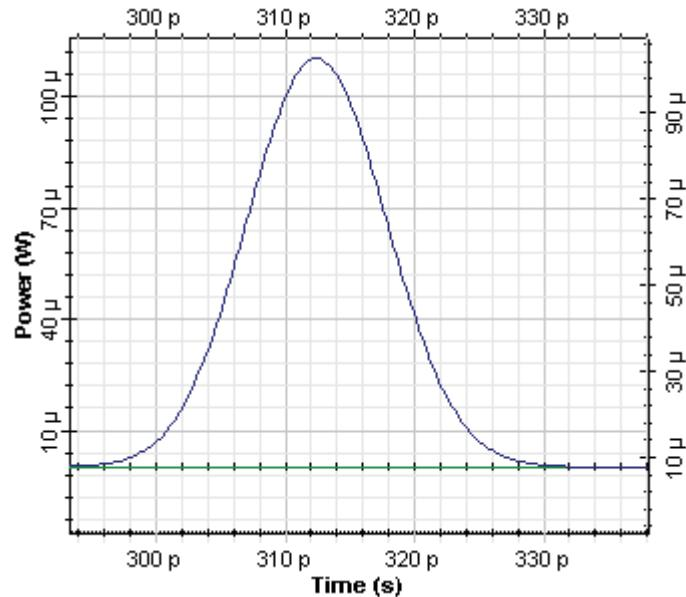


**Figure 5 Grating Definition dialog box**

We consider linear chirped FBG with chirped bandwidth  $\Delta\lambda_{chirp} = 0.35\text{ nm}$ . If we assume the average mode index  $\sim 1.46$  in accordance with the above formula, we get the required length of the grating from  $\sim 6$  mm for the compensation of 160 ps/nm accumulated dispersion in the SMF.

In the presented calculation, we have used the grating with slightly larger length  $\sim 1.6$  cm. Obtained results are saved in the file **Linear chirped FBG.txt**. This file is loaded in the **Linear Chirped FBG** component.

The obtained result of compensation is shown in [Figure 6](#).

**Figure 6 Pulse after dispersion compensation with linear chirped FBG**

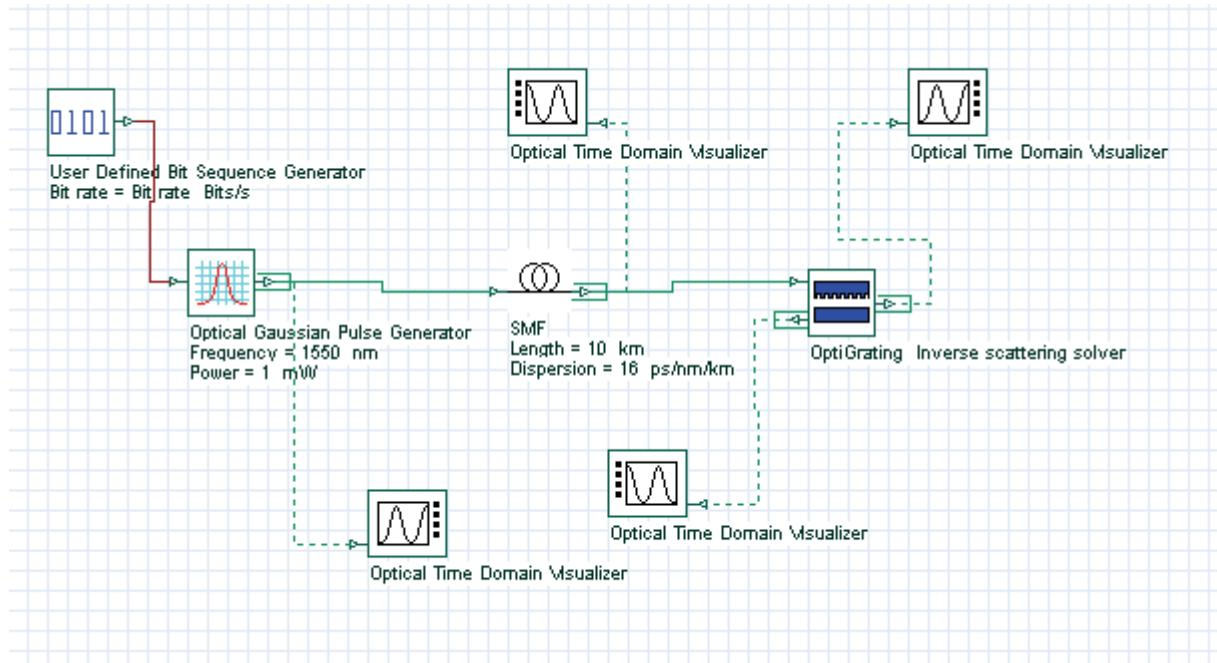
As we see, with designed by means of FBG practically complete dispersion compensation was achieved.

b. Fiber Bragg grating designed by means of inverse scattering algorithm

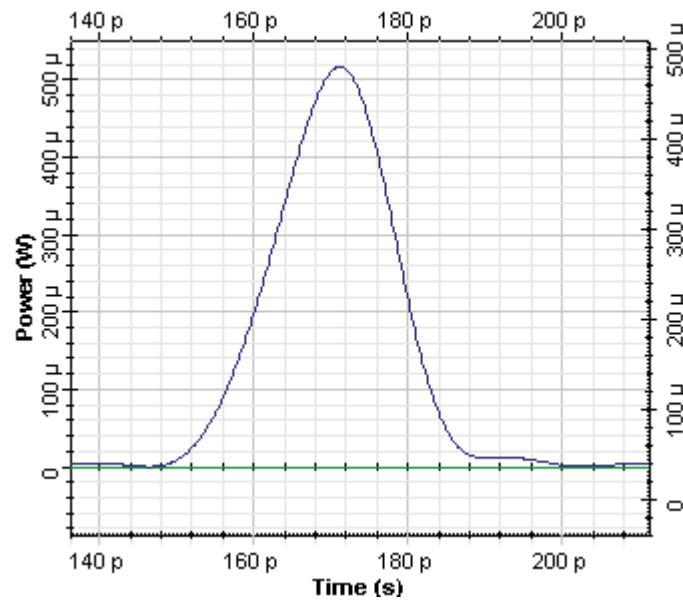
The aim of this layout is to perform dispersion compensation with the help of a fiber Bragg grating, designed with the inverse scattering algorithm of OptiGrating.

Such FBG is created with the help of OptiGrating's file **Lesson7. oad**. The requirement in designing of this FBG is that it has to produce accumulated dispersion of -160 ps/nm. The obtained spectrum is saved in **Complex Spectrum 7 Lesson.txt**.



**Figure 7 Project Layout for dispersion compensation with FBG with inverse scattering algorithm**

The result from the dispersion compensation of accumulated dispersion in SMF is shown in [Figure 8](#).

**Figure 8 Pulse after dispersion compensation with fiber grating FBG generated in OptiGrating with inverse scattering algorithm and - 160 ps/nm accumulated dispersion**

As we see, designed in this way, FBG allows to reduce the pulse width to approximately 17 ps.

To sum up, in this lesson we have demonstrated how the dispersion compensation in OptiSystem can be achieved using a reflection spectrum obtained with the gratings designed by means of OptiGrating.

## References

- [1] G.P. Agrawal, "Fiber-optics communication systems", Wiley Inter-Science, 2002

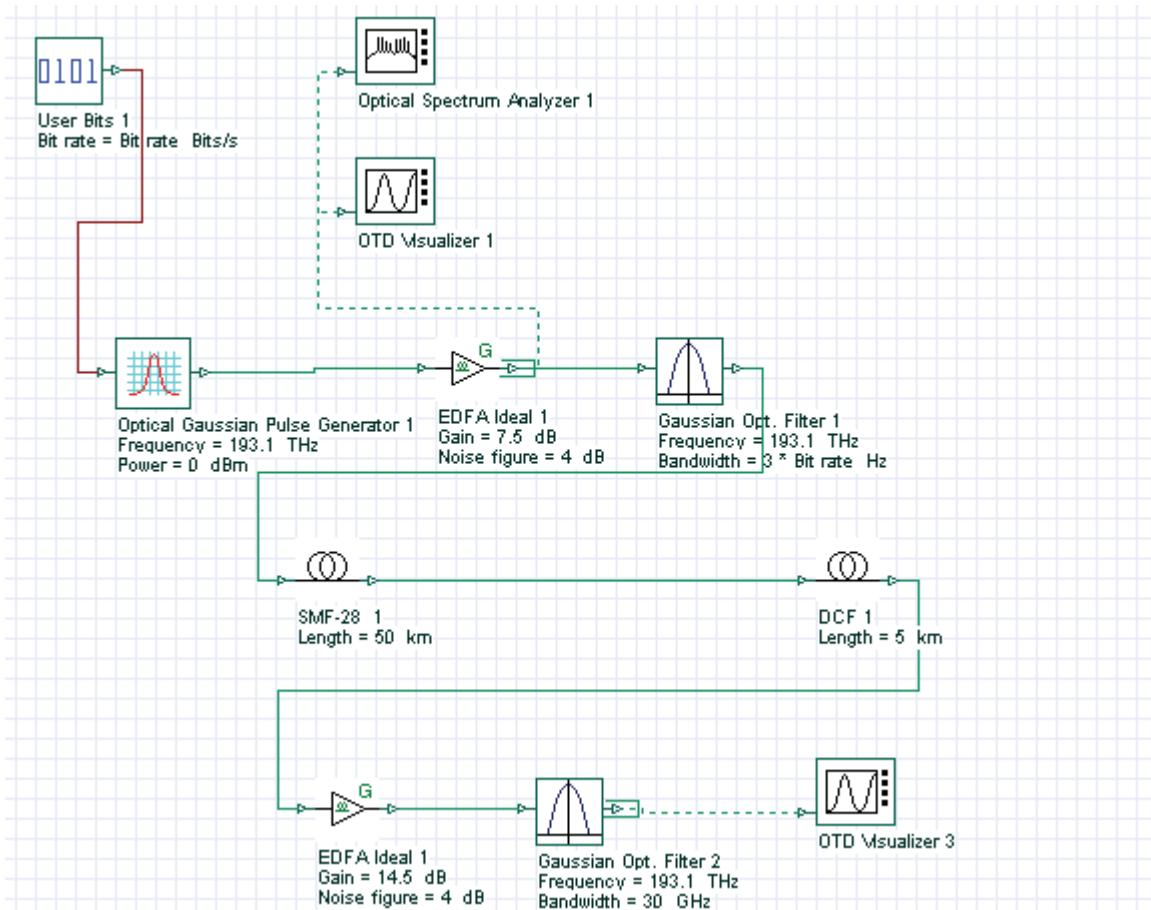


# Dispersion compensation using subsystems

This lesson illustrates how to simulate a simple dispersion compensated link elaborating further the concepts of subsystem definition.

Let us set up the following layout, which includes:

**Figure 1 Dispersion compensated link span**



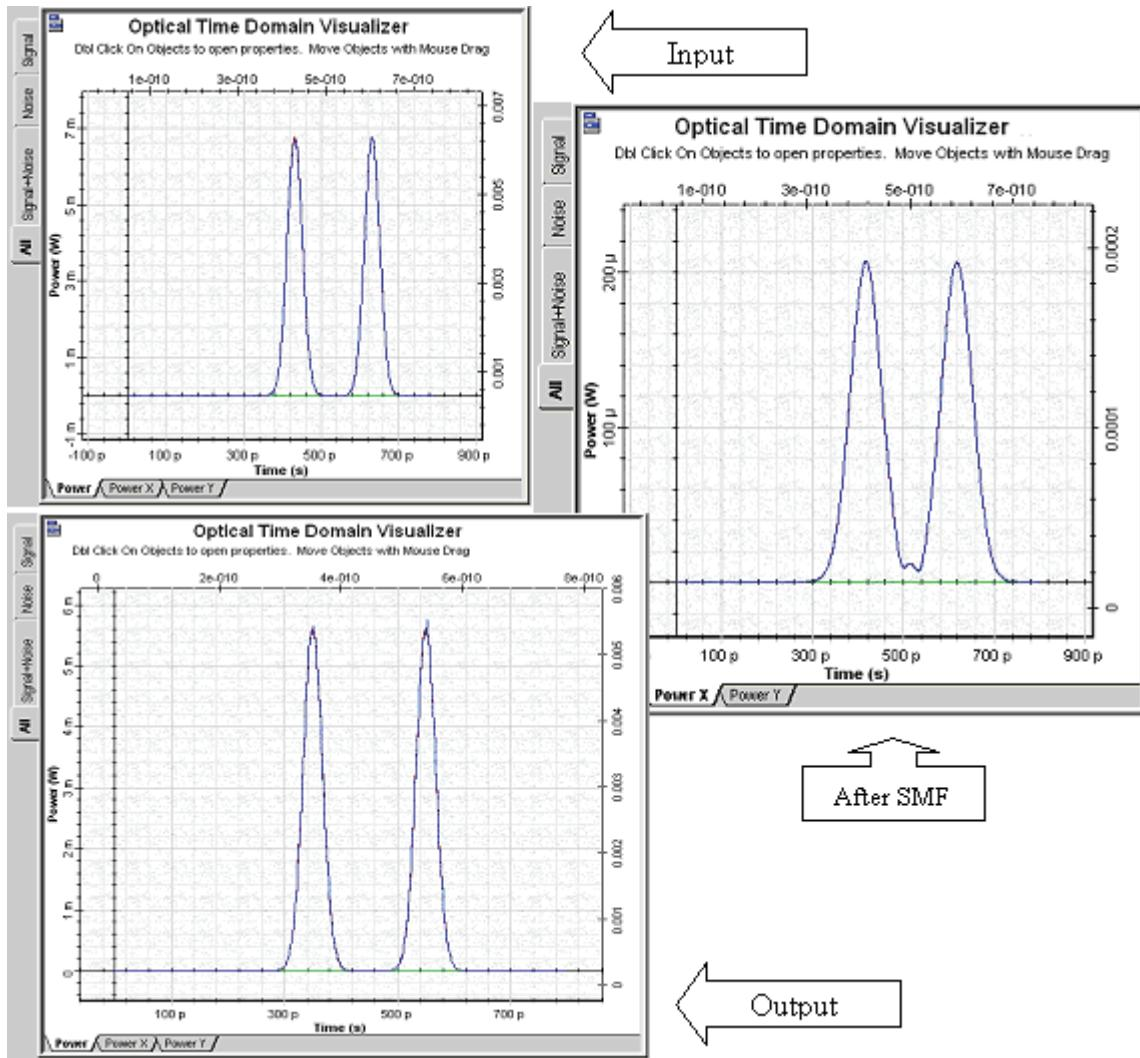
- An abstract source of Gaussian RZ pulses according to a user defined bit sequence
- Booster amplifier and filter
- SMF and DCF
- Inline amplifier and filter
- Visualizers

Let us examine the signal waveforms at the input, after the SMF and at the end of the span. One can observe that after the SMF the signal pulses are attenuated,



broadened by a factor of approximately 2 and that there is considerable inter-symbol interference.

**Figure 2** Signal evolution in a dispersion compensated link span



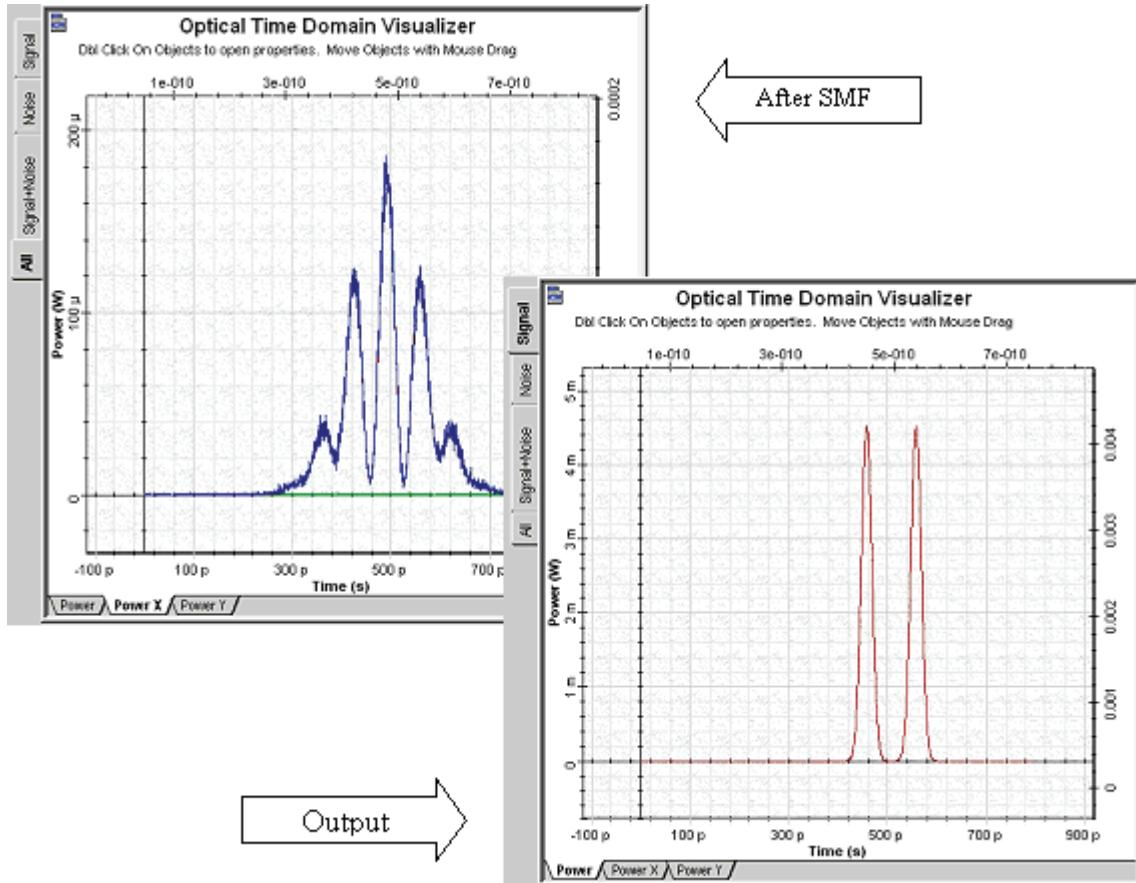
We can now use the powerful scripting feature of OptiSystem in order to avoid the necessity to redefine those of the layout parameters that depend on the signal in case input signals change. One such parameter is the bandwidth of the two inline filters. Open the filter parameter dialog box and switch the **Mode** of the **Bandwidth** to **Script**. Right-click In the value field and select **Bit rate**. Then add **3 \*** so that the whole field reads **3 \* Bit rate**.

Click on the layout work space and show the **Global parameters** dialog box. Increase the bit rate twice and recalculate. The following figure shows that regardless of the



severe dispersive broadening in the SMF, the signal is again preserved after the whole span, both in terms of power and pulse shape.

**Figure 3 Results of the scripted calculations of a dispersion compensated link span**

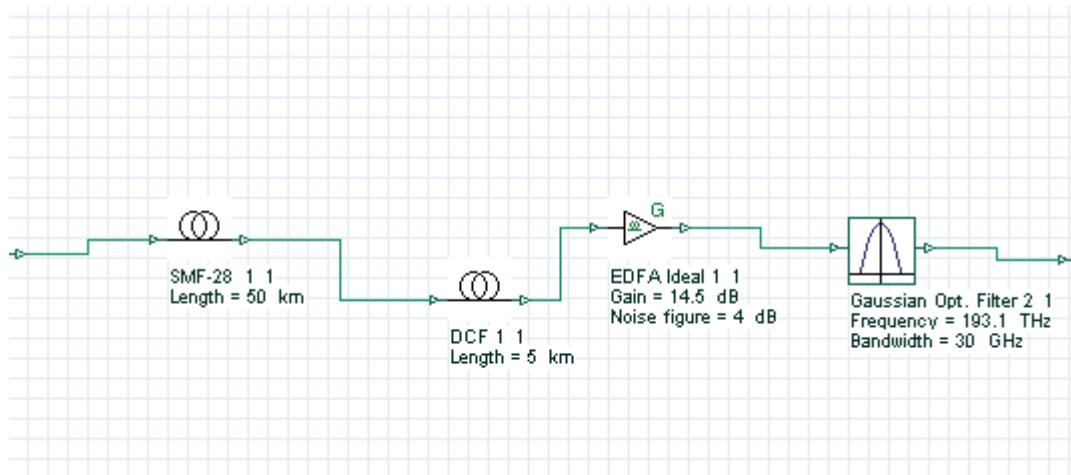


Chances are that this single link might be useful for building longer multi-span systems. In that case it is recommended to encapsulate it into a sub-system, which would later on allow reproducing the same combination of components quickly and efficiently.

We create a new design version, selecting **Design Version/ Add Design Version** from the main menu of OptiSystem and change its name to **Amplified Dispersion Compensating Subsystem**. After that we copy and paste all the components of Version 1 in it.

Next, as shown in [Lesson 2: Subsystems — Hierarchical simulation](#), we select all the components, except the signal source and the booster amplifier (including or skipping the visualizers), and select **Create subsystem** from the right click context menu. Our layout collapses into the visual representation of a subsystem. First we create an output port in the subsystem by selecting **Look Inside** from the right-click menu and using the **Output port** tool. After that we can change the name of the new subsystem to something informative, for instance **Amplified Dispersion Compensated Span**, using the **Component Parameters** menu item.

**Figure 4** The dispersion compensated span represented as a subsystem

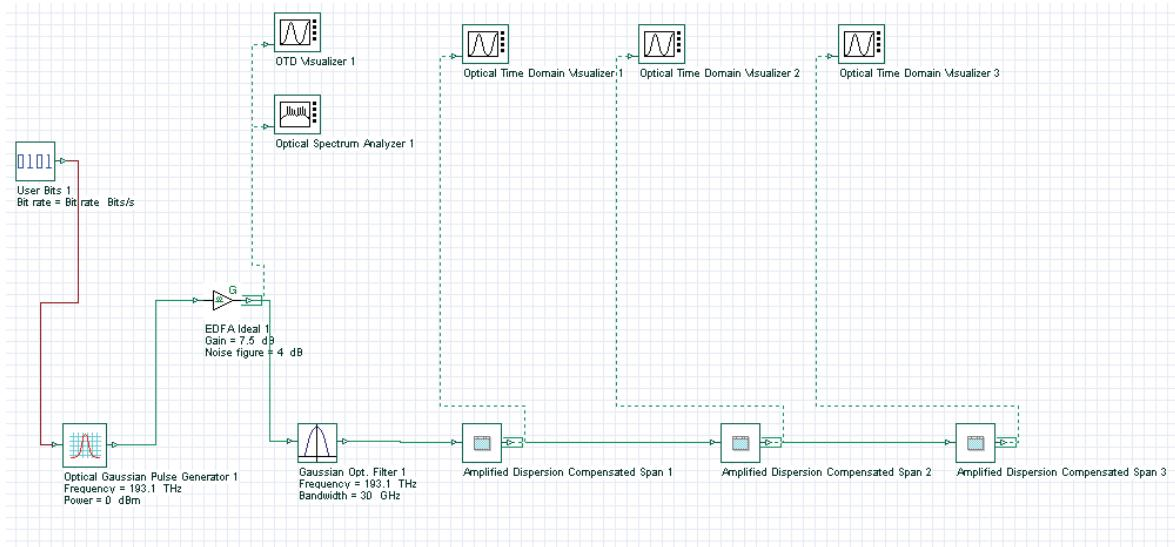


Next we can use the newly created subsystem to build longer multi-span links. Let us create another design version and change its name to "Multi-Span Link". After that, we copy and paste all the components of "Amplified Dispersion Compensating Subsystem" in it.



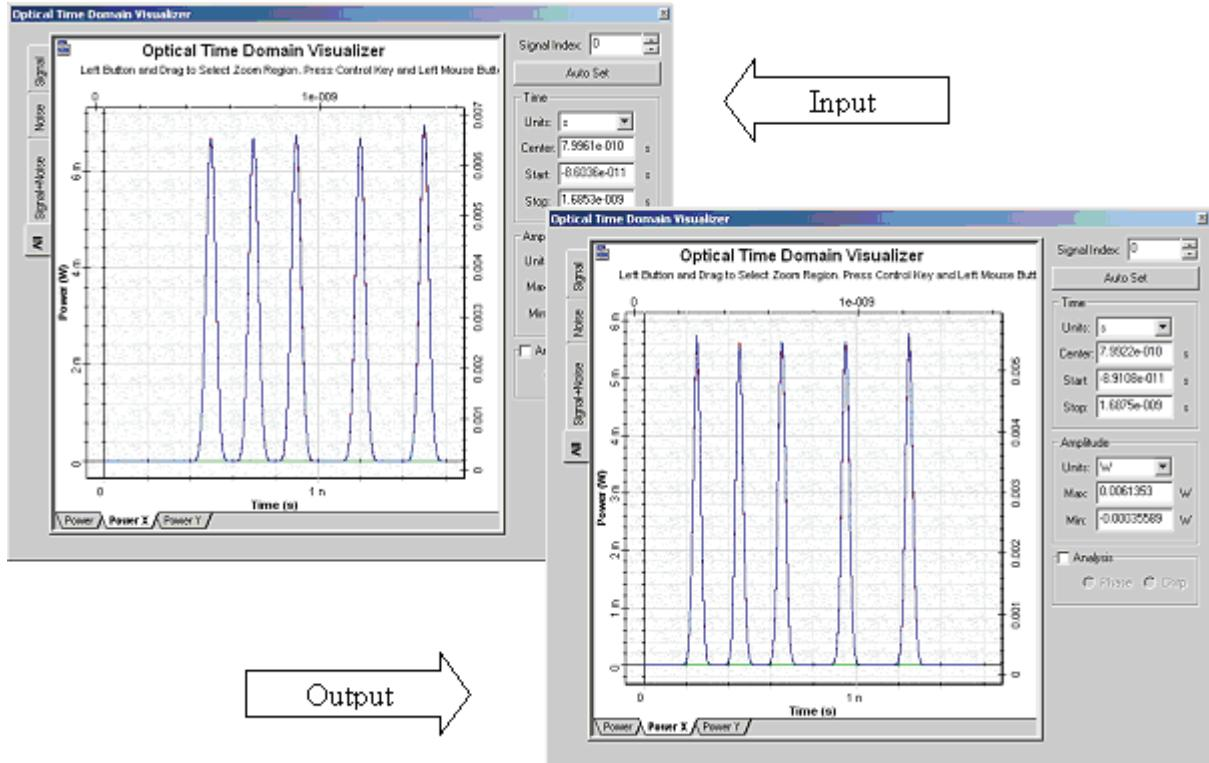
Now we can arrange a three span system by copying and pasting the "Amplified Dispersion Compensated Span" subsystem component and linking the respective input and output ports.

**Figure 5 Building multi-span system using the user defined subsystem**



Let us now define a more complex waveform and perform the calculation. After that we can display and compare the input and output signals in terms of their amplitude and pulse shape.

Figure 6 Input and output waveforms of the dispersion compensated links

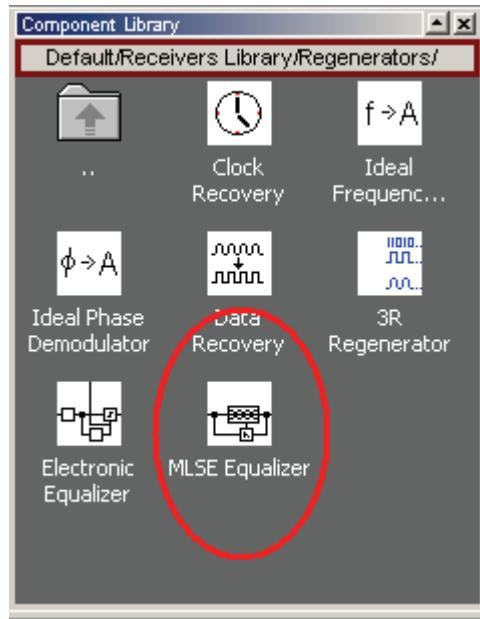


# Maximum-likelihood sequence estimation (MLSE) equalizer

---

This project **MLSE Application.osd** demonstrates the application of the component 'MLSE Equalizer'. The MLSE Equalizer component is available in the OptiSystem component library folder 'Default/Receivers Library/Regenerators' (Figure 1).

Figure 1 OptiSystem component library



The system layout is presented in Figure 2. A 10 GB/s BPSK signal is generated by the 'BPSK Generator' component. The signal is then applied to a propagation channel. The propagation channel is an FIR filter with coefficients [1 0.8 0.3], that simulates a time dispersive channel that causes intersymbol interference (ISI). The signal is then applied to the MLSE equalizer component that will compensate the signal dispersion.

The channel estimation is done in the MLSE equalizer using the same coefficients as the FIR filter. The coefficients are loaded from a text file (FIR.dat -Figure 3).

Figure 2 System layout

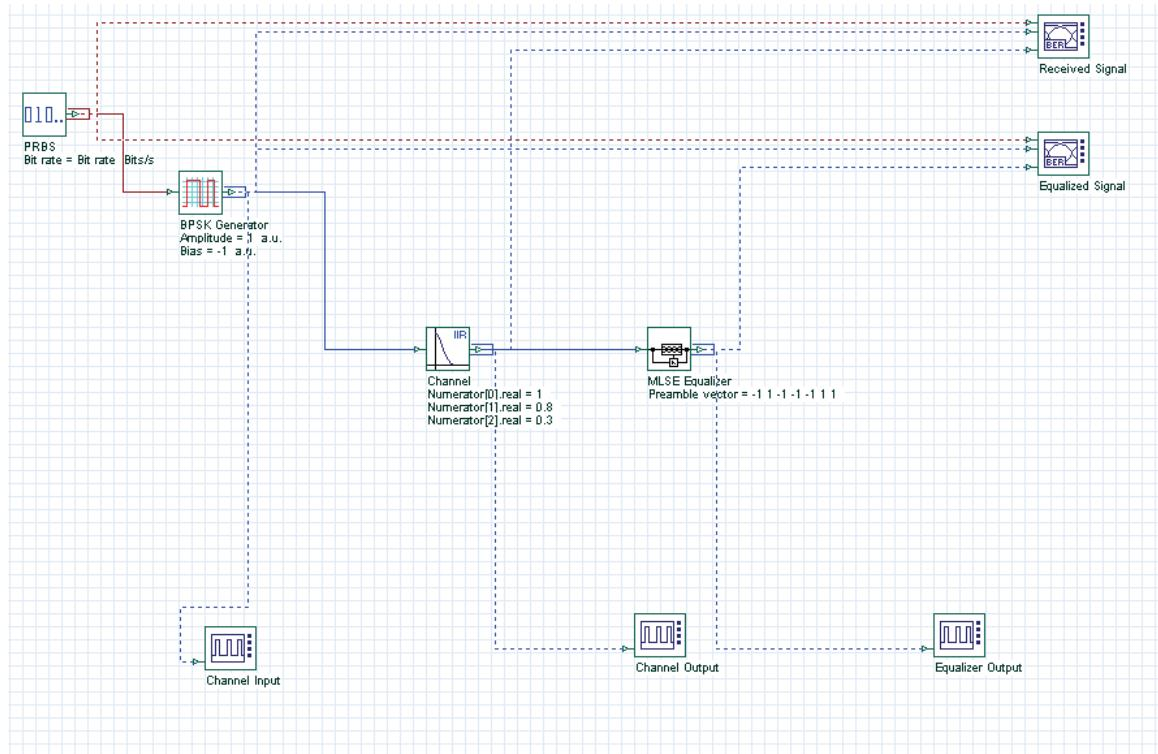
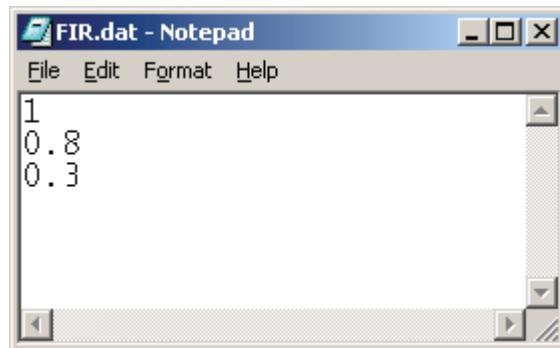
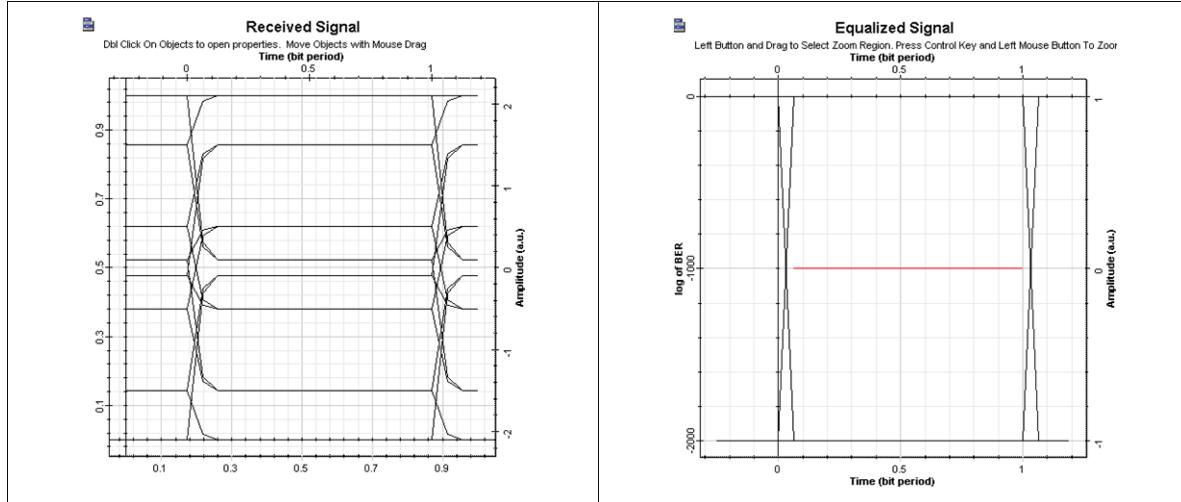
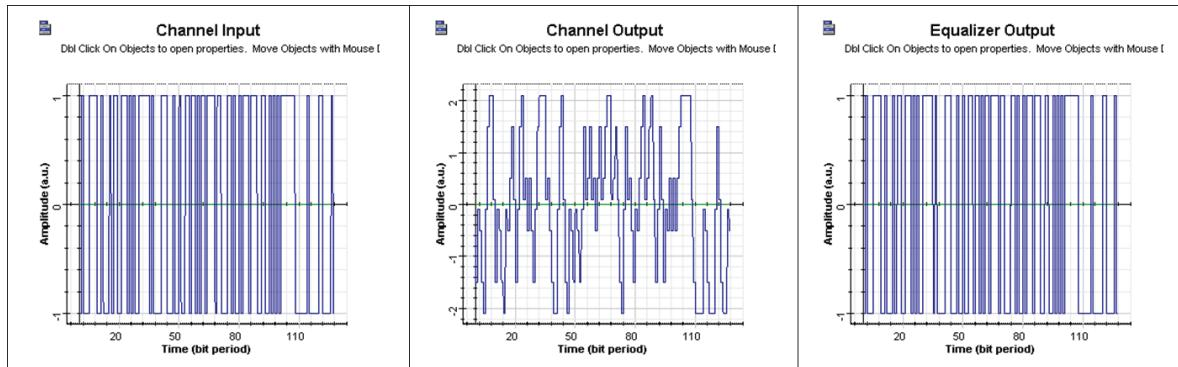


Figure 3 Filter coefficients



The MLSE equalizer can also use an optional preamble. [Figure 4](#) presents the eye diagram before and after the equalizer. [Figure 5](#) presents the signal evolution from the channel input to the equalizer output. The equalizer mitigates ISI and improves the system's performance.



**Figure 4 Eye diagram before and after the equalizer****Figure 5 Signal propagation in the system**

**Notes:**

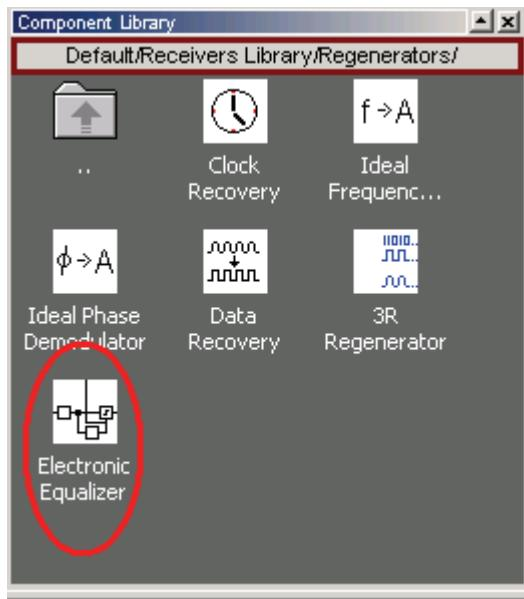


# DFE - Decision-Feedback Equalizer

---

Project **DFE Application.osd** demonstrates the application of the component 'Electronic Equalizer'. The Electronic Equalizer component is available in the OptiSystem component library folder 'Default/Receivers Library/Regenerators' ([Figure 1](#)).

**Figure 1** OptiSystem component library



The system layout is presented in [Figure 2](#). A 10 GB/s BPSK signal is generated by the 'BPSK Generator' component. The signal is then applied to a propagation channel. The propagation channel is an IIR filter with coefficients [1 0.8 0.3], that simulates a time dispersive channel that causes intersymbol interference (ISI). The signal is then applied to the electronic equalizer component that will compensate the signal dispersion.

The channel estimation is done in the MLSE equalizer using the same coefficients as the FIR filter. The coefficients are loaded from a text file (FIR.dat -[Figure 3](#)).

Figure 2 System layout

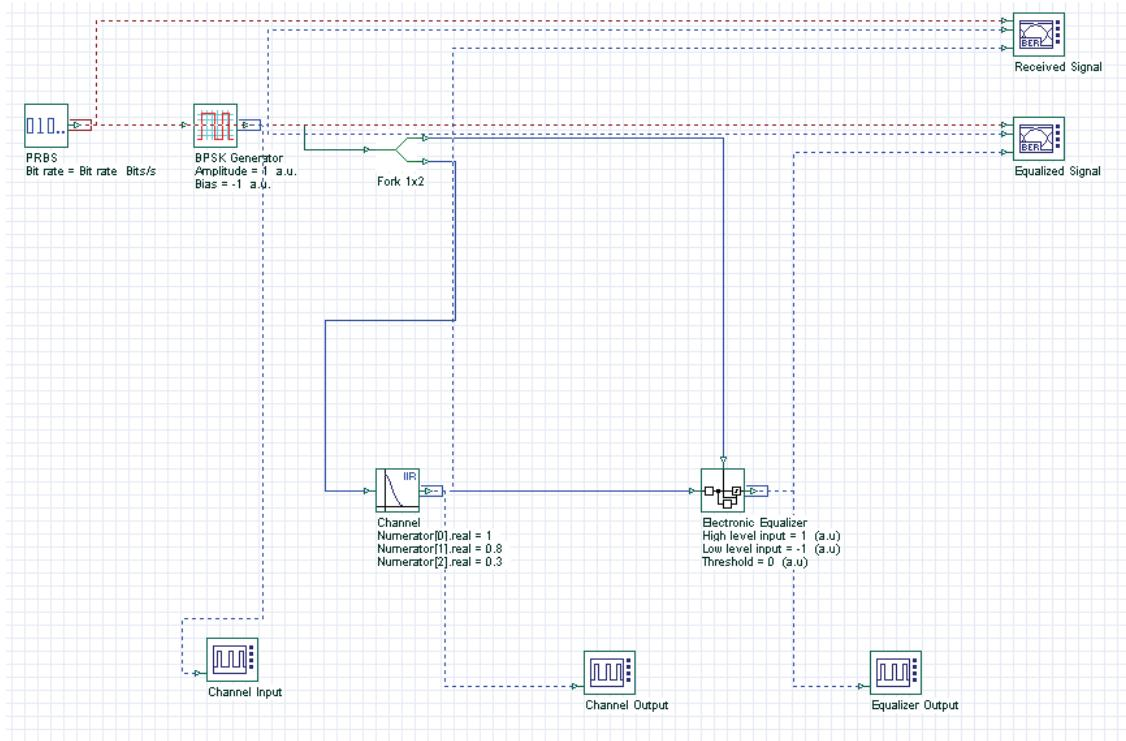
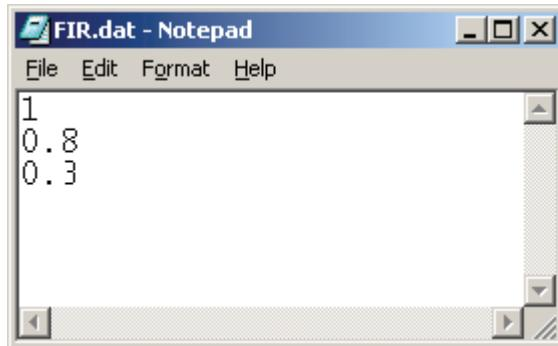
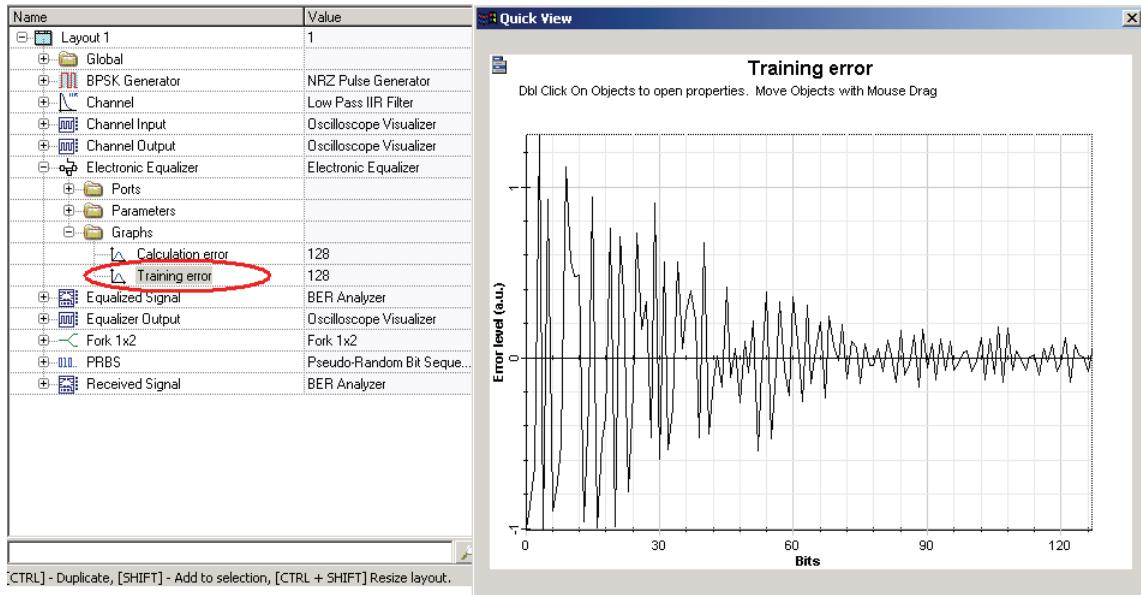
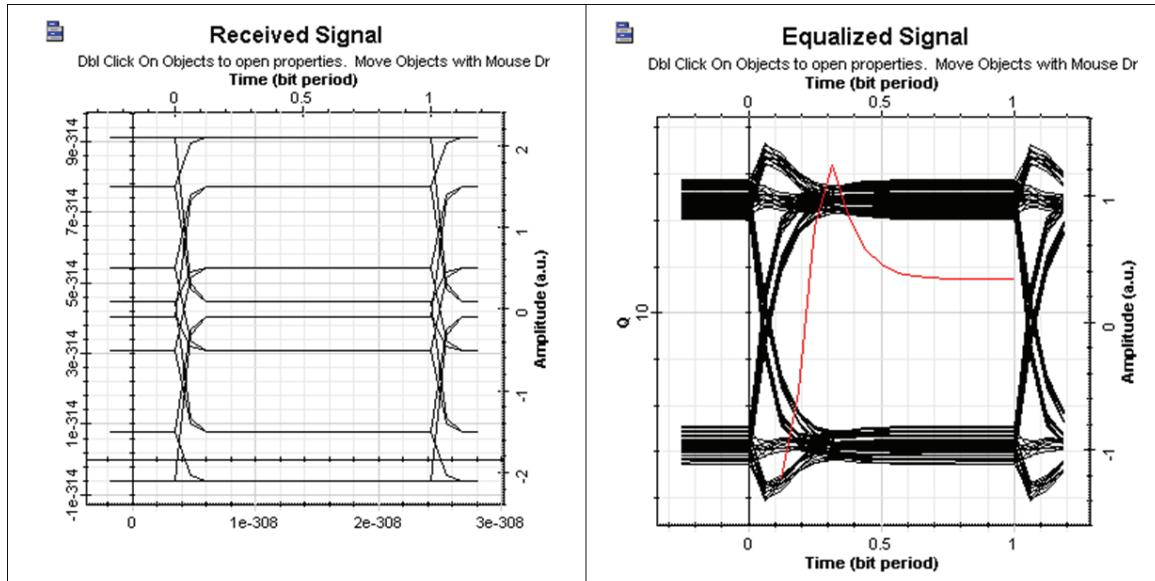


Figure 3 Equalizer coefficients after training

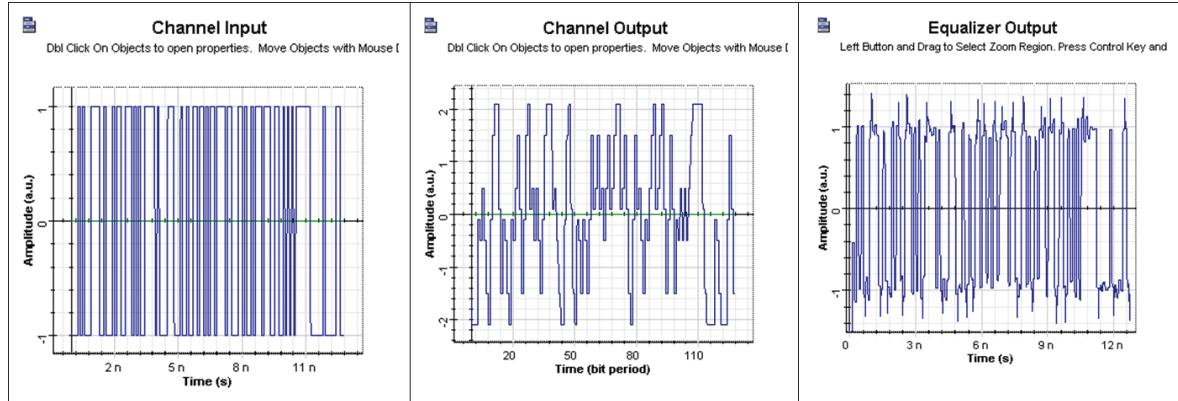


The electronic equalizer will use the original BPSK signal as a training signal to calculate the filter tap coefficients for the FFE and DFE stages. After the calculation, the values of the tap coefficients are available in the parameter Report (Figure 3), and the values for the calculated error during training are available as a graph in the project browser (Figure 4).

Figure 5 presents the eye diagram before and after the equalizer. Figure 6 presents the signal evolution from the channel input to the equalizer output. The equalizer mitigates ISI and improves the system's performance.

**Figure 4 Error level during training****Figure 5 Eye diagram before and after the equalizer**

**Figure 6 Signal propagation in the system**



# Dispersion compensation using electronic equalization

Project **Equalizer GVD.osd** demonstrates the application of the equalizer in an optical link (Figure 1). Figure 2 depicts the eye diagram before and after dispersion compensation.

Figure 1 GVD compensation

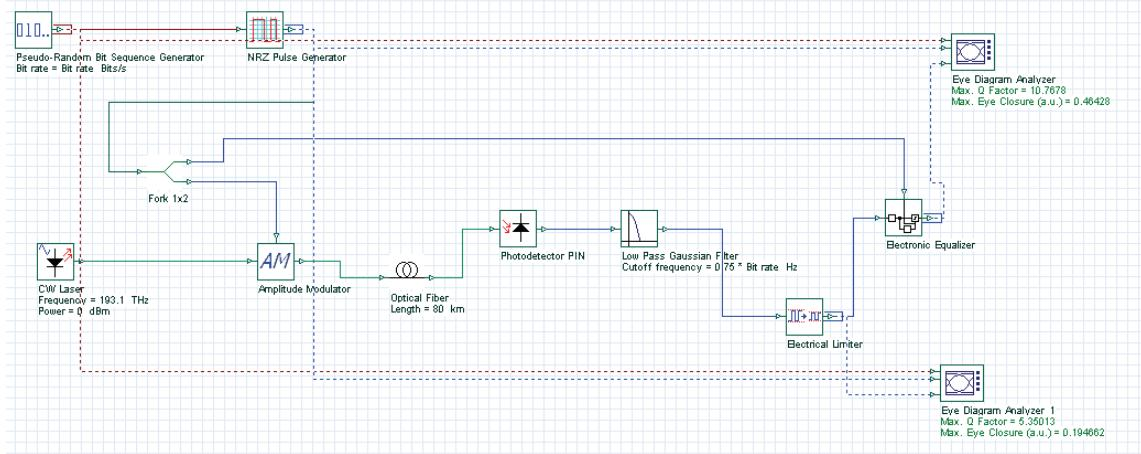
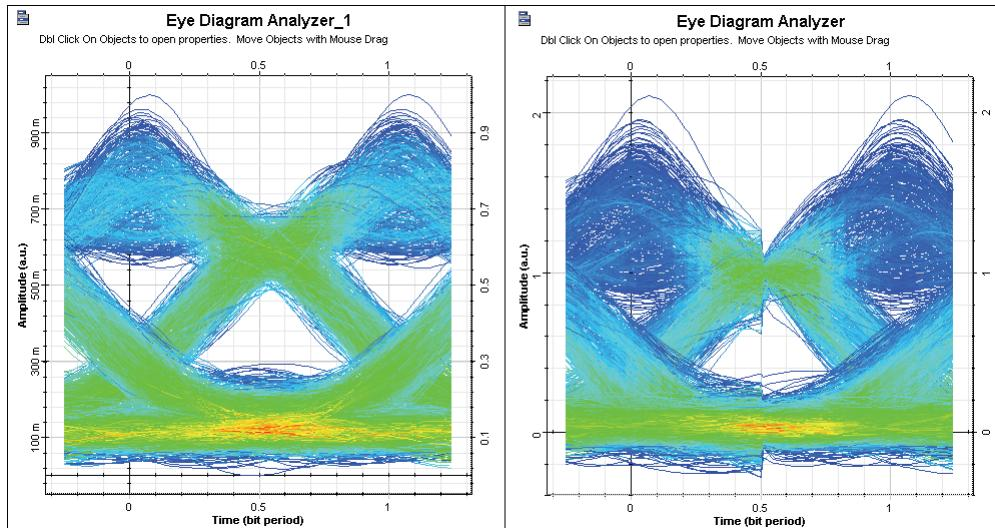


Figure 2 Eye diagram before and after the equalizer



**Notes:**

---

# Lightwave systems

---

This section begins with an introduction to lightwave system components.

This section contains the following advanced and illustrative simulation projects.

- Optimizing the power and dispersion compensation for nonlinear RZ transmission
- 10 Gb/s single channel transmission in standard mode fibers (SMF)
- 40 Gb/s single channel transmission in standard mode fibers (SMF)
- Engineering the fiber nonlinearities and dispersion
- System design — Power budget
- Time Division Multiplexing (TDM)
- Broadband optical system based on a Passive Optical Network (BPON)
- Optical code-division multiple-access system (OCDMA)
- Free Space Optics (FSO)
- Coherent Optical Transmission
- Radio over fiber (RoF)
- Optical Time Domain Multiplexing (OTDM) Design
- System Performance Analysis Using Script Automation

**Notes:**



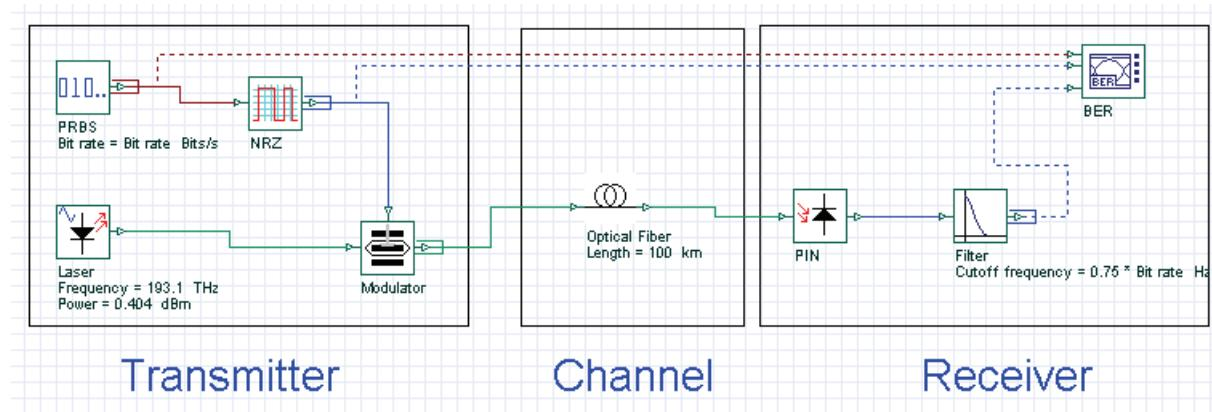
# Lightwave system components

**FOCS Introduction Lightwave System Components.osd** details a generic block diagram of an optical communication system.

An optical communication system consists of a:

- transmitter
- communication channel
- receiver (see [Figure 1](#))

**Figure 1** Lightwave System Components



## Optical transmitter

The role of the optical transmitter is to:

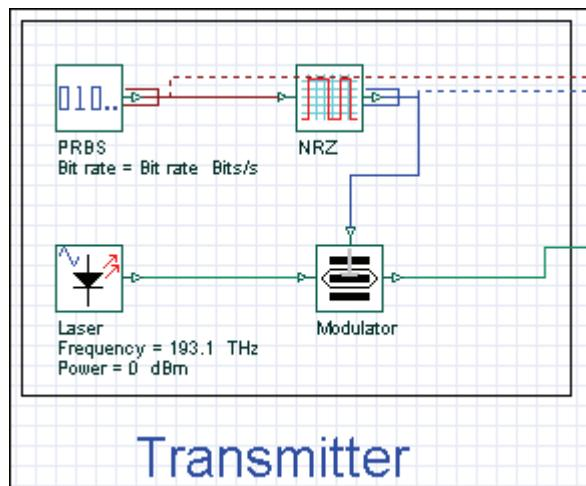
- convert the electrical signal into optical form, and
- launch the resulting optical signal into the optical fiber.

The optical transmitter consists of the following components:

- optical source
- electrical pulse generator
- optical modulator (see [Figure 2](#)).

The launched power is an important design parameter, as it indicates how much fiber loss can be tolerated. It is often expressed in units of dBm with 1 mW as the reference level.

Figure 2 Transmitter components



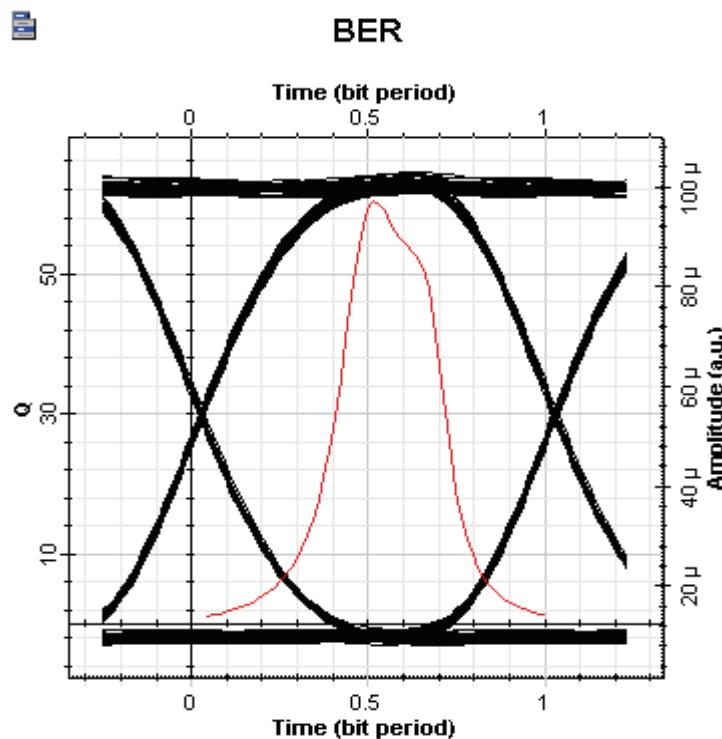
## Communication channel

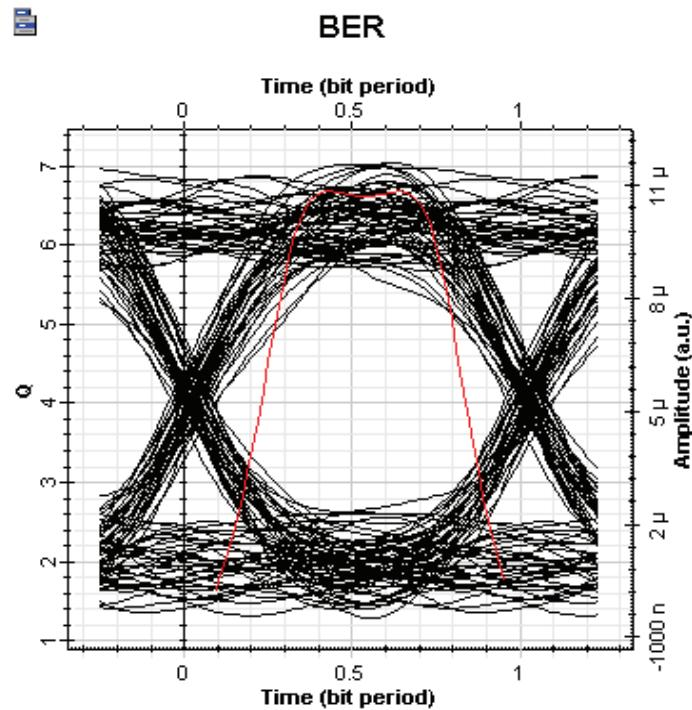
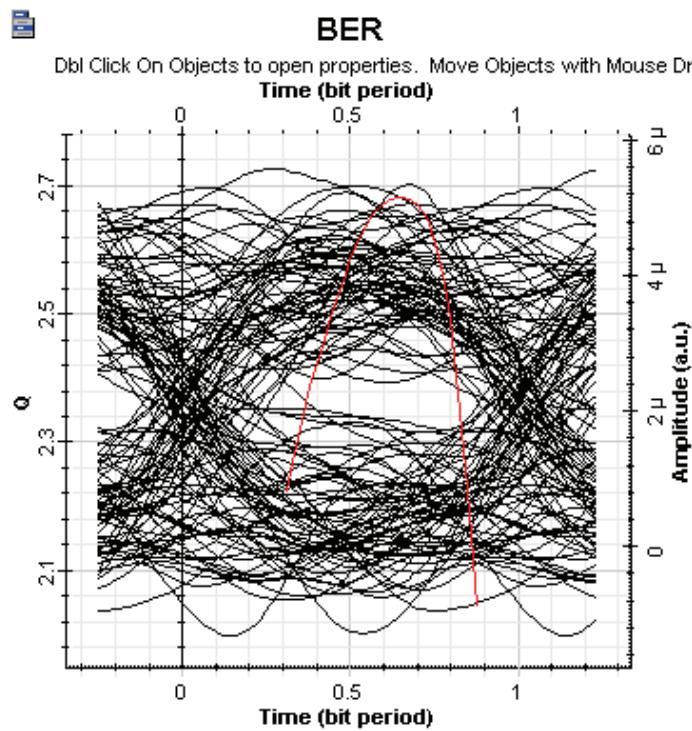
The role of the communication channel is to transport the optical signal from transmitter to receiver without distorting it. Most lightwave communication systems use optical fibers as the communication channel because fibers can transmit light with a relatively small amount of power loss.

Fiber loss is, of course, an important design issue, as it dictates the repeater spacing of a long-haul lightwave system. Another important design issue is fiber dispersion, which leads to broadening of individual pulses inside the fiber.

In order to observe the effects of loss and dispersion in the optical signal, you can change the values of fiber length and visualize the degradation of the signal at the receiver stage.

**Figure 3 Fiber 60 km**



**Figure 4 Fiber 100 km****Figure 5 Fiber 120 km**

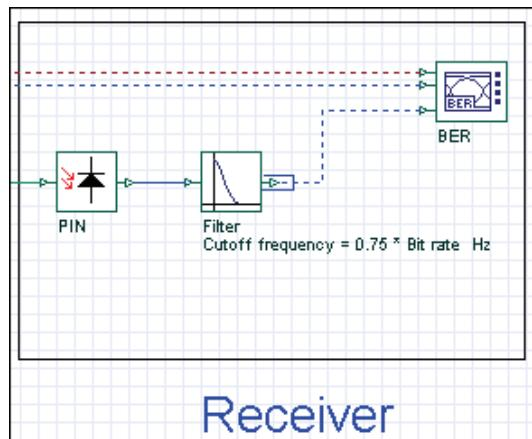
## Optical receivers

An optical receiver converts the optical signal received at the output end of the optical fiber back into the original electrical signal.

The receiver consists of the following components:

- photodetector
- filter
- demodulator (see [Figure 1](#))

**Figure 1 Receiver components**

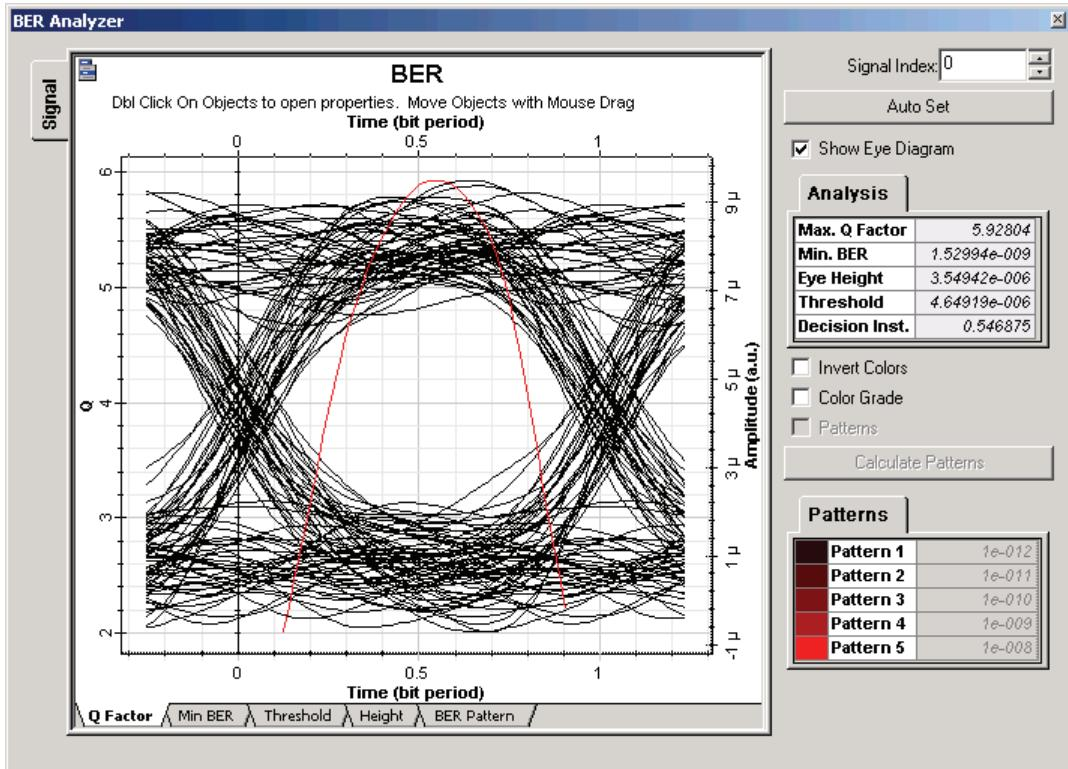


Often the received signal is in the form of optical pulses representing 1 and 0 bits, and is converted directly into an electrical current. Such a scheme is referred to as intensity modulation with direct detection (IM/DD). Demodulation is achieved by a decision circuit that identifies bits as 1 or 0, depending on the amplitude of the electrical current.

The performance of a digital lightwave system is characterized through the bit-error rate (BER). It is customary to define the BER as the average probability of incorrect bit identification. Most lightwave systems specify a BER of  $10^{-9}$  as the operating requirement.

In the sample BER Analyzer diagram shown in [Figure 2](#), a laser output power of 0 dBm and 105 km of fiber length will have a BER close to  $10^{-9}$ .

Figure 2 BER at Fiber 105 km

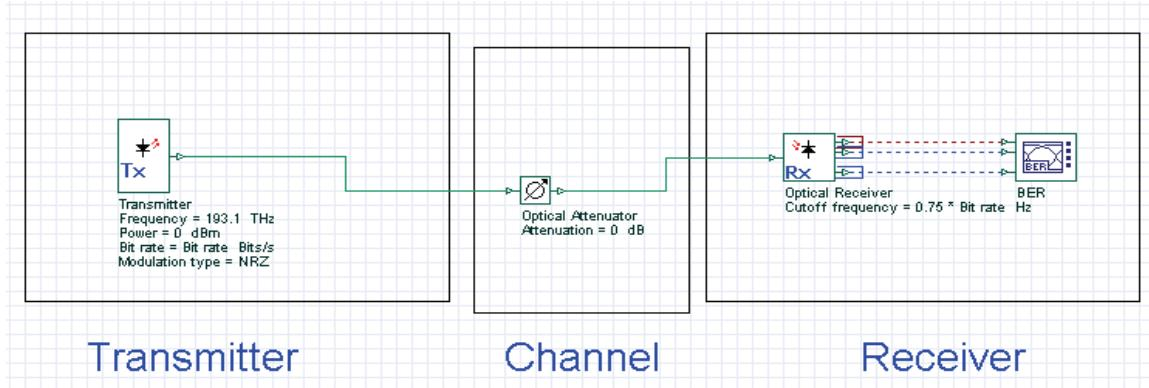


## Receiver design

The design of an optical receiver depends largely on the modulation format used by the transmitter. **Receiver Design.osd** details a digital receiver whose components can be arranged into three groups:

- front end
- linear channel
- data-recovery

**Figure 3 Receiver Design**

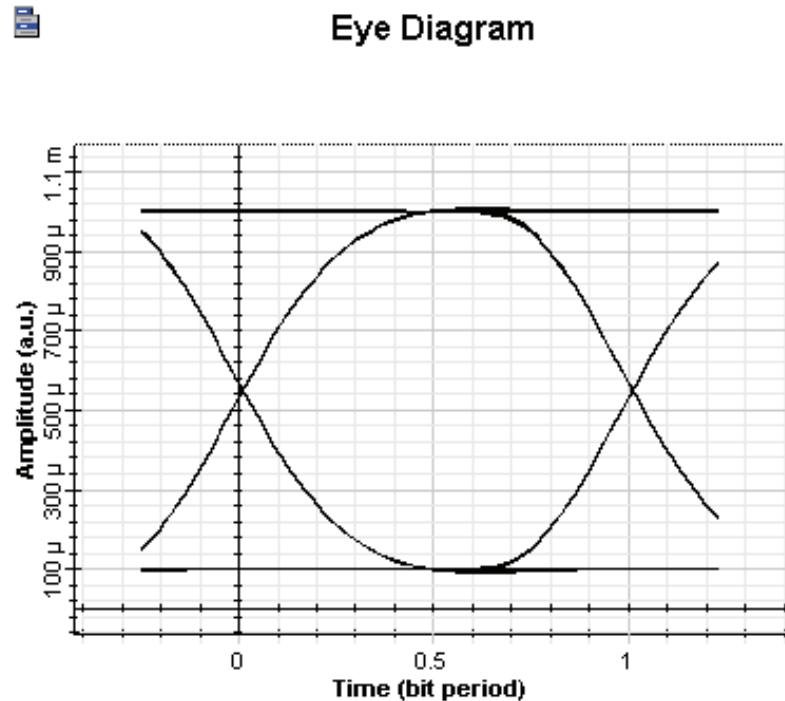


The front-end of a receiver consists of a photodiode with a built-in preamplifier. The linear channel consists of a high-gain amplifier and an low-pass filter. The data recovery is done by the BER Analyzer with a built-in clock recovery and decision circuit.

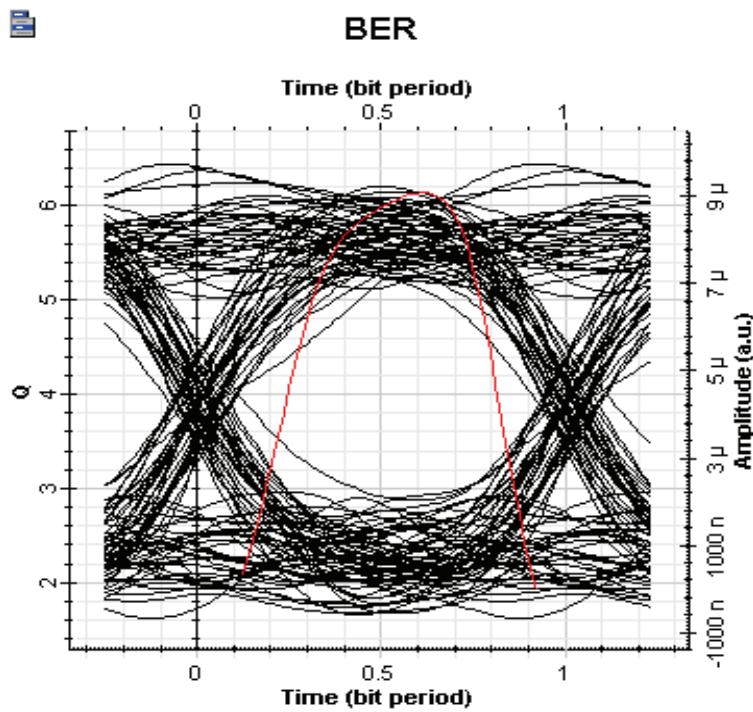
The linear channel has a low pass filter that shapes the pulse. The receiver noise is proportional to the receiver bandwidth and can be reduced by using a low-pass filter whose bandwidth is smaller than the bit rate. The pulse spreads beyond the time slot - the spreading can interfere with the detection of neighboring bits, which is the phenomenon referred to as intersymbol interference (ISI).

When you set the attenuation to 0 dB, the ideal eye diagram seen in Figure 4 is generated.



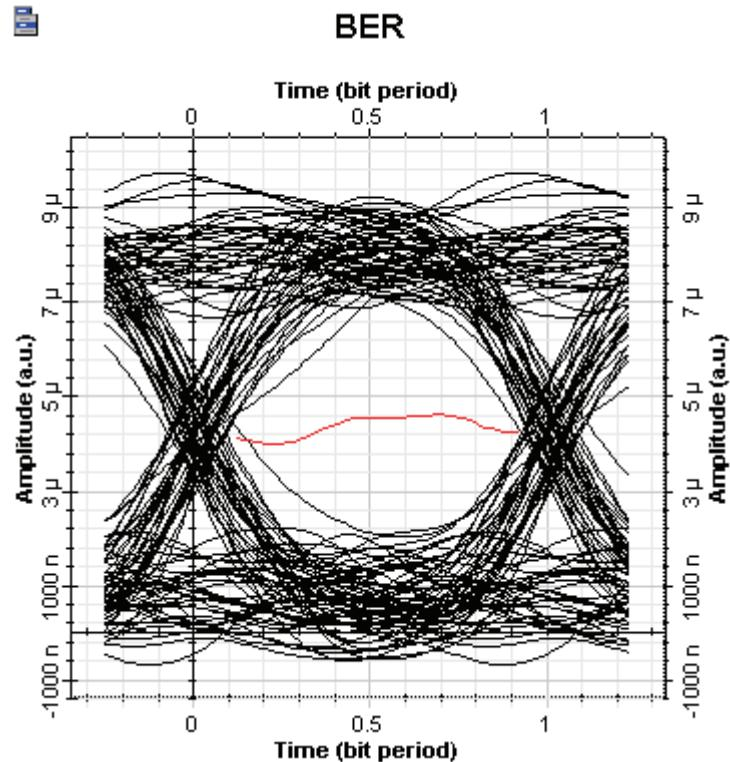
**Figure 4 Receiver EYE Ideal**

If you set the attenuation to 21 dB, the degraded eye diagram seen in Figure 5 is generated.

**Figure 5 Receiver EYE Degraded**

The decision circuit compares the output from the linear channel to a threshold, at a decision instant determined by the clock recovery circuit, and decides whether the signal corresponds to bit 1 or bit 0. The optimum threshold level is calculated for each decision instant in order to minimize the BER (see Figure 6).

Figure 6 Receiver EYE Threshold



**Notes:**



# Optimizing the power and dispersion compensation for nonlinear RZ transmission

---

In this tutorial we show an example of a maximization procedure. We will optimize the launch power and DCF length to maximize the Q factor at the receiver.

Upgrading an existing noise-limited fiber plant requires an increase in launched power, which in turn brings the fiber nonlinearities. It has been shown that nonlinear return to zero (RZ) coding offers significant advantages for high bit rate transmission systems [1][2]. Because the fiber dispersion and Kerr nonlinearities balance each other in this case, the launched power is not limited by self phase modulation (SPM). But this configuration requires careful selection of launch power and dispersion compensating fiber (DCF) length.

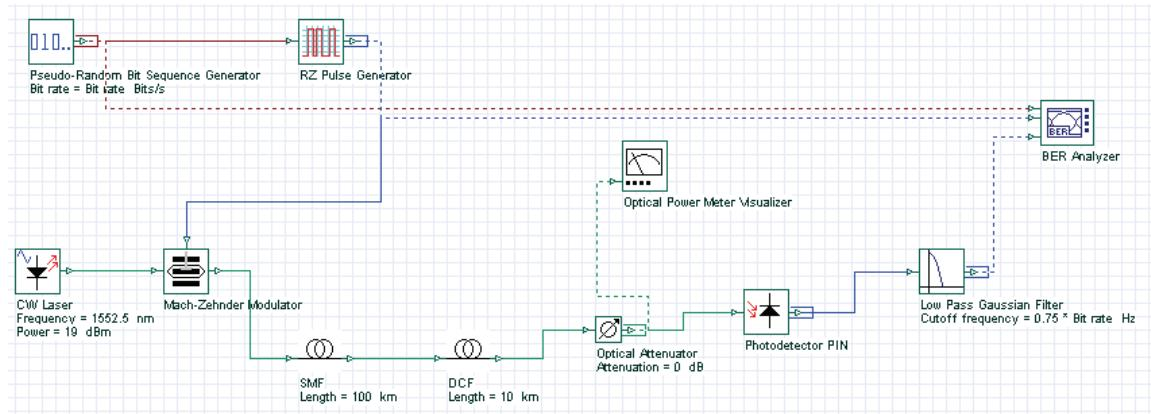
[Figure 1](#) shows the project layout. SMF fiber parameters are as follows: Attenuation is 0.171 dB/km, dispersion is 17.7 ps/nm/km, effective area is 80 micron square,  $n_2 = 2.7 \times 10^{-20} \text{ m}^2/\text{W}$ , length is 100 km.

DCF fiber parameters are as follows: Attenuation is 0.6 dB/km, dispersion is -80 ps/nm/km, effective area is 30 micron square,  $n_2 = 3 \times 10^{-20} \text{ m}^2/\text{W}$ , length is 100 km [3]. Bit rate is 10 Gbps, 7th order PRBS bit sequence and Gaussian beam profile is used. The receiver sensitivity is -17 dBm.

The receiver sensitivity is -17 dBm. An attenuator is used to find the power penalty. Attenuation of the attenuator is initially set to 0 when the optimization is performed. Later, another optimization is carried out to find the power penalty by comparing back-to-back performance transmission and link performance. This is done by varying the attenuation of the attenuator to get the same Q factor (6) as we got from back-to-back transmission. The received power ( $P_{\text{received}}$ ) is then compared with the receiver sensitivity to find the power penalty.

Power penalty is given as  $P_{\text{penalty}} (\text{dB}) = -17 \text{ dBm} - P_{\text{received}} (\text{dBm})$ .

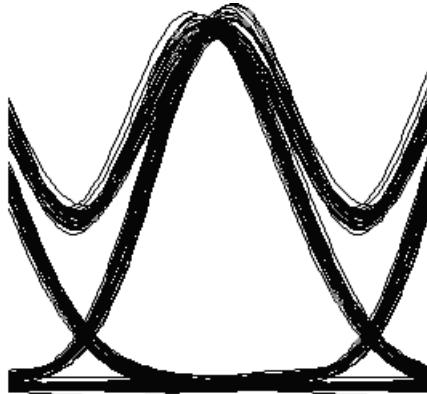
Figure 1 Project layout



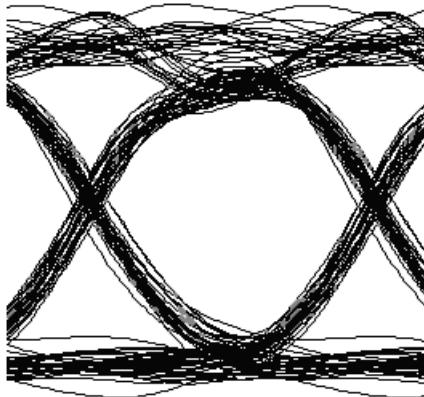
Parameters for the optimization tool are as follows: Initial laser power and DCF length are set to 20 dBm and 20 km respectively. Lower and upper bounds of power are defined as 15 dBm and 25 dBm, 0 and 30 km for DCF length. The termination tolerance of the parameter is 1, that of the result is 0.1.

The Maximum Q Factor is obtained after 15 calculations, when the laser power is about 19 dBm and DCF length is about 10 km. At the optimum point, the Maximum Q Factor is ~20. Received average power is -8.25 dBm.

Figure 2 Eye diagram for RZ modulation with optimum parameters



Maximum Q Factor for back-to-back propagation was about 68. This shows that the optimum dispersion compensation corresponds to about 45 km of compensated SMF (~963 ps/nm residual dispersion) with ~20 dBm launch (~16 dBm average) power. We also found that the power penalty at  $10^{-9}$  BER is 0 dB for optimum values (Required received power to get  $10^{-9}$  BER is around -17 dBm, which is same as the receiver sensitivity). [Figure 2](#) shows the eye diagram after 100 km of propagation with optimum parameters.

**Figure 3 Eye diagram for NRZ modulation with optimum parameters**

In [3], it has been shown that similar results can be obtained from a NRZ modulation format for a single span system, by leaving the correct amount of residual dispersion in the system. In this case, the optimum residual dispersion is lower than that of RZ case.

We have performed similar optimizations for NRZ modulations. The receiver sensitivity is -15.6 dBm. Maximum Q is obtained after 4 calculations when laser power is ~19 dBm (~16 dBm average power), and DCF length is ~18 km. At the optimum point, Maximum Q Factor is ~10 and received average power is -12.3 dBm.

We have found that the power penalty at  $10^{-9}$  BER is ~1 dB for the optimum values when NRZ is used. Optimum dispersion compensation corresponds to about 80 km of compensated SMF (~355 ps/nm residual dispersion).

**Figure 3** shows the eye diagram after 100 km of propagation with optimum parameters when NRZ modulation format is used. The obtained results agree well with the experimental findings of [3] and [4]. Furthermore, comparing the Q factors at optimum points shows that, in fact RZ modulation can tolerate more distortion and reach longer transmission distance.

## References:

- [1] M. L. Dennis, et al., "Long span repeaterless transmission using adiabatic solitons", IEEE Photon. Tech. Lett. 11, 478 (1999).
- [2] C. Furst., et al., "Performance limits of nonlinear RZ and NRZ coded transmission at 10 and 40 Gb/s on different fibers", OFC 2000 2, WM31-302 (2000).
- [3] C. Furst, et al., "RZ verses NRZ coding for 10Gbit/s amplifier free transmission", LEOS 1999 1, MJ1-82 (1999).
- [4] G. Mohs, et al., "Advantages of nonlinear RZ over NRZ on 10 Gb/s single-span links", OFC 2000, FC2-35 (2000).



# 10 Gb/s single channel transmission in standard mode fibers (SMF)

The fundamental limitation to high-speed communication systems over the embedded standard single-mode fiber at  $1.55 \mu\text{m}$  is the linear chromatic dispersion.

Typical value of  $\beta_2 = -20\text{ps}^2 / \text{km}$  at  $1.55 \mu\text{m}$  for SMF leads to  $D = 16 \text{ ps}/(\text{nm} \cdot \text{km})$ . For bit rate  $B = 10 \text{ Gb/s}$ , the slot duration is  $T_B = 100 \text{ ps}$ . If we consider the duty cycle

$$0.5 \rightarrow T_{\text{FWHM}} = 50\text{ps} \rightarrow T_0 = 30\text{ps}$$

the corresponding dispersion length will be approximately  $L_D \sim 45 \text{ km}$ .

This lesson compares RZ- and NRZ-modulation format transmission in SMF at 10 Gb/s, taking into account group velocity dispersion, self-phase modulation due to the Kerr nonlinearity, linear losses, and periodical amplification with ASE noise.

Two tasks will be addressed:

- Compare RZ and NRZ format transmission for lossless cases. The results can be compared to the results of [1], Figure 1(a), and Figure 1(b).
- Investigate linear losses and periodic amplification, taking into account ASE noise.

[Figure 1\(a\)](#), and [Figure 1\(b\)](#) show the layouts used for observing the RZ and NRZ modulation formats.

**Figure 1(a) RZ layout — format transmission for lossless case**

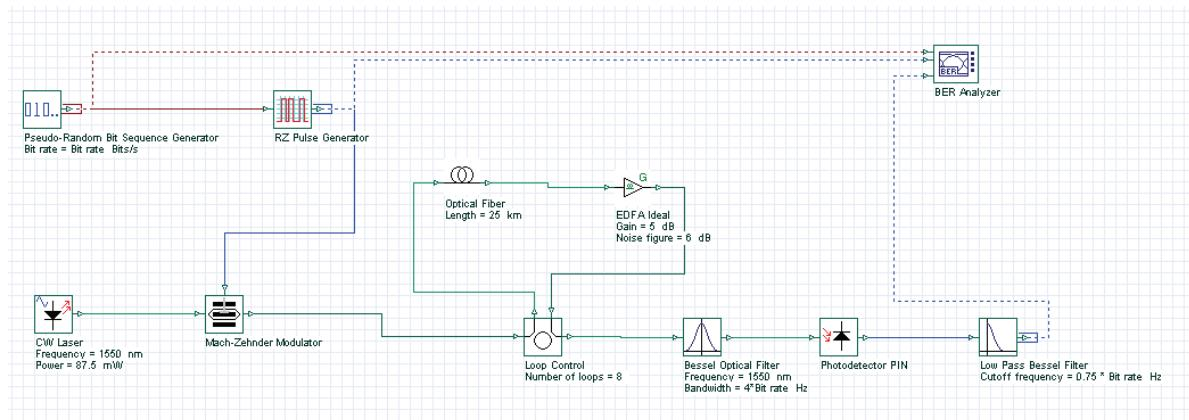
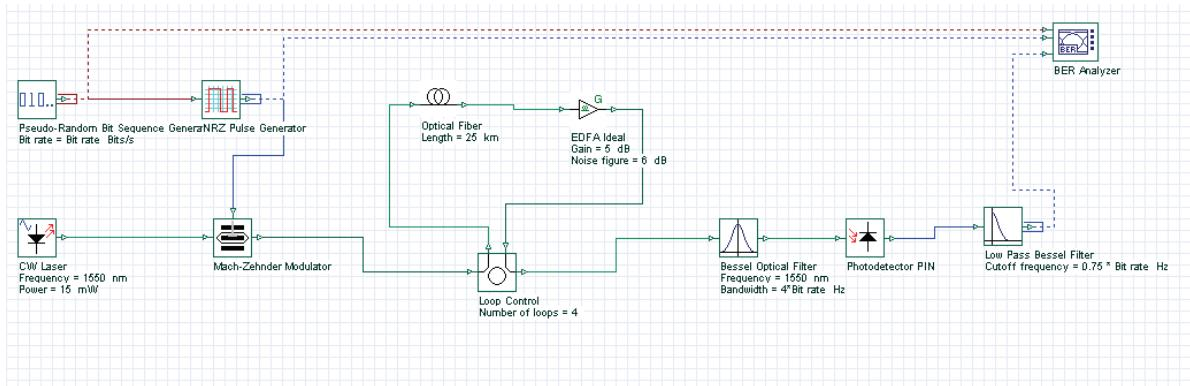


**Figure 1(b) NRZ layout — format transmission for lossless case**



The following global parameters were used:

- Bit rate = 10 Gb/s
- Sequence length = 128 Bits
- Samples per bit = 128

There are no changes in pseudo-random bit sequence generators in either layout.

The RZ-generator has following properties:

- Rectangle shape: Gaussian
- Duty cycle = 0.5 bit
- Rise time = 0.15 bit
- Fall time = 0.25 bit

An externally modulated CW Laser with carrier wavelength  $\lambda = 1550$  nm and line width = 0.1 MHz was used as the optical source.

Standard mode optical fiber has the following properties:

### Dispersion coefficient

$$D = 17 \left[ \frac{\text{ps}}{\text{nm} \cdot \text{km}} \right]$$

### Dispersion slope

$$\frac{\partial D}{\partial \lambda} = 0.08 \left[ \frac{\text{ps}}{\text{nm}^2 \cdot \text{km}} \right]$$

### Nonlinear coefficient

$$\gamma = 1.31 \left[ \frac{1}{\text{km} \cdot \text{W}} \right]$$

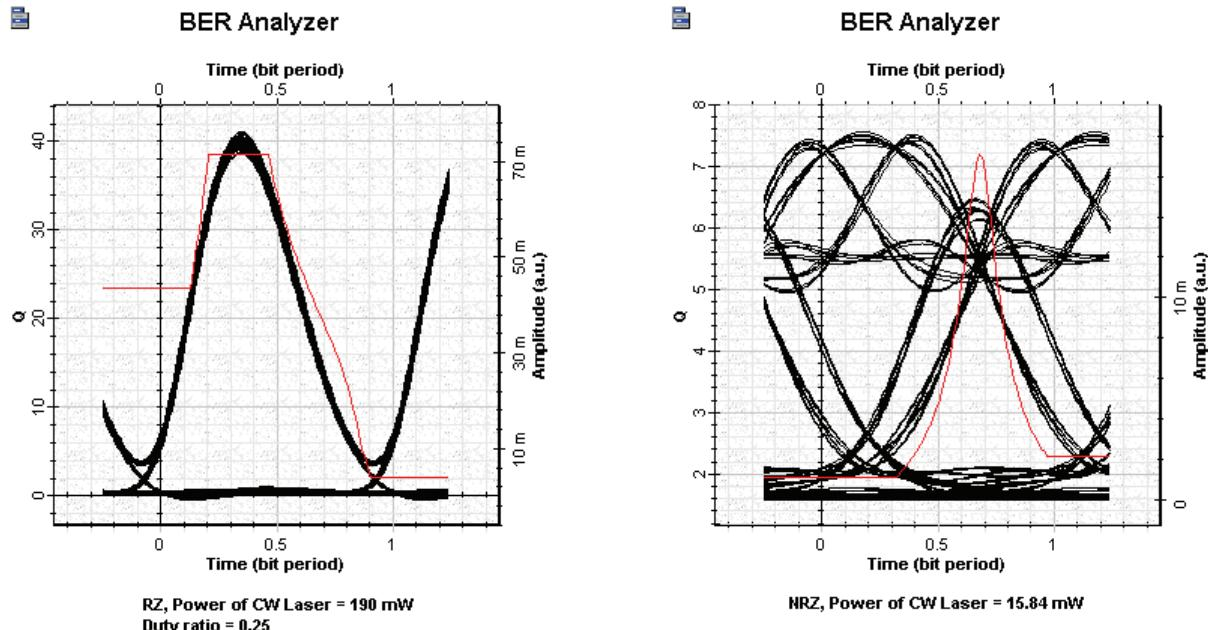
### Linear losses

$$\alpha = 0.2 \text{ dB/km}$$

Properties of the Bessel optical filter are carrier wavelength  $\lambda = 1550 \text{ nm}$  and bandwidth = 4 x Bit rate. The cutoff frequency of the low pass Bessel electrical filter is  $0.75 \times \text{Bit rate}$ . Some of above parameters are chosen in accordance with [1], which allows comparison of the results.

We will compare RZ and NRZ format transmission for a lossless case. Figure 2 shows the eye diagrams for both modulation formats after 100 km transmission at 10 Gb/s in lossless SMF.

**Figure 2 Comparison of RZ and NRZ transmission**



These results can be compared with results of [Figure 1\(a\)](#) and [Figure 1\(b\)](#) from [1]. A good agreement can be identified.

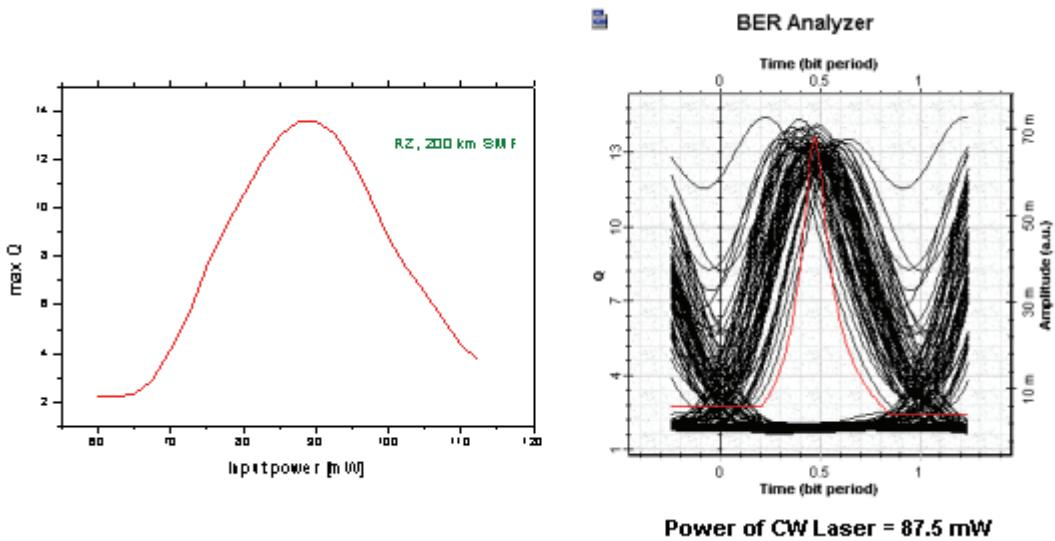
10 Gb/s transmission over SMF will now be analyzed, taking into account linear losses and ideal periodical amplification. Ideal periodical amplification is performed with the help of the OptiSystem Ideal EDFA component, which also takes ASE noise into account.

[Figure 3](#) shows the results obtained with `system applications 10 Gbps in SMF RZ.osd` for 10 Gb/s RZ modulation format (duty ratio = 0.5):

- transmission over common distance from 200 km SMF (8 loops x 25 km)
- periodical amplification after each 25 km: gain = 5 dB
- noise figure = 6 dBm

The dependence of the max Q from the input power is shown in the graph. The BER Analyzer eye diagram represents the optimal point, which according to the graph, is input power  $\sim 87.5$  mW.

**Figure 3 10 Gbps in SMF RZ results**



A well-expressed maximum in the first graph can be seen.

**Note:** We have not performed any fitting of this curve.

At distances greater than 200 km, max Q becomes smaller than 6. Therefore, this is the maximum distance with good Q performance.

[Figure 4](#) shows the results obtained with `system applications 10 Gbps in SMF NRZ.osd` for 10 Gb/s NRZ modulation format:

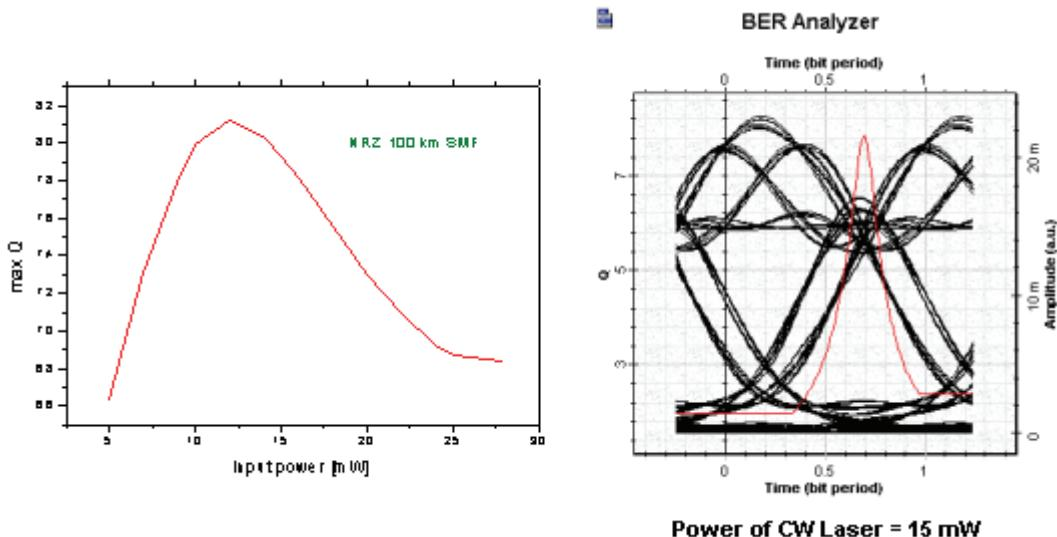
- transmission over common distance from 100 km SMF (4 loops x 25 km)
- periodical amplification after each 25 km: gain = 5 dB



- noise figure = 6 dBm

The dependence of the max Q from the input power is shown in the graph. The BER Analyzer eye diagram represents the optimal point, which according to the graph, is input power  $\sim 15$  mW.

**Figure 4 10 Gbps in SMF NRZ results**



A well-expressed maximum in the first graph can be seen.

**Note:** We have not performed any fitting of this curve.

At distances greater than 100 km, max Q becomes smaller than 6. Therefore, this is the maximum available distance with good Q performance.

Comparing positions of the maximums of the two curves, we can clearly see the shift toward larger input powers for the RZ format.

The general conclusion from this lesson is that for amplifier spacing  $L_A = 25$  km at 10 Gb/s, the maximum transmission length for RZ (duty cycle = 0.5)  $\sim 200$  km, whereas for NRZ  $\sim 100$  km. The RZ is superior when compared to conventional NRZ - modulation format. This observation agrees well with numerical findings of [1] and [2].

## References:

- [1] K. Ennser and K. Petermann, "Performance of RZ- Versus NRZ- Transmission on Standard Single Mode Fibers", IEEE Photonics Technology Letters, Vol. 8, pp. 443-445, 1996.
- [2] M.I. Hayee and A.E. Willner, "NRZ Versus RZ in 10-40 Gb/s Dispersion - Managed WDM Transmission Systems", IEEE Photonics Technology Letters, Vol. 11, pp. 991-993, 1999.

**Notes:**



# 40 Gb/s single channel transmission in standard mode fibers (SMF)

The fundamental limitation to high- speed communication systems over the embedded standard single-mode fiber at 1.55 mm is the linear chromatic dispersion.

Typical value of  $\beta_2 = -20\text{ps}^2/\text{km}$  at 1.55  $\mu\text{m}$  for SMF leads to  $D=16 \text{ ps}/(\text{nm}\cdot\text{km})$ . For bit rate  $B = 40 \text{ Gb/s}$ , the slot duration will be  $T_B = 25 \text{ ps}$ . If we consider the duty cycle

$$0.5 \rightarrow T_{\text{FWHM}} = 12.5\text{ps} \rightarrow T_0 = 7.5\text{ps}$$

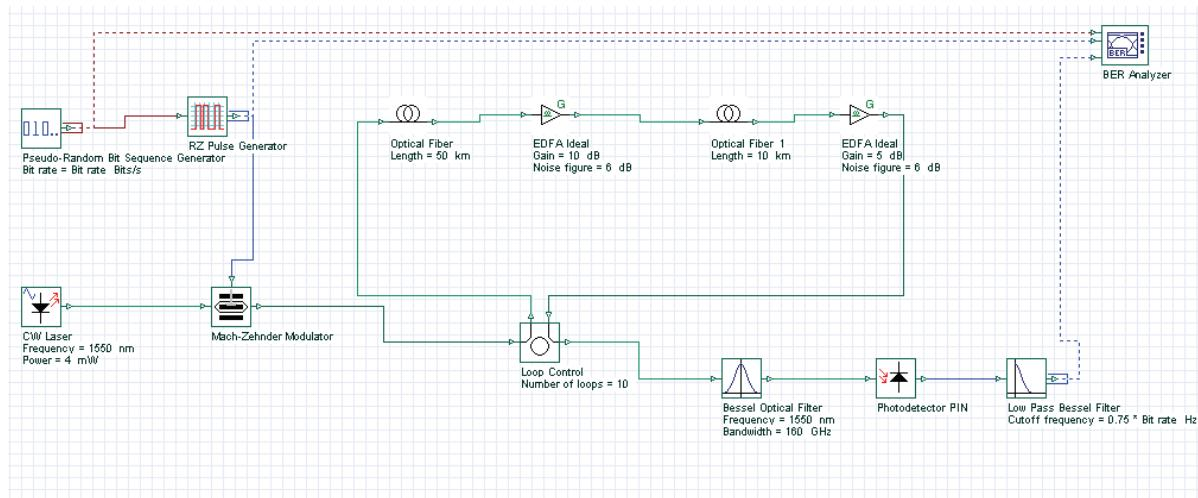
the corresponding dispersion length will be approximately  $L_D \sim 2.8 \text{ km}$ .

This lesson demonstrates the following:

- Compare RZ- and NRZ- modulation format transmission in SMF at 40 Gb/s taking into account: group velocity dispersion, self-phase modulation due to the Kerr nonlinearity, linear losses, and periodical amplification with ASE noise. The large group velocity dispersion is compensated for with a post-dispersion compensation scheme.
- Analyze the influence of accumulated amplifier noise and self-phase modulation for RZ -modulation format transmission in SMF at 40 Gb/s.
- Compare post-dispersion and pre-dispersion compensation schemes for RZ - modulation format transmission in SMF at 40 Gb/s.

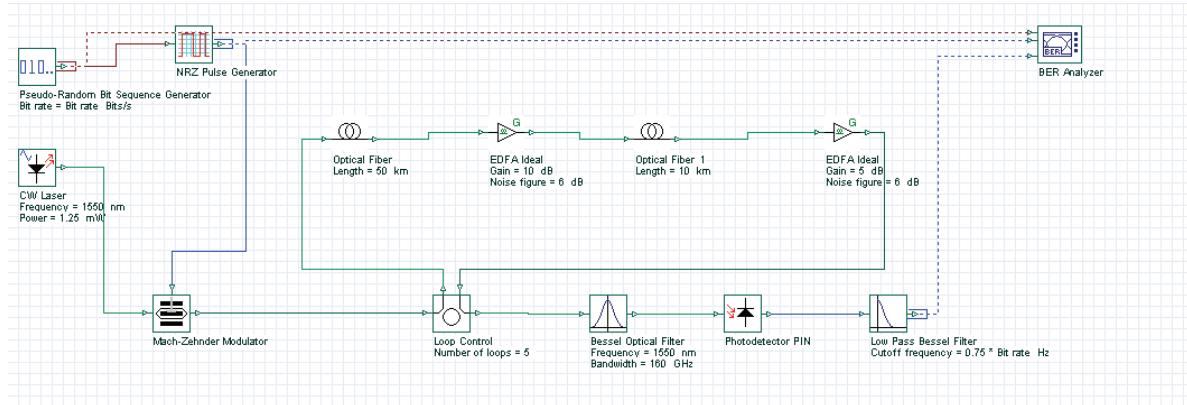
[Figure 1](#) and [Figure 2](#) show the layouts used for observing the RZ- and NRZ- modulation formats.

**Figure 1 RZ layout — modulation format**



## 40 GB/s SINGLE CHANNEL TRANSMISSION IN STANDARD MODE FIBERS (SMF)

**Figure 2 NRZ layout — modulation format**



The setup mode **Set bit rate** with following global parameters was used:

- Bit rate = 40 Gb/s
- Sequence length = 128 Bits
- Samples per bit = 128

Therefore:

- Number of samples = Sequence length \* Samples per bit = 16384
- Time window = Sequence length \* Bit slot = 3.2 ns
- Sampling interval = Time window / Number of samples = 0.195 ps
- Sample rate = 1 / the sampling interval = 5.12 THz

There are no changes in pseudo-random bit sequence generators in either layout. The RZ- generator has the following properties:

- Rectangle shape: Gaussian
- Duty cycle = 0.5 bit
- Rise time = 0.15 bit
- Fall time = 0.25 bit



An externally modulated CW Laser with carrier wavelength  $\lambda = 1550$  nm and line width = 0.1 MHz was used as the optical source.

Standard mode optical fiber has the following properties:

#### **Dispersion coefficient**

$$D = 17 \left[ \frac{\text{ps}}{\text{nm} \cdot \text{km}} \right]$$

#### **Dispersion slope**

$$\frac{\partial D}{\partial \lambda} = 0.08 \left[ \frac{\text{ps}}{\text{nm}^2 \cdot \text{km}} \right]$$

#### **Nonlinear coefficient**

$$\gamma = 1.31 \left[ \frac{1}{\text{km} \cdot \text{W}} \right]$$

#### **Linear losses**

$$\alpha = 0.2 \text{ dB/km}$$

#### **Fiber length**

$$L_{SMF} = 50 \text{ km}$$

After each segment from SMF, an amplifier compensates the linear losses.

Dispersion compensation fiber has the following properties:

#### **Dispersion coefficient**

$$D = -80 \left[ \frac{\text{ps}}{\text{nm} \cdot \text{km}} \right]$$

#### **Dispersion slope**

$$\frac{\partial D}{\partial \lambda} = 0.08 \left[ \frac{\text{ps}}{\text{nm}^2 \cdot \text{km}} \right]$$

#### **Nonlinear coefficient**

$$\gamma = 5.24 \left[ \frac{1}{\text{km} \cdot \text{W}} \right]$$

#### **Linear losses**

$$\alpha = 0.5 \text{ dB/km}$$

### Fiber length

$$L_{DCF} = 10 \text{ km}$$

After each segment from DCF, an amplifier compensates the linear losses.

Properties of Bessel optical filter are carrier wavelength  $\lambda = 1550 \text{ nm}$  and bandwidth =  $4 \times \text{Bit rate}$ .

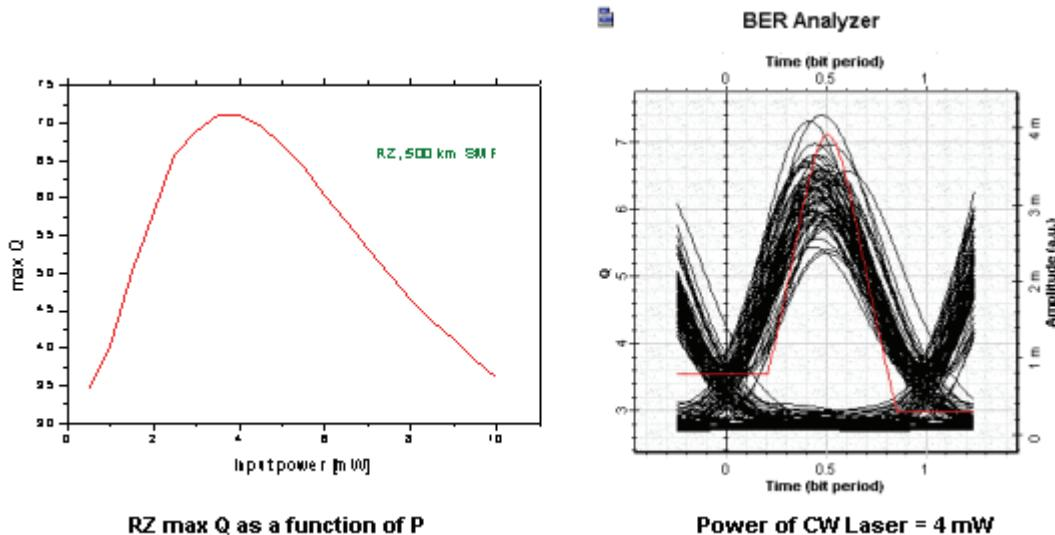
The cutoff frequency of the low pass Bessel electrical filter is  $0.75 \times \text{Bit rate}$ .

Ideal periodical amplification is performed with the help of the OptiSystem Ideal EDFA component, which also takes ASE noise into account. The amplifier after SMF has a gain of 10 dB and noise figure of 6 dB. (This after DCF with 5 dB gain and the same noise figure.)

Note the complete dispersion compensation of the GVD of the standard-mode fiber and the complete compensation of the power losses in both fibers. The post-compensation scheme for the dispersion compensation is used. Some of above parameters are chosen in accordance with [1], which allows comparison of results.

In the first part of this lesson, the comparison of RZ and NRZ formats was observed. [Figure 3](#) shows the results obtained with **high-dispersion fibers 40 Gbps in SMF RZ.osd** for 40 Gb/s RZ modulation format (duty ratio = 0.5) transmission over common distance: from 500 km SMF (10 loops x 50 km) and periodical amplification after each fiber. The dependence of the max Q from the input power is shown in the graph. The BER Analyzer eye diagram represents the optimal point, which according to the graph, is input power  $\sim 4 \text{ mW}$ .

**Figure 3 40 Gbps in SMF RZ results**



A well-expressed maximum in the first graph can be seen.

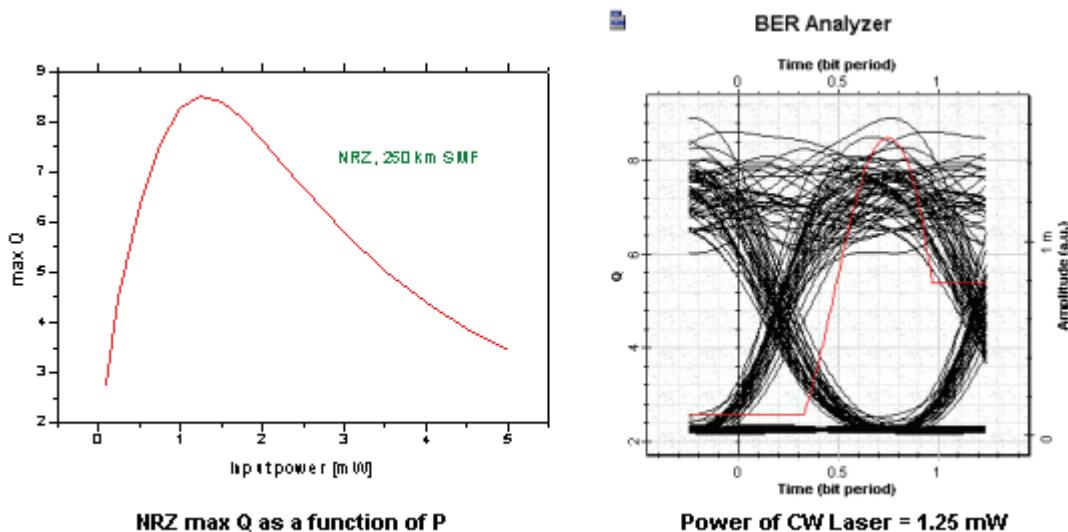
**Note:** We have not performed any fitting of this curve.



At distances greater than 500 km, max Q becomes smaller than 6. Therefore, this is the maximum distance with good Q performance.

**Figure 4** shows the results obtained with **high-dispersion fibers 40 Gbps in SMF NRZ . osd** for 40 Gb/s NRZ modulation format transmission over common distance from 250 km SMF (5 loops x 50 km) and periodical amplification after each fiber. The dependence of the max Q from the input power is shown in the graph. The BER Analyzer eye diagram represents the optimal point, which according to the graph, is input power  $\sim 1.25$  mW.

**Figure 4 40 Gbps in SMF NRZ results**



A well-expressed maximum in the first graph can be seen.

**Note:** We have not performed any fitting of this curve.

At distances greater than 250 km, max Q becomes smaller than 6. Therefore, this is the maximum available distance with good Q performance.

Comparing positions of the maximums of the two curves, we can clearly see the shift toward greater input powers for the RZ format. The results show that the RZ-modulation format duty cycle = 0.5 is superior to the conventional NRZ-modulation format.

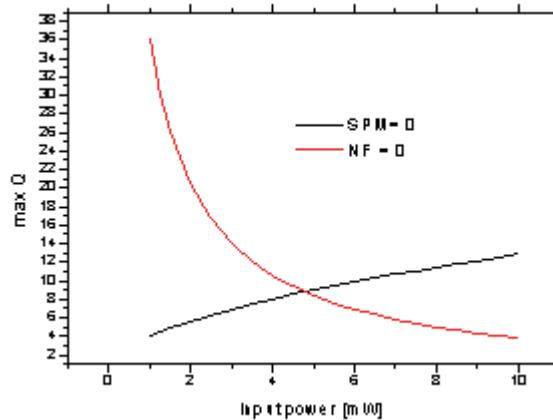
In the second part of this lesson, the influence of accumulated amplifier noise and self-phase modulation on the RZ-modulation transmission in SMF at 40 Gb/s will be analyzed. Two different situations will be considered:

- self-phase modulation is assumed zero
- noise figure is not taken into account

**Figure 5** shows the results.



**Figure 5 Transmission distance 500 km at 40 Gb/s**



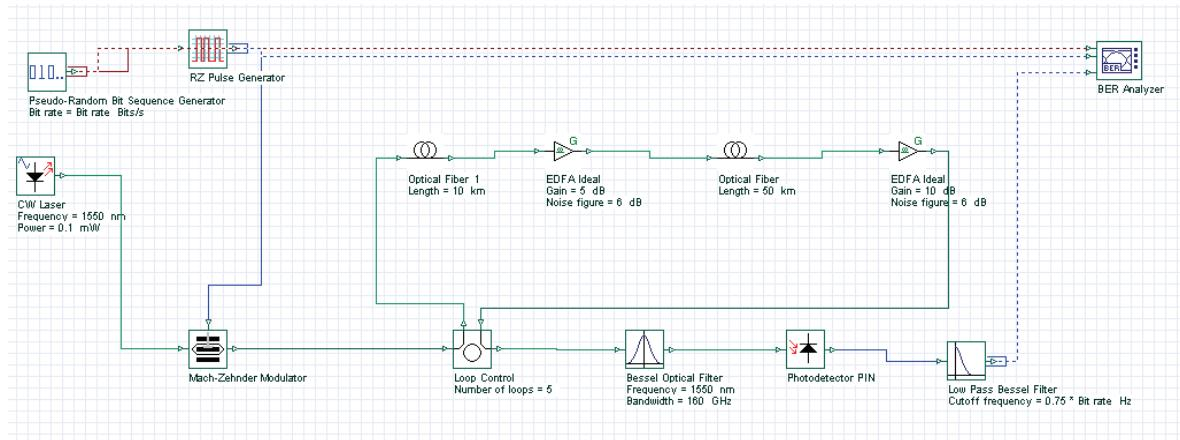
At low power levels, the performance is mainly hampered by the accumulated amplifier noise. At high input power levels, the transmission distance is significantly reduced due to the self-phase modulation. Just these effects determine the well-expressed maximum in the Q curve in the first figure.

In the third part of this lesson, two dispersion compensation schemes will be studied (with **high-dispersion fibers 40 Gbps in SMF RZ pre**):

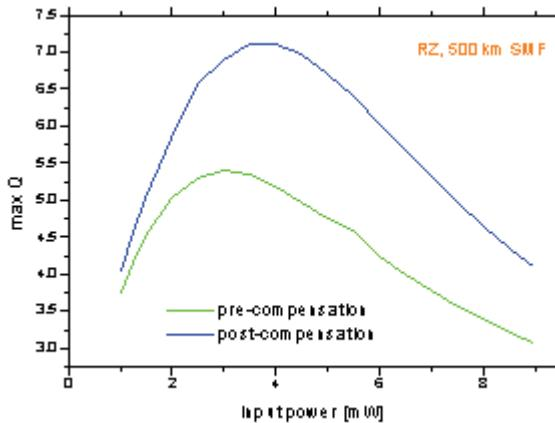
- post-compensation
- pre -compensation

[Figure 6](#) shows the project layout.

**Figure 6 40 Gbps in SMF RZ pre-compensation layout**



[Figure 7](#) shows the corresponding results for the RZ-modulation transmission in SMF at 40 Gb/s.

**Figure 7 RZ modulation format transmission at 40 Gb/s over 500 km in SMF**

The results indicate that the post-compensation scheme is superior compared to the pre-compensation scheme in dispersion compensated systems at 40 Gb/s in SMF.

This lesson demonstrated that for upgrading the existing standard fiber network at 1.55 mm at 40 Gbps:

- Dispersion compensation is necessary
- RZ-modulation is superior compared to conventional NRZ-modulation format
- At low power levels, the performance is mainly hampered by the accumulated amplification
- At higher input powers, the transmission distance is significantly reduced by nonlinear self-phase modulation
- Post-compensation scheme is superior compared to pre-compensation scheme.

The results agree well with the results of [1], [2], and [3].

## References:

- [1] D. Breuer and K. Petermann, "Comparison of NRZ and RZ- Modulation Format for 40 Gbit/s TDM Standard-Fiber System," IEEE Photonics Technology Letters, Vol. 9, pp. 398-400, 1997.
- [2] M.I. Hayee and A.E. Willner, "NRZ Versus RZ in 10-40 Gb/s Dispersion - Managed WDM Transmission Systems," IEEE Photonics Technology Letters, Vol. 11, pp. 991-993, 1999.
- [3] C.M. Weinert, R. Ludvig, W. Papier, H.G. Weber, D. Breuer, K. Petermann, and F. Kuppers, "40 Gbit/s Comparison and 4 x 40 Gbit/s TDM/WDM Standard Fiber Transmission", Journal of Lightwave Technology, Vol. 17, pp. 2276-2284, 1999.



# Engineering the fiber nonlinearities and dispersion

---

The purpose of this example is to investigate the fiber nonlinearity and dispersion related issues in a system.

As long as the optical power within an optical fiber is small, the fiber can be treated as linear medium. However, when the power level is high, we have to consider the impact of nonlinear effects. Nonlinear effects can be classified into two categories:

- Refractive index related
- Scattering related

Some nonlinear effects occur in multi channel WDM systems where interaction of signals at different wavelengths is possible. See [Table 1](#) for more information.

**Table 1** Nonlinear effects in the fiber

Category	Single channel	Multi-channel
<b>Refractive index related</b>	Self-phase modulation (SPM)  Four wave mixing (FWM)	Cross-phase modulation (XPM)
<b>Scattering related</b>	Stimulated Brillouin scattering (SBS)	Stimulated Raman scattering (SRS)

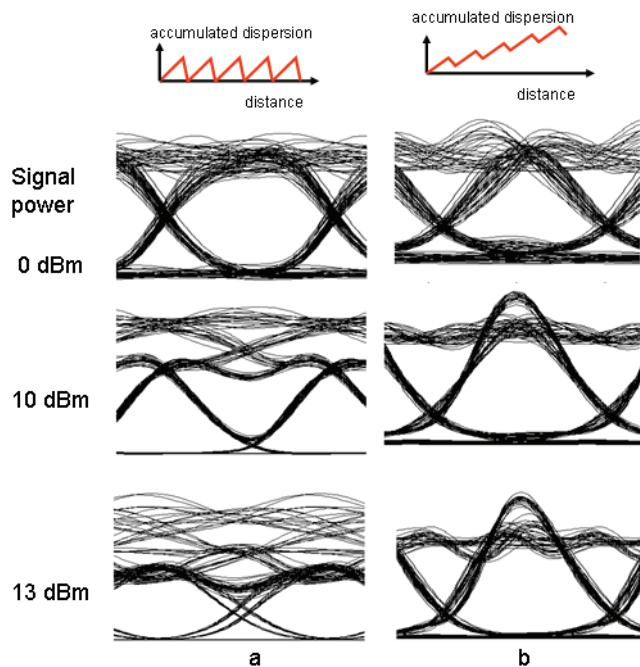
SPM and XPM affect the phase of signals and cause spectral broadening, which in turn leads to increases in dispersion penalties. SBS and SRS provide gains to some channels by depleting power from other channels. The nonlinear interaction depends on transmission length and effective area of the fiber. Since loss in the fiber decreases the signal power, we use an effective instead of physical length. SPM can be a significant consideration in designing 10 Gbps systems, and it restricts the maximum channel power to below a few dBm. XPM becomes an important consideration when the channel spacing is tens of GHz. FWM efficiency depends on signal power and dispersion, as well as channel separation in WDM systems. If the channel is close to the zero dispersion wavelength of the fiber, considerably high power can be transferred to FWM components. Using unequal channel spacing can also reduce effect of FWM.

Dispersion plays a key role in reducing the effects of nonlinearities. However, dispersion itself can cause intersymbol interference. Fortunately, we can engineer systems with zero total dispersion but a certain amount of local dispersion along the link.

In the following example, we will consider the effects of dispersion compensation on system performance in a high power regime where nonlinearities are active. Initially, we will consider a dispersion post-compensated system with a single channel. The project is found in the [Fiber nonlinearities and dispersion single](#)

**channel.osd** file. In this file, we have two different versions of the same project. In the first version, system residual dispersion is 0, whereas it is 800 ps/nm in the second version. The transmission link contains 5 spans and the bit rate is 10 Gbps. The dispersion of 100 km SMF is 16 ps/nm-km and its effective area is 72 square microns. The dispersion of DCF is -80 ps/nm-km. A 20 km DCF is used for the first version to totally compensate the dispersion. For the second version, an 18 km DCF is used to leave some residual dispersion after each span. This adds 800 ps/nm total residual dispersion to the system. The effective area of DCF is 30 square microns. SMF and DCF losses are compensated by an EDFA with 25 dB gain for the first version and with 24.4 dB gain for the second version. The Noise figure of the EDFA is 4 dB. If we consider only the SMF fiber, and include the effect of amplification (5 times), we can estimate the threshold power for SPM [1] [2]. If we do so, we find that after about 10 dBm average power, SPM becomes a limiting effect. We need to investigate if this is the case, and how the residual system dispersion effects it. [Figure 1](#) shows the eye diagrams for two different residual dispersion values and three different signal powers.

**Figure 1** Eye diagrams of the received signal for several received signal powers when system residual dispersion is a) 0, b) 800 ps/nm.



**Note:** Inset on the top shows the dispersion map for each case.

This simulation shows that effect of SPM can be reduced by not completely compensating the dispersion and leaving some residual dispersion in the system. Notice how power increase results closes the eye in the case of zero residual dispersion.



## Multi-channel system

Let us now consider a multi-channel system with 8 channels. For this example, the project layout is shown in [Figure 2](#). The first channel is at 193.1 THz and the channels are separated by 100 GHz. SMF and DCF parameters are the same as in the previous example. In this example, we set the sample per bit parameter to, so as to eliminate effect in fibers. For illustrative purposes, we have set the maximum nonlinear phase shift parameter of the fibers to 100 mrad. This is done to get a fast result. To get more accurate results, this parameter should be set to a lower value. Simulation results are shown in [Figure 3](#).

**Figure 2 Project layout**

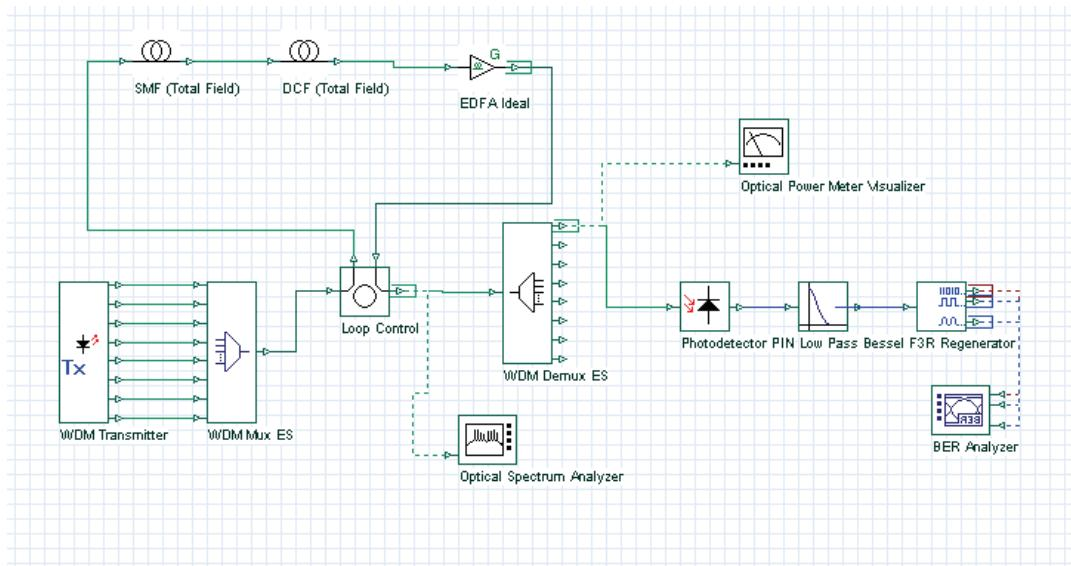
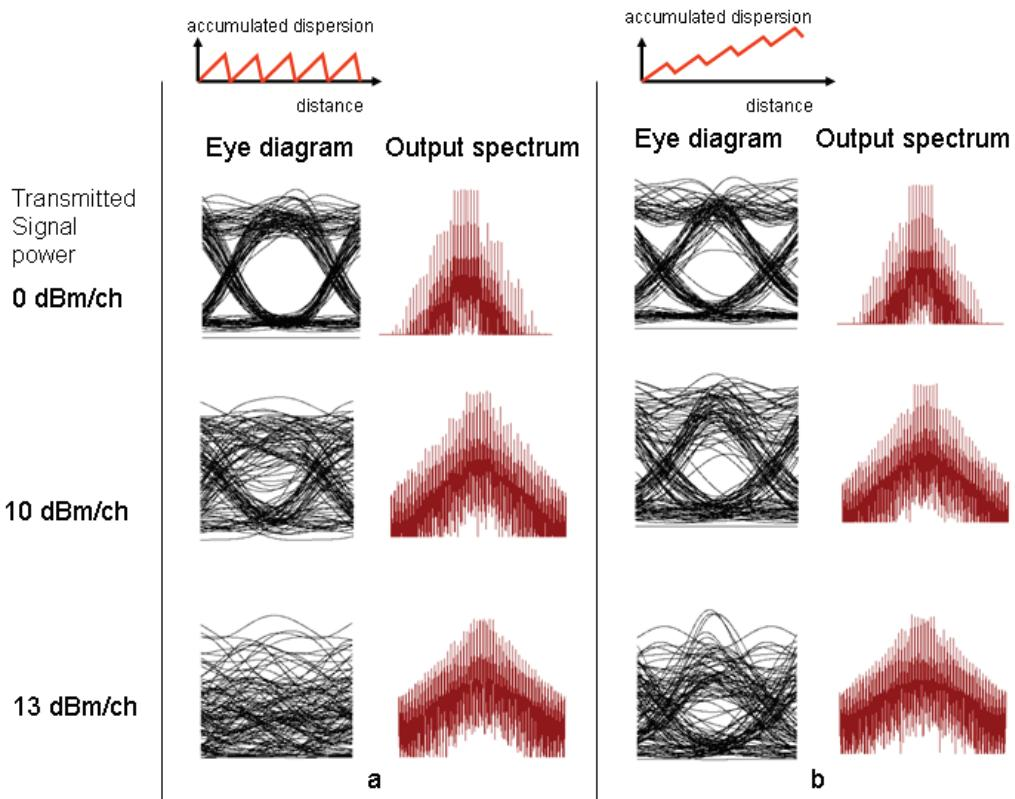


**Figure 3** Eye diagrams of the received signal for several signal powers when a) fiber dispersion is 0; b) and c) when system residual dispersion is 0 and 800 ps/nm respectively.



**Note:** Insets show the power spectrums and dispersion maps for each case.

For an eight-channel system, the threshold power is approximately 10 dBm per channel [1]. In this simulation, both SPM and XPM affect the system performance. The simulation also shows that nonlinear effects can be reduced by local dispersion and better performance is obtained with nonzero residual dispersion [3].

## References

- [1] G. P. Agrawal, *Fiber Optic Communication Systems*, Wiley-Interscience, 1997.
- [2] R. Ramaswami and K. N. Sivarajan, *Optical Networks: A practical Perspective*, Morgan Kaufmann, 1998.
- [3] G. Bellotti et. al., "Dependence of self-phase modulation impairments on residual dispersion in 10 Gb/s based terrestrial transmission using standard fiber", *IEEE Photon. Tech. Lett.* 11, pp. 824, 1999.

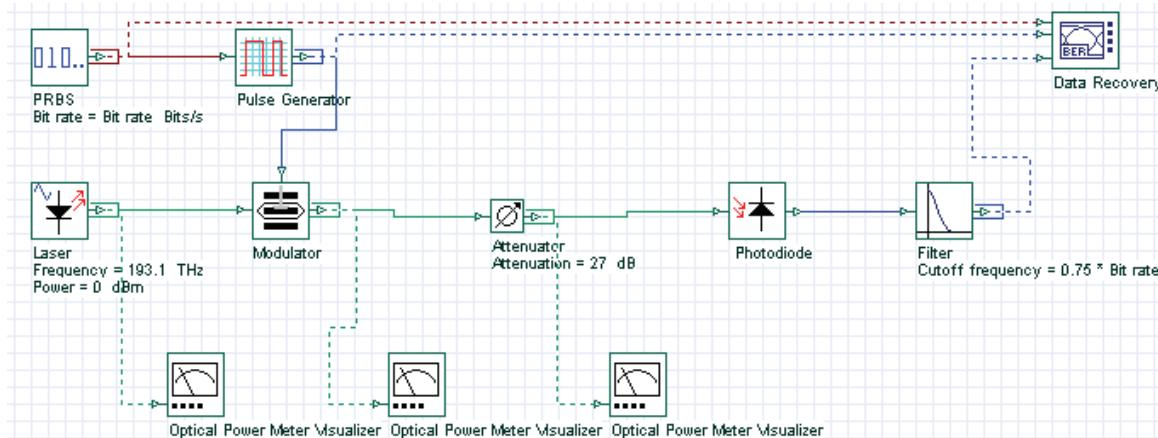
# System design — Power budget

The purpose of power budget is to ensure that enough power will reach the receiver to maintain reliable performance during the entire system lifetime. The minimum average power required by the receiver is the receiver sensitivity. The average launch power is generally specified for each transmitter with optical powers expressed in dBm.

In order to estimate the maximum fiber length we should specify the output power of the transmitter and the receiver sensitivity. We can also specify a system margin. The purpose of the system margin is to allocate a certain amount of power to additional sources of power penalty that may develop during the system lifetime.

**System Design - Power Budget.osd** (see [Figure 4](#)) shows a system designed using a receiver with -30 dBm sensitivity and an external modulated transmitter with output power of -3 dBm.

**Figure 4 Power Budget**



Using a system margin of 0 dB the total loss allocated for the channel will be:

- Channel Loss = System Margin + Receiver Sensitivity + Transmitter power
- Channel Loss = 30 - 3 = 27 dB

For a typical fiber attenuation of 0.25 dB/km, the maximum distance we can propagate in this system is 108 km. In this case, we are not including dispersion effects that will limit the system performance.



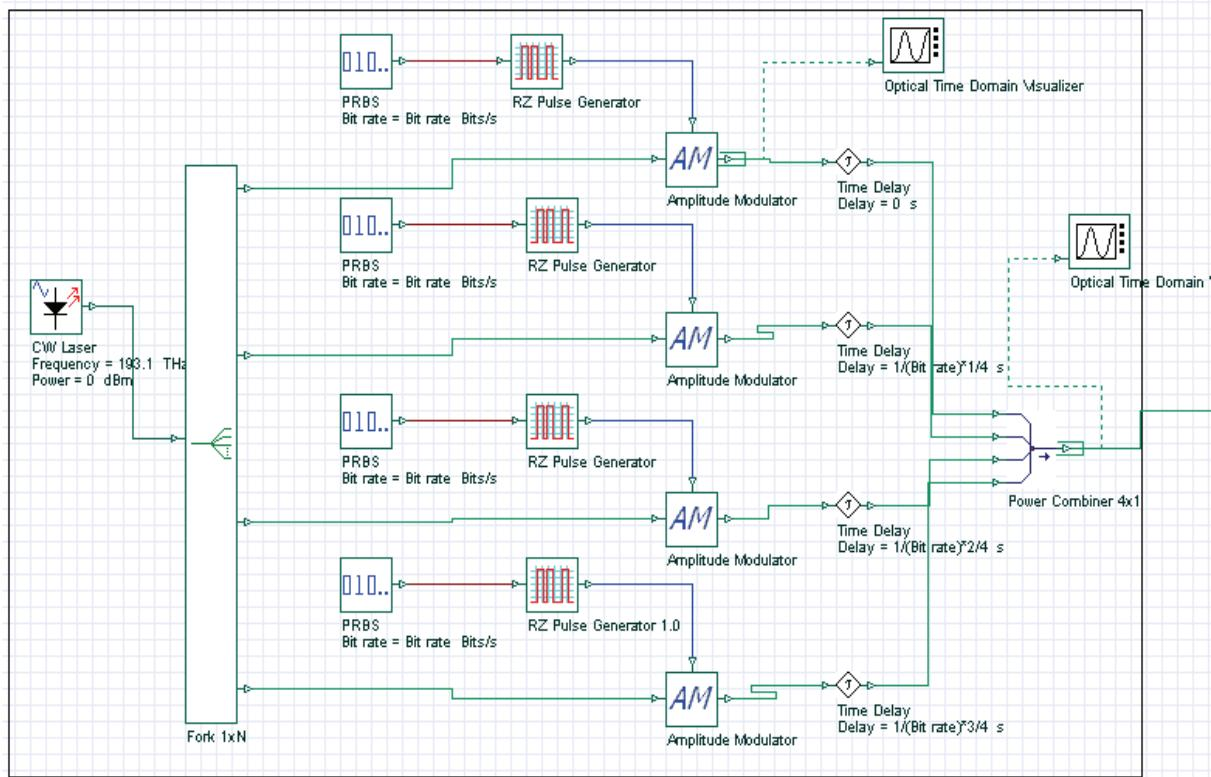
**Notes:**



# Time Division Multiplexing (TDM)

In optical time-division multiplexing (OTDM) systems, several optical signal modulated at the bit rate  $B$  using the same carrier frequency are multiplexed optically to form a composite optical signal at a bit rate  $NB$ , where  $N$  is the number of multiplexed optical channels. **OTDM Multiplexer.osd** (see Figure 5) shows an OTDM transmitter.

Figure 5 OTDM Multiplexer



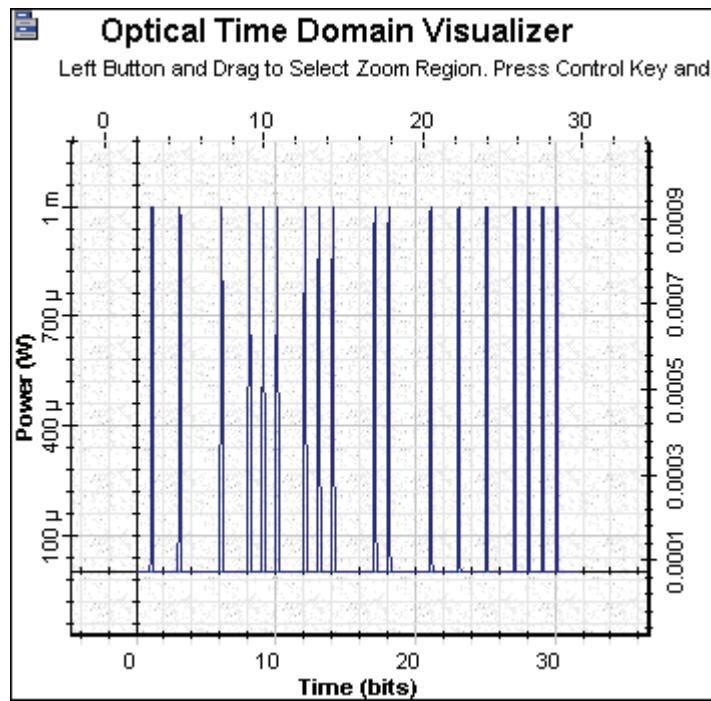
## Multiplexer

Each modulator generates short pulses with 10 GB/s bit rate, the pulse 3 dB pulse width is 0.05 bit period (see Figure 6).



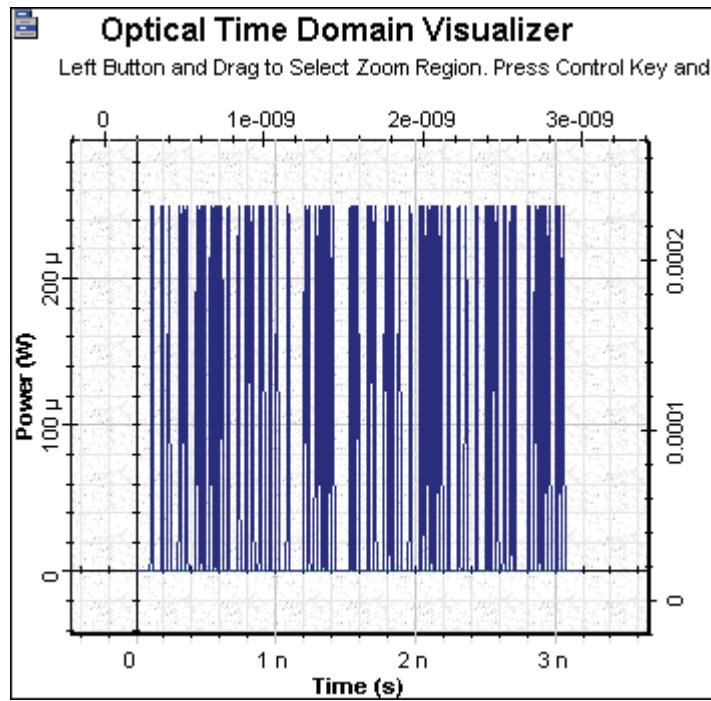
## TIME DIVISION MULTIPLEXING (TDM)

Figure 6 OTDM 10 GBs



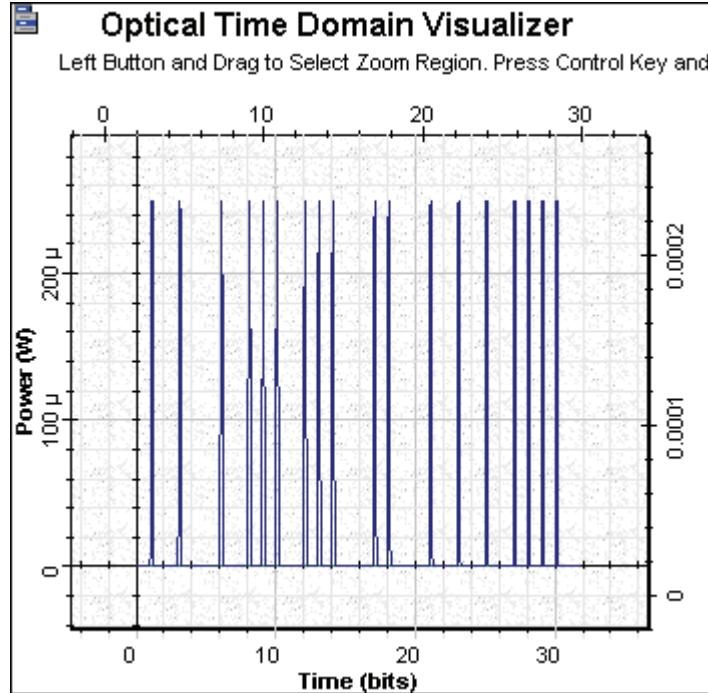
The signals are combined in order to generate an 40 GB/s bit rate at the multiplexer output (see Figure 7).

Figure 7 OTDM 40 GBs



The demultiplexer stage uses a modulator working at 10 GBs clock. [Figure 8](#) shows the output signal as the first channel.

Figure 8 OTDM 10 GBs - Receiver

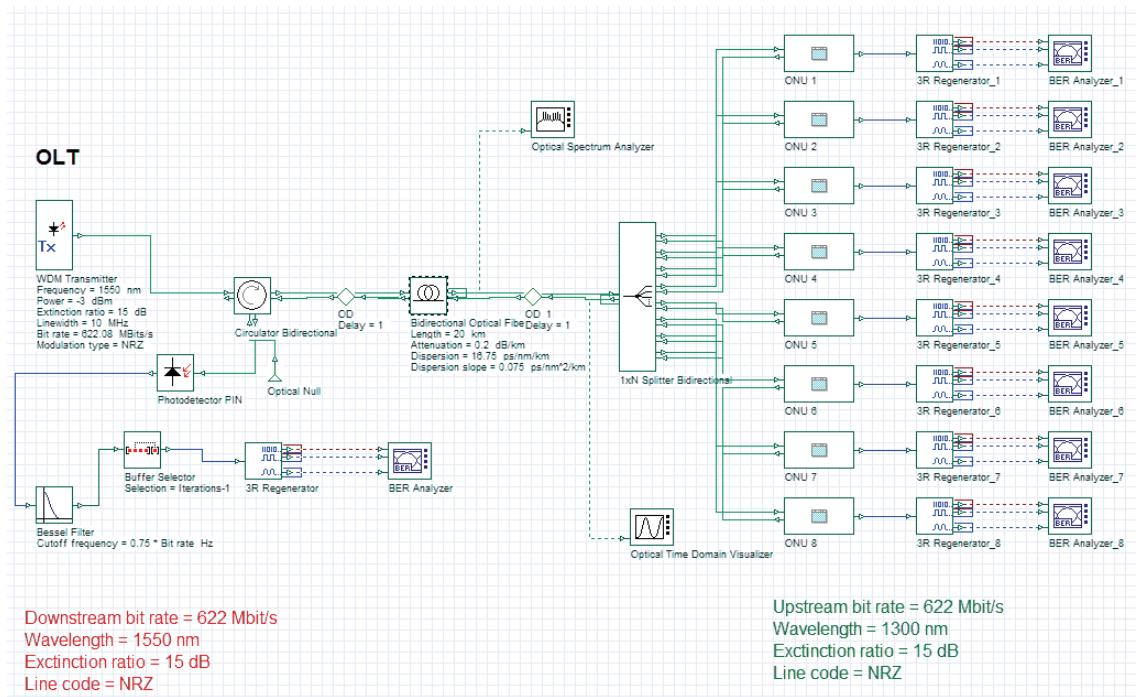


**Notes:**

# Broadband optical system based on a Passive Optical Network (BPON)

The system designed in project **BPON Bidirectional.osd** (Figure 1) provides a 622 Mbps of bidirectional access to multiple sites over a single fiber. It consists of an Optical Line Termination (OLT) at the service provider's central office and 8 Optical Network Units (ONUs) near end users.

**Figure 1** Broadband passive optical network

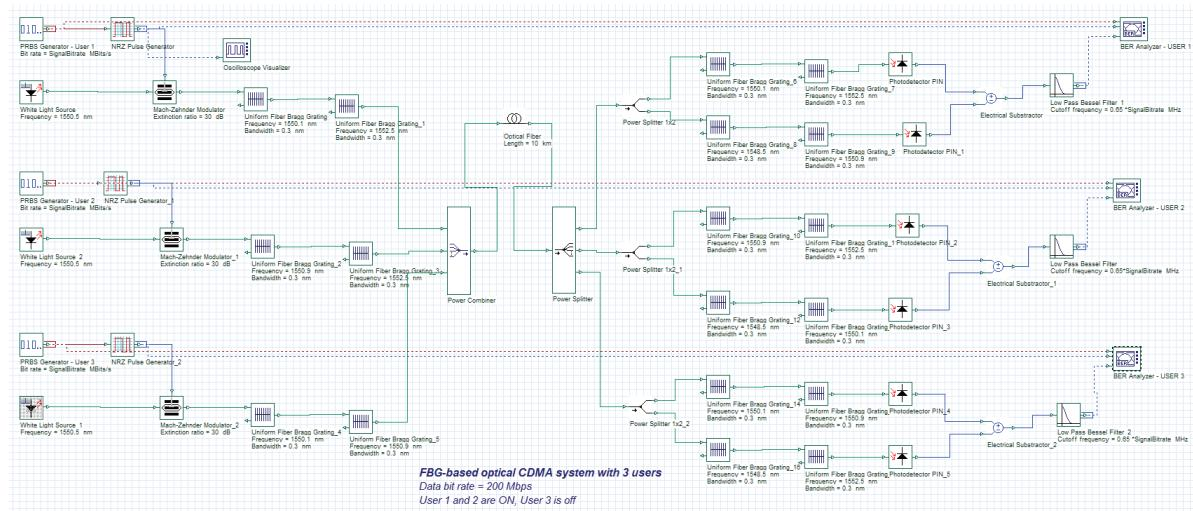


**Notes:**

# Optical code-division multiple-access system (OCDMA)

The system designed in project **SAC OCDMA.osd** (Figure 1) is a spectral-amplitude-coding OCDMA. It has three users, where in this setup two users are transmitting data, while one user is off. The FBGs in the system are working as encoders/decoders for the incoherent optical signal.

**Figure 1** OCDMA system

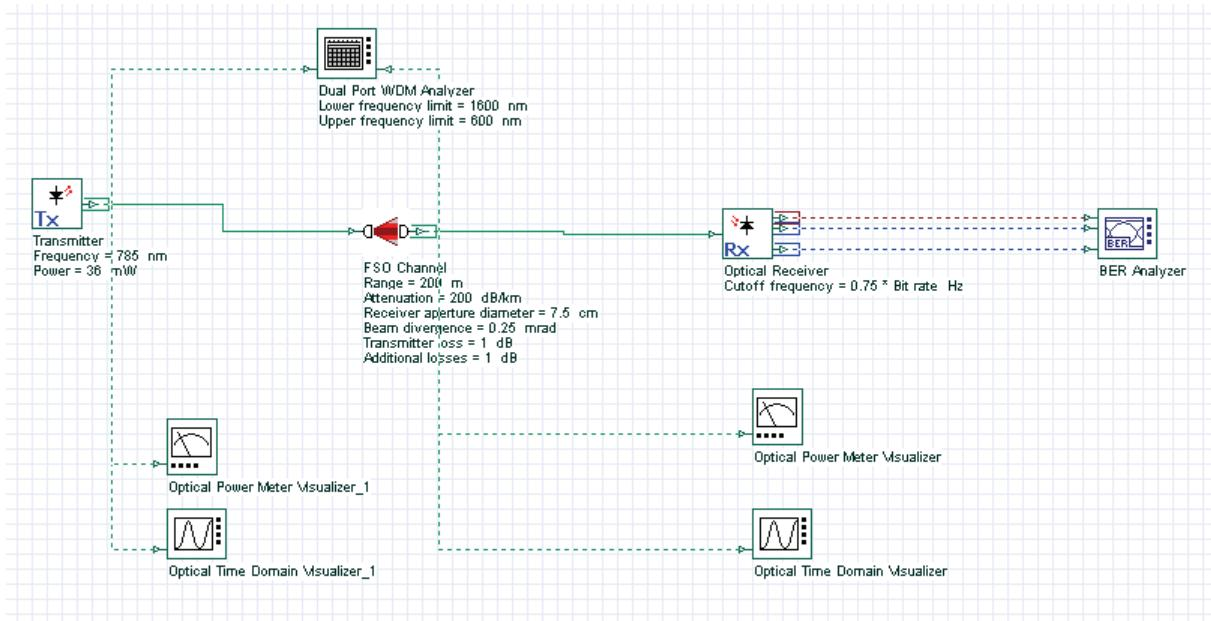


**Notes:**

# Free Space Optics (FSO)

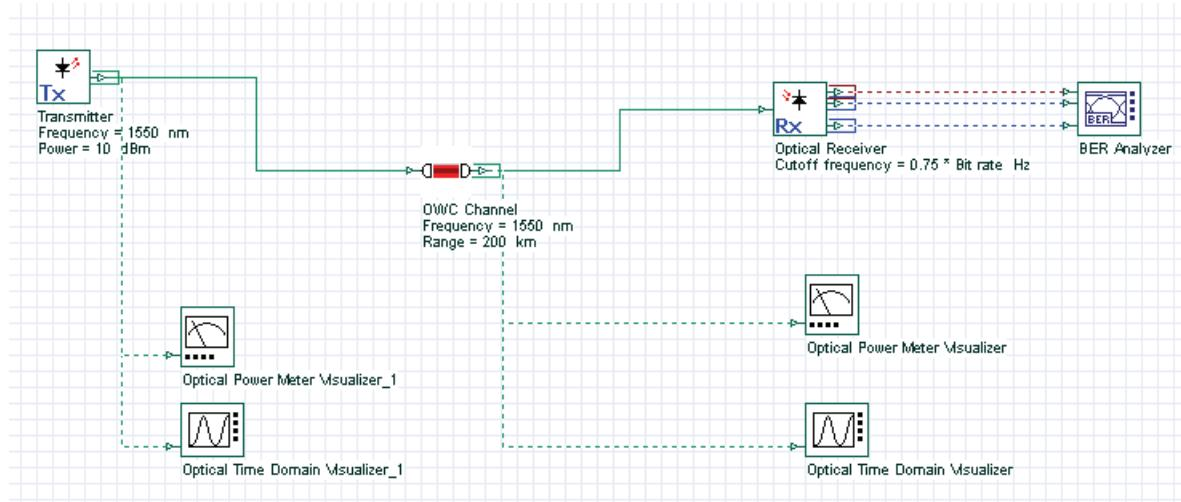
Free Space Optics (FSO) communications [1] refers to the transmission of modulated visible or infrared beams through the atmosphere to obtain optical communications. **FSO.osd** (Figure 1) demonstrates a typical free space optical link operating at 1.25 GB/s, where usually the main source of penalty is the atmospheric attenuation.

Figure 1 FSO Link



The wireless optical channel component, that is also free-space optics, can be used for large distances where the atmospheric attenuation is not the major source of penalties, but the pointing angle is. e.g. satellite communications. **WOC.osd** (Figure 2) demonstrates the impaired link performance from pointing errors between the transmitter and receiver for satellite communications [2][3].

Figure 2 WOC Link



## References

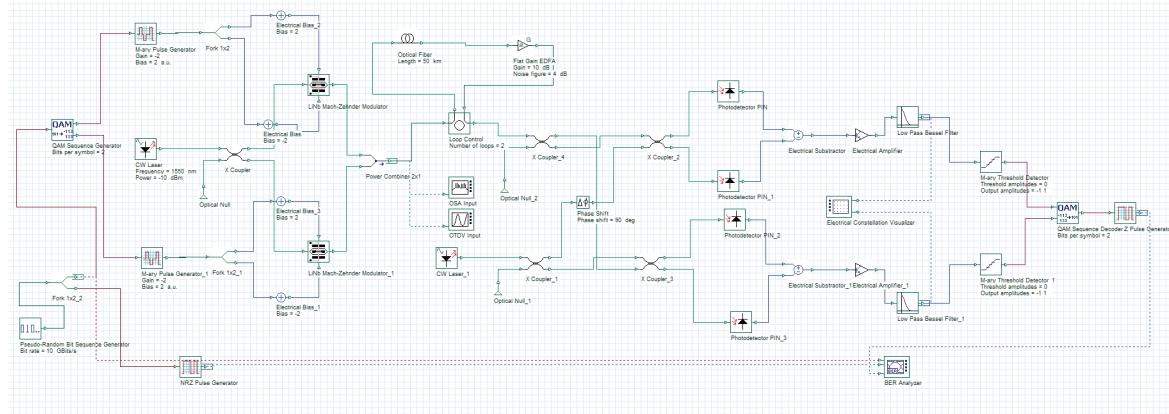
- [1] S. Bloom, E. Korevaar, J. Schuster, H. Willebrand, 'Understanding the performance of free-space optics', Journal of Optical Networking. Vol. 2, No. 6, pp. 178-200, June 2003.
- [2] A. Polishuk, S. Arnon, 'Optimization of a laser satellite communication system with an optical preamplifier', J. Optical Society of America. Vol. 21, No. 7, pp 1307-1315, July 2004..
- [3] S. Arnon, 'Performance of a laser satellite network with an optical preamplifier', J. Optical Society of America. Vol. 22, No. 4, pp 708-715, April 2005.



# Coherent Optical Transmission

**Coherent 4 QAM.osd** (Figure 1) demonstrates a 10 Gbps 4-QAM coherent optical system transmission over 100 km of fiber using homodyne detection.

Figure 1 Coherent optical transmission Link

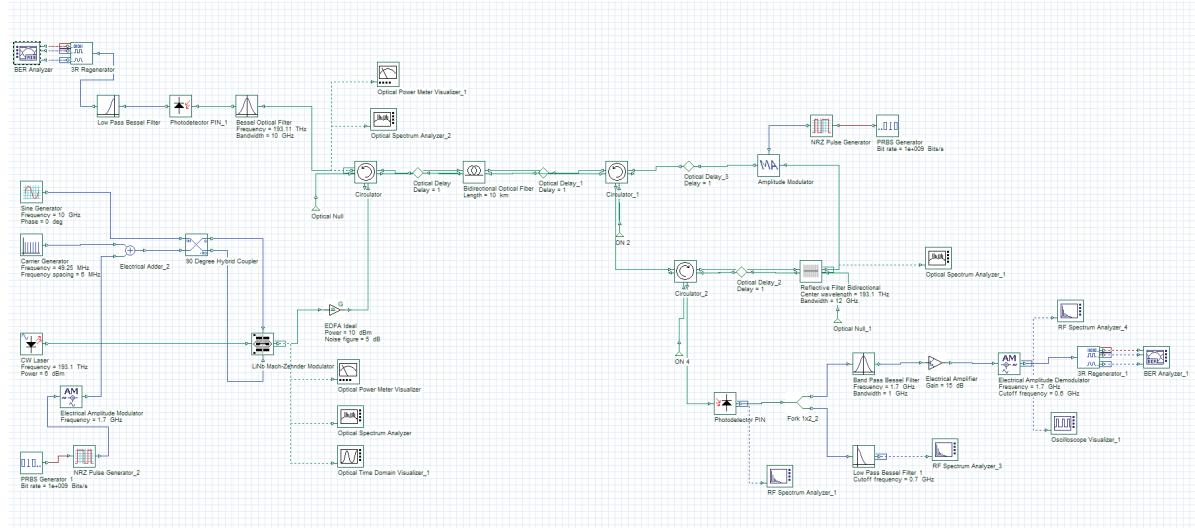


**Notes:**

# Radio over fiber (RoF)

**Radio over Fiber SCM ASK.osd** (Figure 1) demonstrates the use of a subcarrier multiplexing (SCM) architecture to transmit several analog channels and one digital amplitude-shift keying (ASK) signal in a bidirectional setup.

Figure 1 SCM ASK Link



**Notes:**

# Optical Time Domain Multiplexing (OTDM) Design

---

The objective of this lesson is to demonstrate the possibility of simulating a packet-interleaved operation using OptiSystem.

In this case, the data stream externally modulates a periodic stream of narrow pulses.

Because the bit interval is  $T$ , the separation between successive pulses is also  $T$ .

In this way, we have to reduce the interval between successive pulses to  $T_2$ , a high-rate multiplexed signal. This is done by passing the initial sequence through a series of compression stages.

If the size of each packet is  $L$  bits, the output goes through  $K$  compression stages

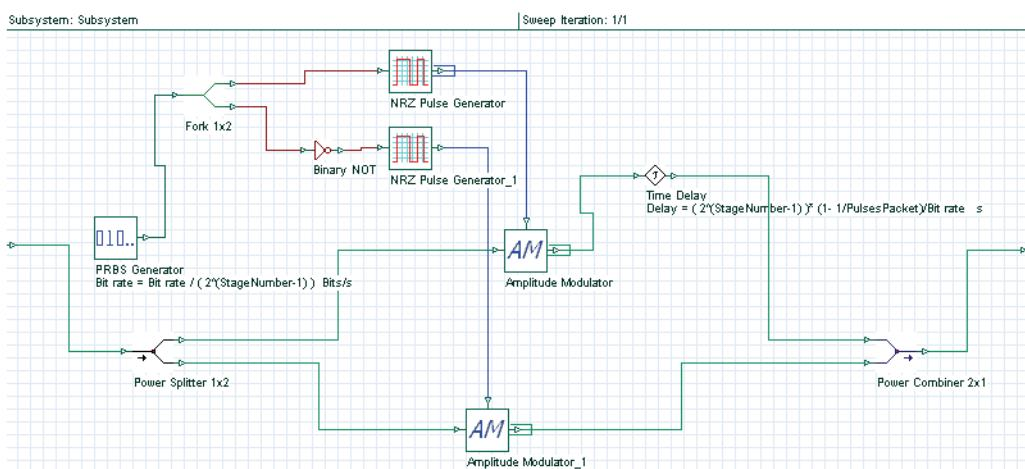
$$K = \log_2(L)$$

We have designed a compression stage with OptiSystem. See Figure 1.

The stage was implemented in a subsystem because each compression stage has the same layout.

The only difference between the compression stages were some parameters such as Bit rate at the PRBS Generator and the Delay at the Time Delay component. However, these parameters were set in script mode to allow the reuse of the subsystem.

**Figure 1 Compression stage**

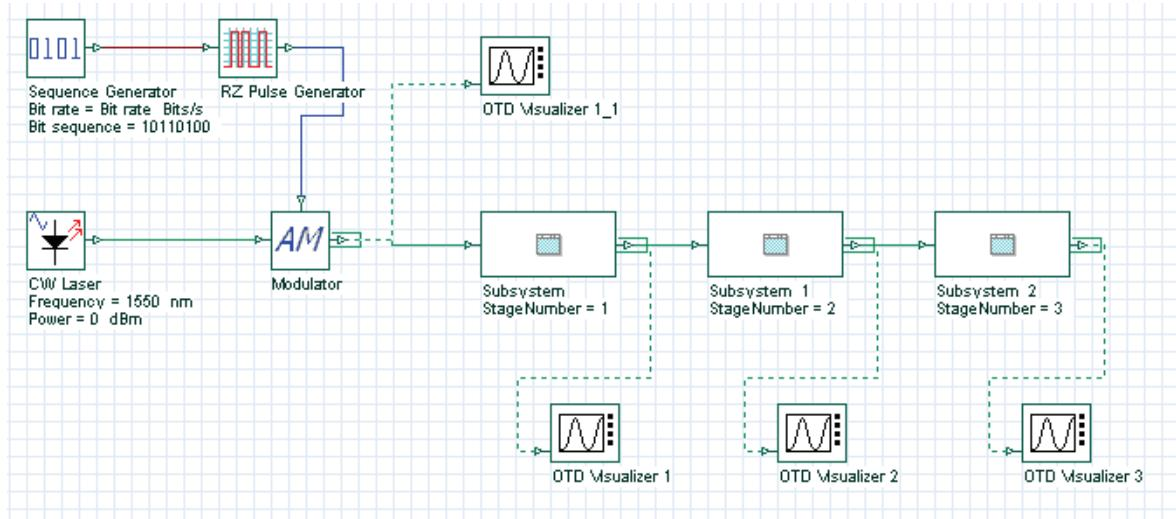


To demonstrate the packet interleaving, we have created a sample in which packets with 6 bits length are created.

The system in Figure 2 shows the layout with three compression stages.

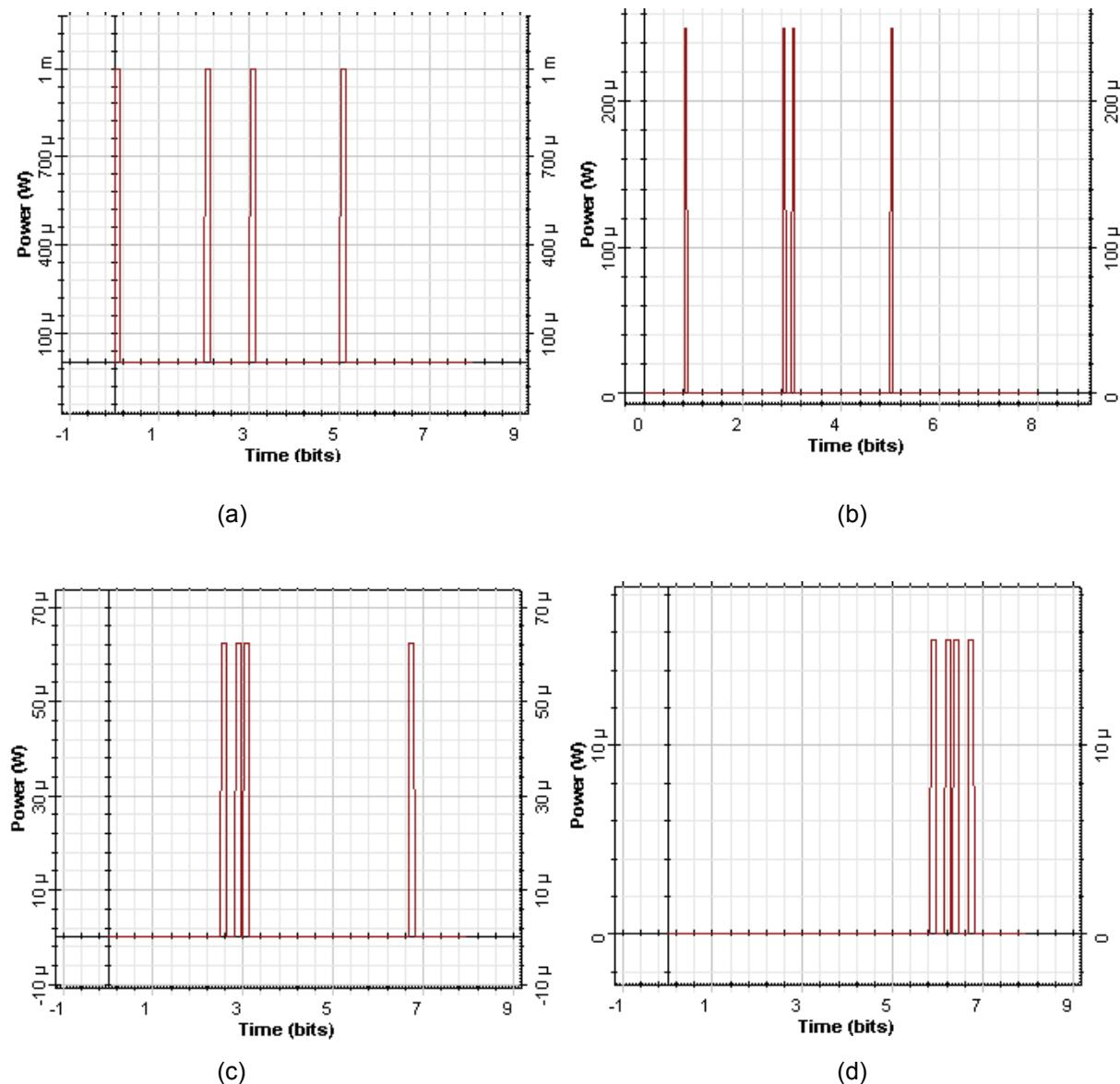
In this layout we have introduced one new tab called Multiplexer. This tab will contain the *PulseTime* parameter that specifies the pulse width and the *PulsesPacket* parameter that specifies the number of bits per packet.

**Figure 2** Packet interleaving with 6 bits/packet



The initial sequence modulated was 10110100 and the behavior of the optical signal along the transmission can be seen in Figure 3.

**Figure 3** (a) Initial bit sequence, (b) bit sequence after CS1, (c) bit sequence after CS2, and (d) bit sequence after CS3

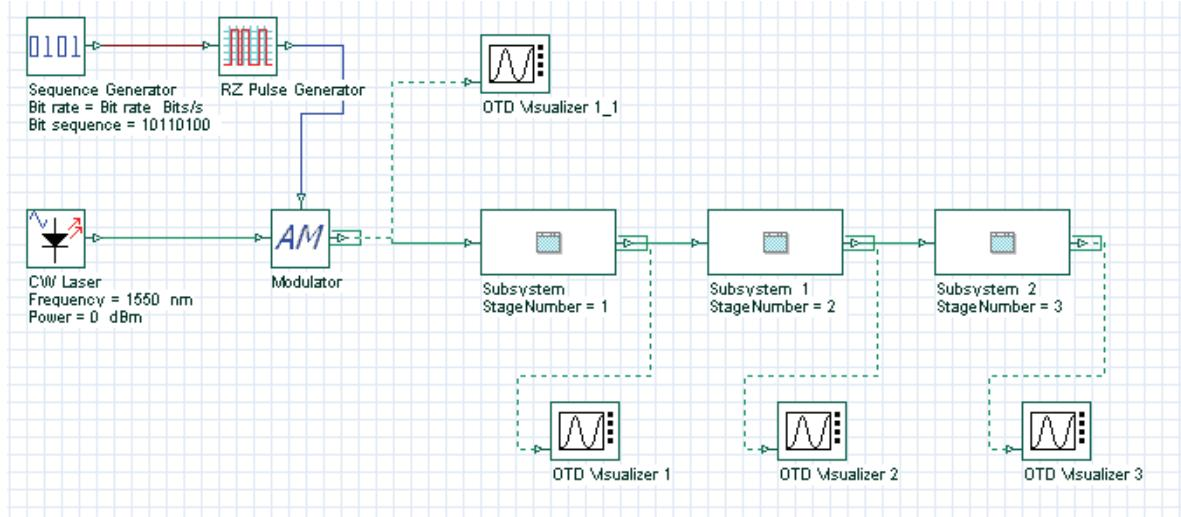


## OPTICAL TIME DOMAIN MULTIPLEXING (OTDM) DESIGN

Another system was created, but this new one has 16 bits/packet and the initial sequence was pseudo-random.

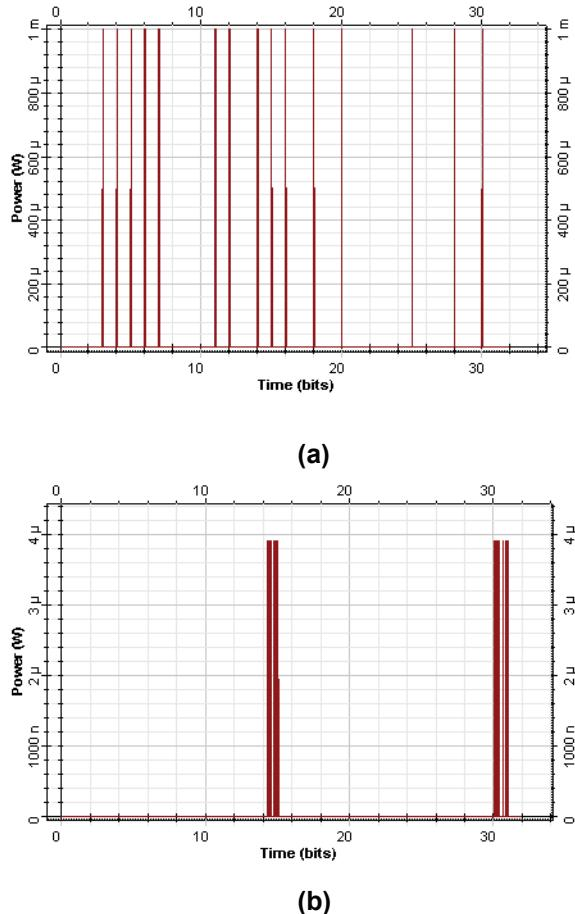
Figure 4 shows the system layout for this case. Because the packet has 16 bits, the number of compression stages must be 4.

**Figure 4** Packet interleaving with 6 bits/packet



With an initial sequence of 32 bits, the formation of 2 packets can be seen in Figure 5.



**Figure 5 (a) Input signal and (b) the two packets at output**

## References

- [1] R. Ramaswami and K. N. Sivarajan. Optical networks: A Practical Perspective - pp. 624

**Notes:**

# System Performance Analysis Using Script Automation

---

The objective of this lesson is to demonstrate the performance analysis of a system using the script page to vary the system parameters and store the results.

Sometimes, to analyze the system performance, several parameters in the system are varied and the results for each different configuration have to be stored.

One way to perform these simulations is to put the parameters in sweep mode.

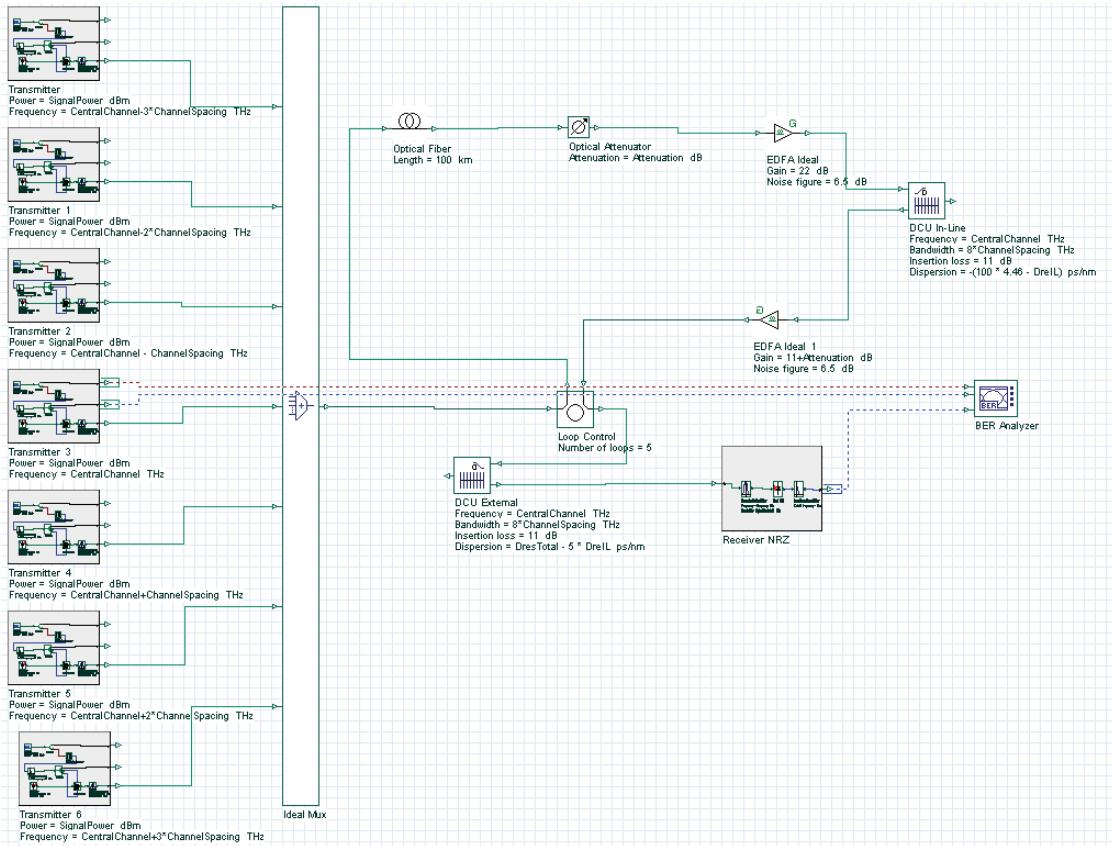
This method can be very effective if we have few parameters to analyze, but when the number of parameters increases, this kind of simulation can become too complex to setup all possible combination of values for each parameter.

Another issue is that all results are stored during the simulations, which can cause the simulations to slowdown because of the increase in the memory used.

The other way to do the simulation is to use the script page to set up the parameter values and store only the necessary results. In this method, the parameter setup is easier and you can specify which results you want to be stored.

In this example, we have 7 channels being propagated along 5 spans with 100 km of fiber and 2 dispersion compensation units (DCU). See Figure 1.

Figure 1 System layout



In this example, we want to vary the dispersion value for each DCU. To do that, we must programme in the script page to vary the parameters "DreIL" and "DresTotal". These are the dispersion of the DCU in line and the DCU external, respectively.

In the code, we select to save the result "Max. Q Factor" from the BER Analyzer and the way the parameters will be varied.

Finally, we allow the parameters and results to be stored in the spreadsheet software Microsoft Excel. The following code was written in the script page.

```

'-----
'OptiSystem Script: Nested Cloops with 2 parameters and 1 result
'      Parameters and Results can be exported to Excel or as Text
'-----
'-----
'Global parameters - Parameter and Result names
'-----
ComponentName1 = "Layout 1"

ParameterName1 = "DreIL"
ParameterName2 = "DresTotal"

VisualizerName1 = "BER Analyzer"

ResultName1 = "Max. Q Factor"

'-----
'Global parameters - Sweep ranges for parameters
'-----
NumberOfSweepIterations1 = 10
ParameterStart1 = -100
ParameterEnd1 = 100

NumberOfSweepIterations2 = 10
ParameterStart2 = -90
ParameterEnd2 = 90

'-----
'Internal parameters - step for each sweep
'-----
ParameterStep1 = ( ParameterEnd1 - ParameterStart1 ) / ( NumberOfSweepIterations1 - 1 )
ParameterStep2 = ( ParameterEnd2 - ParameterStart2 ) / ( NumberOfSweepIterations2 - 1 )

'-----
'Create Excel application - visible must be FALSE
'-----
Dim Excel
Set Excel = CreateObject("Excel.Application")

Excel.Visible = false
Excel.Workbooks.Add

'-----
'OptiSystem SDK specifics - access components and visualizers
'-----
Dim LayoutMgr
Set LayoutMgr = Document.GetLayoutMgr

```

```

Dim Layout
Set Layout = LayoutMgr.GetCurrentLayout

Dim Canvas
Set Canvas = Layout.GetCurrentCanvas

'Dim Component1
'Set Component1 = Canvas.GetComponentByName(ComponentName1)

Dim Visualizer1
Set Visualizer1 = Canvas.GetComponentByName(VisualizerName1)

'-----
' Calculation loop - access parameters and results
'-----

Count = 1

For i = 0 to NumberOfSweepIterations1 - 1

    For j = 0 to NumberOfSweepIterations2 - 1
        'Parameter Values
        ParameterValue1 = ( ParameterStart1 + i * ParameterStep1 )
        ParameterValue2 = ( ParameterStart2 + j * ParameterStep2 )

        'Set component parameters
        Layout.SetParameterValue ParameterName1, ParameterValue1 * 1.0
        Layout.SetParameterValue ParameterName2, ParameterValue2 * 1.0

        'Calculate
        Document.CalculateProject TRUE , TRUE

        'Acces visualizer results
        Set Result1 = Visualizer1.GetResult( ResultName1 )

        'Access resut values
        ResultValue1 = Result1.GetValue( 1 )

        'Send parameters and results to Excel
        Excel.ActiveWorkbook.Worksheets("sheet1").Cells(Count,1) = ParameterValue1
        Excel.ActiveWorkbook.Worksheets("sheet1").Cells(Count,2) = ParameterValue2

        Excel.ActiveWorkbook.Worksheets("sheet1").Cells(Count,3) = ResultValue1

        Count = Count + 1
    Next
Next

```



```
'-----
'Enable Excel application - visible must be TRUE
'-----'
```

Excel.Visible = true

Part of the results obtained when running the script can be seen in Figure 2. In Figure 2, column A is the "DreI1", column B is the "DresTotal" and column C is the Q factor.

**Figure 2 Parameters and results stored**

	A	B	C
1	-100	-90	0
2	-100	-70	2.43978
3	-100	-50	2.865152
4	-100	-30	3.397961
5	-100	-10	3.226432
6	-100	10	3.453008
7	-100	30	3.291738
8	-100	50	3.408063
9	-100	70	0
10	-100	90	0
11	-77.7778	-90	0
12	-77.7778	-70	2.461173
13	-77.7778	-50	2.892471
14	-77.7778	-30	3.418999
15	-77.7778	-10	3.236905
16	-77.7778	10	3.477885
17	-77.7778	30	3.310275
18	-77.7778	50	3.416951
19	-77.7778	70	0
20	-77.7778	90	0
21	-55.5556	-90	0
22	-55.5556	-70	2.530924
23	-55.5556	-50	2.903407
24	-55.5556	-30	3.443426
25	-55.5556	10	3.252275



**Notes:**



---

## **WDM systems**

---

This section contains the following advanced and illustrative simulation projects.

- Comparison of RZ and NRZ modulation formats for 40 Gb/s systems
- 16 channel WDM system design
- WDM components—Tunable filters
- WDM components—AWG demultiplexer
- Broadcast star coupler
- Optical cross-connects
- Configurable optical add-drop multiplexer
- Advanced modulation formats
- Conventional duobinary transmitter
- Modified duobinary transmitter
- Interferometer characterization

**Notes:**

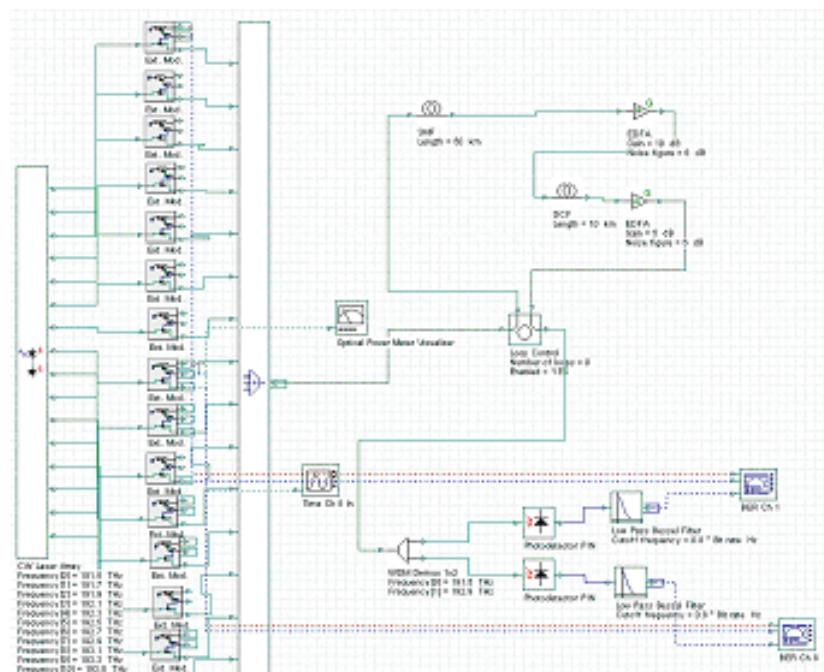
# Comparison of RZ and NRZ modulation formats for 40 Gb/s systems

Most installed fibers are standard single mode fibers (SMF) with high group velocity dispersion values ( $\sim 16\text{ps/nm/km}$ ) at  $1.55 \mu\text{m}$ . To achieve a good level of bit-error-rate (BER) as well as to enable larger repeater spacing and larger signal-to-noise ratio (SNR) in this type of fiber, it is very important to consider the influence of group velocity dispersion, nonlinear effects, PMD, and their interplay on the transmitted signals. Increasing the capacity of optical systems may require either an increase in the bit rate, usage of WDM or ultimately both. At high bit rates, the modulation format, type of dispersion compensation scheme, and channel power become important issues for optimum system design. In particular, it has been demonstrated numerically and experimentally that the conventional nonreturn-to-zero (NRZ) modulation format is superior compared to the return-to-zero (RZ) modulation when dealing with large WDM systems, as RZ modulation causes a significant Eye Closure Penalty near end channels. The results obtained in this tutorial will be used to compare the Eye Closure Penalties for both NRZ and RZ cases, as well as the effects of nonlinearities.

This tutorial will take you through every aspect of the design, from discussions of why certain parameters are chosen, to the significance of these parameters, and finally to the effects that these parameters have on simulated results.

The project file, which shows the layout of the 40 Gb/s system using NRZ modulation, can be found in "[16Ch\\_NRZ\\_40G\\_Variied\\_GVD.osd](#)".

**Figure 1 40 Gb/s using NRZ**



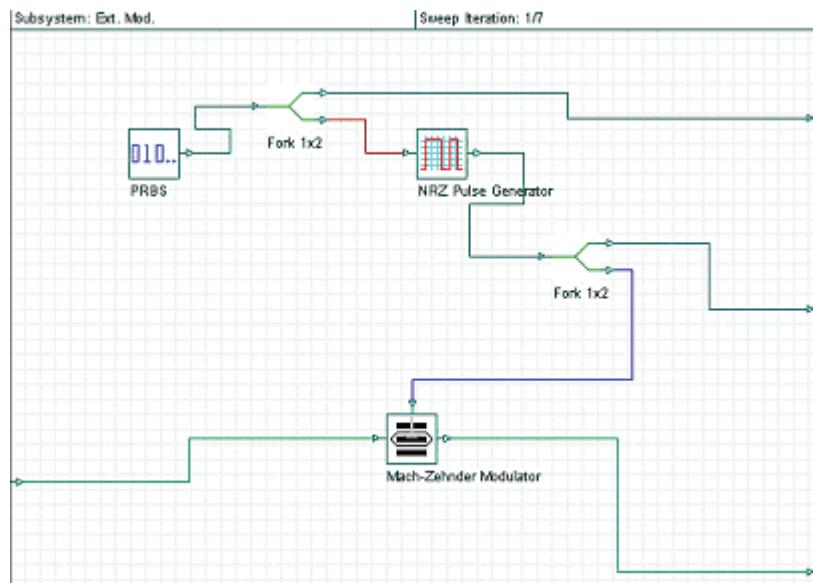
This design has 16 channels, spaced 200 GHz apart, propagating through 300 km of SMF fiber. The results of the 1st channel are then analyzed (as this is the worst-case scenario).

In order to give you a clear picture of the entire design, we will look into each component individually, and discuss which parameters are important and why. We will start with the Externally Modulated Subsystem.

### Externally Modulated Subsystem

The Pseudo Random Bit Sequence (PRBS) generator, NRZ pulse generators, and Mach-Zehnder modulators, are all located inside the Subsystem (see [Figure 2](#)). The use of a subsystem illustrates the hierarchy of the system, and simplifies the entire design process.

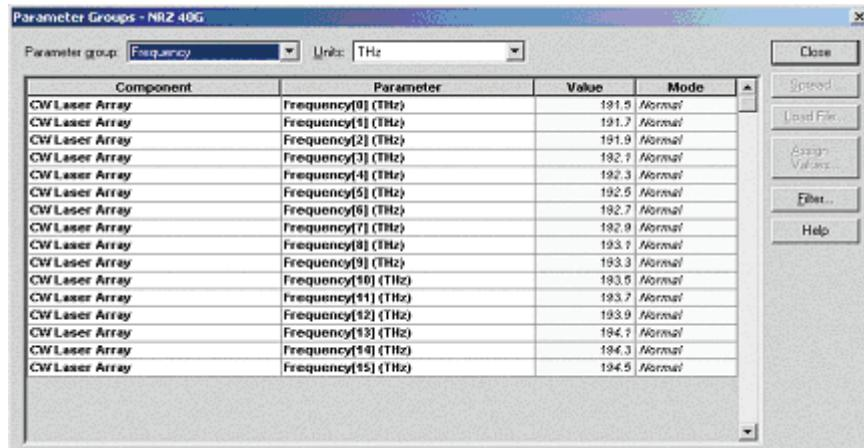
**Figure 2** Externally modulated subsystem



## CW Laser Array

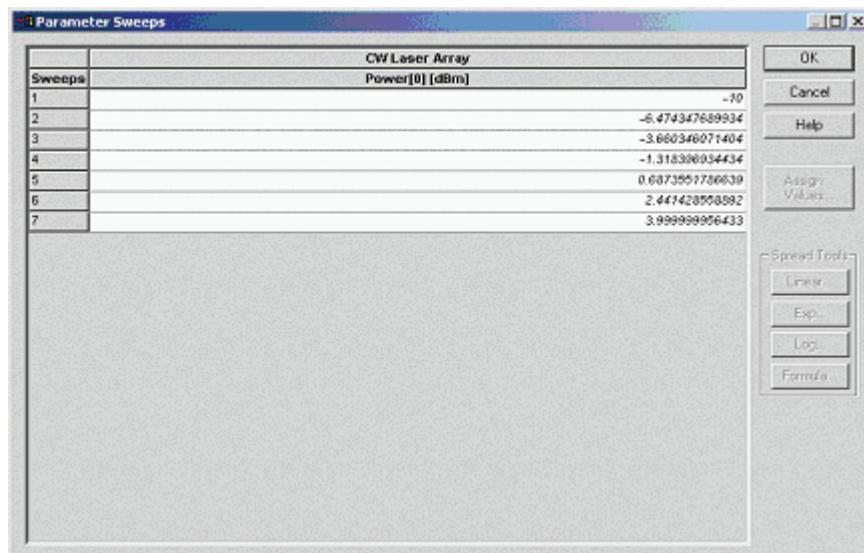
You should first enter the number of output ports, and then start inputting the Frequency values for each channel. The frequency values can be entered individually, copied/pasted from Excel, or entered in the Parameter Groups dialogue box (Figure 3). The **Parameter Groups** dialog box allows you to enter the first frequency value, and then increment every following frequency by a constant value. This method saves time when dealing with several channels.

**Figure 3 Parameter Groups**



Go to the **Power** tab in the CW Laser Array dialog box. You will first notice that the mode for the Power is on 'Sweep'. In this example we have chosen to run 7 different iterations, so the sweep mode allows us to change the input power for each of these 7 iterations (Figure 4). In this case, we made a sweep from -10 dBm to 4 dBm.

**Figure 4 Power Sweep**

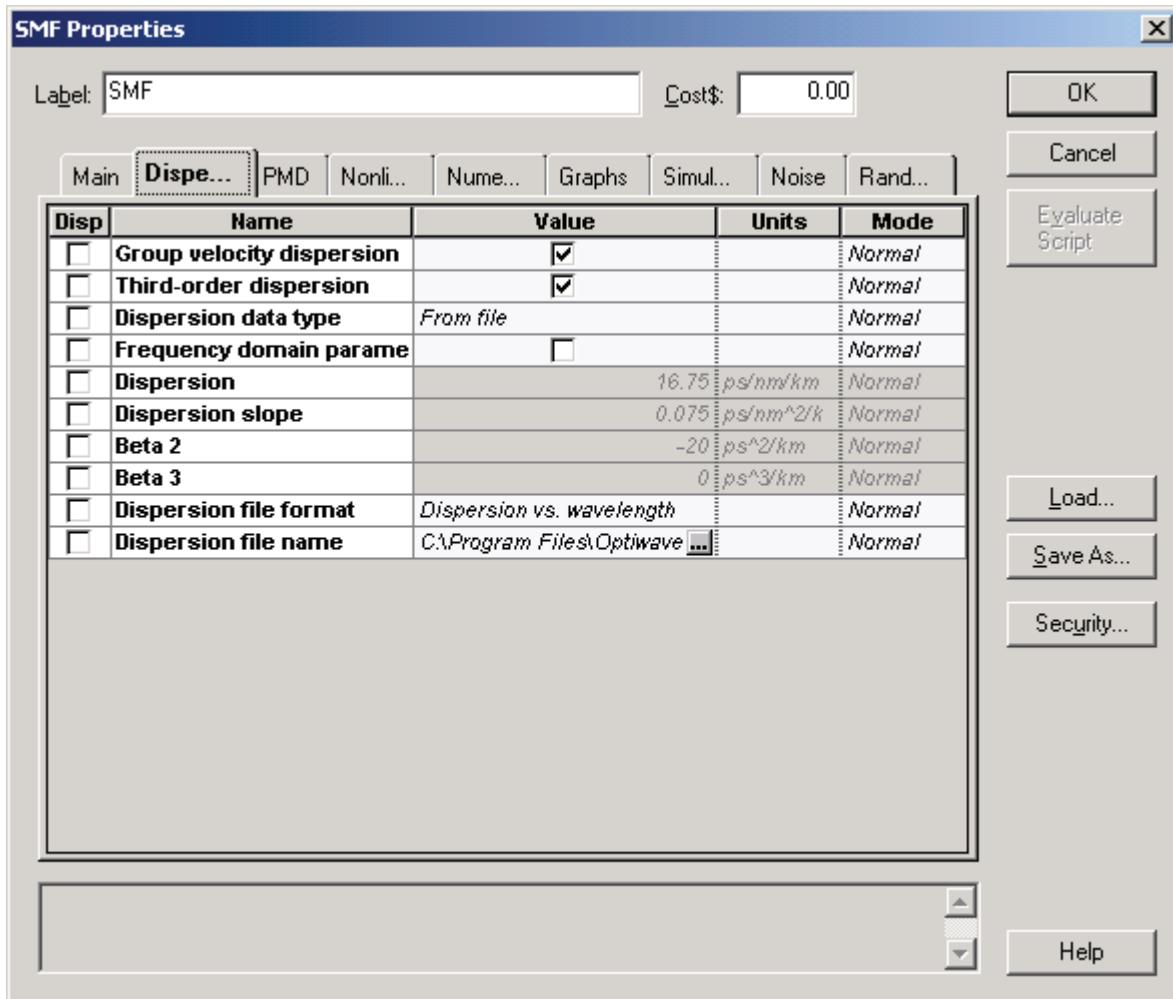


## Single Mode Fiber

The parameters chosen for the SMF are extremely important, and will significantly affect the simulation results. The first tab allows you to choose the length of your fiber (50 km in this case), attenuation, and input/output coupling efficiencies.

Under the **Dispersion** tab, you will notice that we have loaded a GVD data file ([Figure 5](#)). This file will allow us to control the dispersion spectrum. This is very important when dealing with WDM systems, because the constant dispersion slope is not accurate for channels that are located far away from the central channel.

**Figure 5 Dispersion tab**

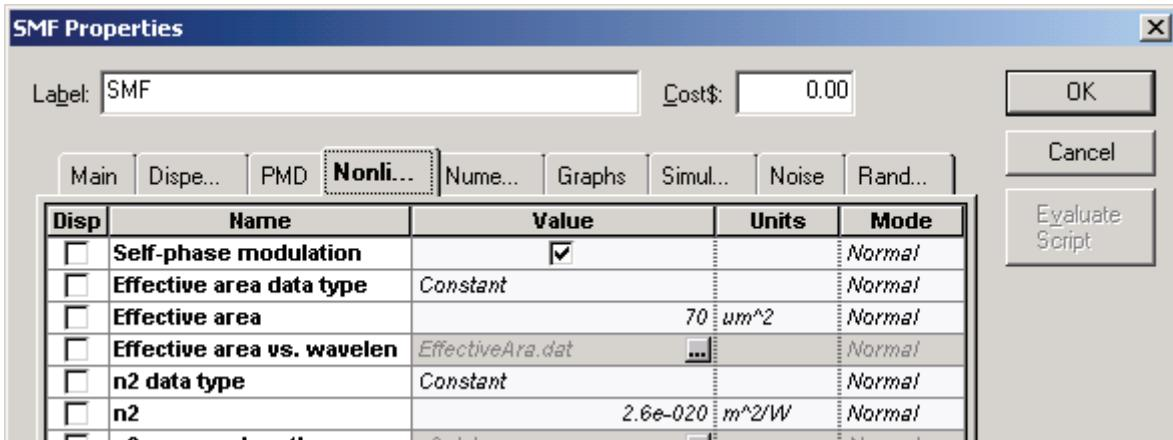


Now we will look at the **Nonlinear** tab ([Figure 6](#)), where you can control all of the nonlinear parameters, such as Effective Area and n2.

The most important parameter in this tab is the Effective Area. This value can be obtained from the fiber vendors.



Figure 6 Nonlinear tab



**Note:** The default values for the numerical parameters will work in most cases, however, when the complexity of the design increases, the importance of these parameters increases.

In summary, here are the most important parameters in the fiber component:

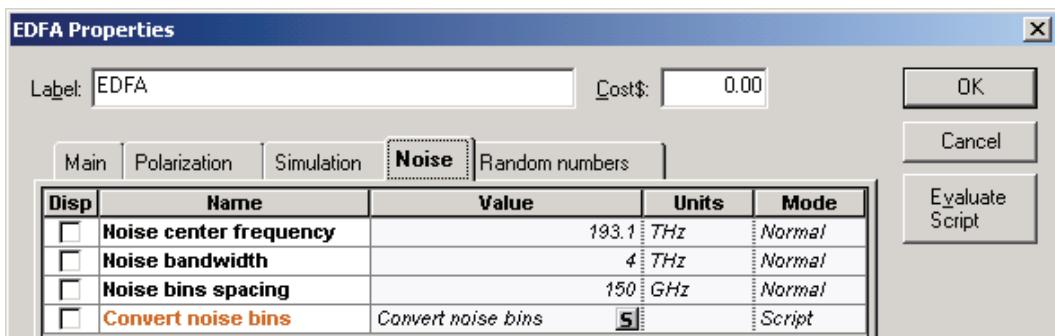
- Length
- Attenuation
- GVD (a data file should be used for WDM systems)
- Dispersion Slope
- Effective Area
- Proper selection of Effects
- Numerical Details (for larger and more complicated systems)

If all these parameters are entered correctly, the accuracy of the simulation will be extremely high. Most of these parameters can be obtained directly from fiber vendors, however, if you are having difficulty finding them, please download some of the scientific papers that are available on our website.

## EDFA

The next component we will look at is the **Erbium Doped Fiber Amplifier**. In this tutorial we use an Ideal EDFA model, which is only concerned with the values of Gain and Noise Figure. These two values are fairly straightforward, as the Gain is set to compensate for the power loss in the fiber, and the Noise Figure is set to a standard value of 6 dB. The next step is to set the Noise parameters to include the noise over the entire simulated bandwidth (Figure 7). In this case, we set the center frequency equal to that of the central channel, and the bandwidth to a value that would include all neighboring channels. Then we choose a bin spacing that will be small enough (to increase accuracy) but not too small.

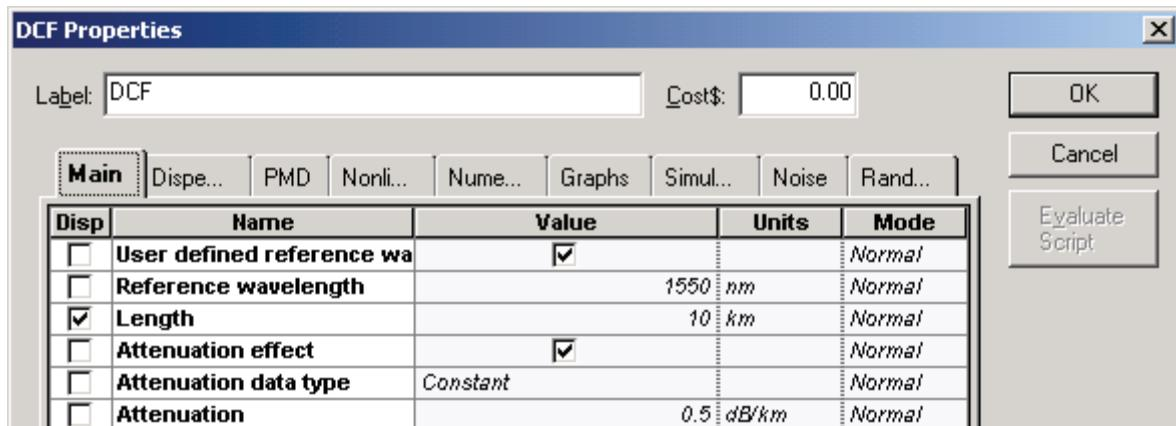
Figure 7 Noise parameters



## DCF

The **Dispersion Compensating Fiber** parameters were chosen similar to the SMF. However, in this case we want to set the Length, GVD, and Dispersion Slope as to perfectly compensate for the dispersion accumulated in the SMF component (see Figure 8).

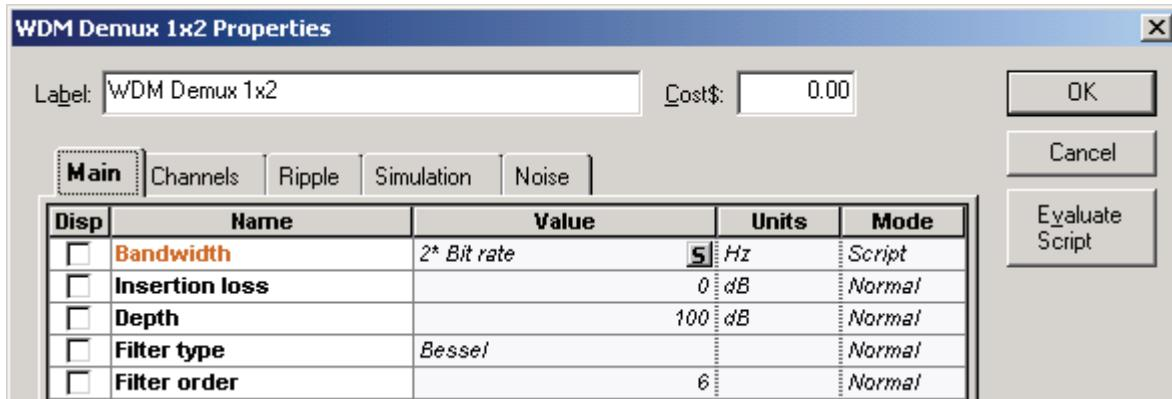
Figure 8 DCF Main properties



## WDM Demux

In this component we are filtering out the 1st and 8th channels, and analyzing the 1st channel using the BER Analyzer (Figure 9). It is very important in the Mux/Demux components to properly set the filter shape and bandwidth, as to properly filter out the channels. The user should also remember to set the appropriate center frequencies for each channel.

**Figure 9 WDM Demux Main properties**



## Remaining Components

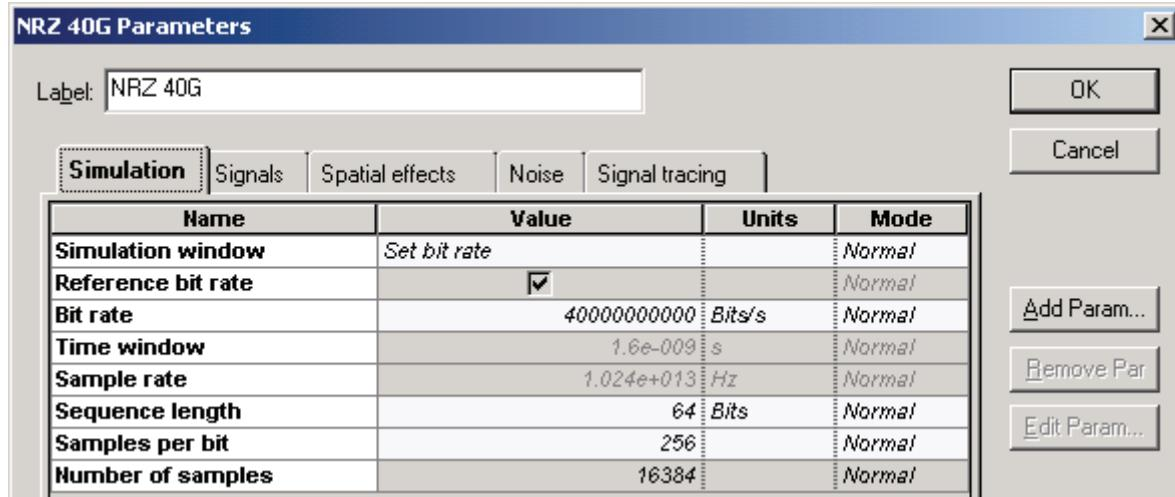
The rest of the components are very simple, and most of the time, will work fine with their default values. I suggest only modifying default parameters, if you are confident that the changes you are making are correct.

Each of these components was modeled from a validated scientific paper. The parameters chosen as defaults were based on industry standards. All references are given in the Technical Background of each component.

## Layout Parameters

Choosing proper global parameters is very crucial when trying to obtain accurate results. The **Layout Parameters** dialog box can be opened by double-clicking anywhere on the layout (Figure 10).

**Figure 10 Layout parameters**



Now here is a set of rules that will help you in your designing process:

### Quick Simulation (fairly accurate results)

- Sequence length = 64
- Samples per bit = 64

**Note:** For large WDM systems, you may want to try decreasing these numbers to 16, however, erroneous results may occur.

### Long Simulation (more accurate results)

- Sequence length > 64 and < 1024
- Samples per bit > 64 and < 1024

**Note:** The best suggestion would be to use 128 for both the length and samples per bit.

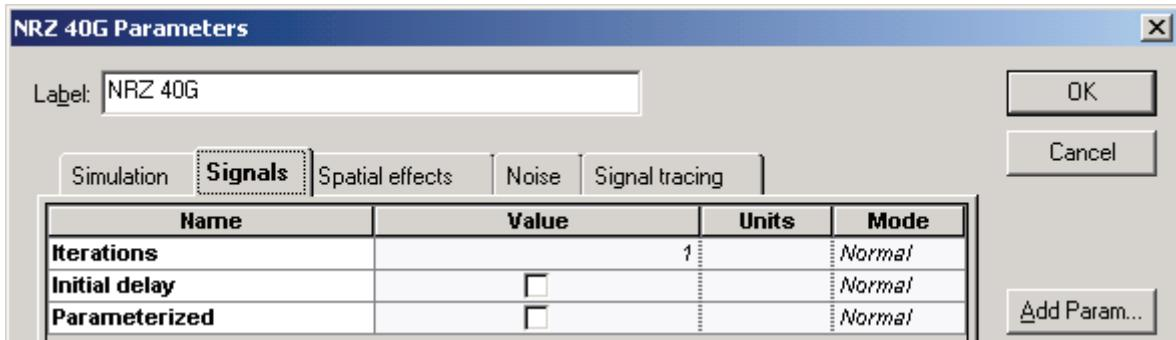


In this tutorial, we use a Sequence length = 64, so that we can properly compare with the following scientific paper: "M.I. Hayee and A.E. Willner, "NRZ Versus RZ in 10-40 Gb/s Dispersion - Managed WDM Transmission systems", IEEE Photon. Technol. Lett., vol. 11, pp.991-993, 1999."

We also use a Sample rate of 10.24 THz, so that all the channels are combined into 1 single band.

The Signals tab, allows you to simulate Parameterized signals (signals that have only 1 power and 1 frequency) instead of Sampled signals (Figure 11). This is very useful for large WDM systems where a power budgeting analysis is required. By parameterizing the signals, the simulation will run almost instantly, allowing you to make designs that are complex, require many iterations/optimizations, and have several channels.

**Figure 11 Signals tab**



The **Noise** tab allows you to convert the noise bins into signals. This will then add the noise and signals together, rather than propagating them as separate arrays.

### Conclusion regarding parameter selection

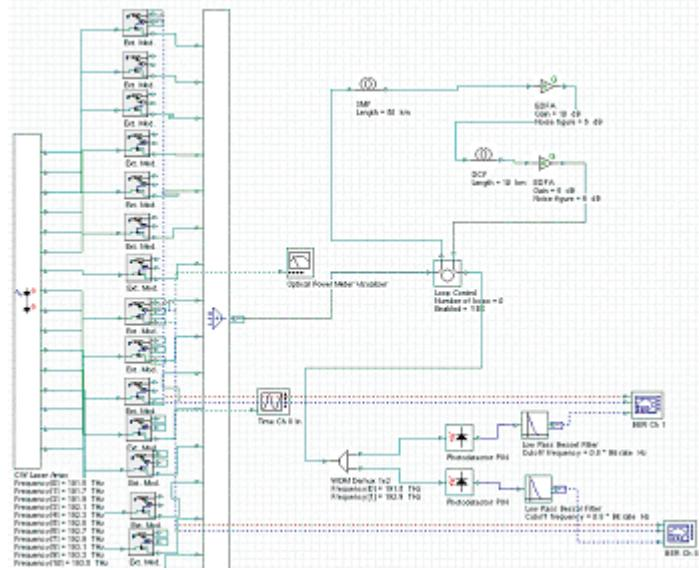
Selecting the proper parameters is the most important step when designing an entire system. Many components/parameters are not known well by users, so they may find it difficult to set all parameters properly. We suggest that at a minimum, the system designer set the proper parameters in the fiber components, amplifiers, and WDM components. These key components have the greatest effect on the outcome of your results.

When you are familiar with the components, you can start simulating. You should start off with fast simulations, in order to narrow down major design problems, and then change the Layout parameters accordingly, to increase the accuracy of your simulation. This will save time in system design, and the outcome should be more satisfying.

## Results of NRZ simulation

After simulating the design, we can analyze any port that has a monitor attached to it. You can identify which ports have monitors attached, because there will be boxes around them (see [Figure 12](#) for an example).

**Figure 12 Monitors**



You can put a monitor on any output port you want—simply click on the monitor tool, and then click on the output ports you wish to analyze. When this is done, you can simulate your project, and all the data will be saved.

**Note:** A monitor is automatically attached if a visualizer is attached to that port.

In this specific design, we have the following 3 types of visualizers connected to our system:

**Optical Power Meter:** shows the total power at a specific location in the system (see [Figure 13](#)).

**Optical Time Domain Visualizer:** displays the Time Domain information for the 8th channel (see [Figure 13](#)).

**BER Analyzers:** displays the Eye Diagram, Q-factor curve, Min BER, Threshold, Eye Height, and BER Patterns for the 1st and 8th channel (see [Figure 14](#)).



Figure 13 OTDV for Channel 8

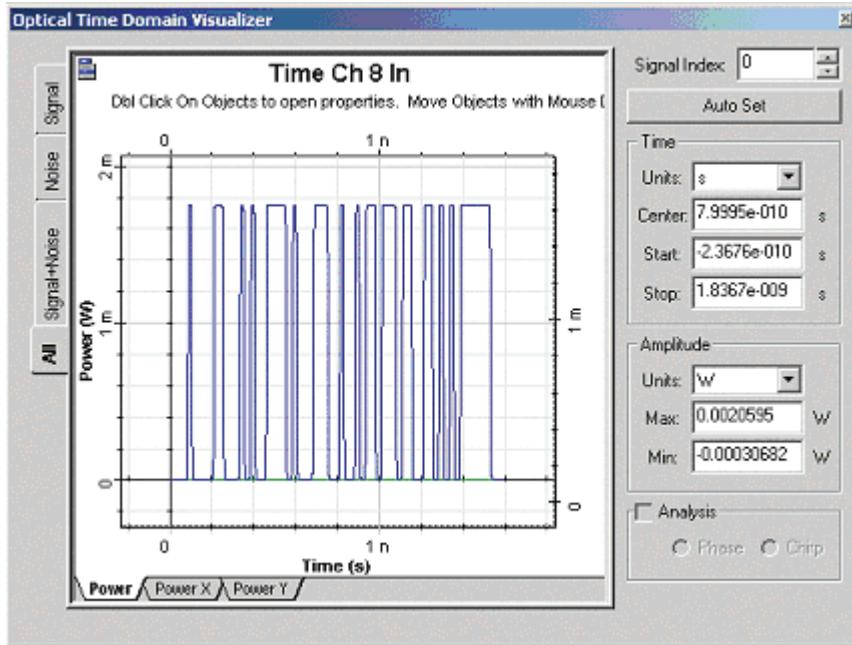
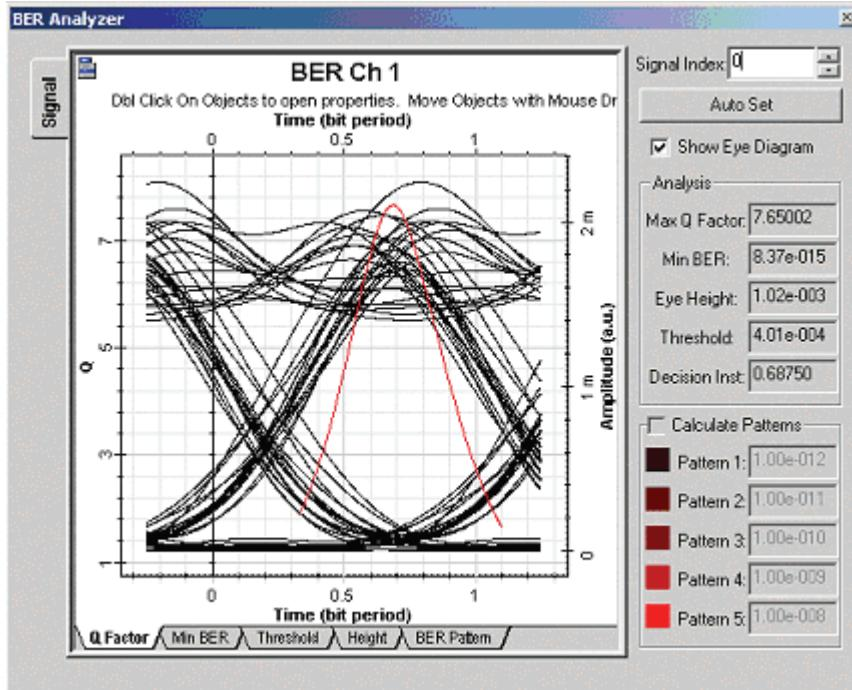


Figure 14 BER Analyzer for Channel 1



For the purposes of this tutorial, we are concerned with the Eye Height values obtained from the best (8th channel) and worst (1st channel) scenarios.

The best way to obtain this information quickly and efficiently is to use the Project Browser. This will allow us to display the data for all iterations on a single spreadsheet.

**Figure 15 Results tab display**

Name	Value
NRZ 40G	7
Global	
BER Ch 1	BE...
Ports	
Parameters	
Results	
BER after FEC at User Defin...	0
BER after FEC at User Defin...	0
BER at User Defined Decisio...	0
BER at User Defined Thresh...	0
Bit Rate [Bits/s]	0
Decision Instant at Min. BER...	0
Extinction Ratio at Min. BER	0
Extinction Ratio at Min. BER ...	0
Extinction Ratio at Min. BER ...	0
Extinction Ratio at User Defi...	0

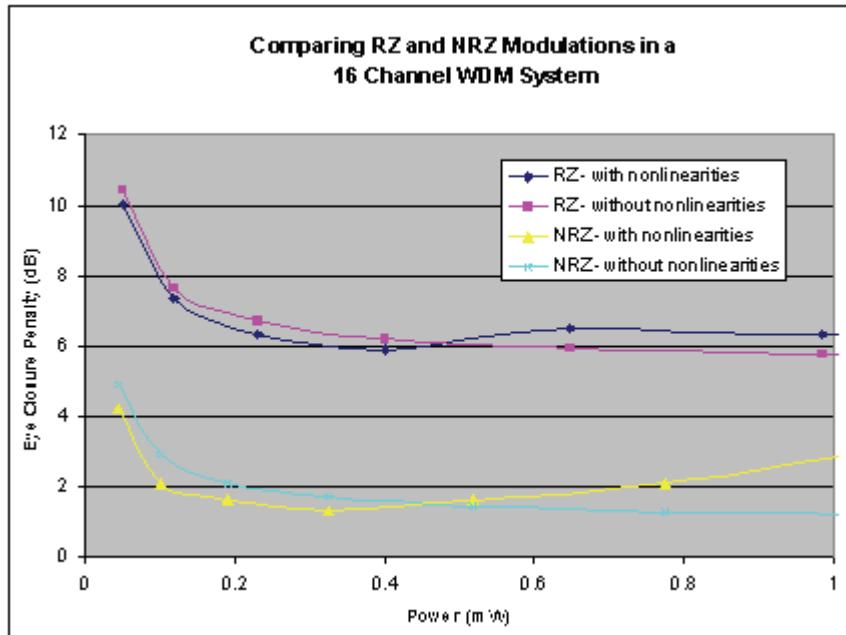
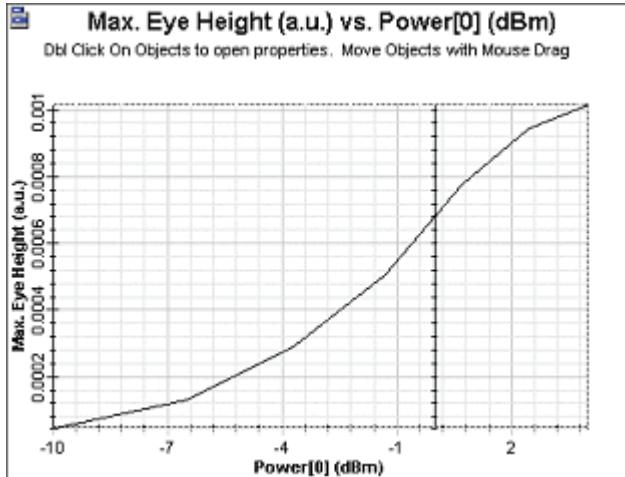
For all 7 iterations, the Max Eye Height for channels 1 & 8 and the Total Input Power have been calculated. This allows us to construct a graph of Eye Closure Penalty vs. Input Power. However, to construct such a Graph, we will need the results from the back-to-back system (MUX ® DEMUX).

These results have been calculated in "16Ch NRZ Ideal.osd". We also calculated the same system without the nonlinear effects in "16Ch NRZ 40G\_varied GVD\_Xnonlinear.osd".

The entire process was then repeated using RZ modulation. When all the data was collected, and the Eye Closure Penalty was calculated, the graph ([Figure 16](#)) was generated.

This graph shows the relationship that RZ and NRZ modulation have on input power. It also shows the difference obtained when taking into account the nonlinear effects. These results have very good agreement with the published results of Willner's paper [\[1\]](#), and suggest to system designers that the use of NRZ modulation becomes very important when dealing with WDM systems that have many channels.



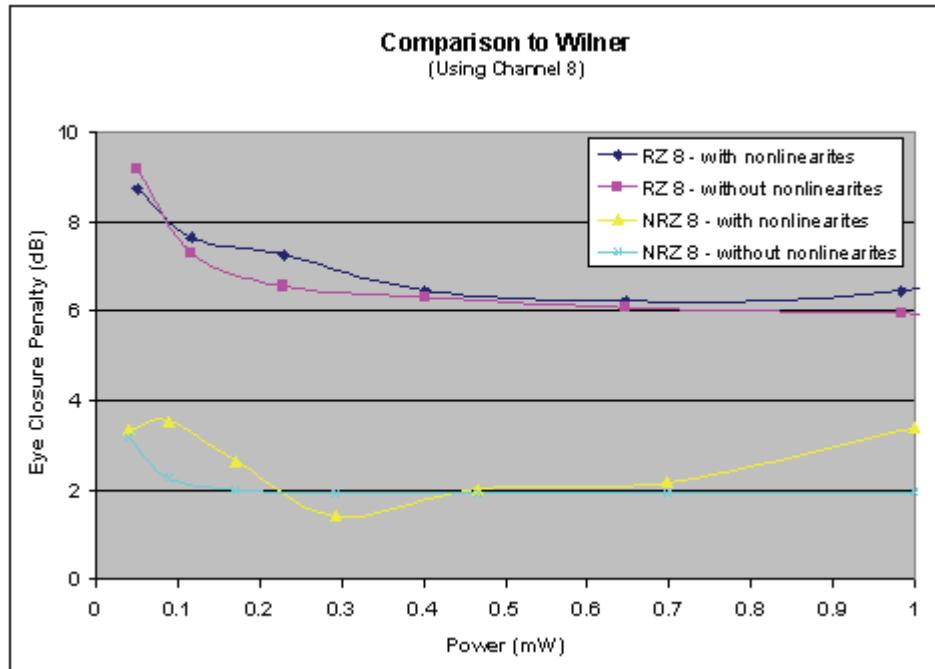
**Figure 16 Eye Closure Penalty for 16 Channel system****Figure 17 Eye Height vs. Power**

## 32 Channels

In this part of the tutorial, we are expanding our system from 16 channels to 32 channels. In this case, we simply added 8 channels at both the beginning and the end of our 16 channel system. The frequencies and powers were then modified, so that they could be integrated with the rest of the system.

After running all 3 simulations (ideal, with nonlinearities, and without nonlinearities) and calculating the results, the graph in [Figure 18](#) was generated.

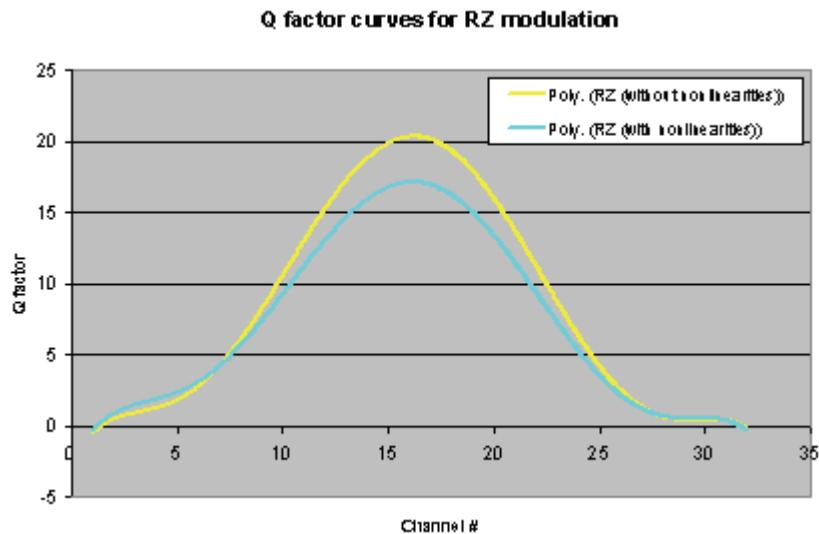
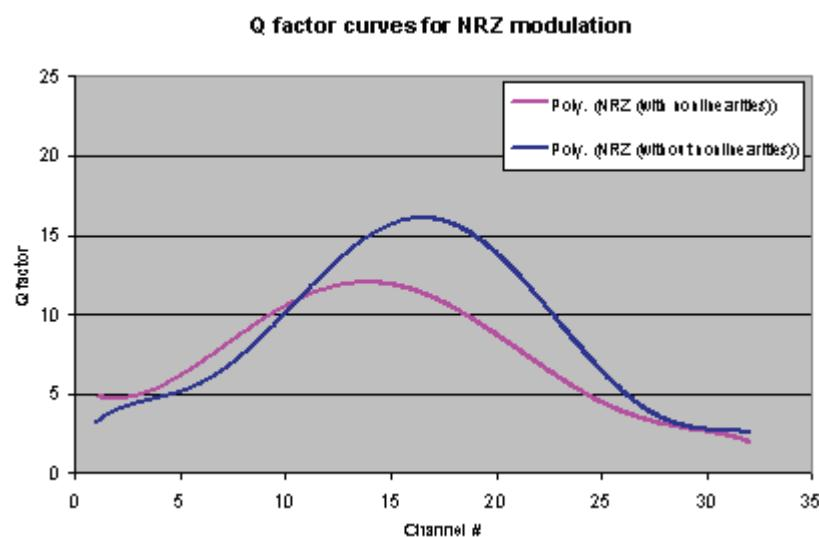
Figure 18 Eye Closure Penalty versus Power (32 Channels)



Since the Eye Closure Penalty was far too high for the end channels (in the case of RZ), the 8th channel was used instead. The results correlate to those in the 16 channel design, and suggest that we have obtained good agreement with Willner's paper [1].

One very important aspect of WDM system design is the Q-factor of the worst-case scenario. In both the RZ and NRZ cases, the worst Q-factor comes from the 1st and 32nd channels (end channels), as they experience the most dispersion. As a full analysis, we have constructed curves to demonstrate the relationship between Q-factor and Channel #, for both the RZ and NRZ cases (Figure 19 and Figure 20).



**Figure 19 Q-factor versus Channel # for RZ modulation****Figure 20 Q-factor versus Channel # for NRZ modulation**

## Discussion

As you went through this tutorial, you have learned that there are many factors that are crucial in obtaining good results, such as fiber and laser settings, layout parameters, and proper setup of the system. Most designers do not have knowledge about every component in an optical system, and usually have less knowledge about the simulation parameters. Therefore, it is suggested that small steps be taken through the design process—start with a few components, test the design, and then slowly add more components to it. Being hasty in the design process can cause you problems in the long run.

When we analyzed a 16 channel, 40 Gb/s system using both RZ and NRZ modulation techniques, the results we obtained agreed well with scientific papers, and suggested that NRZ modulation was the superior technique when dealing with large WDM systems. The curves of Eye Closure Penalty versus Input Power demonstrated that NRZ modulation works better for both low and high input powers, regardless of the fact that NRZ is more affected by the nonlinearities in the high power regime.

We then expanded our system to 32 channels, where we obtained results that correlated well with those of the 16 channel system. As a further investigation into the system performance, we graphed the Q-factors versus Channel #, and found that the Q-factors for the RZ modulation dropped off much quicker than those for the NRZ modulation. This demonstrates once again that RZ modulation performs worse than NRZ when the number of channels in the system becomes significant.

**Note:** The default layout parameters have been set slightly different from those used in this tutorial, in order to provide you with a much quicker analysis of the design.

## Reference:

- [1] M.I. Hayee, and A.E. Willner, "NRZ Versus RZ in 10-40-Gb/s Dispersion managed WDM transmission systems", IEEE Photon. Technol. Lett., vol. 11, pp.991-993, 1999.



# 16 channel WDM system design

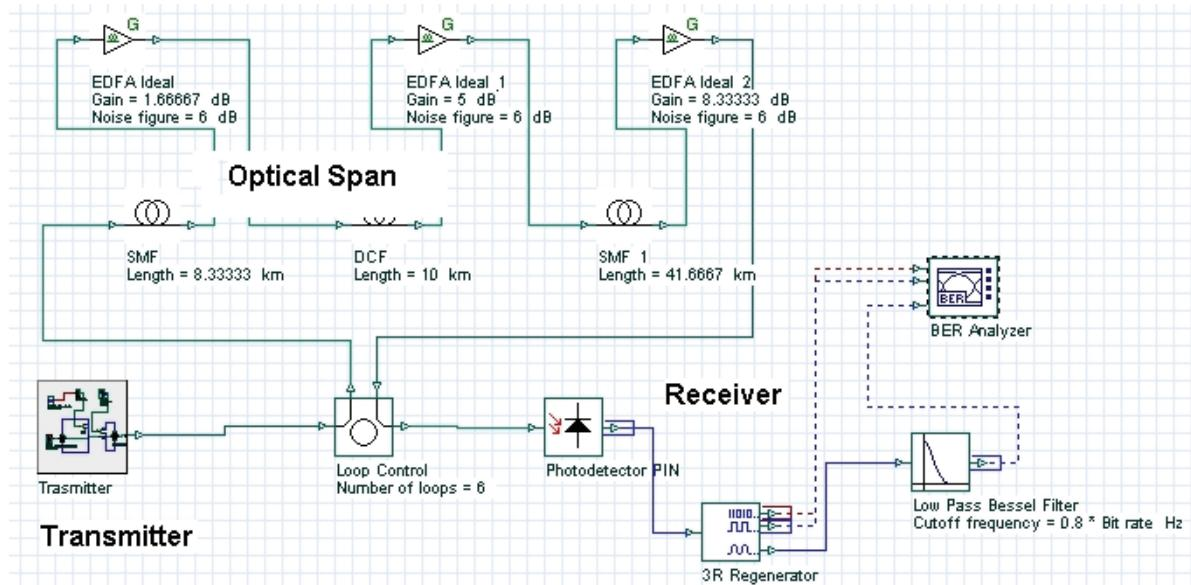
This lesson demonstrates the basic features of a typical WDM optical communication system and shows the basic design steps with OptiSystem.

In this lesson we will develop a simple, realistic WDM communication system. The performance of the system will be shown and compared with published results. The impact of various physical effects accompanying the light propagation in optical fibers on the signal transmission will be analyzed. Because the analysis of a multi-channel system is useful, the natural starting point is with the analysis of a simple one-channel system.

## Single-channel transmission

Figure 1 shows the layout that we use to analyze the performance of such a system. The layout is followed with detailed explanations of its components.

**Figure 1 Single channel system layout**



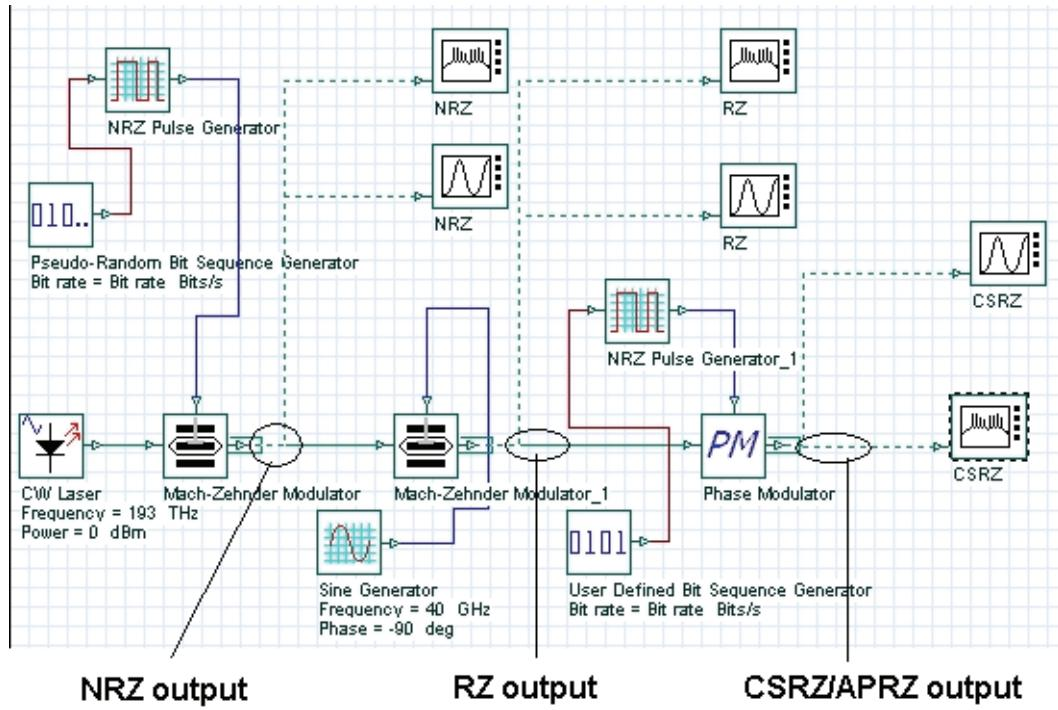
The three main blocks of each communication system shown in Figure 1 are the transmitter, the optical span, and the receiver.



## Transmitter

The process of converting the digital data stream (a sequence of logical "ones" and "zeros") into sequence of light pulses (where the presence of the pulse corresponds to "one" and the absence of a pulse corresponds to "zero") is known as modulation. At bit rates as high as 40 Gb/s (considered here) the direct switching "on" and "off" the laser (known as direct modulation) is impossible due to the transient effects taking place within the laser. Therefore, we use external modulation, which means that the laser will operate in a continuous wave mode and an external device (the modulator), will convert the data into a sequence of pulses.

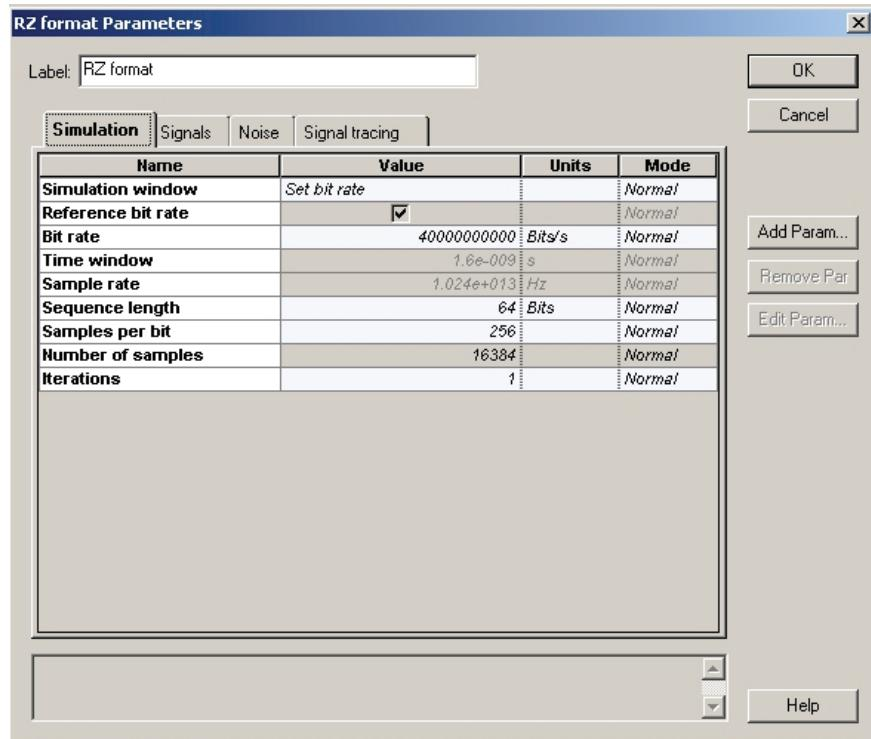
**Figure 2 Transmitter subsystem layout**



The exact way this conversion is carried out depends on the modulation format. The global parameters of the layout shown in Figure 2 are detailed in [Figure 3](#).

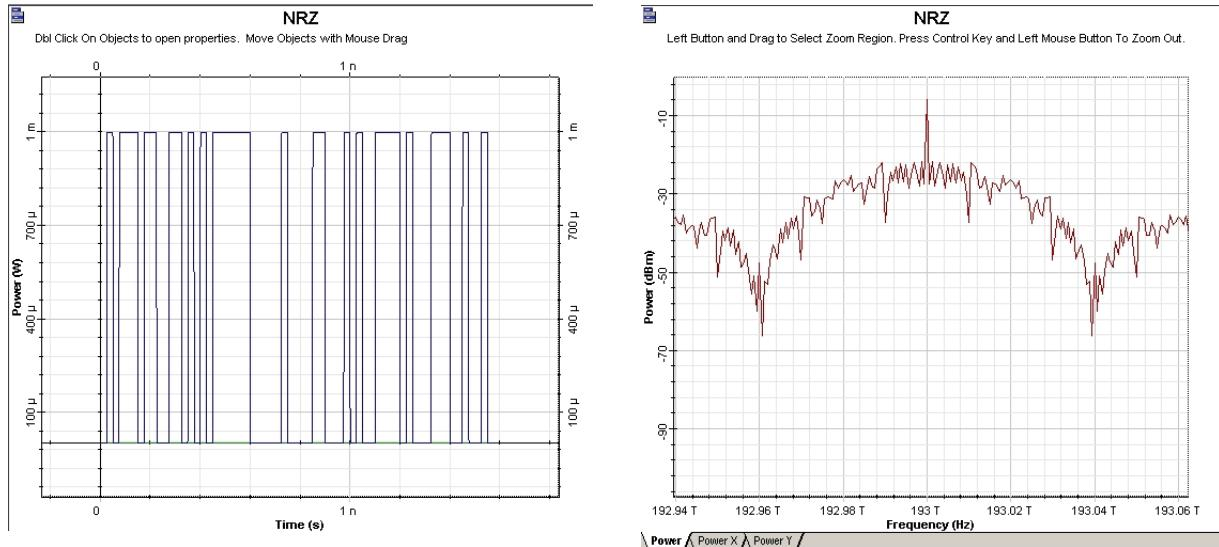
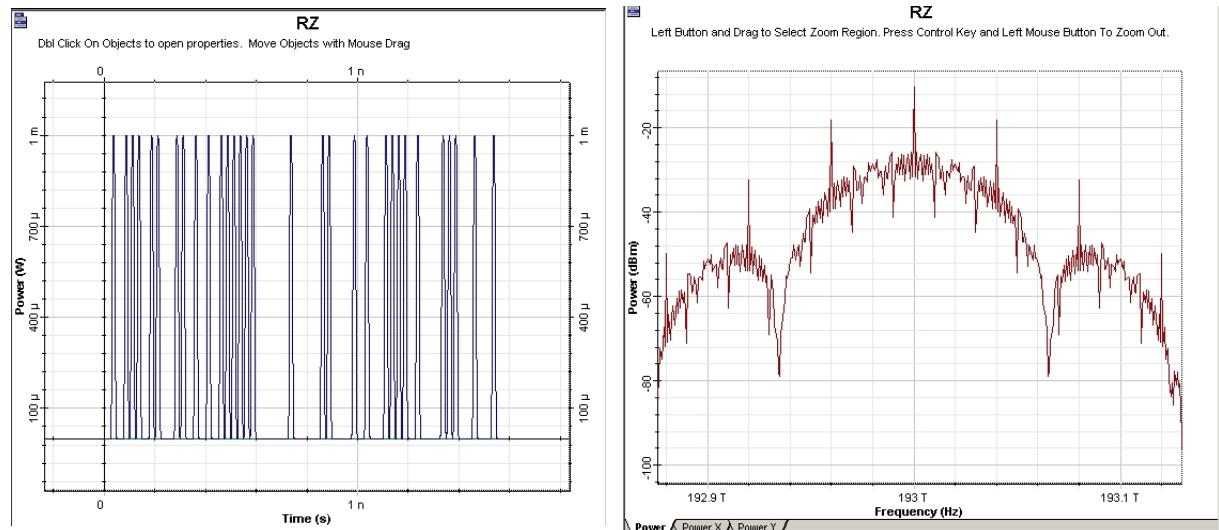


Figure 3 Global parameters



The laser is considered as ideal, so its line-width is set to zero. The phase-deviation parameter of phase modulator is set to 180°. The "10" sequence is used in the "User-defined bit sequence generator". The modulator shown in Figure 3 has three stages. After each stage, the modulation formats known as NRZ (non-return-to-zero), RZ (return-to-zero) and CSRZ (carrier-suppressed-return-to-zero) modulation formats are produced.

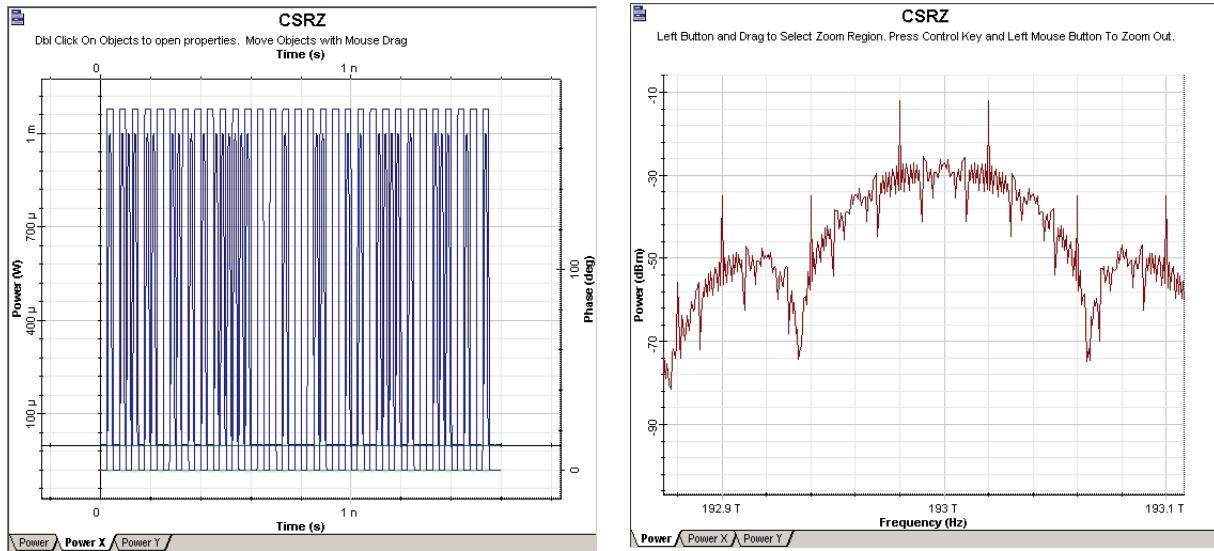
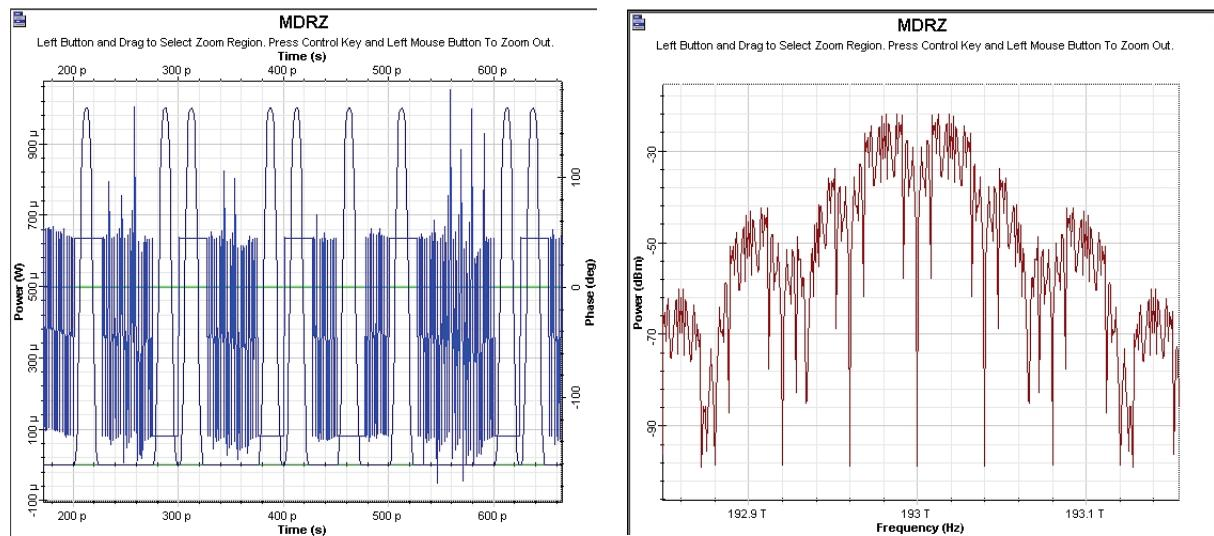
The graphs produced by the time- and frequency-domain visualizers after the first, second, and third modulation stage, are shown in Figure 4, Figure 5, and Figure 6. Figure 6A shows a frequency and time domain visualization of a modulation format known as modified duobinary return-to-zero (known also as carrier suppressed duobinary return-to-zero, see [4], [29]).

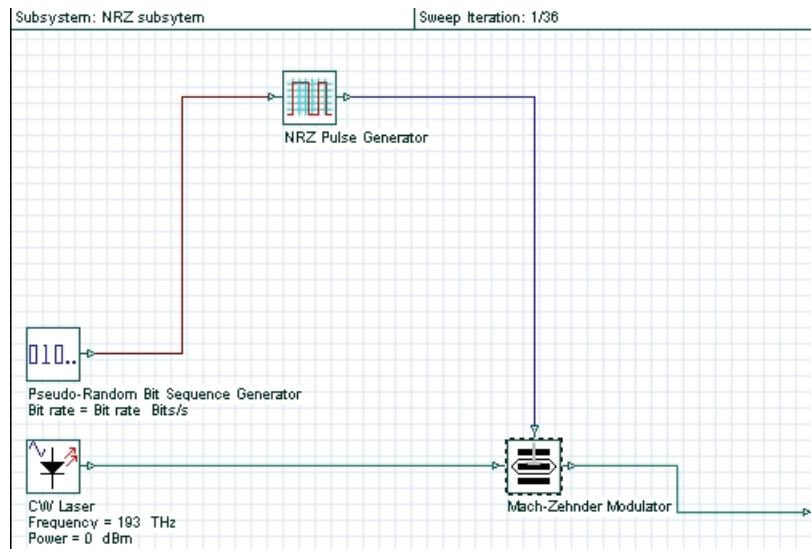
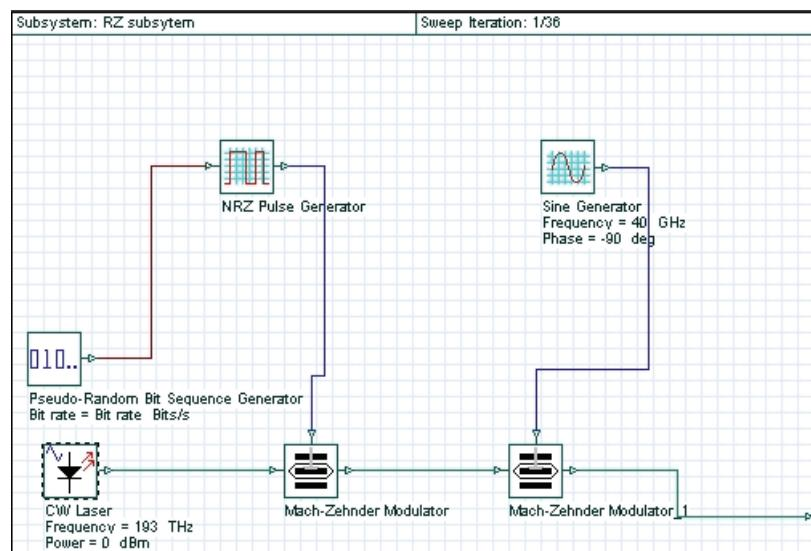
**Figure 4 NRZ time- and frequency-domain visualizers****Figure 5 RZ time- and frequency-domain visualizers**

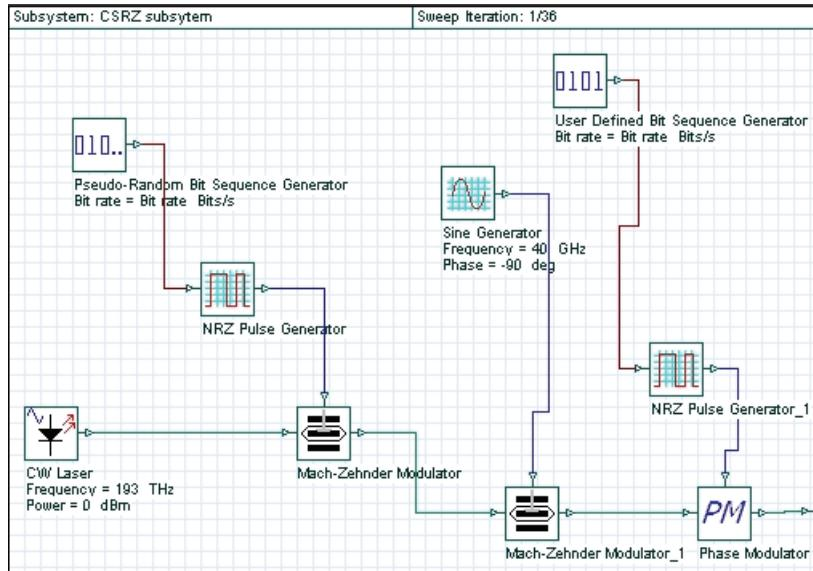
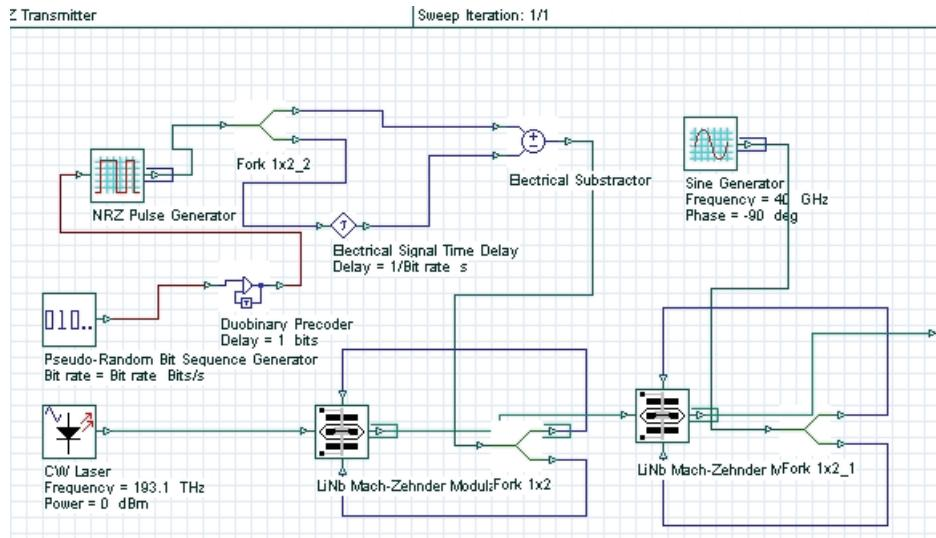
Note, that the spectra of the modulation formats shown coincide with those presented in references [1],[2],[29].

We can convert each of the modulators into a subsystem, which is convenient for the further design. These subsystems are shown in [Figure 7](#), [Figure 8](#), [Figure 9](#) and [Figure 9.1](#). By varying the phase deviation parameter of the phase modulator ([Figure 2](#)) a set of formats can be produced known as alternating-phase return-to-zero [3]. At one extreme (zero phase deviation) this corresponds to the ordinary RZ, while at  $180^\circ$  phase deviation CSRZ will be generated.



**Figure 6 CSRZ time- and frequency-domain visualizers****Figure 6A MDRZ time- and frequency-domain visualizers**

**Figure 7 NRZ subsystem design****Figure 8 RZ subsystem design**

**Figure 9 CSRZ subsystem design****Figure 9.1 MDRZ subsystem design**

The practical aspects of the generation of some of the most frequently used modulation formats are discussed in [2], [3], [4], [29]. The second stage (amplitude) modulator and the third stage (phase) modulator are replaced by a single dual-drive modulator with the presence (absence) of the phase modulation achieved by the appropriate biasing and alteration of the frequency of the sine generator (Bit rate/2 for 180° phase alternation and Bit rate for no phase modulation, see [2] for details).

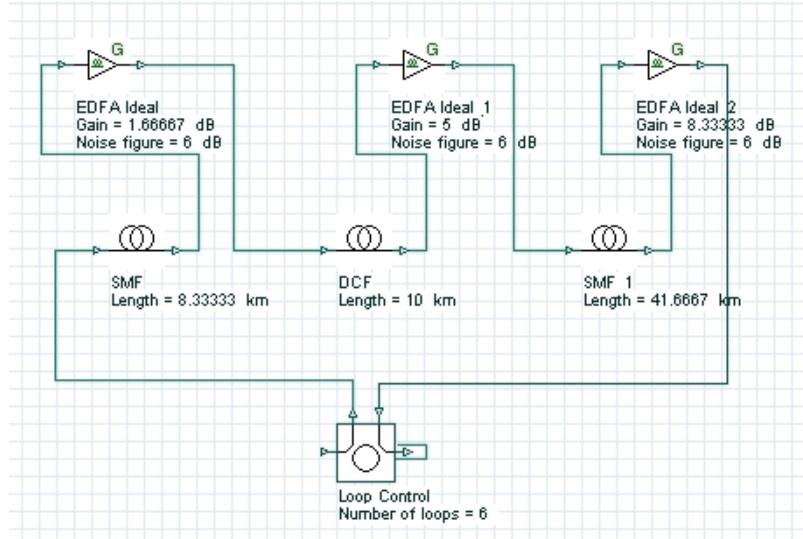
**Figure 9.1** shows a design of a MDRZ modulator [4], [29].

The differences between NRZ and RZ are obvious. Additional phase modulation is introduced to RZ to convert it to APRZ/CSRZ - i.e. a phase variation between every two bits. For MDRZ this phase modulation is somewhat different. The phase of all the "zero" bits is kept constant and a 180° phase variation between all the consecutive "ones" is introduced.

## Optical span

The next step is to design the transmission span (see [Figure 10](#)). The transmission span that we use consists of "cells" i.e. it is periodic. The "Loop control" component will actually perform the multiplication of our cell the necessary number of times.

**Figure 10** Transmission span layout



The use of cells stems from the necessity of dispersion compensation. At bit rates as high as 40 Gb/s, the design of the cell is crucial. The dispersion length at 1.55 micrometers, assuming standard single-mode fibers (SMF), and Gaussian pulses with 0.5 duty ratio is of the order of 3 km [5], [6]. As [Figure 10](#) shows, the period of the cell is 50 km (the length of the dispersion compensating fiber (DCF) is not included). This means that during the propagation, within one cell, not only is there a strong overlap between the adjacent pulses, but the original bit stream will be totally scrambled due to the dispersion-induced pulse broadening. This regime of propagation known as "pulse-overlapped" is of very high practical importance, since in this case the impact of the nonlinear effects taking place due to the interaction of the overlapping pulses that belong to one and same information channel (known as intra-channel nonlinearities) are reduced [7], [8]. The concept involves spreading of the pulses as far as possible and as quickly as possible in the time domain in order to create a rapidly varying intensity pattern, in order to combat the impact of the nonlinearity [12].



Figure 11 SMF parameters

SMF Properties					
Label: SMF Cost\$: 0.00 <input checked="" type="radio"/> Main <input type="radio"/> Disp... <input type="radio"/> PMD <input type="radio"/> Nonli... <input type="radio"/> Num... <input type="radio"/> Graphs <input type="radio"/> Simul... <input type="radio"/> Noise <input type="radio"/> Rand...					
Disp	Name	Value	Units	Mode	
<input type="checkbox"/>	User defined reference wavelength	<input type="checkbox"/>	1550 nm	Normal	
<input checked="" type="checkbox"/>	Length	8.33333	km	Sweep	
<input type="checkbox"/>	Attenuation effect	<input checked="" type="checkbox"/>		Normal	
<input type="checkbox"/>	Attenuation data type	Constant		Normal	
<input type="checkbox"/>	Attenuation	0.2	dB/km	Normal	
<input type="checkbox"/>	Attenuation vs. wavelength	Attenuation.dat		Normal	
<input checked="" type="radio"/> Main <input type="radio"/> Disp... <input type="radio"/> PMD <input type="radio"/> Nonli... <input type="radio"/> Num... <input type="radio"/> Graphs <input type="radio"/> Simul... <input type="radio"/> Noise <input type="radio"/> Rand...					
Disp	Name	Value	Units	Mode	
<input type="checkbox"/>	Group velocity dispersion	<input checked="" type="checkbox"/>		Normal	
<input type="checkbox"/>	Third-order dispersion	<input checked="" type="checkbox"/>		Normal	
<input type="checkbox"/>	Dispersion data type	Constant		Normal	
<input type="checkbox"/>	Frequency domain parame	<input type="checkbox"/>		Normal	
<input type="checkbox"/>	Dispersion	17	ps/nm/km	Normal	
<input type="checkbox"/>	Dispersion slope	0.075	ps/nm^2/k	Normal	
<input type="checkbox"/>	Beta 2	-20	ps^2/km	Normal	
<input type="checkbox"/>	Beta 3	0	ps^3/km	Normal	
<input type="checkbox"/>	Dispersion file format	Dispersion vs. wavelength		Normal	
<input type="checkbox"/>	Dispersion file name	Dispersion.dat		Normal	
<input checked="" type="radio"/> Main <input type="radio"/> Disp... <input type="radio"/> PMD <input type="radio"/> Nonli... <input type="radio"/> Num... <input type="radio"/> Graphs <input type="radio"/> Simul... <input type="radio"/> Noise <input type="radio"/> Rand...					
Disp	Name	Value	Units	Mode	
<input type="checkbox"/>	Birefringence type	Deterministic		Normal	
<input type="checkbox"/>	Differential group delay	0.2	ps/km	Normal	
<input type="checkbox"/>	PMD coefficient	0.5	ps(km)^0.5	Normal	
<input type="checkbox"/>	Mean scattering section le	500	m	Normal	
<input type="checkbox"/>	Scattering section dispers	100	m	Normal	
<input checked="" type="radio"/> Main <input type="radio"/> Disp... <input type="radio"/> PMD <input type="radio"/> Nonli... <input type="radio"/> Num... <input type="radio"/> Graphs <input type="radio"/> Simul... <input type="radio"/> Noise <input type="radio"/> Rand...					
Disp	Name	Value	Units	Mode	
<input type="checkbox"/>	Self-phase modulation	<input checked="" type="checkbox"/>		Normal	
<input type="checkbox"/>	Effective area data type	Constant		Normal	
<input type="checkbox"/>	Effective area	70	μm^2	Normal	
<input type="checkbox"/>	Effective area vs. wavelen	EffectiveAra.dat		Normal	
<input type="checkbox"/>	n2 data type	Constant		Normal	
<input type="checkbox"/>	n2	2.6e-020	m^2/W	Normal	
<input type="checkbox"/>	n2 vs. wavelength	n2.dat		Normal	
<input type="checkbox"/>	Self-steepening	<input type="checkbox"/>		Normal	
<input type="checkbox"/>	Full Raman Response	<input type="checkbox"/>		Normal	
<input type="checkbox"/>	Intrapulse Raman Scatt.	<input type="checkbox"/>		Normal	
<input type="checkbox"/>	Raman self-shift time1	14.2	fs	Normal	
<input type="checkbox"/>	Raman self-shift time2	3	fs	Normal	
<input type="checkbox"/>	Fract. Raman contribution	0.18		Normal	
<input type="checkbox"/>	Orthogonal Raman factor	0.75		Normal	
<input checked="" type="radio"/> Main <input type="radio"/> Disp... <input type="radio"/> PMD <input type="radio"/> Nonli... <input type="radio"/> Num... <input type="radio"/> Graphs <input type="radio"/> Simul... <input type="radio"/> Noise <input type="radio"/> Rand...					
Disp	Name	Value	Units	Mode	
<input type="checkbox"/>	Model type	Scalar		Normal	
<input type="checkbox"/>	Propagator type	Exponential		Normal	
<input type="checkbox"/>	Calculation type	Noniterative		Normal	
<input type="checkbox"/>	Number of iterations	2		Normal	
<input type="checkbox"/>	Step size	Variable		Normal	
<input type="checkbox"/>	Max. nonlinear phase shift	5	mrad	Normal	
<input type="checkbox"/>	Boundary conditions	Periodic		Normal	
<input type="checkbox"/>	Filter steepness	0.005		Normal	
<input type="checkbox"/>	Lower calculation limit	1400	nm	Normal	
<input type="checkbox"/>	Upper calculation limit	1700	nm	Normal	



Figure 12 DCF parameters

**DCF Properties**

Label:	DCF	Cost\$:	0.00	
<input checked="" type="radio"/> Main <input type="radio"/> Disp... <input type="radio"/> PMD <input type="radio"/> Nonli... <input type="radio"/> Num... <input type="radio"/> Graphs <input type="radio"/> Simul... <input type="radio"/> Noise <input type="radio"/> Rand...				
Disp	Name	Value	Units	Mode
<input type="checkbox"/>	User defined reference wa	<input type="checkbox"/>		Normal
<input type="checkbox"/>	Reference wavelength	1550	nm	Normal
<input checked="" type="checkbox"/>	Length	10	km	Normal
<input type="checkbox"/>	Attenuation effect	<input checked="" type="checkbox"/>		Normal
<input type="checkbox"/>	Attenuation data type	Constant		Normal
<input type="checkbox"/>	Attenuation	0.5	dB/km	Normal
<input type="checkbox"/>	Attenuation vs. wavelength	Attenuation.dat	<input type="checkbox"/>	Normal

<input checked="" type="radio"/> Disp... <input type="radio"/> Main <input type="radio"/> PMD <input type="radio"/> Nonli... <input type="radio"/> Num... <input type="radio"/> Graphs <input type="radio"/> Simul... <input type="radio"/> Noise <input type="radio"/> Rand...				
Disp	Name	Value	Units	Mode
<input type="checkbox"/>	Group velocity dispersion	<input checked="" type="checkbox"/>		Normal
<input type="checkbox"/>	Third-order dispersion	<input checked="" type="checkbox"/>		Normal
<input type="checkbox"/>	Dispersion data type	Constant		Normal
<input type="checkbox"/>	Frequency domain paramete	<input type="checkbox"/>		Normal
<input type="checkbox"/>	Dispersion	-85	ps/nm/km	Normal
<input type="checkbox"/>	Dispersion slope	-0.3	ps^2/nm^2/km	Normal
<input type="checkbox"/>	Beta 2	-20	ps^2/km	Normal
<input type="checkbox"/>	Beta 3	0	ps^3/km	Normal
<input type="checkbox"/>	Dispersion file format	Dispersion vs. wavelength		Normal
<input type="checkbox"/>	Dispersion file name	Dispersion.dat	<input type="checkbox"/>	Normal

<input type="radio"/> Main <input checked="" type="radio"/> Disp... <input type="radio"/> PMD <input type="radio"/> Nonli... <input type="radio"/> Num... <input type="radio"/> Graphs <input type="radio"/> Simul... <input type="radio"/> Noise <input type="radio"/> Rand...				
Disp	Name	Value	Units	Mode
<input type="checkbox"/>	Birefringence type	Deterministic		Normal
<input type="checkbox"/>	Differential group delay	0.2	ps/km	Normal
<input type="checkbox"/>	PMD coefficient	0.5	ps/(km)^0.5	Normal
<input type="checkbox"/>	Mean scattering section le	500	m	Normal
<input type="checkbox"/>	Scattering section dispers	100	m	Normal

<input type="radio"/> Main <input type="radio"/> Disp... <input checked="" type="radio"/> PMD <input type="radio"/> Nonli... <input type="radio"/> Num... <input type="radio"/> Graphs <input type="radio"/> Simul... <input type="radio"/> Noise <input type="radio"/> Rand...				
Disp	Name	Value	Units	Mode
<input type="checkbox"/>	Self-phase modulation	<input checked="" type="checkbox"/>		Normal
<input type="checkbox"/>	Effective area data type	Constant		Normal
<input type="checkbox"/>	Effective area	22	μm^2	Normal
<input type="checkbox"/>	Effective area vs. wavelen	EffectiveAra.dat	<input type="checkbox"/>	Normal
<input type="checkbox"/>	n2 data type	Constant		Normal
<input type="checkbox"/>	n2	2.6e-020	m^2/W	Normal
<input type="checkbox"/>	n2 vs. wavelength	n2.dat	<input type="checkbox"/>	Normal
<input type="checkbox"/>	Self-steepening	<input type="checkbox"/>		Normal
<input type="checkbox"/>	Full Raman Response	<input type="checkbox"/>		Normal
<input type="checkbox"/>	Intrapulse Raman Scatt.	<input type="checkbox"/>		Normal
<input type="checkbox"/>	Raman self-shift time1	14.2	fs	Normal
<input type="checkbox"/>	Raman self-shift time2	3	fs	Normal
<input type="checkbox"/>	Fract. Raman contribution	0.18		Normal
<input type="checkbox"/>	Orthogonal Raman factor	0.75		Normal

<input type="radio"/> Main <input type="radio"/> Disp... <input type="radio"/> PMD <input type="radio"/> Nonli... <input checked="" type="radio"/> Num... <input type="radio"/> Graphs <input type="radio"/> Simul... <input type="radio"/> Noise <input type="radio"/> Rand...				
Disp	Name	Value	Units	Mode
<input type="checkbox"/>	Model type	Scalar		Normal
<input type="checkbox"/>	Propagator type	Exponential		Normal
<input type="checkbox"/>	Calculation type	Noniterative		Normal
<input type="checkbox"/>	Number of iterations	2		Normal
<input type="checkbox"/>	Step size	Variable		Normal
<input type="checkbox"/>	Max. nonlinear phase shift	5	mrad	Normal
<input type="checkbox"/>	Boundary conditions	Periodic		Normal
<input type="checkbox"/>	Filter steepness	0.005		Normal
<input type="checkbox"/>	Lower calculation limit	1400	nm	Normal
<input type="checkbox"/>	Upper calculation limit	1700	nm	Normal

Figure 11 and Figure 12 give the parameters of SMF and DCF. They are the same as those used in [9]. The gain of the EDFA placed after each fiber is such that it compensates the losses of the preceding fiber. The noise figure of the amplifiers is constant and set to 6 dB [9]. Note that the "Model type" parameter of both fibers is set



to Scalar, so no birefringence effects are considered, and consequently PMD is not taken into account.

Our first task is to analyze the performance of the single channel system depending on the dispersion cell design and input power for different modulation formats. To achieve this, we need to "sweep" a range of input power levels and, simultaneously, a range of lengths for the transmission fibers, keeping the cell length constant and equal to 50 km. This is done by using the "sweep" mode for the lengths of both transmission fibers in the cell and for the amplifier gains. The total number of iterations is set to 36. If a finer grid is needed, this number can be increased, however this will increase the total computation time. [Table 2](#) gives an example of such a setup. The lengths of the transmission fibers (SMF and SMF\_1) are chosen in such a way that the dispersion compensation scheme ranges from pre-compensation to post-compensation.

## Receiver

[Figure 13](#) shows the receiver that we use. It consists of a PIN photo-detector, fourth order low-pass Bessel electrical filter with 32 GHz ( $0.8 \times$  Bit rate) cut-off frequency and a BER Analyzer with its default settings kept. The thermal noise of the photo-detector is not taken into account.

**Figure 13 Receiver layout**

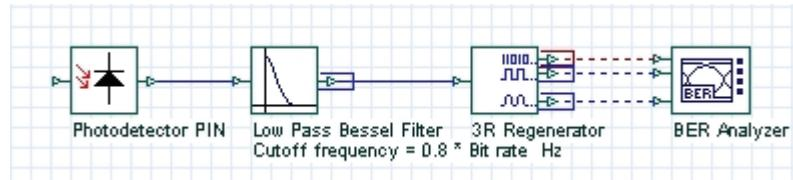


**Table 2**

EDFA Ideal 2	SMF_1	EDFA Ideal	SMF	CW Laser
Gain [dB]	Length [km]	Gain [dB]	Length [km]	Power [mW]
8.33333	41.66667	1.66667	8.33333	0.5
8.33333	41.66667	1.66667	8.33333	1.2
8.33333	41.66667	1.66667	8.33333	1.9
8.33333	41.66667	1.66667	8.33333	2.6
8.33333	41.66667	1.66667	8.33333	3.3
8.33333	41.66667	1.66667	8.33333	4
6.66667	33.33333	3.33333	16.66667	0.5
6.66667	33.33333	3.33333	16.66667	1.2
6.66667	33.33333	3.33333	16.66667	1.9
6.66667	33.33333	3.33333	16.66667	2.6
6.66667	33.33333	3.33333	16.66667	3.3

EDFA Ideal 2	SMF_1	EDFA Ideal	SMF	CW Laser
Gain [dB]	Length [km]	Gain [dB]	Length [km]	Power [mW]
6.66667	33.33333	3.33333	16.66667	4
5	25	5	25	0.5
5	25	5	25	1.2
5	25	5	25	1.9
5	25	5	25	2.6
5	25	5	25	3.3
5	25	5	25	4
3.33333	16.66667	6.66667	33.33333	0.5
3.33333	16.66667	6.66667	33.33333	1.2
3.33333	16.66667	6.66667	33.33333	1.9
3.33333	16.66667	6.66667	33.33333	2.6
3.33333	16.66667	6.66667	33.33333	3.3
3.33333	16.66667	6.66667	33.33333	4
1.66667	8.33333	8.33333	41.66667	0.5
1.66667	8.33333	8.33333	41.66667	1.2
1.66667	8.33333	8.33333	41.66667	1.9
1.66667	8.33333	8.33333	41.66667	2.6
1.66667	8.33333	8.33333	41.66667	3.3
1.66667	8.33333	8.33333	41.66667	4
0	0	10	50	0.5
0	0	10	50	1.2
0	0	10	50	1.9
0	0	10	50	2.6
0	0	10	50	3.3
0	0	10	50	4

In our case, no special calibration of the receiver has been performed. The impact of the receiver calibration on the system performance estimation can be eliminated by using the eye closure penalty instead of the Q-factor as a measure of the system performance [2], [9], [10]. The receiver calibration however can be performed by sweeping the thermal noise parameter until a given value of the Q-factor (say Q=6) is achieved at a specified input power level. It should be noted however that the optimum receiver design is crucial and it is a subject of intensive research (see e.g. [23]-[27]).

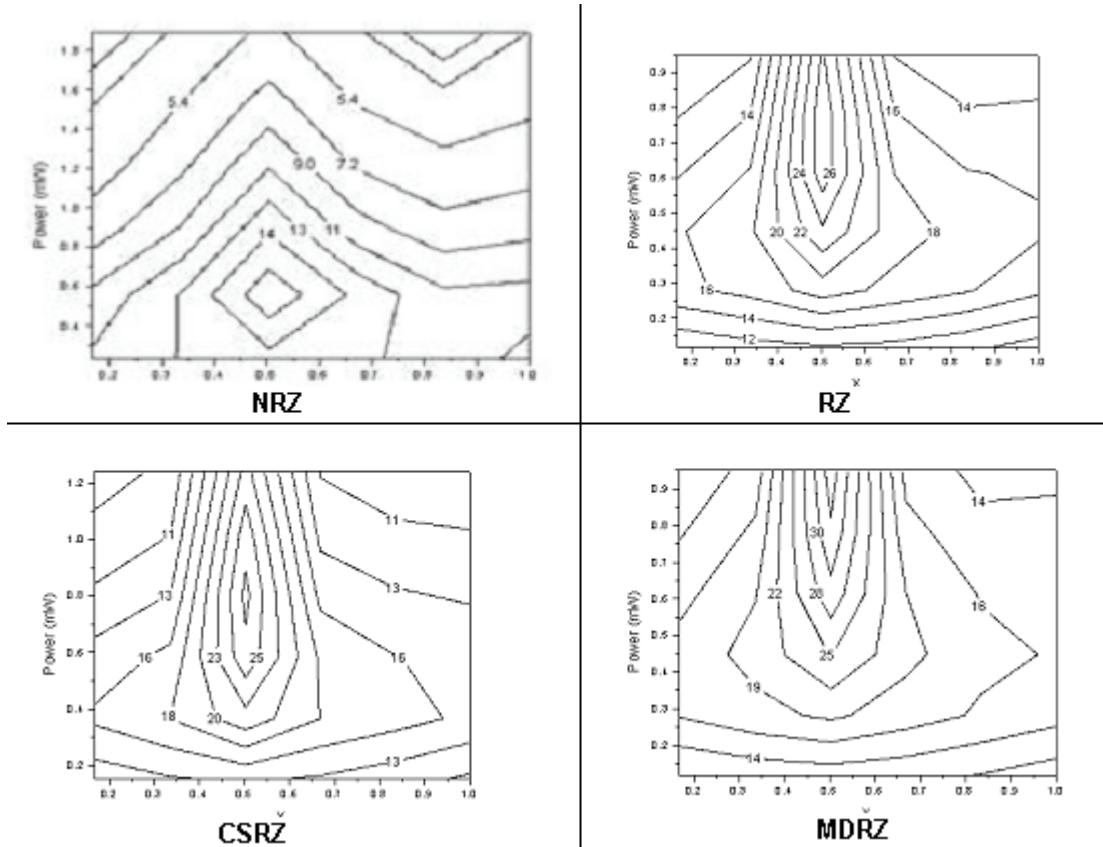


## Results

Using the layout shown in [Figure 1](#), and performing the simulations, the following results are obtained for performance of the single-channel system studied ([Figure 14](#)) depending on the input power, dispersion compensation scheme and modulation format. These results are published in part in [\[11\]](#).

As [Figure 14](#) shows, optimum performance is obtained with symmetric dispersion compensation. This is a well established result [\[12\]-\[15\]](#) and it does not depend on the modulation format since the intra-channel nonlinear effects depend on pulse-to-pulse interactions. A simple explanation (e.g. [\[15\]](#)) for this is that the nonlinear distortions accumulated in the first part of the cell are balanced by those in the second part of it.

**Figure 14 Dependence of the Q-factor of a single-channel on averaged power and dispersion compensation scheme**



**Note:** X denotes the fraction of the SMF length preceding the DCF. X=0 corresponds to precompensation, X=1 to postcompensation. Bit sequences containing 1024 bits are used.

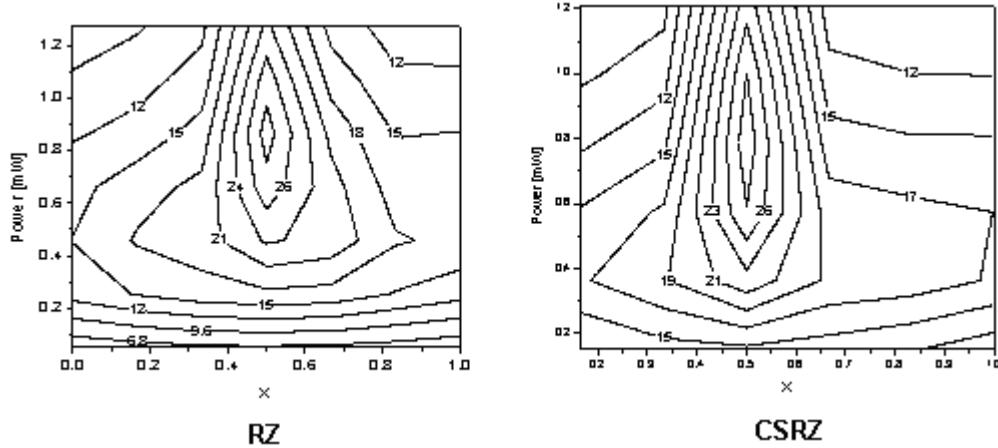
A comparison between NRZ and RZ shows that in single channel dispersion compensated systems, RZ performs better than NRZ (see e.g. [\[9\]](#), [\[10\]](#)). The explanation is that because dispersion is compensated, RZ would perform better because it tolerates nonlinearities [\[10\]](#). This situation changes however in situations

where incomplete dispersion compensation is used [9] because NRZ has a narrower spectrum and therefore tolerates residual dispersion better.

The existence of an optimum input power can be explained with the interplay between the amplifier noise and the nonlinear distortions. At low power values the performance improves with the increase of power resulting from the better signal-to-noise ratio. At higher power levels however nonlinear distortions dominate [10].

The location of the maximum of the Q factor with respect to the averaged launched power shows that nonlinearity tolerance of the different formats studied is quite different. NRZ has the lowest nonlinearity tolerance. The pulse-width is not constant for NRZ which leads to different interplay between dispersion and self-phase modulation. The other reason is related to the inter-channel cross-phase modulation and four-wave-mixing. As it has been already mentioned (see [12]) the faster and further the pulse spreading occurs the smaller the impact of the intra-channel nonlinearities would be [7, 12]. This is the basic idea behind the "pulse-overlapped" transmission. Obviously, the shorter RZ pulses will spread faster which will combat the intra-channel nonlinearities better.

**Figure 15 Dependence of the Q-factor of a single-channel on averaged power and dispersion compensation scheme**



**Note:** X denotes the fraction of the SMF length preceding the DCF.  $X=0$  corresponds to precompensation,  $X=1$  to postcompensation. Bit sequences containing 256 bits are used.

If, however, the distortions caused by intra-channel nonlinearities depended merely on the pulse width, all RZ-based modulation formats (RZ, CSRZ and MDRZ) would perform in exactly the same way. This however is not the case. As it has been shown (see e.g. [4]) and Figure 14 shows MDRZ has a superior performance to CSRZ and RZ. This can be attributed to the fact that the spectrum of the MDRZ formats lacks discrete tones [4], which counteracts the intra-channel four-wave mixing. It has been suggested in [16] that the  $180^\circ$  phase inversion between the consecutive "marks" (that takes place for MDRZ) will lead to a suppression of the energy of the four-wave-mixing product that appears in a space bit (the so-called ghost pulse [14]) generated by two blocks of marks surrounding this "space".

Figure 15 shows the results for RZ and CSRZ formats presented in Figure 14 with 256 bits Qualitatively the same results are obtained.

**Figure 16 Eye closure penalty versus averaged power for different modulation formats and compensation schemes - post-compensation (a) and symmetric compensation (b). Bit stream with 256 bits is used.**

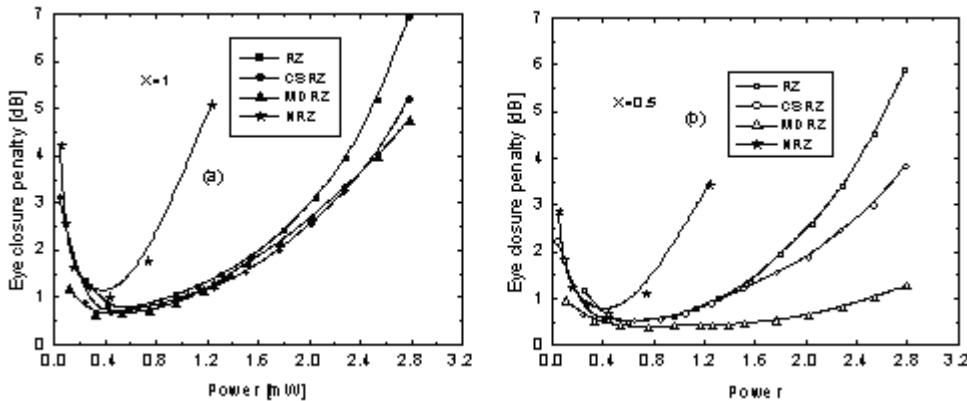


Figure 15 compares the performance of all the four studied formats in terms of eye closure penalties [2], [9], [10] as a function of the launched power for the cases of post-compensation and symmetric dispersion compensation. In the case of post-compensation all the RZ-based formats show similar performance. The similar performance of RZ and CSRZ is to be expected based on the considerations of [3] and [17]. Superior performance of MDRZ has been reported earlier in [4], however different dispersion cell has been used in [4] and besides the power range covered is between 3 mW and 13 mW in [4]. With symmetric dispersion compensation scheme used the situation presented in Figure 16 (a) changes. Although all the formats improve their performance due to the suppression of the "ghost-pulses", the improvement is different for all the formats. As Figure 16 (b) shows, the superiority of MDRZ format exists for power levels above 1 mW. Besides, for power values above 1.5 mW the difference between RZ and CSRZ becomes well pronounced. The combination of MDRZ (also called carrier-suppressed duobinary) and symmetric dispersion map has been studied experimentally for the first time in [18].

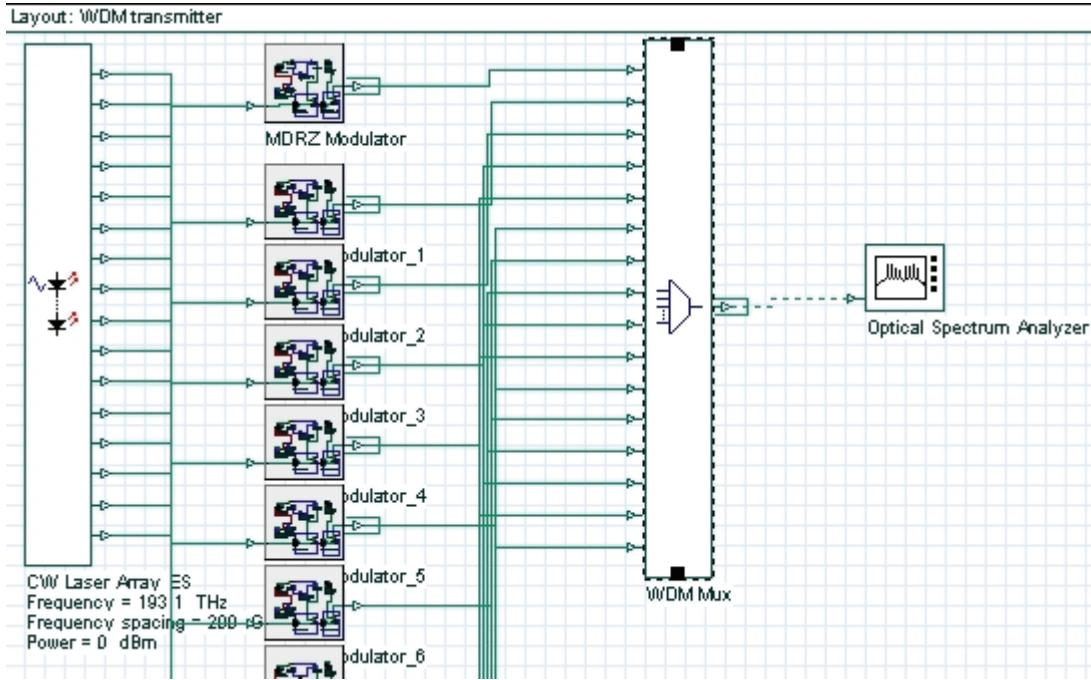
## 16 channels at 40 GB/s WDM transmission

This part of the tutorial discusses the design of a multi-channel WDM system. With all the blocks necessary to build a typical single channel system with OptiSystem already explained, only small modifications are needed to extend the design to multi-channel systems. The transmission span remains the same. A multiplexer must be added at the receiver site to combine all the channels so that they can be transmitted through the optical fibers. Respectively, a de-multiplexer must be added at the receiver site which will provide the separation of the channels in the frequency domain and they can be analyzed separately.

## WDM Transmitter

One possible design of a WDM transmitter (using MDRZ modulation) is shown in Figure 17. Note that the same design can be used to transmit any desired modulation format provided that the external modulators are replaced accordingly.

**Figure 17 WDM transmitter using MDRZ modulation**



The parameters of the CW Laser Array component is shown in Figure 18.

**Figure 18 CW Laser Array parameters**

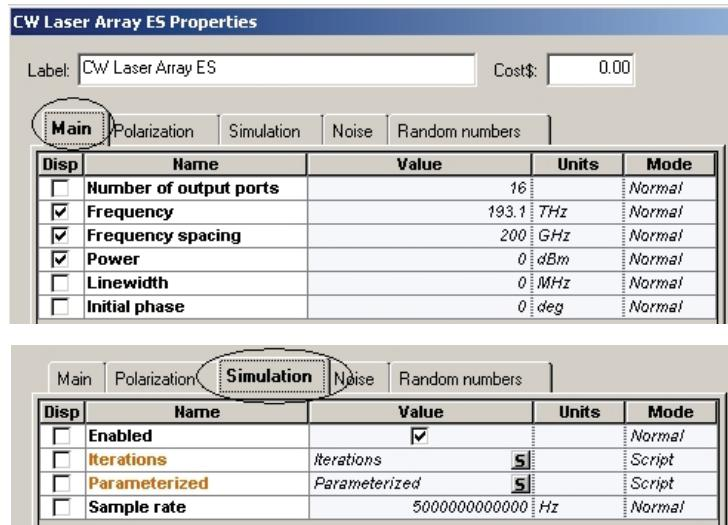


Figure 19 details the parameters of the WDM multiplexer.

**Figure 19 WDM multiplexer parameters**

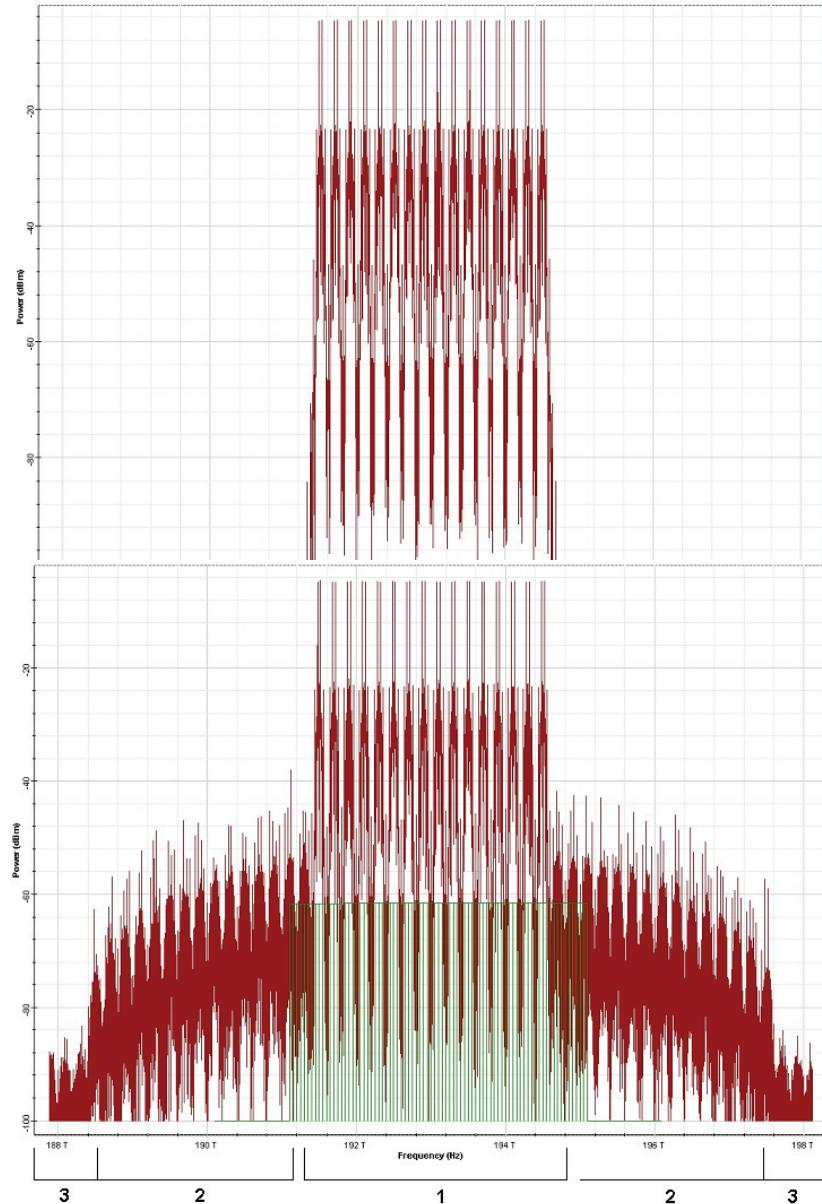
The screenshot shows two stacked dialog boxes for 'WDM Mux Properties'. The top dialog has a 'Main' tab selected, showing parameters like Number of input ports (16), Bandwidth (160000000000 Hz), Insertion loss (0 dB), Depth (100 dB), Filter type (Bessel), and Filter order (2). The bottom dialog has a 'Channels' tab selected, showing 16 frequency channels from Frequency[0] to Frequency[15], each set to 193.1 THz.

Disp	Name	Value	Units	Mode
<input type="checkbox"/>	Number of input ports	16		Normal
<input type="checkbox"/>	Bandwidth	160000000000	Hz	Normal
<input type="checkbox"/>	Insertion loss	0	dB	Normal
<input type="checkbox"/>	Depth	100	dB	Normal
<input type="checkbox"/>	Filter type	Bessel		Normal
<input type="checkbox"/>	Filter order	2		Normal

Disp	Name	Value	Units	Mode
<input type="checkbox"/>	Frequency[0]	193.1	THz	Normal
<input type="checkbox"/>	Frequency[1]	193.3	THz	Normal
<input type="checkbox"/>	Frequency[2]	193.5	THz	Normal
<input type="checkbox"/>	Frequency[3]	193.7	THz	Normal
<input type="checkbox"/>	Frequency[4]	193.9	THz	Normal
<input type="checkbox"/>	Frequency[5]	194.1	THz	Normal
<input type="checkbox"/>	Frequency[6]	194.3	THz	Normal
<input type="checkbox"/>	Frequency[7]	194.5	THz	Normal
<input type="checkbox"/>	Frequency[8]	194.7	THz	Normal
<input type="checkbox"/>	Frequency[9]	194.9	THz	Normal
<input type="checkbox"/>	Frequency[10]	195.1	THz	Normal
<input type="checkbox"/>	Frequency[11]	195.3	THz	Normal
<input type="checkbox"/>	Frequency[12]	195.5	THz	Normal
<input type="checkbox"/>	Frequency[13]	195.7	THz	Normal
<input type="checkbox"/>	Frequency[14]	195.9	THz	Normal
<input type="checkbox"/>	Frequency[15]	196.1	THz	Normal

The signal consists of 16 channels (the first one being at 193.1 THz) with 200 GHz channel spacing [9]. Although the channel spacing that we use is one and same for the channels, WDM transmission with unequal channel spacing has also been considered in the literature [19] to counteract the effect of the inter-channel FWM.

**Figure 20 Expansion of signal bandwidth as a result of the inter-channel four-wave-mixing.**

**Note:** Upper plot shows the input signal. Lower plot is the signal after 300 km transmission. 1 - input signal bandwidth, 2 - FWM products of interactions between the input signals (first-order), 3 - second order FWM products - result of interactions between waves that were not present at the fiber input, but are generated by nonlinear interactions between the input signals.



To ensure separation between the channels in the frequency domain (linear cross-talk suppression), before multiplexing, each channel is optically filtered with a second-order Bessel filter with a bandwidth equal to four times the Bit rate (or 160 GHz).

Although we keep the value of this parameter fixed throughout the design, it should be noted that this value depends on the modulation format used [9]. The length of the pseudo-random bit sequences used is 256 bits. Total field approach will be used to model the light propagation in the optical fiber component [5],[6][21]. This means that the global sample rate will be such that all the sampled signals will form a single band - i.e. the simulated bandwidth (numerically equal to the sample rate) will be large enough to accommodate all the sampled signals. In our case we have 16 channels with 200 GHz channel spacing, which means that the total channel bandwidth will be  $15 \times 200 \text{ GHz} = 3\text{THz}$ . Due to the inter-channel four-wave mixing (FWM) - see e.g. [19]-[21] - however the initial signal bandwidth will expand after the transmission through a nonlinear optical fiber. A typical example of this is shown in [Figure 20](#). Recalling that the wave frequencies interacting through FWM obey  $f_1+f_2=f_3+f_4$ , it is easy to see that if only interactions between input signal frequencies are taken into account, their products will lead to a bandwidth expansion by a factor of three. These continuously generated new frequencies (known also as "spurious waves"[20]) can further interact among each other leading to further bandwidth expansion. Since only a finite bandwidth is available, it is clear that the FWM products outside the simulated bandwidth will be aliased - i.e. they will be falsely translated into the simulated bandwidth. By choosing the simulated bandwidth to be at least three times [9], [22], that of the input signal (as in our simulation) we can ensure that only "second-order" and higher FWM products (i.e. products of the products) will be aliased. As expected, (and as [Figure 20](#) shows) their power is much smaller than that of the first order products.

To summarize, bandwidth at least three times that of the input signal must be considered if the FWM in the system is significant - which will be the case in systems with low local dispersion and/or higher input power. You should however keep in mind that the increase of the simulated bandwidth leads to an increase in the computation time.



## WDM Receiver

Figure 21 shows a WDM receiver design. It consists of 1 to 16 de-multiplexer and a "single-channel" receiver (Figure 13) connected to each output port.

Figure 21 WDM receiver layout

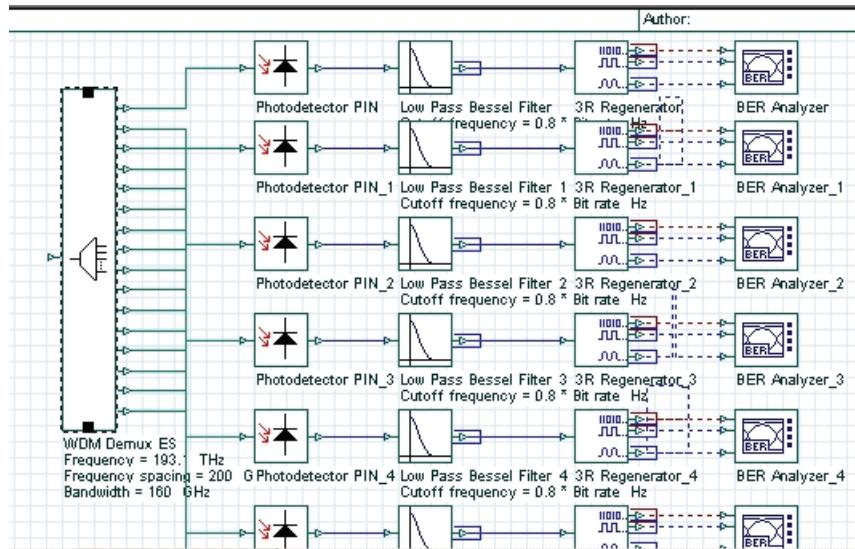
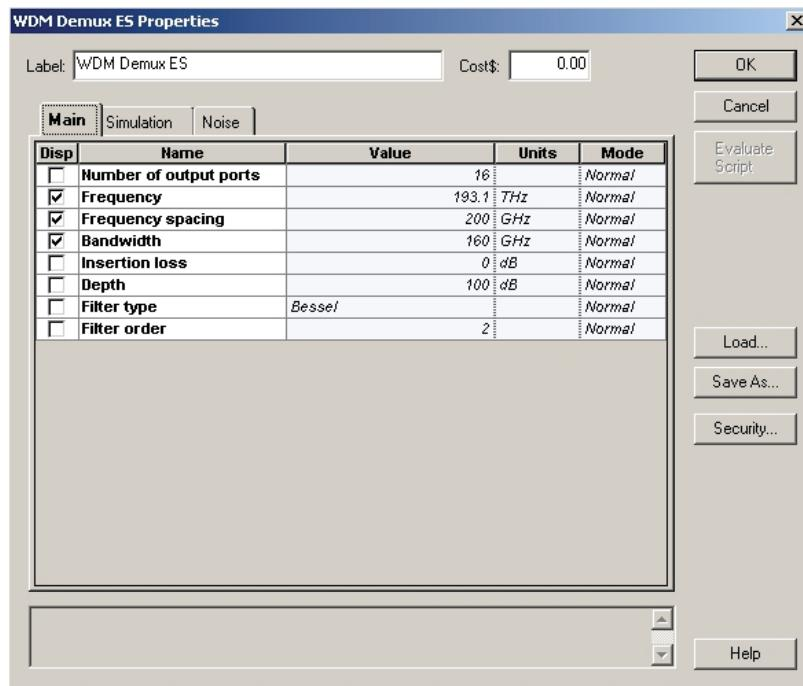


Figure 22 shows the parameters of the WDM de-multiplexer component.

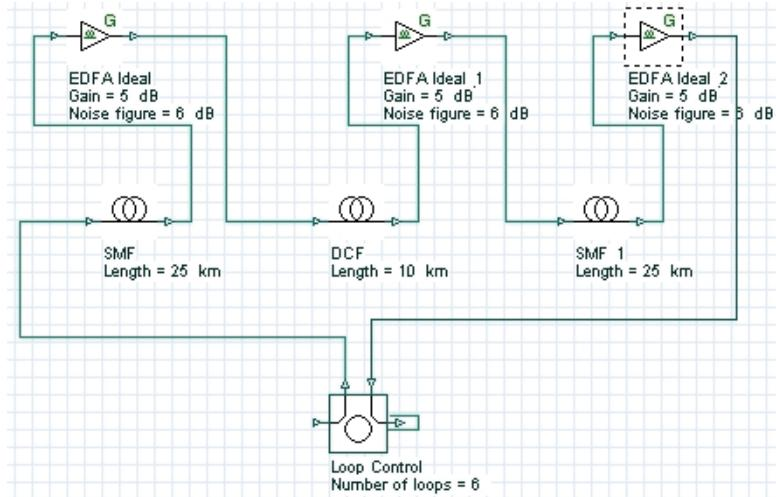
Figure 22 WDM de-multiplexer component parameters



## Transmission span

Based on the results obtained in the single-channel case we are going to use symmetric dispersion compensation (Figure 23). The values of the fiber parameters (attenuation, dispersion, nonlinearities etc.) are exactly the same as in the single-channel case (see Figure 12 and Figure 13) The cell length (50km) is split to equal parts 25km each. The DCF is placed in the middle of the cell.

Figure 23 Transmission span layout



The gains of the EDFAs are such that each amplifier compensates the losses of the preceding fiber. The noise figure of the EDFAs is 6 dB. Examination of the fiber parameters (Figure 12 and Figure 13) shows that the first-order dispersion is compensated exactly (i.e. the equality  $D_{\text{SMF}}L_{\text{SMF}}=D_{\text{DCF}}L_{\text{DCF}}$  holds where  $D$  means the first-order dispersion parameter [ps/nm/km] of the corresponding fiber and  $L$  stands for the total SMF or DCF length per cell). The second-order dispersion (dispersion slope) is not compensated exactly, which means that in total dispersion, compensation takes place only at a certain wavelength. This is the carrier wavelength, which (since it is not explicitly specified in the set-up) is assumed by the fiber components to correspond to the center frequency of the simulated bandwidth. Due to the incomplete dispersion compensation, the longest-wavelength channel accumulates approximately 9 ps/nm (positive) dispersion per single cell. The shortest wavelength channel accumulates -9 ps/nm dispersion per cell. One of our tasks is to identify how the interplay between this residual dispersion and the nonlinearity (SPM) influences the performance of the system depending on the modulation format.

Variable step-size is used with the maximum (over the time window) nonlinear phase shift allowed equal to five mrad. This is consistent with what is used in the literature (e.g. one mrad is used in [9] and three mrad in [21]). In the presence of loss, the impact of the nonlinearities will decrease along the fiber length (or more specifically, the nonlinearities will be important until the propagation distance is less than the effective length [5]) which subsequently allows larger step-sizes to be used - the variable step size calculation is advantageous in this case. It is well established that if the step size is improperly chosen (too big), the FWM effects will be artificially exaggerated [28]. Boundary conditions must be set to periodic.

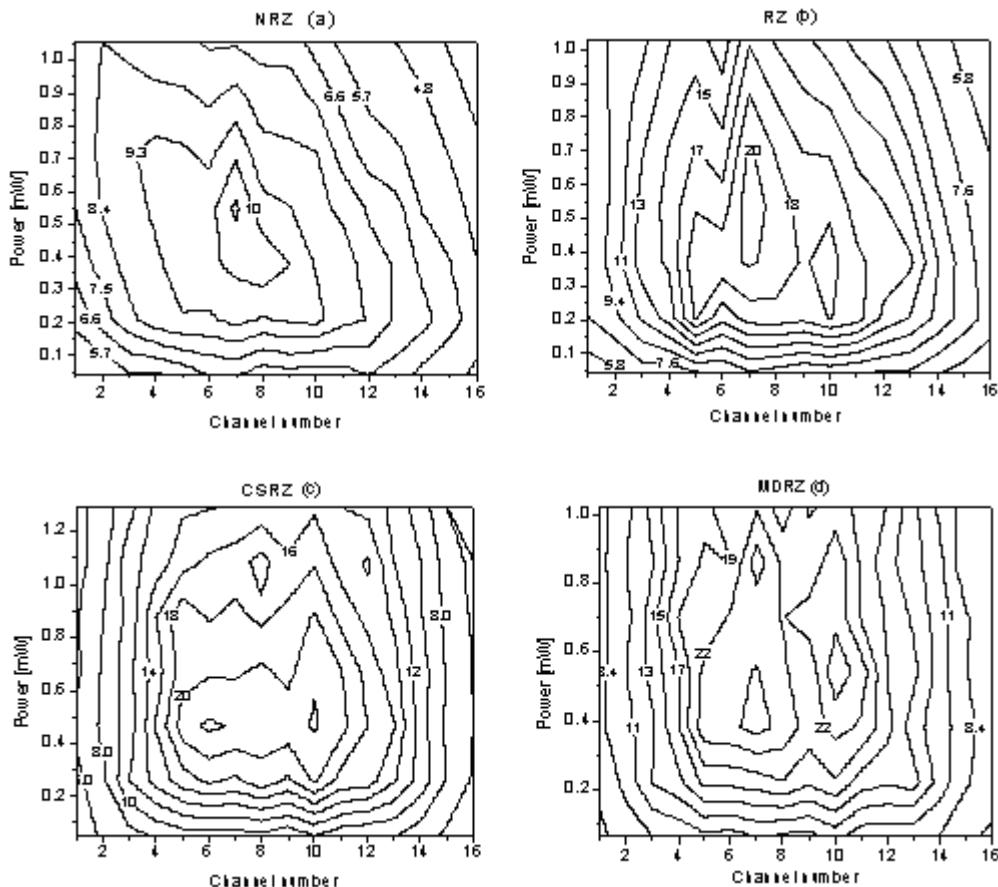


## Results

Figure 24 shows the dependence of the Q-factor of the system on the channel power and channel number (that is, the amount of the residual dispersion).

The largest area with best performance, i.e. the largest number of channels and largest region of powers with maximum Q, is obtained for MDRZ. The CSRZ has the second best performance. This observation is consistent with results from the single channel analysis, in accordance with the very basic idea that the intra-channel nonlinear interactions are more important than the inter-channel one.

**Figure 24** Q-factor of a 16 x 40 Gb/s WDM system depending on the channel number (i.e. the amount of residual dispersion) and averaged channel power.



**Note:** Symmetric compensation scheme is used. Channel number one is the longest wavelength channel.

As Figure 24 shows, there is a noticeable asymmetry in the performance of NRZ. With the increase of the channel power, the outer channels with longer wavelengths (with numbers from 1 to 4) improve their performance with the power increase, while the performance of the shorter-wavelength channels (with numbers from 12 to 16) degrades. This feature can be attributed to the interplay between the residual dispersion and nonlinearity. As already mentioned, the longest-wavelength channel



(channel number 1) accumulates approximately 9 ps/nm positive dispersion per single cell. The resulting negative chirp tends to compensate the positive one created by nonlinearity, with the degree of compensation increasing with the increase of power, which explains the observed improvement in performance. On the other hand, the residual dispersion is negative for the shorter-wavelength channels, and the effects of residual dispersion and nonlinearity are added together, which degrades the performance of these channels with the power increase.

In a weaker form, this effect could also be seen for the RZ. At the same time, MDRZ and CSRZ demonstrate almost complete symmetry in the performance of the outer channels. The smaller resistance of NRZ compared to RZ to the interplay between dispersion and nonlinearity is a well established fact (see e.g. [10]).

## References:

- [1] D. Dahan and G. Eisenstein, Journ. Lightwave. Technol. 20, 379 (2002).
- [2] A. Hodzik, B. Konrad and K. Petemann, Journ. Lightwave. Technol. 20, 598, (2002).
- [3] P. Johannsson, D. Anderson, M. Marklund, A. Berntson, M. Forzati and J. Martensson, Opt. Lett. 27, 1073, (2002).
- [4] K.S. Cheng and J. Conradi, IEEE Phot. Technol. Lett., 14p. 98, (2002).
- [5] G. P. Agrawal, Nonlinear Fiber Optics, Academic press (2001).
- [6] G. P. Agrawal, Applications of Nonlinear Fiber Optics, Academic press (2001).
- [7] P.V. Mamyshev and N.A. Mamysheva, Opt. Lett. 24, 1454, (1999).
- [8] A. Mecozzi, C.B. Clausen, M. Schtaif, IEEE Phot. Technol. Lett., 12, 392 (2000).
- [9] M.I. Hayee and A.E. Willner, IEEE Phot. Technol. Letters, 11, 991, (1999).
- [10] D. Breuer and K. Petermann, IEEE Phot. Technol. Lett. 9, 398, (1997).
- [11] K. Marinov, I. Uzunov, M. Freitas and J. Klein, Optical amplifiers and their applications (OSA Topical meeting), 76 - 78, Otaru, Japan, July 6 - 9 (2003).
- [12] A. Mecozzi, C.B. Clausen, M. Schtaif, IEEE Phot. Technol. Lett., 12, 1633, (2000).
- [13] A. Mecozzi, C.B. Clausen, M. Shtaif, IEEE Phot. Technol. Lett., 13, 445 (2001).
- [14] P. Johannsson, D. Anderson, A. Bernutson and J. Martensson, Opt. Lett., 26, 1227, (2001).
- [15] R. I. Killey, H. J. Thiele, V. Mikhailov and P. Bayvel, IEEE Phot. Technol. Lett., 12, 1624, (2000).
- [16] X. Liu, X. Wei, A. H. Gnauck, C. Xu and L. K. Wickham, Opt. Lett. 27, 1177, (2002).
- [17] Forzati, and J. Martensson, A. Bernutson, A. Djupsjobaska, P. Johannsson, IEEE Phot. Technol. Lett., 14, 1285, (2002).
- [18] Y. Miyamoto, A. Hirano, S. Kuwahara, Y. Tada, H. Masuda, S. Aozasa, K. Murata, and H. Miyazawa, Technical Digest of OAA 2001, post-deadline paper PD6, July, (2001).
- [19] F. Forghieri, R. W. Tkach and A. R. Chraplyvy, Journ. Lightwave. Technol., 13, 889, (1995).
- [20] D. Marcuse, A. R. Chraplyvy and R. W. Tkach, Journ. Lightwave. Technol, 9, 121, (1991).
- [21] R. W. Tkach, A. R. Chraplyvy, F. Forghieri, A. H. Gnauck, and R. M. Derosier, Journ. Lightwave. Technol, 13, 841, (1995).
- [22] F. Matera and M. Settembre, Journ. Lightwave. Technol., 14, 1, (1996).
- [23] L. Boivin and J. Pendock, Optical amplifiers and their applications, 292, (1999).
- [24] P. Winzer, M. Pfennigbauer, M. Strasser and W. Leeb, Journ. Lightwave Technol. 19, 1263, (2001).
- [25] P. Winzer and A. Kalmar, Journ. Lightwave Technol., 17, 171, (1999).
- [26] M. Pauer, P. Winzer and W. Leeb, Journ. Lightwave. Technol. 9, 1255, (2001).
- [27] C. H. Kim, H. Kim, P. J. Winzer and R. Jopson, IEEE Phot. Technol. Lett. 14, 1629, (2002).
- [28] O. Sinkin, R. Holzlöhner, J. Zweck and C. R. Menyuk, Journ Lightwave Technol. 21, 61 (2003).
- [29] Y. Miyamoto, K. Yonenaga, A. Hirano and M. Tomizawa, IEICE Trans. Commun., E85-B, 374, (2002).



# WDM components—Tunable filters

OptiSystem component library includes different types of components for WDM systems, the tunable optical filters include Fabry-Perot filters, Mach-Zehnder interferometers, and grating based filters.

## Fabry-Perot filters

**Fabry-Perot filter.osd** shows the transmission of a Fabry-Perot filter used as a tunable optical filter (see [Figure 1](#)). The frequency spacing between two successive transmission peaks is known as free spectral range (see [Figure 2](#)).

**Figure 1** Fabry-Perot filter

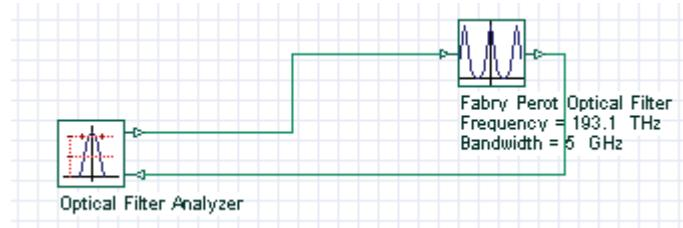
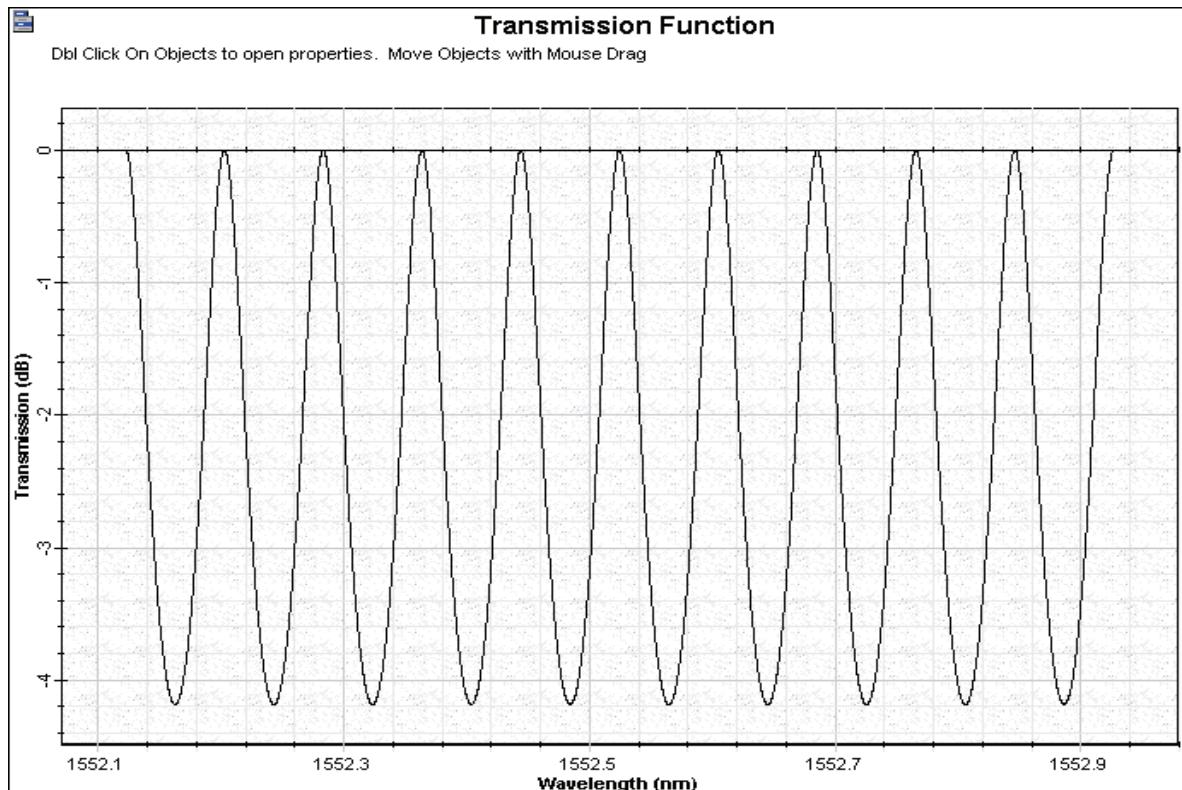


**Figure 2** Fabry-Perot filter transmission



## Uniform FBG Filters

A separate class of optical filters makes use of the wavelength selectivity provided by a Bragg grating (see Figure 3). **FBG filter.osd** shows the transmission of a uniform FBG filter (see Figure 4).

**Figure 3 FBG filter**

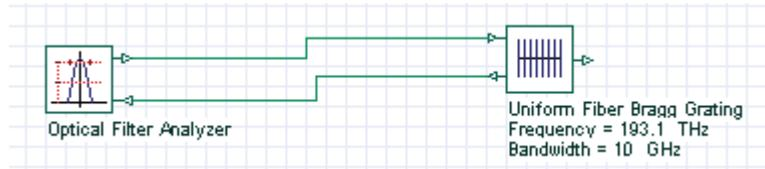
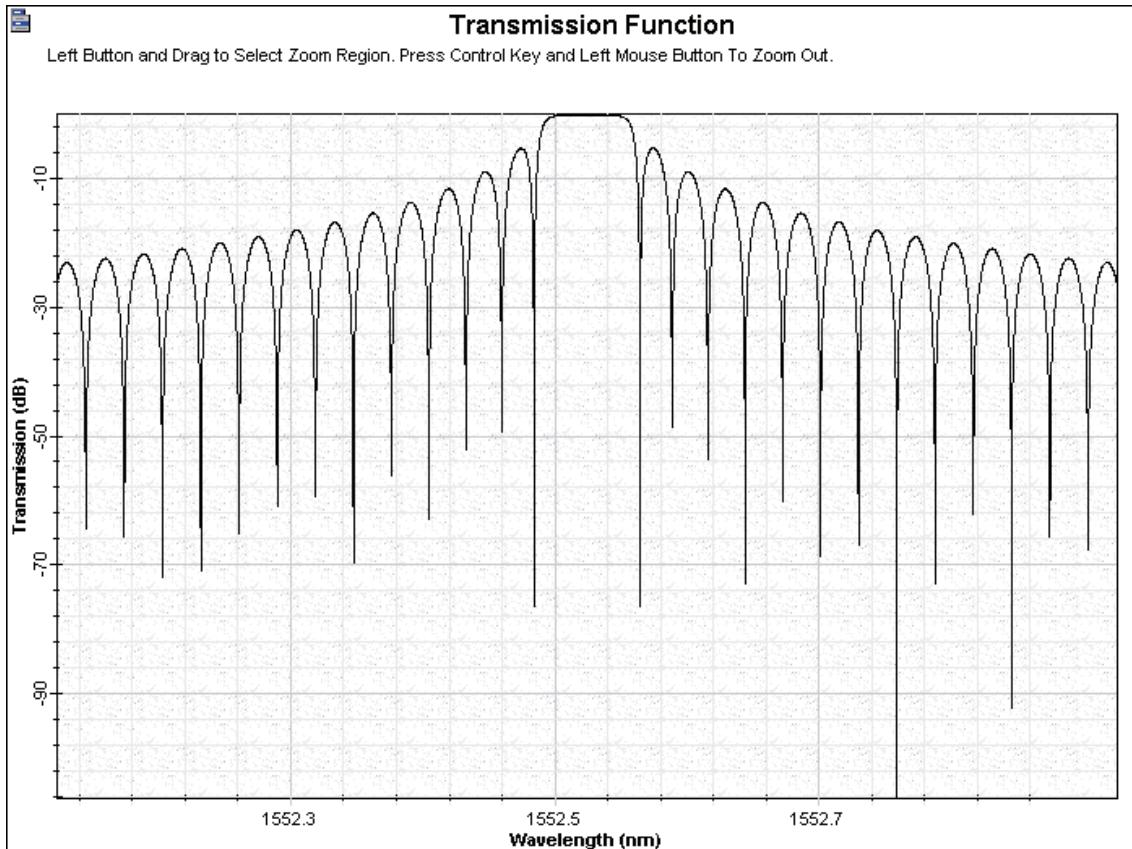


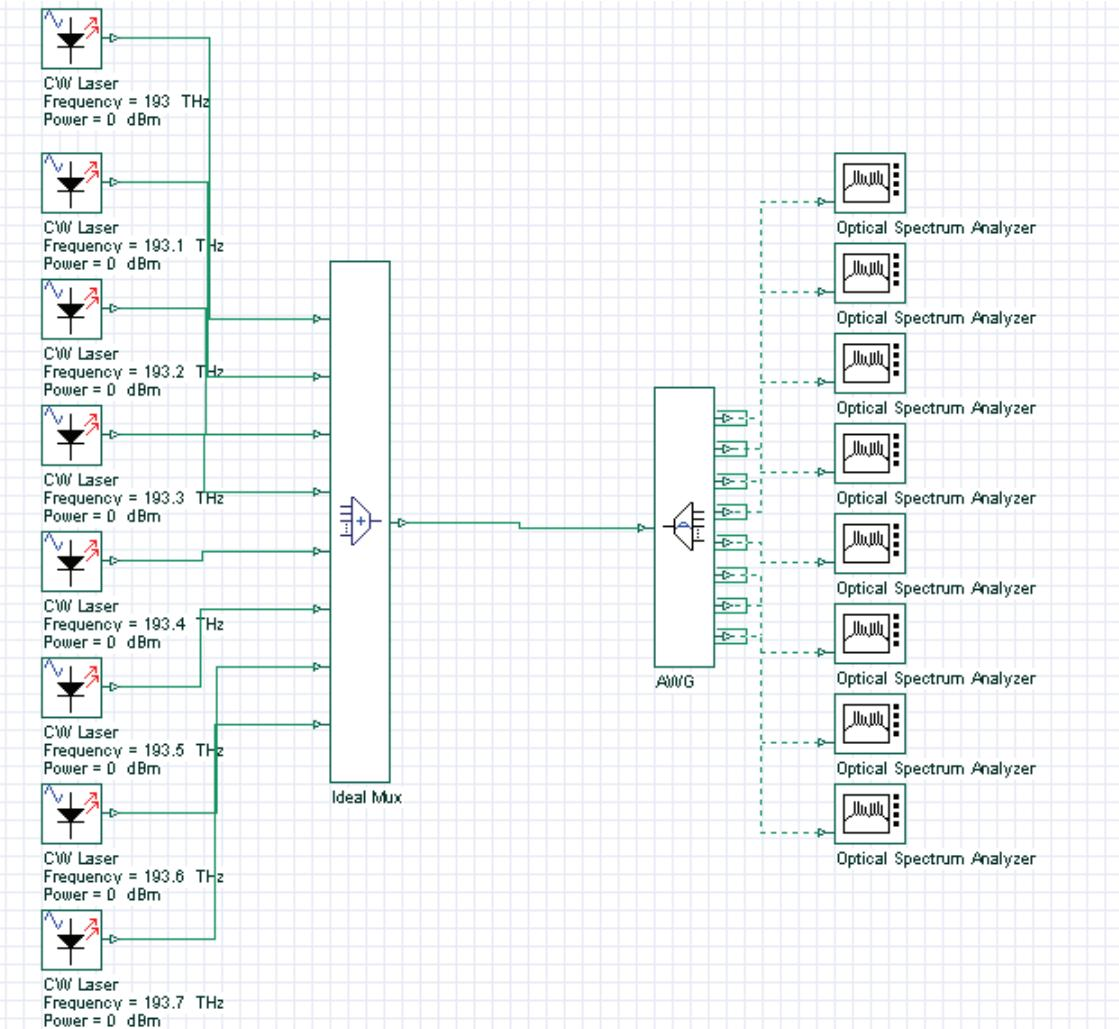
**Figure 4 FBG filter transmission**



# WDM components—AWG demultiplexer

Fiber Bragg gratings can be used for making all fiber demultiplexers. **AWG Demultiplexer.osd** (see [Figure 5](#)) shows an Array waveguide grating (AWG) demultiplexer.

**Figure 5 AWG Demultiplexer**

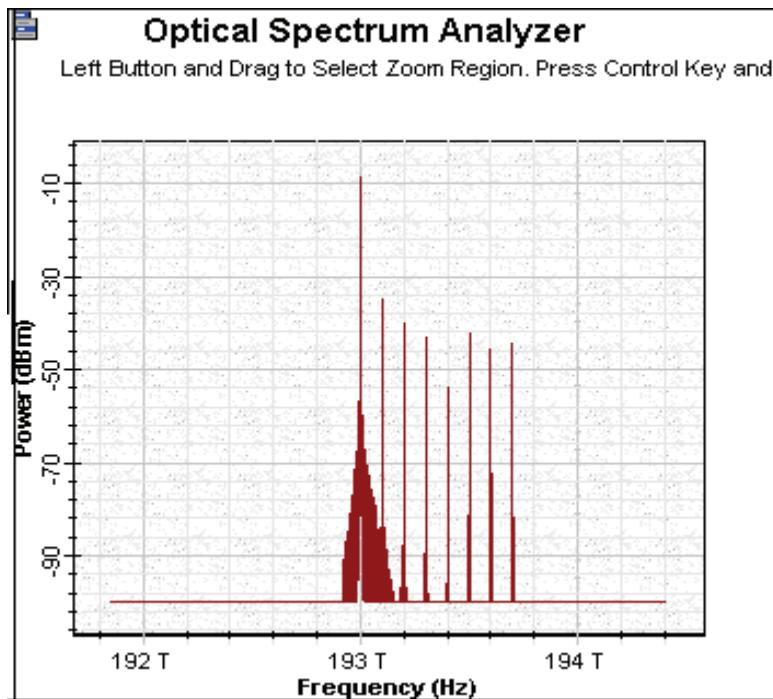


The OSA at the AWG output shows the selected WDM channel.

For the first channel, the results are shown in [Figure 6](#).

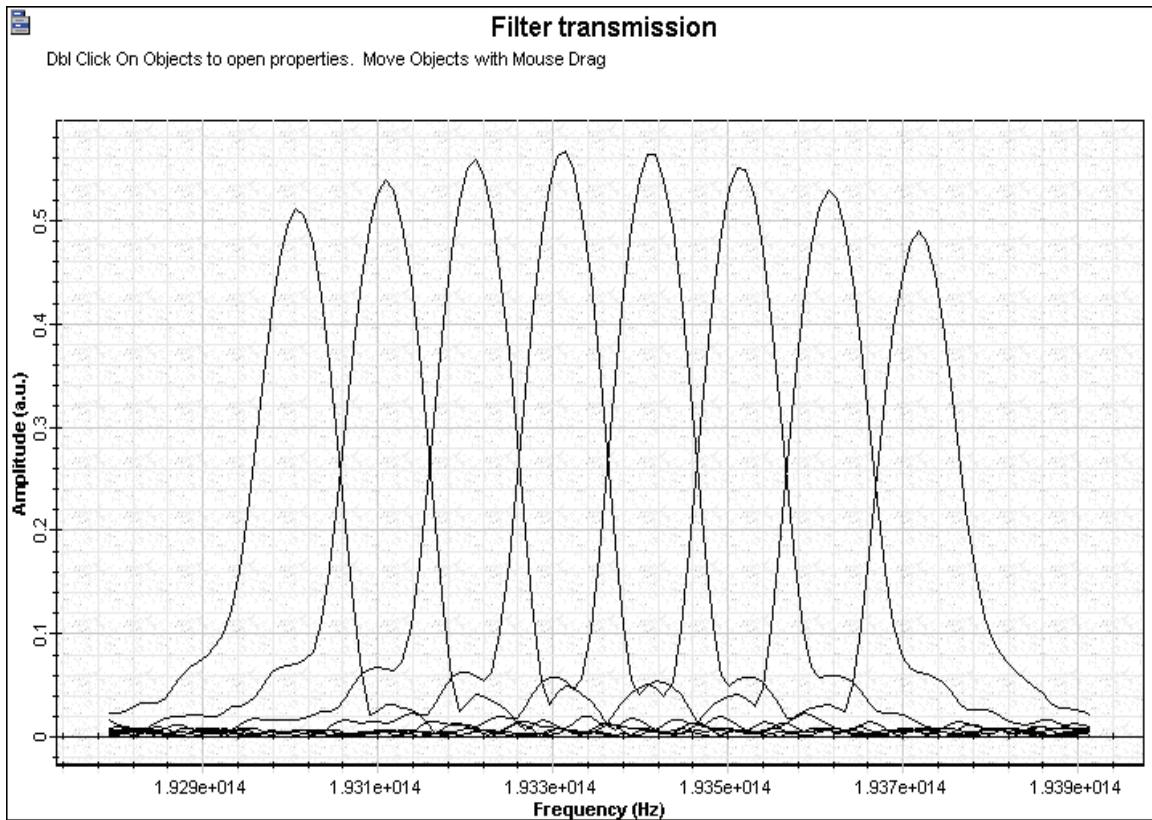


Figure 6 AWG OSA Input



The AWG transmission is shown in Figure 7.



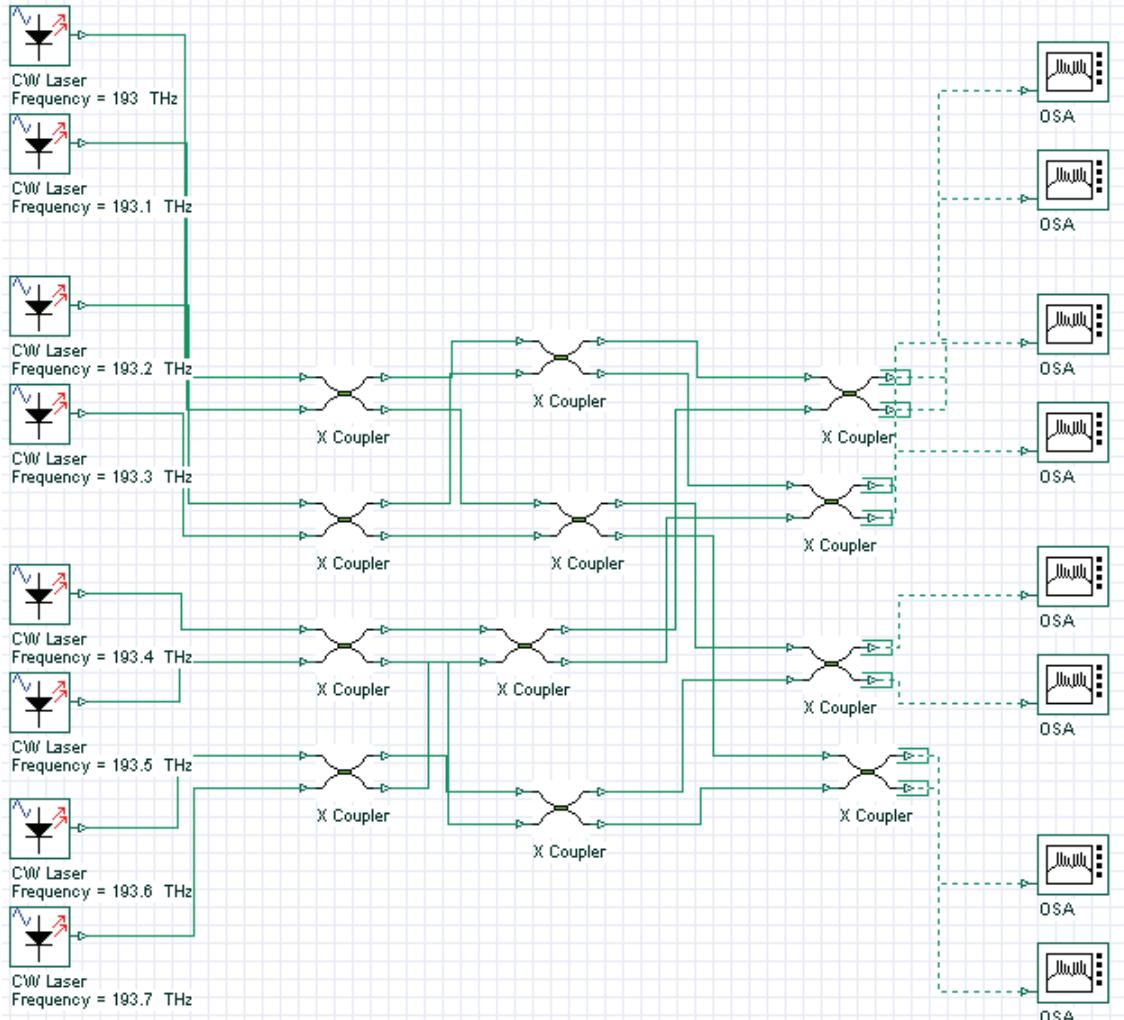
**Figure 7 AWG transmission**

**Notes:**

# Broadcast star coupler

The role of a star coupler is to combine the optical signals entering from its multiple input ports and divide it equally among its output ports. **Broadcast Star Couplers.osd** show a star coupler with 8 input ports; each port has a transmitter working in different wavelengths.

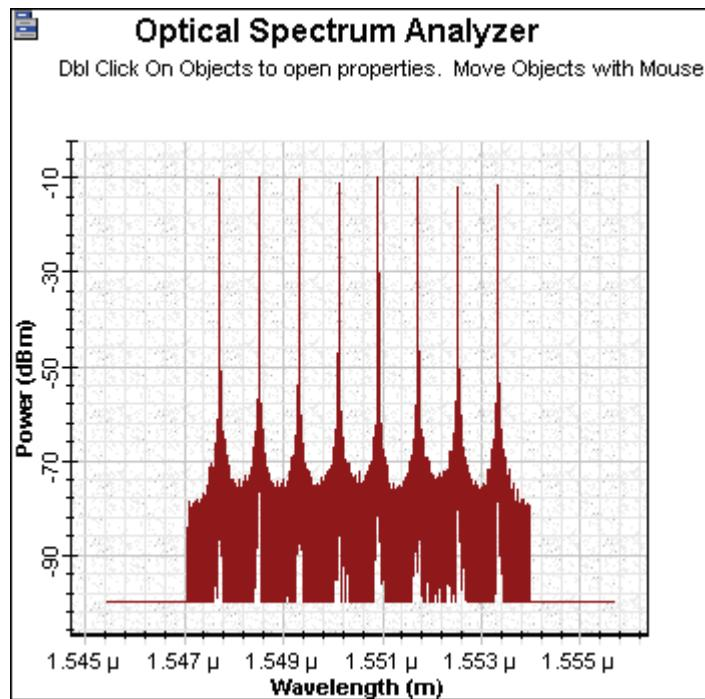
**Figure 8 Broadcast Star Couplers**



The output of the star coupler can be visualized by attaching an OSA at any of the output ports (see [Figure 9](#)).



Figure 9 Broadcast Star Couplers OSA

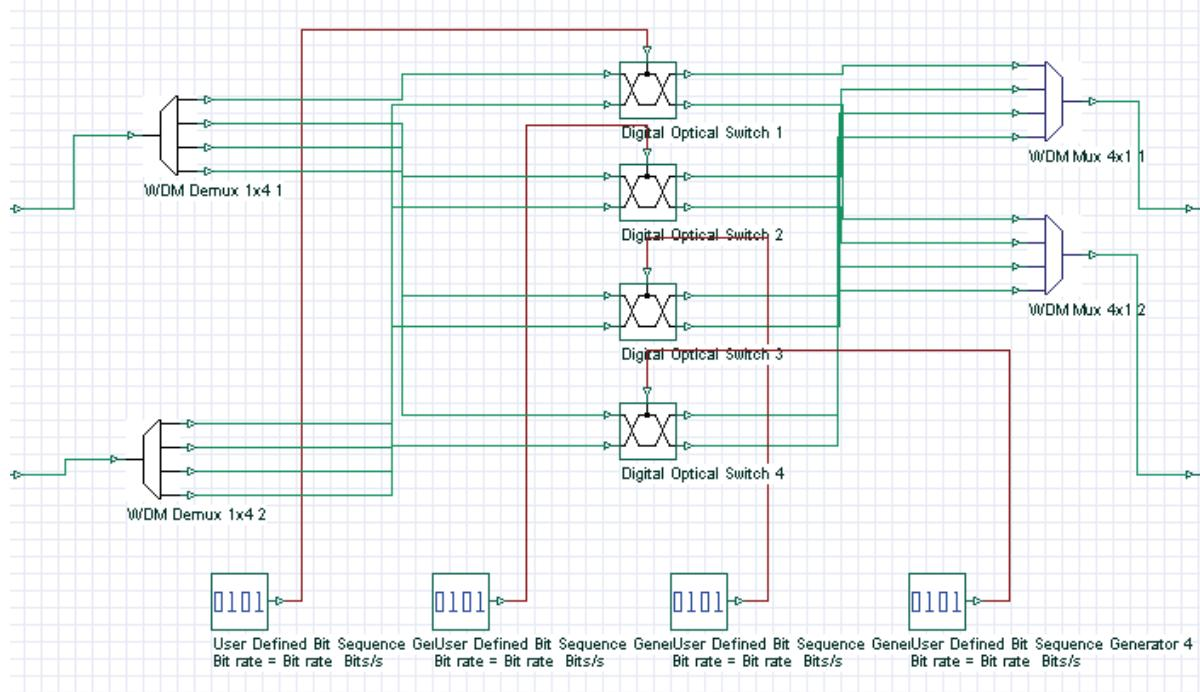


# Optical cross-connects

---

The development of wide-area WDM networks requires wavelength routing that can be reconfigure the network while maintaining its transparent nature. **OXC Project.osd** shows an optical cross connect with 2 input and 2 outputs, each port accommodate 4 wavelengths:

**Figure 10 Optical Cross-Connect**



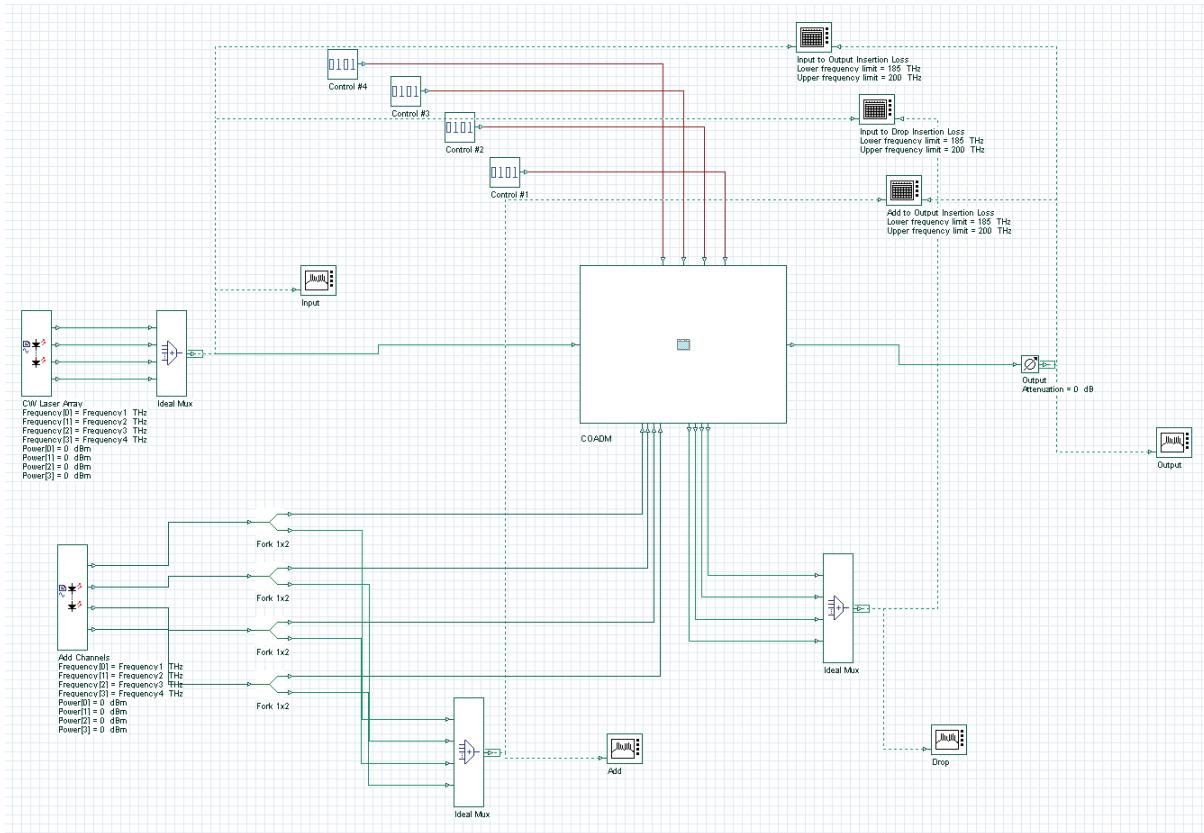
**Notes:**

# Configurable optical add-drop multiplexer

Designed to deliver increased functionality and flexibility necessary for today's advanced optical networks, the COADM demonstrated in project **COADM 4x4.osd** enables up to 4 channels to be independently added and dropped at will.

The system layout is presented in Figure 1; the input of the COADM is connected to a CW Laser Array, which generates 4 wavelength signals. The second laser array generates the channels connected to the ADD input ports. The input signals will have linewidths of 1 MHz, and the added signals will have linewidths of 10 MHz. This difference was added intentionally, to allow for easy identification of the signal sources when using the OSAs. The control components configure the COADM, by changing the switch positions from cross-state to bar-state.

Figure 1 COADM layout



**Notes:**

# Advanced modulation formats

---

The objective of this lesson is to demonstrate the ability to modulate optical signals in formats different of the common RZ and NRZ.

In this tutorial our goal is to generate a 40 Gb/s optical signal in the proposed modulation formats:

- duobinary
- modified-duobinary (MDRZ)
- Carrier-suppressed RZ (CSRZ), DPSK and DQPSK formats

To generate the optical signals we have used a CW laser source, Mach-Zehnder modulators, NRZ pulse pattern generator and a sinusoidal electrical signal generator.

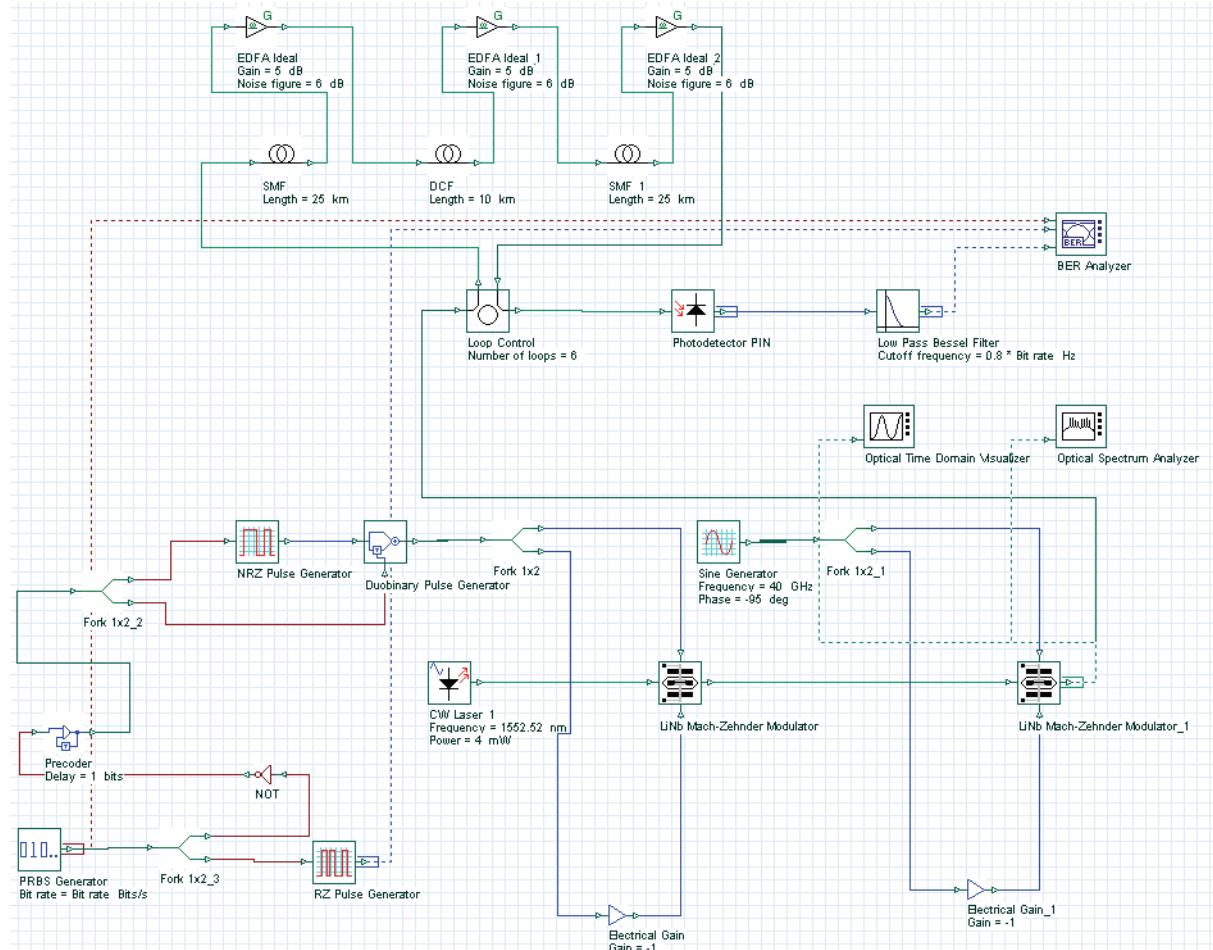
Furthermore, we have used a duobinary precoder for the duobinary and MDRZ signals in order to avoid recursive decoding in the receiver.

Figure 1 shows a system transmitting a Duobinary signal at 40 Gb/s (sample [Duobinary\\_Signal.osd](#)).

The Duobinary was generated by first creating an NRZ duobinary signal using a precoder and a duobinary pulse generator. The generator drives the first MZM, and then concatenates this modulator with an second modulator that is driven by a sinusoidal electrical signal with the frequency of 40 GHz.

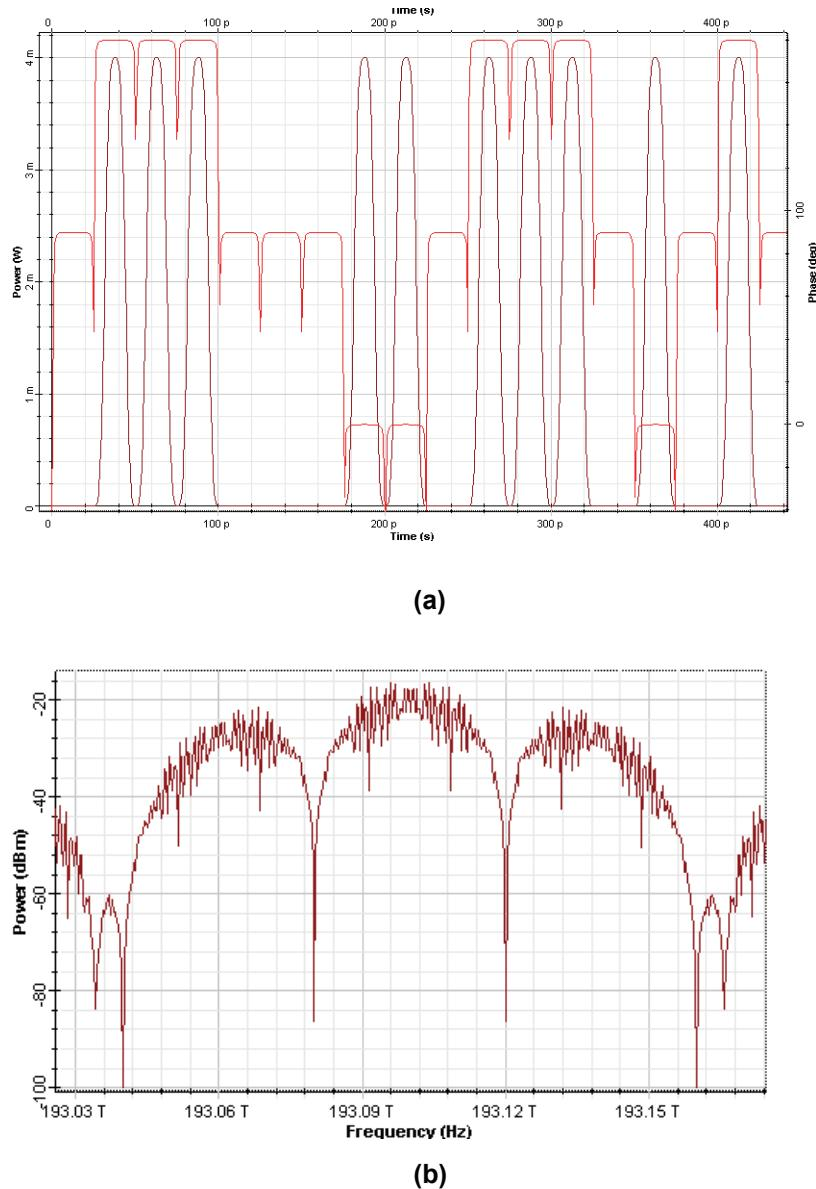
The duobinary precoder used here was composed of an exclusive-or gate with a delayed feedback path.

Figure 1 Duobinary system layout



The optical signal at the output of the second MZ modulator is shown in Figure 2.

**Figure 2 Duobinary signal (a) Time domain, and (b) spectra**

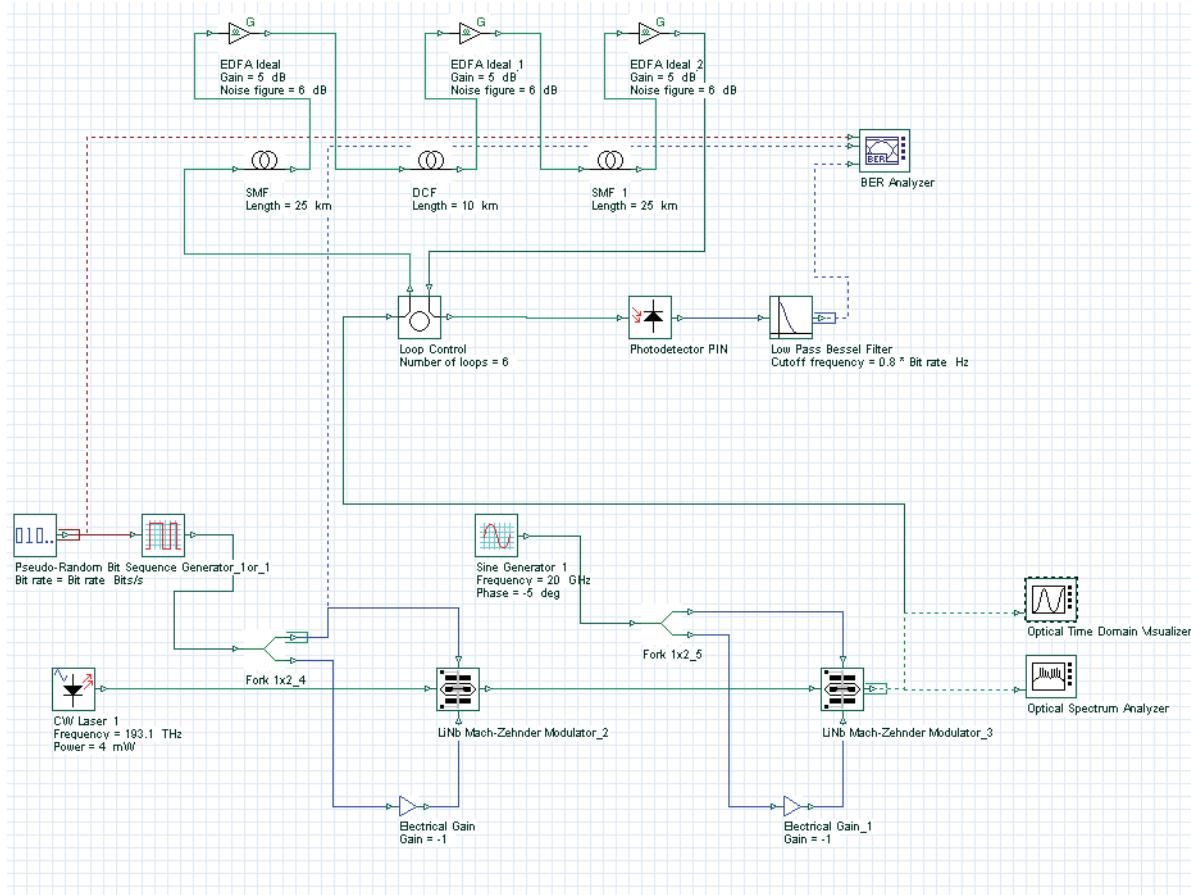


The CSRZ signal is generated in a similar way to the RZ format. However, the frequency of the sinusoidal electrical signal applied in the second MZM has half of the bit rate, 20 GHz.

The second MZM was biased in a way to provide alternating optical phases between 0 to  $\pi$  for the neighboring time slots.

Figure 3 shows a system transmitting a CSRZ signal at 40 Gb/s (sample CSRZ\_Signal.osd).

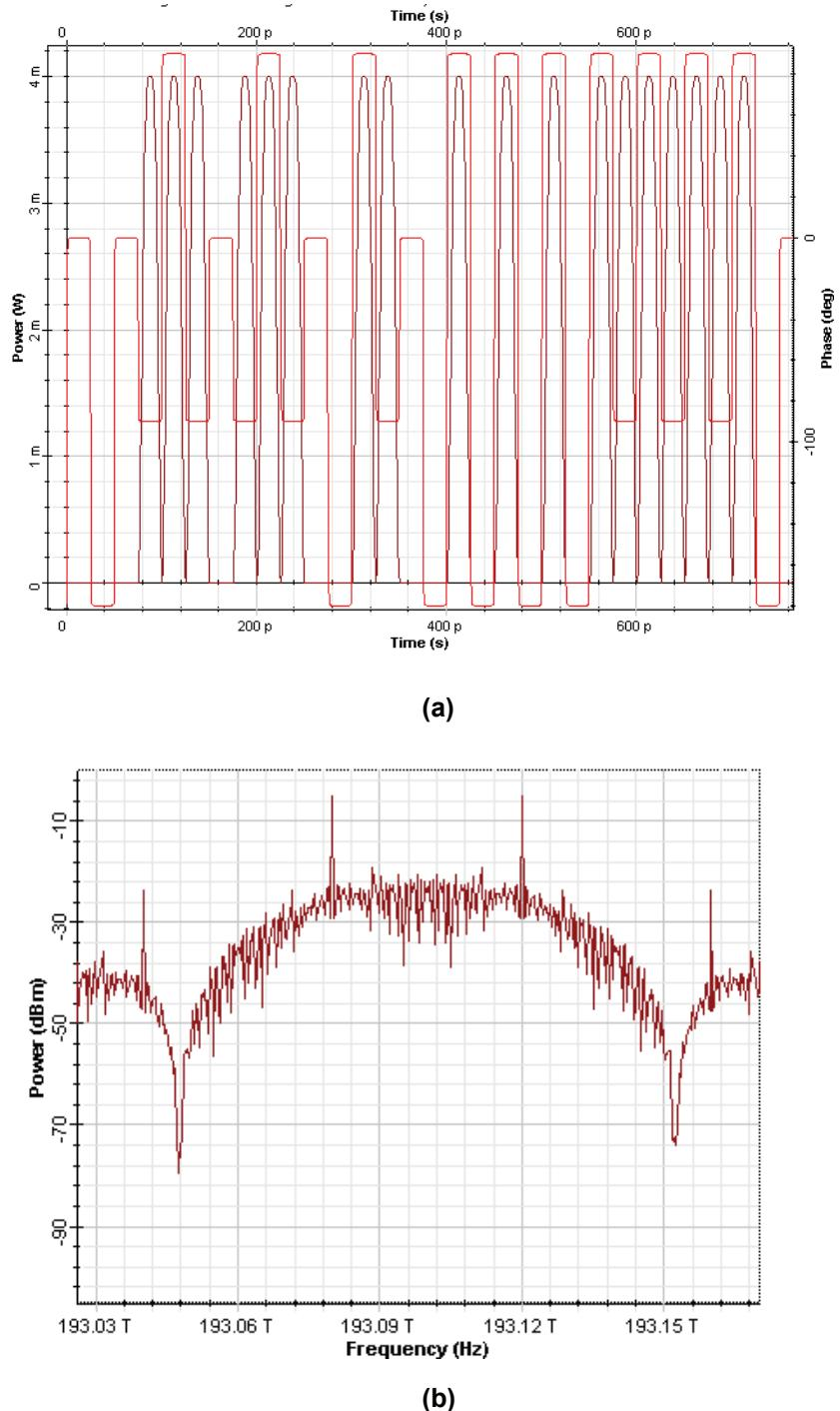
**Figure 3 Carrier-suppressed RZ system layout**



The CS-RZ optical signal is shown in Figure 4.

We can see in Figure 4(a) that the phase of bits '1's are alternating with a difference of  $\pi$  ( $180^\circ$ ). This phase difference causes the elimination of the carrier at 193.1 THz.



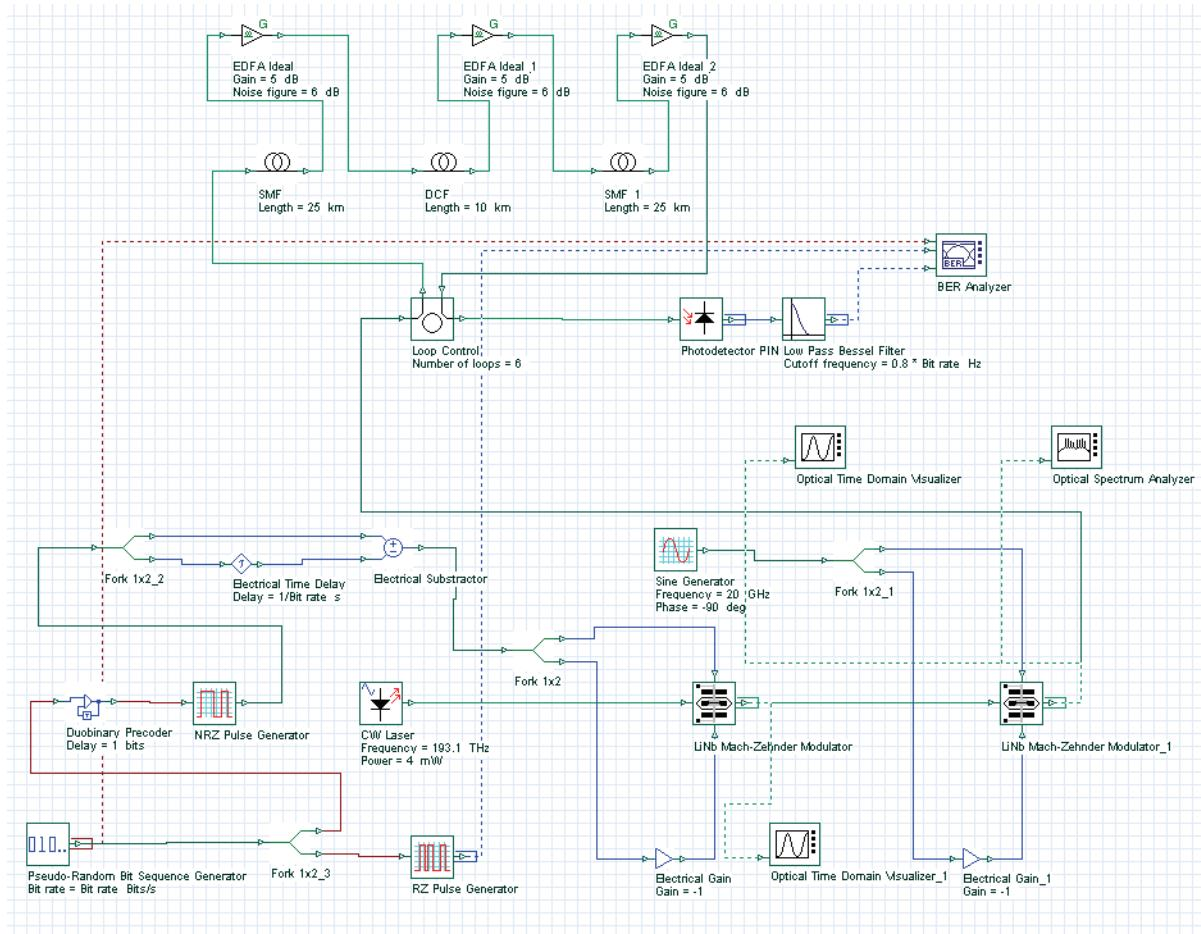
**Figure 4 CSRZ signal (a) Time domain, and (b) spectra**

The MDRZ was generated by first creating an NRZ duobinary signal using an delay-and-subtract circuit that drives the first MZM [1], and then concatenating this modulator with a second modulator that is driven by a sinusoidal electrical signal with the frequency of 40 GHz.

The duobinary precoder used here was composed of an exclusive-or gate with a delayed feedback path.

Figure 5 shows a system transmitting a MDRZ signal at 40 Gb/s (sample [MDRZ\\_Signal.osd](#)).

**Figure 5 Modified duobinary RZ system layout**

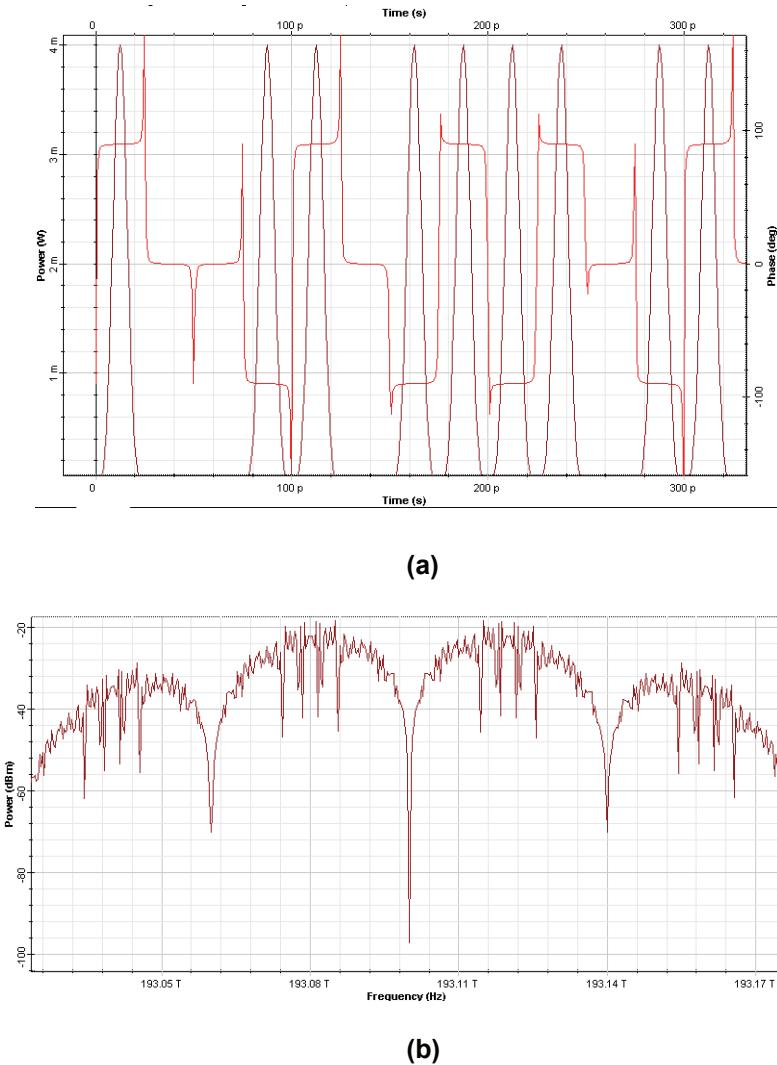


The MDRZ signal is shown in Figure 6.

Different of the duobinary signal where the phase of bits '1's are modified only after a bit '0' appear, in the modified duobinary signal the phase is alternated between 0 and  $\pi$  for the bits '1'.

This will cause the difference in the signal spectra shown at Figure 6(b).

**Figure 6 MDRZ signal (a) Time domain, and (b) spectra**



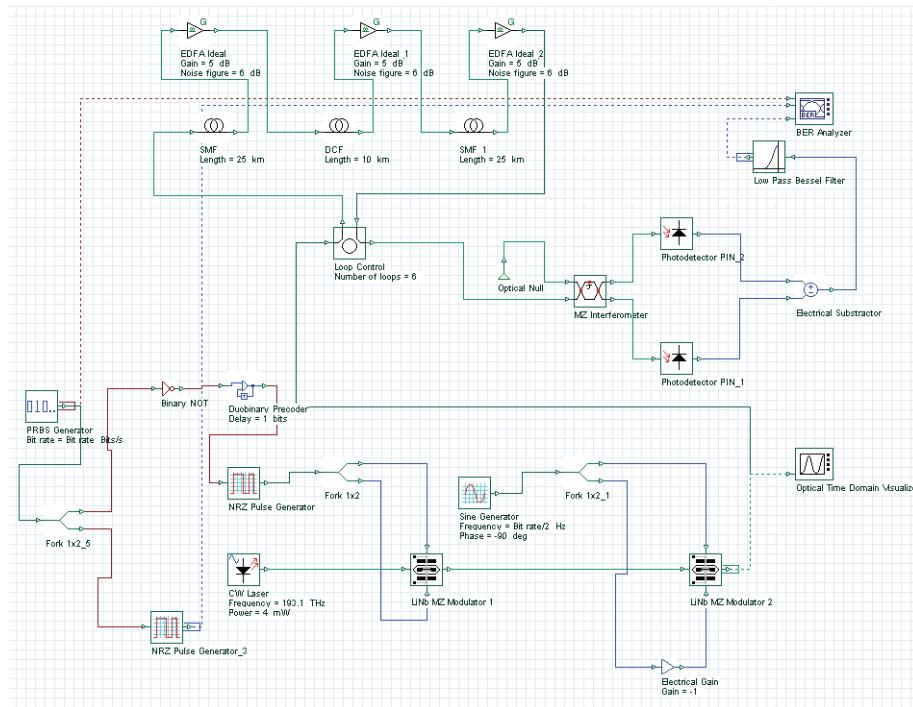
For the DPSK signal generation, we continue to use two concatenated modulators.

The phase modulation was generated by first encoding the NRZ signal using a duobinary precoder that drives the first MZ and modulates the phase of the CW signal, and then concatenating this modulator with an second modulator driven by a sinusoidal electrical signal with the frequency of 20 GHz.

The encoding in the initial bit sequence will allow the demodulation of the transmitted signal at the receiver by using a Mach-Zehnder interferometer and balanced photodiodes.

Figure 7 shows a system transmitting a DPSK RZ with 33% of duty-ratio signal at 40 Gb/s (sample **DPSK\_33%\_Signal.osd**).

**Figure 7 DPSK RZ 33% system layout**

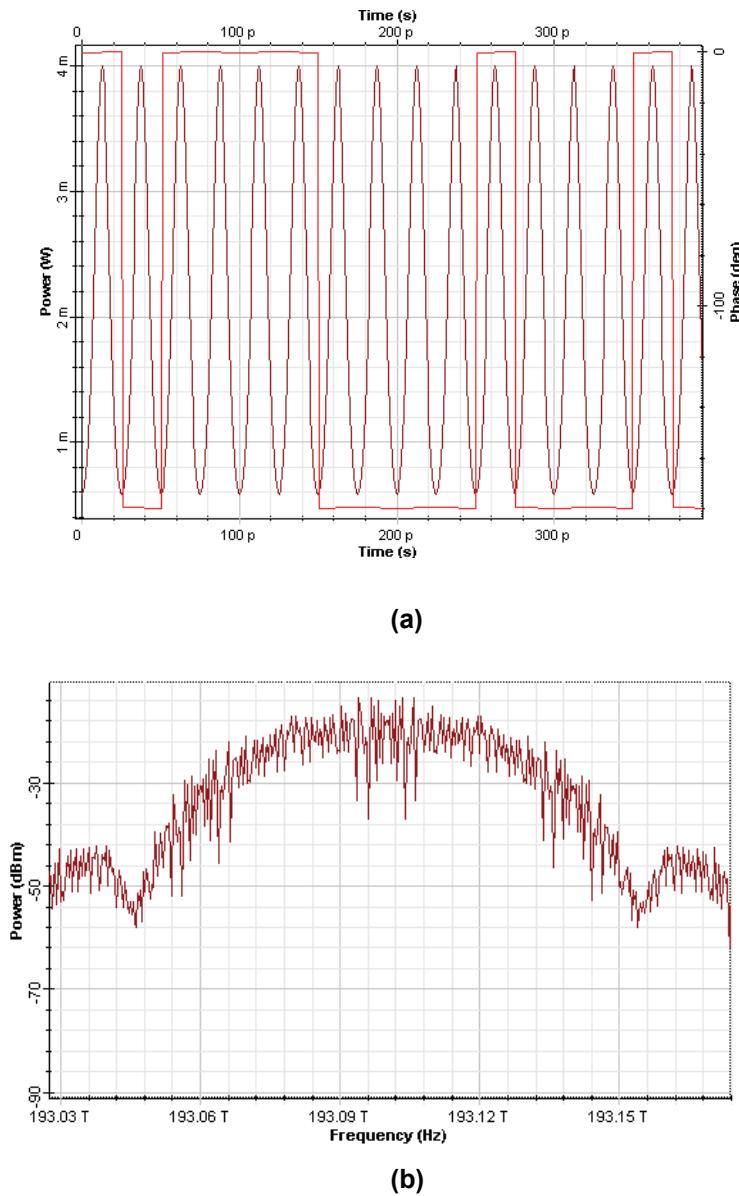


The DPSK signal is shown in Figure 8.

We can verify a sequence of bit '1' with the information modulated in the phase of if bit '1' (0, p).

The corresponding signal spectrum is shown at Figure 8(b).

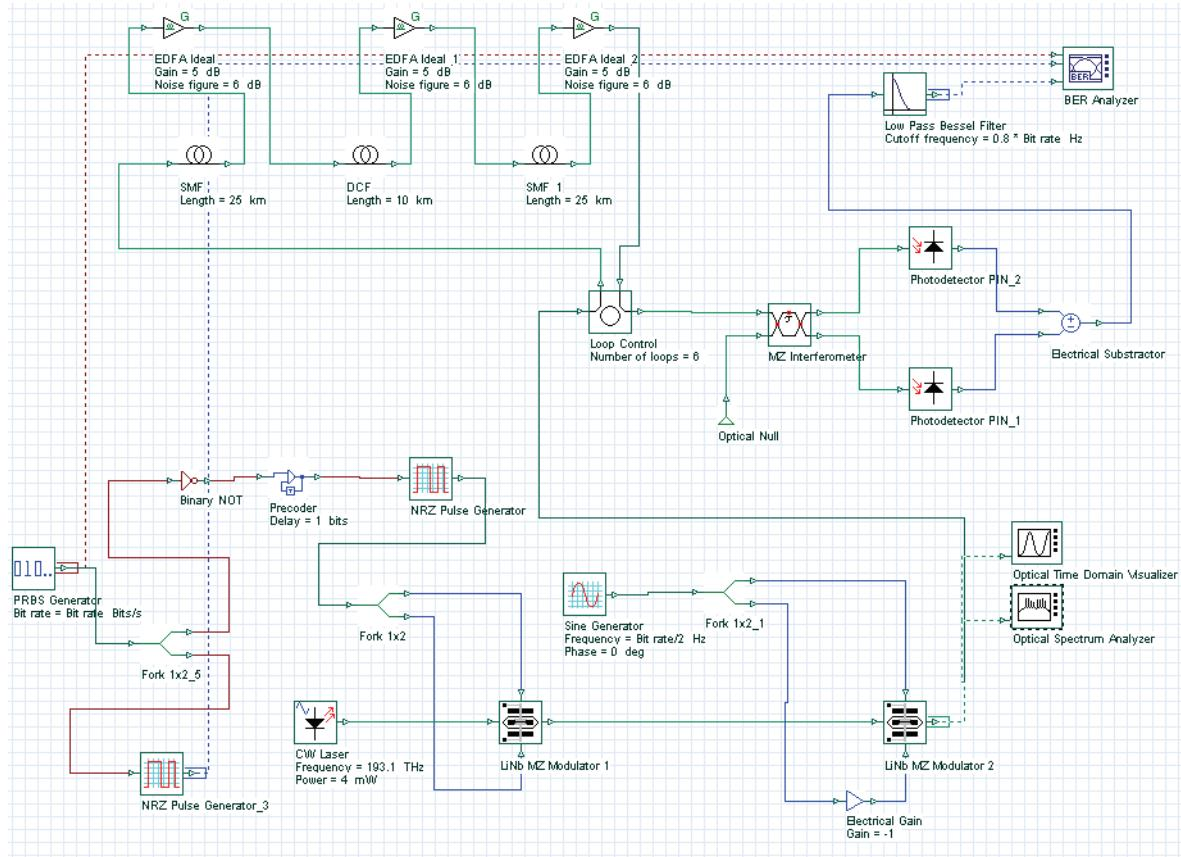
**Figure 8 DPSK 33% RZ signal (a) Time domain, and (b) spectra**



The generation of a DPSK signal with 66% of RZ duty-ratio is very similar to the system in the last layout. Only the phase and amplitude in sinusoidal electrical signal and the bias voltage in the second MZM are modified to generate the RZ signal with 66% of the duty-ratio.

The new layout can be seen in Figure 9 (sample **DPSK\_33%\_Signal.osd**).

**Figure 9 DPSK RZ 66% system layout**

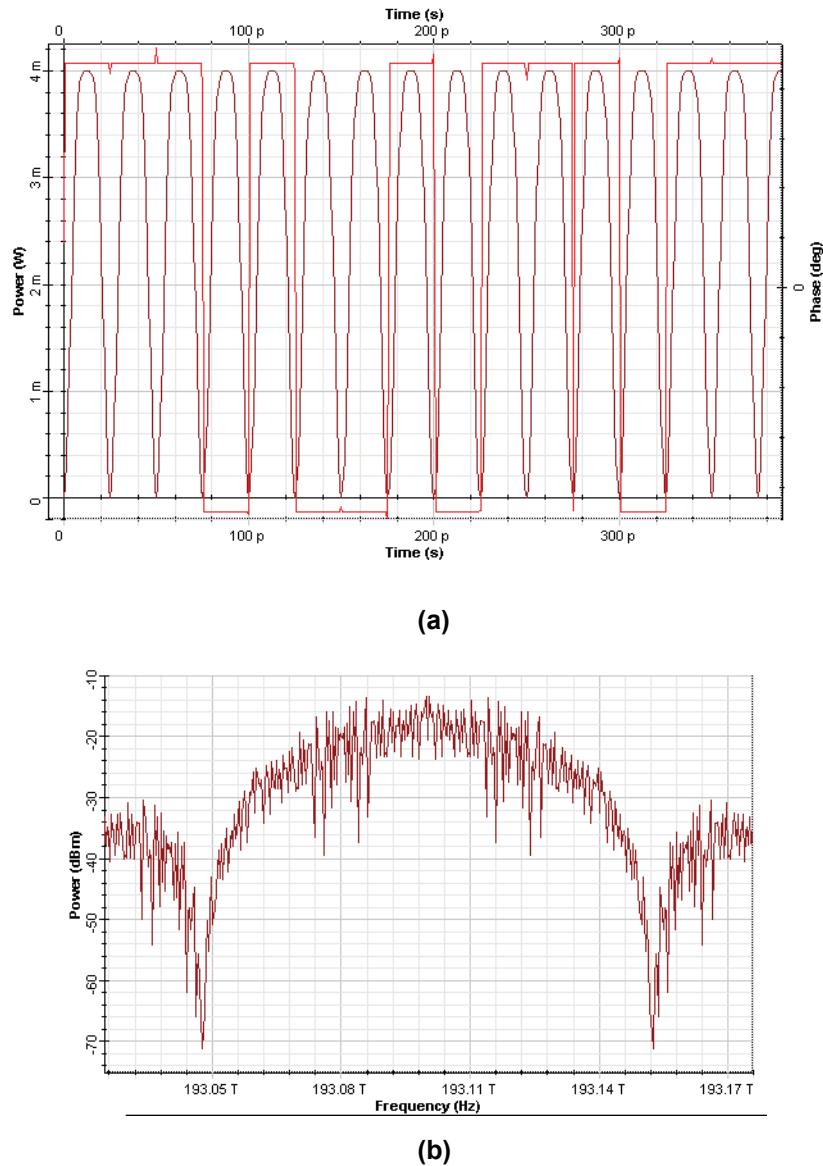


The DPSK signal is shown in Figure. 10.

We can verify a sequence of bits '1' with the information modulated in its phase.

The correspondent signal spectrum is shown at Figure 10(b).

**Figure 10 DPSK 66% RZ signal (a) Time domain, and (b) spectra**



Finally, using three MZ modulators concatenated can generate the DQPSK signal format.

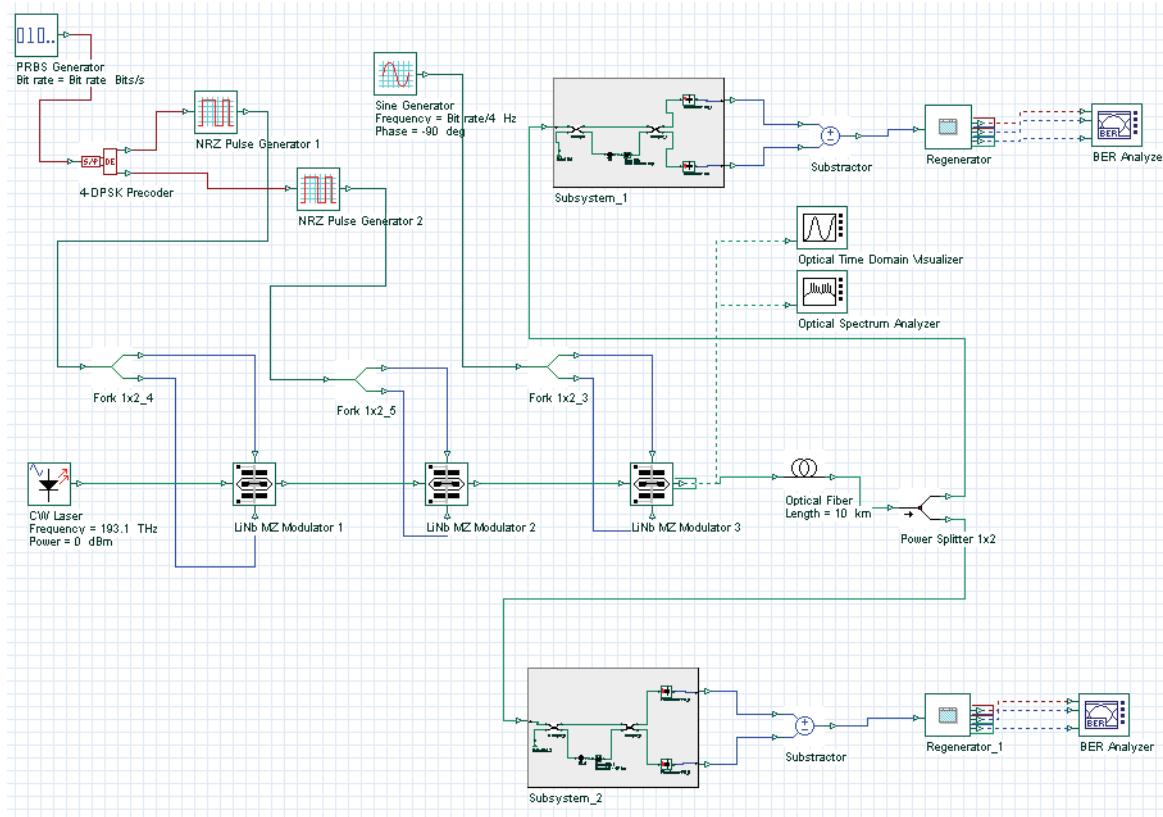
However, to do that, the information has to be encoded in way to allow the demodulation in the reception using two set of interferometers and balanced receivers.

The codification in the initial information was done using the DPSK component (precoder) that will simulate a precoder and generate two encoded signals that will modulate the first and second MZ modulator.

The last modulator will generate the RZ signal.

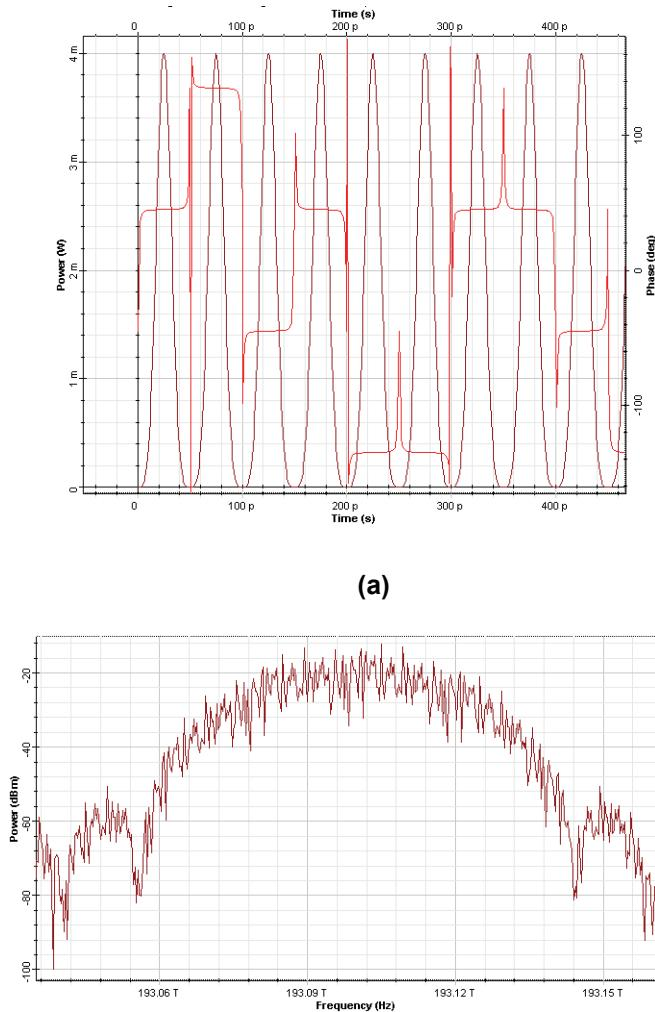
Figure 11 shows the DQPSK layout (see sample **DQPSK\_Signal\_33%.osd**).

**Figure 11 DQPSK system layout**



Each transmitted symbol conveys two bits, encoded in four possible phase differences between successive symbols as can be seen in Figure 12(a).

**Figure 12 DQPSK signal (a) Time domain, and (b) spectrum**



## References

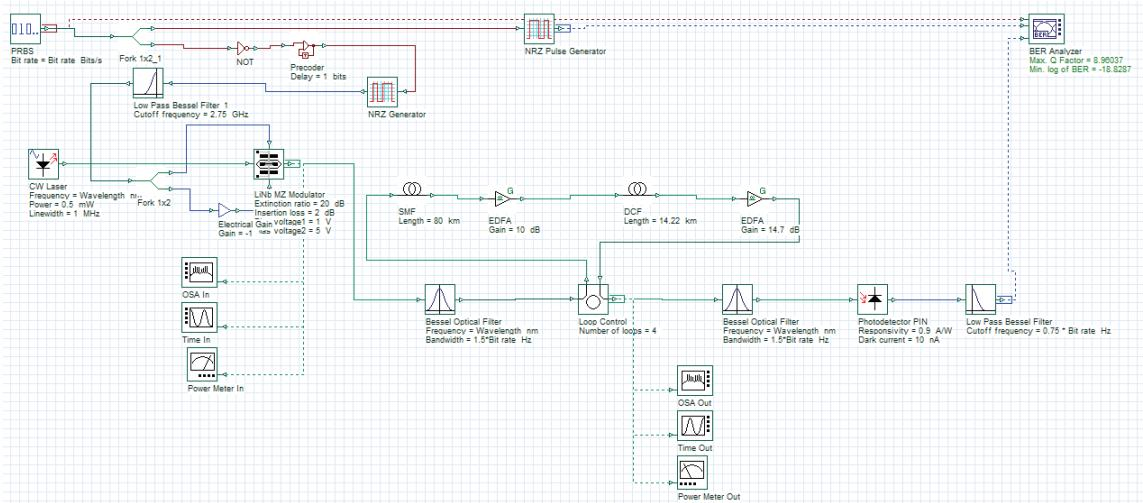
- [1] Y. Miyamoto, K. Yonenaga, A. Hirano and M. Tomizawa "Nx40 - Gbit/s DWDM transport system using novel return-to-zero formats with modulation bandwidth reduction", IEICE Transaction Communications, vol. E85-B, 374-385, (2002).

**Notes:**

# Conventional duobinary transmitter

Project **ODB with Filters ModulationSystem.osd** (Figure 1) demonstrates a system that is an optical duobinary system based on a conventional duobinary transmitter implemented by using a Mach-Zehnder modulator driven with three-level signals generated by using electrical low-pass filters.

Figure 1 Optical duobinary system



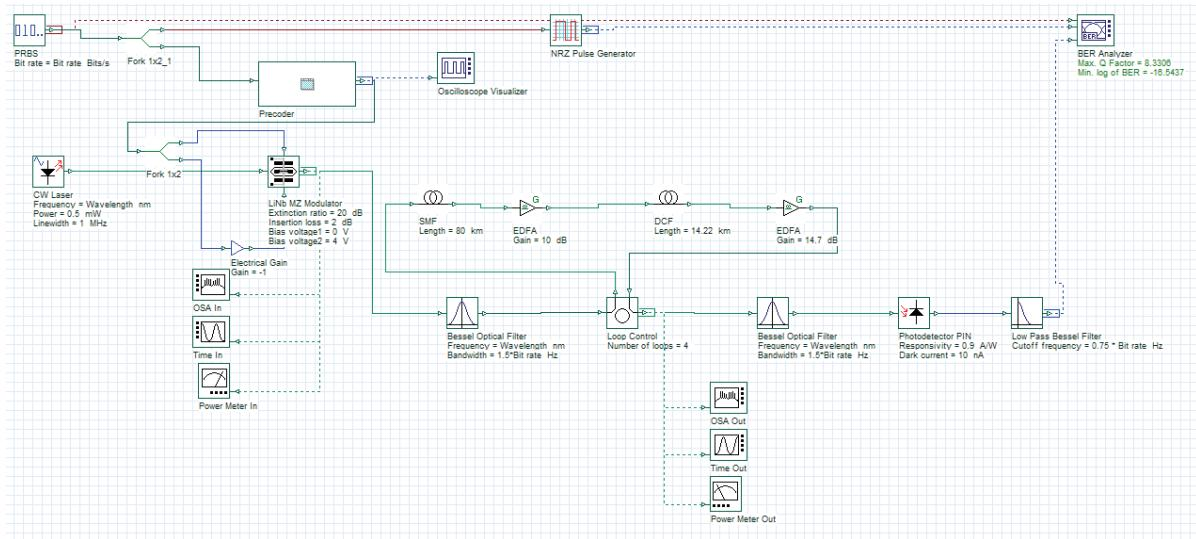
**Notes:**



# Modified duobinary transmitter

Project **MODB\_ModulationSystem.osd** (Figure 1) demonstrates a system that is an optical modified duobinary RZ transmission system, which is equivalent to a duobinary carrier suppressed.

**Figure 1 Modified duobinary system**



**Notes:**



# Interferometer characterization

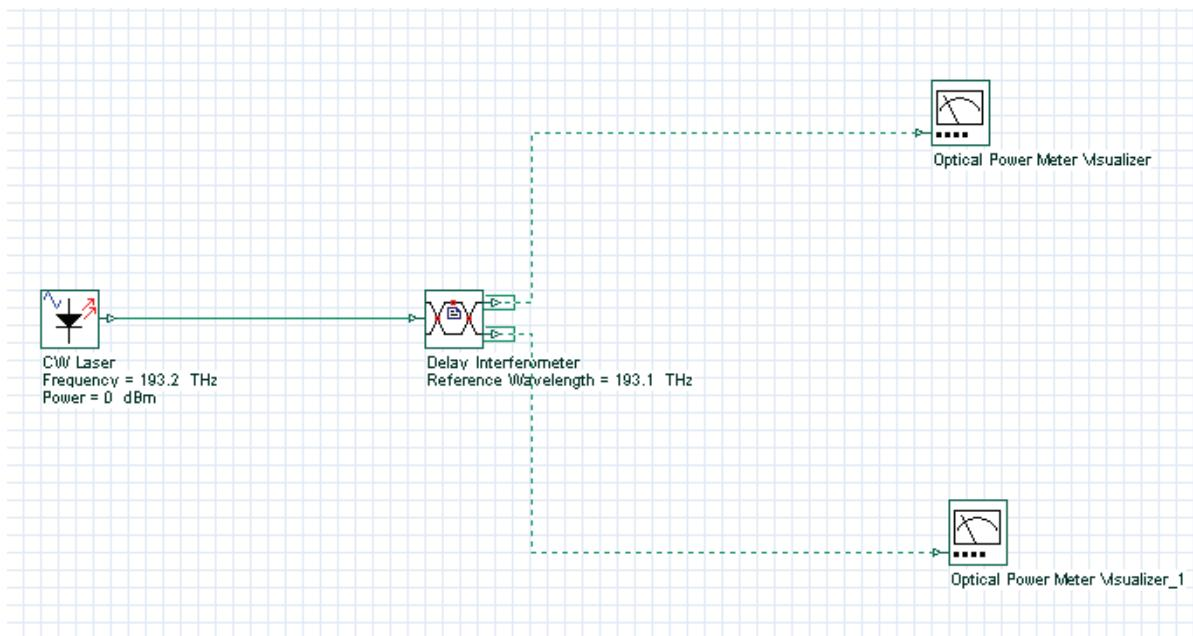
---

The objective of this lesson is to demonstrate the response of the delay interferometer when the wavelength and polarization of the input signal changes.

Initially, we are going to characterize the interferometer response to the variation in the signal wavelength.

Figure 1 shows the system layout designed. See sample InterferometerCharacterization.osd.

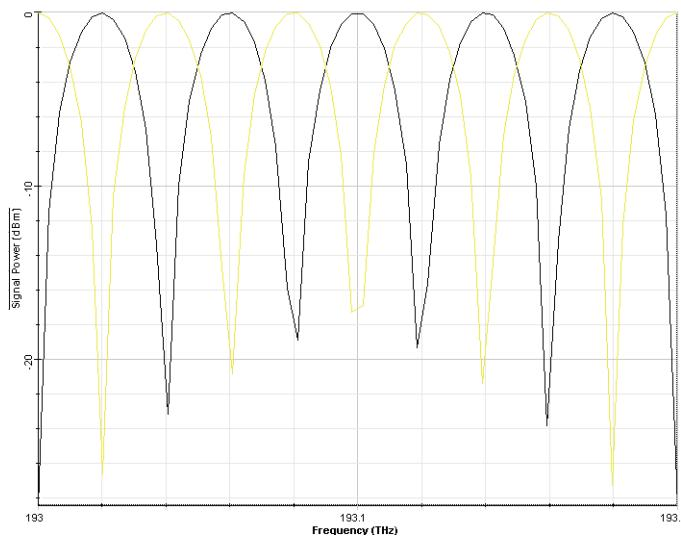
**Figure 1 Output Power x Signal wavelength system layout**



The Frequency parameter in the CW laser is in sweep mode and the frequency vary from 193.0 THz to 193.2 THz.

The maximum IL in the Interferometer is 30 dB, the delay is 0.025 ns and the reference frequency is 193.1 THz.

Figure 2 shows the response in the two output ports for each frequency simulated.

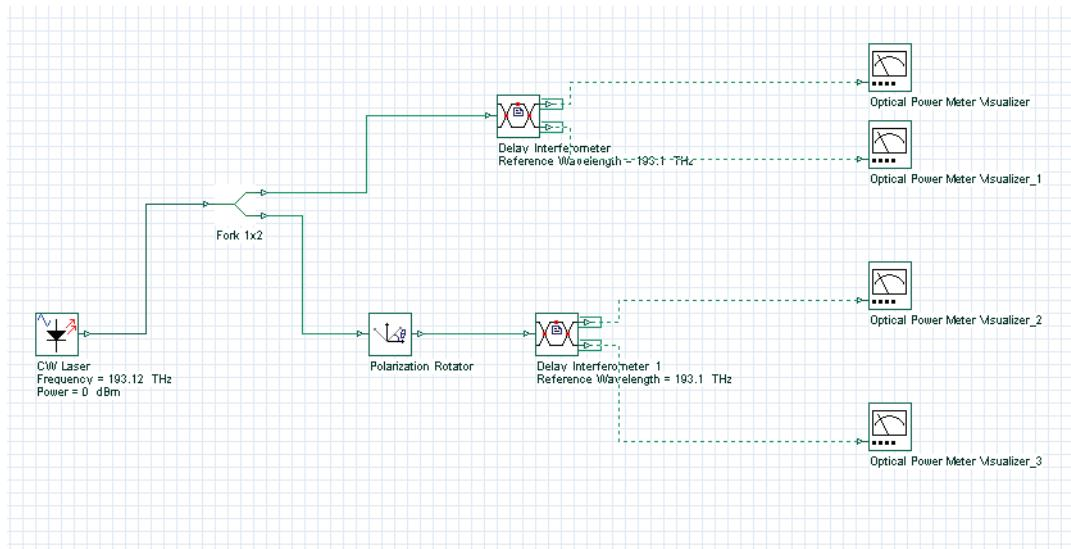
**Figure 2 Output signal power at Output port 1 and 2**

The curve that presents the 0 dBm at 193.1 THz is the response at output port 1. At the same frequency, for output port 2 the signal power should be around -30 dBm. The frequency spacing between the maximum power peaks at each curve is 40 GHz (1/0.025 ns).

To be able to see the effect of the parameter *PDF*, "polarization-dependent frequency shift", we simulate a system with two delay interferometers.

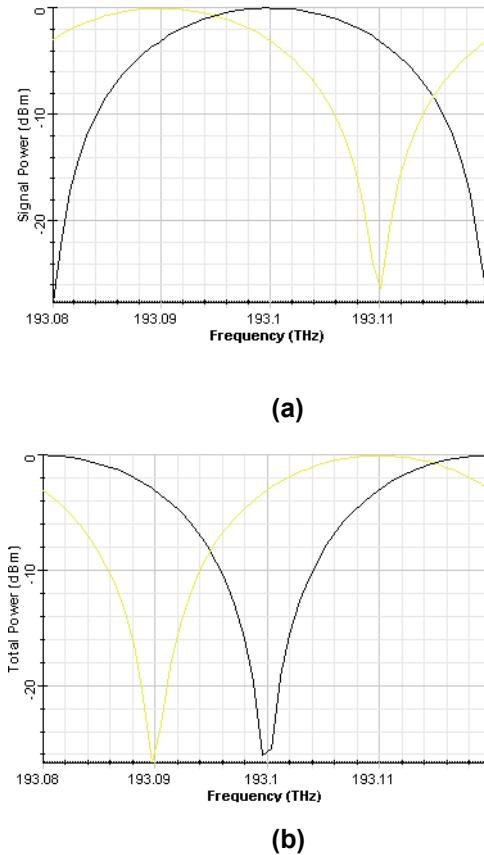
One of delay interferometers will have an input signal orthogonally polarized compared to the other. At this time the signal frequency will vary from 193.08 THz to 193.12 THz.

Figure 3 shows the system layout.

**Figure 3 System layout to compare two signals with different polarizations**

The *Polarization-dependent Frequency Shift* parameter value for each interferometer simulated was 10 GHz.

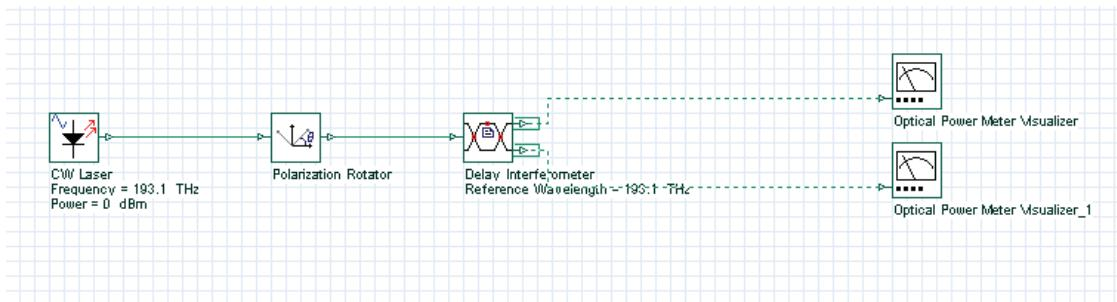
The responses are plotted in Figure 4(a) for output ports 1 and Figure 4(b) for output ports 2.

**Figure 4 Output signal power (a) at output port 1 and (b) output port 2**

We can see in Figure 4 that the difference in the input signal polarization causes a shift of 10 GHz in the curves from different interferometers. This shift is the polarization-dependent frequency shift specified in the interferometers.

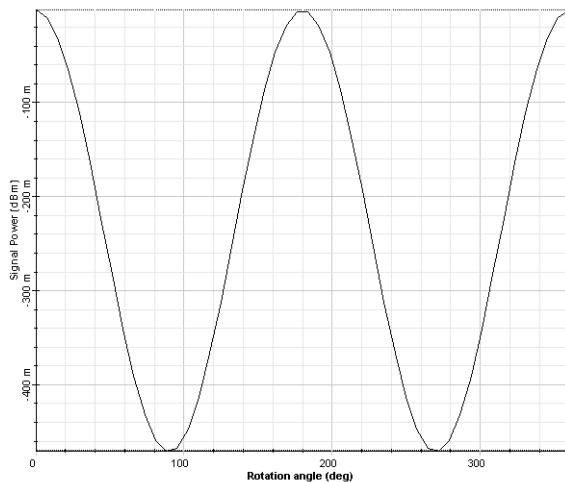
Finally, we analyze the variation in the polarization in the input signal using a polarization rotator varying the angle from 0 to 360 degrees.

Figure 5 shows the system simulated

**Figure 5** Polarization analysis system layout

In this case, we have put the PDF value as zero, and the polarization dependent loss, PDL, of 0.5 dB was specified.

In Figure 6 we can see that the variation in the polarization causes an additional loss and its maximum value is 0.5 dB for signals orthogonally polarized.

**Figure 6** Output signal power x polarization angle

**Notes:**

---

# Solitons and soliton systems

---

This section contains the following advanced and illustrative simulation projects.

## Solitons

- Fundamental and higher order solitons
- Interactions of optical solitons
- Decay of higher order solitons in the presence of third-order dispersion
- Decay of higher order solitons in the presence of intrapulse Raman scattering
- Decay of higher order solitons in the presence of self-steepening
- Stability of solitons in birefringent optical fibers
- Orthogonal Raman gain

## Soliton systems

- Average soliton regime
- SOA as in-line amplifier in soliton communication systems

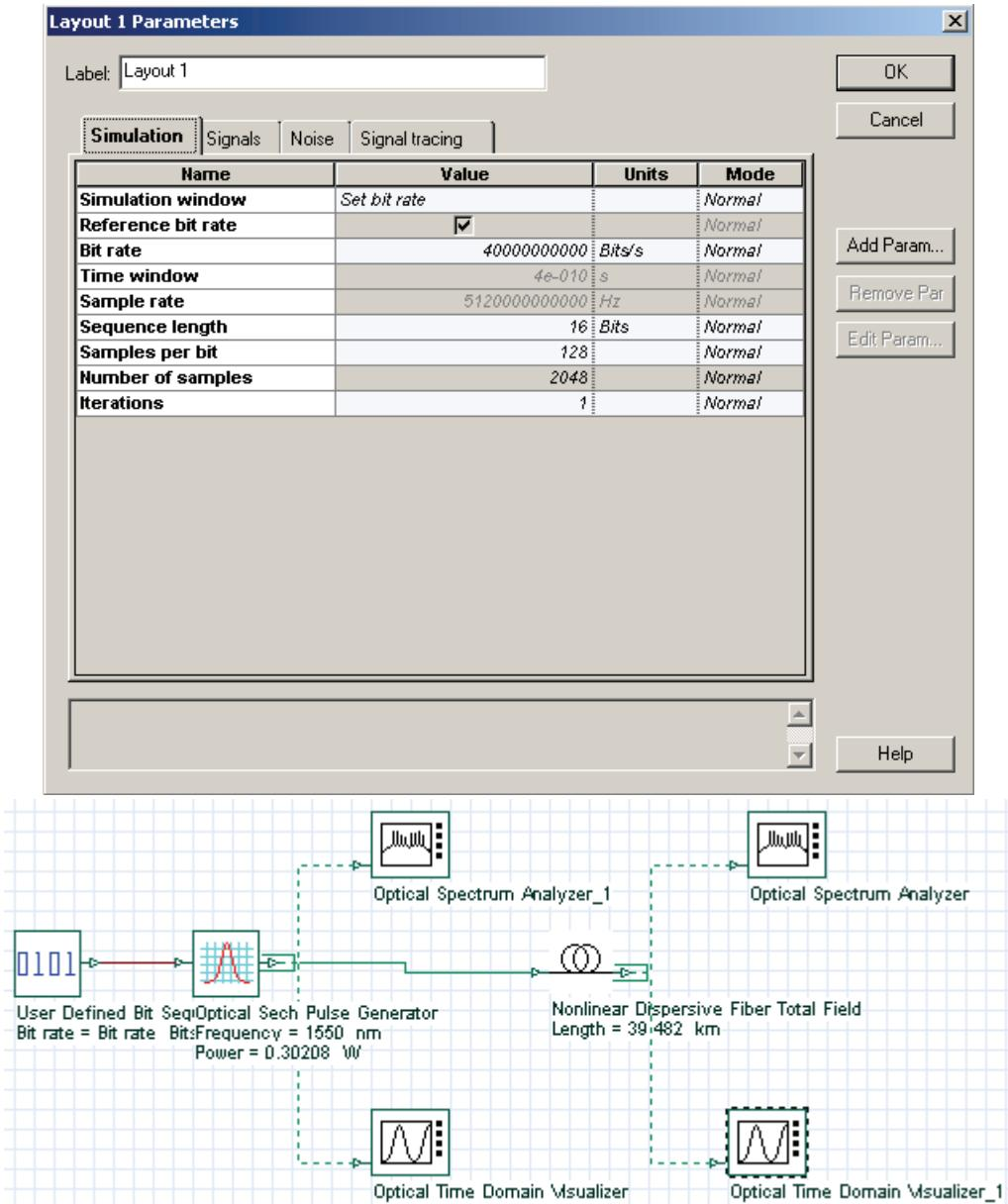
**Notes:**



# Fundamental and higher order solitons

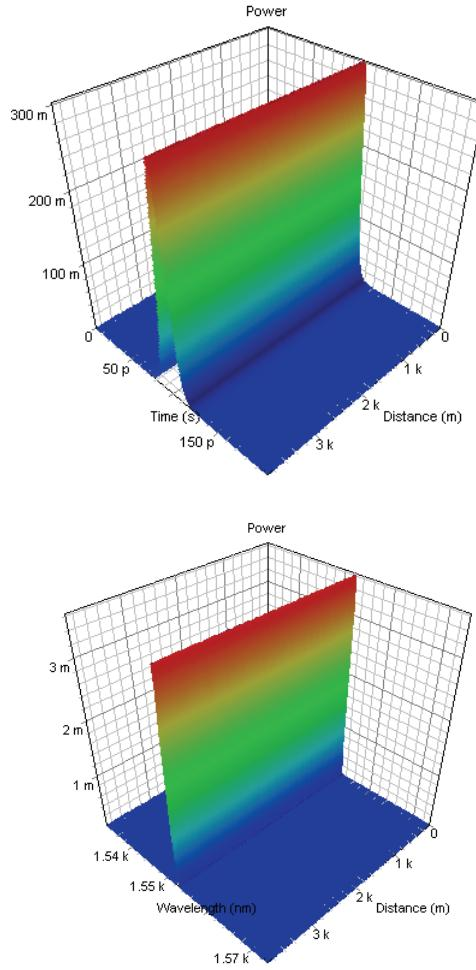
This lesson demonstrates that the exact balance between the effects of SPM and GVD leads to the formation of a fundamental soliton - a light pulse that propagates without changing its shape and spectrum, and shows some basic features of the higher-order solitons. [Figure 1](#) shows the layout and its global parameters.

**Figure 1** System layout and global parameters



The compensation between the effects of SPM and GVD is not complete for Gaussian pulses since the SPM induced chirp is different from that induced by the GVD. The exact compensation occurs when the pulse shape is that of a fundamental soliton. The peak power necessary to launch a N-order soliton can be calculated in the following way [1].

**Figure 2 Evolution of pulse shape (top) and spectrum (bottom) corresponding to the fundamental (N=1) soliton. One soliton period is shown.**



At 40Gb/s the bit slot is 25 ps and the pulse width is  $T_{FWHM} = 12.5ps$ .

The relation between the  $T_0$  parameter in (2) and  $T_{FWHM}$  for sech-pulses is:

$$T_0 = \frac{T_{FWHM}}{1.763} \text{ hence } T_0 = 7.0902ps.$$

The values  $n_2 = 2.6 \times 10^{-20} m^2/W$  and  $A_{eff} = 80 \mu m^2$  are used.



The power value is.. [1].

$$P_N = N^2 \frac{|\beta|^2}{\gamma T_0^2} = N^2 \frac{20}{1.317(7.0902)^2} = 0.30208N^2[W]$$

The dispersion length is.

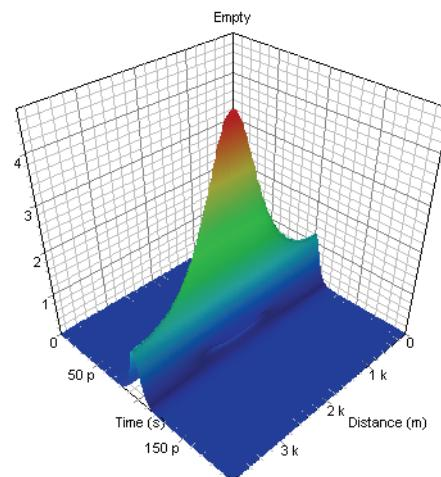
$$L_D = \frac{T_0^2}{|\beta|^2} = \frac{7.0902^2}{20} = 2.5135km$$

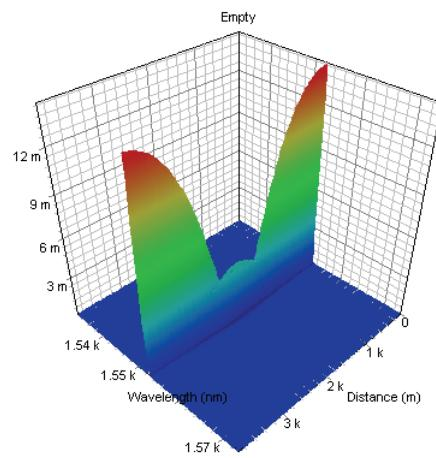
The quantity  $z_0 = \frac{\pi}{2}L_D$  is the soliton period [1] and in our case is  $z_0 = 3.9482km$ .

**Figure 2** shows the evolution of a fundamental soliton within one soliton period. The fundamental soliton remains unaffected by both SPM and GVD, since in this case they cancel each other completely. The pulse remains chirpless, due to the exact compensation that occurs between the SPM-induced and GVD-induced frequency modulations.

While the fundamental ( $N=1$ ) soliton does not change its shape and spectrum with propagation the evolution of all higher order solitons ( $N>1$ ) is spatially periodic with the period equal to  $z_0$ . Figures 3 and 4 represent the evolution of pulse shape and spectrum corresponding to second-order ( $N=2$ ) and third-order ( $N=3$ ) solitons.

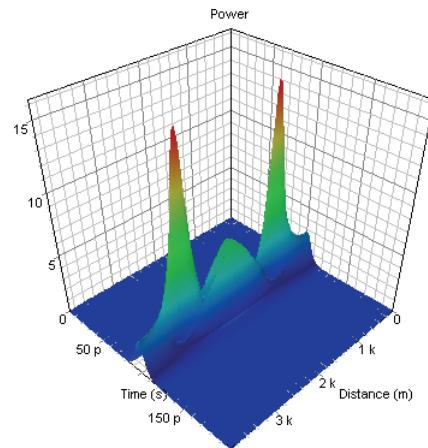
**Figure 3 Evolution of pulse shape (first plot) and spectrum (second plot) corresponding to a second-order soliton. One soliton period is shown.**

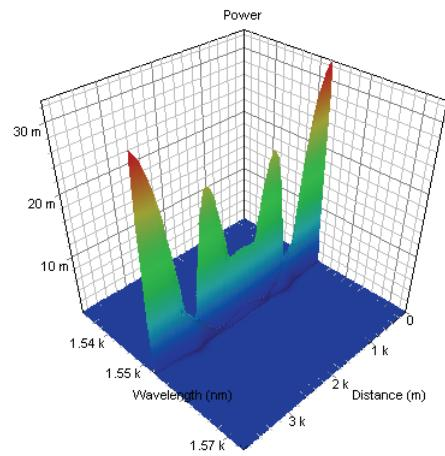




After one complete period initial pulse shape is restored. The evolution of the spectrum also follows a periodic pattern.

**Figure 4 Evolution of N=3 soliton over one soliton period**





## Reference

- [1] G. P. Agrawal Nonlinear Fiber Optics, Academic Press (2001).

**Notes:**

# Interactions of optical solitons

---

This lesson demonstrates the particle-like nature of the solitons through some basic features of their interactions.

The fundamental optical soliton propagates (see "Self-phase modulation and group velocity dispersion" from the Tutorials) undistorted due to the exact balance between the nonlinear (SPM) and dispersive (GVD) effects. Thus the soliton propagates as a "particle" (i.e. maintains its shape) rather than as a linear wave packet.

The particle-like nature of solitons manifests itself clearly through the interactions between neighboring solitons. Soliton pulses remain unaffected after interacting with each other. Besides, soliton interaction is phase-sensitive. In-phase solitons "attract"  $\pi$  - but out-of-phase ones repel each other. The intermediate cases (phase difference between zero and  $\pi$ ) pertain to an initial attraction followed by repulsion.

When two identical, in-phase solitons, separated in time by  $T$ , interact with each other, the time separation between them evolves periodically and the period (the collision length) given by the inverse scattering theory [1] is:

$$L_{coll} = L_D \frac{\pi \sinh \frac{T}{T_0} \cosh \frac{T}{2T_0}}{\frac{T}{T_0} + \sinh \frac{T}{T_0}} \quad (1)$$

In [Equation 1](#),  $L_D$  is the dispersion length, and  $T_0$  is the pulse width. At 40 Gb/s, and 0.5 bit pulse width for sech pulses,  $T_0 = 7.0902\text{ps}$ .

The dispersion length is then:

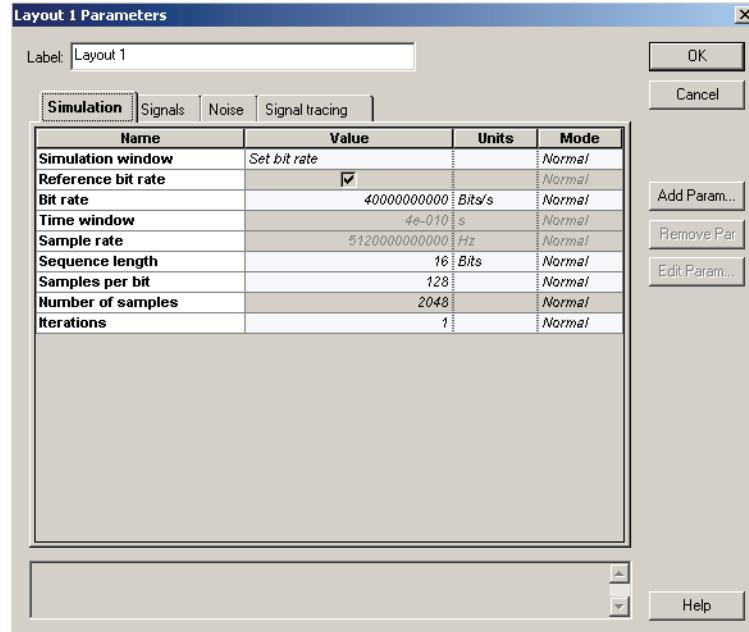
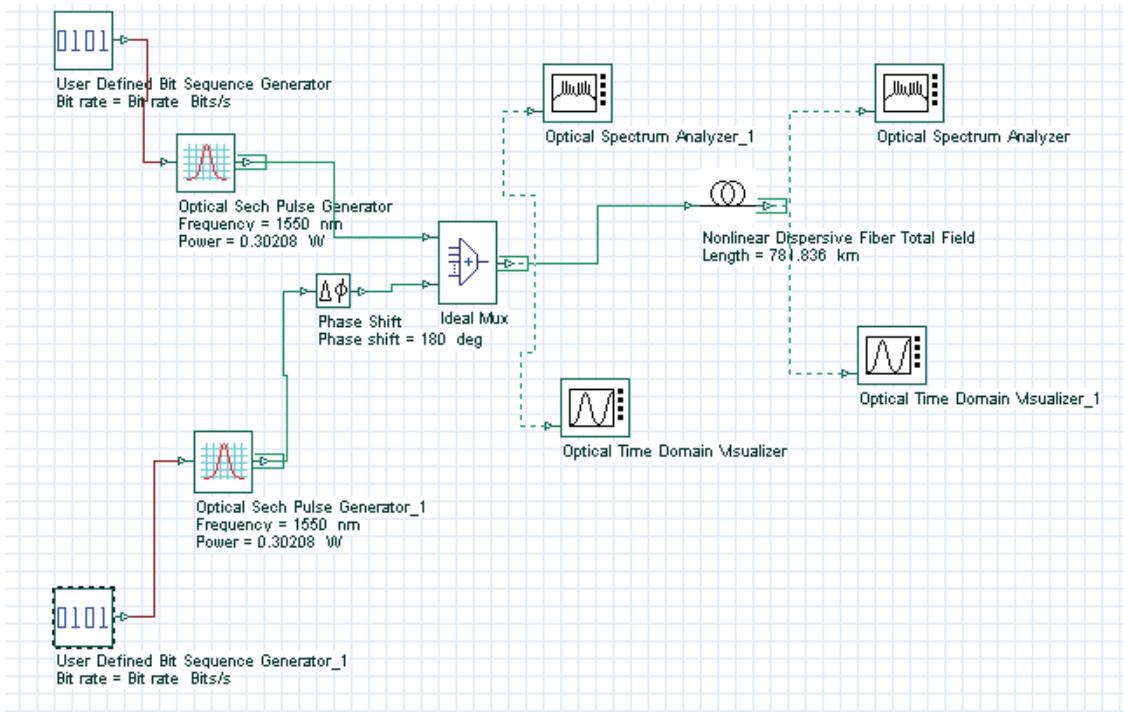
$$L_D = \frac{T_0^2}{|\beta_2|} = \frac{7.0902^2}{20} = 2.5135\text{km}.$$

With time separation of 75 ps chosen here from [Equation 1](#), we see that the collision length is  $L_{coll} \approx 782\text{km}$ .

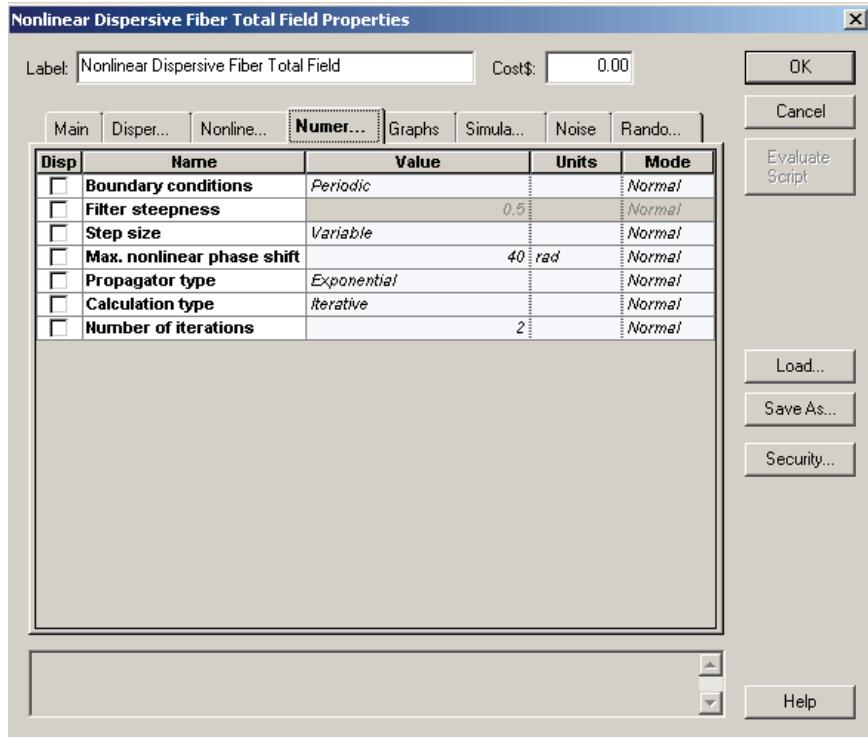
To demonstrate the periodic behavior of soliton interactions we create the following layout ([Figure 1](#)).



Figure 1 The setup to observe soliton interactions



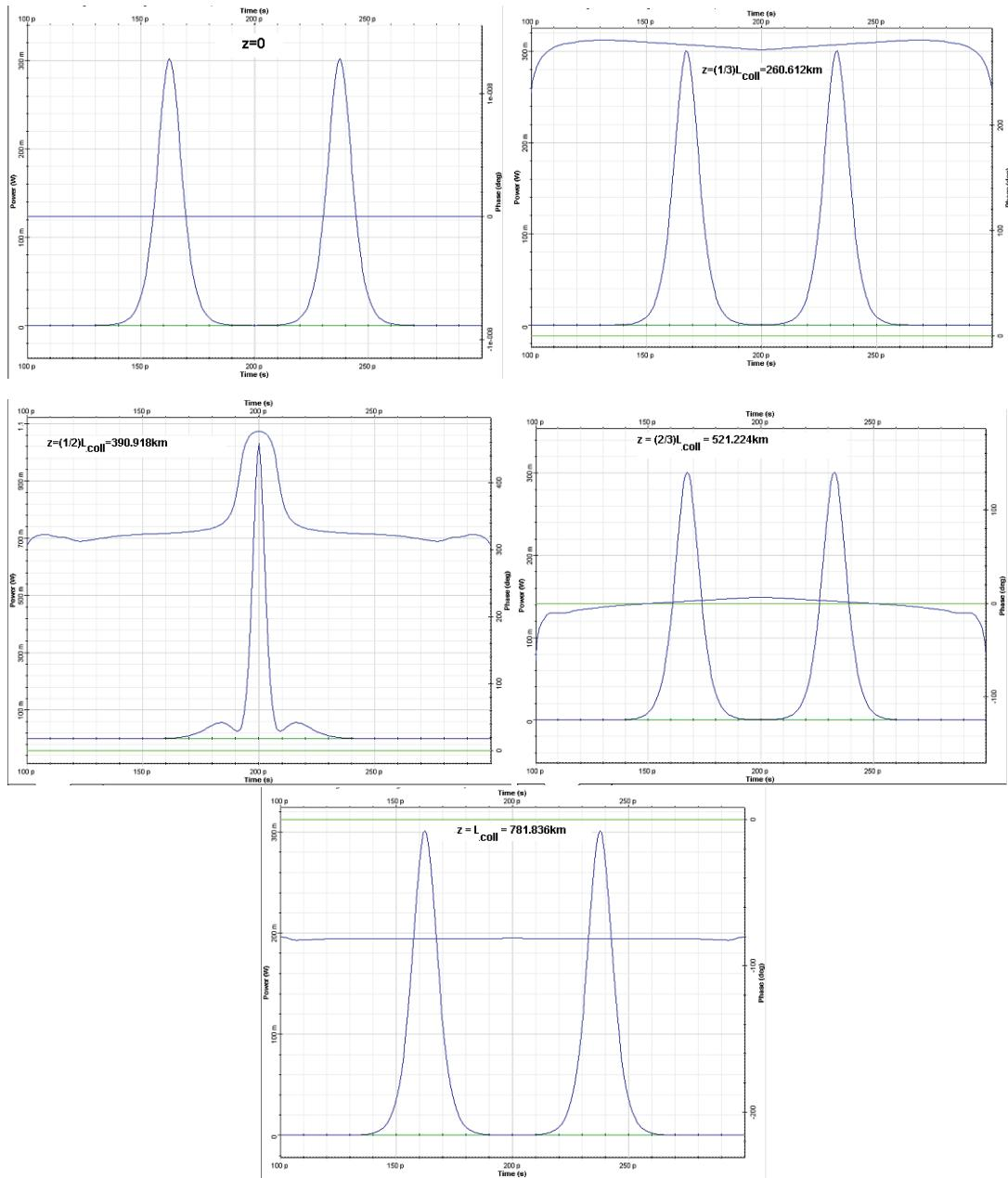
To achieve the necessary accuracy we use the iterative implementation of the split-step Fourier method (Figure 2).

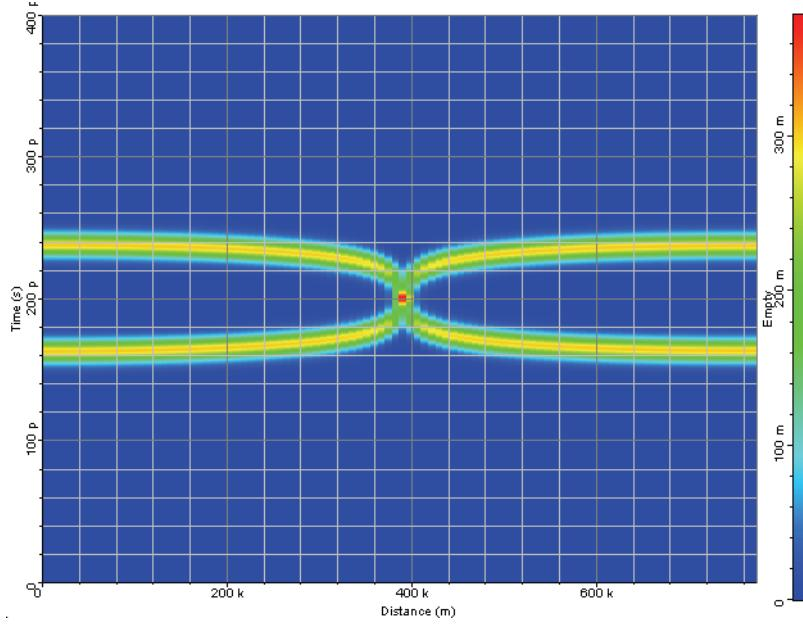
**Figure 2 Iterative implementation of the split-step Fourier method**

At first we consider interaction between two identical in-phase solitons. In this case they form a bound pair.

Figure 3 shows the evolutions of the soliton pair separated initially by 75 ps within one collision length (782 km in this case). The solitons attract each other and become superimposed at a distance equal to half the collision length. Then at a distance equal to the collision length, the initial configuration is restored completely (the pulses are again separated by 75 ps in time).

This picture repeats itself with further propagation with the initial configuration being restored at fiber length equal to multiples of the collision length.

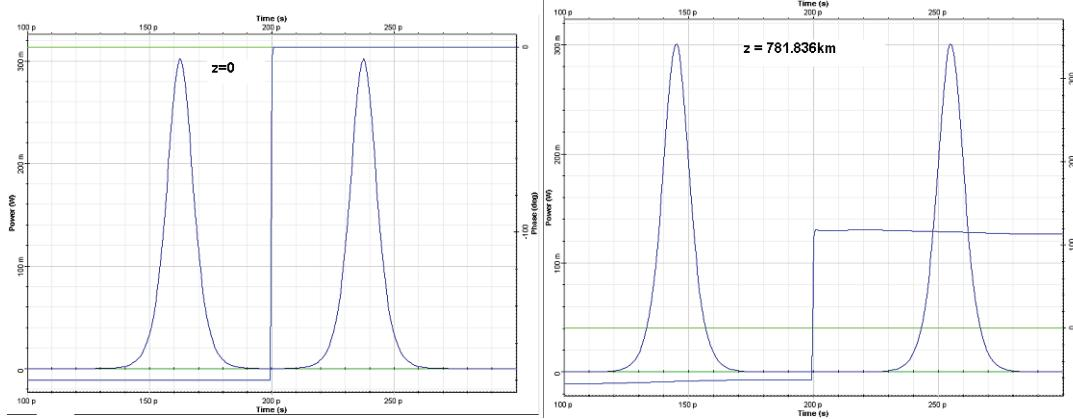
**Figure 3** Interaction between identical, in-phase solitons within one collision length



The second case we consider is an interaction of an  $\pi$  out-of-phase soliton pair. In this case the time separation  $T_z$  after propagation in a fiber with length equal to  $z$  can be obtained by treating the interaction as a perturbation, an assumption that is valid in the case of weak overlap between the neighboring solitons [1]. The result is:

$$T(z) = T(z=0) + 2T_0 \ln\left(\cosh\left(\frac{2z}{L_D} \exp\left(-\frac{T(z=0)}{2T_0}\right)\right)\right) \quad (2)$$

**Figure 4 Interaction of identical,  $\pi$ -out of phase solitons. Repulsion is evident.**



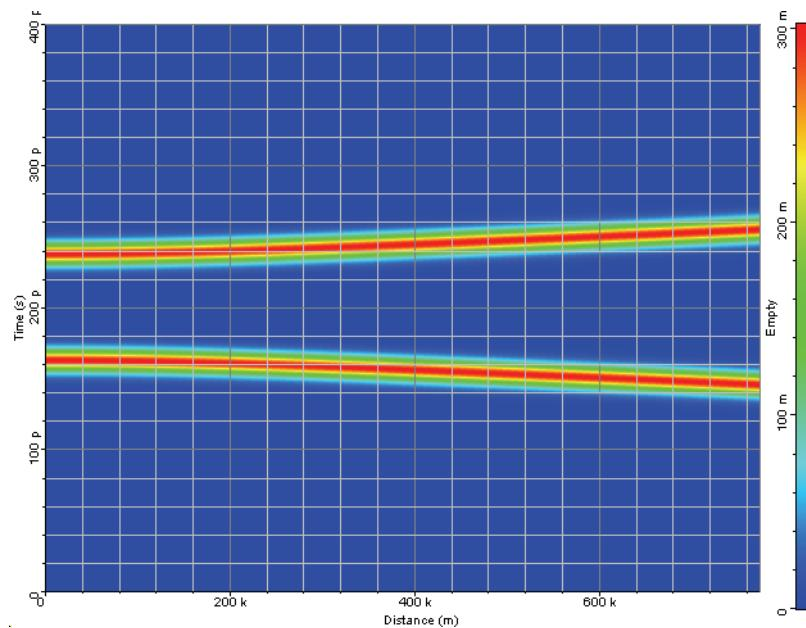


[Table 1](#) compares the results obtained from the perturbation theory, ([Equation 1](#)), and those calculated using the layout shown in [Figure 1](#). A good agreement between both is observed.

**Table 1 Perturbation theory results**

$Z(\text{km})$	$T(z)[\text{ps}]$	
	Perturbation theory	OptiSystem
260.612	81.660	81.2
390.918	88.033	88.0
521.224	95.066	95.3
651.53	102.348	103.1
781.836	109.719	109.3

## Reference:

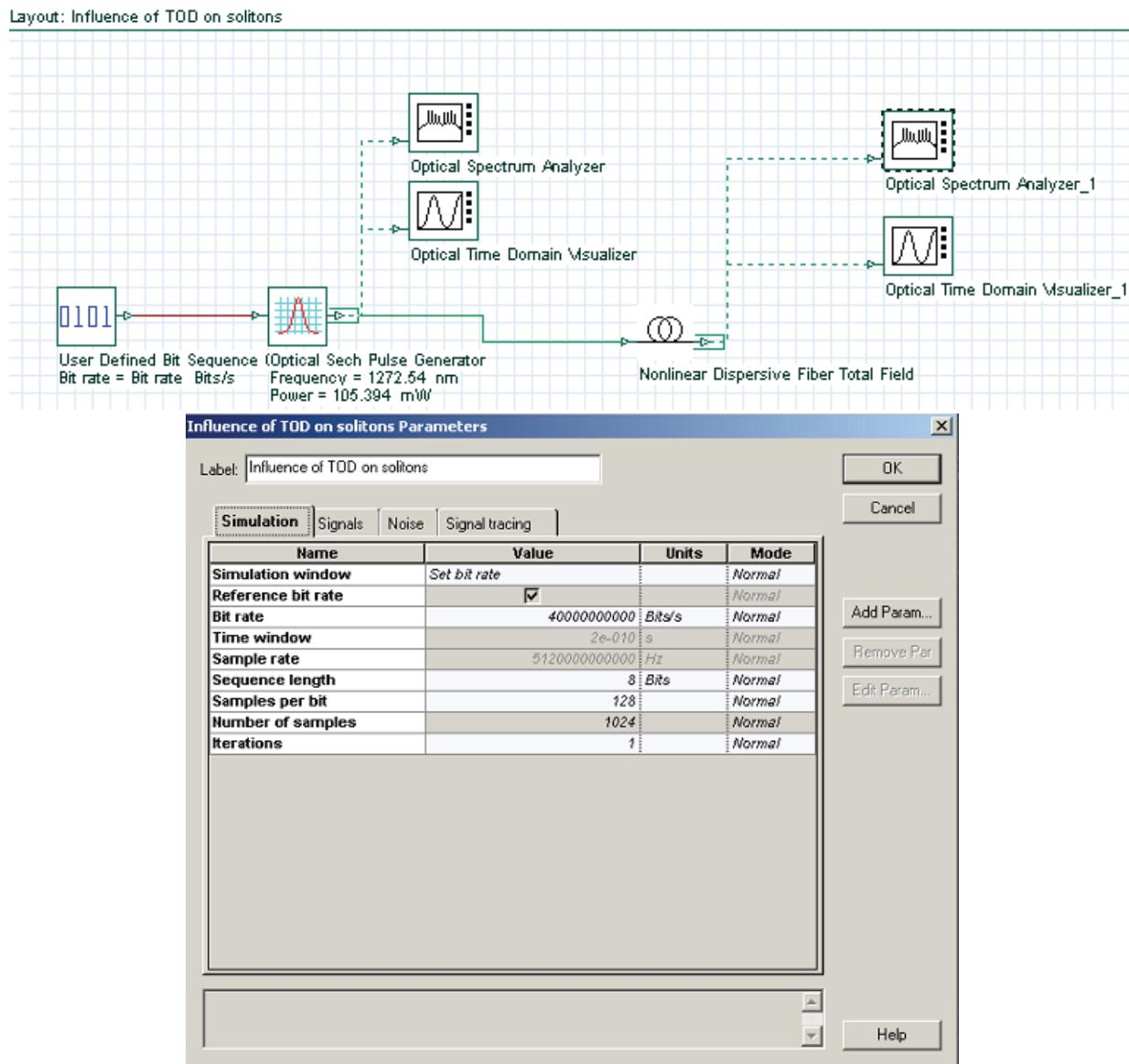
- [1] G. P. Agrawal Nonlinear Fiber Optics, Academic Press (2001).

# Decay of higher order solitons in the presence of third-order dispersion

This lesson demonstrates the effect of third-order dispersion on the fundamental and higher-order solitons.

The layout that we use and its global parameters are shown in [Figure 1](#).

**Figure 1 System layout with parameters**



The setups for the bit sequence generator and for the sech-pulse generators are displayed in [Figure 2](#) and [Figure 3](#).

**Figure 2** Setup for the bit sequence generator

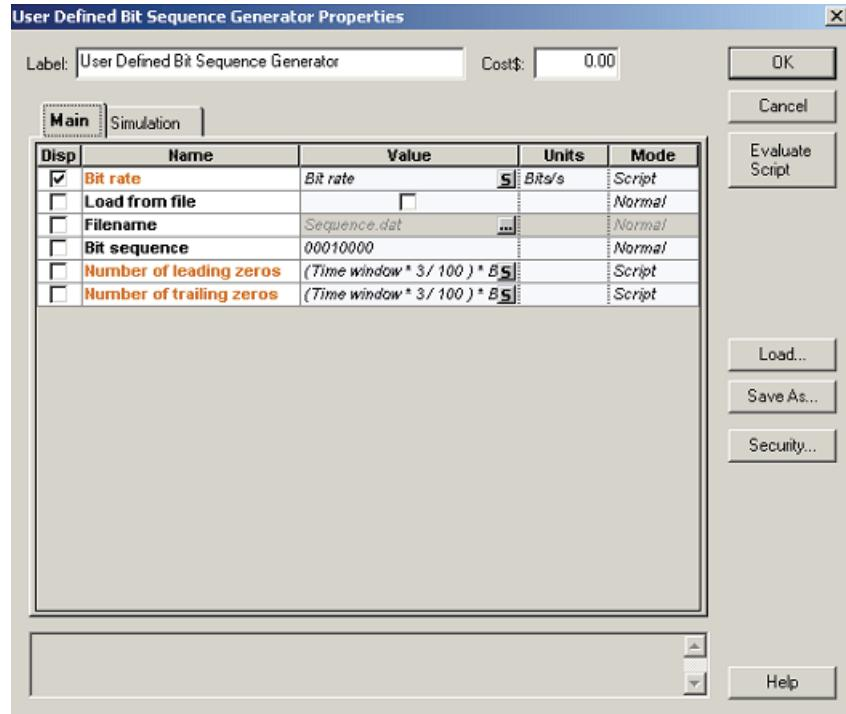


**Figure 3** Setup for the sech-pulse generator

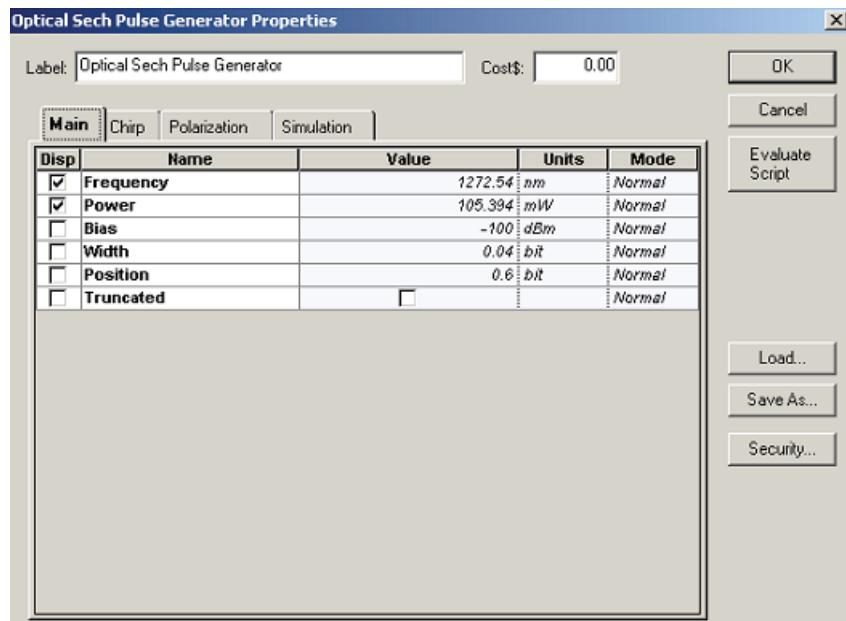
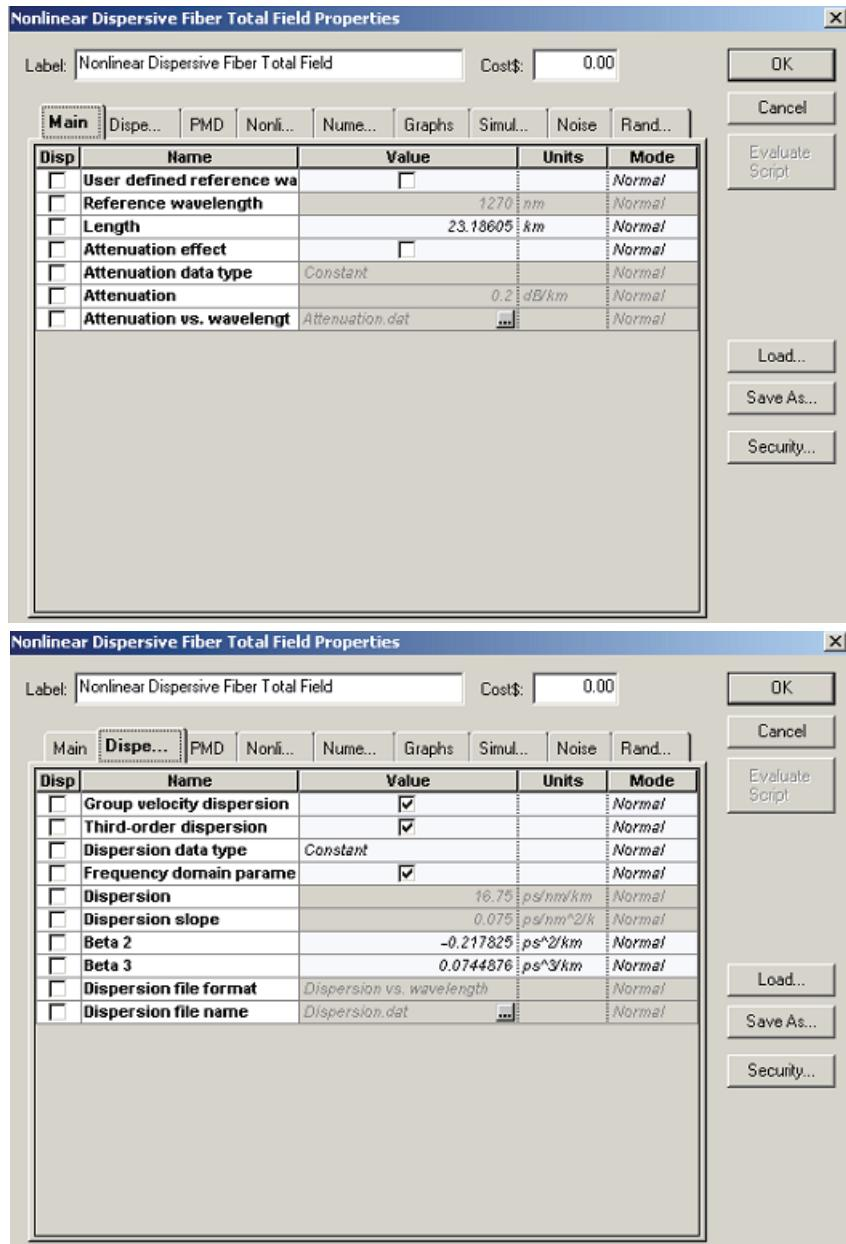


[Figure 4](#) shows the setup for the nonlinear dispersive fiber component.

Figure 4 Setup for the nonlinear dispersive fiber component



**Nonlinear Dispersive Fiber Total Field Properties**

Label: Nonlinear Dispersive Fiber Total Field Cost\$: 0.00

Main Disp... PMD Nonli... Num... Graphs Simul... Noise Rand... OK Cancel Evaluate Script

Disp	Name	Value	Units	Mode
<input type="checkbox"/>	Self-phase modulation	<input checked="" type="checkbox"/>		Normal
<input type="checkbox"/>	Effective area data type	Constant		Normal
<input type="checkbox"/>	Effective area	20	μm <sup>2</sup>	Normal
<input type="checkbox"/>	Effective area vs. wavelength	C:\Kirk\fiberfrom_ramanan...		Normal
<input type="checkbox"/>	n <sup>2</sup> data type	Constant		Normal
<input type="checkbox"/>	n <sup>2</sup>	2.6e-020	m <sup>2</sup> /W	Normal
<input type="checkbox"/>	n <sup>2</sup> vs. wavelength	n2.dat		Normal
<input type="checkbox"/>	Self-steepening	<input type="checkbox"/>		Normal
<input type="checkbox"/>	Full Raman Response	<input type="checkbox"/>		Normal
<input type="checkbox"/>	Intrapulse Raman Scatt.	<input type="checkbox"/>		Normal
<input type="checkbox"/>	Raman self-shift time1	14.2	fs	Normal
<input type="checkbox"/>	Raman self-shift time2	3	fs	Normal
<input type="checkbox"/>	Fract. Raman contribution	0.18		Normal
<input type="checkbox"/>	Orthogonal Raman factor	0.75		Normal

Load... Save As... Security... Help

**Nonlinear Dispersive Fiber Total Field Properties**

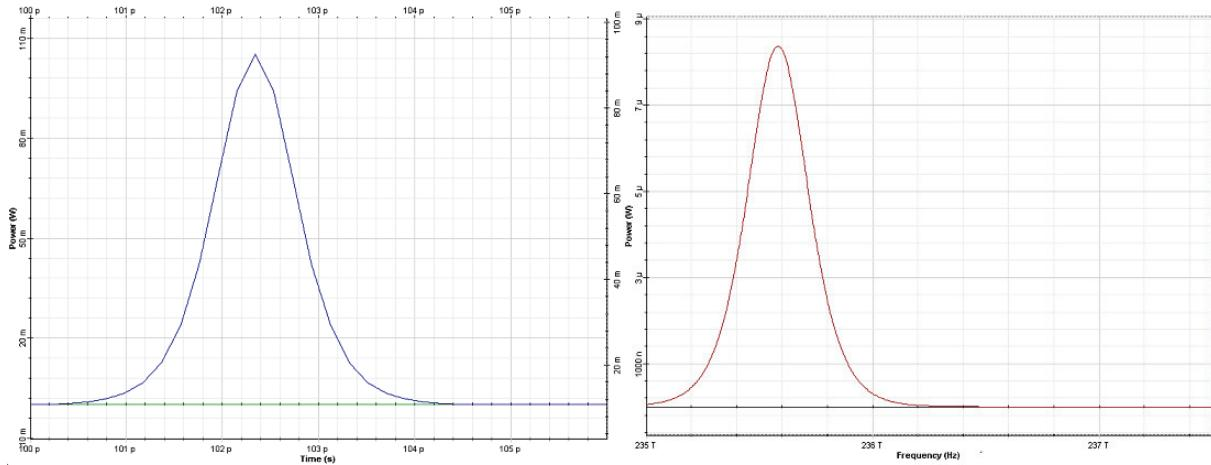
Label: Nonlinear Dispersive Fiber Total Field Cost\$: 0.00

Main Disp... PMD Nonli... Num... Graphs Simul... Noise Rand... OK Cancel Evaluate Script

Disp	Name	Value	Units	Mode
<input type="checkbox"/>	Model type	Scalar		Normal
<input type="checkbox"/>	Propagator type	Exponential		Normal
<input type="checkbox"/>	Calculation type	Noniterative		Normal
<input type="checkbox"/>	Number of iterations	2		Normal
<input type="checkbox"/>	Step size	Constant		Normal
<input type="checkbox"/>	Max. nonlinear phase shift	40	mrad	Normal
<input type="checkbox"/>	Boundary conditions	Periodic		Normal
<input type="checkbox"/>	Filter steepness	0.005		Normal

Load... Save As... Security... Help



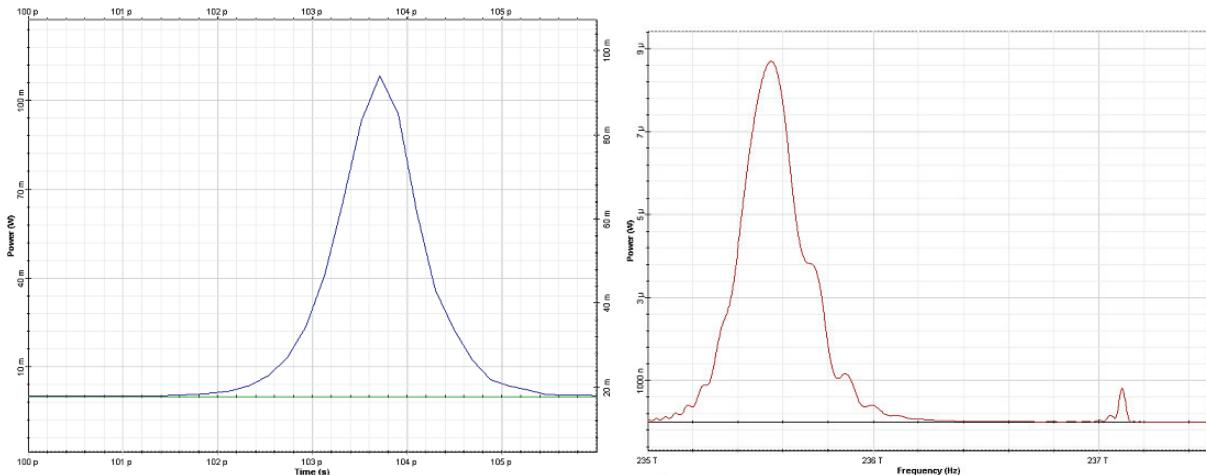
**Figure 5 Input pulse shape (left) and spectrum (right)**

The input pulse (Figure 1) is a 1 ps wide (FWHM) fundamental soliton propagating near the zero-dispersion wavelength [1].

The output pulse shape and spectrum are shown in Figure 6.

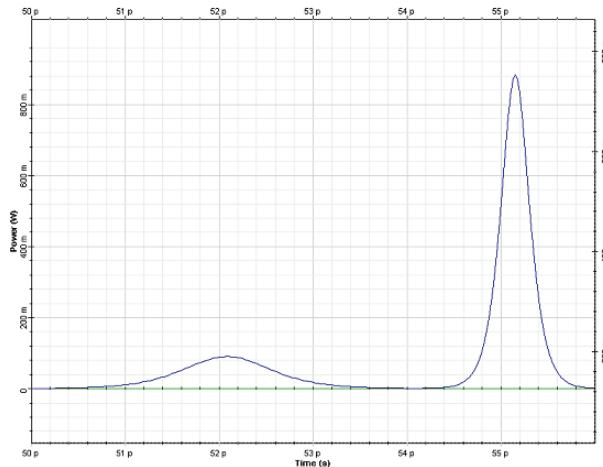
The principal effect of the third-order dispersion term is to stimulate radiation resonantly at a frequency:

$$\omega - \omega_0 \approx \frac{3|\beta_2|}{\beta_3} [1].$$

**Figure 6 Output (at 10 soliton periods or 23.18 km) pulse shape (left) and spectrum (right). Resonance radiation peak is evident**

Good agreement can be seen between the results presented in [1] and in Figure 6.

**Figure 7 Output pulse shape after 11.6 km (or 5 soliton periods) of propagation. Second order soliton has been split into its constituents by the effect of TOD [1]**



The second part of this tutorial considers TOD-induced decay of  $N=2$  soliton. To simulate this phenomenon, the following changes of the parameters are applied. The sequence length is set to four bits and the samples per bit parameter is set to 1024. The bit sequence in the user defined bit sequence generator is changed to "0100". The power of the sech-pulse generator is set to  $421.576\text{mW}$  (corresponding to second order soliton). The fiber length is changed to  $11.593\text{km}$ , which corresponds to five soliton periods. Beta 3 dispersion parameter in the optical fiber component is set to  $0.019366776 \text{ ps}^3/\text{km}$ .

The output pulse shape is presented in [Figure 7](#). The second-order soliton has been split into its constituents by the effect of TOD [1].

## References

- [1] P. K. A. Wai, C. R. Menyuk, Y. C. Lee, and H. H. Chen Optics Letters, 11, No. 7, (1986).

# Decay of higher order solitons in the presence of intrapulse Raman scattering

This lesson demonstrates the influence of stimulated Raman scattering on short soliton pulses.

The layout and its global parameters are shown in [Figure 1](#).

**Figure 1 Layout and global parameters**

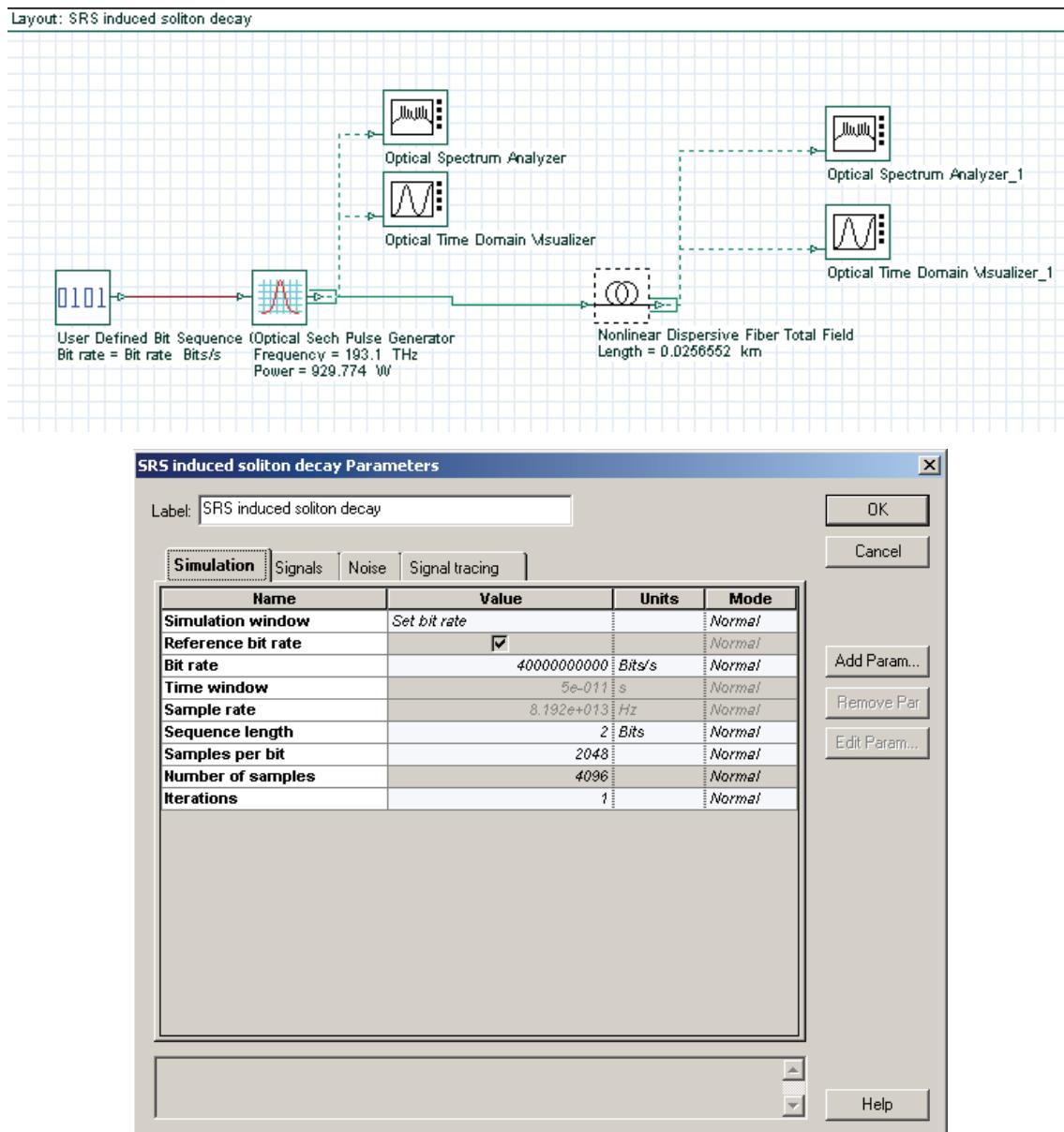


Figure 2 Setup for the Bit sequence generator

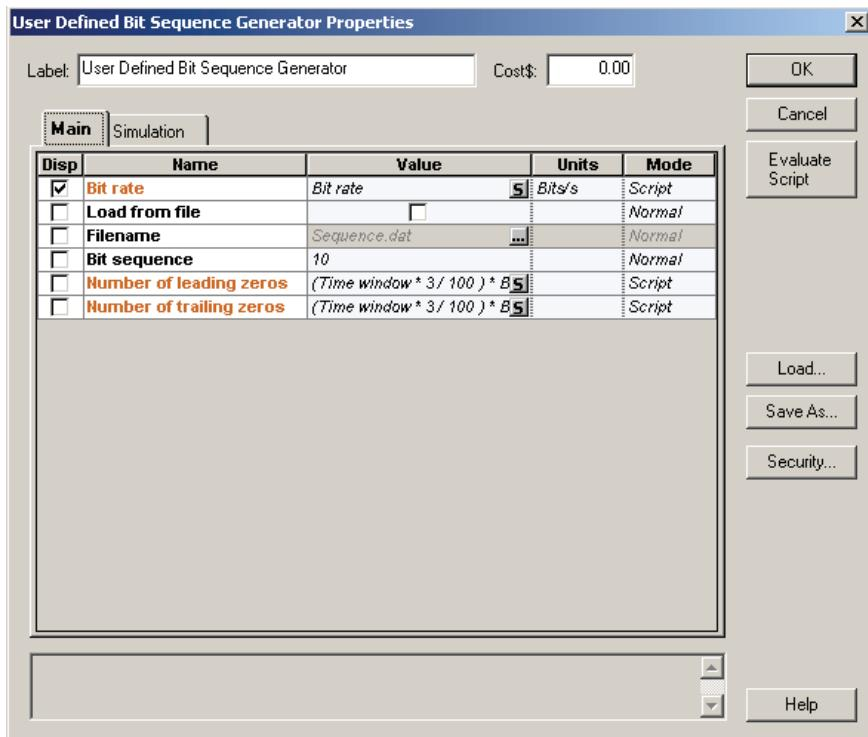
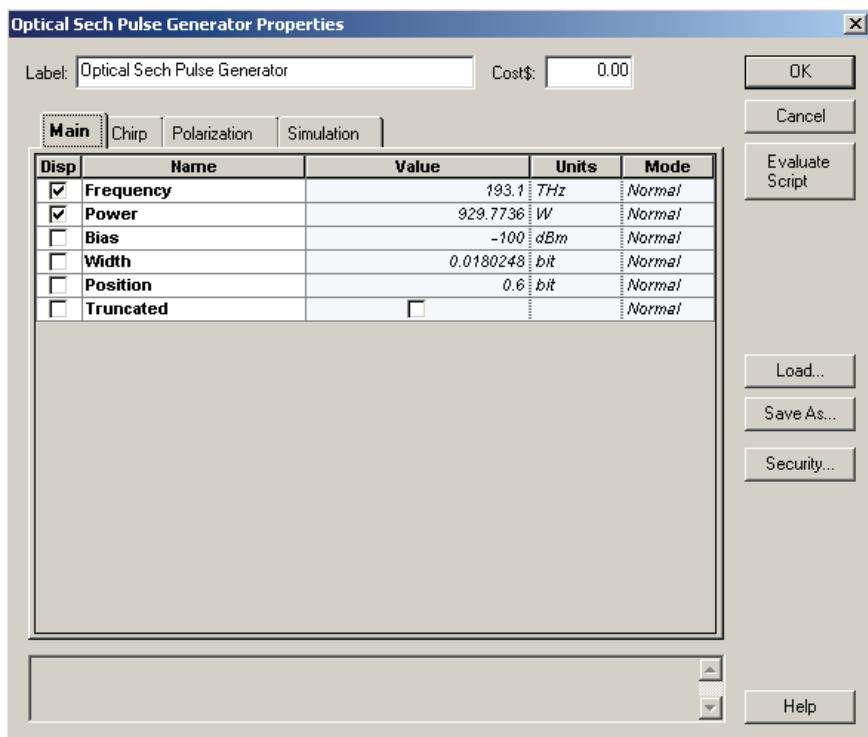


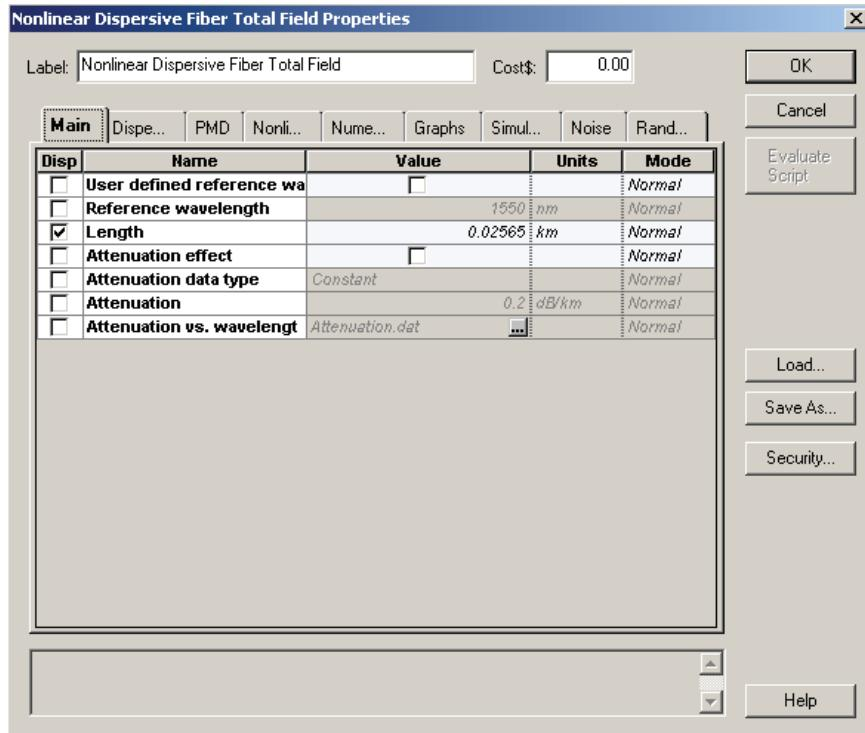
Figure 3 Setups for the Sech-pulse generator



The parameters of the nonlinear dispersive fiber component are shown in [Figure 4](#). The layout simulates N=2 soliton pulse propagation within five soliton periods [1].

The pulse width (FWHM) is 450.62fs, with the corresponding value of  $T_0$  being  $T_0 \approx (T_{FWHM}/1.763) = 255.6fs$ .

**Figure 4 Parameters of the nonlinear dispersive fiber component**



**Nonlinear Dispersive Fiber Total Field Properties**

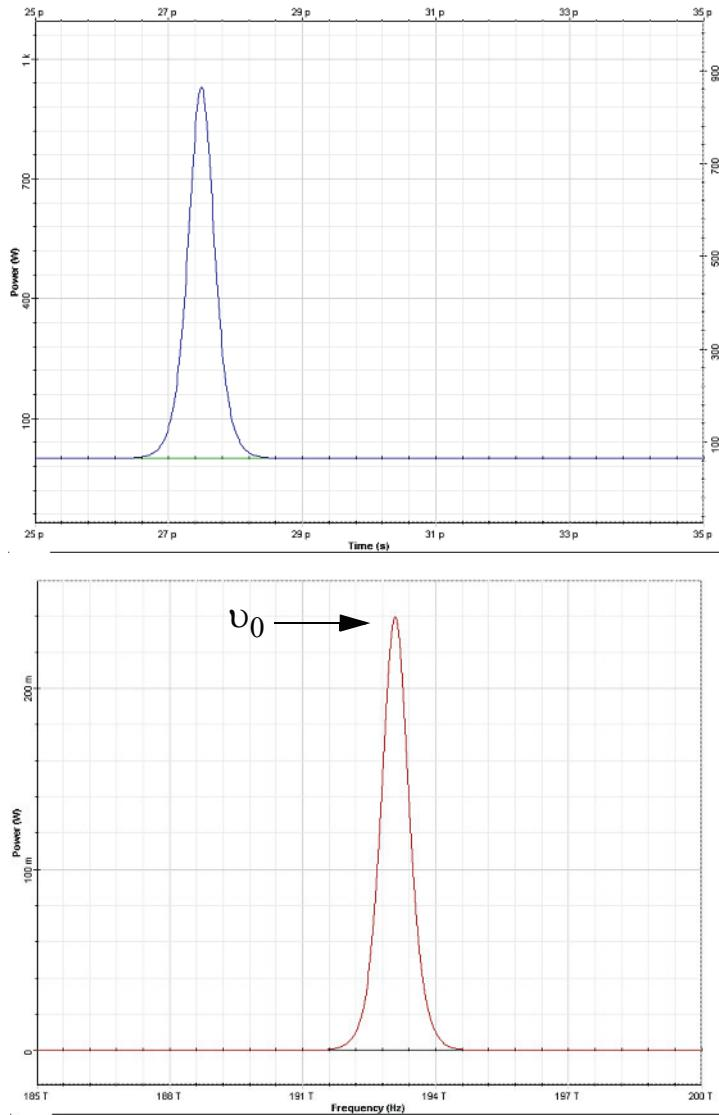
Label:	Nonlinear Dispersive Fiber Total Field	Cost\$:	0.00	OK																																																																															
Main	Dispe...	PMD	<b>Nonli...</b>	Num...	Graphs	Simul...	Noise	Rand...																																																																											
<table border="1"> <thead> <tr> <th>Disp</th> <th>Name</th> <th>Value</th> <th>Units</th> <th>Mode</th> </tr> </thead> <tbody> <tr> <td><input type="checkbox"/></td> <td>Self-phase modulation</td> <td><input checked="" type="checkbox"/></td> <td></td> <td>Normal</td> </tr> <tr> <td><input type="checkbox"/></td> <td>Effective area data type</td> <td>Constant</td> <td></td> <td>Normal</td> </tr> <tr> <td><input type="checkbox"/></td> <td>Effective area</td> <td>93</td> <td>um^2</td> <td>Normal</td> </tr> <tr> <td><input type="checkbox"/></td> <td>Effective area vs. wavelength</td> <td>EffectiveAra.dat</td> <td>[...]</td> <td>Normal</td> </tr> <tr> <td><input type="checkbox"/></td> <td>n2 data type</td> <td>Constant</td> <td></td> <td>Normal</td> </tr> <tr> <td><input type="checkbox"/></td> <td>n2</td> <td>3e-020</td> <td>m^2/W</td> <td>Normal</td> </tr> <tr> <td><input type="checkbox"/></td> <td>n2 vs. wavelength</td> <td>n2.dat</td> <td>[...]</td> <td>Normal</td> </tr> <tr> <td><input type="checkbox"/></td> <td>Self-steepening</td> <td><input type="checkbox"/></td> <td></td> <td>Normal</td> </tr> <tr> <td><input type="checkbox"/></td> <td>Full Raman Response</td> <td><input type="checkbox"/></td> <td></td> <td>Normal</td> </tr> <tr> <td><input type="checkbox"/></td> <td>Intrapulse Raman Scatt.</td> <td><input checked="" type="checkbox"/></td> <td></td> <td>Normal</td> </tr> <tr> <td><input type="checkbox"/></td> <td>Raman self-shift time1</td> <td>14.2</td> <td>fs</td> <td>Normal</td> </tr> <tr> <td><input type="checkbox"/></td> <td>Raman self-shift time2</td> <td>3</td> <td>fs</td> <td>Normal</td> </tr> <tr> <td><input type="checkbox"/></td> <td>Fract. Raman contribution</td> <td>0.18</td> <td></td> <td>Normal</td> </tr> <tr> <td><input type="checkbox"/></td> <td>Orthogonal Raman factor</td> <td>0.75</td> <td></td> <td>Normal</td> </tr> </tbody> </table>									Disp	Name	Value	Units	Mode	<input type="checkbox"/>	Self-phase modulation	<input checked="" type="checkbox"/>		Normal	<input type="checkbox"/>	Effective area data type	Constant		Normal	<input type="checkbox"/>	Effective area	93	um^2	Normal	<input type="checkbox"/>	Effective area vs. wavelength	EffectiveAra.dat	[...]	Normal	<input type="checkbox"/>	n2 data type	Constant		Normal	<input type="checkbox"/>	n2	3e-020	m^2/W	Normal	<input type="checkbox"/>	n2 vs. wavelength	n2.dat	[...]	Normal	<input type="checkbox"/>	Self-steepening	<input type="checkbox"/>		Normal	<input type="checkbox"/>	Full Raman Response	<input type="checkbox"/>		Normal	<input type="checkbox"/>	Intrapulse Raman Scatt.	<input checked="" type="checkbox"/>		Normal	<input type="checkbox"/>	Raman self-shift time1	14.2	fs	Normal	<input type="checkbox"/>	Raman self-shift time2	3	fs	Normal	<input type="checkbox"/>	Fract. Raman contribution	0.18		Normal	<input type="checkbox"/>	Orthogonal Raman factor	0.75		Normal
Disp	Name	Value	Units	Mode																																																																															
<input type="checkbox"/>	Self-phase modulation	<input checked="" type="checkbox"/>		Normal																																																																															
<input type="checkbox"/>	Effective area data type	Constant		Normal																																																																															
<input type="checkbox"/>	Effective area	93	um^2	Normal																																																																															
<input type="checkbox"/>	Effective area vs. wavelength	EffectiveAra.dat	[...]	Normal																																																																															
<input type="checkbox"/>	n2 data type	Constant		Normal																																																																															
<input type="checkbox"/>	n2	3e-020	m^2/W	Normal																																																																															
<input type="checkbox"/>	n2 vs. wavelength	n2.dat	[...]	Normal																																																																															
<input type="checkbox"/>	Self-steepening	<input type="checkbox"/>		Normal																																																																															
<input type="checkbox"/>	Full Raman Response	<input type="checkbox"/>		Normal																																																																															
<input type="checkbox"/>	Intrapulse Raman Scatt.	<input checked="" type="checkbox"/>		Normal																																																																															
<input type="checkbox"/>	Raman self-shift time1	14.2	fs	Normal																																																																															
<input type="checkbox"/>	Raman self-shift time2	3	fs	Normal																																																																															
<input type="checkbox"/>	Fract. Raman contribution	0.18		Normal																																																																															
<input type="checkbox"/>	Orthogonal Raman factor	0.75		Normal																																																																															
<input type="button" value="Load..."/> <input type="button" value="Save As..."/> <input type="button" value="Security..."/>																																																																																			
Help																																																																																			

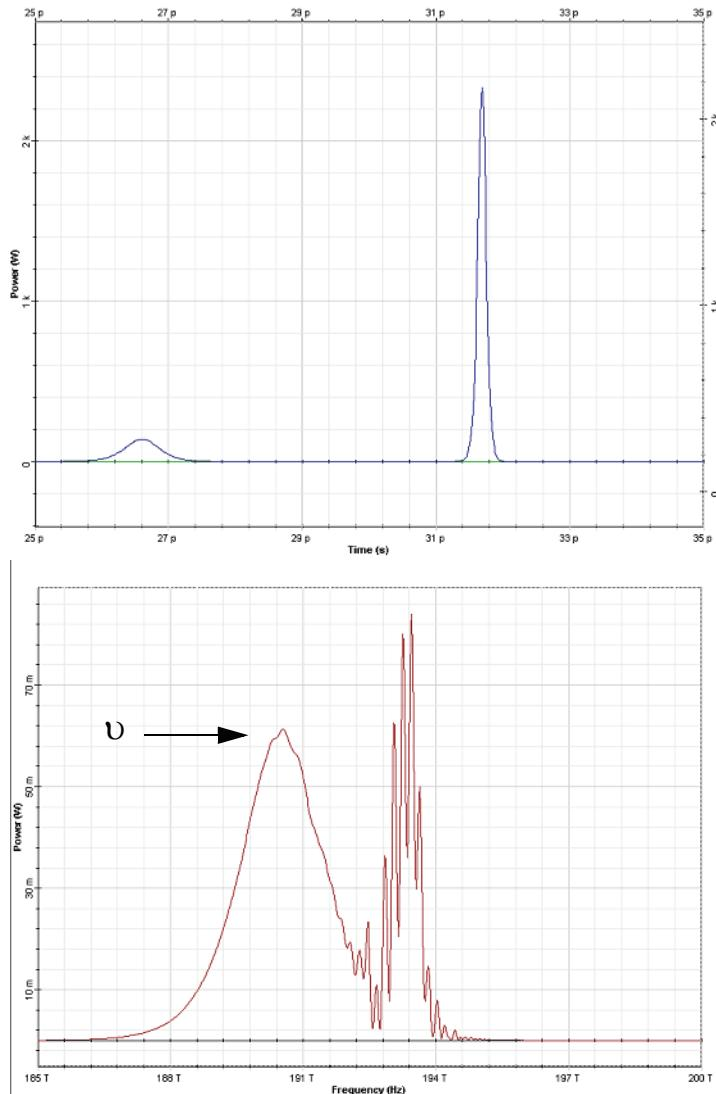
**Nonlinear Dispersive Fiber Total Field Properties**

Label:	Nonlinear Dispersive Fiber Total Field	Cost\$:	0.00	OK																																																	
Main	Dispe...	PMD	<b>Nonli...</b>	<b>Num...</b>	Graphs	Simul...	Noise	Rand...																																													
<table border="1"> <thead> <tr> <th>Disp</th> <th>Name</th> <th>Value</th> <th>Units</th> <th>Mode</th> </tr> </thead> <tbody> <tr> <td><input type="checkbox"/></td> <td>Model type</td> <td>Scalar</td> <td></td> <td>Normal</td> </tr> <tr> <td><input type="checkbox"/></td> <td>Propagator type</td> <td>Exponential</td> <td></td> <td>Normal</td> </tr> <tr> <td><input type="checkbox"/></td> <td>Calculation type</td> <td>Noniterative</td> <td></td> <td>Normal</td> </tr> <tr> <td><input type="checkbox"/></td> <td>Number of iterations</td> <td>2</td> <td></td> <td>Normal</td> </tr> <tr> <td><input type="checkbox"/></td> <td>Step size</td> <td>Constant</td> <td></td> <td>Normal</td> </tr> <tr> <td><input type="checkbox"/></td> <td>Max. nonlinear phase shift</td> <td>20</td> <td>mrad</td> <td>Normal</td> </tr> <tr> <td><input type="checkbox"/></td> <td>Boundary conditions</td> <td>Periodic</td> <td></td> <td>Normal</td> </tr> <tr> <td><input type="checkbox"/></td> <td>Filter steepness</td> <td>0.005</td> <td></td> <td>Normal</td> </tr> </tbody> </table>									Disp	Name	Value	Units	Mode	<input type="checkbox"/>	Model type	Scalar		Normal	<input type="checkbox"/>	Propagator type	Exponential		Normal	<input type="checkbox"/>	Calculation type	Noniterative		Normal	<input type="checkbox"/>	Number of iterations	2		Normal	<input type="checkbox"/>	Step size	Constant		Normal	<input type="checkbox"/>	Max. nonlinear phase shift	20	mrad	Normal	<input type="checkbox"/>	Boundary conditions	Periodic		Normal	<input type="checkbox"/>	Filter steepness	0.005		Normal
Disp	Name	Value	Units	Mode																																																	
<input type="checkbox"/>	Model type	Scalar		Normal																																																	
<input type="checkbox"/>	Propagator type	Exponential		Normal																																																	
<input type="checkbox"/>	Calculation type	Noniterative		Normal																																																	
<input type="checkbox"/>	Number of iterations	2		Normal																																																	
<input type="checkbox"/>	Step size	Constant		Normal																																																	
<input type="checkbox"/>	Max. nonlinear phase shift	20	mrad	Normal																																																	
<input type="checkbox"/>	Boundary conditions	Periodic		Normal																																																	
<input type="checkbox"/>	Filter steepness	0.005		Normal																																																	
<input type="button" value="Load..."/> <input type="button" value="Save As..."/> <input type="button" value="Security..."/>																																																					
Help																																																					



**Figure 5** Input pulse shape (top) and spectrum (bottom)

**Figure 5** shows the input pulse shape and spectrum. The output (after five soliton periods of propagation) pulse shape and spectrum are shown in [Figure 6](#). It can be seen that the effect of stimulated Raman scattering on the higher-order soliton is to split it into its constituents [\[1\]](#).

**Figure 6 Output (at five soliton periods) pulse shape (top) and spectrum (bottom)**

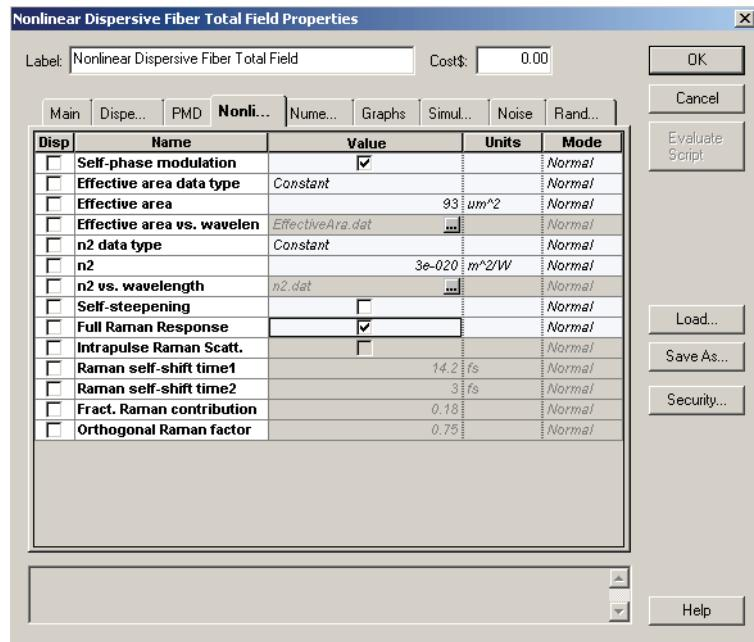
Moreover, the frequency domain manifestation of this effect (soliton self-frequency shift) can be clearly seen upon comparing the input and output pulse spectrum.

The normalized frequency shift:

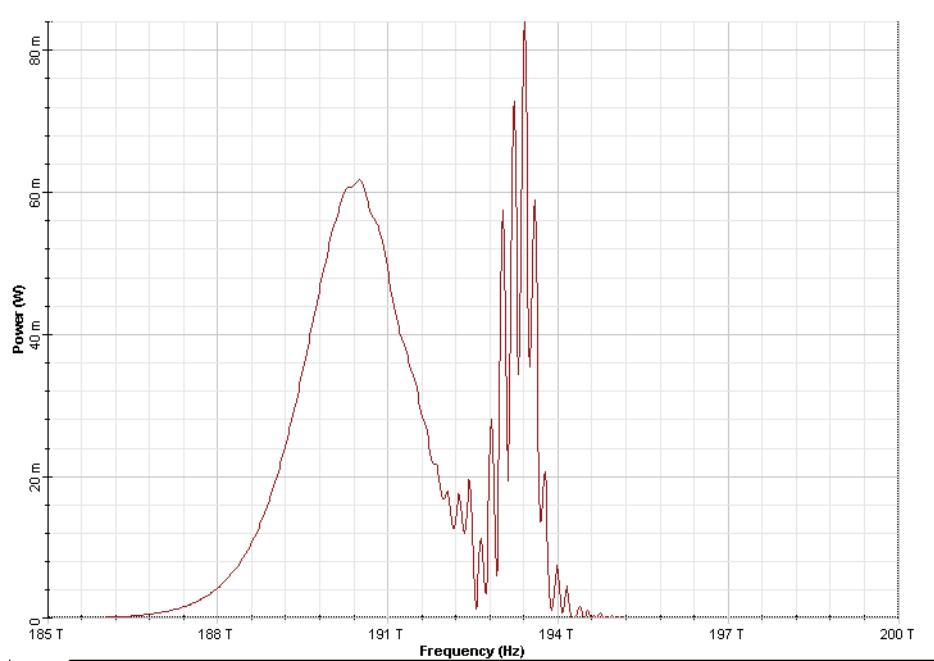
$$(v - v_0)T_0 = (193.1\text{ THz} - 190.35\text{ THz}) \times 255.6\text{ fs} \approx 0.7$$

agrees well with that presented in [1].

The same layout can be used to demonstrate the applicability of the approximation of the full Raman response of the material with the intrapulse Raman scattering in the case when the signal bandwidth is much narrower compared to the Raman gain spectrum [1], which is the case considered here. To achieve this we choose "Full Raman response" in the Nonlinear dispersive fiber (Non-linearities tab) (Figure 7).

**Figure 7 Full Raman response in the nonlinear dispersive fiber**

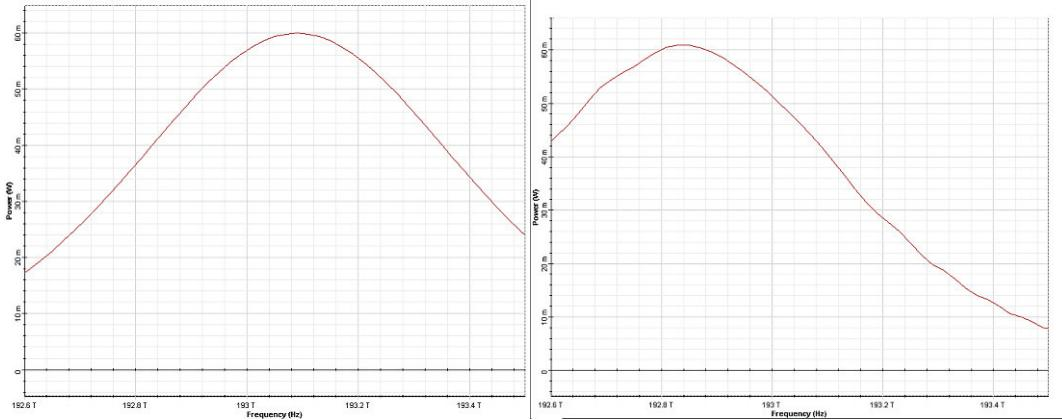
The rest of the setup remains unchanged. The obtained output spectrum is shown in [Figure 8](#).

**Figure 8 Output pulse spectrum at five soliton periods. "Full Raman response" is used in the nonlinear dispersive fiber.**

The remainder of this lesson demonstrates a phenomenon known as soliton self-frequency shift.

In order to do this, we make the following changes to the layout (see Figure 9):

**Figure 9 Input (left) and output at 50 soliton periods (right) pulse spectra**



The normalized red shift of the soliton frequency is:

$$(\nu_0 - \nu)T_0 = (193.1 \text{ THz} - 192.84 \text{ THz}) \times 0,2556 \text{ ps} = 0.066.$$

On the other hand, the same quantity if arrived at with the following expression [1]:

$$(\nu - \nu_0)T_0 = \frac{8}{30\pi} \frac{|\beta_2| \rho \tau_1 z}{T_0^3} = \frac{8}{94.24} \frac{20 \times 0.0142 \times 0.18 \times 0.2565}{0.2536^3} = 0.067,$$

which agrees with the results we obtained.

## Reference:

- [1] G. P. Agrawal Nonlinear Fiber Optics, Academic Press (2001).

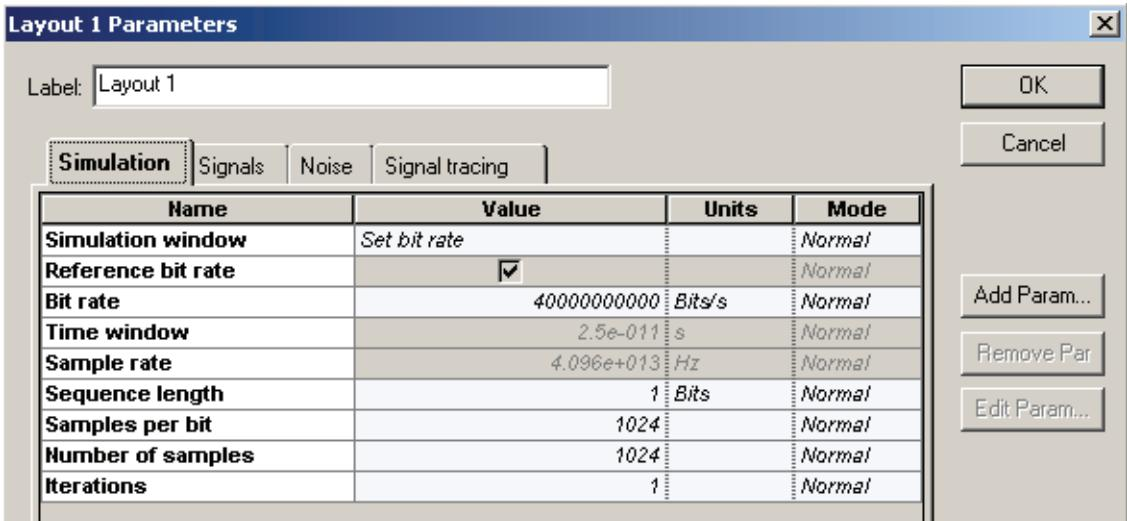
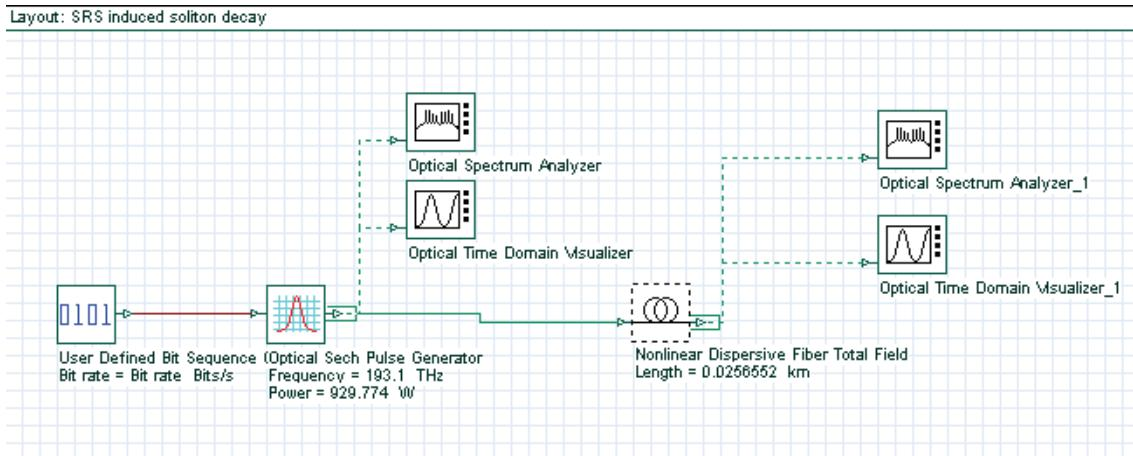


# Decay of higher order solitons in the presence of self-steepening

This lesson demonstrates the influence of self-steepening effect on short soliton pulses and to compare it with that of the intrapulse Raman scattering.

The layout and global parameters are shown in [Figure 1](#).

**Figure 1 Layout and parameters**



The setups for the Bit sequence generator and the sech-pulse generator are shown in figures 2 and 3, respectively.

Figure 2 Bit sequence generator parameters

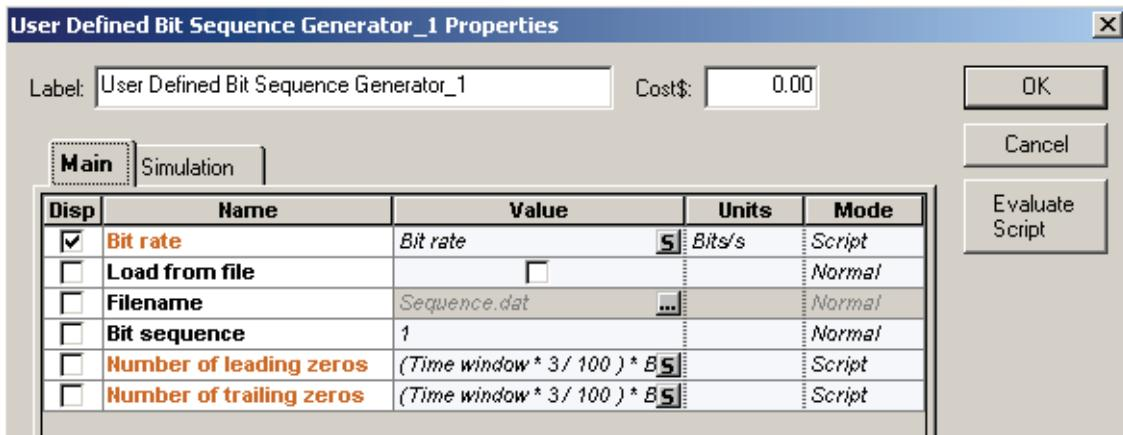
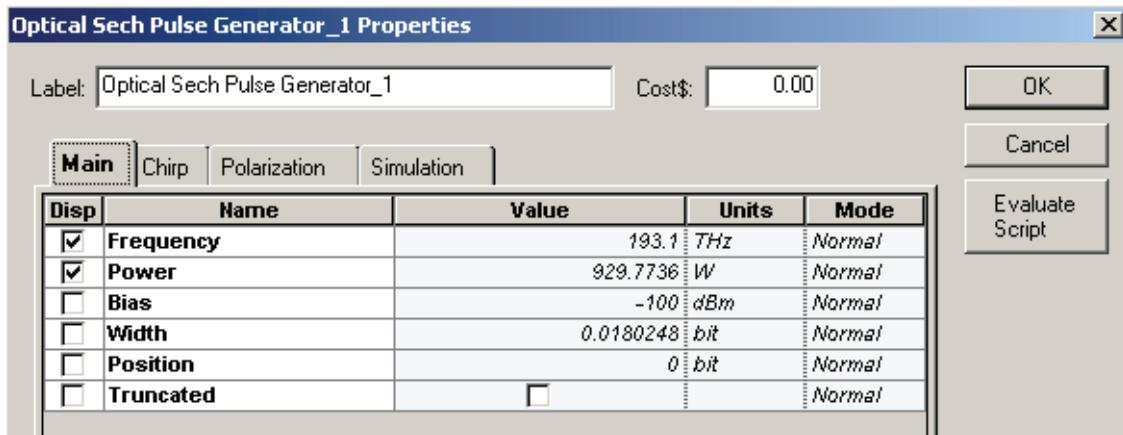


Figure 3 Sech-pulse generator parameters



The parameters of the nonlinear dispersive fiber component are shown in figure 4. The layout simulates N=2 soliton pulse propagation within five soliton periods [1]. The pulse width (FWHM) is 450.62fs, with the corresponding value of  $T_0$  being  $T_0 \approx (T_{FWHM}/1.763) = 255.6\text{fs}$ .

Note that we consider the same pulse and fiber parameters as those considered in the "Decay of higher-order solitons in the presence of intrapulse Raman scattering" except that here we enable the self-steepening effect instead of the intrapulse Raman scattering effect.

Figure 4 Fiber parameters

**Nonlinear Dispersive Fiber Total Field Properties**

Main		Disp...	PMD	Nonli...	Num...	Graphs	Simul...	Noise	Rand...		
Disp	Name	Value		Units		Mode					
<input type="checkbox"/>	User defined reference wavelength	<input type="checkbox"/>		nm		Normal					
<input checked="" type="checkbox"/>	Length	1550		nm		Normal					
<input type="checkbox"/>	Attenuation effect	0.02565		km		Normal					
<input type="checkbox"/>	Attenuation data type	Constant				Normal					
<input type="checkbox"/>	Attenuation	0.2		dB/km		Normal					
<input type="checkbox"/>	Attenuation vs. wavelength	Attenuation.dat		<input type="button" value="..."/>		Normal					

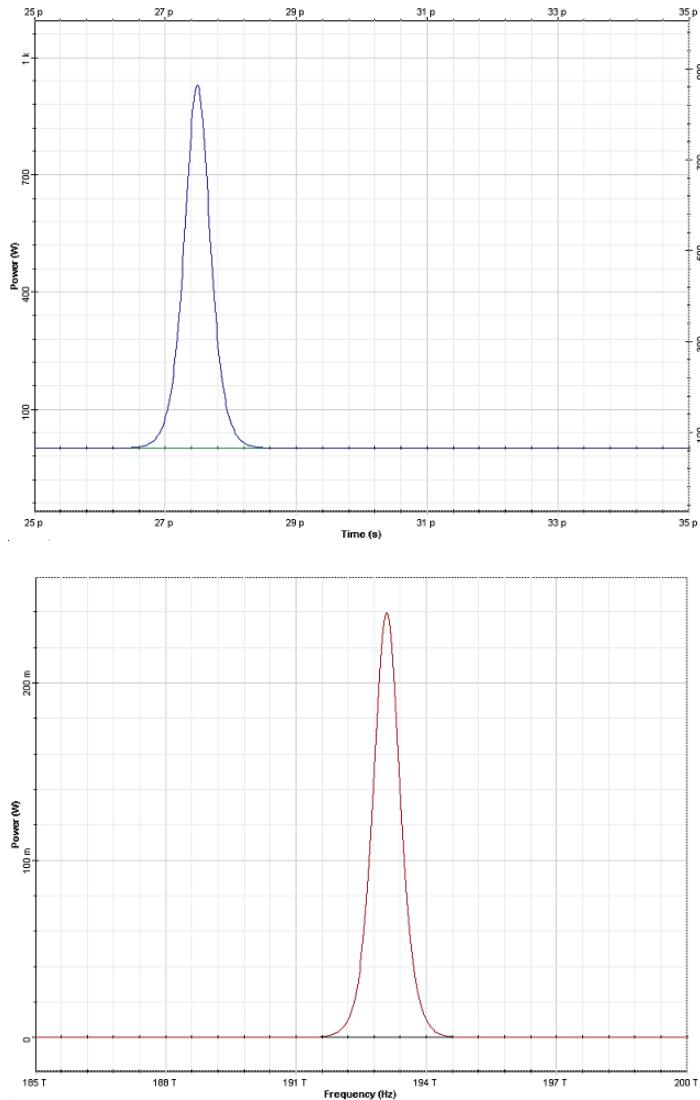
Main		Disp...	PMD	Nonli...	Num...	Graphs	Simul...	Noise	Rand...		
Disp	Name	Value		Units		Mode					
<input type="checkbox"/>	Group velocity dispersion	<input checked="" type="checkbox"/>				Normal					
<input type="checkbox"/>	Third-order dispersion	<input type="checkbox"/>				Normal					
<input type="checkbox"/>	Dispersion data type	Constant				Normal					
<input type="checkbox"/>	Frequency domain parameter	<input checked="" type="checkbox"/>				Normal					
<input type="checkbox"/>	Dispersion	16.75		ps/nm/km		Normal					
<input type="checkbox"/>	Dispersion slope	0.075		ps/nm^2/km		Normal					
<input type="checkbox"/>	Beta 2	-20		ps^2/km		Normal					
<input type="checkbox"/>	Beta 3	0		ps^3/km		Normal					
<input type="checkbox"/>	Dispersion file format	Dispersion vs. wavelength		<input type="button" value="..."/>		Normal					
<input type="checkbox"/>	Dispersion file name	Dispersion.dat		<input type="button" value="..."/>		Normal					

Main		Disp...	PMD	Nonli...	Num...	Graphs	Simul...	Noise	Rand...		
Disp	Name	Value		Units		Mode					
<input type="checkbox"/>	Model type	Scalar				Normal					
<input type="checkbox"/>	Propagator type	Exponential				Normal					
<input type="checkbox"/>	Calculation type	Noniterative				Normal					
<input type="checkbox"/>	Number of iterations	2				Normal					
<input type="checkbox"/>	Step size	Constant				Normal					
<input type="checkbox"/>	Max. nonlinear phase shift	20		mrad		Normal					
<input type="checkbox"/>	Boundary conditions	Periodic				Normal					
<input type="checkbox"/>	Filter steepness	0.005				Normal					
<input type="checkbox"/>	Lower calculation limit	1000		nm		Normal					
<input type="checkbox"/>	Upper calculation limit	2000		nm		Normal					

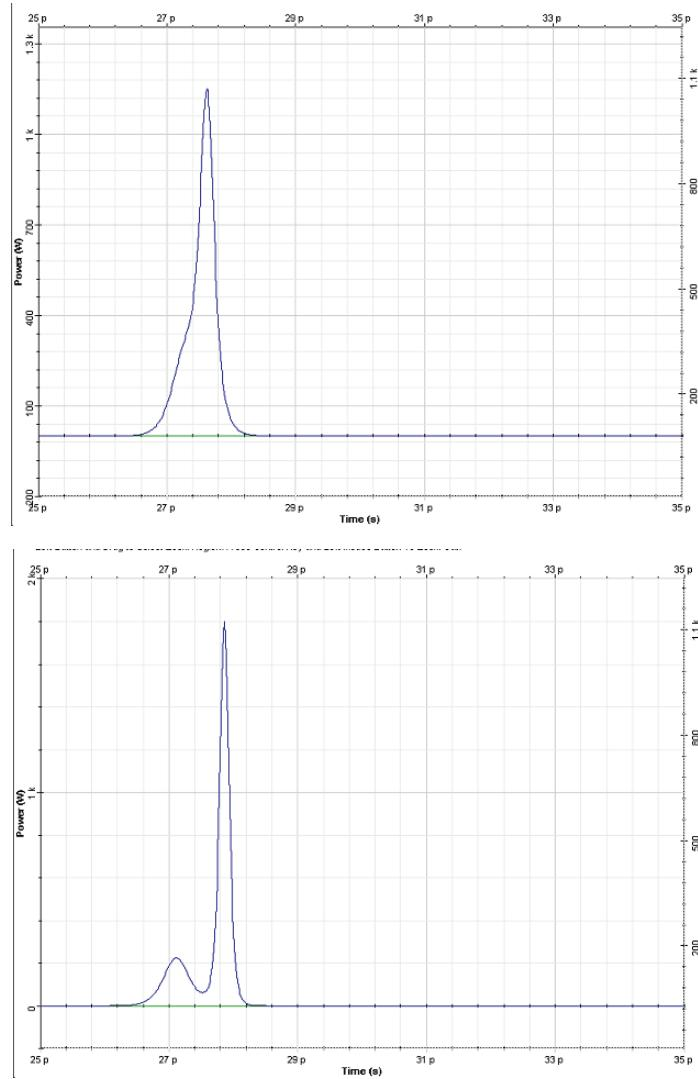
  

Main		Disp...	PMD	Nonli...	Num...	Graphs	Simul...	Noise	Rand...		
Disp	Name	Value		Units		Mode					
<input type="checkbox"/>	Self-phase modulation	<input checked="" type="checkbox"/>				Normal					
<input type="checkbox"/>	Effective area data type	Constant				Normal					
<input type="checkbox"/>	Effective area	93		μm^2		Normal					
<input type="checkbox"/>	Effective area vs. wavelength	EffectiveAra.dat		<input type="button" value="..."/>		Normal					
<input type="checkbox"/>	n2 data type	Constant				Normal					
<input type="checkbox"/>	n2	3e-020		m^2/W		Normal					
<input type="checkbox"/>	n2 vs. wavelength	n2.dat		<input type="button" value="..."/>		Normal					
<input type="checkbox"/>	Self-steepening	<input checked="" type="checkbox"/>				Normal					
<input type="checkbox"/>	Full Raman Response	<input type="checkbox"/>				Normal					
<input type="checkbox"/>	Intrapulse Raman Scatt.	<input type="checkbox"/>				Normal					
<input type="checkbox"/>	Raman self-shift time1	14.2		fs		Normal					
<input type="checkbox"/>	Raman self-shift time2	3		fs		Normal					
<input type="checkbox"/>	Fract. Raman contribution	0.18				Normal					
<input type="checkbox"/>	Orthogonal Raman factor	0.75				Normal					

**Figure 5 Input pulse shape (top) and spectrum (bottom)**

**Figure 5** shows the input pulse shape and spectrum. The output pulse shape after five and ten soliton periods of propagation are shown in [Figure 6](#). It can be seen that the effect of self-steepening on the higher-order soliton is to split it into its constituents [1].



**Figure 6 Output pulse shape at five (top) and ten (bottom) soliton periods**

**Note:** Ten soliton periods correspond to 51.3 m fiber length.

While the soliton splitting has occurred within a distance of five soliton periods in the case when the intrapulse Raman scattering acts as a perturbing effect, the splitting is still in its initial stage (for the same input configuration) in the case considered here. This shows that the self-steepening effect is weaker than the stimulated Raman scattering [1].

## Reference:

- [1] G. P. Agrawal Nonlinear Fiber Optics, Academic Press (2001).

**Notes:**

# Stability of solitons in birefringent optical fibers

---

This lesson demonstrates that the Kerr nonlinearity, which stabilizes solitons against spreading due to GVD, also stabilizes them against splitting due to birefringence [1] - [3].

The "single-mode" fibers are actually bimodal because of the presence of birefringence. This means that the group velocity is different for pulses polarized along the two principal axes.

If the pulse contains both polarization components, in addition to spreading due to GVD, the partial pulses will tend to split apart because of birefringence [1], [2].

In the anomalous GVD regime, the Kerr nonlinearity can compensate the spreading due to GVD, leading to formation of a soliton. The similar fact is true for the birefringent walk-off.

Above a certain soliton number, which increases with the strength of the linear birefringence, the two polarizations interact to form a soliton consisting of both polarizations. The physical effect responsible for this type of behavior is the cross-phase modulation between the two polarization components.

Mathematically [1], [2], the propagation of a pulse in linear birefringent fiber, in the absence of loss, with an arbitrary polarization with respect to the principal polarization axes is described by the following system of coupled NLS equations:

$$\begin{aligned} i\left(\frac{\partial u}{\partial \xi} + \delta \frac{\partial u}{\partial \tau}\right) + \frac{1}{2} \frac{\partial^2 u}{\partial \tau^2} + \left(|u|^2 + \frac{2}{3}|v|^2\right)u &= 0 \\ i\left(\frac{\partial v}{\partial \xi} - \frac{\partial v}{\partial \tau}\right) + \frac{1}{2} \frac{\partial^2 v}{\partial \tau^2} + \left(|v|^2 + \frac{2}{3}|u|^2\right)v &= 0 \end{aligned} \quad (1)$$

In Equation 1  $\delta = (\beta_{1x} - \beta_{1y})T_0/(2|\beta_2|)$  is the normalized group velocity mismatch between the two polarization components.

$\tau = (t - \bar{\beta}_1 z)/T_0$  is the normalized time, where

$\bar{\beta}_1 = \frac{1}{2}(\beta_{1x} + \beta_{1y})$  is inversely related to the average group velocity,

and  $z = \xi L_D$ .

The electric field envelopes are normalized according to  $(u, v) = \sqrt{\gamma L_D}(E_x E_y)$ .

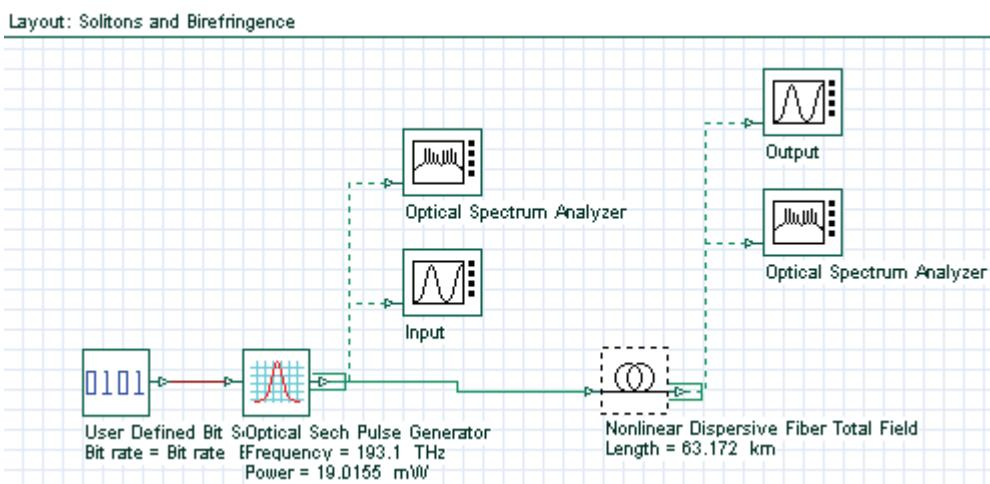
The initial (at  $z=0$ ) conditions we are going to use are in the form:

$$\begin{aligned} u(z = 0, \tau) &= N \cos \theta \operatorname{sech}(\tau) \\ v(z = 0, \tau) &= N \sin \theta \operatorname{sech}(\tau) \end{aligned} \quad (2)$$

$$\text{where } N^2 = \frac{L_D}{L_{NL}} = \frac{\gamma P_0 T_0^2}{|\beta_2|}$$

is the soliton number (see "Self-phase modulation and group velocity dispersion" from the Tutorials). The layout is shown in [Figure 1](#).

**Figure 1 Solitons and birefringence layout**



We set the bit rate to 10 Gb/s and the pulse width to 0.5 bit (50 ps).

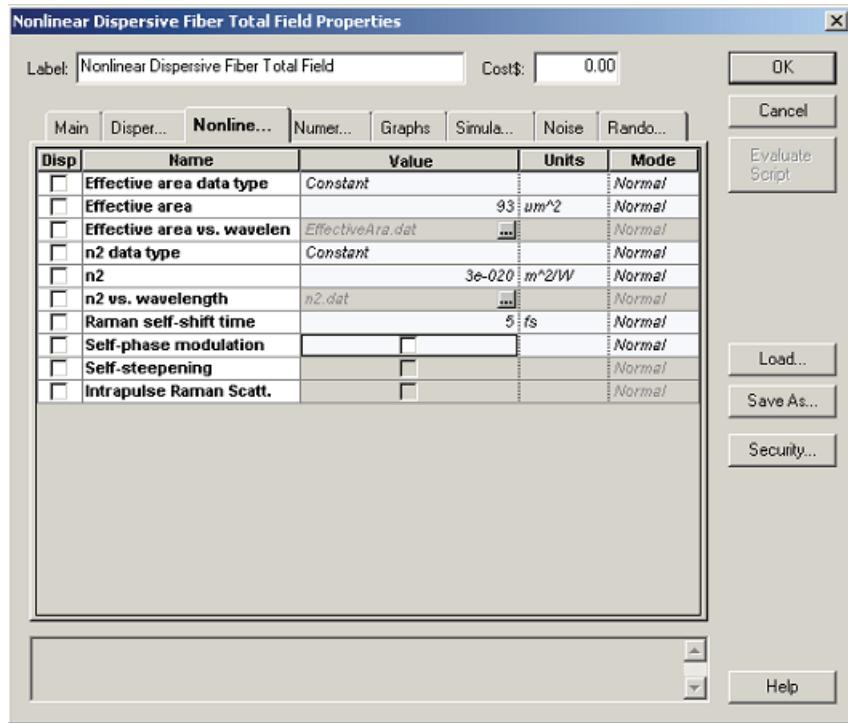
With  $n_2 = 3.10^{-20} m^2/W$ ,  $A_{eff} = 93 \mu m^2$ , and  $\beta_2 = -20 ps^2/km$

(corresponding to 1550 nm, in the anomalous GVD regime of the fiber), the power necessary to launch the fundamental soliton is  $P_0 = 19.0155 mW$  and the soliton period is  $z_0 = 63.172 km$ .

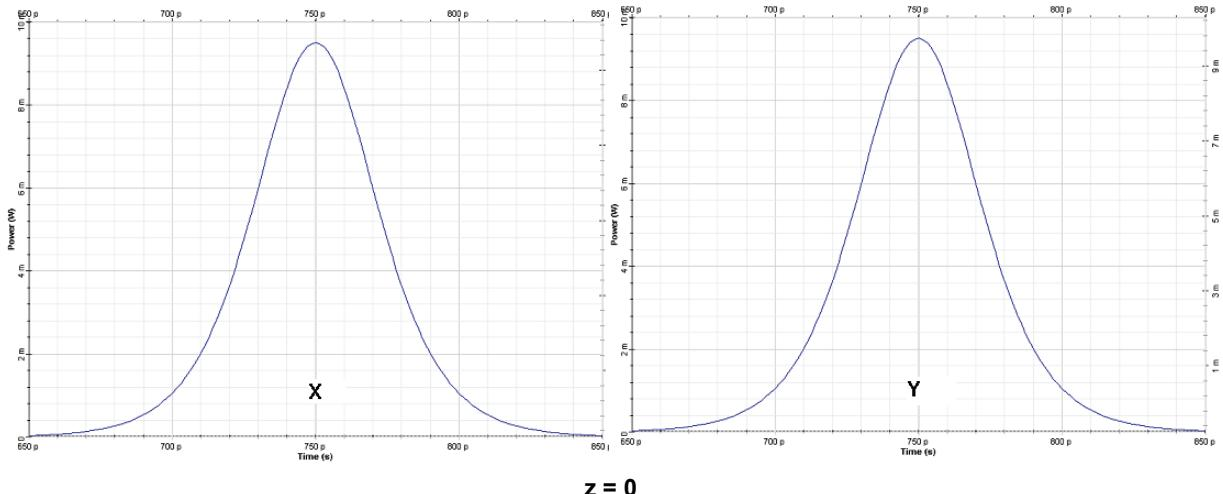
We set the value of the birefringence to  $\Delta n = n_x - n_y = 2.1187 \times 10^{-7}$ , where  $n_x$  and  $n_y$  are the effective mode indices for x and y polarized components respectively.

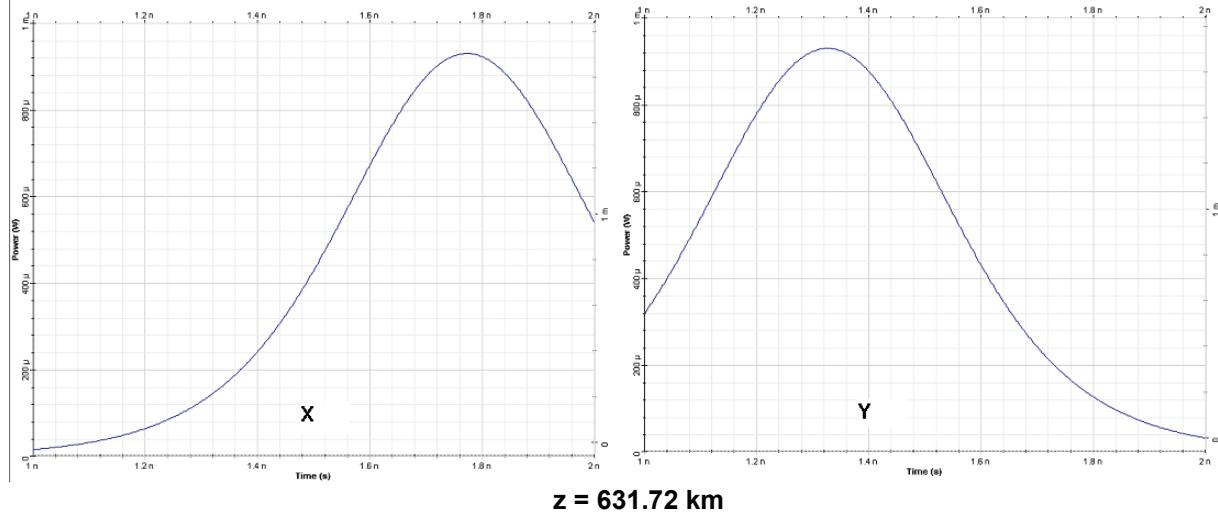
The difference in the group delays per unit fiber length between both polarization components is then  $\Delta n/c = 0.7067 ps/km$ . Since  $T_0 = 28.3607 ps$ , the value of the group velocity mismatch parameter  $\delta$  is  $\delta = 0.5$ . To see the birefringence-induced time delay between both polarization components, we set azimuth in the optical sech pulse generator equal to  $45^\circ$ , fiber length to 631.72 km (10 soliton periods) and switch the nonlinear effects OFF (see [Figure 2](#)).



**Figure 2 Fiber parameters**

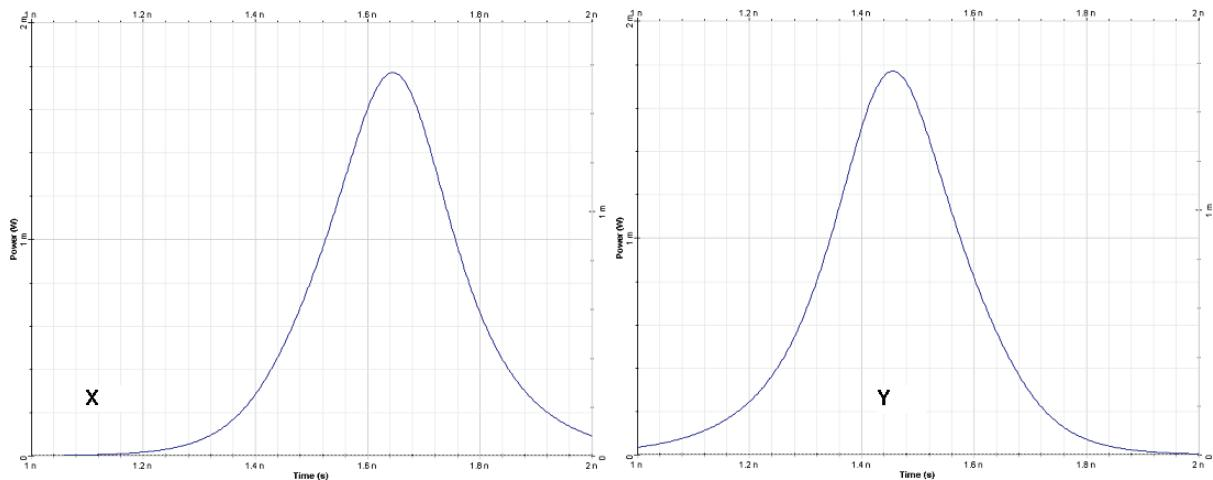
**Figure 3(a)** shows the input and output partial pulses after 631.72 km propagation in a loss-free fiber. Both partial pulses are broadened by GVD and shifted in time by 440 ps with respect to each other, which corresponds to a difference in the arrival times of 0.7 ps for 1 km of fiber length. This shift can be attributed to the birefringence.

**Figure 3(a) Input polarization components x (left) and y (right) for a sech-pulse in linear regime**

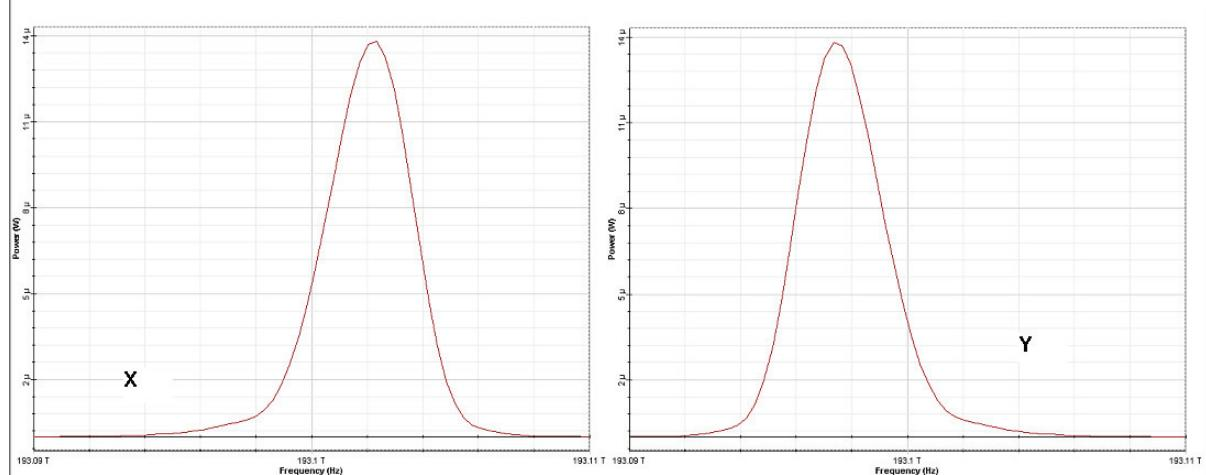
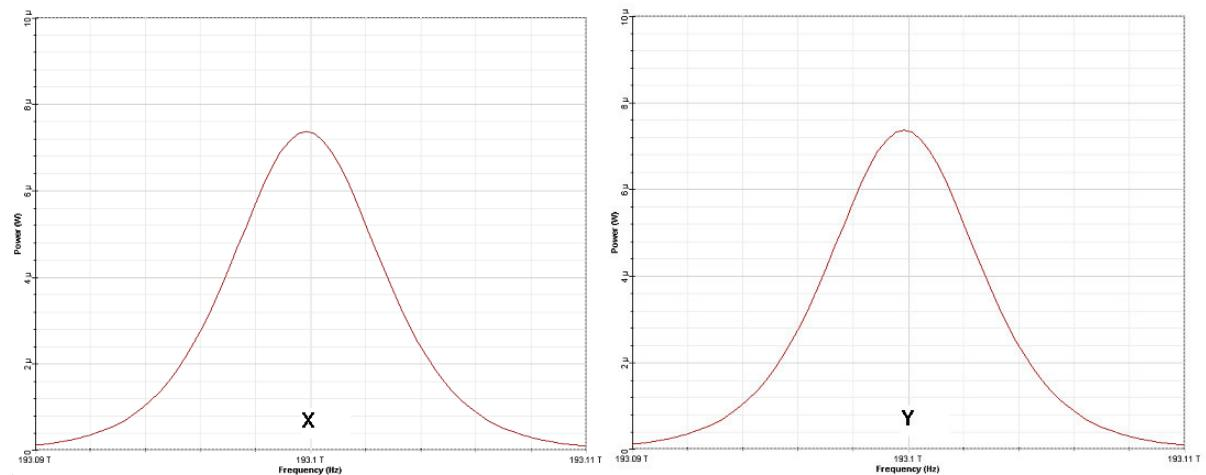
**Figure 3(b) Output polarization components x (left) and y (right) for a sech-pulse in linear regime**

When the nonlinearity is taken into account, the two polarization components remain bound together if  $N$  in [Equation 2](#) exceeds some critical value  $N_{th}$  that increases with the increase  $\delta$ . For  $\delta = 0.5$ , this value is [\[1\]](#), [\[2\]](#)  $N_{th} \approx 1$ .

To see this, we switch the nonlinear effects ON in the fiber component. The output pulses for 631.72 km of propagation are shown in [Figure 4](#).

**Figure 4 Partial pulses after propagating in 631 km of fiber taking into account the nonlinear effects**

Comparing [Figure 4](#) and [Figure 3\(a\)](#), we can see that the impact of the nonlinearity is twofold: Nonlinear effects reduce the GVD induced pulse broadening for each of the polarization components, and the time delay between both is reduced with respect to case of linear propagation (i.e. neglecting the nonlinear effects, [Figure 3\(a\)](#)).

**Figure 5(a) Input pulse spectra evolution over 10 soliton periods x (slow axis) and y (fast axis)****Figure 5(b) Output pulse spectra evolution over 10 soliton periods x (slow axis) and y (fast axis)** **$z = 631.72 \text{ km}$** 

When the nonlinear effects are taken into account, the time delay is roughly 200 ps, which is more than a factor of two smaller compared to the case of linear-regime propagation. It can be concluded that Kerr nonlinearity reduces the birefringent walk-off [2].

To understand this phenomenon in somewhat more detail, we can look at the evolution of the pulse spectra corresponding to the pulse shapes presented in Figure 4. The spectra are presented in Figure 5(a) and Figure 5(b).

Initially the spectra for both x (slow) and y (fast) polarization components are identical. However, due to the action of the cross-phase modulation between both polarization components, the spectrum of the x-polarization component acquires a blue shift, while the spectrum of the y-polarization component turns out to be red-shifted.



In the case of the anomalous GVD considered here, the high frequency (blue) components travel faster than the low frequency (red) components.

Hence, as a result of the action of the cross-phase modulation between both polarization components (the last terms in the system [Equation 1](#)), the faster polarization component is slowed down while the slower polarization component is accelerated and consequently the birefringent walk-off is reduced.

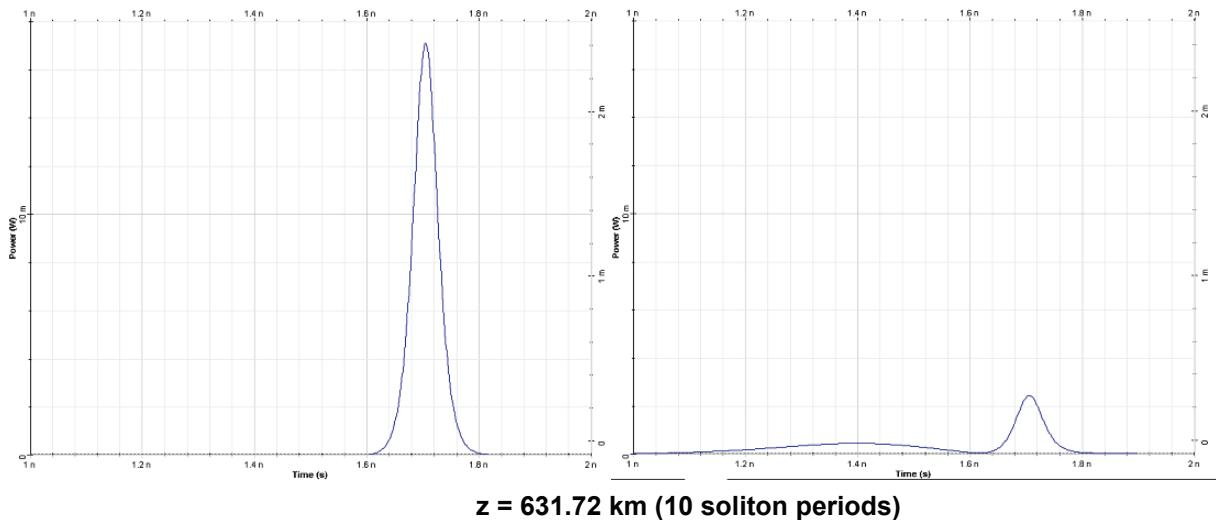
When  $\theta \neq 45^\circ$  in [Equation 2](#), the two components have different amplitudes initially. In this case, when  $N$  exceeds  $N_{th}$ , the evolution scenario is qualitatively different, depending on the value of the birefringence ( $\delta$ -parameter in [Equation 1](#)). With  $\theta = 30^\circ$ , this is illustrated in [Figure 6](#) and [Figure 7](#) for different values of the birefringence.

For the case  $\delta = 0.15$ , ([Figure 6](#)), the smaller pulse is captured by the larger and two move together. However, when  $\delta = 0.5$ , the larger one captures a fraction of the energy in the smaller pulse and the rest of it is dispersed with propagation.

The results shown in [Figure 6](#) and [Figure 7](#) indicate that under certain conditions the two orthogonally polarized components of the soliton move with a common group velocity despite of their different modal indices. This phenomenon is known as soliton trapping [3].

**Figure 6 Pulse evolution over 20 soliton periods for:**

$$P_0 = 12.1699 \text{ mW}, \Delta n = 6.3561 \times 10^{-8}, (N = 0.8, \delta = 0.15), \theta = 30^\circ$$



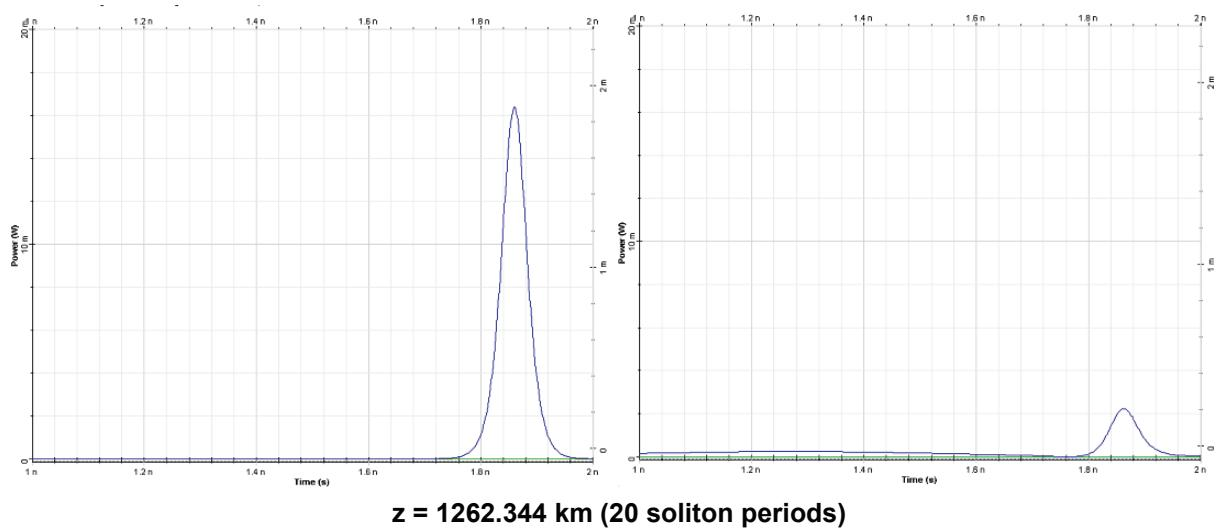
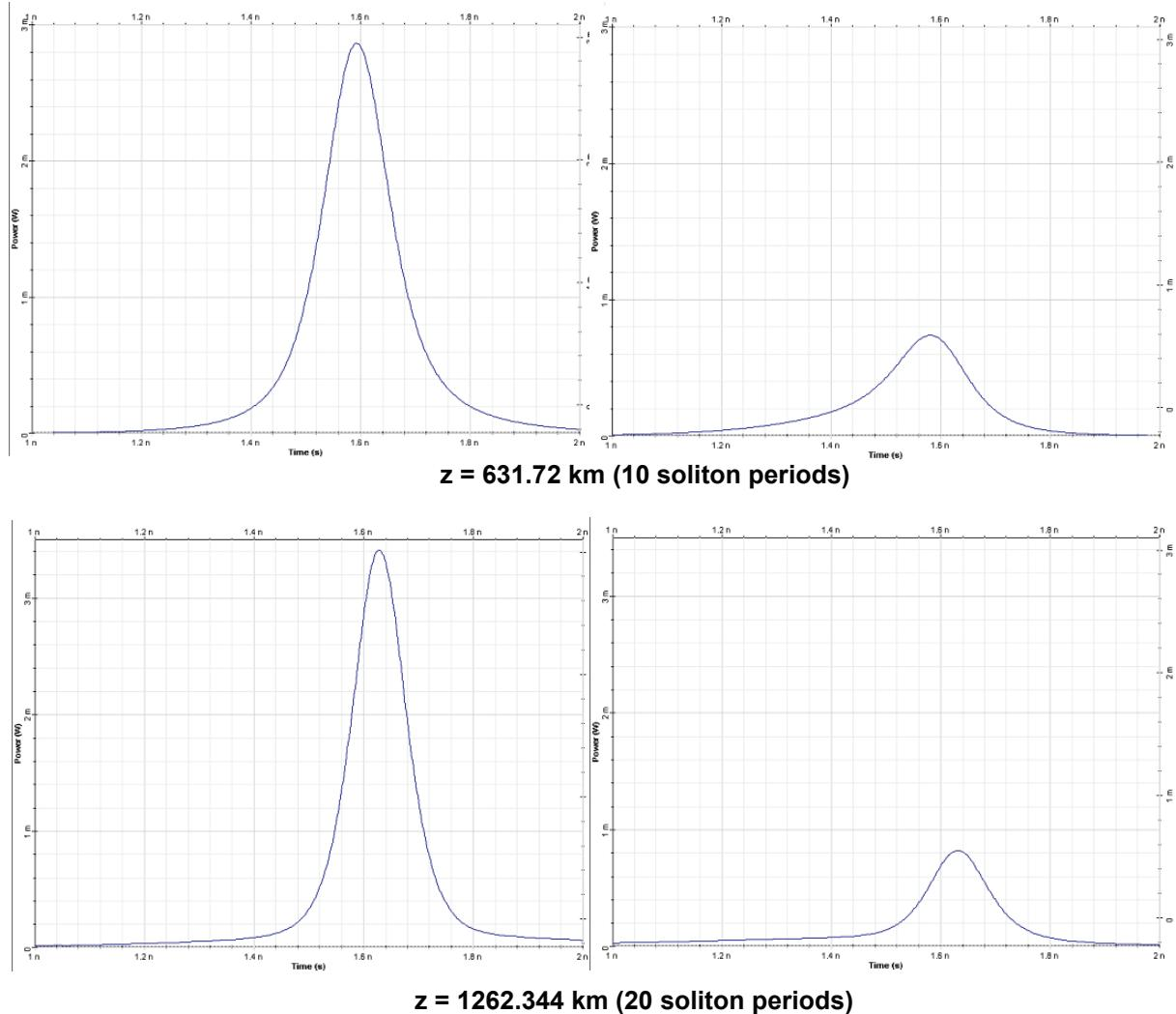


**Figure 7 Pulse evolution over 20 soliton periods for:**

$$P_0 = 12.1699 \text{ mW}, \Delta n = 6.3561 \times 10^{-8}, (N = 0.8, \delta = 0.15), \theta = 30^\circ$$



## References:

- [1] C. R. Menyuk, Opt. Lett., 12, p. 614 (1987).
- [2] C. R. Menyuk, JOSA B, 5, p. 392(1988).
- [3] G. P. Agrawal Nonlinear Fiber Optics, Academic Press (2001).

# Orthogonal Raman gain

---

This lesson demonstrates the energy exchange between two optical solitons with orthogonal polarizations associated with the orthogonal Raman gain [1].

Using equations (17a) from the technical description of the Nonlinear dispersive fiber component it can be shown [1] that the energy exchange between two solitons:

$$E_X = \sqrt{P_1} \operatorname{sech} \left( \sqrt{\frac{\gamma P_1}{|\beta_2|}} (t - \beta_2 \Delta\omega z) \right) \exp(-i\Delta\omega t) \quad (1)$$

where  $P_1 \gg P_2$  and  $\Delta\omega > 0$  is approximately given by the following expression [1]:

$$I_\gamma(z) - I_\gamma(0) = 2\rho(\tau_1 - \tau_2) \sqrt{P_1 P_2} \tanh(\sqrt{\gamma P_2 |\beta_2|} \Delta\omega z) \quad (2)$$

Equation 2 denotes the energy of the weaker (low frequency) soliton.

## ORTHOGONAL RAMAN GAIN

The layout and its global parameters are shown in Figure 1.

**Figure 1 System layout and global parameters**

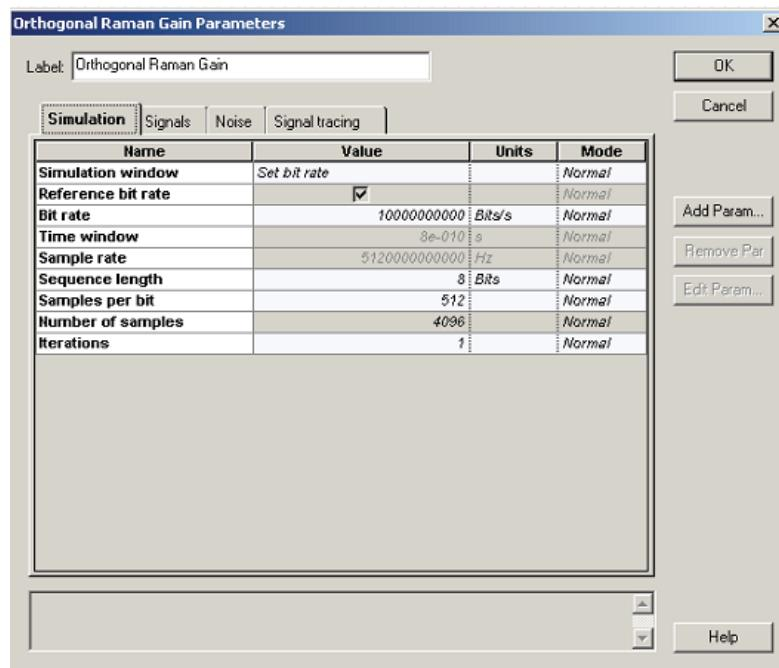
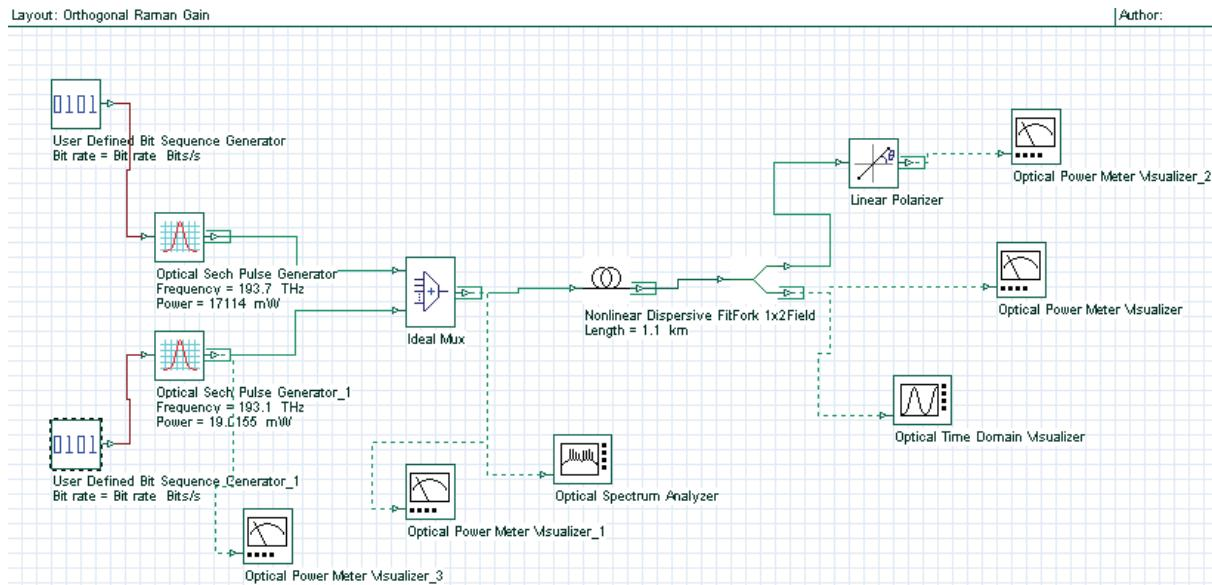
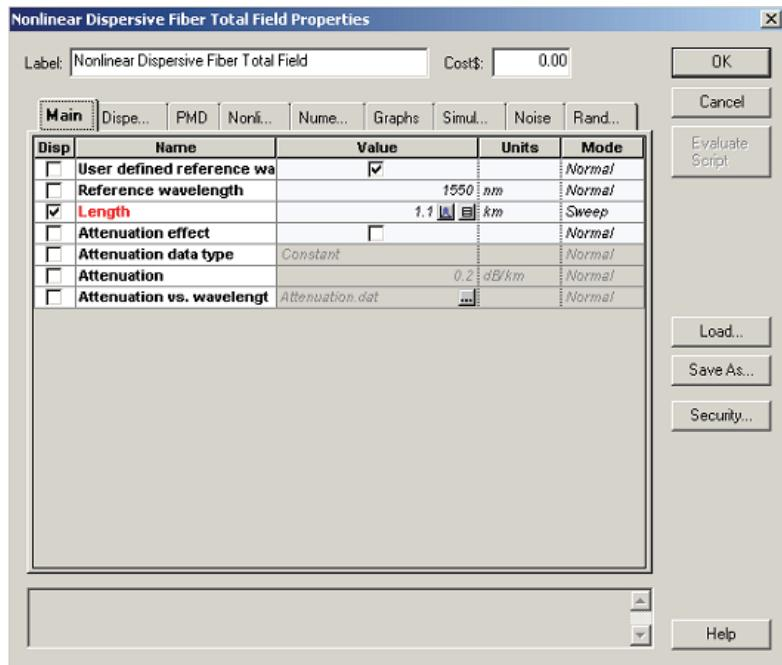


Figure 2 gives the setup for the nonlinear dispersive fiber component.



Figure 2 Setup parameters



## ORTHOGONAL RAMAN GAIN

Nonlinear Dispersive Fiber Total Field Properties				
Label: Nonlinear Dispersive Fiber Total Field		Cost\$: 0.00	<input type="button" value="OK"/> <input type="button" value="Cancel"/> <input type="button" value="Evaluate Script"/>	
<input type="button" value="Main"/> <input checked="" type="button" value="Disp..."/> <input type="button" value="PMD"/> <input type="button" value="Nonli..."/> <input type="button" value="Nume..."/> <input type="button" value="Graphs"/> <input type="button" value="Simul..."/> <input type="button" value="Noise"/> <input type="button" value="Rand..."/>				
<b>Disp</b>	<b>Name</b>	<b>Value</b>	<b>Units</b>	<b>Mode</b>
<input type="checkbox"/>	Group velocity dispersion	<input checked="" type="checkbox"/>		Normal
<input type="checkbox"/>	Third-order dispersion	<input type="checkbox"/>		Normal
<input type="checkbox"/>	Dispersion data type	Constant		Normal
<input type="checkbox"/>	Frequency domain parameter	<input checked="" type="checkbox"/>		Normal
<input type="checkbox"/>	Dispersion	16.75	ps/nm/km	Normal
<input type="checkbox"/>	Dispersion slope	0.075	ps/nm <sup>2</sup> /km	Normal
<input type="checkbox"/>	Beta 2	-20	ps <sup>2</sup> /km	Normal
<input type="checkbox"/>	Beta 3	0	ps <sup>3</sup> /km	Normal
<input type="checkbox"/>	Dispersion file format	Dispersion vs. wavelength		Normal
<input type="checkbox"/>	Dispersion file name	Dispersion.dat	<input type="button" value="..."/>	Normal

Nonlinear Dispersive Fiber Total Field Properties				
Label: Nonlinear Dispersive Fiber Total Field		Cost\$: 0.00	<input type="button" value="OK"/> <input type="button" value="Cancel"/> <input type="button" value="Evaluate Script"/>	
<input type="button" value="Main"/> <input type="button" value="Disp..."/> <input checked="" type="button" value="PMD"/> <input type="button" value="Nonli..."/> <input type="button" value="Nume..."/> <input type="button" value="Graphs"/> <input type="button" value="Simul..."/> <input type="button" value="Noise"/> <input type="button" value="Rand..."/>				
<b>Disp</b>	<b>Name</b>	<b>Value</b>	<b>Units</b>	<b>Mode</b>
<input type="checkbox"/>	Birefringence type	Deterministic		Normal
<input type="checkbox"/>	Differential group delay	0	ps/km	Normal
<input type="checkbox"/>	PMD coefficient	0.5	ps <sup>2</sup> (km) <sup>0.5</sup>	Normal
<input type="checkbox"/>	Mean scattering section length	500	m	Normal
<input type="checkbox"/>	Scattering section dispersion	100	m	Normal



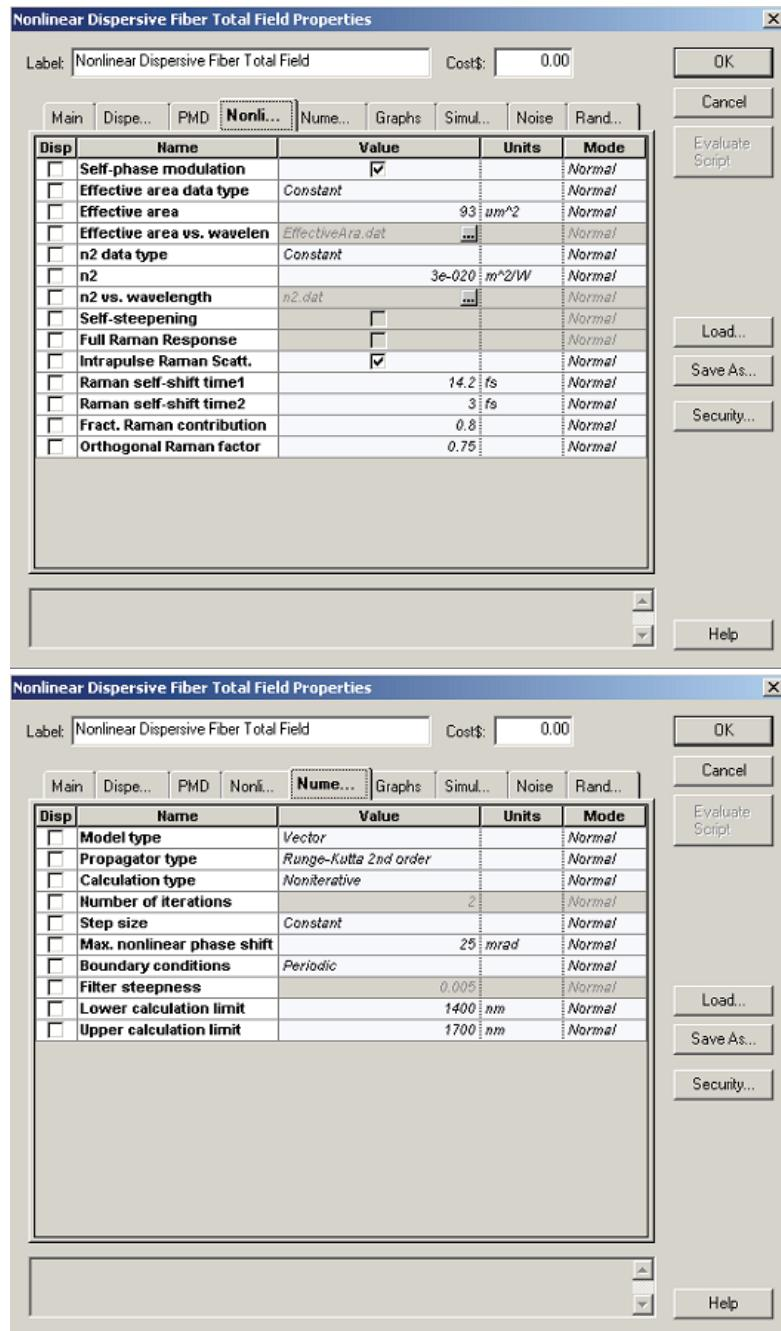
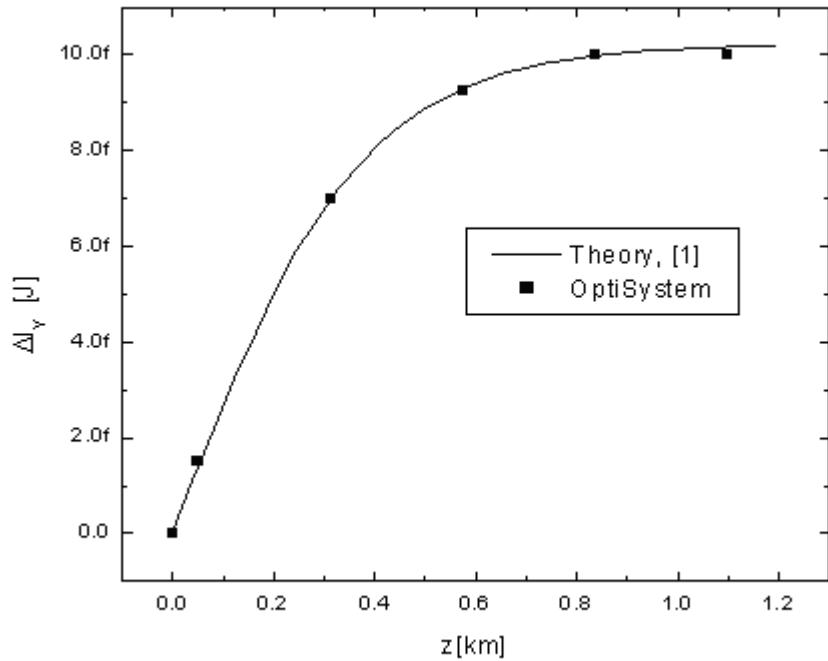


Figure 3 gives the comparison between the analytical result of Equation 2 and the results obtained with OptiSystem.

Figure 3 Experimental and OptiSystem results



## References

- [1] C. R. Menyuk, M. N. Islam and J. P. Gordon, Optics Letters 16 p.566 (1991).



# Average soliton regime

---

This lesson demonstrates the average soliton regime at 10 Gb/s transmission over a 500 km optical link consisting of SMF.

Figure 1 shows the layout that was used.

**Figure 1 Average soliton regime layout**

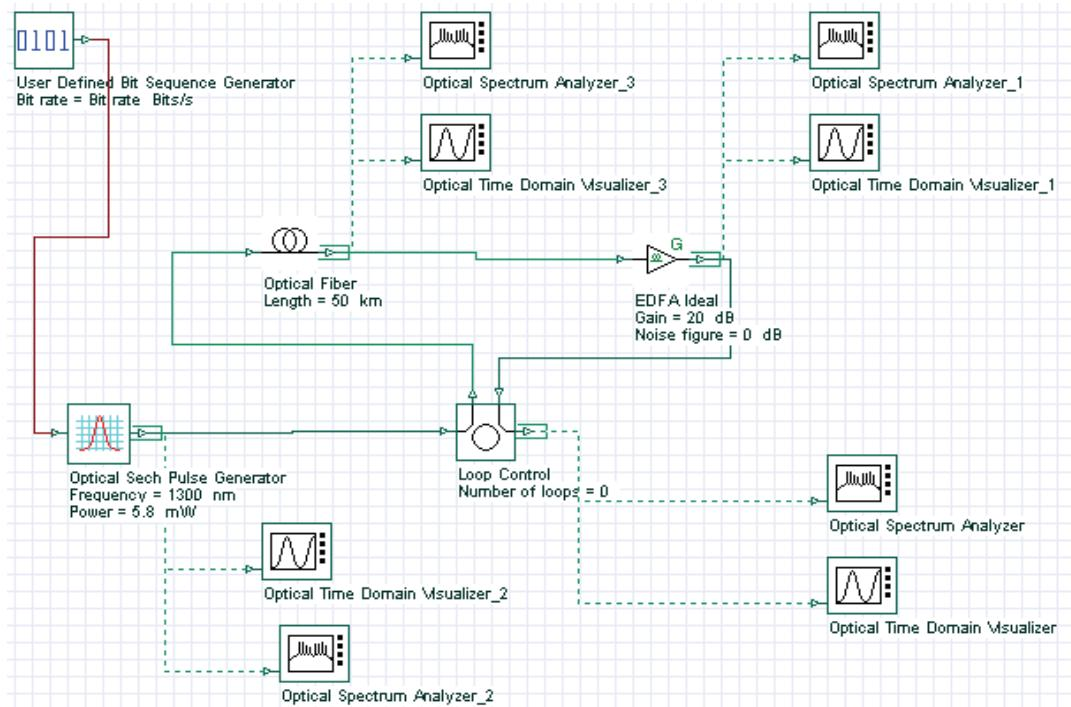
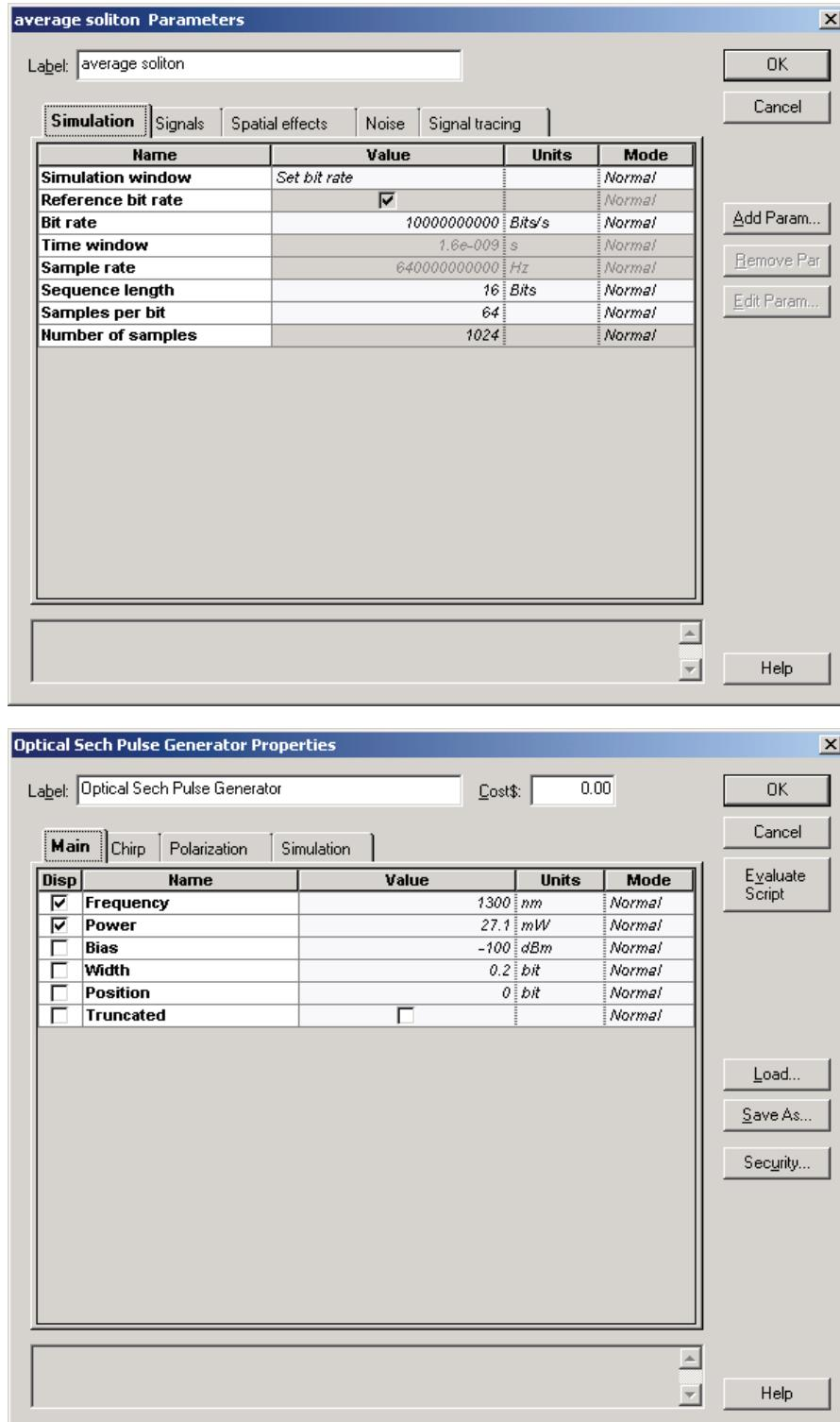


Figure 2 shows the global and pulse parameters used to achieve transmission at 10 Gb/s.

Figure 2 Simulation and Main parameters for 10 GB/s transmission

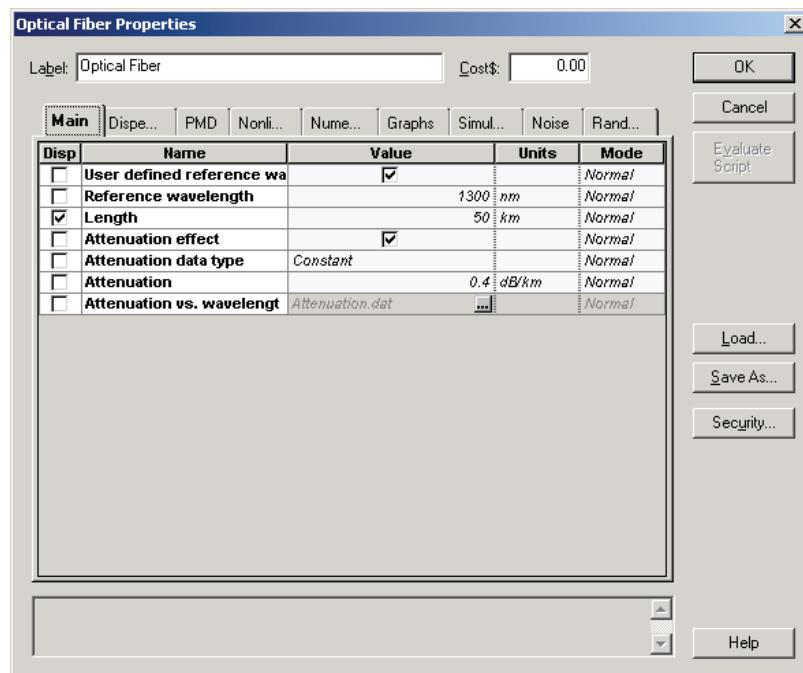


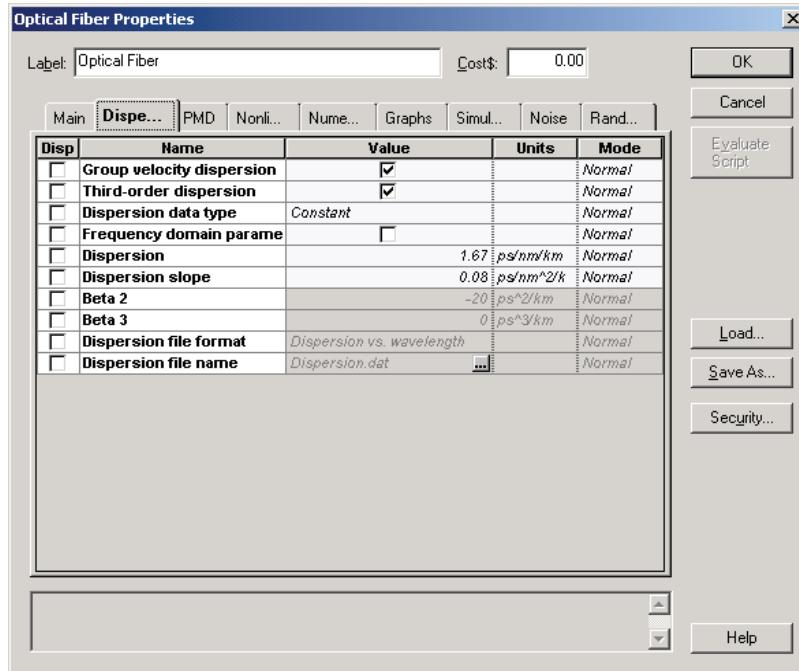
We fixed  $B = 10 \text{ Gb/s} \rightarrow T_B = 100 \text{ ps}$ .

Sequence length	16 bits
Carrier wavelength of the pulse	$\lambda \sim 1300 \text{ nm}$
$T_{\text{FWHM}} = 20 \text{ ps}$	$\rightarrow T_0 = 0.567 T_{\text{FWHM}} \sim 11.34 \text{ ps}$
Input peak power	21.7 mW

Figure 3 and Figure 4 show the selected parameters.

**Figure 3 Fixing Nonlinear Dispersive Fiber Main parameters**



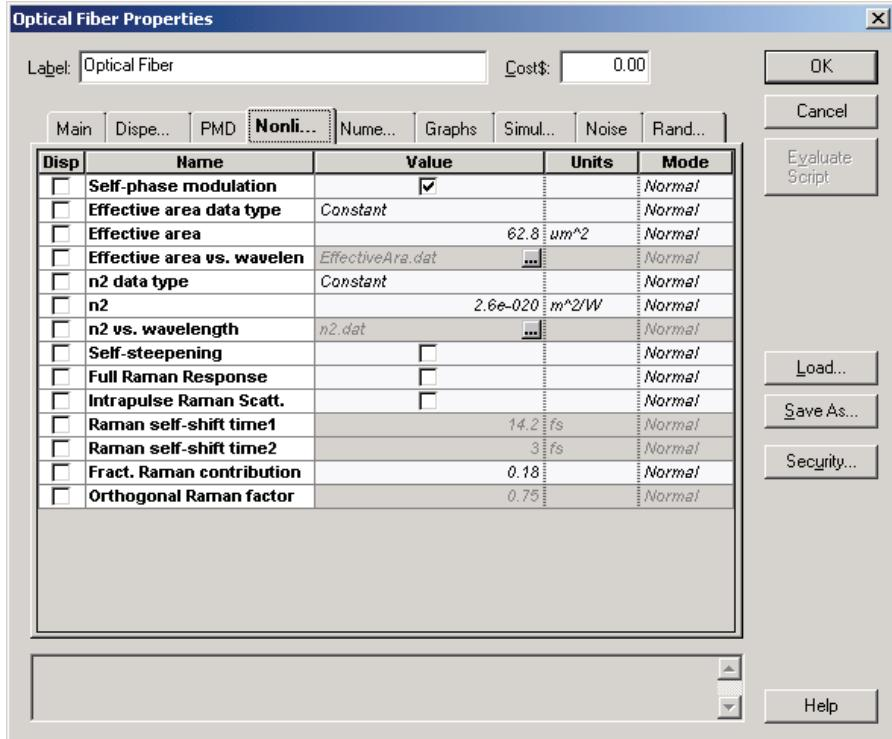
**Figure 4 Fixing Nonlinear Dispersive Fiber Dispersion parameters**

We will consider SMF with a length of 50 km and losses of 0.4 dB/km.

$$k_2 = (-\lambda_2 D) / (2\pi c) \sim -1.5 \text{ (ps}^2/\text{km}) \rightarrow D = 1.67 \text{ (ps/nm.km)} \rightarrow L_D = T_0^2 / |k_2| \sim 85 \text{ km}$$

**Note:** The effects of group delay and third order of dispersion are not taken into account.

After each fiber, the signal is amplified with SOA. Therefore,  $L_A \sim 50$  km. Note that the condition  $L_A < L_D$  is satisfied (see [Figure 5](#)).

**Figure 5 Nonlinear Dispersive Fiber Nonlinearities parameters**

The Kerr nonlinearity coefficient  $\gamma = n_2 \omega_0 / c A_{eff}$  for the fixed values of nonlinear refractive index  $n_2 = 2.6 \cdot 10^{-20} [\text{m}^2/\text{W}]$ ,

$$\omega_0 / c = 2\pi / \lambda = 2\pi / 1.310^{-6} [\text{m}^{-1}], A_{eff} = 62.8 [\mu\text{m}^2]$$

will be 2 [1/km.W]

The linear losses for 50 km SMF are 20 dB. The losses are periodically compensated with the Ideal EDFA with 20 dB gain.

Soliton peak power for this SMF is 5.8 mW. The input power of the average soliton is 27.1 mW. To demonstrate the importance of the input power of the average soliton, we will consider soliton propagation in a 500 km SMF with two different input powers:

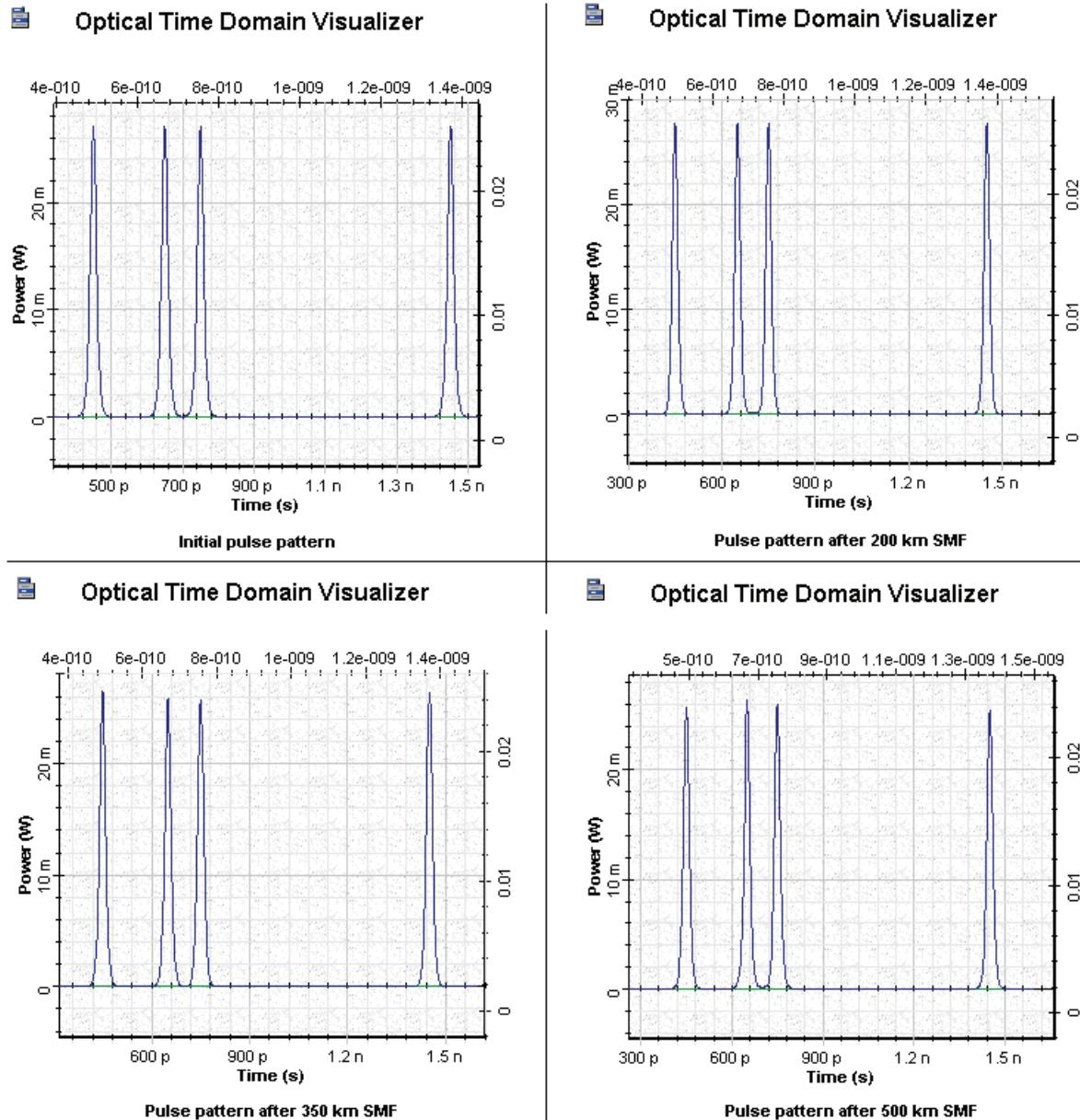
5.8 mW — usual soliton peak power (Version insufficient power)

27.1 mW — modified soliton peak power which takes into account the periodical amplification (Version average soliton)

Each version includes sweeps on the number of loops 0, 4, 7, and 10 with which to represent the propagation distances 0, 200, 350, and 500 km in SMF.

[Figure 6](#) shows the initial pattern of pulses, and the same pattern of pulses after 200, 350, and 500 km transmission in SMF and periodic amplification with EDFA at every 50 km with the 27.1mW — modified soliton peak power which takes into account the periodical amplification.

**Figure 6 Average soliton pulse patterns**

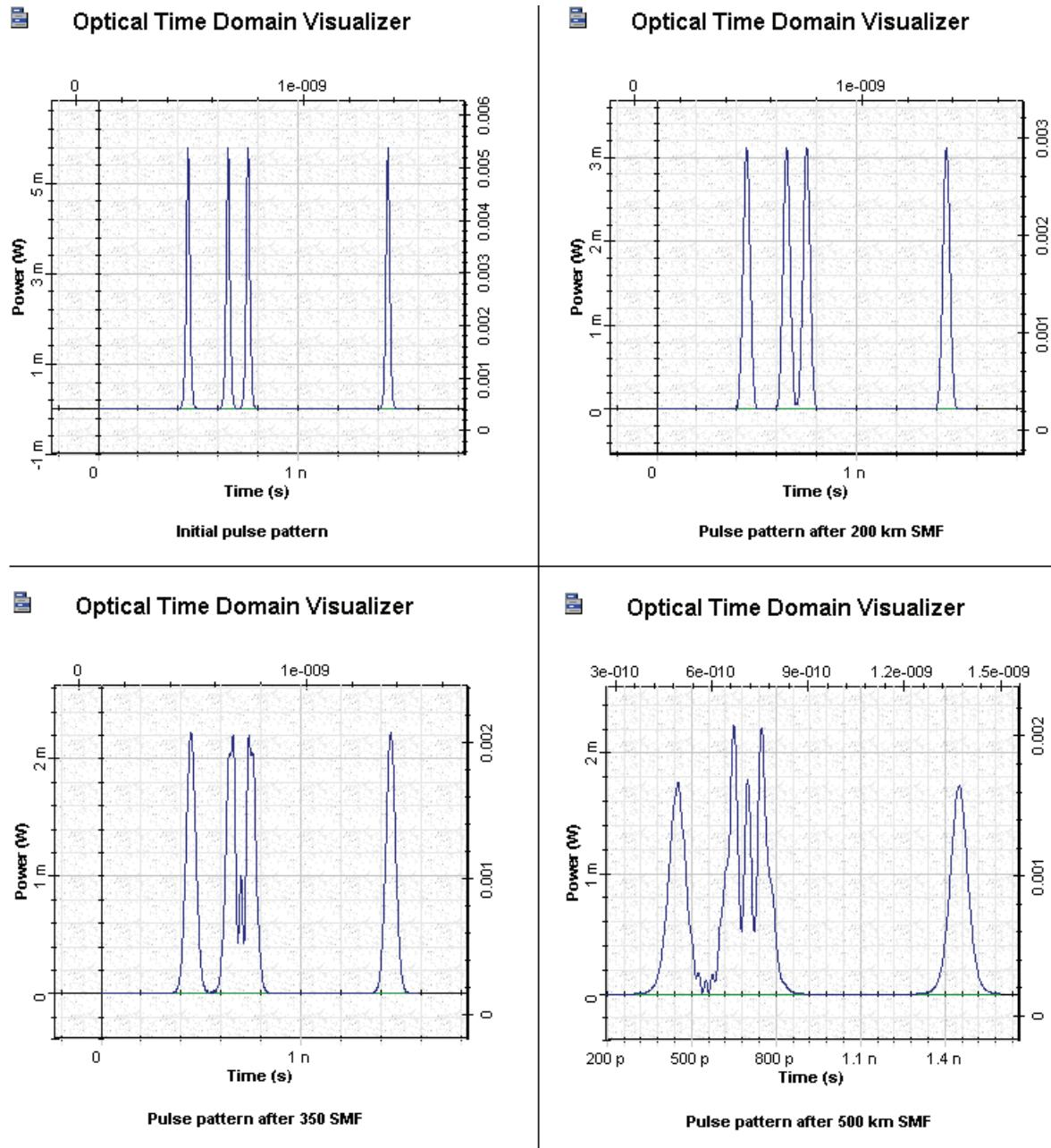


Good preservation of the pattern of pulses can be clearly seen. The average soliton concept is valid for these pulse, fiber, and amplification parameters.



[Figure 7](#) shows the initial pattern of pulses, and the same pattern of pulses after 200, 350, and 500 km transmission in SMF and periodic amplification with EDFA at every 50 km with the 5.8 mW — soliton peak power which doesn't take into account the periodical amplification.

**Figure 7 Insufficient power pulse patterns**



Because of the improper pulse power used, the pulses in the pattern do not preserve their forms. As a result, pulses broaden and complicated structures appear.

This lesson demonstrated the average soliton concept. It requires:

- fulfilment of adiabatic condition  $L_A < L_D$
- proper pulse peak power which to take into account the process of periodical amplification

## References

- [1] G.P. Agrawal, "Applications of Nonlinear Fiber Optics", Academic Press, 2001.
- [2] G.P. Agrawal, "Fiber Optic Communication Systems", 2nd Edition, John Wiley & Sons Inc., 1997.



# SOA as in-line amplifier in soliton communication systems

---

One possible way to upgrade an existing network from previously installed standard optical fibers is to exploit the 1.3 mm optical window, where the step index fibers have a zero-dispersion wavelength using SOA.

The advantages of using SOA as in-line single-channel optical amplifiers are:

- low dispersion of the SMF at this carrier wavelength
- attractive features of semiconductor optical amplifiers

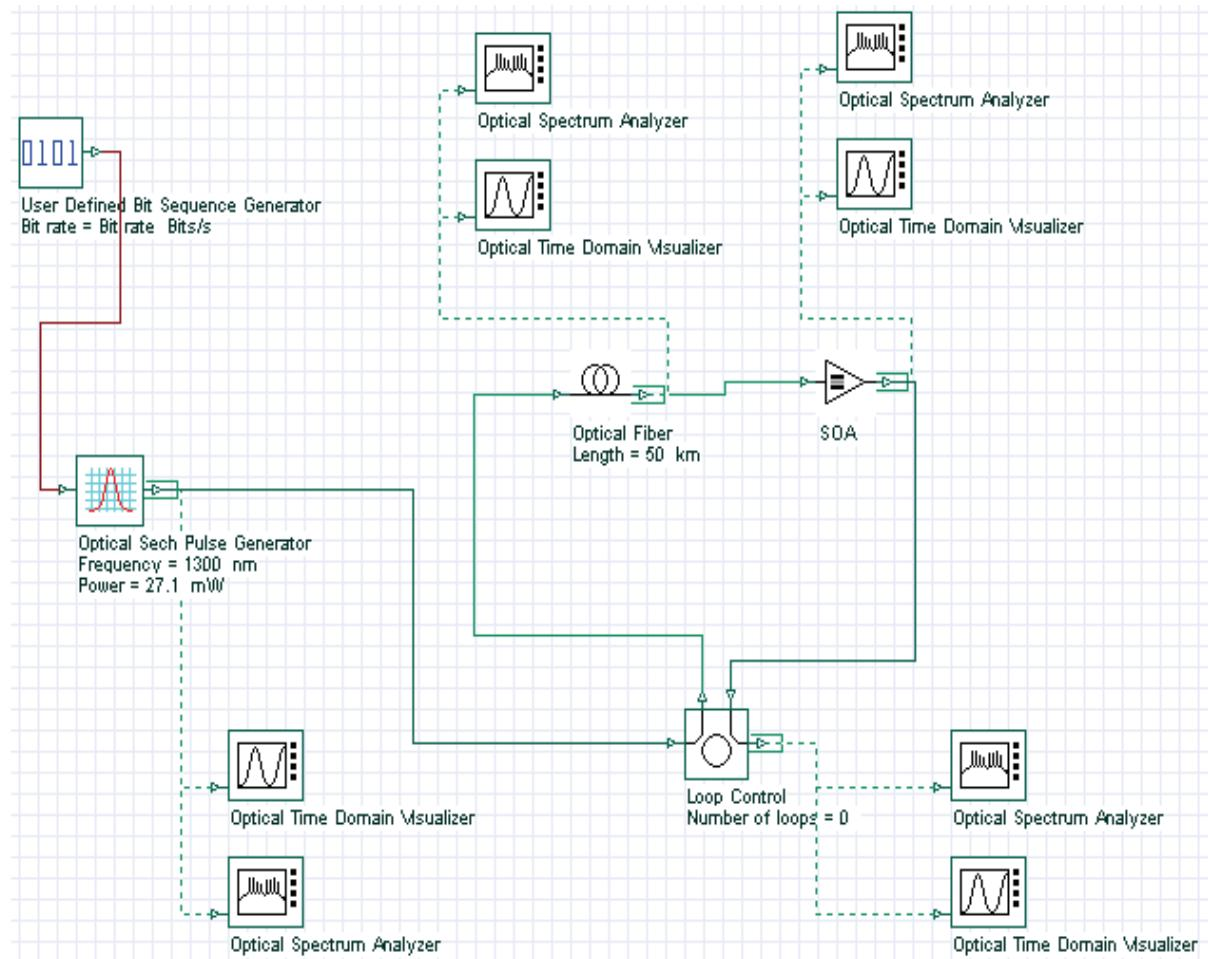
Two disadvantages of using SOA as in-line single-channel optical amplifiers are:

- gain-saturation effects, which lead to non-equal amplification of pulses in the pattern (so called pattern effect)
- chirp that the pulse acquires after amplification

This lesson demonstrates the pattern effect at 10 Gb/s transmission over a 500 km optical link consisting of SMF and in-line SOA's [1]. We will try to use parameters similar to the parameters in [1].

Figure 1 shows the project layout.

**Figure 1 Layout of pattern effect at 10 Gb/s transmission over 500 km optical link**



The following global and pulse parameters are used to achieve transmission at 10 Gb/s (see [Figure 2](#) and [Figure 3](#)).

**Figure 2** Simulation parameters for transmission at 10 Gb/s

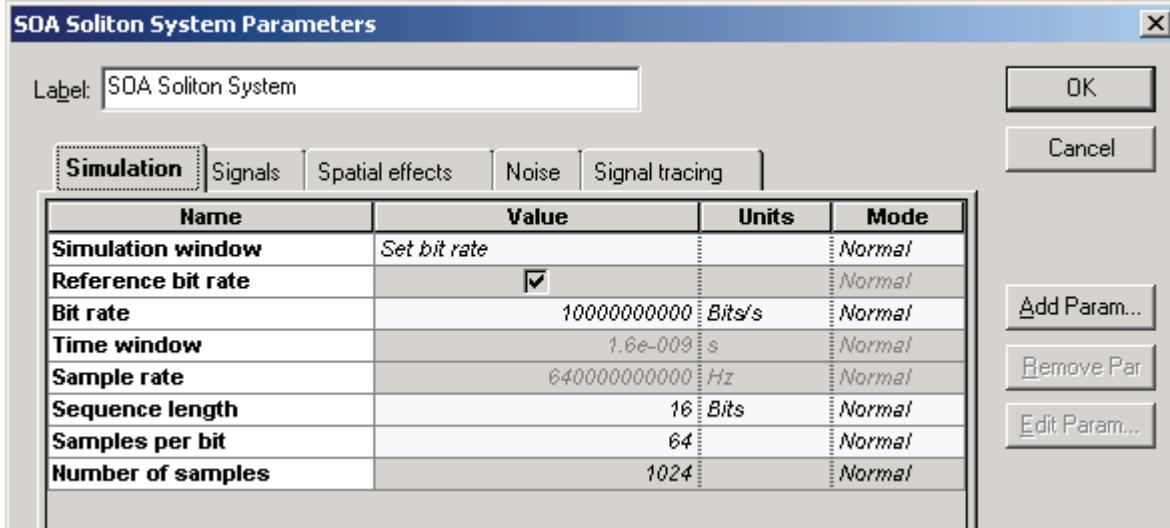
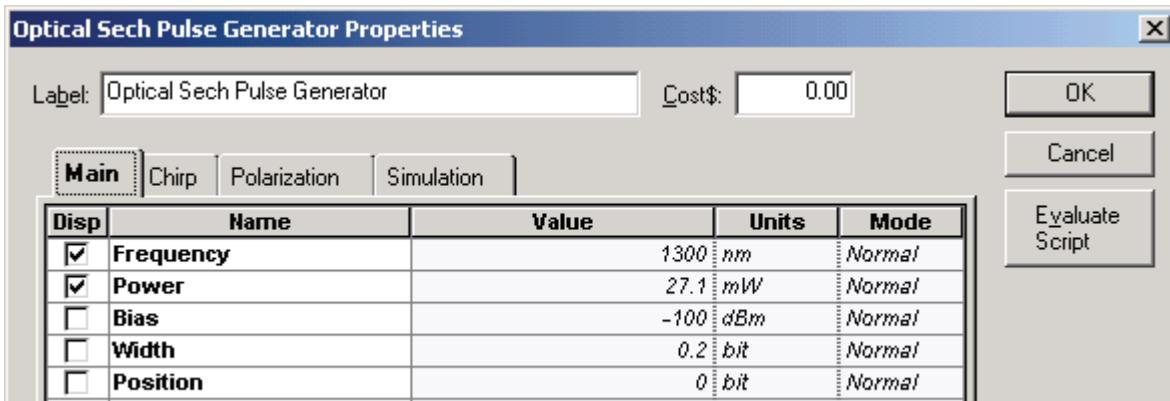


**Figure 3** Optical Sech Pulse Generator Main parameters for transmission at 10 Gb/s



We fixed  $B = 10 \text{ Gb/s} \rightarrow T_B = 100 \text{ ps}$ .

Sequence length                            16 bits

Carrier wavelength of the pulse       $\lambda \sim 1300 \text{ nm}$

$T_{\text{FWHM}} = 20 \text{ ps}$                              $\rightarrow T_0 = 0.567 T_{\text{FWHM}} \sim 11.34 \text{ ps}$

Input peak power                        21.7 mW

[Figure 4](#) and [Figure 5](#) show the selected fiber parameters.

Figure 4 Nonlinear Dispersive Fiber Main parameters

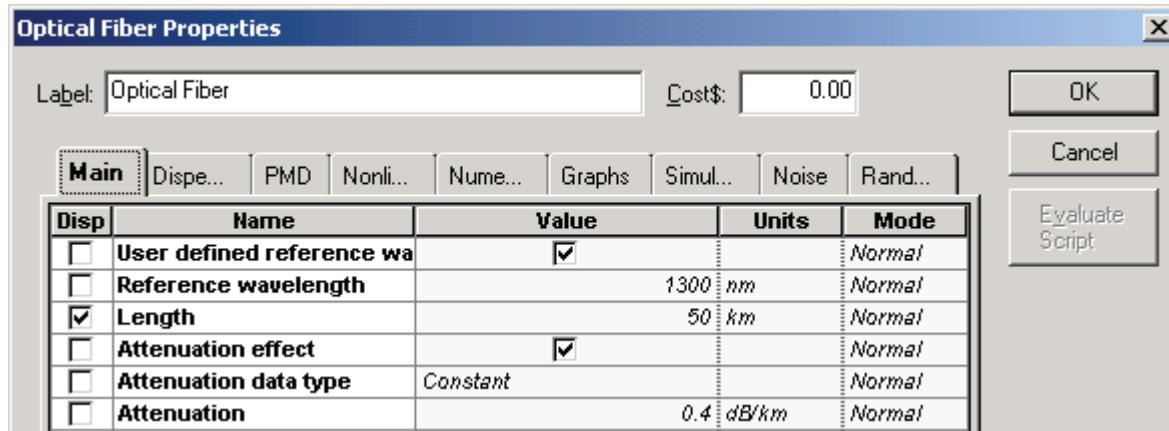
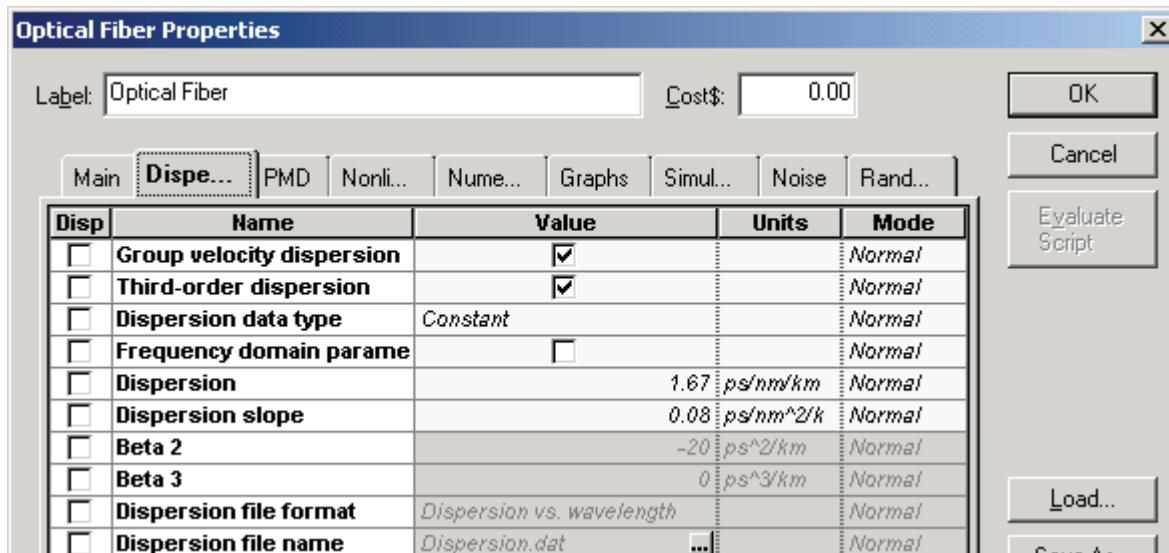


Figure 5 Nonlinear Dispersive Fiber Dispersions parameters



We will consider SMF with a length of 50 km and losses of 0.4 dB/km.

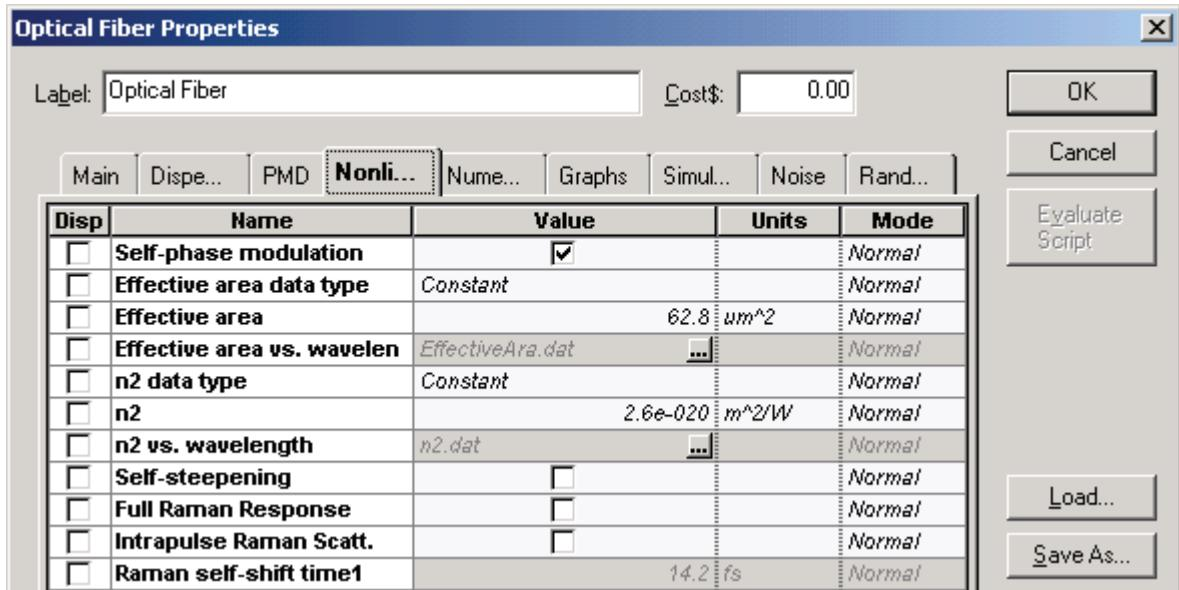
$$K_2 = \frac{(-\lambda^2 D)}{(2\pi c)} \sim -1.5 \text{ (ps}^2/\text{km}) \rightarrow D = 1.67 \text{ (ps/nm.km)} \rightarrow L_D = T_0^2 / |K_2| \sim 85 \text{ km}$$

**Note:** The effects of group delay and third order of dispersion are not taken into account.

After each fiber, the signal is amplified with SOA. Therefore,  $L_A \sim 50$  km. The condition  $L_A < L_D$  is satisfied.

Figure 6 shows the nonlinear parameters.

Figure 6 Nonlinear Dispersive Fiber NonLinear parameters



The Kerr nonlinearity coefficient

$$\gamma = \frac{n_2 w_0}{c A_{eff}}$$

for the fixed values of nonlinear refractive index

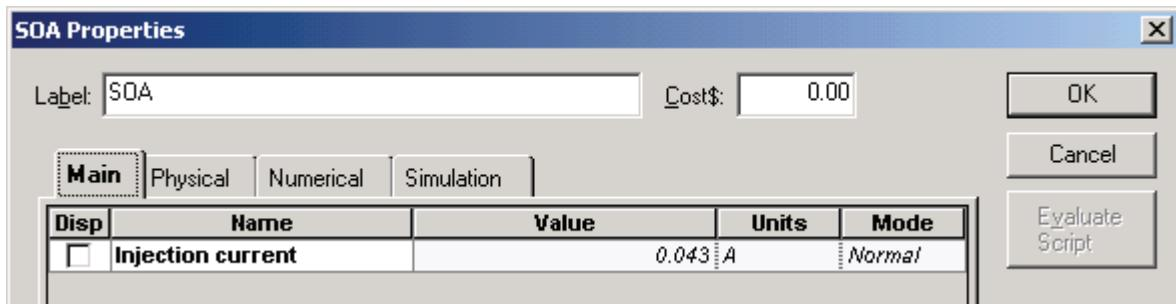
$$n_2 = 2.6 \cdot 10^{-20} [\text{m}^2/\text{W}], w_0/c = 2\pi/\lambda = 2\pi/1.3 \cdot 10^{-6} [\text{m}^{-1}], (A_{eff} = 62.8 [\mu\text{m}^2])$$

will be:

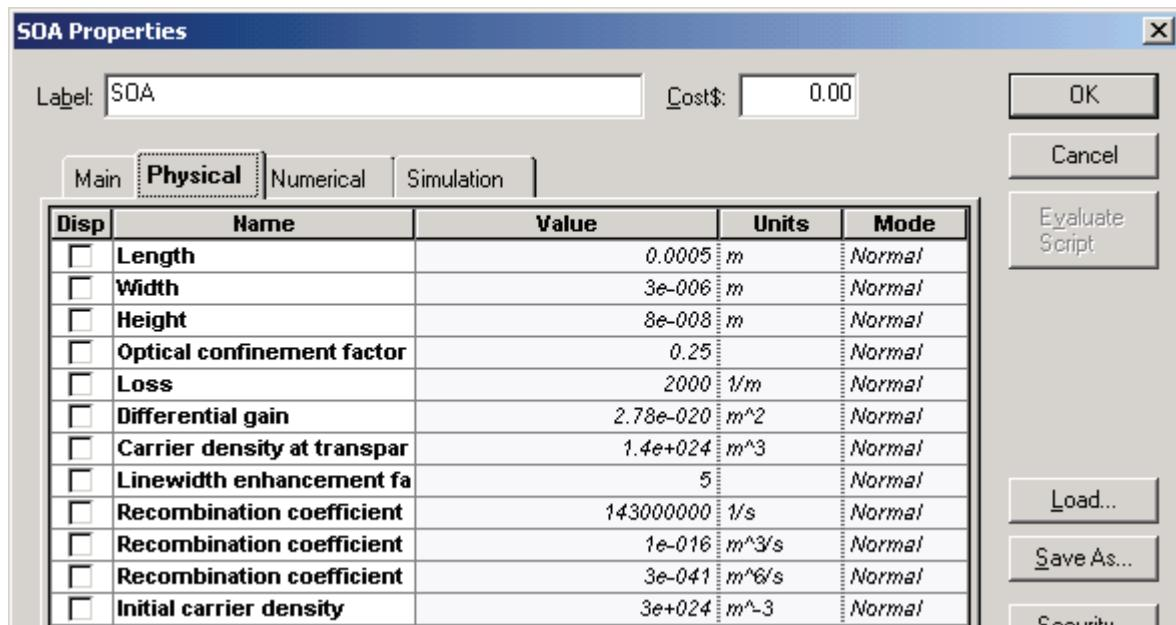
$$\gamma = 2 \left[ \frac{1}{\text{km} \cdot \text{W}} \right]$$

The linear losses for 50 km SMF are 20 dB. This is unsaturated single pass gain required from SOA. To obtain this gain, the following parameters have been used (see [Figure 7](#) and [Figure 8](#)).

**Figure 7 SOA Main parameters**

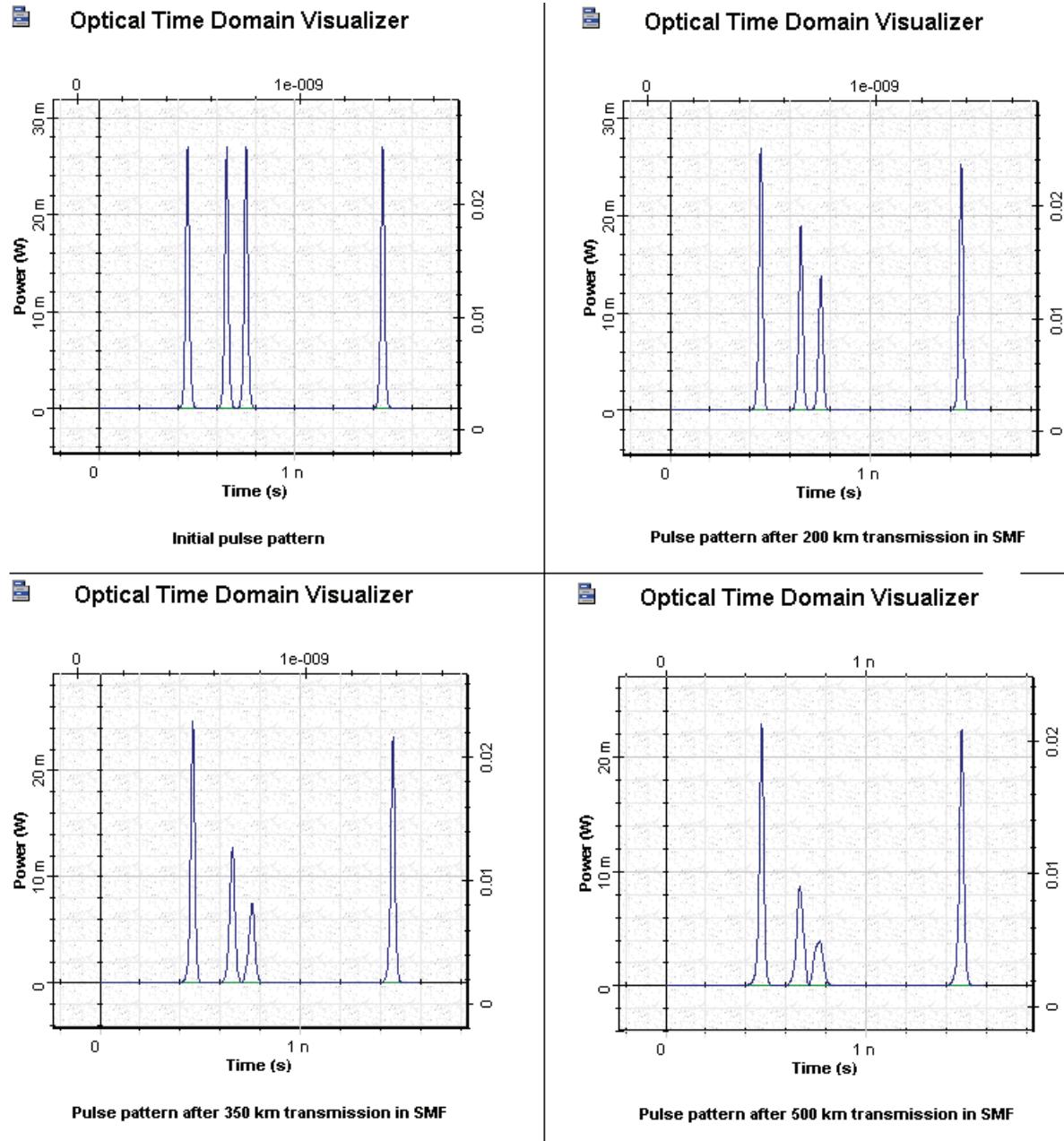


**Figure 8 SOA Physical parameters**



The inner losses are  $2000[m^{-1}]$  and the line width enhancement factor = 5.  $P_{sat} \sim 30$  mW and carrier lifetime  $t_C = 200$  ps in [1]. Therefore,  $E_{sat} \sim 6$  pJ. Our default values of the SOA component and  $\Gamma = 0.25 \rightarrow E_{sat} \sim 5.2\mu J$ .

[Figure 9](#) shows the initial pattern of pulses, and the same pattern of pulses after 200, 350, and 500 km transmission in SMF and periodic amplification with SOA at every 50 km.

**Figure 9 SOA pulse patterns**

In this figure, we can see the pattern effect that leads to a reduction in the gain of the pulses after the first one in the first group. Regarding our default parameters, the carrier lifetime is approximately 1.4 ns even for the last pulse, which is at a distance of approximately 1 nm from the first one. There is not enough time for the gain to recover completely.

This lesson demonstrated two basic problems associated with using the SOA as an in-line amplifier:

- pattern effect, which is a consequence of the gain saturation properties of the SOA
- nonlinear crosstalk [3]

## References:

- [1] M. Settembre, F. Matera, V. Hagele, I. Gabitov, A. W. Mattheus, and S. Turitsyn, "Cascaded optical communication systems with in-line semiconductor optical amplifiers", Journal of Lightwave Technology, Vol. 15, pp. 962-967, 1997.
- [2] F. Matera and M. Settembre, "Study of 1.3 mm transmission systems on standard step-index fibers with semiconductor optical amplifiers", Optics Communications, Vol. 133, pp.463-470, 1997.
- [3] G.P. Agrawal, "Fiber Optic Communication Systems", 2nd Edition, John Wiley & Sons Inc., 1997.



---

## Metro systems

---

This section contains the following advanced simulation projects.

- Power level management in optical Metro networks
- Migrating to 10Gbps in Metro networks
- Negative dispersion fiber for Metro networks
- Interchannel crosstalk in Metro networks
- WDM Ring—Wavelength independent subscriber equipment

**Notes:**

# Power level management in optical Metro networks

---

## Design without amplification

In this example, our goal is to design a basic transparent ring network without amplification and discover the power related issues.

Metro networks using ring topology are expected to have more dynamic traffic patterns compared to most long-haul networks. They are also expected to have optically transparent nodes with a minimum number of regenerators. Therefore, we need to consider all the optical power variations that may result from several factors:

- wavelength dependent loss in fibers
- wavelength dependent gain in amplifiers
- channel to channel insertion loss variation in the multiplexers/demultiplexers

These optical degradations accumulate along the links until the optical termination is reached. Due to dynamic nature of the network, only proper dynamic power level management can reduce them.

Optical Add/Drop Multiplexers (OADMs) introduce insertion loss that contains two parts: deterministic and random. In fact, loss varies with the wavelength. The loss of fiber depends on fiber type and wavelength. Variation of optical switch types and different path lengths in the network will result in a random loss, which is difficult to predict.

There are several limiting factors in terms of power in optical networks, including:

- nonlinear effects
- receiver sensitivity
- losses in the fiber, OADMs, OXCs

We will consider all these effects in our design and simulations.

Typical loss, transmitter power, and receiver sensitivity values are given in [Table 1](#) and [Table 2](#).

**Table 1 Typical losses for components used in metro links**

<b>Symbol</b>	<b>Description</b>	<b>Loss value</b>
$L_{mon}$	Tap loss for monitoring	0.2 dB
$L_{conn}$	Loss of a connector	0.25 dB
$L_{splice}$	Loss of a splice	0.15 dB
$L_{span}$	Loss of a fiber span	0.25 dB/km
$L_{mux}$	Loss of a multiplexer	4 dB
$L_{demux}$	Loss of a demultiplexer	4 dB
$L_{foadm}$	Loss of a fixed OADM	2 dB
$L_{roadm}$	Loss of a re-configurable OADM	10 dB

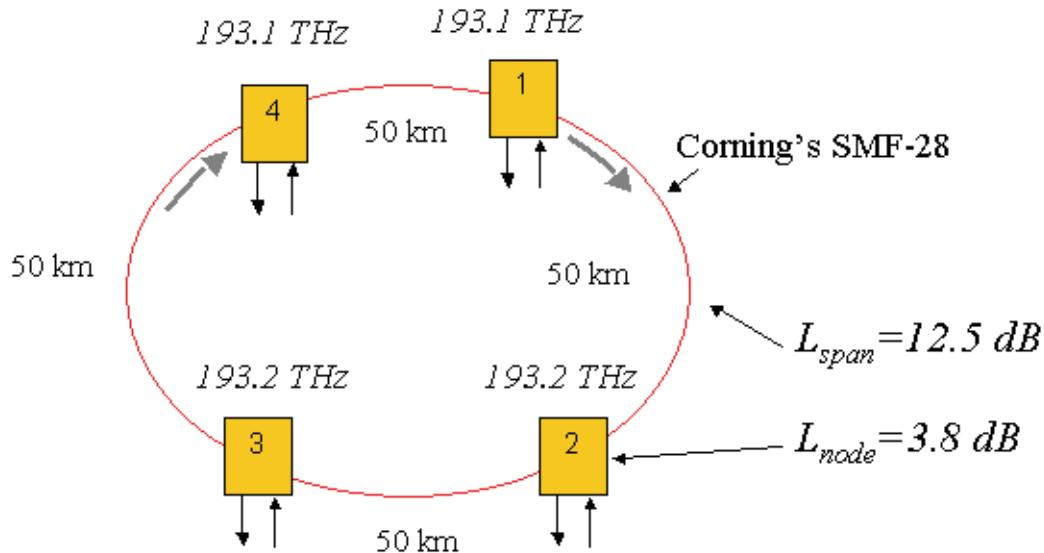
**Table 2 Typical values for transmitter and receiver**

<b>Symbol</b>	<b>Description</b>	<b>Optical Power/ Receiver Sensitivity</b>
$P_{T-DM@2.5}$	2.5 Bbps/DM output power	3 dBm
$P_{T-EM@10}$	10 Gbps/EM output power	0 dBm
$P_{R-sen@2.5}$	2.5 Gbps pin diode receiver sensitivity	-23 dBm
$P_{R-sen@10}$	10 Gbps pin diode receiver sensitivity	-16 dBm

Total allowable loss from transmitter to receiver depends on the transmitted power and receiver sensitivity. As shown in [Table 2](#), receiver sensitivity is also a function of bit rate. The allowable loss is given by  $L_{allowable} = P_T - P_{R-sens}$ . Assuming two splices and six connectors, total loss at each node is given by  $L_{node} = 2L_{splice} + 6L_{conn} + L_{foadm}$ .

Let us consider a typical WDM metro ring at 2.5 Gbps, with a 200 km circumference and four intermediate fixed OADMs, as shown in [Figure 1](#). In this network, node 1 and 4 communicate on channel 1, whereas node 2 and 3 communicate on channel 2. The project is found in the [Optical power level management in metro networks\\_Linear.osd](#) and [Optical power level management in metro networks\\_NA.osd](#) files. These are two versions of the same project, one with linear fibers and one with nonlinear fibers. We will first investigate the system performance without fiber nonlinearities. Then we will enable fiber nonlinearities to see if a design without considering nonlinearities really works in real life.



**Figure 1 A basic optical ring network with four node and two channel**

Without any inline amplification, the allowable loss by using direct modulated source is  $L_{allowable} = 3(-23) = 26 \text{ dB}$ . Node (including two splices and six connectors) and span losses are  $L_{node} = 2 \times 0.15 + 6 \times 0.25 + 6 \times 0.25 + 2 = 3.8 \text{ dB}$  and  $L_{span50\text{km}} = 13.5 \text{ dB}$ . Therefore total loss will be  $3 \times (13.5 + 3.8) = 51.9 \text{ dB}$ .

Comparing the allowable loss and total loss in the network shows that it is not a good idea to make a design without amplification. Of course, increasing power is another option, but nonlinear effects may become important impairments at high powers. In this case, allowing 3 dB system margin, the required launch power will be the following:

$$51.9 + 3 - 23 = 31.9 \text{ dBm/channel}$$

Now let us try to estimate the threshold values for fiber nonlinearities.

### **Self-Phase Modulation**

The effect of SPM is to chirp the pulse and broaden its spectrum. As a rough design guideline, SPM effects are negligible when  $P_0 < \alpha/\gamma$  where  $\gamma = n_2 \omega_0 / c A_{eff}$  [1/(W/km)] is the nonlinearity coefficient,  $P_0$  is the peak power, and  $\alpha$  is the loss parameter.

For the fiber, we used  $\gamma \approx 1.5 \text{ W}^{-1} \text{ km}^{-1}$ . Therefore, SPM effects can be negligible when the total peak power is below 180 mW or 19 dBm average power.

### **Cross-Phase Modulation**

When two or more pulses of different wavelengths propagate simultaneously inside fibers, their optical phases are affected not only by SPM but also by XPM. Fiber dispersion converts phase variations into amplitude fluctuations. XPM induced phase shift should not affect the system performance if the GVD effects are negligible. As a

rough estimate, the channel power is restricted with  $P_{ch} < \alpha / [\gamma(2N_{ch}-1)]$ , where  $N_{ch}$  is the number of channels.

For a two channel system, limiting power is around *60 mW (14.5 dBm per channel)*. Separation between channels also affects the XPM. An increase in the separation will decrease the penalty which originates from XPM.

## Four-Wave Mixing

FWM is the major source of nonlinear cross-talk for WDM communication systems. It can be understood from the fact that beating between two signals generates harmonics at difference frequencies. If the channels are equally spaced new frequencies coincide with the existing channel frequencies. This may lead to nonlinear cross-talk between channels. When the channels are not equally spaces, most FWM components fall in between the channels and add to overall noise. FWM efficiency depends on signal power, channel spacing, and dispersion.

If the GVD of the fiber is relatively high  $|\beta^2| > 5\text{ps}^2/\text{km}$ , the FWM efficiency factor almost vanishes for a typical channel spacing of 50 GHz or more. If the channel is close to the zero dispersion wavelength of the fiber, considerably high power can be transferred to FWM components. To reduce the effect of FWM on system performance, you can use either uneven channel spacing or a dispersion-management technique.

## Stimulated Raman Scattering

Because of SRS, short wavelength channels act as pumps for longer wavelength channels. In a WDM system, the SRS impairs the system performance because energy is transferred from the short-wavelength to the long-wavelength channels. The Raman threshold for a single channel system is given by:

$$P_{th} \approx 16A_{eff}/g_R L_{eff} \text{ where } L_{eff} = \frac{1 - \exp(-\alpha L)}{\alpha}$$

and it is approximately equal to  $1/\alpha$  for long fibers. In fact, it is a function of the number of the channels and channel power. For a single channel system it is around 500 mW near 1.55 micrometer if  $g_R = 1 \times 10^{-13} \text{m/W}$ . For a 20 channel system  $P_{th}$  exceeds 10 mW whereas it is around 1 mW for a 70 channel system. It has little impact on system performance.

## Stimulated Brillouin Scattering

SRS is the result of the interaction of light with acoustic waves in fiber which scatters power backward. Back scattered light is downshifted in frequency from the original signal frequency. Threshold level depends on:

- source line-width
- effective core area
- effective fiber length

$$P_{th} \approx 21A_{eff}/g_B L_{eff}$$

Typical value for  $g_B$  is approximately  $5 \times 10^{-11} \text{m/W}$ . The threshold value also depends on modulation format and duration of pulse. Some values for threshold power are given below:

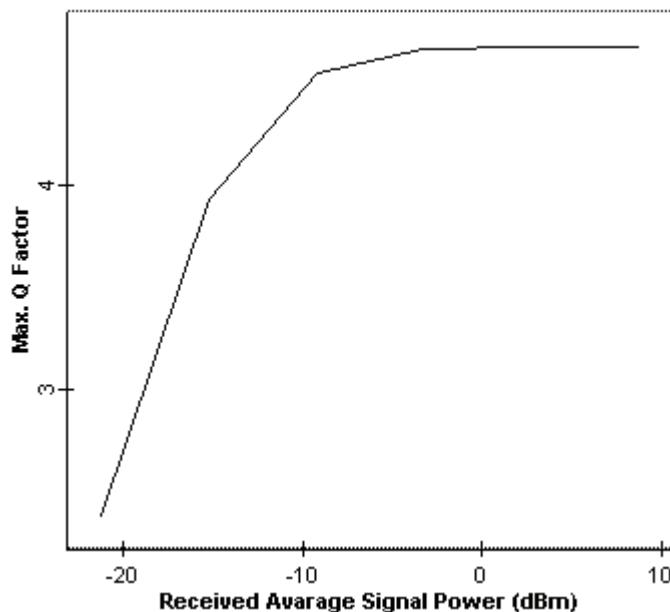


- 9 dBm for CW light
- 12 dBm for externally modulated transmitter
- >18 dBm for externally modulated transmitter with source wavelength dither

Generally speaking, SBS has little effect on system performance.

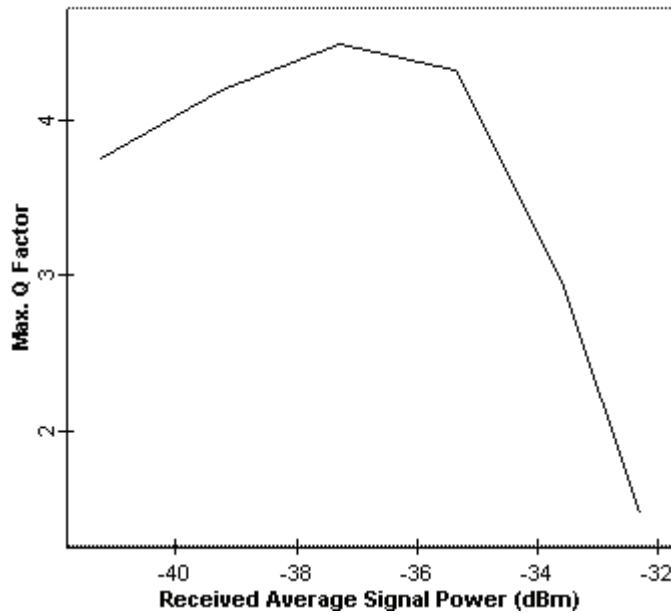
**Figure 2** shows the Q factor for channel 1 at the receiver end versus received average power, when no in-line amplifier is used and non-linearities of the fibers are disabled. To obtain this figure, we have used directly modulated sources with 3 dBm output power. We have inserted a power amplifier after Node 1 to adjust the signal power. Thermal noises of the receivers are adjusted to obtain -2.5 Gbps sensitivity at 2.5 Gbps. When we enable the non-linearity, the eye is always closed.

**Figure 2 Q factor versus received average power at node 4 when no amplifier is used and fiber non-linearity is disabled**



To investigate the effect of non-linearity, we disabled the thermal noise of the PIN (which is the dominant noise in this design) and repeated the simulation. The results are shown in [Figure 3](#). This figure shows that after about 14 dBm launch power (as predicted), non-linearity becomes an issue and Q factor starts to decay. From these figures, we can conclude that the limiting factor below the 18 dBm region is mainly thermal noise, whereas above 14 dBm, it is non-linearity. Therefore, non-linearity is an important factor in the design of transparent optical metro networks without amplification.

**Figure 3 Q factor versus average received power at node 4 when no amplifier is used and thermal noise of the PIN is disabled**



We have also seen that a simple power budgeting is not enough to design a transparent ring network. However, you need to run a whole detailed simulation to see the effects of fiber non-linearities on the system performance.



## Design with Lumped Amplification

In this example, we will consider design of a transparent ring network with lumped amplification.

Metro ring networks have a more dynamic traffic pattern than most long-haul networks. In these types of configurations, we need to consider:

- all the optical power variations resulting from wavelength dependent losses in fibers
- wavelength dependent gain in amplifiers
- channel to channel insertion loss variations in multiplexers/demultiplexers

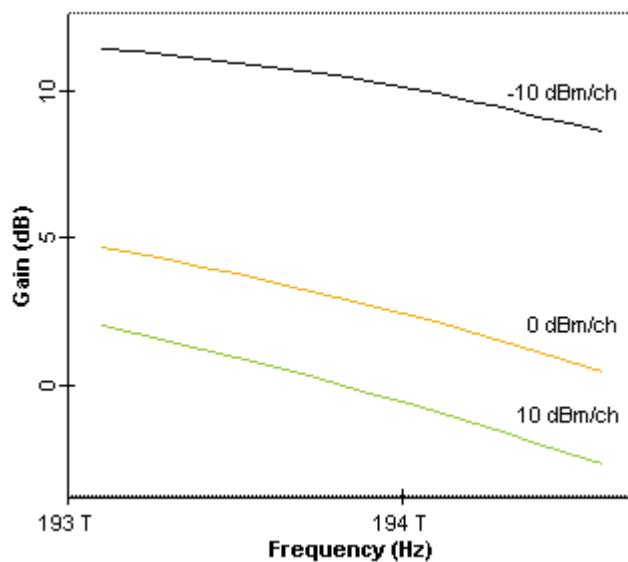
These optical degradations accumulate along the links and may increase very quickly, depending on the path followed by the wavelength. Due to dynamic nature of the network, only proper dynamic power level management can reduce them. Typical values for the loss elements can be found in “Design without amplification” on page 369.

Let us first investigate optical amplifiers.

### Optical Amplifier

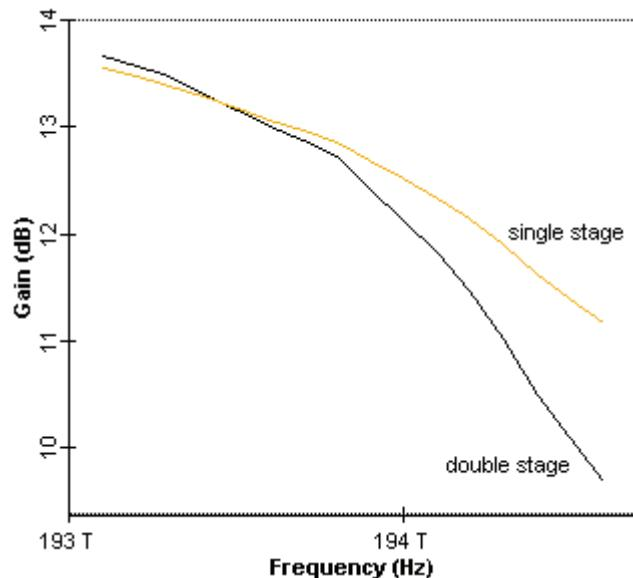
Gain and gain tilt of optical amplifiers changes with the input power. This can be seen in [Figure 1](#) for EDFA (length of the fiber is 4 m, pump power at 980 nm is 100 mW). (See gain variation of EDFA.osd.) When the span losses of each span in the ring are different, the input power of each amplifier will be different. Depending on the path of the signal, each communication link between two nodes will experience different amplification. Furthermore, amplifier tilt can accumulate depending on the path followed. To eliminate this effect, pump control, variable attenuator at the input, or gain tilt compensating amplifier/filters can be used.

**Figure 1 Value and shape of optical amplifiers**

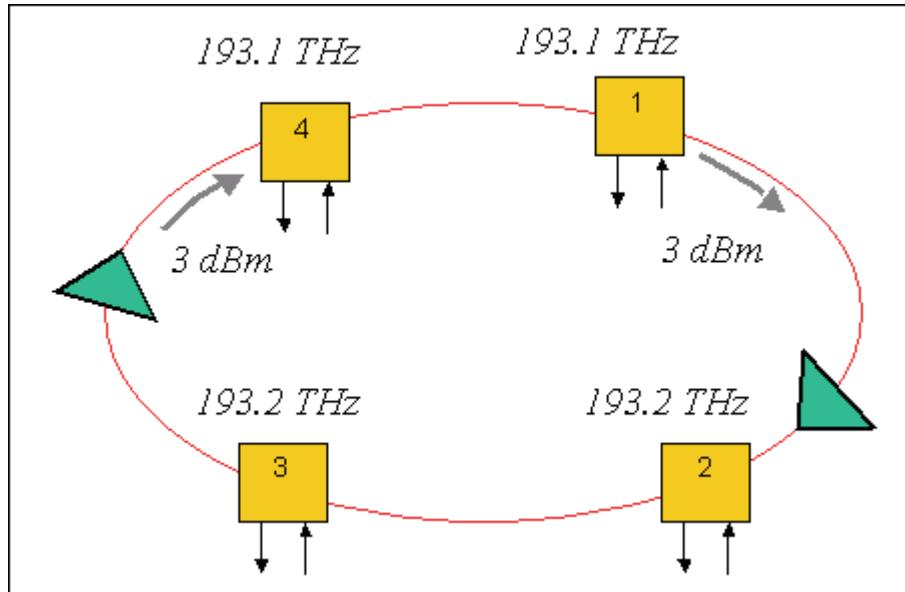


[Figure 2](#) shows the results of two cascaded EDFAs (length of the fiber is 4 m, pump power at 980 nm is 35 mW, input power 17.3 dBm/channel or -133 dBm total power). (See gain variation of cascaded EDFAs.osd.) Here, we consider a 16.4 dB loss between amplifiers to model the total span and node loss. It is clear from this figure that tilt of the two-stage amplifier is increased. A channel near 193 THz will see a gain of approximately 14 dB after a two node pass, whereas it is approximately 12 dB for a channel at 194 THz. Therefore, this effect may be an issue for a 100 GHz separated 10 channel system, even though each channel passes through the same number of amplifiers.

**Figure 2 Gain profile of one and two cascaded amplifiers**



A typical WDM metro ring at 2.5 Gbps, with a 200 km circumference and four intermediate fixed OADMs, is shown in [Figure 3](#). In this network, node 1 and 4 communicate on channel 1, whereas node 2 and 3 communicate on channel 2, as in the previous example. The project is found in the `Optical power level management in metro networks lumped amplification.osd` file

**Figure 3** Ring network layout with two amplifiers

Assuming a launch power of 3 dBm per channel, the amount of amplification needed in the ring is

$$G_{\text{required}} = -(3 - 4 \times 0.25 \times 50 - 4 \times 3.8 - (-23) - 3) = 42.2 \text{dB}$$

This gain can be obtained by using two amplifiers as shown in [Figure 3](#). In this configuration, two amplifiers with 15 dB gain are placed just before node 2 and node 4. Note that required gain is higher than the gain target value for metro EDFAs (see [Table 1](#)). Therefore, a single amplifier configuration is not practical for metro applications. Keep in mind that even though this amplifier design gives sufficient performance, scalability of this configuration will be complicated.

**Table 1** Typical values for amplifiers

Name	Metro target
<b>Gain</b>	10 to 20 dB
<b>Power</b>	10 to 15 dBm
<b>Noise figure</b>	6 dB
<b>Gain flatness</b>	1 dB

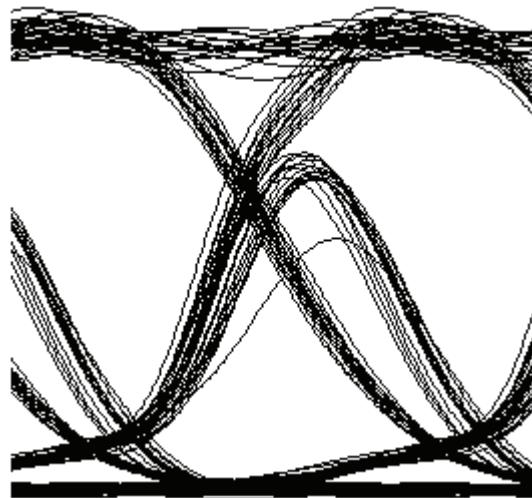
[Figure 4](#) shows Q factor versus received average power for two-amplifier configurations.

**Figure 4 Measured signal power and OSNR**

Frequency (THz)	Signal Power (dBm)	Noise Power (dBm)	OSNR (dB)
193.1	-19.169929	-40.899899	21.72997
193.2	-92.554518	-100	7.4454824

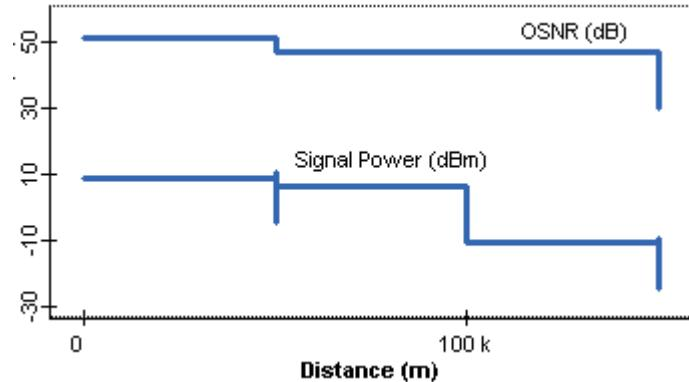
This figure shows about -11 dBm average received power. Q factor is maximum and below 4.5. [Figure 5](#) shows the eye diagram for this case. [Figure 6](#), on the other hand, shows the trace of OSNR and signal power as obtained by using Trace Paths tool.

**Figure 5 Eye diagram at node 4 when two amplifiers with 15 dB gain each are inserted before node 4 and node 2**



[Figure 6](#) shows the eye diagram when the gain of the two amplifiers are 25 dB each. In this case, the Q factor is 38, and OSNR is approximately 31 dB.

Frequency (THz)	Signal Power (dBm)	Noise Power (dBm)	OSNR (dB)
193.1	0.82416429	-30.229305	31.053469
193.2	-82.554598	-100	17.445402

**Figure 6 Trace of the OSNR and power from node 1 to node 4**

These results show that this configuration provides a better system performance compared to design without amplification. Q factor that we can get from this configuration is about 4.5, due to unoptimized add/drop multiplexers and electrical filters. System performance can be further improved by carefully adjusting the transmitter and filter parameters.

Even though this configuration may give satisfactory performance for a static configuration, it will not allow addition of a new node or complex wavelength routing schemes where one signal may follow different paths depending on the routing.

## Unity Gain Design

In this example we will show an alternative approach, the “unity gain” approach, in which each amplifier matches the loss of one.

In optical ring topology, we need to consider all the optical power variations resulting from

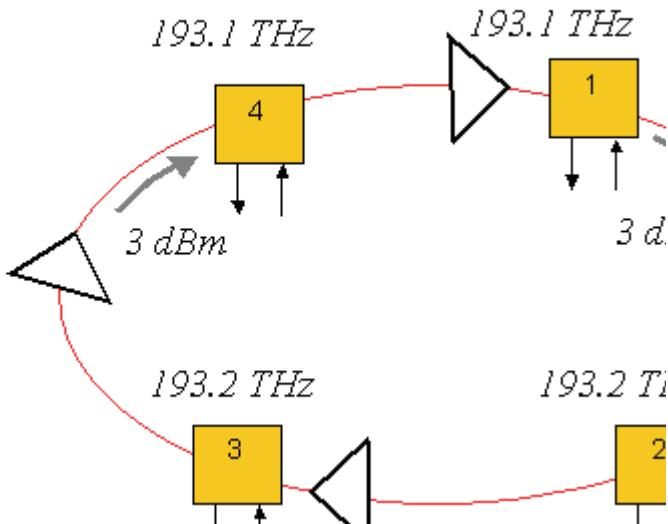
- wavelength dependent loss in the fiber
- wavelength dependent gain in amplifiers
- channel to channel insertion loss variation in the multiplexers/demultiplexers

These optical degradations accumulate along the links and may increase very rapidly depending on the path followed by the wavelength. Due to the dynamic nature of the network, only proper dynamic power level management can reduce them. In these previous two sections, we have seen that design without amplification is not a good option, because required high power levels can trigger fiber nonlinearity.

For this approach, an amplifier with a modest gain of 17.3 dB at every node can be used. This approach is only economically feasible with a low cost-compact optical amplifier, but it is the best one considering the dynamic routing in the network.

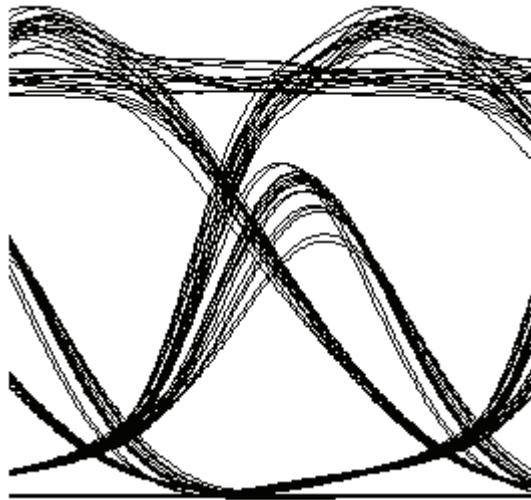
Let us now consider a typical WDM metro ring at 2.5 Gbps with 200 km in circumference with four intermediate fixed OADMs as shown in Figure 1. In this network, node 1 and 4 communicate on channel 1 whereas node 2 and 3 communicate on channel 2, as in the previous cases. Loss of each span and node is compensated at the node following the span. The gain of each amplifier is 17.3 dB. The project is found in the [Optical power level management in metro networks unity gain.osd](#) file. This configuration is scalable, since regardless of the path followed by a certain wavelength, the power is always balanced.

**Figure 1** Ring network layout with amplifier at each node

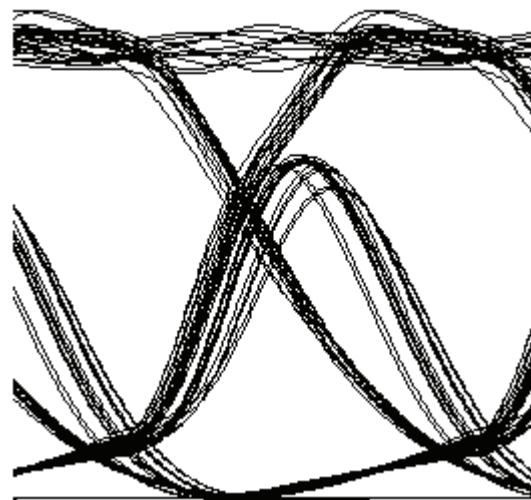


Eye diagrams of channel 1 at node 4 is shown in [Figure 2](#), where received average power is 0 dBm. [Figure 3](#) shows the eye diagram at node 4 when average received power is 12 dBm. [Figure 4](#) shows Q factor versus received average signal power.

**Figure 2** Eye diagram of channel 1 at node 4 when received average power is about 0 dBm and bit rate is 2.5 Gbps



**Figure 3** Eye diagram of channel 1 at node 4 when received average power is about 12 dBm and bit rate is 2.5 Gbps



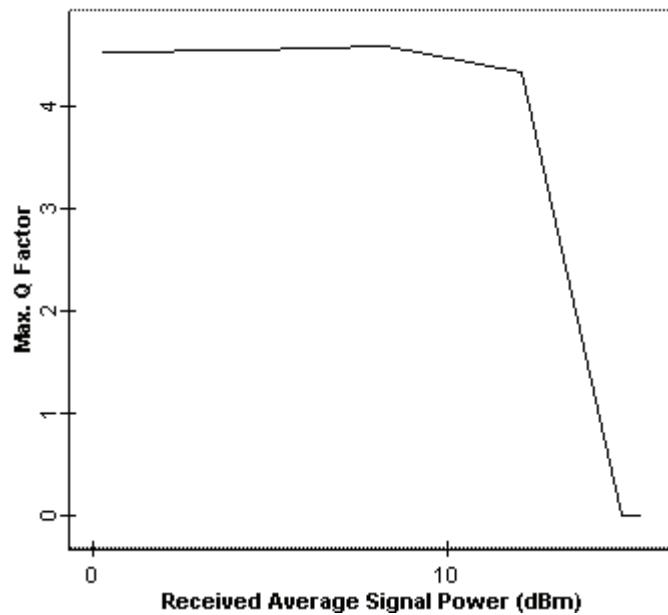
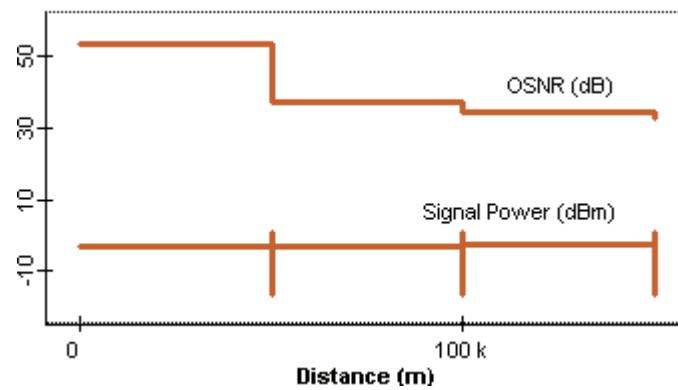
**Figure 4 Q factor versus average received power at node 4 when bit rate is 2.5 Gbps**

Figure 6 shows the trace of OSNR and signal power as obtained by using Trace Path tool. This figure shows that the signal power is balanced throughout the light path for channel 1, at 193.1 THz. Of course, this will increase the scalability of the optical metro network. Moreover, dynamic wavelength routing can be easily implemented in this type of network. Also note that this configuration is less sensitive to power changes. This is a result of balanced power throughout the network.

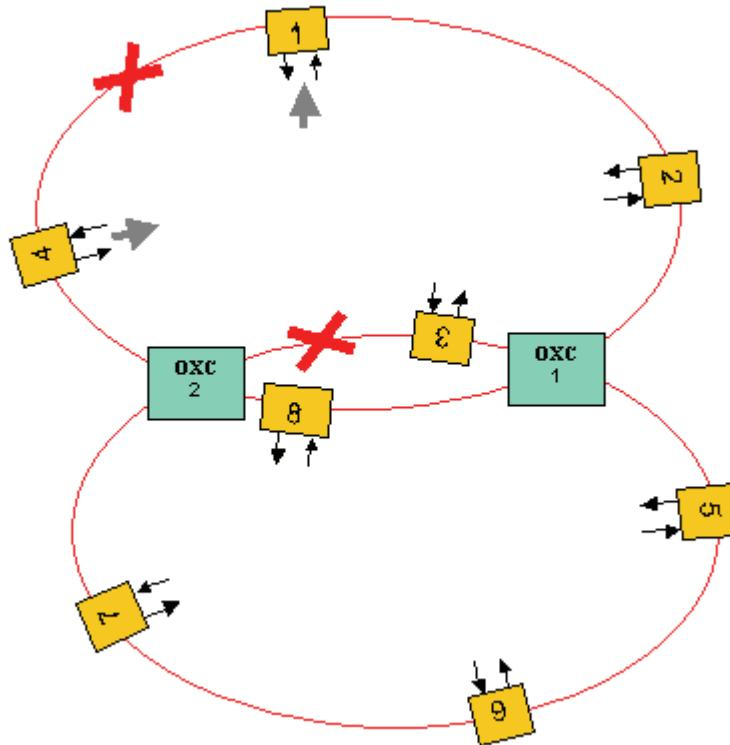
**Figure 5 Trace of OSNR/power from node 1 to node 4 when received signal power is about 0 dBm**

## Considering the Non-Ideal Characteristics of EDFAs

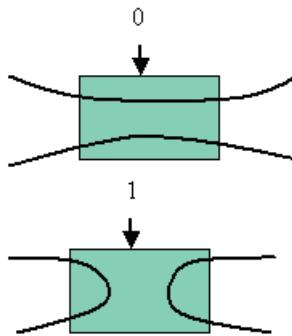
In this example, we will consider an all optical two-ring network connected with OXCs and investigate the effects of amplifier control mode to network performance.

We will consider a two-ring system as shown in [Figure 1](#). The project is found in the [Considering nonideal characteristics of EDFA\\_power.osd](#) file.

**Figure 1** Two interconnected ring network layout

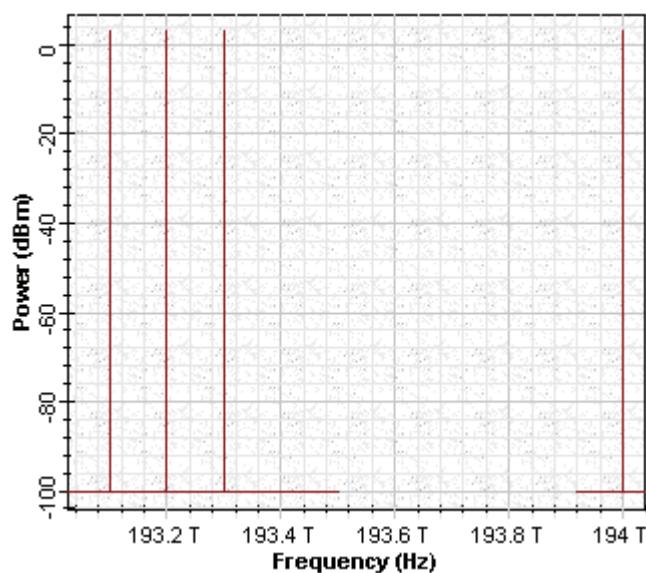


In this system, each ring can be used as a protection path for the other. A functional diagram of OXCs is shown in [Figure 2](#).

**Figure 2 Functional diagram of OXCs**

Each span between nodes is made up of a single mode fiber and an EDFA (to compensate the span loss). In this project, we used Black Box EDFA models. For the sake of simplification, we have used the Directly Modulated Laser Measured model for transmitters and set chirp-related factors to zero. Therefore, we neglect any system penalty related to initial chirp on the signal.

Chirp-related issues will be discussed in the Negative Dispersion Fiber for Metro Networks tutorial. In this network, node 1 communicates with node 4 on channel 1, node 5 communicates with node 7 on channel 2, node 6 communicates with node 8 on channel 3, and node 2 communicates with node 3 on channel 4. The frequency spectrum of the channels is shown in [Figure 3](#). Node 1 can send data following a path passing through 1, 2, OXC 1, 3, OXC 2, 4. This path requires 4 amplifications.

**Figure 3 Power spectrum of the 4 channel-8 node ring network**

For this example, we will presume that there is a fiber break between OXC 1 and OXC 2 or a problem at node 3, while node 1 wants to send data to node 4. Depending on the switching of OXC 1 and OXC 2, there is more than one path that the signal on channel 1 can follow. Let us assume that node 1 communicates with node 4 following the path passing through 1, 2, OXC 1, 5, 6, 7, OXC 2, 4, by using the second ring as the recovery path. This path will require 6 amplifications.

Because of the dynamic nature of the metro network, total power at the input of each amplifier will be different depending on the wavelength routing. Moreover, the gain spectrum is not flat, but tilted, so it will require some extra planning to balance the power through the network.

We first set all the amplifiers to work in power control mode and set the power on the output amplifiers to 6 dBm. Considering each ring individually, this seems to be a good choice, where the power of each channel is kept at a certain level. Interaction between the rings, on the other hand, will influence the performance of the amplifiers. This is shown in [Figure 4](#) and [Figure 5](#).

These two figures show the eye diagrams for the two different paths, before and after the fiber break, respectively.

**Figure 4** Eye diagram of the signal at node 4 when the first path (node 1, node 2, OXC 1, node 3, OXC node 2, and node 4) is followed

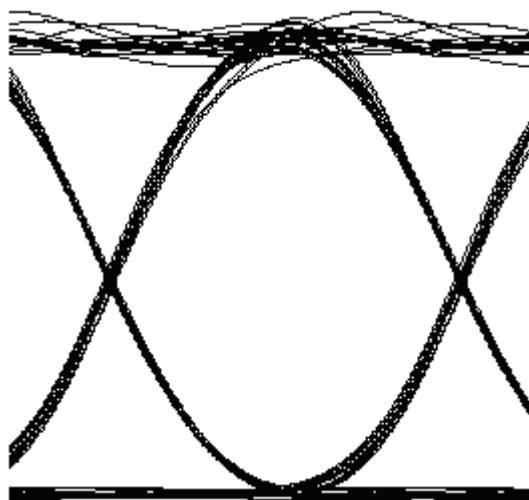
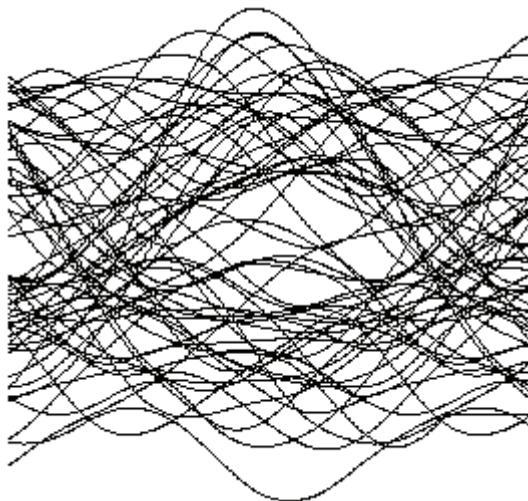


**Figure 5 Eye diagram of the signal at node 4 when the second path (node 1, node 2, OXC 1, node 5, node 6, node 7, OXC node 2, and node 4) is followed after a fiber break**



This example shows that due to dynamic nature of metro network, a careful and intelligent power budget planning and control should be exercised. Several strategies can be followed to solve this problem. Let us assume that the gains of the EDFA are flattened and stabilized with respect to input power change. To model this condition, we set the EDFA to work in gain control mode with 17.3 dB gain. The project is found in the [Considering nonideal characteristics of EDFA\\_gain.osd](#) file.

Simulation results are shown in [Figure 6](#) and [Figure 7](#), before and after the fiber break, respectively. These figures show that we can obtain a better performance for a dynamic metro network when gain-controlled amplifiers are used. We note an extra eye closure in [Figure 7](#). This is partly related to lower SNR at node 4 when the signal follows the protection path, since there are two extra amplifiers on this path. Moreover, there will be more non-linear interaction between channels due to extra fibers that signal passes and extra channels that increase the total power in the fiber.

The results show that gain control of amplifiers is important for metro applications, and dynamic routing can be done easily without any problem when the unity gain approach is used (see “Unity Gain Design” on page 380).



Figure 6 Eye diagram of the signal at node 4 when the first path (node 1, node 2, OXC 1, node 3, OXC node 2, and node 4) is followed and gain-controlled amplifiers are used

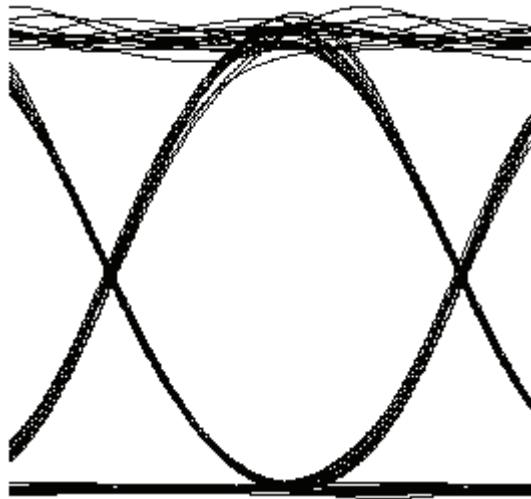
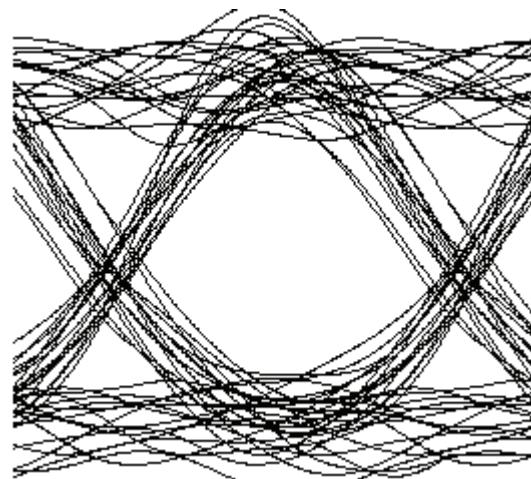


Figure 7 Eye diagram of the signal at node 4 when the second path (node 1, node 2, OXC 1, node 5, node 6, node 7, OXC node 2, and node 4) after a fiber break is followed and gain-controlled amplifiers are used



## References:

- [1] K. M. Sivalingam and S. Subramaniam, Optical WDM Networks: Principles and Practice, Kluwer Academic Publishers, 2001.
- [2] Sidney Shiba et. al., "Optical Power Level Management in Metro Networks", NFOEC'01, 2001.
- [3] R. Ramaswami and K.N. Sivarajan, Optical Networks: A practical Perspective, Morgan Kaufmann, 1998.
- [4] Tarek S. El-Bawab et. al., "Design considerations for transmission systems in optical metropolitan networks", Opt. Fib. Tech. 63, p. 213, 2000.
- [5] I. Tomkos et. al., Filter concatenation in metropolitan optical networks utilizing directly modulated lasers", IEEE Photon. Tech. Lett. 13, p. 1023, 2001.



# Migrating to 10Gbps in Metro networks

---

In this example, we will investigate the issues at high data bit rate, particularly 10 Gbps (OC-192) systems in metro area ring networks. At higher bit rates, in addition to loss compensation, we may also need to consider the chromatic dispersion compensation. Different options related to dispersion and initial chirp will be investigated.

For this case, the receiver sensitivity is -16 dBm which reduces the allowable loss to  $L_{allowable} = 3 - (-16) = 13 \text{ dB}$ . Assuming a power of 3 dBm per channel, the amount of amplification needed in the ring is  $G_{required} = -(3 \times 13.5 - 3 \times 3.8 - (-16) - 3) = 35.9 \text{ dB}$ . We can again use the unity gain segment approach for power compensation. By using this approach, migration from 2.5 Gbps to 10 Gbps is easily done in terms of power budgeting since the total loss is not changed, even though the allowable loss is changed. In this case, the received power will be well above the receiver sensitivity. See “Unity Gain Design” on page 380.

In the case of directly modulated DFB lasers, the limiting transmission distance is

$$L < \frac{1}{4B|D|\lambda_2}$$

where  $\lambda_2$  is root-mean-square spectral width, with a typical value of 0.15 nm for  $D=16\text{ps}/(\text{km-nm})$  and 2.5 Gbps, and  $L \approx 42\text{km}$ .

For externally modulated sources, the limiting transmission distance is

$$L < \frac{2\pi c}{16|D|\lambda^2 B^2}$$

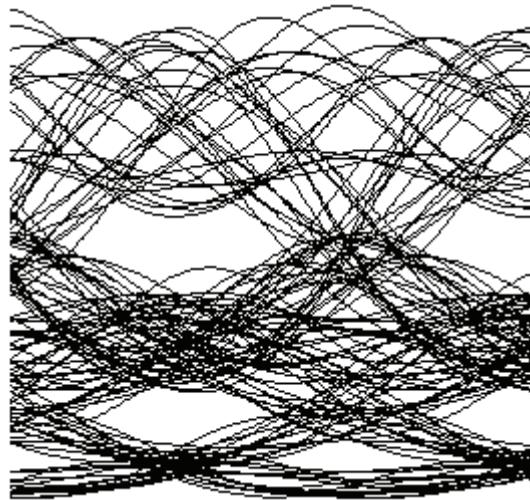
with  $D=16\text{ps}/(\text{km-nm})$  and 2.5 Gbps,  $L \approx 500\text{km}$ . Therefore, Group Velocity Dispersion (GVD) is not a limiting effect for a 2.5 Gbps communications network.

## No dispersion compensation

At high bit rates, GVD may become a limiting factor for the transmission distance. When the bit rate increased to 10 Gbps, GVD-limited transmission distance drops to 30 km for externally modulated sources and to 10.5 km for directly modulated sources. [Figure 1](#) shows the eye diagram when the bit rate is 10 Gbps and transmitter power is 3 dBm/channel and directly modulated sources are used. Ever increasing transmitter power does not open the eye. In fact, the shape of the eye shows that pulse direction distortion is related to dispersion. In this example, we have used the unity gain segment approach, which means that loss in each fiber span and node is compensated immediately at the following node. This project is given in [Migrating to 10 Gbps no dispersion compensation.osd](#) file.

For simplicity, in this project we have used the “Directly Modulated Laser Measured” model for directly modulated sources and set the alpha parameter to -5.



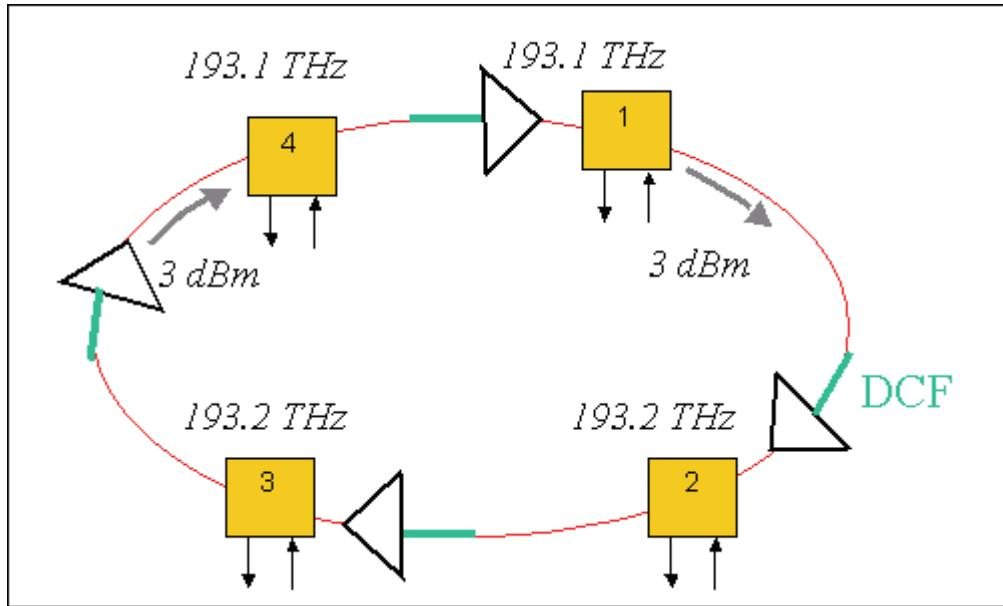
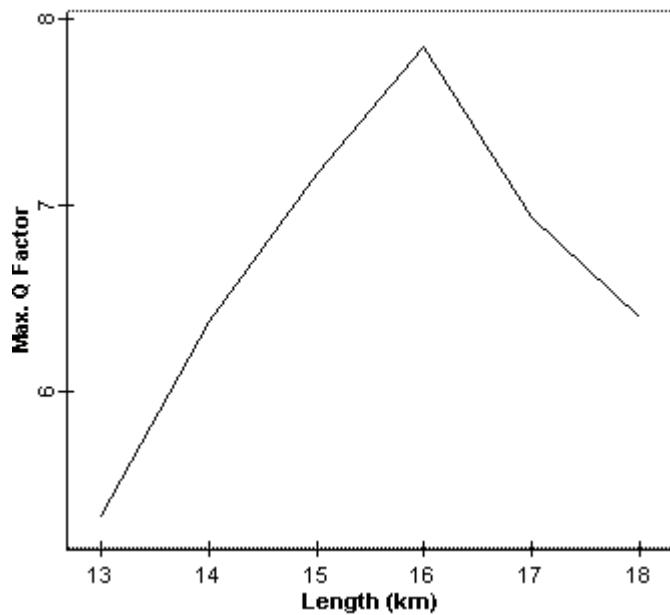
**Figure 1 Eye diagram of channel 1 at node 4 when the transmitter power is 3 dBm and bit rate is 10 Gbps**

Therefore, at 10 Gbps bit rate, you have to use dispersion compensation. Total dispersion per 50 km span is around  $16 \times 50 = 800 \text{ ps / nm}$ . This will require 10.25 km of dispersion compensating fiber (DCF) with  $D = -80 \text{ ps / nm / km}$  for each fiber span. There are several avenues to compensate for the accumulated dispersion that we will investigate in the following sections.

### "Per span" dispersion compensation

DCF can be used after each span, or total accumulated dispersion can be compensated at a certain point. To preserve the scalability of the network, and keeping in mind the dynamic structure of the metro traffic, it seems to be the best choice to distribute the dispersion compensation to every node. This will also ensure that dispersion experienced by dynamically routed signals will be compensated properly. The project is found in the [Migrating to 10 Gbps dispersion compensation at each node.osd](#) file. [Figure 2](#) shows the network layout when unity gain approach and per node dispersion compensation is used.

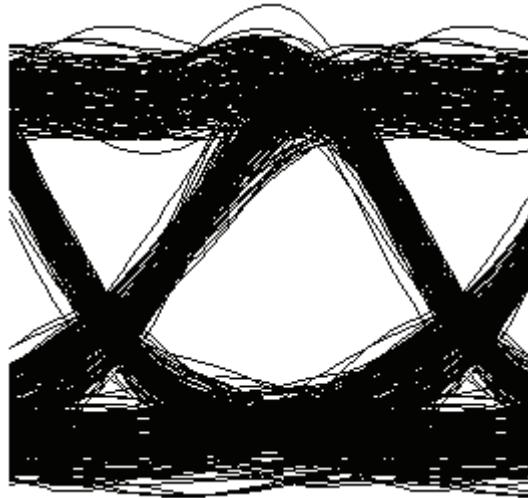
In this project, we again used directly modulated transmitters as described in previous sections. To find the optimum length for dispersion compensation, we swept the length of the DCFs from 13 km to 18 km. [Figure 4](#) shows the simulation results in terms of Q factor when transmitter power is 3 dBm. As you can see from this figure, maximum Q factor is observed when the length of DCFs is about 18 km. You can also identify from this figure that there is  $\pm 2$  km of tolerance for each DCF for a minimum Q factor of 6. [Figure 5](#) shows the eye diagram when maximum Q factor is observed.

**Figure 2** Ring network layout when unity gain approach and per span dispersion compensation is used**Figure 3** Q factor vs. DCF length when directly modulated transmitter is used

To investigate the effect of transmitter type, we have replaced directly modulated sources with externally modulated ones. The project is given in the **Migrating to 10 Gbps dispersion compensation at each nodeEM.osd** file. The results are shown in **Figure 5** in terms of Q factor for different DCF lengths. Maximum Q factor is observed when the length of DCF is about 14 km. Compared to the directly modulated transmitter case, this curve is broader and dispersion compensation

tolerance is higher; 14 km for this case, which is related to initial chirp on the signal. The influence of the initial chirp on system performance will be investigated in the [Negative dispersion fiber for Metro networks](#).

**Figure 4** Eye diagram at node 4 when per span dispersion compensation is used and DCF length is 16 km

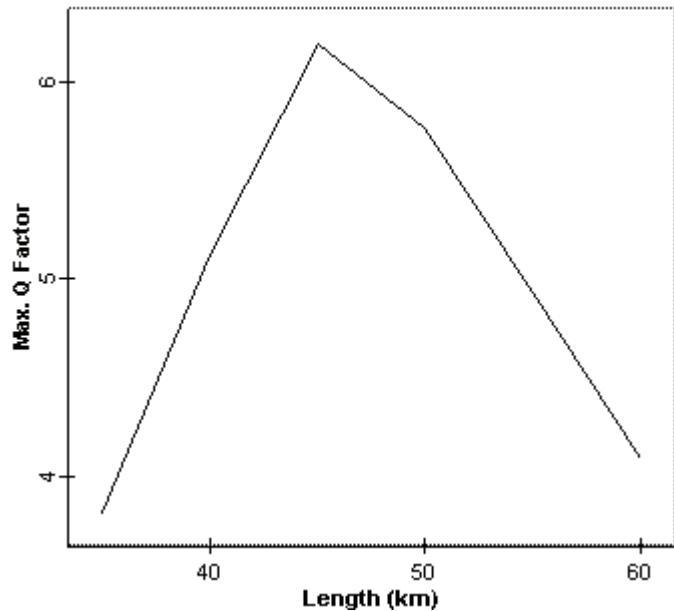


### "Lumped" dispersion compensation

In the "lumped" dispersion compensation case, one DCF and an extra amplifier is inserted just before node 2 to compensate the total dispersion. This project is found in the [Migrating to 10 Gbps lumped dispersion compensation.osd](#) file. [Figure 5](#) shows Q factor versus DCF length at node 4 when directly modulated laser is used and transmitter power is 3 dBm. As can be seen from this figure, this configuration definitely improves the network performance compared to the uncompensated case, but is worse than the case with distributed compensation.

In the case of lumped dispersion compensation, DCF length tolerance is about  $\pm 1.5$  where maximum Q factor is observed, DCF is 45 km, and maximum Q factor is about 6.2. Furthermore, this type of dispersion compensation is not suitable for metro networks in which the wavelength routing path cannot be estimated. For example, consider the path recovery schemes in a much more complex network with more than one ring. Depending on the structure of the network, one particular wavelength can follow a path that does not pass over the single dispersion compensation fiber in the network.



**Figure 5 Q factor versus DCF length at node 4 when "lumped" dispersion compensation is used**

## References

- [1] G. P. Agrawal, Fiber-Optic Communication Systems, Wiley-Interscience, 1997.
- [2] R. Ramaswami and K. N. Sivarajan, Optical Networks: A practical Perspective, Morgan Kaufmann, 1998.

**Notes:**

# Negative dispersion fiber for Metro networks

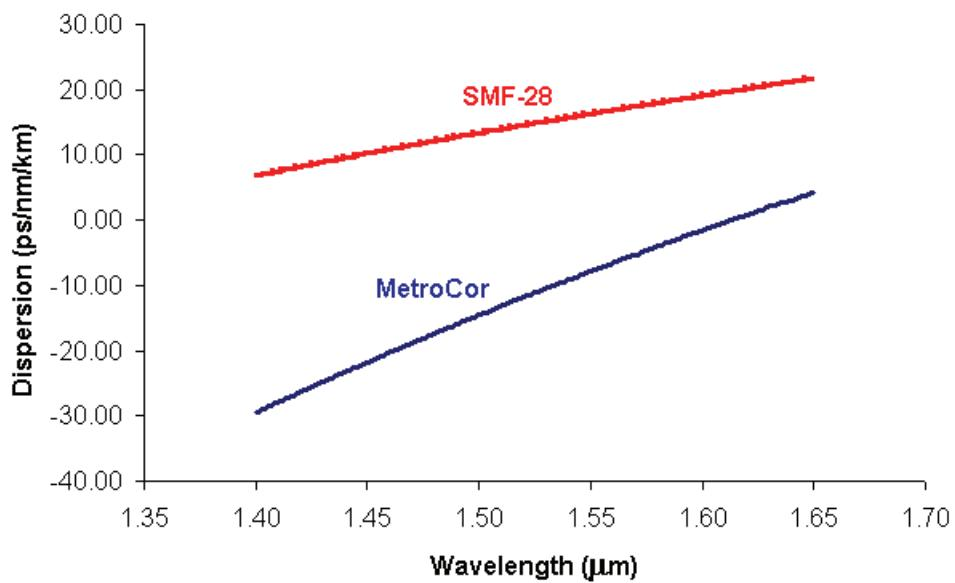
---

In this example, we compare two types of fibers, Corning's MetroCor and SMF-28 fibers for metro network applications. MetroCor Fiber has a negative dispersion, whereas SMF-28 has a positive dispersion in the EDFA bands. Dispersion characteristics of these two fibers are shown in [Figure 1](#). For metro applications, directly modulated lasers (DMLs) are preferred because of their low cost, but they have a higher chirp compared to externally modulated lasers and this results in more penalty due to dispersion when standard positive dispersion SMF is used.

Typically, DMLs are rated for 100 km transmission distances over SMF-28 fiber with less than 2 dB dispersion-induced penalty. One option to overcome this effect is to use a fiber with negative dispersion that can take advantage of the positive chirp characteristics of DMLs to enhance transmission distances.

MetroCor fiber has a zero dispersion wavelength near 1630 to 1640 nm. As a result, this fiber has an average dispersion of about -3 ps/nm/km in L-band and about -8 ps/nm/km in C-band. The loss, the dispersion slope and effective area are typical of other conventional NZ-DSF fibers.

**Figure 1** Dispersion characteristics of MetroCor and SMF-28 fibers



## Modeling Directly Modulated Lasers

We will first investigate DMLs that we are going to use in our simulations. We have modeled two types of DMLs by using our Laser Rate Equations model. One is strongly adiabatic chirp dominated (DML-1) and the other one is strongly transient chirp dominated (DML-2). The model parameters are extracted from the measured parameters of [1]. Laser parameters are given in [Figure 2](#) and [Figure 3](#).

**Figure 2 Extracted parameter values of DML-1**

Name	Value	Units
<b>Active layer volume</b>	5.8e-012	cm^3
<b>Quantum efficiency</b>	0.19	
<b>Spontaneous emission factor</b>	2.34e-005	
<b>Gain compression coefficient</b>	5e-018	cm^3
<b>Carrier density at transparency</b>	1e+017	cm^-3
<b>Differential gain coefficient</b>	5.12e-017	cm^2
<b>Group velocity</b>	8500000000	cm/s
<b>Linewidth enhancement factor</b>	2.2	
<b>Mode confinement factor</b>	0.4	
<b>Carrier lifetime</b>	3.74e-010	s
<b>Photon lifetime</b>	2.91e-012	s

**Figure 3 Extracted parameter values of DML-2**

Name	Value	Units
<b>Active layer volume</b>	5.8e-012	cm^3
<b>Quantum efficiency</b>	0.19	
<b>Spontaneous emission factor</b>	2.34e-005	
<b>Gain compression coefficient</b>	5e-018	cm^3
<b>Carrier density at transparency</b>	1e+017	cm^-3
<b>Differential gain coefficient</b>	5.12e-017	cm^2
<b>Group velocity</b>	8500000000	cm/s
<b>Linewidth enhancement factor</b>	2.2	
<b>Mode confinement factor</b>	0.4	
<b>Carrier lifetime</b>	3.74e-010	s
<b>Photon lifetime</b>	2.91e-012	s

## Transmission Characteristics of DMLs

To understand the chirp characteristics of directly modulated lasers to address the dispersion-induced deformation on the transmitted signals at 2.5 Gbps, we performed a series of simulations. We also compared our simulation results with the results of [1] to validate our model. The project is shown in \*\*figure 4.

This project is found in the `Tomkos_JSTQE_May_June2001.osd` file. This project contains four different layouts. The first two layouts use DML-1 and the last two layouts use DML-2. Layout 1 and Layout 3 use SMF-28 fiber whereas Layout 2 and Layout 4 use MetroCor fiber. As in [1], attenuations of fibers are disabled to isolate the



effect of chirp and dispersion. Rise and fall times of the NRZ electrical pulse are 0.5 bit and exponential shapes are selected.

**Figure 4** Project layout to investigate the effect of laser chirp on transmission performance

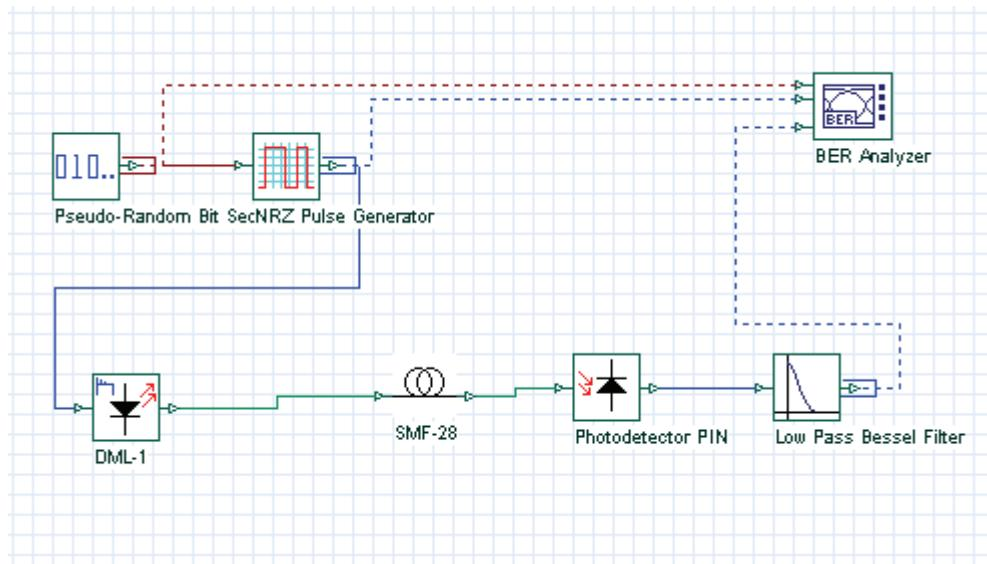


[Figure 5](#) shows the received eye diagram for the case of an adiabatic chirp dominated transmitter (DML-1) after transmitting over 300 km of SMF-28 fiber. The received eye is deformed but not completely closed.

[Figure 6](#) on the other hand, shows the received eye diagram for the case of an adiabatic chirp dominated transmitter (DML-1) after transmitting over 300 km of MetroCor fiber. In this case, deformation is smaller because MetroCor fiber has a small absolute value of dispersion that is less than half of that for SMF-28.

[Figure 7](#) shows the received eye diagram for the case of a transient chirp dominated transmitter (DML-2) after transmitting over 300 km of SMF-28 fiber. In this case, the received eye pattern is severely closed due to significant intersymbol interference.

[Figure 8](#), on the other hand, shows the received eye diagram for the case of a transient chirp dominated transmitter (DML-2) after transmitting over 300 km of MetroCor fiber. The only noticeable effect in this case is the formation of some peaks on the top of ones. The received eye is completely open. These simulation results are in perfect agreement with the results of [1].

Figure 5 Eye diagram at the receiver side after 300 km propagation on SMF-28 fiber when DML-1 is used

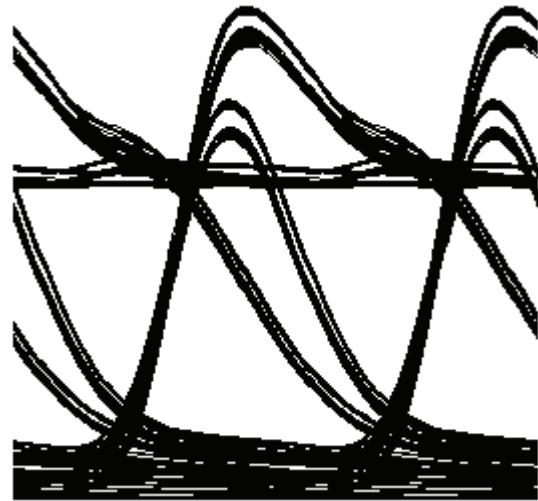
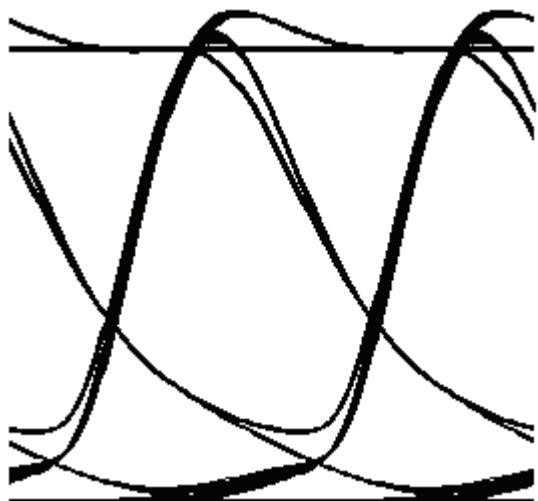
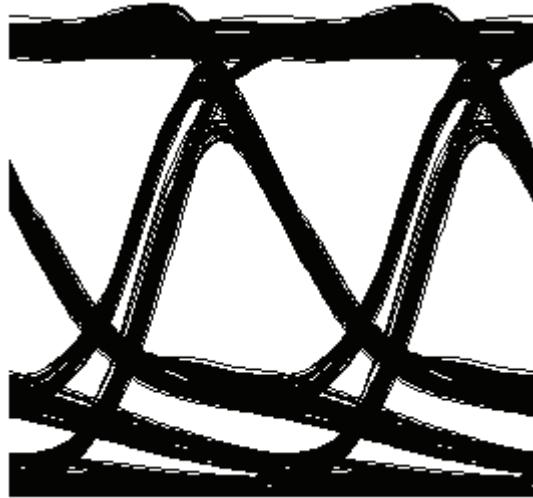


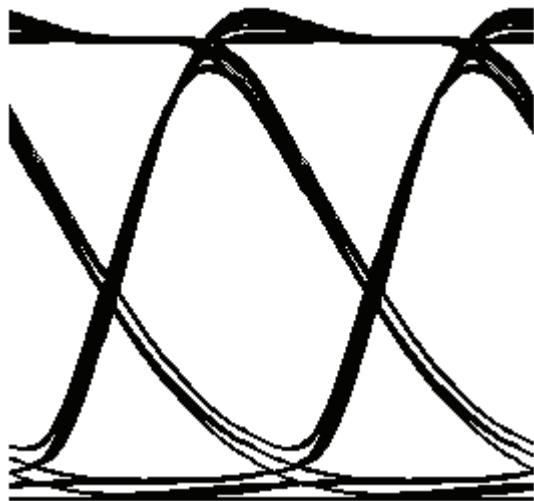
Figure 6 Eye diagram at the receiver side after 300 km propagation on MetroCor fiber when DML-1 is used



**Figure 7** Eye diagram at the receiver side after 300 km propagation on SMF-28 fiber when DML-2 is used



**Figure 8** Eye diagram at the receiver side after 300 km propagation on MetroCor fiber when DML-2 is used



## Transmission at higher bit rates

In this section, we will show the simulation results at 10 Gbps bit rate. The project is found in `Tomkos_JSTQE_May_June2001_10Gbps.osd` file. Here we have used the same DML-1 that we used in previous sections for 2.5 Gbps transmission. The signal propagates over 120 km SMF-28 or MetroCor fiber. The extinction ratio of the transmitter is set to about 9 dB, in this case. [Figure 9](#) and [Figure 10](#) show the eye diagrams after 120 km propagation over either SMF-28 or MetroCor fiber, respectively. When MetroCor is used, the eye is still open after 120 km of propagation.

Figure 9 Eye diagram at the receiver side after 120 km propagation at 10 Gbps on SMF-28 fiber

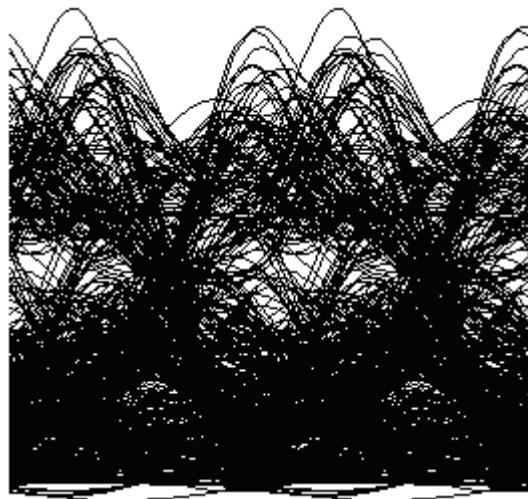
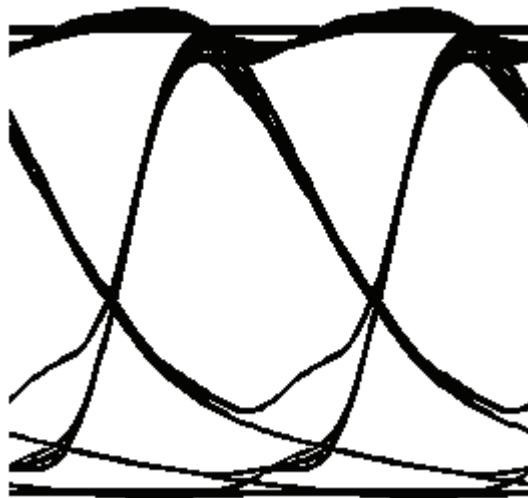


Figure 10 Eye diagram at the receiver side after 120 km propagation at 10 Gbps on MetroCor fiber



### 32 Channel DWDM system simulation at 2.5 Gbps

In this section, we reproduce the experimental results of [1] for the 32 channel DWDM system at 2.5 Gbps. The project is found in the `32 Channel DWDM Metro.osd` file. The 32 channels are between 1533.5 and 1558.2 nm with 100 GHz spacing on the ITU-T and are multiplexed.

In this design, DMLs are used. Transmitted power is about -3 dB/channel. Multiplexed channels are propagated either over 300 km of SMF-28 fiber or 300 km of MetroCor fiber. EDFA with 18 dB gain and 4 dB noise are inserted after every 100 km of fiber. The received signal is filtered to get channel 21 and channel 30.



The eye diagrams for these channels for MetroCor fiber simulation are shown in [Figure 11](#) and [Figure 12](#). For these channels, Q is about 10 dB as defined  $10\log(Q)$ .

[Figure 13](#) and [Figure 14](#), on the other hand, show the eye diagrams for these channels for SMF-28 fiber simulation. For these channels, Q is about 5 dB, which is below 9 dB. A Q of 9 dB corresponds to a BER of  $10^{-15}$ . These results are in perfect agreement with the experimental findings of [1].

**Figure 11** Eye diagram of channel 21 at the receiver side after 300 km propagation at 2.5 Gbps over MetroCor fiber

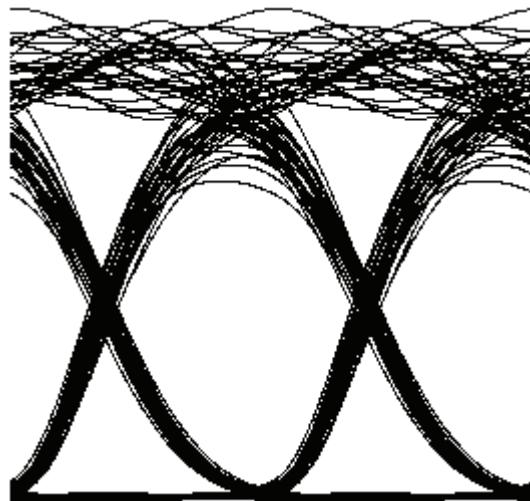


**Figure 12** Eye diagram of channel 30 at the receiver side after 300 km propagation at 2.5 Gbps over MetroCor fiber

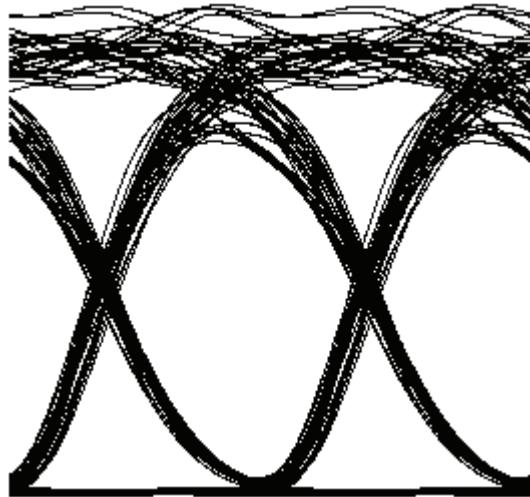


Figure 13 Eye diagram of channel 21 at the receiver side after 300 km propagation at 2.5 Gbps over SMF-28 fiber

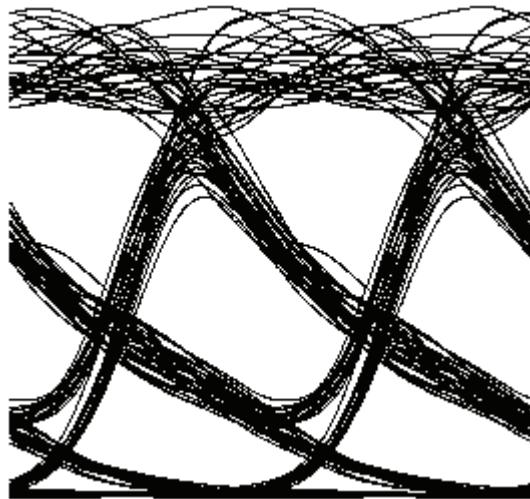
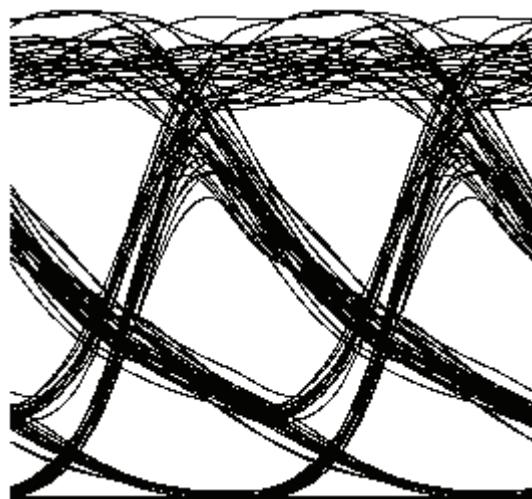


Figure 14 Eye diagram of channel 30 at the receiver side after 300 km propagation at 2.5 Gbps over SMF-28 fiber



## References

- [1] I. Tomkos et. al., "Demonstration of negative dispersion fibers for DWDM metropolitan networks", IEEE J. of Select. Top. in Quan. Elec. 7, p.439, 2001.
- [2] Chris Kennedy et. al., "The performance of negative dispersion fiber at 10 GBps and significance of externally and directly modulated lasers", NFOEC'01, 2001.
- [3] David Culverhouse et. al., "Corning MetroCor Fiber and its Application in Metropolitan Networks", Corning's White Paper WP5078.
- [4] G. P. Agrawal, Nonlinear Fiber Optics, Second Edition, Academic Press, 1995.

# Interchannel crosstalk in Metro networks

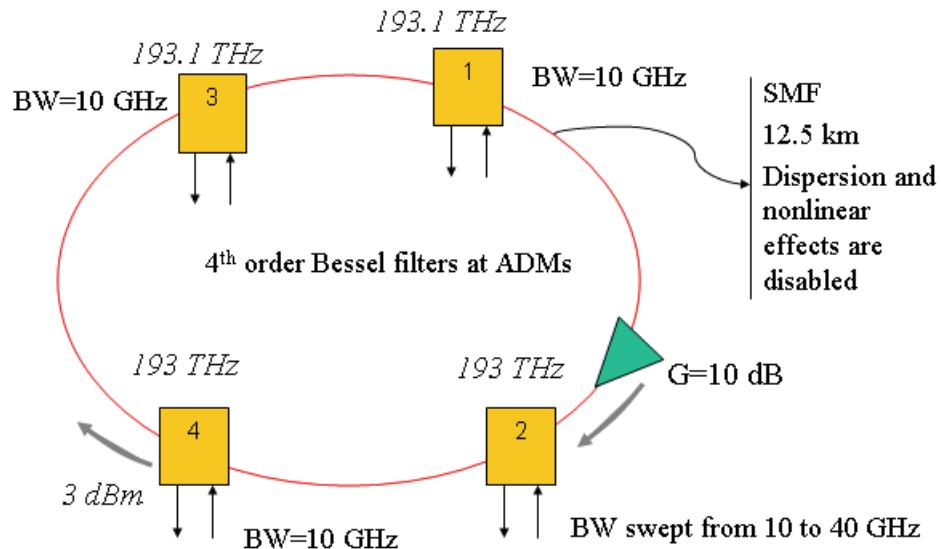
---

Inter-channel cross-talk can arise from a variety of sources. These sources may include [1]:

- An optical filter or ADM that selects one channel (drop) and passes others over the network
- An optical switch switching between different wavelengths creates cross-talk from the imperfect isolation between the switch ports
- Other cross-talk types include amplifier induced, router induced, and XPM induced

A particular signal can accumulate cross-talk from different elements and channels over the network. Cross-talk can be reduced by using several techniques such as wavelength dilation or filter cascading. In this example, we will investigate the effect of interchannel cross-talk at ADM to a ring network. The project is found in the **Interchannel crosstalk at ADM in a ring network.osd** file. This network contains 4 nodes that communicate over two channels at 193 THz and 193.1 THz, as shown in [Figure 1](#). The bit rate is 10 Gbps. ADMs at each node is modeled by using WDM add and WDM drop components. WDM add and drop components are created by using 4th order Bessel filters. The ring is ended with a ring control component which can circulate the signals around ring for a given number of times. The distance between nodes is 12.5 km and we inserted an ideal amplifier just before node 2 to compensate for the total fiber loss in the ring. Dispersion and nonlinear effects of fibers are disabled to isolate the crosstalk effect.

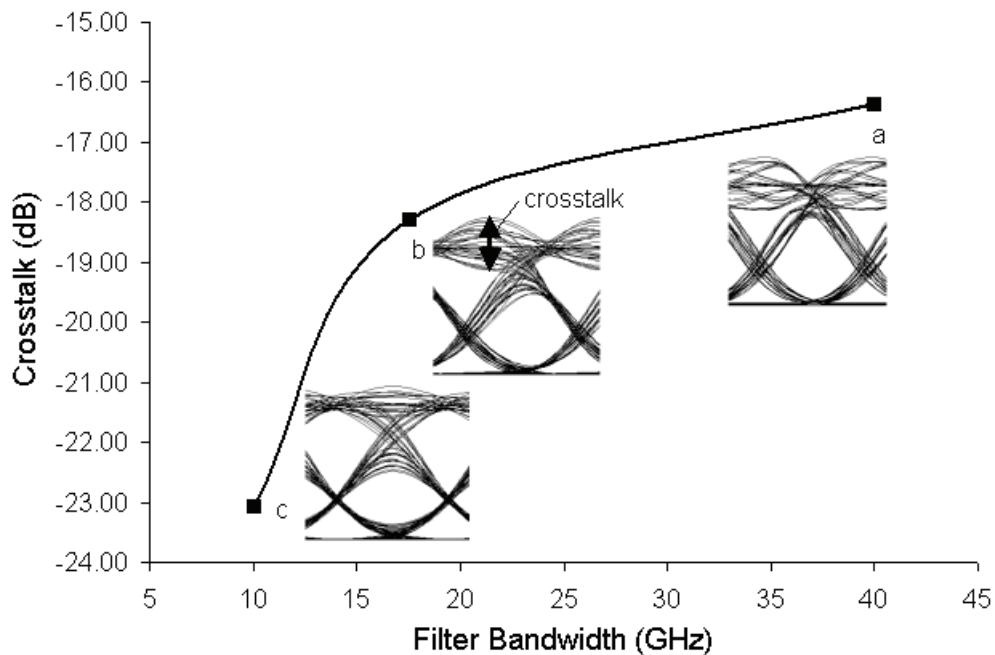
Figure 1 A basic ring network with 4 nodes



To show the effect of interchannel cross-talk, we have swept the band width of the filters in ADM of node 2 from 10 to 40 GHz. The eye diagrams at node 2 for several bandwidths are given in Figure 2. This figure also shows the cross-talk [1], [2], and [3], as defined  $10\log(V_{xt}/V_{sig})$  versus filter bandwidth.



**Figure 2** Cross talk versus filter bandwidth at node 2. Insets show the eye diagrams when filter bandwidth is a) 40 GHz, b) 17.5 GHz, and c) 10 GHz.



## References:

- [1] G. P. Agrawal, Fiber Optic Communication Systems, Wiley-Interscience, 1997.
- [2] Tim Gyselings et. al, "Crosstalk analysis of multi-wavelength optical cross connects", J. Light. Tech. 17, pp. 1273, 1999.
- [3] R. Ramaswami and K. N. Sivarajan, Optical Networks: A practical Perspective, Morgan Kaufmann, 1998.

**Notes:**

# WDM Ring—Wavelength independent subscriber equipment

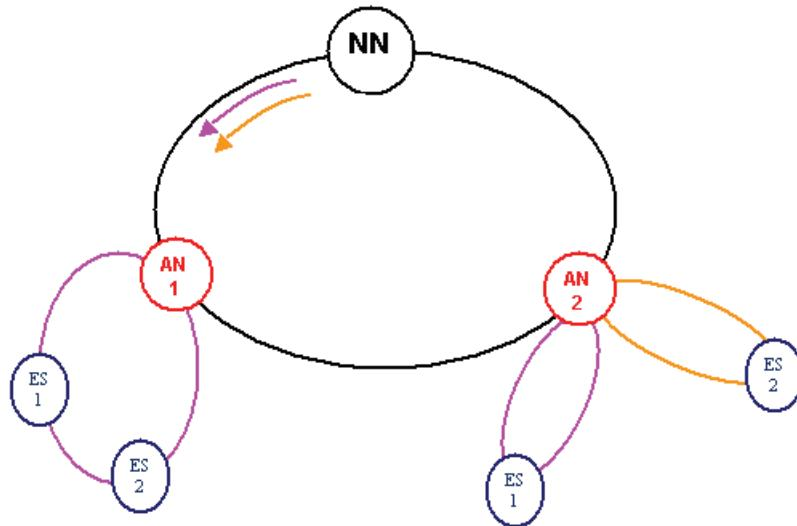
---

In this example, we will show realization of a WDM ring network using wavelength independent subscriber equipment to share bandwidth [1].

The metro-ring network we modeled operates with 2 wavelength carriers as shown in Figure 1. In this configuration, several subscribers share the bandwidth. For illustration purposes, the network contains one Network Node (NN) and one Access Node (AN). By using a packet format, multiple users can share a single wavelength. All wavelengths are sourced at the NN whose output wavelengths are multiplexed on the ring fiber. NN also contains an associated set of WDMs. The resulting architecture can simultaneously support:

- cost-shared virtual rings (the distribution ring network connected to AN, single wavelength goes around this sub-rings)
- distribution stars with a dedicated wavelength per user (every End Station (ES) uses a different wavelength)
- a combination

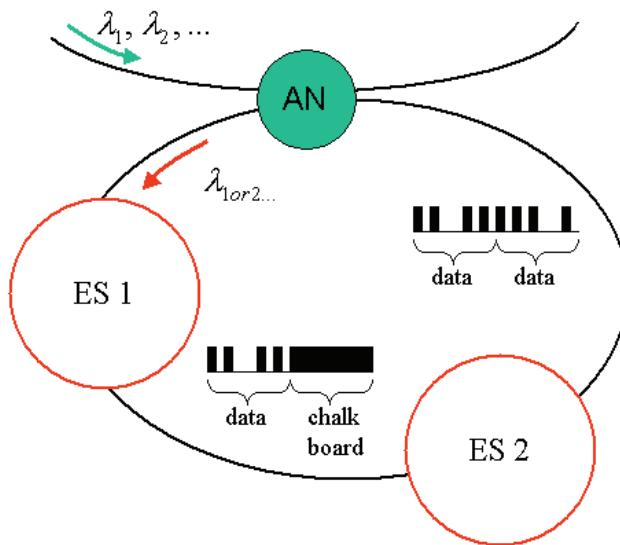
**Figure 1** Ring network with 4 end stations (subscribers) and 2 access nodes



In the example shown in Figure 1, we have one NN and two ANs (AN1, AN2). In this configuration, two end stations (ES1 and ES 2) share the same wavelength. End users, via a packet protocol as shown in Figure 2, share this wavelength. Incoming packet data is directed to user's receiver via a 3 dB splitter. Each outgoing packet is created by modulating an incoming "optical chalkboard", which consists of a string of all ones sourced at the NN. In our example, we modulated two optical carriers at ES1

and ES3. Note that the modulation and packet organization can take place at any sub-ring or star (at any ES that wants to communicate with any other ES). In [1] and [2], SOAs are used to amplify and modulate the incoming signal at every ES. To model this, we have used a combination of an ideal amplifier with 14 dB gain and an ideal amplitude modulator. Therefore, we did not consider any penalty from the SOA characteristics. Details of the ES subsystem is shown in [Figure 3](#).

**Figure 2** Details of end stations and writing data on a "chalkboard"



The project is found in the **WDM Ring WISE\_NRZ\_DM.osd** file. Here, the bit rate is 2.5 Gbps and laser power at NN is 3 dBm. In this example, ES1 sends data to ES3 by modulating the signal originated from NN on channel 1, over a virtual path marked as "ch1 from ES1 to ES3" in Path manager. In the same way, ES4 communicates with NN on channel 2, over a virtual path marked as "ch2 form ES4 to NN" in Path manager. [Figure 4](#) shows Q factor versus received power at ES3. [Figure 5](#), on the other hand, shows the variation of OSNR and its signal power from ES1 to ES3 as obtained from the Trace tool. [Figure 6](#) shows the eye diagram at ES3 when the received power is about -18 dBm.

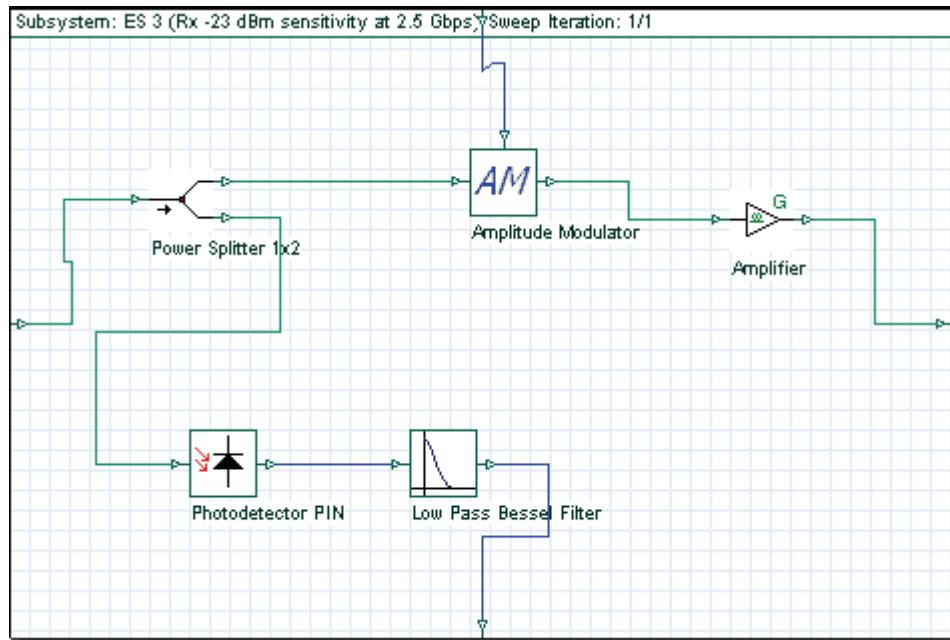
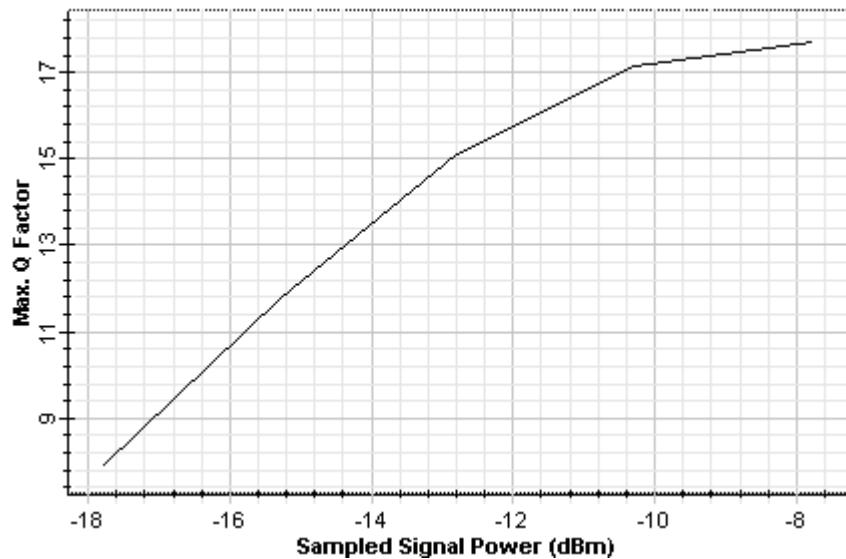
**Figure 3 Details of ES subsystem****Figure 4 Q factor versus received power at node ES3**

Figure 5 OSNR and signal power vs. transmission distance from ES1 to ES3

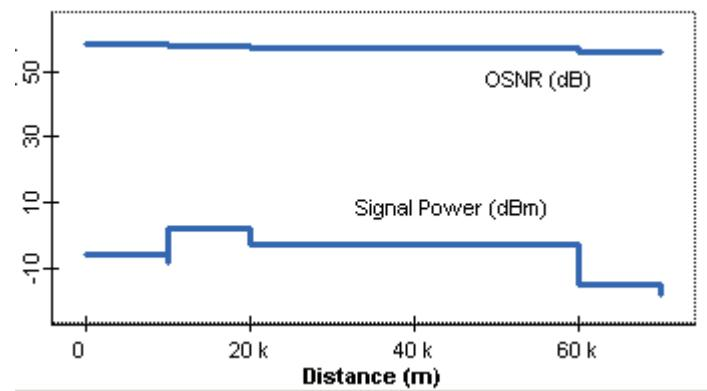
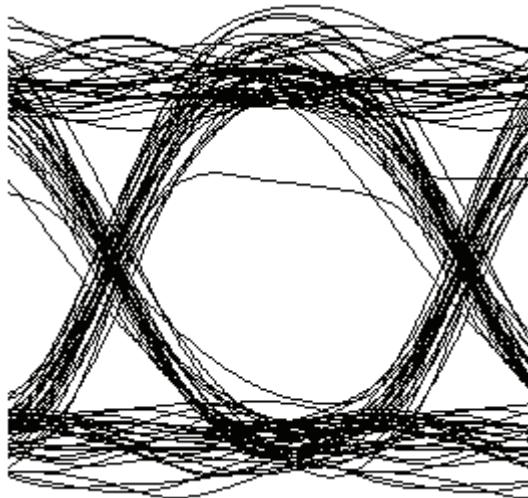


Figure 6 Eye diagram at ES 3 when received power is about -18 dBm



## References

- [1] P. P. Iannone et. al., "A flexible metro WDM ring using wavelength-independent subscriber equipment to share bandwidth", OFC'00, paper PD38, 2000.
- [2] P. P. Iannone et. al., "A transparent WDM network featuring shared virtual rings", J. Lightwave Tech., vol. 18, pp 1955, 2000.
- [3] G. P. Agrawal, Nonlinear Fiber Optics, Second Edition, Academic Press, 1995.

---

## Digital modulation

---

This section contains the following advanced and illustrative simulation projects.

- Digital modulation—DPSK
- Digital modulation—OQPSK
- Digital modulation—QAM
- Manchester and PAM Coding/Decoding

**Notes:**

# Digital modulation—DPSK

---

The purpose of this lesson is to demonstrate how to design an 8 DPSK pulse generator using the OptiSystem component library. This tutorial includes references to project files that demonstrate some of the steps presented here. Refer to the end of the tutorial for the project file names. You should use the OptiSystem Component Library manual to read the technical description of the individual components presented here.

The first step when creating a project using OptiSystem is to define the global parameters.

## Global parameters

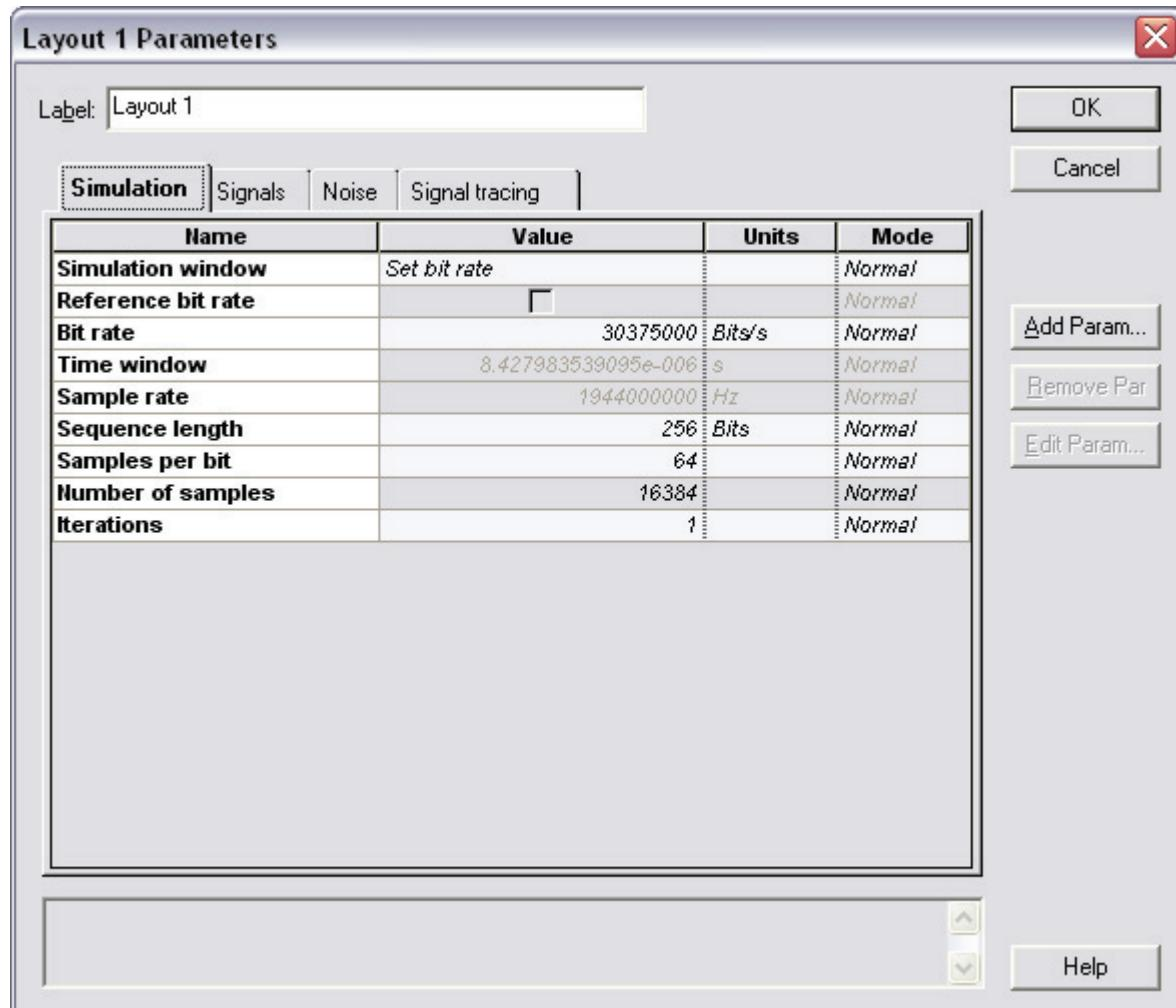
To view the global parameters, perform the following procedure.

**Step    Action**

- 1      From the **File** menu, select **New**.  
*A blank **Main layout** appears in the **Project layout** window.*
- 2      Double-click anywhere in the **Main layout**.  
*The **Layout 1 Parameters** dialog box appears (see [Figure 1](#)).*  
The global parameters used for this simulation are:
  - **Bit rate:** 30375000 Bits/s
  - **Sequence length:** 256 bits
  - **Sample rate:** 1.944 GHz

The sample rate can be controlled by changing the number of samples per bit.

**Figure 1 DPSK Transmitter global parameters**



As you are aware, OptiSystem requires a power of two sequence length, e.g. 64, 128, 256, 512... In this example we will also use an 8 DPSK modulation, which uses 3 bits per symbol. This means that we will have not only a binary sequence that will use the parameter sequence length, but also a M-ary sequence with sequence length divided by 3 (after the DPSK sequence generator). The user should choose the right value for the sequence length that matches the value for the bits per symbol. In order to calculate this value, divide the global sequence length by the bits per symbol, and then take the closest integer number.

For example (8 DPSK):

$$X = 256 / 3 = 85.33$$

$$N = 85$$

The integer N should be lower than or equal to X, and 256 is a valid value for the sequence length.

Another example if using sequence length of 128:

$$X = 512 / 3 = 170.67$$

$$N = 171$$

In this case, N is greater than X, and you should use another value for the sequence length. This is critical, because the decoders always convert the M-Ary sequences back to binary, and they will convert the sequence length to the next power of two. This means that if you have 512 bits, N=171, and  $3 \times 171 = 513$ . 513 will be converted to 1024 and the decoder will add zeros to the bit sequence. The received binary sequence will not be correct.

This is not a problem for 256 bits, because N=85, and  $3 \times 85 = 255$ . 255 will be converted to 256 - the original sequence length. If the bits per symbol are a multiple of 2, in this case X is equal to N.

### ***Creating a project***

After setting the global parameters, we can start adding the components to design the DPSK transmitter.

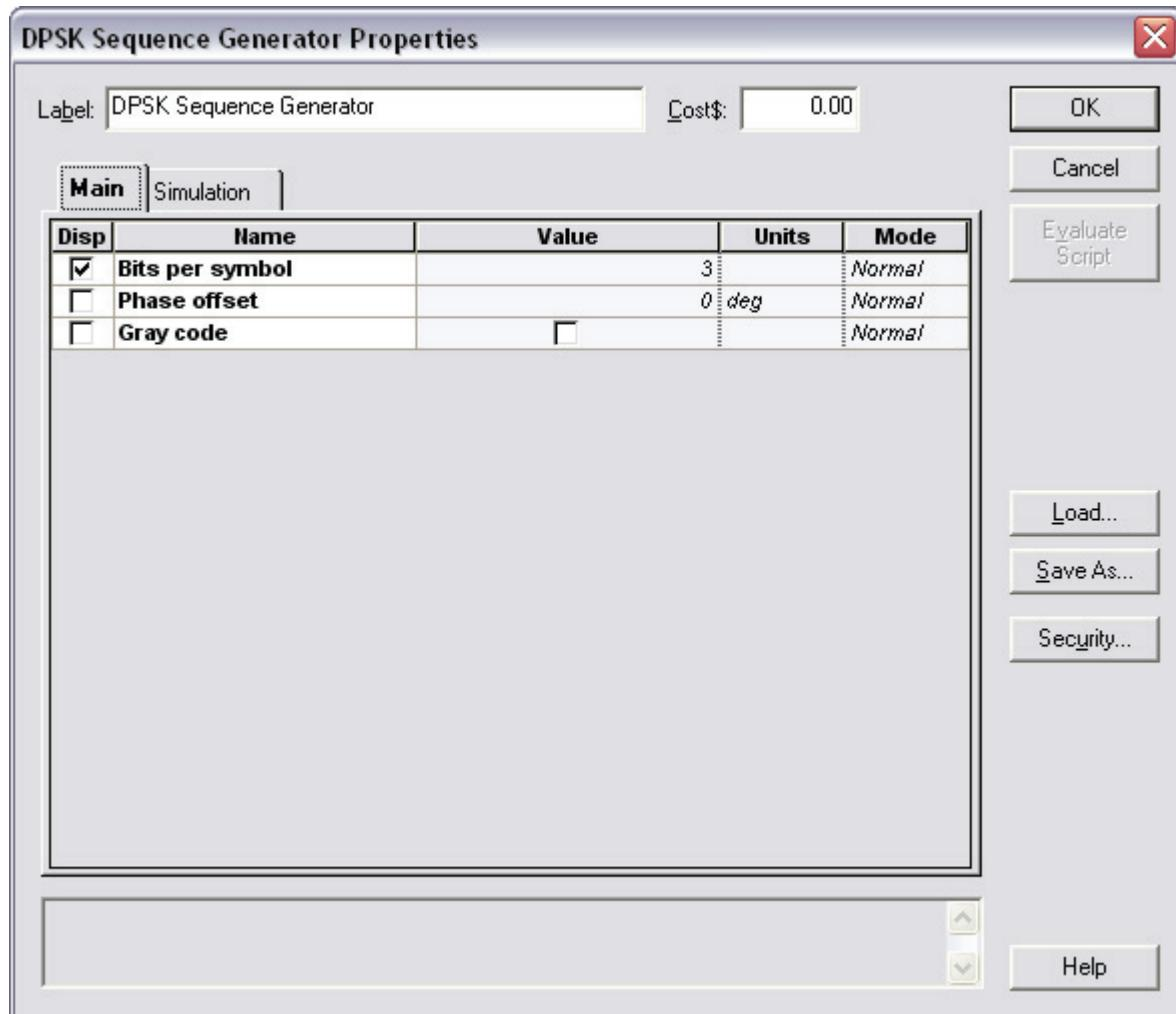
From the component library, drag and drop the following components into the layout:

<b>Step</b>	<b>Action</b>
-------------	---------------

- 1 From the Component Library, select **Default > Transmitters Library > Bit Sequence Generators**.
- 2 Drag the **Pseudo-Random Bit Sequence Generator** to the **Main layout**.
- 3 From the Component Library, select **Default > Cable Access Library > Transmitters > Sequence Generators**.
- 4 Drag the **DPSK Sequence Generator** to the **Main layout**.
- 5 From the Component Library, select **Default > Transmitters Library > Pulse Generators > Electrical**.
- 6 Drag two of the **M-ary Pulse Generators** components to the **Main layout**.
- 7 From the Component Library, select **Default > Visualizers Library > Electrical**.
- 8 Drag two of the **Oscilloscope Visualizer** components to the **Main layout**.
- 9 From the Component Library, select **Default > Visualizers Library > Electrical**.
- 10 Drag the **Electrical Constellation Visualizer** to the **Main layout**.

The next step is to set the parameters and connect the components. In this design, for the DPSK Sequence Generator component, we will use the parameters presented in [Figure 2](#). The other component parameters will use their default values.

Figure 2 DPSK Sequence Generator component parameters

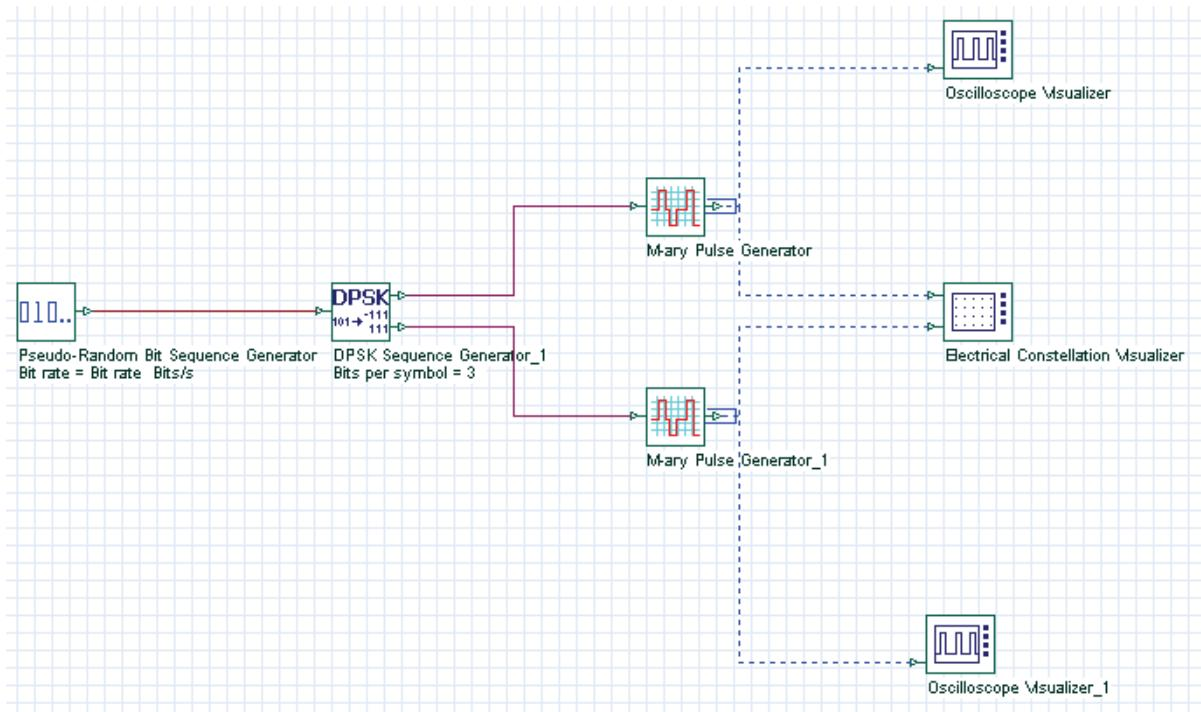


The components and visualizers should be connected according to Figure 3.

This layout is equivalent to a DPSK pulse generator. Refer to the OptiSystem project file: "DPSK Step 1 - Pulse Generator.osd"



Figure 3 DPSK pulse generator



To demonstrate how the global and DPSK parameters affect the simulation results, we can run this simulation and analyze the results of the visualizers.

### **Running the simulation**

To run a simulation, perform the following procedure.

**Step    Action**

- 1      From the **File** menu, select **Calculate**.  
*The OptiSystem Calculations dialog box appears.*
- 2      In the **OptiSystem Calculations** dialog box, click **Run** to start the simulation.  
*The calculation output appears in the dialog box, and the simulation results appear below the components that were included in the simulation in the Main layout.*

### **Viewing simulation results**

After running the calculation, we can analyze the results from the visualizers.

To display results from a visualizer, perform the following action.

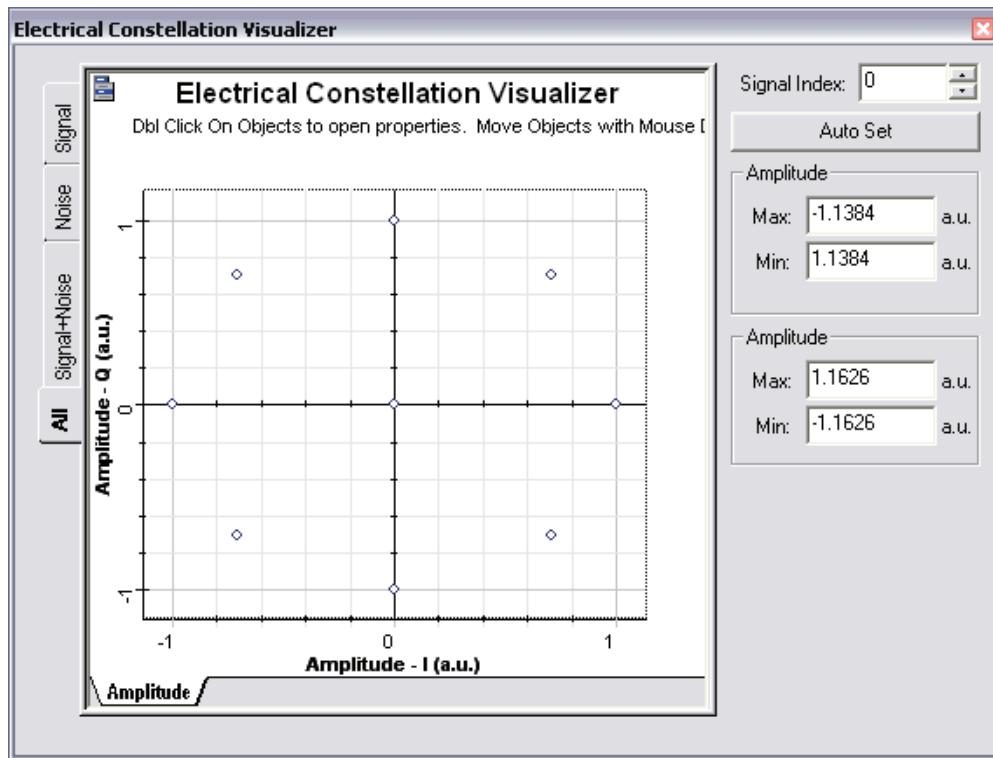
**Action**

- Double-click on the **Electrical Constellation Visualizer** to view the graphs and results that the simulation generated.

**Note:** Double-click again to close the dialog box.

You should see the constellation diagram showing the In-phase and Quadrature-phase on the X- and Y-axis respectively. [Figure 4](#) presents the results of the simulation. This is a well known result for DPSK modulation, using 3 bits per symbol, without phase shift - 8 DPSK. Since we are simulating only 64 bits, not all combinations for 8 DPSK are shown.

**Figure 4** Constellation diagram for a 8 DPSK modulation (3 bits per symbol)



#### Action

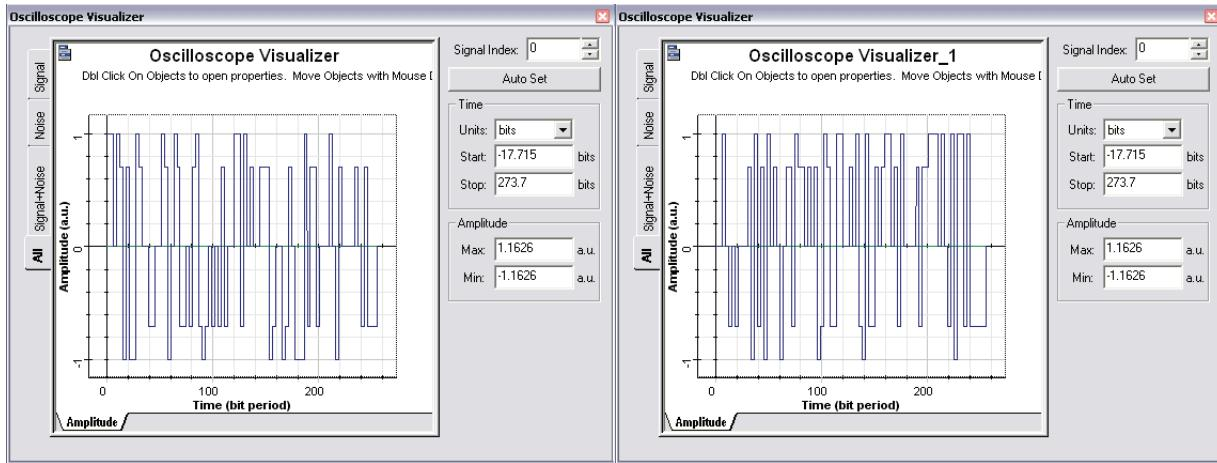
- Double-click on the **Oscilloscope Visualizer** to view the graphs and results that the simulation generated.

**Note:** Double-click again to close the dialog box.

Note the amplitude of the signal. This is a signal with multiple levels; also known as M-ary signal.

For the DPSK there are 5 possible values:  $-1, -\sqrt{2}/2, 0, \sqrt{2}/2$  and  $1$  for both I and Q signals (see [Figure 5](#)).



**Figure 5 In-phase and Quadrature phase M-ary signals**

## Using the DPSK Sequence Decoder

We already have the I and Q M-ary signals, however before modulating these signals using a quadrature modulator, we can test to see if the signals can be properly decoded into the original binary sequence. This can be done using a different layout, or reorganizing the previous one.

In order to compare the binary signals before and after coding/decoding, we should modulate the original binary sequence and the decoded sequence using electrical pulse generators, such as the RZ Pulse Generator.

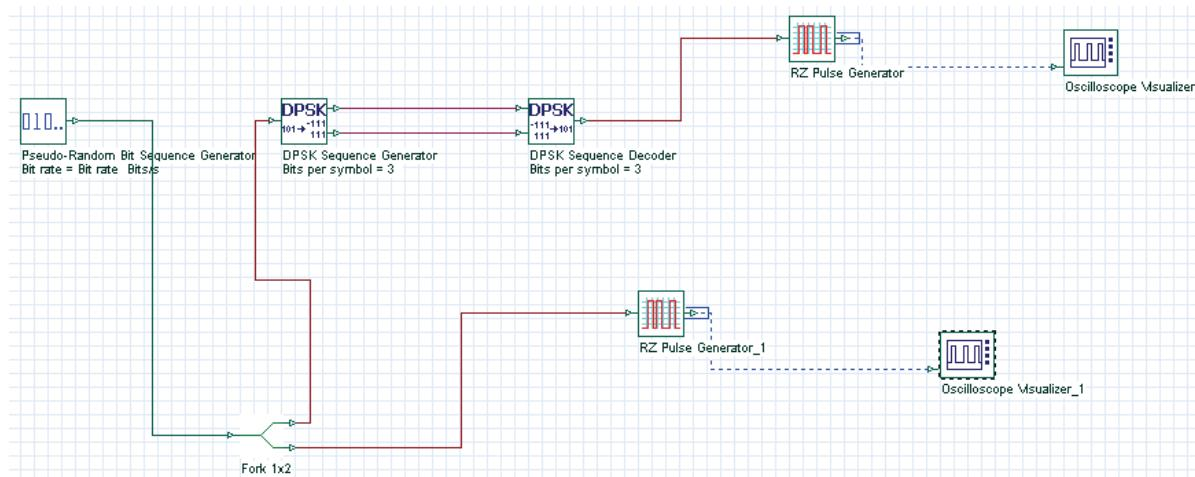
### Step Action

- 1** From the Component Library, select **Default > Cable Access Library > Receivers > Decoders**.
- 2** Drag the **DPSK Sequence Decoder** to the **Main layout**.
- 3** In the **Main layout**, double click the **DPSK Sequence Decoder**. *The DPSK Sequence Decoder Properties dialog box appears.*
- 4** Enter the same parameters as defined for the **DPSK Sequence Generator** (see [Figure 2](#)).
- 5** From the Component Library, select **Default > Cable Access Library > Transmitters > Sequence Generators**.
- 6** Drag the **DPSK Sequence Generator** to the **Main layout**.
- 7** From the Component Library, select **Default > Tools**.
- 8** Drag the **Fork 1x2** to the **Main layout**.
- 9** From the Component Library, select **Default > Transmitters Library > Pulse Generators > Electrical**.
- 10** Drag two of the **NRZ Pulse Generators** components to the **Main layout**.
- 11** Reorganize the previous layout according to [Figure 6](#) (refer to the OptiSystem project file: "DPSK Step 2 - Coding and Decoding.osd")
- 12** From the **File** menu, select **Calculate**.

The OptiSystem Calculations dialog box appears.

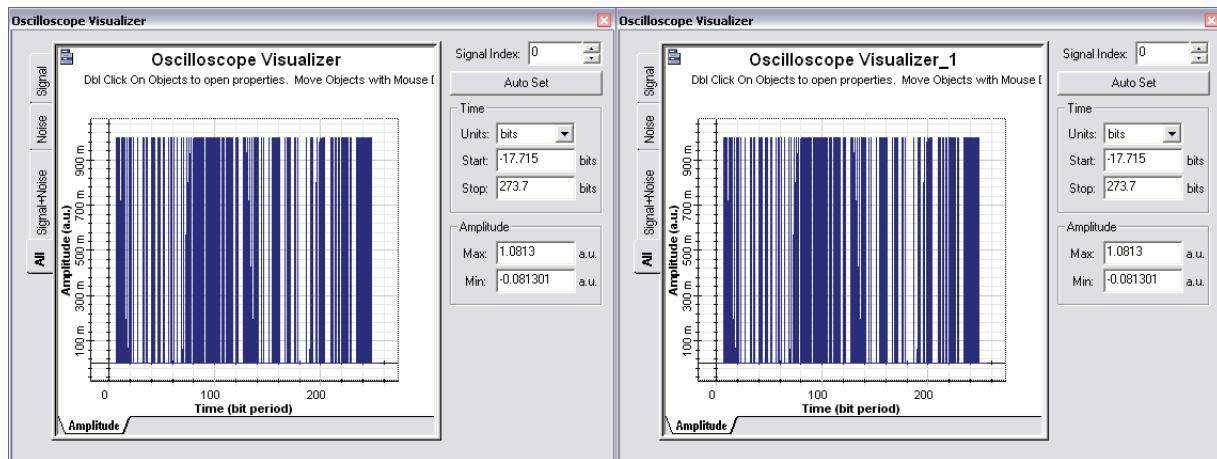
- 13 In the **OptiSystem Calculations** dialog box, click **Run** to start the simulation.  
*The calculation output appears in the dialog box, and the simulation results appear below the components that were included in the simulation in the Main layout.*

**Figure 6 Testing the DPSK sequence coding and decoding**



We should see that the electrical signals are the same in both oscilloscopes, since we coded, then decoded the same binary signal. This is demonstrated in [Figure 7](#).

**Figure 7 Electrical signals before and after DPSK coding/decoding**



## Using the M-ary Threshold Detector

The next step is to detect the I and Q electrical signals using a M-ary Threshold Detector. By using the threshold detector, we can recover the original DPSK sequence, and then decode the sequence into the original binary signal. You can use the system from [Figure 3](#) and the components from [Figure 6](#). However, you will need one additional component:

**Step Action**

- 1 From the Component Library, select **Default > Cable Access Library > Receivers > Detectors**.
- 2 Drag the **M-ary Threshold Detector** to the **Main layout**.

The main challenge is to set the proper values of the threshold and output amplitudes in the **M-ary Threshold Detector** component.

Since we know that this is an 8 DPSK, the output amplitudes should be  $-1, -\sqrt{2/2}, 0, \sqrt{2/2}$  and  $1$ .

The detector will require the threshold values to evaluate the input signal to determine the equivalent output level, assuming that the input values are the same as the output values ([Figure 8](#)), we will set the threshold values according to the signal input:  $((-1 - \sqrt{2/2})/2, -\sqrt{2/4}, (1 + \sqrt{2/2})/2, \sqrt{2/4}$ , or the equivalent numerical values: -0.85, -0.353, 0.353 and 0.85.

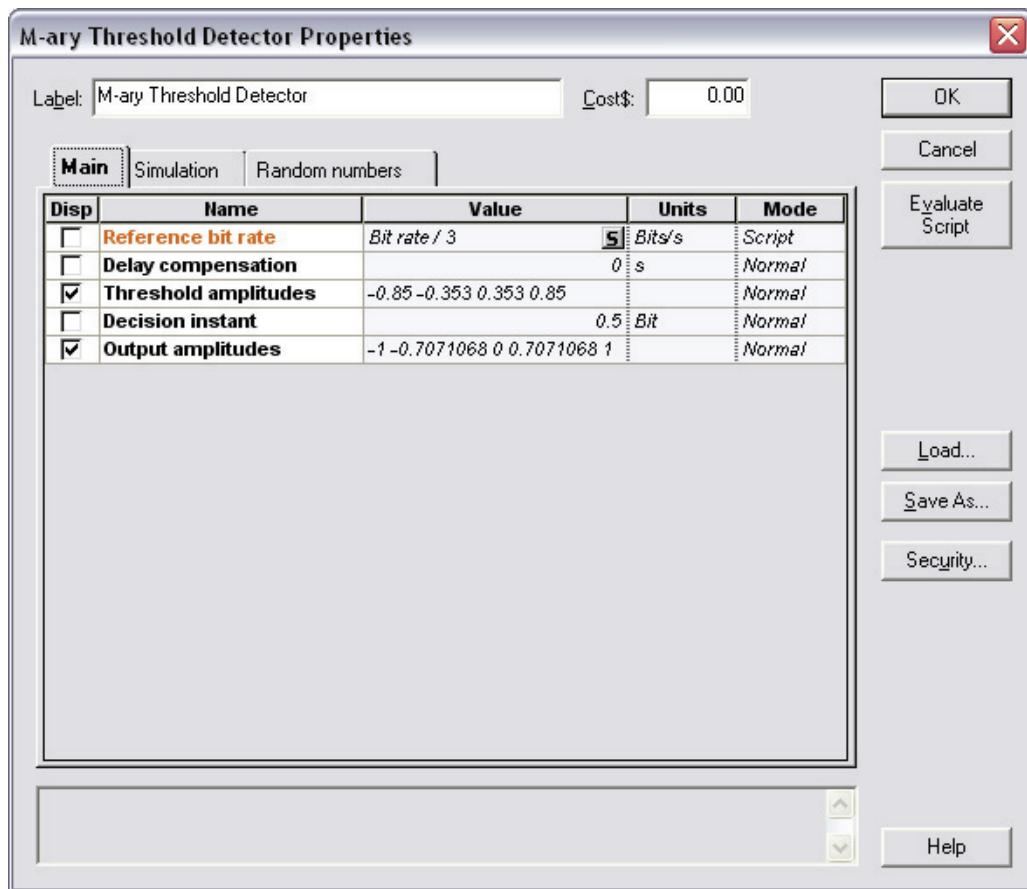
These values are used to compare the input signal with the threshold according to:

**Table 2 Input and output based on threshold amplitudes**

Input Amplitude	Output Amplitude
$< -0.85$	-1
$> -0.85$ and $< -0.353$	$-\sqrt{2/2}$
$> -0.343$ and $< 0.353$	0
$> 0.35$ and $< 0.85$	$\sqrt{2/2}$
$> 0.85$	1

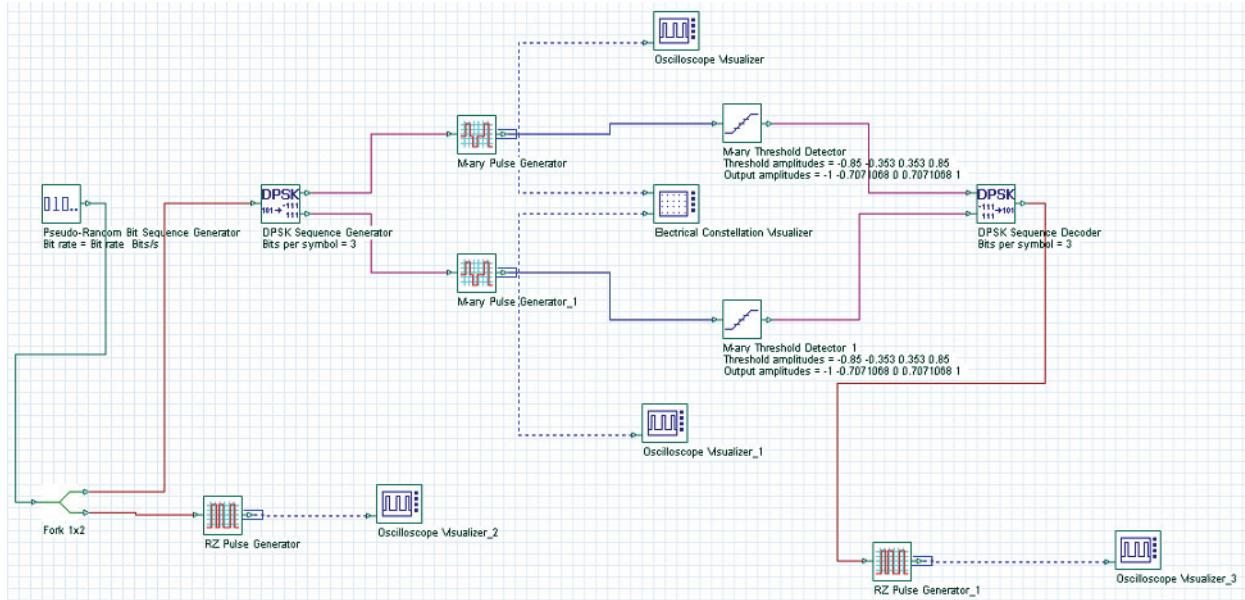
Also, the parameter **Reference bit rate** should be the same bit rate as the input M-ary signal, and this is the original bit rate of the binary sequence divided by the number of bits per symbol: the global bit rate / 3. [Figure 8](#) presents the parameters for both detectors.

Figure 8 M-ary Threshold Detector parameters



- 3 Connect the components according to the layout presented in Figure 9 (refer to the OptiSystem project file: "DPSK Step 3 – Pulse Generator and Decoding.osd").
- 4 Run the simulation.

Figure 9 DPSK pulse generator and detector



After running the simulation, you will see that the results for the oscilloscopes at the binary source and at the decoder output are the same (Figure 7). If you don't have the proper values for the global sequence length, for example, 512 bits, the graphs will be different.

## Adding Quadrature Modulation

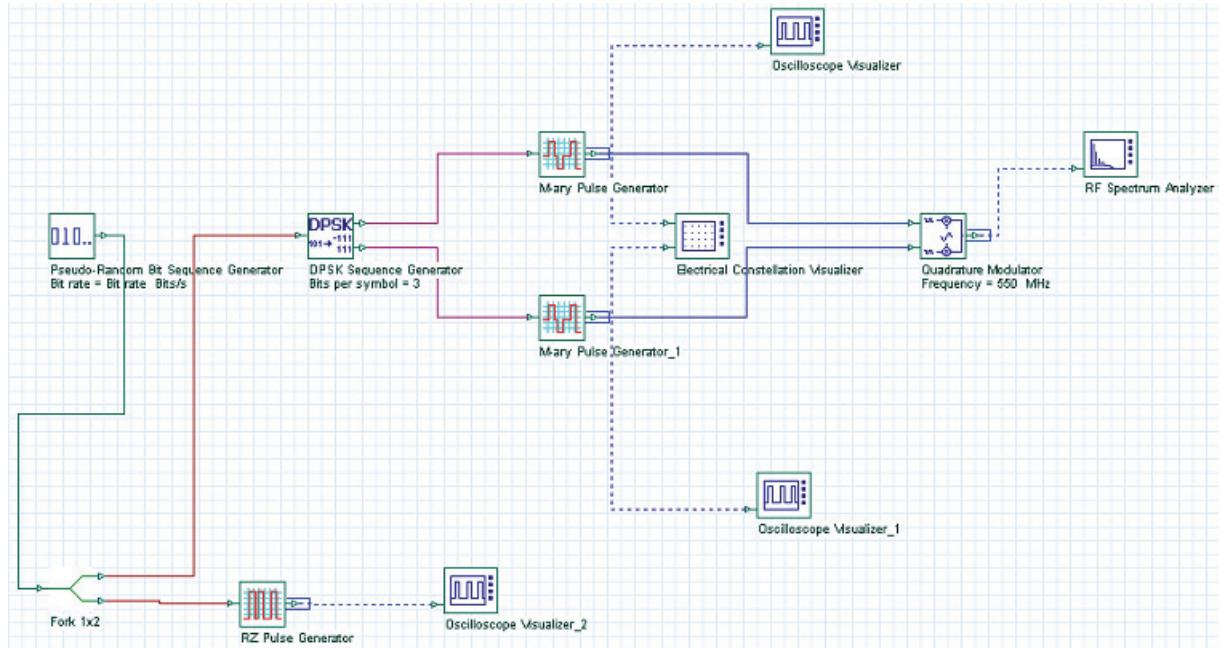
We already know how to code and decode a DPSK signal; now we can modulate the M-ary signal using quadrature modulation.

### Step Action

- 1 From the Component Library, select **Default > Cable Access Library > Transmitters > Modulators**.
- 2 Drag the **Quadrature Modulator** to the **Main** layout.
- 3 Set the parameter **Frequency** in the **Quadrature Modulator** to 550 MHz.
- 4 From the Component Library, select **Default > Visualizers Library > Electrical**.
- 5 Drag the **RF Spectrum Analyzer** to the **Main** layout.

- 6** Connect the components according to the layout in Figure 10 (refer to the OptiSystem project file: "DPSK Step 4 - Transmitter.osd").

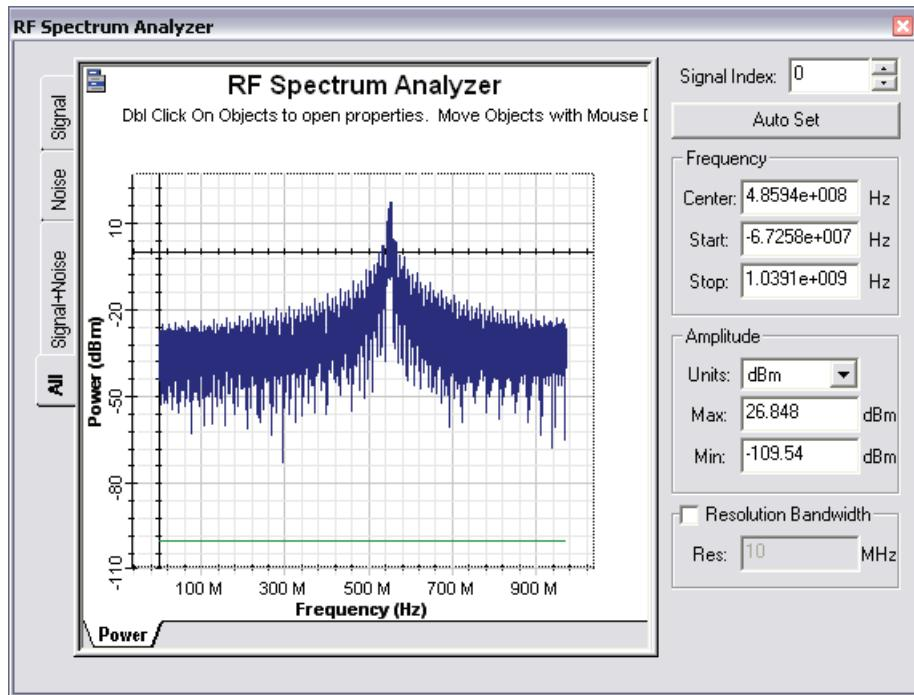
**Figure 10 DPSK Transmitter**



This was the last step to build our DPSK transmitter, now run the simulation and visualize the spectrum of the signal output (Figure 11).



Figure 11 DPSK Transmitter output



Observe that the center frequency of the signal is the modulation frequency 550 MHz, and that the simulation bandwidth is defined by half or the value of the global parameter sample rate ( $1.944 \text{ GHz} / 2 = 972 \text{ MHz}$ ). This means that if you want to increase the simulation bandwidth to accommodate a higher modulation frequency ( $>900 \text{ MHz}$ ), you should change the number of samples per bit in the global parameters window.

### Adding Quadrature Demodulation

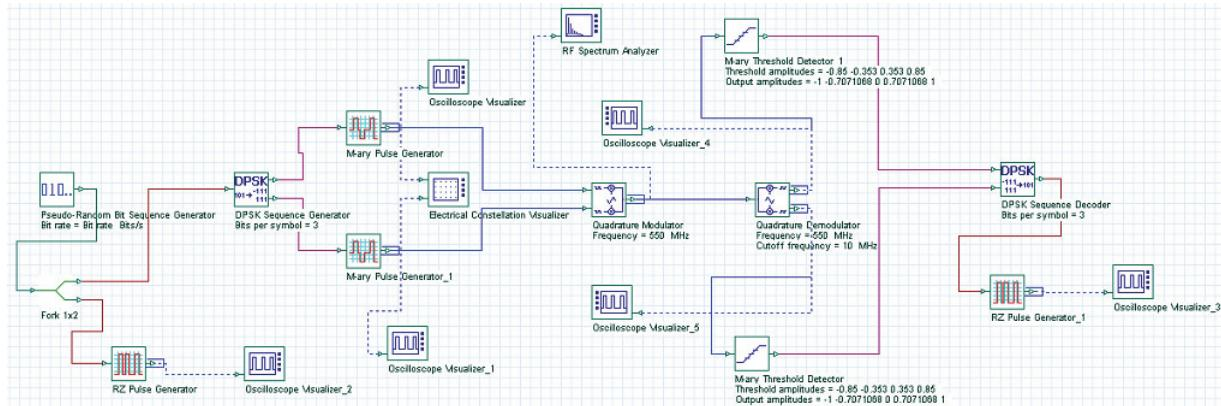
We already know how to code, decode and modulate a DPSK signal; now we can demodulate the DPSK signal using quadrature demodulation.

#### Step Action

- 1 From the Component Library, select **Default > Cable Access Library > Receivers > Demodulators**.
- 2 Drag the **Quadrature Demodulator** to the **Main layout**.
- 3 Set the parameter **Frequency** in the **Quadrature Demodulator** to 550 MHz, the **Cutoff frequency** to 10 MHz and the **Gain** to 2.
- 4 Using the components from the previous layouts (Figure 9 and Figure 10), and additional oscilloscopes, connect the components according to the layout

in [Figure 12](#) (refer to the OptiSystem project file: "DPSK Step 5 – Transmitter and Receiver.osd").

**Figure 12 DPSK transmitter and receiver**

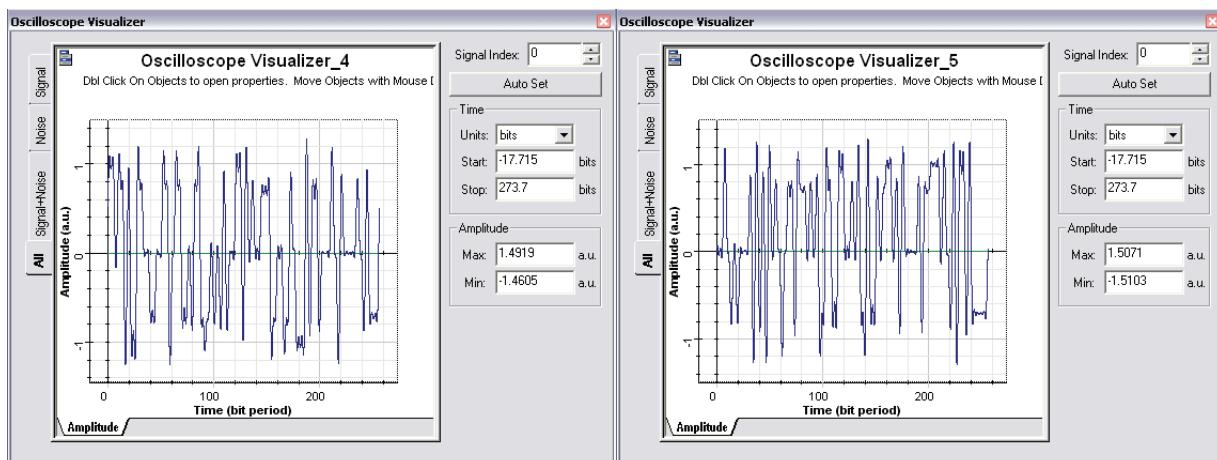


For the quadrature demodulator, the **Frequency** parameter should be the same value as the carrier transmitter frequency. The cutoff frequency again should be adjusted accordingly in order to shape and scale the output signal properly.

- 5 Run the simulation
- 6 Compare the oscilloscopes connected at the M-ary pulse generators and at the quadrature demodulator outputs.

The output signals at the quadrature demodulator are presented in [Figure 13](#), the signals are virtually the same as presented in [Figure 5](#), however they are distorted by the quadrature demodulator low-pass filter. If you add a channel between the transmitter and receiver, the signal may have additional distortion and noise.

**Figure 13 In-phase and Quadrature phase M-ary demodulated signals**



The next step is to compare the binary signals at the transmitter and at the receiver. If the system parameters are correct, you should have the same results as presented in [Figure 7](#).



The layout presented in [Figure 12](#) is a complete project for an 8 DPSK transmitter and receiver. You can use this project as a starting point for other types of modulation, such as QAM and OQPSK. Refer to the OptiSystem Component Library documents for the description of different types of modulation available in the software.

## Saving Design Time Using the Modulators Library

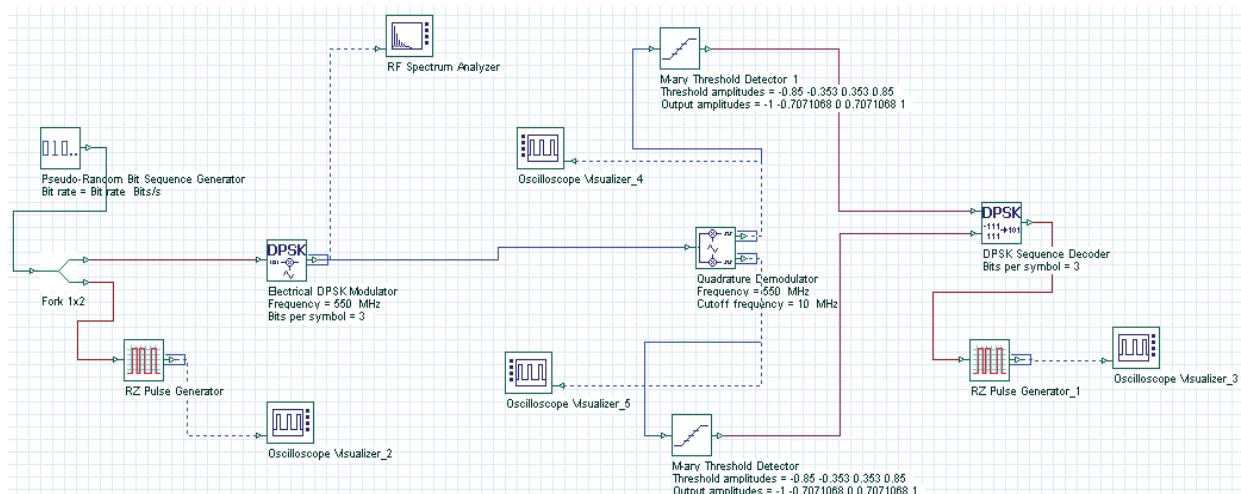
The previous transmitter design required multiple components to code the signal, generate the M-ary pulses, and to finally modulate the signal. You can use components from the pulse generator library that include the coders and pulse generators, or components from the modulators library that include the pulse generators and the quadrature modulators.

In the previous layout ([Figure 12](#)), delete the **DPSK Sequence Generator**, the **M-ary Pulse Generators**, and the **Quadrature Modulator** and the visualizers connected to them.

### Step Action

- 1 From the Component Library, select **Default > Cable Access Library > Transmitters > Modulators**.
- 2 Drag the **Electrical DPSK Modulator** to the **Main layout**.
- 3 Set the parameter **Frequency** in the **Electrical DPSK Modulator** to 550 MHz, and the **Number of Bits** per symbol to 3.
- 4 Connect the component according to the layout presented in [Figure 14](#) (refer to the OptiSystem project file: "DPSK Step 6 - Transmitter and Receiver II.osd").

**Figure 14 DPSK transmitter (using DPSK modulator) and receiver**



As you can see, by using the DPSK modulator instead the multiple components, the system is faster in making the design than the one in [Figure 12](#). On the other hand, you cannot access all the internal signals that helps you to test and understand the challenges when designing digital modulation transmitters.

## Plotting eye diagrams for M-ary signals

OptiSystem can plot and estimate the BER of an optical system for two level (binary) signals. When using M-ary signals, you cannot estimate the values of BER directly, however you can still plot the eye diagrams.

Step	Action
1	In the previous layout ( <a href="#">Figure 14</a> ), from the Component Library, select <b>Default &gt; Visualizers &gt; Electrical</b> .
2	Drag the <b>Eye Diagram Analyzer</b> to the <b>Main layout</b> .
3	From the Component Library, select <b>Default &gt; Transmitters Library &gt; Bit Sequence Generators</b> .
4	Drag the <b>Bit Sequence Generator</b> to the <b>Main layout</b> .
5	In the second bit sequence generator, divide the parameter <b>Bit rate</b> by 3, in order to match the bit rate of the M-ary sequence. Set the parameter <b>Operation mode</b> to <b>Alternate</b> ( <a href="#">Figure 15</a> ).
6	From the Component Library, select <b>Default &gt; Transmitters Library &gt; Pulse Generators &gt; Electrical</b> .
7	Drag the <b>NRZ Pulse Generators</b> components to the <b>Main layout</b> .

- 1 In the previous layout ([Figure 14](#)), from the Component Library, select **Default > Visualizers > Electrical**.
- 2 Drag the **Eye Diagram Analyzer** to the **Main layout**.
- 3 From the Component Library, select **Default > Transmitters Library > Bit Sequence Generators**.
- 4 Drag the **Bit Sequence Generator** to the **Main layout**.
- 5 In the second bit sequence generator, divide the parameter **Bit rate** by 3, in order to match the bit rate of the M-ary sequence. Set the parameter **Operation mode** to **Alternate** ([Figure 15](#)).
- 6 From the Component Library, select **Default > Transmitters Library > Pulse Generators > Electrical**.
- 7 Drag the **NRZ Pulse Generators** components to the **Main layout**.



- 8 Connect the components according to [Figure 16](#) (refer to the OptiSystem project file: "DPSK Step 7 - Transmitter and Receiver with Eye Diagram.osd").

**Figure 15** PRBS generator for parameters used to generate M-ary eye diagrams

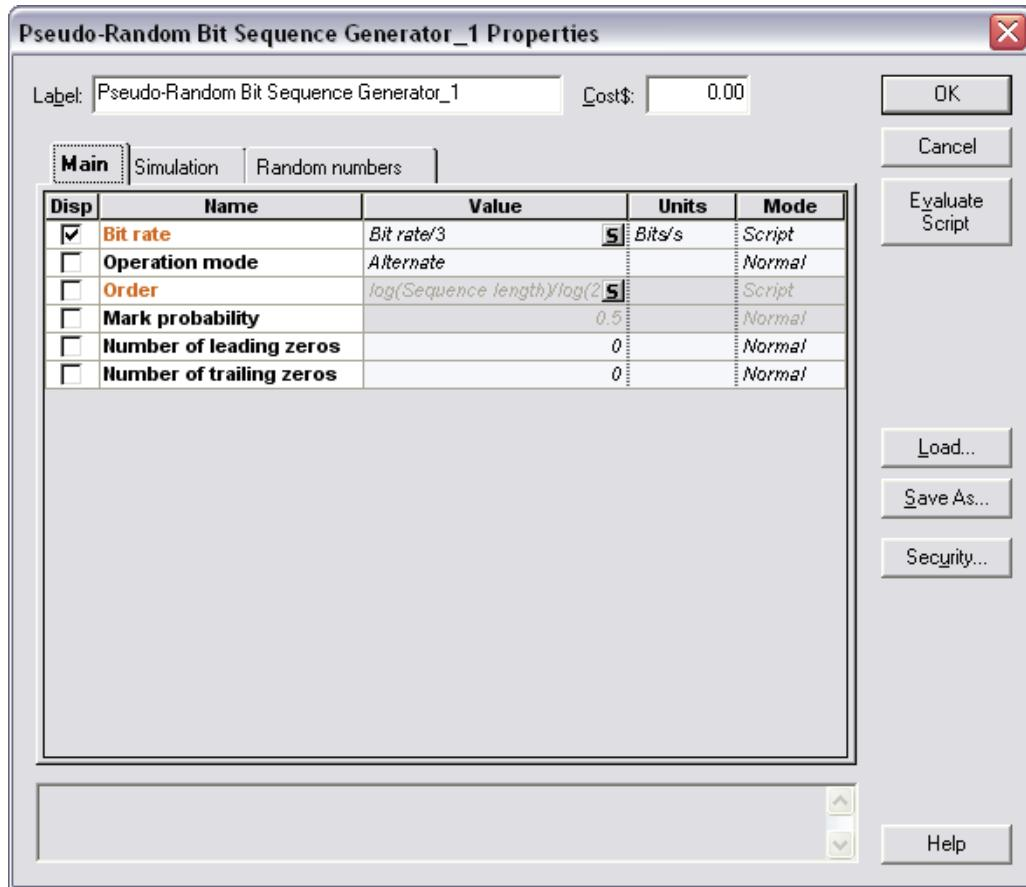
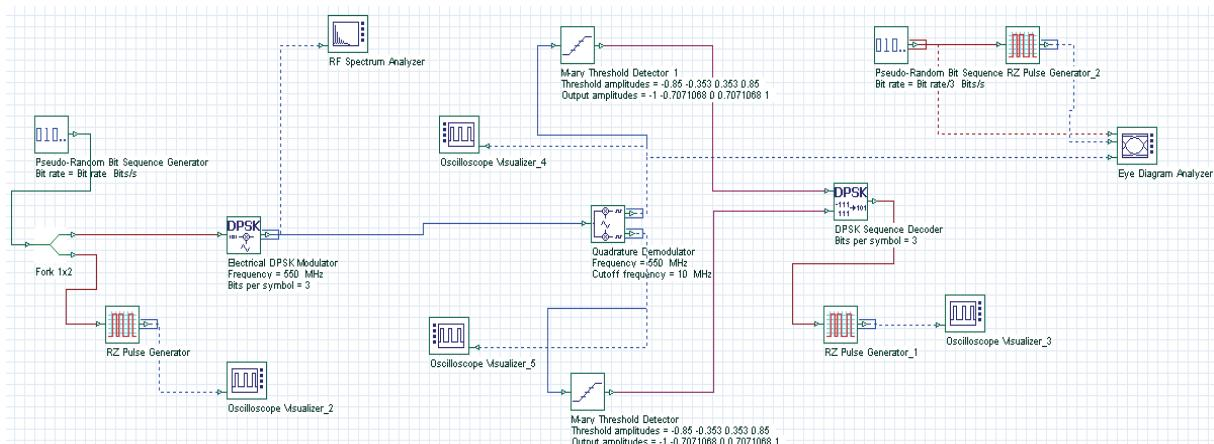


**Figure 16** DPSK system, including components to generate eye diagrams

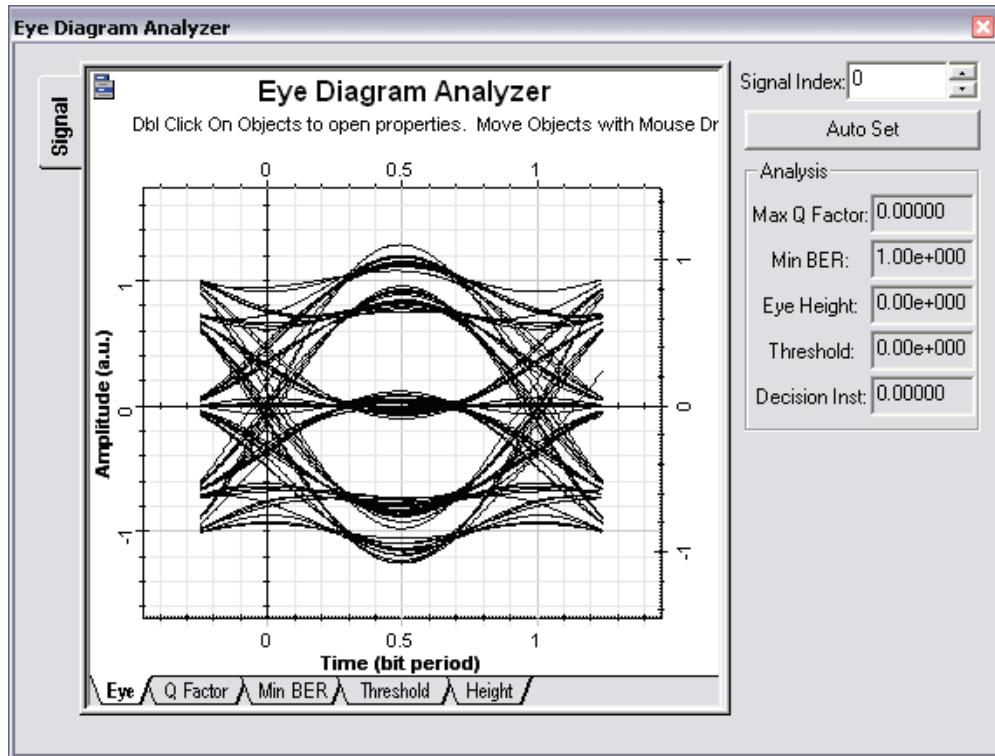


In this example, we added the Eye diagram tool to plot the M-ary signal at the quadrature modulator output, for the In-phase signal.

- 9 Run the simulation and then view at the Eye diagram. The results should be the same as those seen in [Figure 17](#).

The main parameter is the bit rate at the PRBS. It should be the binary bit rate divided by the number of bits per symbol, e.g. M-ary bit rate. This is the same value used in the Threshold detector.

**Figure 17 DPSK Eye diagram at the receiver for an 8 DPSK system**



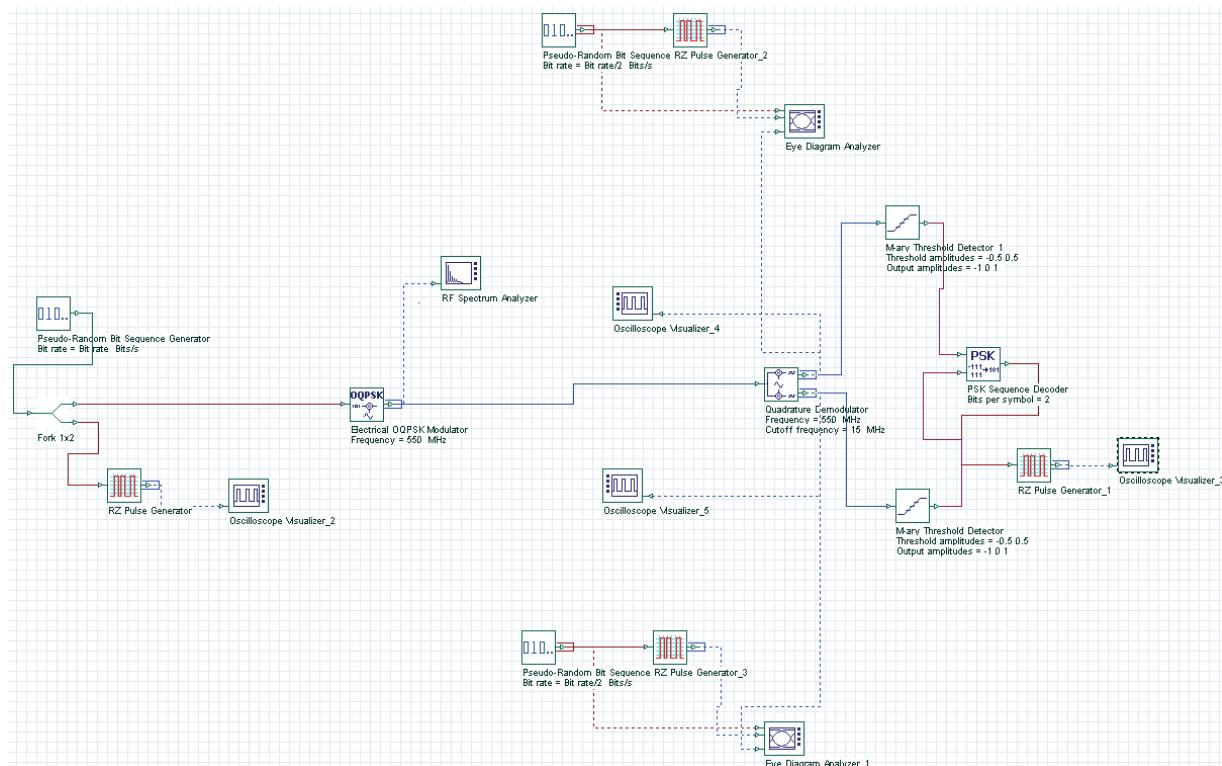
# Digital modulation—OQPSK

## Introduction

The OQPSK modulation is a PSK modulation, using 2 bits per symbol and a delay of one bit in the in quadrature signal (refer to OptiSystem component library, **OQPSK Pulse Generator**). The project file "OQPSK – Transmitter and Receiver.osd" has an OQPSK transmitter and receiver (Figure 1).

This project was based on the project from Figure 16, but replaces the DPSK modulator with the OQPSK modulator, and the DPSK sequence decoder with the PSK sequence decoder.

**Figure 1 OQPSK System**



The main difference from the DPSK project is the bits per symbol (2), the threshold and output amplitudes for the detector (-1,0,1) and the decision instant for the in quadrature threshold detector (0.75). The decision instant difference is related to the delay added to the quadrature signal in the transmitter stage.

## Simulation Results

After running the simulation you can visualize the results from the Eye diagrams (Figure 2), and also compare the input and output bit sequence (Figure 3). The input and output signals should be the same.

**Figure 2 OQPSK Eye diagrams: In-phase and In-quadrature signals**

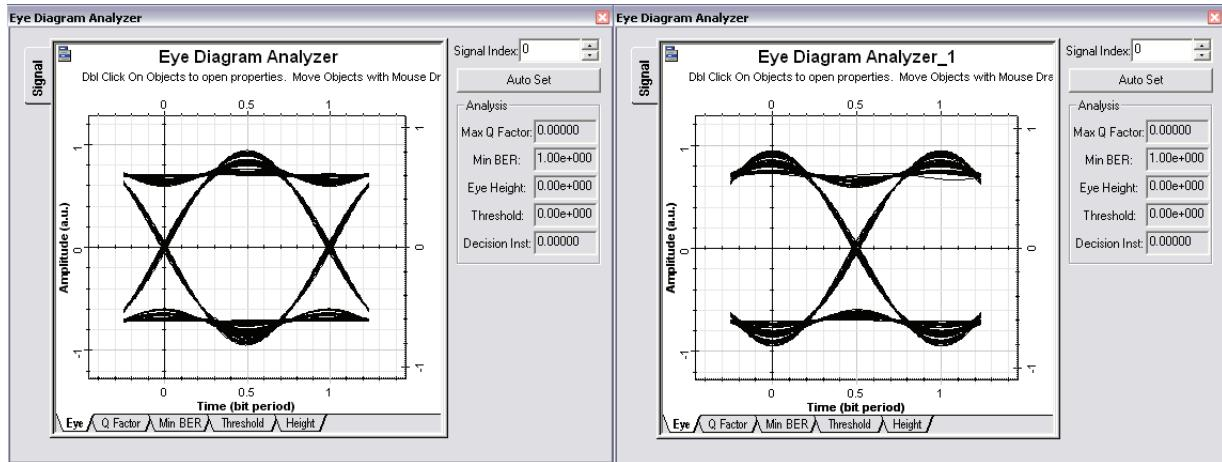
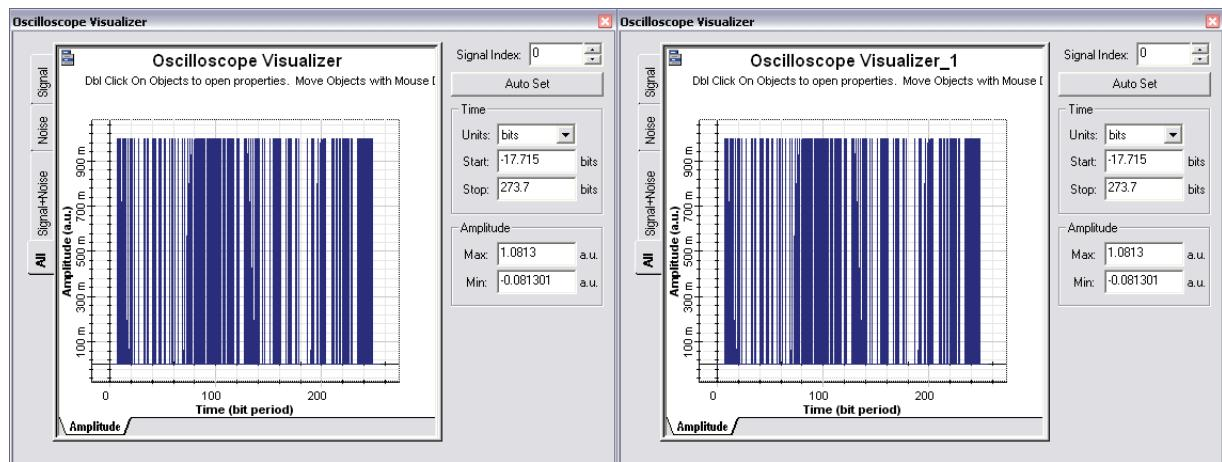


**Figure 3 Electrical signals before and after OQPSK coding/decoding**

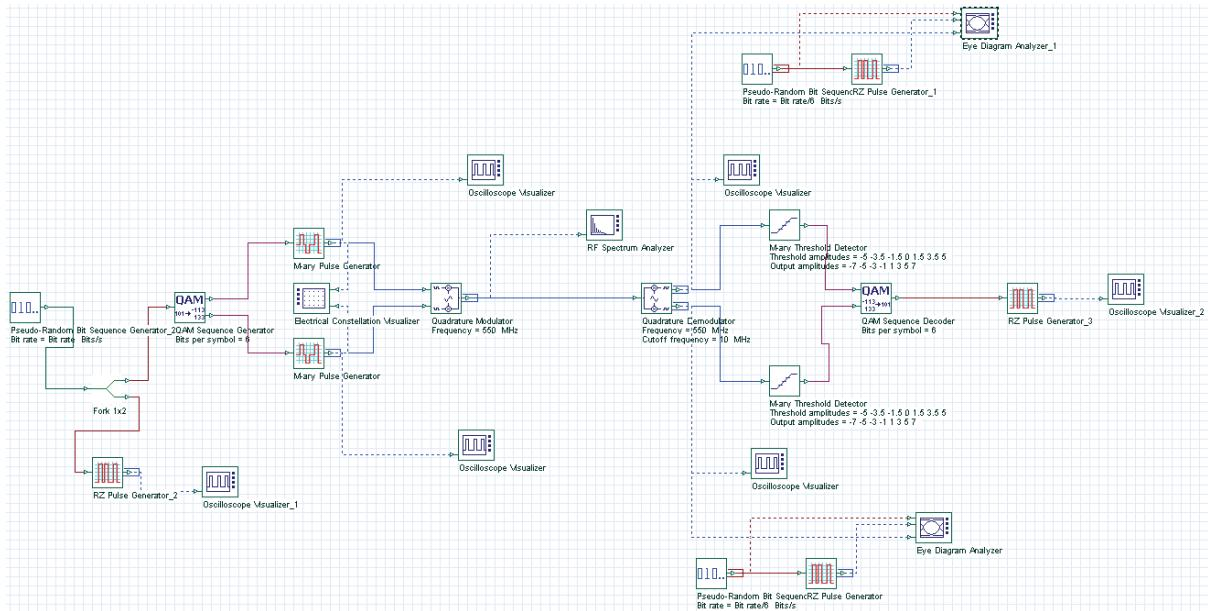


# Digital modulation—QAM

## Introduction

The QAM modulation is typically used in CATV system for cable modem transmission. The project file "QAM - Transmitter and Receiver.osd" has an QAM transmitter and receiver (Figure 1) using a 64 QAM transmission (6 bits per symbol).

**Figure 1 64 QAM System**



The main difference from the DPSK project is the bits per symbol (6), the threshold and output amplitudes for the detector (-7, -5, -3, -1, 1, 3, 5 and 7). Also the global sequence length is 2048.

## Simulation Results

After running the simulation you can visualize the results from the Eye diagrams (Figure 2). Additionally you can visualize the constellation diagram (Figure 3), with the expected results for the In-phase and quadrature points for a 64 QAM modulation scheme.

**Figure 2 64 QAM Eye diagrams: In-phase and In-quadrature signals**

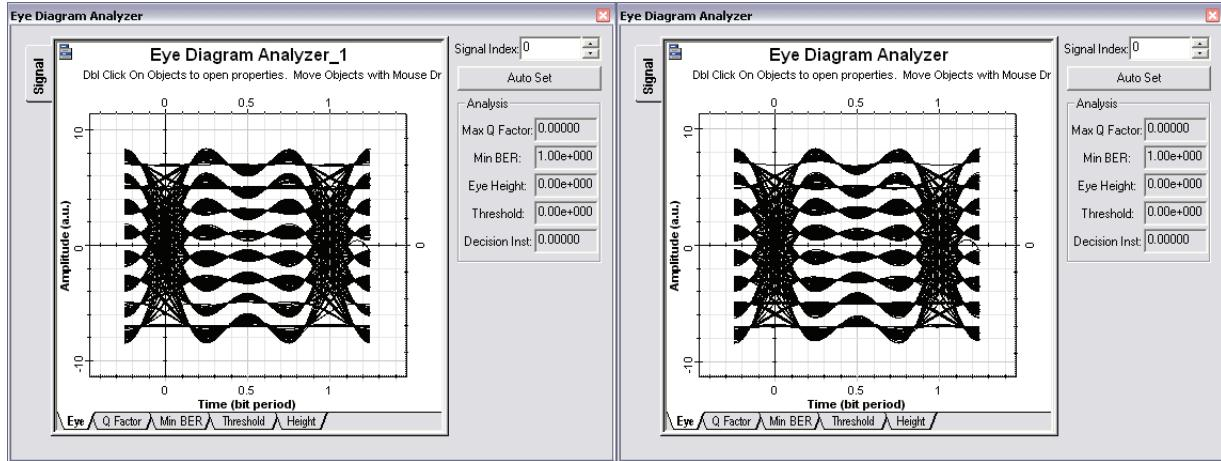
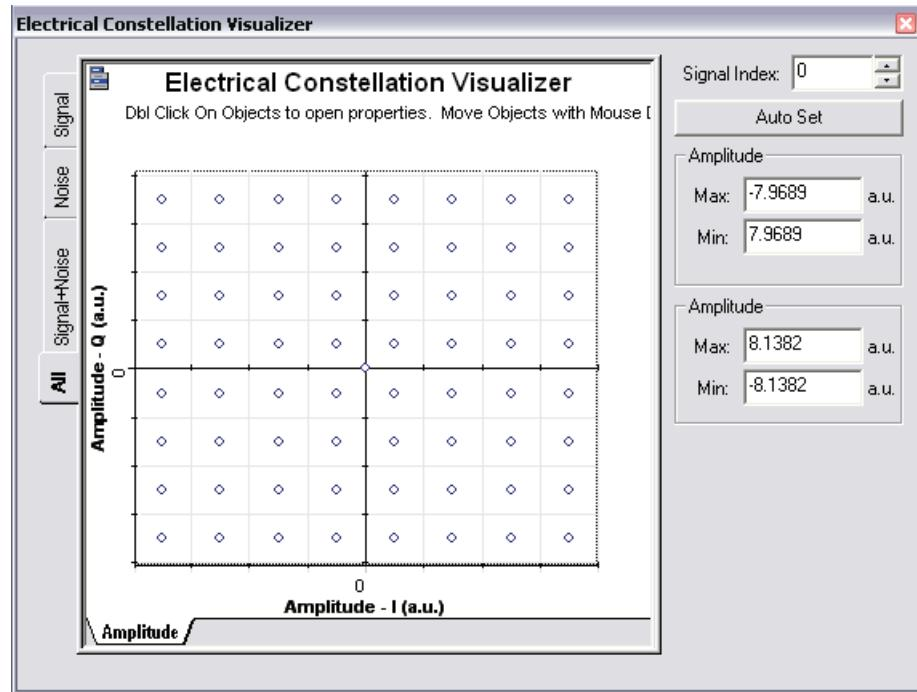


**Figure 3 Constellation diagram for a 64 QAM modulation (6 bits per symbol)**



# Manchester and PAM Coding/Decoding

A Manchester encoded signal contains frequent level transitions which allow the receiver to extract the clock signal and correctly decode the value and timing of each bit. To allow reliable operation, the transmitted bit stream must contain a high density of bit transitions. Manchester encoding ensures this, allowing the receiving to correctly extract the clock signal. Projects **Manchester Coding - Decoding.osd** and **Manchester - Fiber Link.osd** (Figure 1) demonstrate the usage of this type of coding. Project **PAM - Fiber Link.osd** demonstrates the bipolar non-return-to-zero scheme that is known as pulse amplitude modulation or PAM (Figure 2).

**Figure 1** Manchester coding and decoding.

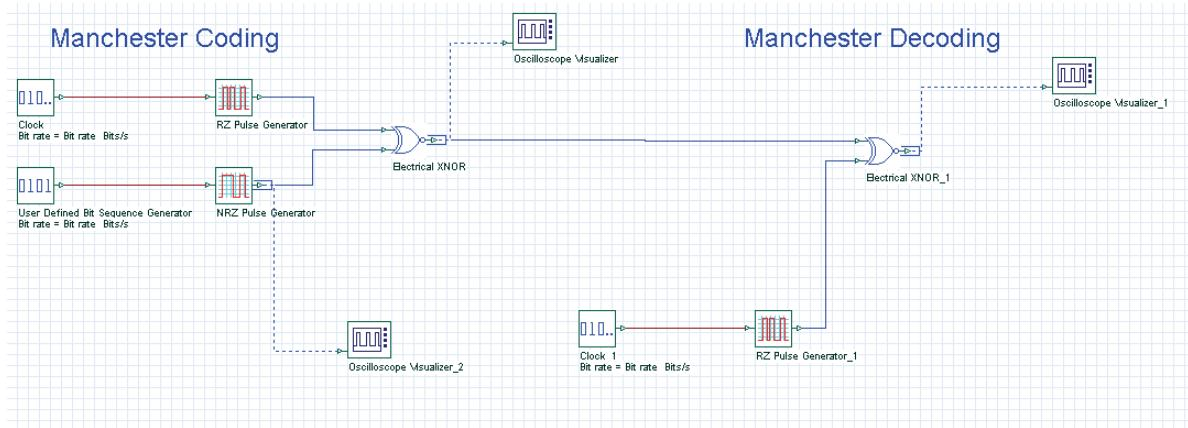
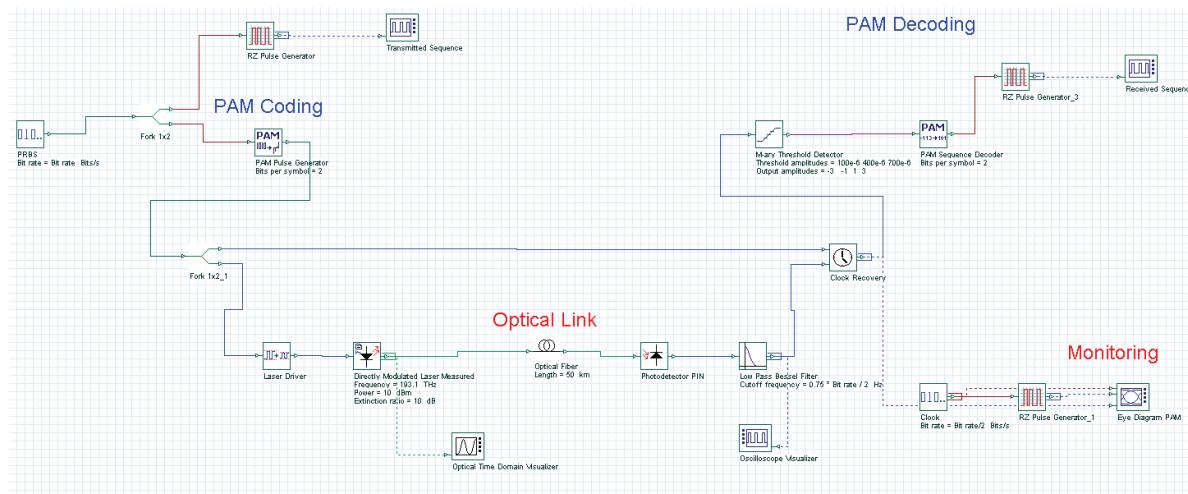


**Figure 2** PAM coding and decoding.



**Notes:**

---

## CATV

---

This section contains the following advanced and illustrative simulation projects.

- Using OptiSystem to analyze CATV systems

**Notes:**

# Using OptiSystem to analyze CATV systems

---

The aim of this material is to show the possibilities of using OptiSystem to analyze CATV systems.

In Part I, we demonstrate the basic nonlinear distortions that result from the propagation of the multiple carrier frequencies through a laser diode.

Observation of harmonic and intermodal products is presented. Although the appearance of the nonlinear distortions is a deterministic process, it is considered to contribute to the laser noise.

In Part II, as a typical application example, direct modulation of a laser diode is considered.

We analyze:

- a) laser frequency response
- b) laser clipping with single sinusoid modulation
- c) RIN
- d) propagation of the signal with harmonic distortions, RIN and phase noise through standard fiber

To demonstrate these topics, different layouts in the sample file have been designed.

Global parameters of the layouts have been chosen to allow enough frequency resolution for the reliable observation of the studied phenomena. We used a sample rate 160 GHz, and a number of points 65536, with 2.44 MHz frequency resolution.

In most of the cases, our laser diode (described by the laser rate equation component) has threshold current 33.457 mA, bias current 38 mA, and modulation peak current 3.8 mA.

In some cases, in order clearly to observe different effects, RIN and phase noise of laser diode, and noise sources in PIN were disabled.

## Part Basic Nonlinear Distortions

### Harmonic distortions

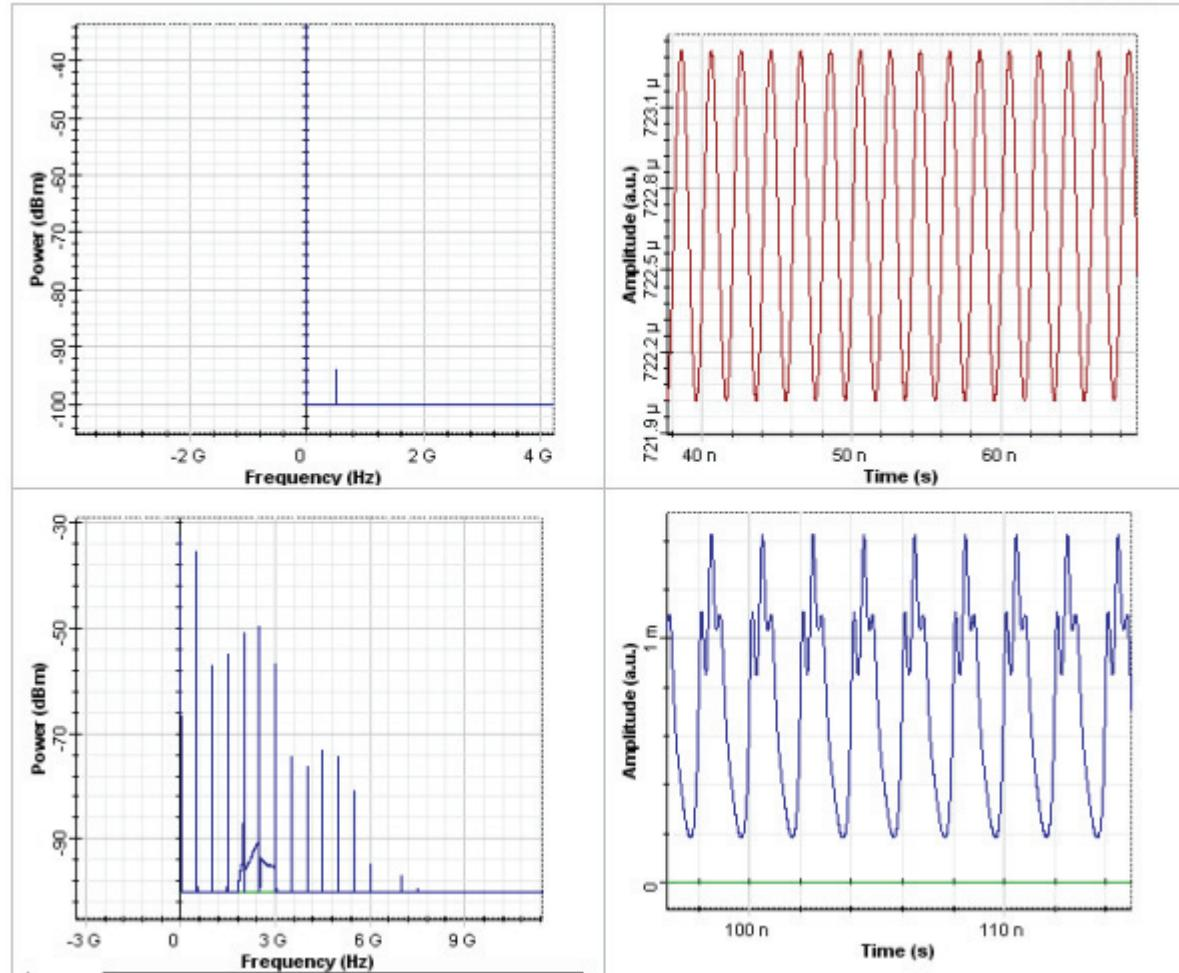
For the analysis of harmonic distortions (layout Harmonic distortions), we use one-tone modulation  $f_1$  at 500 MHz.

The values of carrier generator amplitude are swept: 0.001, 0.1, 0.2, 0.8, 1, 1.2, and 1.5. Both the RIN and phase noise of laser rate equations and noise sources in PIN are disabled.

In the following figures, the spectrums and time domain shapes of the signal from the first (initial signal) and fourth iterations are presented.



Figure 1 Harmonic distortions



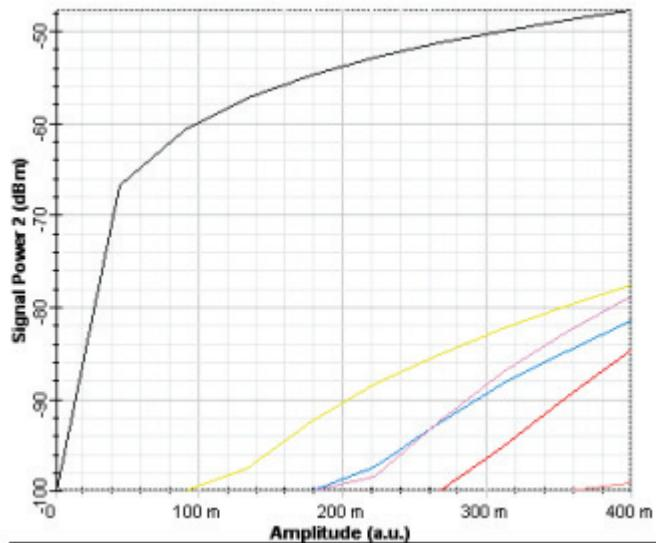
As we can see, the harmonic distortions can be seen at the tones  $nf_1$ ,  $n$  is the integer number. The appearance of the new harmonic frequencies in the spectrum leads to a shape deformation of the signal in time, which can be seen in the fourth graph.

We also perform an analysis of the dependence of the magnitudes of the harmonic products as a function of the modulation index. This is accomplished by means of the layout Harmonic distortions modulation index.

In this layout, the modulation index is swept through the change of the amplitude of the carrier generator (between 0.001 and 0.4).

The powers of the original signal at  $f_1 = 500$  MHz, and the harmonics at  $2f_1 = 1$  GHz,  $3f_1 = 1.5$  GHz,  $4f_1 = 2$  GHz,  $5f_1 = 2.5$  GHz, and  $6f_1 = 3$  GHz, are measured with the Electrical Carrier Analyzer.

Results are shown in the next figure, where the black, yellow, green, pink, red, and the second pink (just at the bottom right corner of the figure) curves correspond to 500 MHz, 1GHz, 1.5 GHz, 2 GHz, 2.5 GHz, and 3 GHz, respectively.

**Figure 2 Magnitudes of the harmonic products**

As we can see, the software allows the detailed quantitative analysis of the development of the different harmonic distortions.

### Intermodulation distortions

For the analysis of intermodulation distortions (layout Intermodulation distortions), two-tone modulation is applied  $f_1 = 500MHz$ ,  $f_2 = 525MHz$ .

To change the modulation index, the amplitude of the carrier generator is swept between 0.001 and 0.15. Both the RIN and phase noise of laser rate equations, and noise sources in PIN were disabled.

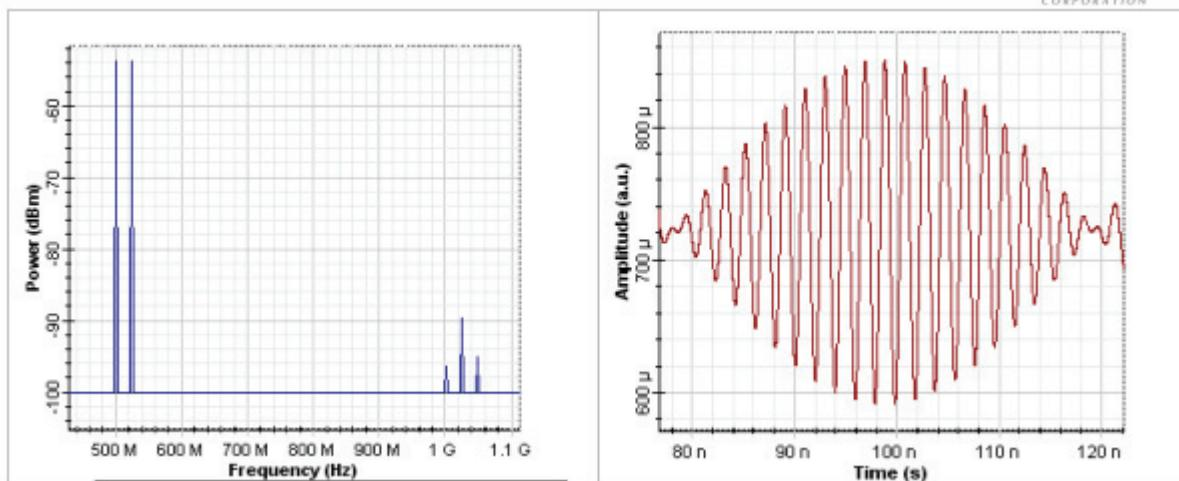
In all cases, the product of 3.8 mA with the amplitude of the carrier generator (which gives the modulation index) is smaller than  $38 \cdot 33.457 = 4.543$  mA.

Therefore, we cannot expect laser clipping.

Proceeding through the five iterations of the RF Spectral Analyser\_1, we will see the appearance of new intermodulation products: second- and third-order intermodulation distortions.

The second-order intermodulation distortions will be given by  $|f_1 - f_2| = 25MHz$  and  $|f_1 + f_2| = 1025MHz$ .

In the following figures, the spectrum and corresponding time-domain form of the signals is shown.

**Figure 3 Spectrum and corresponding time-domain form of the signals**

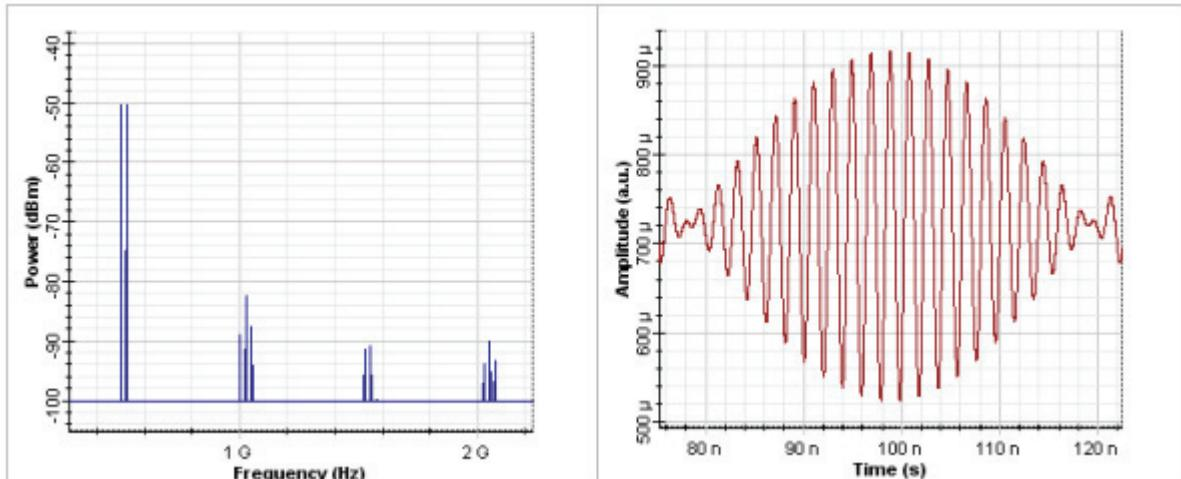
In the first figure we see on the left our original frequencies:  
 $f_1 = 500\text{MHz}$ ,  $f_2 = 525\text{MHz}$ .

On the right side of the first figure, we see the second-order distortion  $|f_1 + f_2| = 1025\text{MHz}$  (the largest between the three components), and the next order of the second-order distortions between  $f_3 = |f_1 + f_2| = 1025\text{MHz}$ , and  $f_4 = |f_1 - f_2| = 25\text{MHz}$ , namely  $f_5 = |f_3 + f_4| = 1.05\text{GHz}$ , and  $f_6 = |f_3 - f_4| = 1\text{GHz}$ .

The corresponding time shape of the signal is shown in the second figure.

Let us now continue with the analysis of third-order intermodulation distortions. The third-order distortions will be given by  $|2f_1 - f_2| = 475\text{MHz}$  (also called two-tone third-order IM products), and  $|2f_1 + f_2| = 1525\text{MHz}$ , respectively.

The following figure shows the results from the calculation of the fifth iteration of this layout.

**Figure 4 Calculation of the fifth iteration**

In the first figure we see already four groups of frequencies.

The first group is our initial two-tone signal.

The second group has been explained by second-order distortions.

The third group consists of two frequencies components:

$$f_7 = |2f_1 + f_2| = 1.525 \text{ GHz}, \text{ and } f_8 = |2(f_1 + f_2) - f_1| = 1.55 \text{ GHz}.$$

As we can see, both of these frequency components are related to the corresponding two-tone third-order IM distortions.

The frequencies in the fourth group are  $f_9 = 2.025 \text{ GHz}$ ,  $f_{10} = 2.05 \text{ GHz}$ , and  $f_{11} = 2.075 \text{ GHz}$ .

They can be interpreted as following triple-beat IM products:  $f_9 = |f_7 + f_8 - f_5|$ ,  $f_{10} = |f_7 + f_8 - f_3|$ , and  $f_{11} = |f_7 + f_8 - f_6|$ .

The further increasing of the number of the intermodulation products leads ultimately to deformation of the time shape of the signals.

The contributions of the different second-order and third-order intermodulation distortions (triple-beat IM products and two-tone IM products) can be estimated precisely using the Electrical Carrier Analyzer in the way already demonstrated in the layout Harmonic distortions.

Using standard formulas, the composite second order (CSO) and composite triple beat (CTB) can be calculated that describe the performance of the arbitrary multichannel AM links.



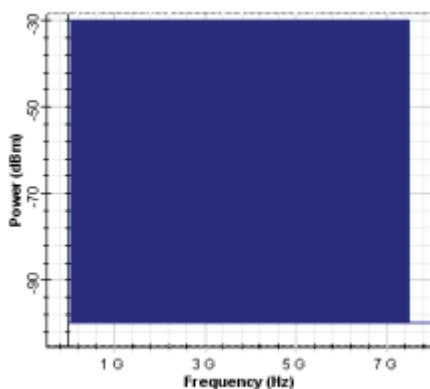
## Direct Modulation of Laser Diode

### Laser frequency response

Next, we analyze the laser frequency response.

We use a carrier generator, which creates 298 channels with 25 MHz frequency separations, starting at 50 MHz. This initial signal can be seen in the figure below:

**Figure 5 298 channels with 25 MHz frequency separations**



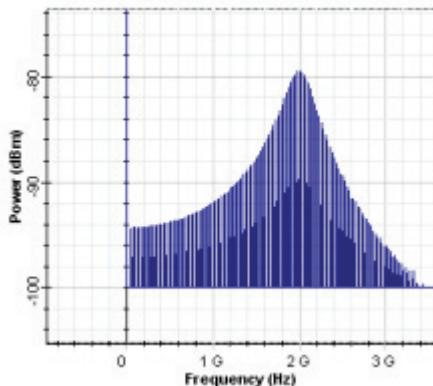
This signal is applied to the laser diode. The RF spectrum analyzer is used after the PIN in order to display the laser frequency response. Noise and phase noise of laser rate equations, and noise sources in our PIN were disabled.

In this project, three different values of the amplitude of the carrier generator were used: 0.001, 0.01, and 0.8.

For only the first value, we drive the laser without generating laser nonlinearities. This is the way to obtain the correct laser frequency response.

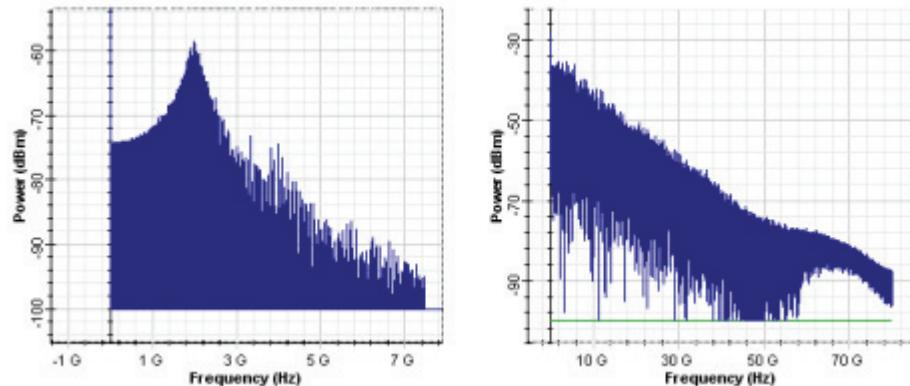
For a laser driver without nonlinearities (iteration 1, the amplitude of the carrier generator = 0.001), the observed frequency response of our directly modulated laser is shown in the next figure.



**Figure 6 Frequency response of our directly modulated laser**

As can be seen, for the default values of the physical parameters of our laser rate equation model, the relaxation frequency is approximately 2 GHz.

By increasing the values of the amplitude of the carrier generator, the nonlinearities of the laser are triggered. As a result, the observed frequency response changes dramatically. The obtained results for the displayed output for the next two iterations can be seen in the next two figures.

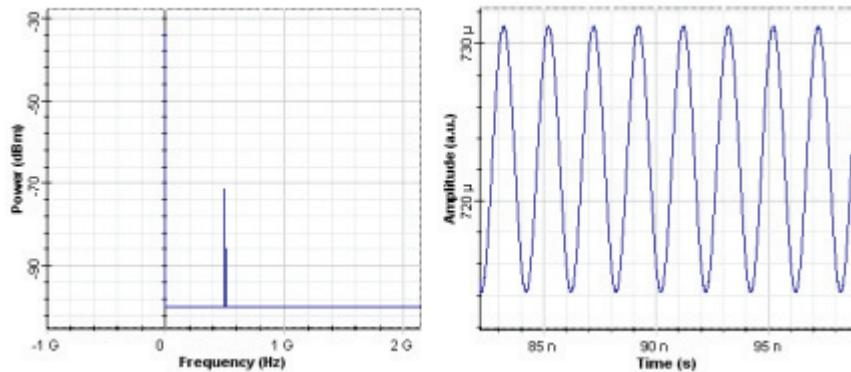
**Figure 7 Output for the next two iterations**

## Clipping

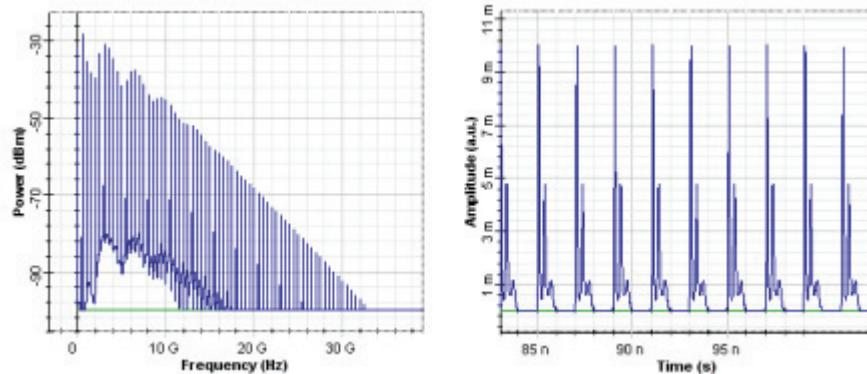
For the analysis of clipping (layout Clipping), the amplitude of the carrier generator is fixed at 0.25.

In this case, the modulation peak current is swept between 0.2, 11.5, 21, 30.5, and 40. Noise and phase noise of laser rate equations, and noise sources in our PIN were disabled.

In the first iteration, linear transformation of the electrical signal to optical and back to electrical can be seen.

**Figure 8 First iteration**

After the third iteration, the drive current goes below a threshold and the laser output power goes to zero in the time domain presentation of the signal. This phenomenon is called clipping. Clipping is best demonstrated in the fifth iteration.

**Figure 9 Third iteration**

## RIN

Here we analyze the relative intensity noise (RIN) of our laser diode.

In our laser rate equation model, we enabled the option *Include noise* in the Noise tab. Noises in PIN were disabled.

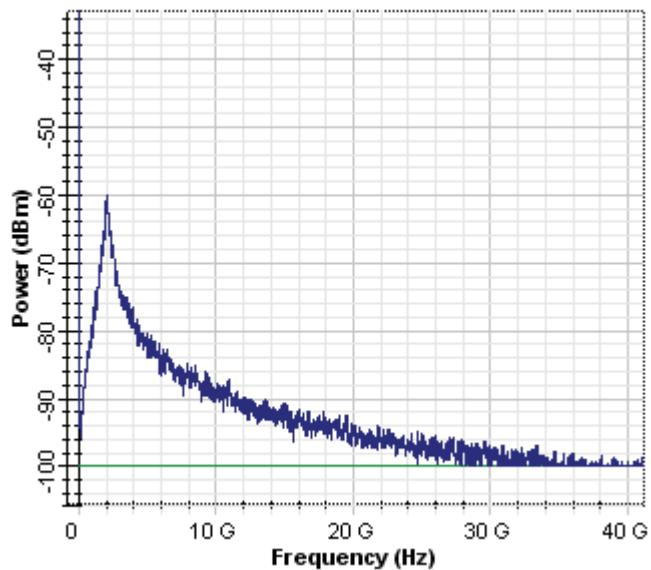
We will sweep the amplitude parameter of carrier generator: 0.001, 0.045, and 0.6.

Note that in this layout, we increased the resolution bandwidth in the RF Spectrum analyzer to 50 MHz.

Contribution from harmonic distortions is minimal in the first iteration. A typical spectral presentation of RIN is observed by using the RF Spectrum analyzer.



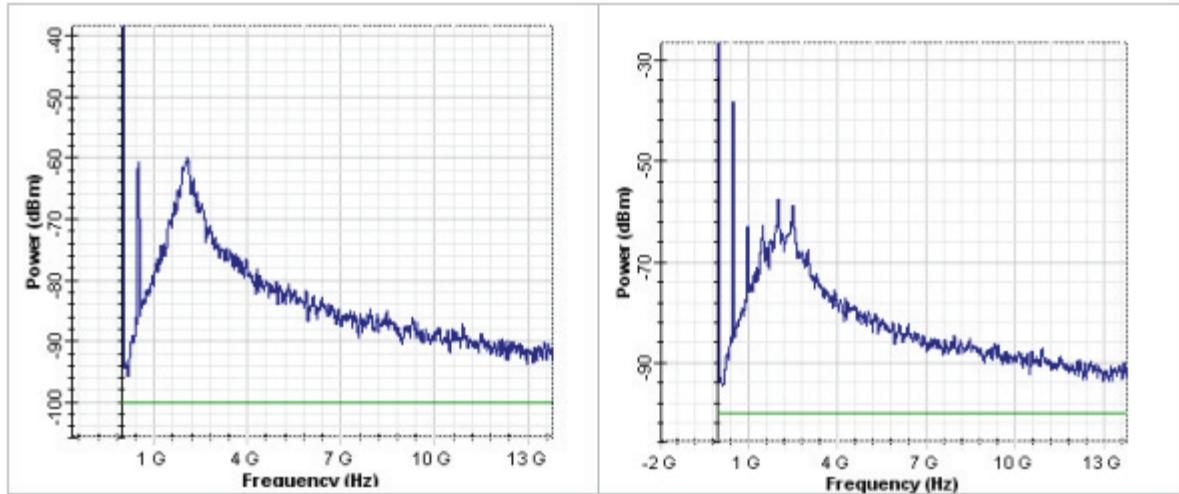
Figure 10 Spectral presentation of RIN is observed by using the RF Spectrum analyzer



RIN spectral dependence peaks at frequency 2 GHz.

As mentioned previously, at the same frequency, the maximum laser frequency response was seen. The same default values of the physical parameters of the laser model have been used. This is what we expect from the laser theory.

In the next two figures, we illustrate the relative intensity noise in the presence of harmonic distortions.

**Figure 11 Relative intensity noise in the presence of harmonic distortions**

Note the appearance of the harmonics at the top of the RIN spectrum (50 MHz resolution bandwidth in the RF Spectrum analyzer has been used.)

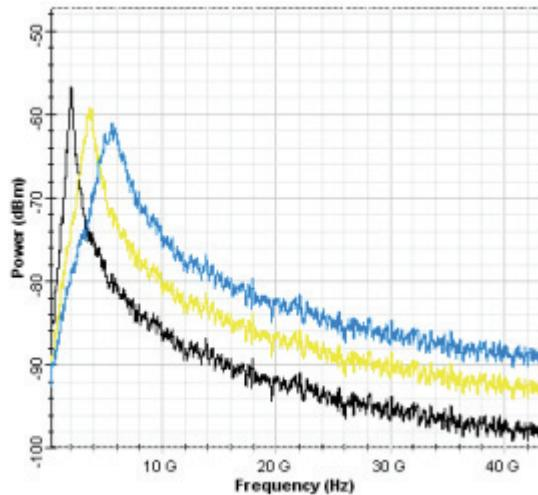
Next, we analyze the power dependence of the RIN.

It is well known that increasing the power lead to the reduction of RIN peak. This effect is demonstrated with the Layout RIN power dependence.

Here, we swept the bias current between 38, 58, and 68 A. As a result, the average power changes from 0.72 mW to 2.3 mW, and 5.5 mW.

The observed RIN spectrums are shown in the next figure, where black, yellow, and blue correspond to 0.72 mW to 2.3 mW, and 5.5 mW, respectively.



**Figure 12 Decrease in the peak of the RIN with the increase of the power**

The expected decrease in the peak of the RIN with the increase of the power can be clearly observed.

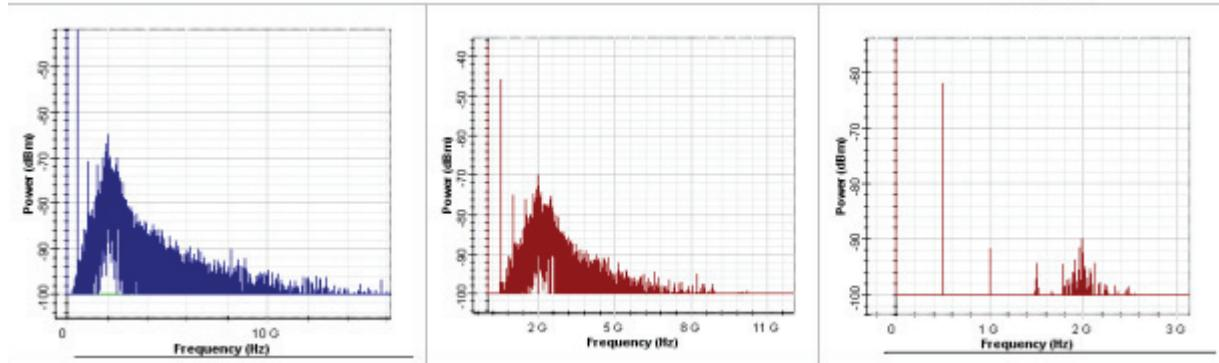
### **Harmonic distortions, RIN, phase noise and propagation in 50 km SMF**

Here we continue to analyze the influence of the relative intensity noise of our laser rate equation model on the harmonic distortions - layout RIN phase noise fiber.

In our laser rate equation model, we enable the options *Include noise* and *Include phase noise* in the Noise tab. Noise sources in PIN are disabled. We use the amplitude parameter of carrier generator 0.6. The resolution bandwidth in the RF Spectrum analyzer is 50 MHz.

We propagated our signal through 0, 10, and 50 km SMF. The parameters of the fiber can be seen in the tabs of the fiber component.

The corresponding results are shown in the next three figures.

**Figure 13 Powers of all signals were reduced by approximately 20 dB**

As we can see, at 50 km, due to the linear losses, the powers of all signals were reduced by approximately 20 dB.

If the power of the input light radiation is increased, a complex interaction between the harmonics generated in the laser will occur in the optical fiber because of the fiber nonlinearities.



---

## Multimode

---

This section contains the following advanced and illustrative simulation projects.

- Differential Mode Delay and Modal Bandwidth
- Encircled Flux

**Notes:**

# Differential Mode Delay and Modal Bandwidth

---

For the differential mode delay measurement (DMD), an 850 nm probe is scanned at small radial increments across the core of the multimode fiber under test.

At each position the temporal response to a short impulse is recorded. After removal of the reference pulse temporal width, the DMD temporal width is determined at the 25% threshold level between the first leading edge and the last trailing edge of all traces encompassed between specified radial positions.

The DMD Analyzer tool encapsulates the necessary equipment to do this measurement in one component.

The fiber modal bandwidth can be measured in time domain, using a pulse of light launched into one end of the fiber and the temporal response of the output is measured. Conversion into the frequency domain reveals the bandwidth from the transfer function  $H(f)$ , which is defined as the earliest frequency at which the amplitude drops 3 dB below the amplitude at zero frequency.

The Filter Analyzer component combined with the multimode generator can easily measure the fiber bandwidth.

## DMD Measurement

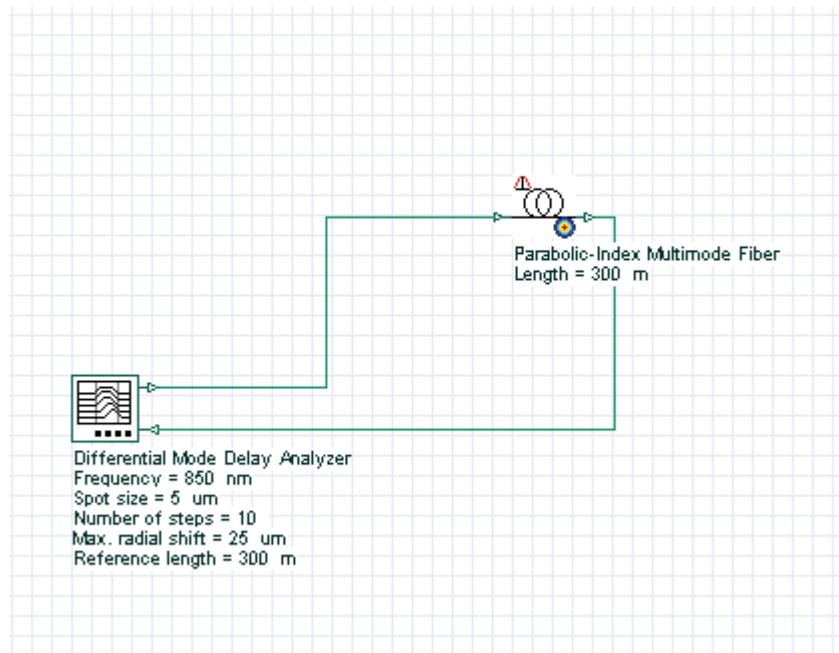
### System setup for a 50- $\mu\text{m}$ Fiber

Using the default global parameters, we can start adding the components to analyze the fiber DMD.

From the component library, drag and drop the following component in to the layout:

- From "Default/Visualizers Library/Optical", drag and drop the "Differential Mode Delay Analyzer" into the layout.
- From "Default/Optical Fibers/Multimode", drag and drop the "Parabolic-Index Multimode Fiber" into the layout.
- For the fiber, set the parameter Attenuation to 0 dB/km and the Length to 300 m.

The next step is to connect the components according to the Figure 1.

**Figure 1 DMD measurement layout**

For this example, the DMD Analyzer will generate one Laguerre-Gaussian spatial mode LG00, with the spot size equal to  $5 \mu\text{m}$ . The reference length is 300 m for the fiber and for the analyzer. The analyzer will generate 10 signals shifting the transverse mode from 0 to  $25 \mu\text{m}$ . The expected result is the  $50 \mu\text{m}$  fiber DMD graphs.

## Running the simulation

We can run this simulation and analyze the results:

- To run the simulation, you can go to the File menu and select Calculate. You can also press Control+F5 or use the calculate button in the toolbar. After you select Calculate, the calculation dialog box should appear.
- In the calculation dialog box, press the Play button. The calculation should perform without errors.

## Viewing the results

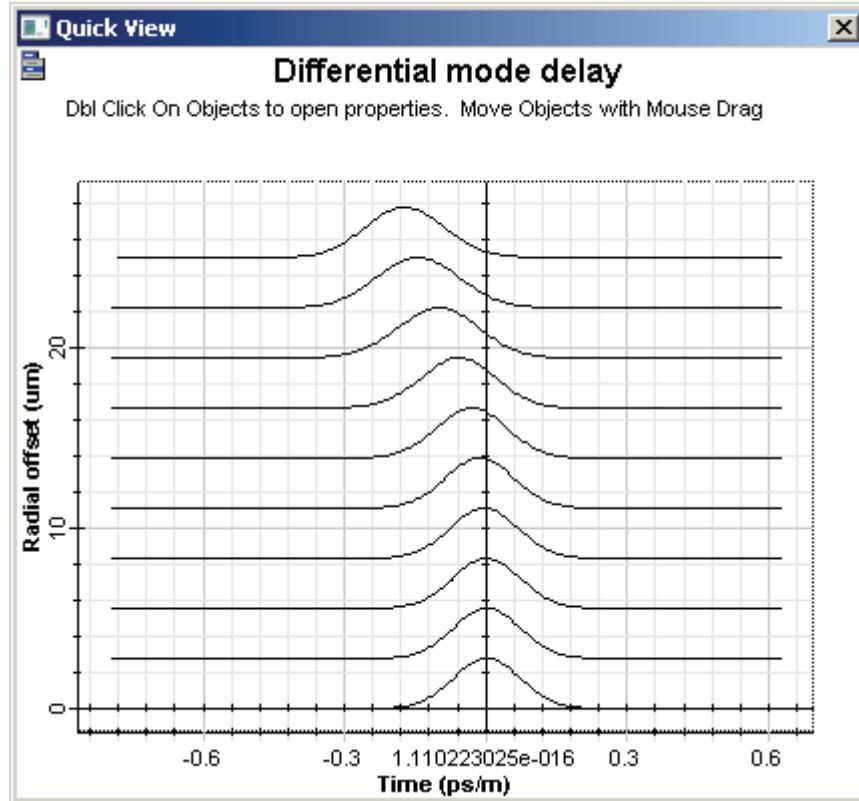
In order to see the results, go to the project browser and select the Graphs folder under the Differential Mode Delay Analyzer (Figure 2).



**Figure 2 Differential Mode Delay Analyzer graphs**

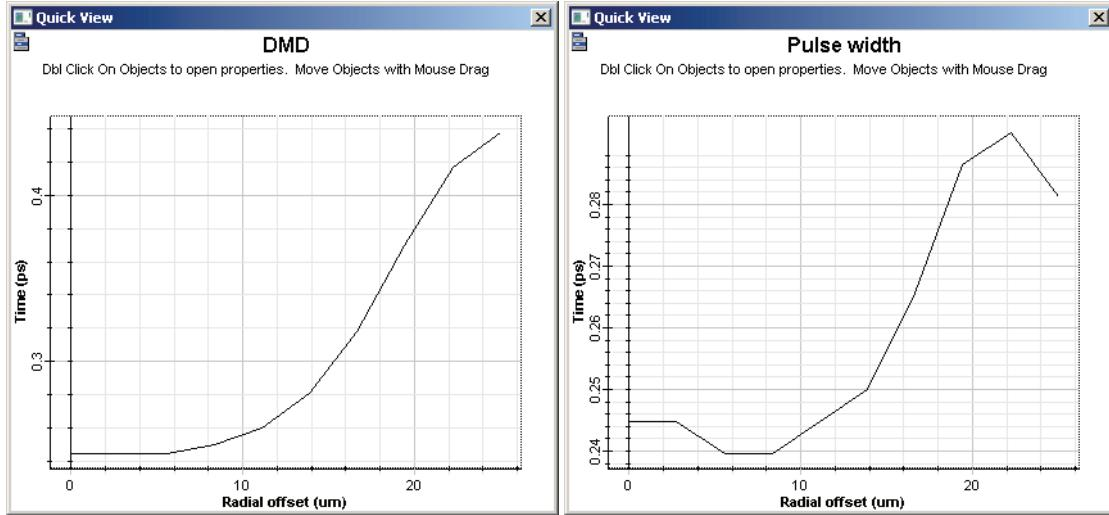
Name	Value
Layout 1	1
Global	
Differential Mode Delay Analyzer	Differential Mode Delay Analyzer
Ports	
Parameters	
Graphs	
Bandwidth	0
Differential mode delay	0
DMD	0
Pulse width	0
Transfer function	0
Unscaled differential mode ...	0
Parabolic-Index Multimode Fiber	Parabolic-Index Multimode Fiber

The main graph is the “Differential mode delay” graph (Figure 3). It shows the temporal-radial evolution of the fiber output pulse.

Figure 3 Differential mode delay graph for a 50  $\mu m$  fiber

The analyzer can also calculate the DMD and the pulse width versus radial offset. Additionally, the fiber transfer function and bandwidth for a given input pulse can be calculated.



**Figure 4 DMD and pulse width graphs for a 50  $\mu m$  fiber**

### System setup for a 30 $\mu m$ Fiber

We can repeat the same analysis for a fiber with 15  $\mu m$  radius:

- For the fiber, set the parameter Core radius to 15  $\mu m$ .
- For the analyzer, set the parameter Max. radial shift to 15  $\mu m$ .
- Run the simulation

### Viewing the results

Figures 5 and 6 present the results for the 30  $\mu m$  fiber.

## DIFFERENTIAL MODE DELAY AND MODAL BANDWIDTH

Figure 5 Differential mode delay graph for a 30  $\mu m$  fiber

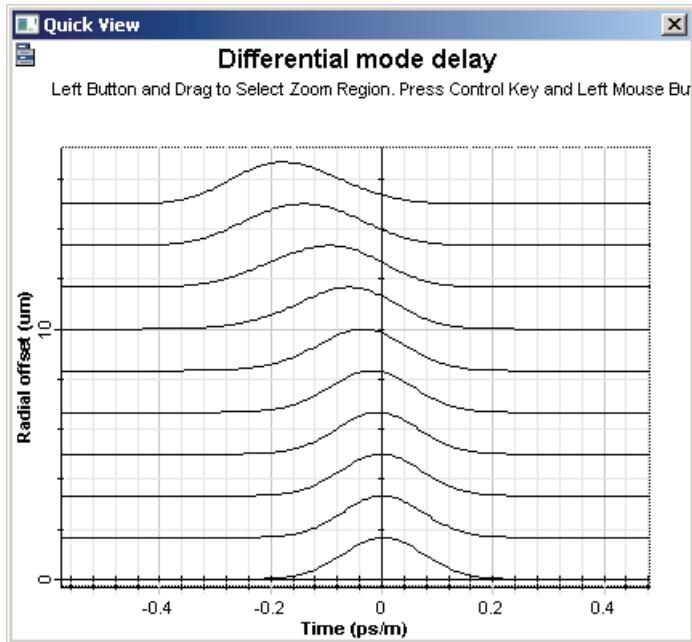
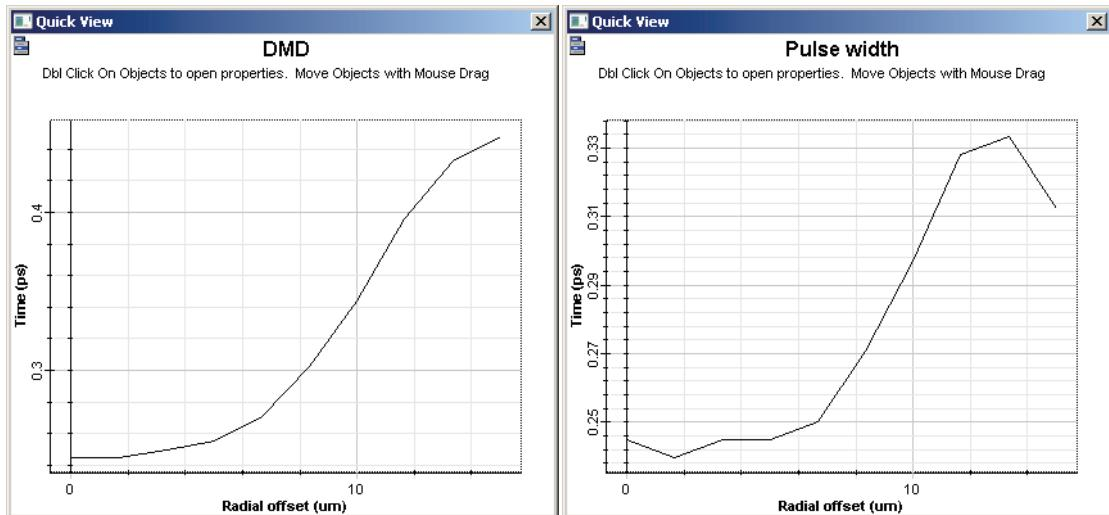


Figure 6 DMD and pulse width graphs for a 30  $\mu m$  fiber



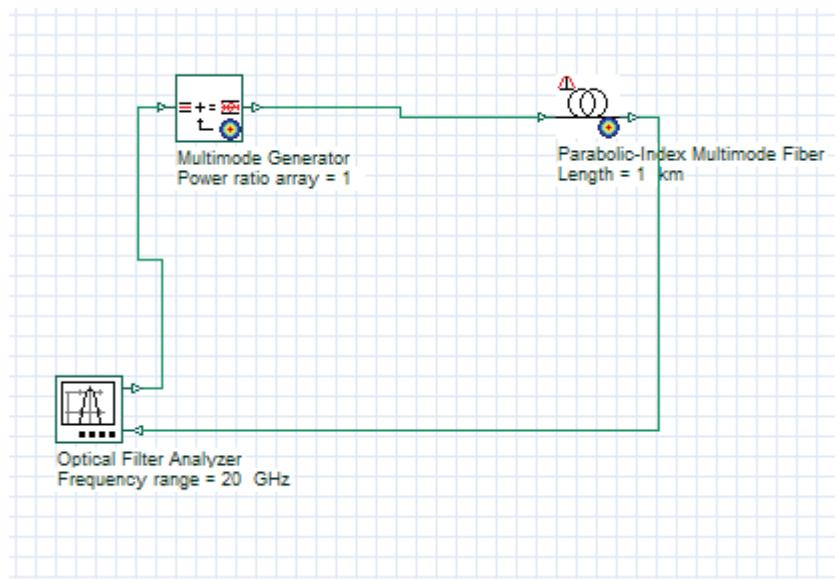
## Modal Bandwidth Measurement

### System setup

Using the previous 50 mm fiber, we can setup the measurement of the modal bandwidth:

- From "Default/Filter Library/Filter Analyzers", drag and drop the "Optical Filter Analyzer" into the layout.
- For the filter analyzer, set the parameter *Frequency* to 850 nm, *Frequency range* to 20 GHz, *Time domain* to true, and the Frequency unit to Hz.
- From "Default/Transmitters Library/Multimode", drag and drop the "Multimode Generator" into the layout.
- For the fiber, enable the parameter *Const. mode power dist.* (Numerical tab) and the parameter *Length* to 1 km.
- Connect the components according to Figure 7.

**Figure 7 Modal bandwidth measurement setup**



The filter analyzer will generate a time domain impulse and will measure the fiber response. The fiber will generate a constant power distribution for the modes (MPD), which imitates an overfilled launch condition.

- Run the simulation

## Viewing the results

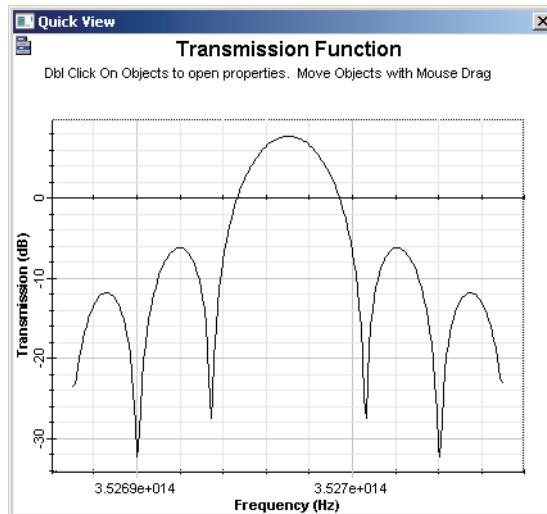
The filter analyzer also generates graphs and results using the project browser (Figure 8).

**Figure 8 Filter Analyzer graphs and results**

Name	Value
Layout 1	1
Global	
Multimode Generator	Multimode Generator
Optical Filter Analyzer	Optical Filter Analyzer
Ports	
Parameters	
Results	
Filter Bandwidth [BandPass] at Cut off (Hz)	5.39063e+009
Filter Bandwidth [BandPass] at Cut off (nm)	0.0129914
Filter Bandwidth [Band-Reject] at Cut off (Hz)	7.34375e+009
Filter Bandwidth [Band-Reject] at Cut off (nm)	0.0176991
Frequency at Max. Transmission (Hz)	3.52697e+014
Frequency at Max. Transmission (nm)	850
Frequency at Min. Transmission (Hz)	3.5269e+014
Frequency at Min. Transmission (nm)	850.017

The fiber bandwidth can be calculated by the filter bandwidth parameter ( $5.39 \text{ GHz} / 2 = 2.695 \text{ GHz}.\text{km}$ ). Additionally, the fiber transfer function can be displayed selecting the Transmission Function graph (Figure 9).

**Figure 9 Fiber transfer function**



# Encircled Flux

---

Encircled flux, as the name implies, describes the flux encircled within a circular radius inside the fiber.

Encircled flux is often quantified as the radius from the center of the fiber required to encircle 25% and 75% of the light energy through the fiber.

The power distribution of a fiber described by the encircled flux value is a crucial factor in ensuring the required data transmission rate in Gigabit Ethernet systems.

This tutorial describes the encircled flux simulation using the Encircled Flux Analyzer.

## System setup

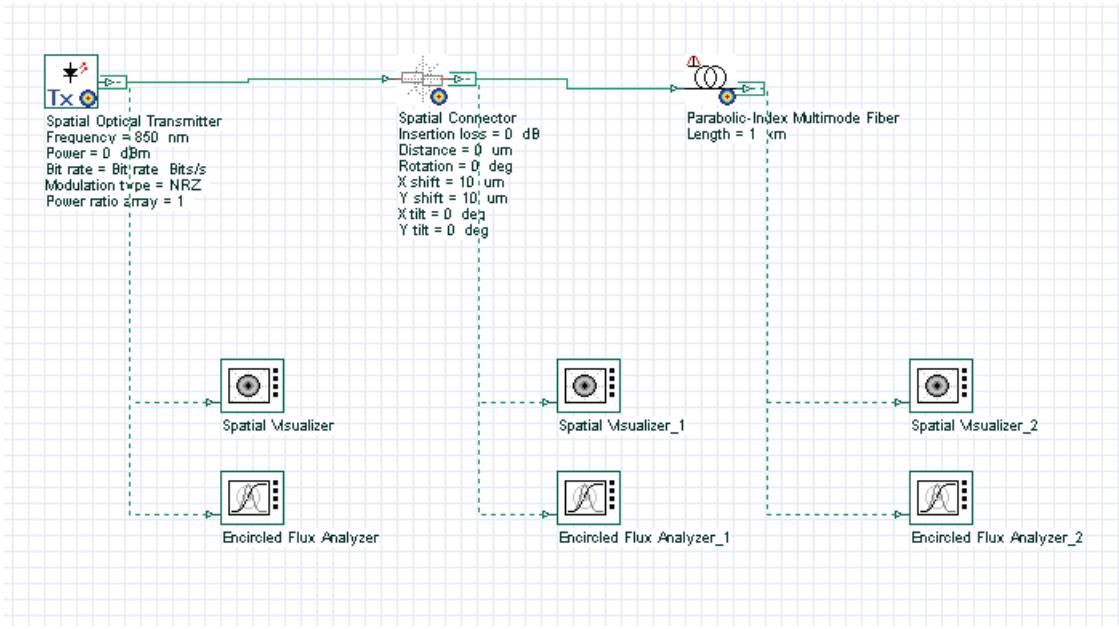
Using the default global parameters, we can start adding the components to design the basic encircled flux simulation layout.

From the component library drag and drop the following component in to the layout:

- From "Default/Transmitters Library/Optical Transmitters", drag and drop the "Spatial Optical Transmitter" into the layout.
- From "Default/Passives/Optical/Connectors", drag and drop the "Spatial Connector" component into the layout. Set the parameters X and Y shift to 10  $\mu m$ .
- From "Default/Optical Fibers/Multimode", drag and drop the "Parabolic-Index Multimode Fiber" into the layout.
- From "Default/Visualizers Library/Optical", drag and drop three instances of the "Spatial Visualizer" into the layout.
- From "Default/Visualizers Library/Optical", drag and drop three instances of the "Encircled Flux Analyzer" into the layout.

The next step is to connect the components according to the Figure 1.



**Figure 1 Multimode link and encircled flux measurement**

For this example, the optical transmitter will generate one Laguerre-Gaussian spatial mode  $LG_{00}$ , with spot size equal to  $10 \mu m$ .

The spatial connector has an X and Y-axis shift of  $10 \mu m$ . The fiber has  $25 \mu m$  radius and this is the same analysis radius for the encircled flux analyzers.

## Running the simulation

We can run this simulation and analyze the results:

- To run the simulation, you can go to the File menu and select Calculate. You can also press Control+F5 or use the calculate button in the toolbar. After you select Calculate, the calculation dialog box should appear.
- In the calculation dialog box, press the Play button. The calculation should perform without errors.

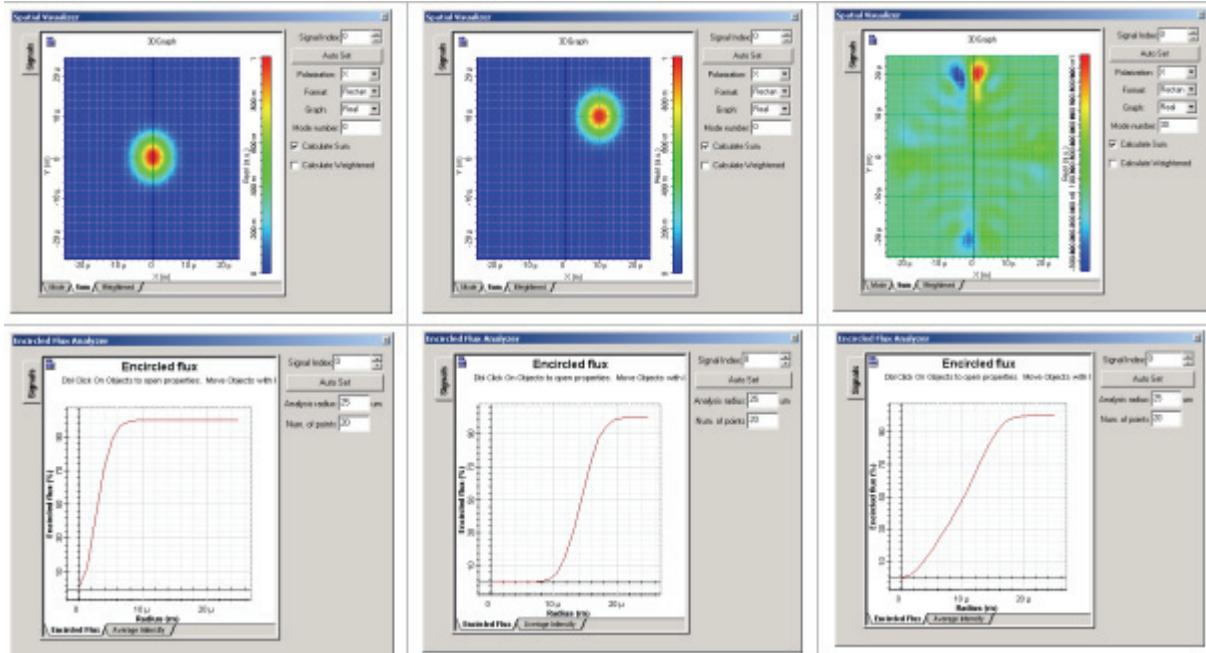
## Viewing the results

In order to see the results, double click the Encircled Flux Analyzer.

Using the Encircled Flux Analyzer, you can see the encircled flux and average intensity of the signals.

Figure 2 presents the total signal output (spatial) and the encircled flux graphs for each of the analyzers.

**Figure 2 Spatial profile of the total field using the spatial visualizer and the encircled Flux Analyzer displaying the encircled flux graph for each signal**



The first graph (left) shows the transverse mode at the transmitter output. The mode is centered at 0,0 and the encircled flux graphs show the maximum flux approximately at  $10 \mu m$ .

After the spatial connector, the transverse mode (center graph) is shifted by  $10 \mu m$  and the maximum flux is at approximately  $20 \mu m$ , as expected after the X and Y-axis shift.

The last graph (right) shows the sum of the transverse modes at the fiber output. The signal is centered at 0,0 and the encircled flux graph shows the maximum flux at  $20 \mu m$ .

The Encircled Flux Analyzer can be added to any output port and the user can easily recalculate the graphs by changing the analysis radius or number of points and pressing <ENTER>.

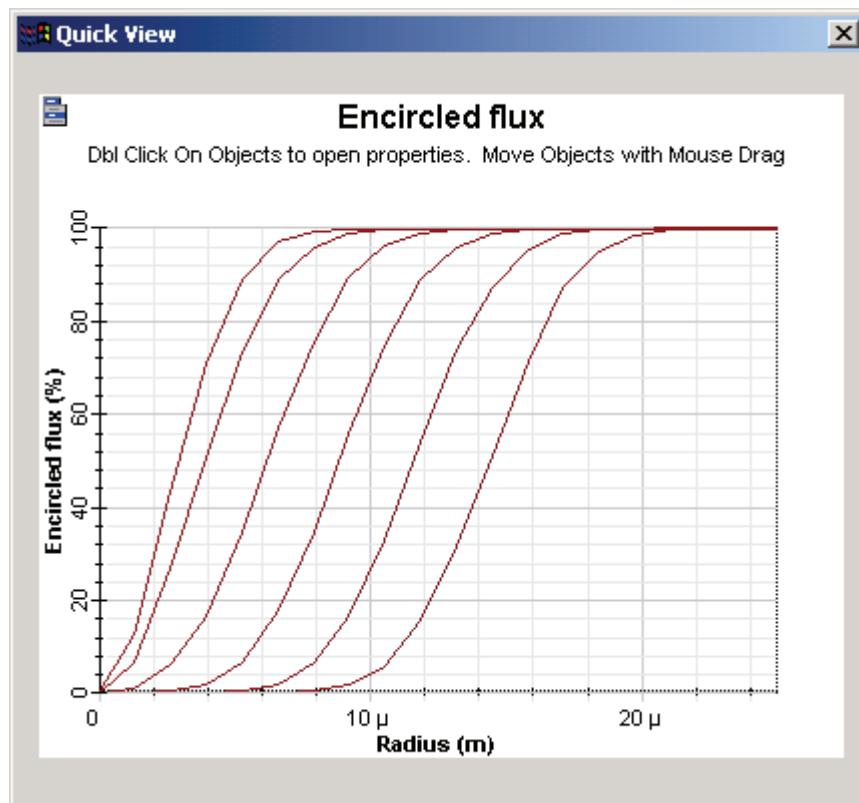


The user can also create a parameter sweep of the connector shift and see the changes of the encircled flux graph.

- Remove the multimode fiber and the visualizers connected to the fiber from the layout
- In the spatial connector, set the parameter X and Y shift mode to sweep.
- Set the sweep values to 0,2,4,6,8,10 mm for both parameters.
- Run the simulation

Using the Project browser, we can compare the encircled flux graphs per each sweep (Figure 3).

**Figure 3 Encircled flux graphs for each sweep of the X and Y shift**







**Optiwave**  
**7 Capella Court**  
**Ottawa, Ontario, K2E 7X1, Canada**

Tel.: 1.613.224.4700  
Fax: 1.613.224.4706

E-mail: [support@optiwave.com](mailto:support@optiwave.com)  
URL: [www.optiwave.com](http://www.optiwave.com)